POLYPUBLIE
Polytechnique Montréal

POLYTECHNIQUE MONTRÉAL
UNIVERSITÉ D'INGÉNIERIE

Titre: Title:	Experimental and Thermodynamic Investigation of RE-Mg-Zn (RE=Sc, Y, La, Ce, Pr, Nd, Pm, Sm, Eu, Gd, Tb, Dy, Ho, Er, Tm, Yb and Lu) Systems
Auteur: Author:	Zhijun Zhu
Date:	2015
Type:	Mémoire ou thèse / Dissertation or Thesis
Référence: Citation:	Zhu, Z. (2015). Experimental and Thermodynamic Investigation of RE-Mg-Zn (RE=Sc, Y, La, Ce, Pr, Nd, Pm, Sm, Eu, Gd, Tb, Dy, Ho, Er, Tm, Yb and Lu) Systems [Ph.D. thesis, École Polytechnique de Montréal]. PolyPublie. https://publications.polymtl.ca/1798/

Document en libre accès dans PolyPublie
Open Access document in PolyPublie

URL de PolyPublie: PolyPublie URL:	https://publications.polymtl.ca/1798/
Directeurs de recherche: Advisors:	Arthur Pelton, & Michael Gharghouri
Programme: Program:	Génie métallurgique

Ce fichier a été téléchargé à partir de PolyPublie, le dépôt institutionnel de Polytechnique Montréal
This file has been downloaded from PolyPublie, the institutional repository of Polytechnique Montréal

https://publications.polymtl.ca

UNIVERSITÉ DE MONTRÉAL

EXPERIMENTAL AND THERMODYNAMIC INVESTIGATION OF RE-Mg-Zn (RE=Sc, Y, La, Ce, Pr, Nd, Pm, Sm, Eu, Gd, Tb, Dy, Ho, Er, Tm, Yb and Lu) SYSTEMS

ZHIJUN ZHU

DÉPARTEMENT DE GÉNIE CHIMIQUE

ÉCOLE POLYTECHNIQUE DE MONTRÉAL

THÈSE PRÉSENTÉE EN VUE DE L'OBTENTION

DU DIPLÔME DE PHILOSOPHIAE DOCTOR

(GÉNIE MÉTALLURGIQUE)

AOÛT 2015

© Zhijun Zhu, 2015.

UNIVERSITÉ DE MONTRÉAL

ÉCOLE POLYTECHNIQUE DE MONTRÉAL

Cette thèse intitulée:

EXPERIMENTAL AND THERMODYNAMIC INVESTIGATION OF RE-Mg-Zn (RE=Sc, Y, La, Ce, Pr, Nd, Pm, Sm, Eu, Gd, Tb, Dy, Ho, Er, Tm, Yb and Lu) SYSTEMS

présentée par: ZHU Zhijun

en vue de l'obtention du diplôme de : Philosophiae Doctor

a été dûment acceptée par le jury d'examen constitué de :

M. CHARTRAND Patrice, Ph. D., président

M. PELTON Arthur, Ph, D., membre et directeur de recherche

M. GHARGHOURI Michael, Dr., membre et codirecteur de recherche

M. BALE Christopher, Ph. D., membre

M. DAVIS Boyd Robert, Ph. D., membre externe

DEDICATION

To my wife Yan Yang and my daughter Sirui Zhu

ACKNOWLEDGEMENTS

This research work was carried out at Center for Research in Computational Thermochemistry (CRCT) at École Polytechnique de Montréal under the guidance of Prof. A.D. Pelton. I gratefully acknowledge Prof. A. D. Pelton for his supervision and patience during my research. Prof. A.D. Pelton is a paragon of virtue and learning. Although he is very easygoing and easy to get along with, it is not the case when it comes to research-he is always strict on my research work. Needless to say, I benefit a lot from his instruction.

I am also indebt to my co-director Dr. Michael Gharghouri for his guidance of my experiments; to Prof. Mamoun Medraj for allowing me to use all the facilities at TMG lab in Concordia University; I would like to express my appreciation to both of you for your important suggestions to the Neutron Powder Diffraction experiments.

Special thanks goes to Prof. In-Ho Jung for proposing the current project; to Prof. Chistopher Bale for your excellent course on FactSage software; to Prof. Patrice Chartrand for your suggestion to the research; to Dr. Christian Robelin for your detailed explanation of the solution file and french translation of the Abstract; to Aimen Gheribi for your *ab-initio* calculation and French translation of “CONDENSÉ EN FRANÇAIS”; to Drs. Dmytro Kevorkov and Mostafa Ahmad for helping me prepare the samples; to Dr. Sooyeol Lee for helping with the neutron diffraction experiments; to Dr. Liling Jin for all your help during my research, to Dr. James Sangster for checking my thesis.

I also thank Dr. Jacques Melançon and Eve Belisle for helping with all the technical issue related to the computer or FactSage software.

I am grateful to all the staff members at Canadian Neutron Beam Center, without your help all the experimental work could not be finished.

All the members from CRCT: Mme Catherine Boucher, Dr. Sergei Degterov, Dr. Jean-Philippe Harvey, Dr. Wan-Yi Kim, Dr. Adarsh Shuklar, Dr. Guillaume Lambotte, Dr. Denis Shishin, Dr. Viktoria Prostakova, Mme Evgenii Nekhoroshev, Dr. Jian Wang, to name a few, are greatly appreciated for your friendship.

The financial support from the Natural Sciences and Engineering Research Council of Canada (NSERC) Magnesium Strategic Research Network are greatly appreciated.

I am particularly indebted to my wife, Yan Yang, for your support and understanding; to my daughter, Sirui Zhu, for all the happiness you bring to me; to all my family members and friends for your support and encouragement. I love you all!

RÉSUMÉ

Lors d'une "optimisation" / modélisation thermodynamique, des paramètres du modèle ajustables sont affinés à partir de toutes les données thermodynamiques et d'équilibres de phases disponibles de façon à obtenir un ensemble d'équations du modèle dépendant de la température et de la composition. A partir de ces équations du modèle, toutes les propriétés thermodynamiques et tous les diagrammes de phases peuvent être calculés par minimisation de l'énergie de Gibbs à l'aide d'un logiciel tel que FactSage. En général, l'optimisation d'un système ternaire commence par l'optimisation des trois sous-systèmes binaires. Les paramètres binaires du modèle sont ensuite utilisés pour estimer les propriétés des phases ternaires, et ces estimations sont ensuite améliorées par l'introduction de paramètres ternaires si nécessaire de façon à reproduire les données ternaires disponibles.

Tous les systèmes binaires Mg-Zn et Mg-RE (où RE = terre rare) ont déjà été optimisés auparavant et les paramètres du modèle pour ces systèmes sont disponibles dans le logiciel FactSage. Dans le présent projet, tous les systèmes binaires RE-Zn et la plupart des systèmes ternaires RE-Mg-Zn sont optimisés.

En premier lieu, toutes les données thermodynamiques et de diagrammes de phases disponibles pour les systèmes Re-Zn (Sc, Y, La, Ce, Pr, Nd, Pm, Sm, Eu, Gd, Tb, Dy, Ho, Er, Tm, Yb, Lu) ont été rassemblées et évaluées de manière critique. Les terres rares ont des propriétés très similaires. Les diagrammes de phases de tous les systèmes Re-Zn sont très semblables. Les tendances observées dans les propriétés des systèmes terre rare (RE)-Zn pour toute la séquence des terres rares ont été exploitées pour estimer les données manquantes et pour vérifier la cohérence des données existantes. Le Modèle de Miedema est également utilisé dans le présent projet pour évaluer l'enthalpie de mélange des phases liquides. A partir de toutes les données disponibles, une évaluation critique et une optimisation thermodynamiques de ces systèmes a été effectuée et des paramètres du modèle pour les propriétés thermodynamiques de toutes les phases ont été obtenus.

En second lieu, des expériences de diffraction de neutrons (DN) *in-situ* ont été réalisées pour des échantillons choisis dans les systèmes Ce-Mg-Zn et Nd-Mg-Zn de façon à identifier les phases et les températures de transition. Grâce à la grande capacité de pénétration des neutrons, des échantillons de grande taille (10-20 grammes) peuvent être utilisés dans le présent travail,

conduisant à un meilleur contrôle de la composition et à une résistance à l'oxydation accrue. Des informations plus précises à propos des relations de phases et du comportement en transformation découlent des présentes expériences de DN car celles-ci sont réalisées *in-situ* à des températures élevées. Toutes les données expérimentales de DN sont utilisées pour valider et affiner le modèle thermodynamique.

Finalement, toutes les données de diagrammes de phases pour les systèmes RE-Mg-Zn ont été évaluées de manière critique et tous les systèmes ternaires RE-Mg-Zn (à l'exception de Sc-Mg-Zn, Pm-Mg-Zn, Eu-Mg-Zn et Yb-Mg-Zn) ont été optimisés à partir des systèmes binaires Mg-Zn, Mg-RE et RE-Zn. Les tendances et régularités observées sont utilisées à nouveau lors de l'optimisation des systèmes ternaires. Comme on pouvait s'y attendre, tous les systèmes RE-Mg-Zn sont liés de près. Les systèmes Ce-Mg-Zn et Nd-Mg-Zn sont optimisés de façon critique en prenant en compte les nouvelles données de DN. L'optimisation thermodynamique de tous les autres systèmes RE-Mg-Zn est grandement facilitée par l'optimisation simultanée des systèmes Ce-Mg-Zn et Nd-Mg-Zn.

Il faut noter que le Modèle Quasichimique Modifié (MQM) est utilisé dans le présent projet pour décrire la phase liquide. Puisque l'ordre à courte distance est pris en compte par ce modèle, on s'attend à une meilleure description de la phase liquide.

Le présent projet a pour but de construire une banque de données thermodynamiques la plus complète et la plus précise possible pour les systèmes RE-Mg-Zn. Les chercheurs s'intéressant aux alliages de Mg pourront en bénéficier.

ABSTRACT

In a thermodynamic "optimization/modeling", adjustable model parameters are refined based on all available thermodynamic and phase-equilibrium data in order to obtain one set of model equations as functions of temperature and composition. From the model equations, all the thermodynamic properties and phase diagrams can be back-calculated by Gibbs energy minimization using software such as FactSage. Generally, in the optimization of a ternary system one begins by optimizing the three binary sub-systems. The binary model parameters are then used to estimate the properties of the ternary phases, and these estimates are then refined by introducing ternary model parameters where required to reproduce available ternary data.

All binary Mg-Zn and Mg-RE (where RE = rare earth) systems have already been optimized and the model parameters of these systems are readily available in the FactSage software. In the present project, all binary RE-Zn and most of the ternary RE-Mg-Zn systems are optimized.

Firstly, all available phase diagram and thermodynamic data for the RE-Zn (Sc, Y, La, Ce, Pr, Nd, Pm, Sm, Eu, Gd, Tb, Dy, Ho, Er, Tm, Yb, Lu) systems have been collected and critically assessed. The rare earth elements have very similar properties. The phase diagrams of all RE-Zn systems are very similar. Trends in the properties of the rare earth (RE)-Zn systems as one traverses the rare earth series have been exploited for purposes of estimating missing data and for checking existing data for consistency. The Miedema Model is also used in the present project to estimate the enthalpy of mixing of the liquid phases. Based on all available data, critical thermodynamic evaluation and optimization of these systems have been carried out and model parameters for the thermodynamic properties of all phases have been obtained.

Secondly, *in-situ* neutron diffraction (ND) experiments have been performed on selected samples in the Ce-Mg-Zn and Nd-Mg-Zn systems to identify phases and transition temperatures. Due to the high penetrating power of neutrons, large samples (10-20 grams) are used in the present work, leading to better control of composition and increased resistance to oxidation. More accurate information about phase relationships and transformation behavior can also be expected from the present ND experiments because they are performed *in-situ* at high temperatures. All the ND experimental data are used to validate and refine the thermodynamic modelling.

Finally, all phase diagram data for the RE-Mg-Zn systems have been critically assessed and all ternary RE-Mg-Zn (excluding Sc-Mg-Zn, Pm-Mg-Zn, Eu-Mg-Zn and Yb-Mg-Zn) systems have been optimized, based on the binary Mg-Zn, Mg-RE and RE-Zn systems. Observed trends and regularities are again used in the optimization of the ternary systems. As expected, all RE-Mg-Zn systems are similarly closely related. The Ce-Mg-Zn and Nd-Mg-Zn systems are critically optimized taking into account the new ND data. Thermodynamic optimization of all other RE-Mg-Zn systems is greatly aided by simultaneous optimization of the Ce-Mg-Zn and Nd-Mg-Zn systems.

It should be noted that the Modified Quasichemical Model (MQM) is used in the present project to describe the liquid phase. Since short range ordering (SRO) is taken into account by this model, better description of the liquid phase is expected.

The present project is aimed at building the most complete and accurate thermodynamic database for the RE-Mg-Zn systems from which all investigators of Mg alloys can benefit.

CONDENSÉ EN FRANÇAIS

Le secteur des transports contribue pour environ un quart des émissions des gaz à effet de serre du Canada. Une des possibilités pour réduire ces émissions, en ce qui concerne le secteur des transports, est de réduire la masse des véhicules. Celle-ci peut être réalisé en remplaçant les composantes actuelles en acier soit par soit par le magnésium ou par des alliages d'aluminium puisque les alliages *à* base de magnésium sont parmi les plus légère matériaux de structure. Cependant, le magnésium à des propriétés mécaniques faibles par rapport à l'acier et aux alliages d'aluminium : à savoir une mauvaise de résistance mécanique et une mauvaise maniabilité. Des éléments d'alliage doivent être ajoutés pour améliorer les propriétés mécaniques du magnésium.

Le zinc est souvent ajouté dans les alliages magnésium pour augmenter la résistance mécanique par renforcement de la solution solide. Le magnésium et le zinc ont la même structure hexagonale compacte, la même valence et une électronégativité similaire. Les tailles des deux éléments diffèrent entre de 15 *à* 18%. Selon les règles de Hume-Rothery, le zinc est l'un des éléments les plus appropriés pour le renforcement des solutions solides dans les alliages de magnésium. L'aluminium est un autre élément d'alliage important dans les alliages magnésium. L'addition d'aluminium peut également augmenter la résistance mécanique des alliages magnésium en formant la phase $Al_{12}Mg_{17}$ dans la matrice de magnésium. L'effet de renforcement de la phase $Al_{12}Mg_{17}$ est limité parce que cette phase devient molle à haute température. Par conséquent, les alliages Al-Mg ne peuvent être utilisés à hautes températures.

L'un des inconvénients *à* l'ajout de zinc et d'aluminium and le magnésium est qu'ils ne peuvent pas augmenter la capacité de mise en forme d'alliages de magnésium. Il est communément accepté que les systèmes de glissement au sein du magnésium soient très limités. Par conséquence, la capacité de déformation des alliages de magnésium demeure marginale. L'ajout d'éléments de terres rares peut augmenter la déformabilité des alliages de magnésium, possiblement du à la capacité des terres rares de changer l'énergie de défaut d'empilement dans les alliages de magnésium. Les terres rares peuvent également augmenter la résistance mécanique des alliages de magnésium, soit par durcissement de la solution solide ou renforcement via la précipitation.

Les bases de données thermodynamiques sont essentielles pour le développement de nouveaux alliages de magnésium. Avec une base de données appropriée, il est toujours possible

de prédire les propriétés thermodynamiques et les phases présentes dans un alliage donné. Dans cette étude, une nouvelle base de données thermodynamique pour les systèmes RE-Mg-Zn (RE désignant un élément de terre rare) a été construite en utilisant la méthode de CALPHAD (Acronyme anglais de CALculation of PHAse Diagram)

L'optimisation thermodynamique des systèmes RE-Mg-Zn ont été réalisées selon les étapes suivantes:

1) Toutes les données expérimentales relatives aux systèmes binaires RE-Zn sont examinées de manière critique. En se basant sur les données expérimentales, les modèles thermodynamiques appropriés sont choisis pour toutes les phases binaires possibles. En particulier, le modèle Quasichimique modifié (MQM) est utilisé pour décrire la phase liquide. Le MQM a la particularité de rendre compte des interactions à courte distance au sein de la phase liquide et peut ainsi amener à de meilleures extrapolations dans les systèmes d'ordre supérieur.
2) Des tendances entre les propriétés de tous les systèmes binaires de type RE-Zn ont été établis sur la base de l'analyse de données expérimentales disponibles (à savoir : les points de fusion des éléments purs de terres rares ainsi que les composes RE-Zn similaires; les paramètres de maille des composés RE-Zn). Les tendances ont été utilisées pour estimer les données absentes de la littérature telles que les points de fusion et l'enthalpie de formation de composés. Comme tous les éléments de terre rare ont des propriétés très similaires, des composés stœchiométriques similaires sont attendus dans les différents systèmes RE-Zn. Par conséquent, des composés stœchiométriques de plusieurs systèmes ont été proposés alors qu'aucune évidence expérimentale n'est disponible dans la littérature. Le modèle semi-empirique de Miedema a également été utilisé pour estimer l'enthalpie de mélange des phases liquide et l'enthalpie de formation des phases solides.
3) En prenant compte de toutes les données, estimés ou expérimentales disponible dans littérature, 17 systèmes binaires RE-Zn (avec RE = Sc, Y, La, Ce, Pr, Nd, Pm, Sm, Eu, Gd, Tb, Dy, Ho, Er, Tm, Yb et Lu) ont été optimisés simultanément. En considérant les tendances trouvées, les paramètres du modèle ont également été proposés pour les phases métastables et aussi instables.

4) Toutes les données expérimentales sur les systèmes RE-Mg-Zn ternaires ont été recherchées dans la littérature et soumises à une étude critique. Seules les données compatibles avec les systèmes binaires déjà optimisés furent utilisées dans la procédure d'optimisation. Les systèmes ternaire RE-Mg-Zn ont ensuite été optimisés en fonction des systèmes binaires limite de et de toutes les données expérimentales disponibles dans la littérature.
5) Des expériences in situ diffraction de neutrons (ND) ont été réalisées sur des échantillons choisis dans les systèmes Ce Mg-Zn et Nd-Mg-Zn. Les transformations de phase au sein de ces échantillons ont été étudiées *in situ*. Les données ND ont ensuite été utilisées soit pour valider ou pour affiner la modélisation thermodynamique.
6) En tenant compte des tendances établies lors de l'optimisation de tous les systèmes binaires RE-Zn, les paramètres du modèle de toutes les phases ternaires ont été établis. Certains ajustements des paramètres du modèle pour les phases binaires ont été effectues pour une meilleure description des systèmes binaires et ternaires RE-Zn et RE-Mg-Zn.

Les résultats de la présente étude sont présentés dans six articles, dont deux ont déjà été acceptés pour publication et quatre autres ont été soumis dans des revues a comite de lecture. Les six articles sont présentés dans les chapitres 4, 5, 6, 7, 8 et 9.

Évaluation thermodynamique et l'optimisation des plus léger systèmes binaires RE-Zn (La-Zn, Ce-Zn, Pr-Zn, Nd, Pm-Zn-Zn et Sm-Zn ainsi que Sc-Zn) ont été acceptés pour publication dans la revue "Journal of alloys and compounds" et présenté dans le chapitre 4. Les diagrammes de phase de tous les systèmes RE-Zn sont très similaires, sauf pour Sc-Zn. Des phases avec la même stœchiométrie peuvent être trouvées dans la plupart des systèmes RE-Zn. Par conséquent, les composés stœchiométriques nous avons supposé que le système Pm-Zn a les même composés stœchiométries que ceux des systèmes Nd-Zn et Sm-Zn même si aucune étude poussée n'a été effectuée pour le système Pm-Zn en raison sa nature radioactive. Toutes les données expérimentales disponibles sont examinées pour vérifier leur cohérence. Il a été supposé dans la présente étude que toutes les propriétés des systèmes RE-Zn obéissent aux mêmes tendances lorsque l’on parcourt la série RE. Les tendances ont été utilisées dans la présente étude pour estimer les données absentes de la littérature telle que l'enthalpie de mélange de la phase liquide, l'enthalpie de formation des composés stœchiométriques, les points de fusion des composés, etc. Les données de force électromotrice (FEM) et de pression de vapeur saturante ont directement été

utilisées dans la procédure d'optimisation. Cette approche est différente de la précédente optimisation ou les données thermodynamiques sont dérivées de la force électromotrice et des données de pression de vapeur saturante ont été utilisées. Aucune donnée de solubilité n'a été trouvée pour les composés. De plus tous les composés ont été exclusivement traités comme des composés stœchiométriques. La capacités calorifique de tous les composés sont supposés obéir à l'équation dite de Neumann-Kopp : $Cp=xC_P(RE)+(1-x)C_p(Zn)$. La Solubilité du zinc dans les solutions terminales de structure cubique centré peuvent être observées dans les diagrammes de phases mesurées pour les systèmes : Ce-Zn, Zn-Pr, Nd-Zn et Sm-Zn et la limite de solubilité était d'environ la même pour tous ces systèmes. Par conséquent, la limite de solubilité a été supposée pour le système Sc-Zn, La-Zn et Pm-Zn. L'enthalpie des solutions liquides calculées à partir du modèle Miedema sont comparable à celles obtenues par l'optimisation thermodynamique. Le modèle semi-empirique de Miedema a été utilisé pour prédire l'enthalpie de mélange des solutions liquide dans les systèmes plus lourd RE-Zn la où aucune données thermodynamiques concernant les phases liquides ne sont disponibles dans la littérature. L'enthalpie de formation de plusieurs composés dans le système Zn-La a été calculée avec des calculs ab-initio. Une forte tendance à former des composés a été observée dans tous les systèmes RE-Zn, ce qui est un indice de l'ordre à courte distance dans la phase liquide. Le MQM est ainsi utilisé pour décrire la phase liquide.

Le chapitre 5 présente l'évaluation et l'optimisation thermodynamique des systèmes plus lourds RE-Zn (Eu-Zn, Gd-Zn, Tb-Zn, Dy-Zn, Ho-Zn, Er-Zn, Tm-Zn, Yb-Zn, Lu- Zn et Y-Zn). Les résultats ont été publiés dans la revue "Journal of alloys and compounds". Pour les systèmes plus lourd RE-Zn les données thermodynamiques sont très limitées, excepté pour le système Y-Zn. Les diagrammes de phase de l'Eu-Zn, Tm-Zn et Lu-Zn n'ont pas encore été établies. Des composés ont été signalés pour ces trois systèmes et leurs points de fusion sont proposés dans la présente étude, en utilisant les tendances établies plus tôt. Les diagrammes de phase des systèmes : Eu-Zn Tm-Zn et Lu-Zn ont ensuite été proposés. Tous les diagrammes de phase des systèmes plus lourds RE-Zn sont également très similaires, a l'exception des deux systèmes Eu-Zn et Yb-Zn, comme cela pouvait être attendu, puisque Eu et Yb ont une sous-couche électronique f a moitie remplis. Les points de fusion et les propriétés thermodynamiques des composés ainsi que les propriétés thermodynamiques des phases liquides ont ensuite été estimées à partir des tendances puis l'optimisation thermodynamique de l'ensemble des systèmes plus

lourd RE-Zn a été effectuée en tenant compte des données expérimentales et estimées. Il est à noter que les points de fusion et les propriétés thermodynamiques des phases métastables et instables ont également été proposés à partir des tendances obtenues au préalable et que l'ensemble de ces phases ont été incluses dans la procédure d'optimisation. Des paramètres sensés pour le modèle ont été proposés pour les phases métastables et instables. Les capacités calorifiques des composés des systèmes plus lourd RE-Zn ont également été formulées via l'équation Neumann-Kopp. Les capacités de calorifiques calculées sont en excellent accord avec celles mesurées pour les composes YZn, Y_2Zn_{17}, Gd_2Zn_{17}, TbZn, Tb_2Zn_{17}, HoZn et Yb_2Zn_{17}, ce qui indique la validité de l'équation Neumann-Kopp pour ces composés. On peut donc également supposer que l'équation Neumann-Kopp est valide pour tous les composés dans le système binaire RE- Zn et ternaire RE-Mg-Zn.

Le troisième article (chapitre 6) présente la modélisation thermodynamique et l'étude in situ du système Ce-Mg-Zn par diffraction de neutrons. L'article a été soumis à la revue Acta Materialia. Il n'existe aucune donnée thermodynamiques pour le système Ce-Mg-Zn dans la littérature. Toutes les sections isothermes et isoplèthes existantes ont été prises en compte dans l'optimisation thermodynamique. Les structures cristallines de toutes les phases ont été analysées de façon critique et des modèles thermodynamiques appropriés ont été choisis pour ces phases. Toutes les phases ternaires existantes ($\tau 1$ à $\tau 7$ dans la présente étude) ont été examinées. En outre, les phases binaires et CeZn et CeMg ont été modélisées comme une solution; la solubilité du zinc dans les phases $CeMg_3$ et $CeMg_{12}$ ainsi que la solubilité du magnésium dans $\tau 1$ et $\tau 3$ a été prises en compte. On a supposé que toutes les autres phases binaires ne sont étendues dans la région ternaire et toutes les autres phases ternaires ont été supposées être stœchiométriques. Des expériences in-situ de diffraction des neutrons (ND) ont été réalisées sur des échantillons pour étudier les transitions de phases afin de valider ainsi que d'affiner la modélisation thermodynamique. Ainsi, quatre échantillons ont été sélectionnés en se basant sur l'optimisation préliminaire. Tous les échantillons sont situés dans les régions triphasées car ils sont censés présenter le plus grand nombre de transitions, ce qui permet d'obtenir plus d'informations. Pour chaque échantillon des spectres de diffraction ont été prélevés tous les 5 °C, tout en étant refroidi à partir de l'état liquide; les séquences des températures de transition et des précipitations ont été obtenus par l'analyse des spectres de diffraction. Tous les paramètres du modèle ont été finalisés en tenant compte des données ND.

Le quatrième article (chapitre 7) présente la modélisation thermodynamique et d'étude in situ du système Nd-Mg-Zn par diffraction de neutrons. L'article a été également soumis à la revue Acta Materialia. Les phases correspondant à la plupart des phases ternaires observées dans le système Ce-Mg-Zn ($\tau2$, $\tau3$, $\tau4$, $\tau5$ et $\tau7$) ont également été observées dans le système Nd-Mg-Zn. L'existence de la phase $\tau1$ est encore incertaine et aucune étude n'a été effectuée dans le domaine de composition où $\tau6$ pourrait exister. Les deux phases n'ont également pas été observées dans aucun autre des systèmes RE-Mg-Zn. Par conséquent, ils n'ont pas été pris en compte dans la présente optimisation. Tous les systèmes RE-Mg-Zn ont été optimisés simultanément et des tendances établies pour les systèmes binaires Zn-RE ont été utilisés. Les expériences in situ de ND ont été également effectuées sur des échantillons du système Nd-Mg-Zn. Les données ND dans cette étude ont été privilégiées dans l'optimisation thermodynamique car les expériences ont été réalisées à haute température avec la présence de la phase liquide. En outre, en raison de la force de pénétration élevée des neutrons, de grands échantillons ont été utilisés dans les expériences de ND, conduisant à un meilleur contrôle de la composition et une résistance accrue à l'oxydation. La plupart des données expérimentales (en particulier les données du liquidus) obtenues dans la littérature ainsi que les expériences actuelles de ND ont été bien reproduites.

Dans le cinquième article (chapitre 8) la modélisation thermodynamique des systèmes légers RE-Mg-Zn (La-Mg-Zn, Pr-Mg-Zn et Sm-Mg-Zn) sont présenté. Le système Sc-Mg-Zn n'a pas été optimisé lors de cette étude, car aucune étude expérimentale n'a été trouvée dans la littérature. Puisque le système binaire Sc-Zn est différent des autres systèmes RE-Zn, le système ternaire Sc-Mg-Zn devrait donc être différent des autres systèmes ternaires RE-Mg-Zn. Par conséquent, il est impossible de proposer des phases ternaires dans le système Mg-Sc-Zn. Le système Pm-Mg-Zn n'a également pas été pris en compte dans la présente étude car la description thermodynamique du système Pm-Mg n'est pas disponible. Seule une phase ternaire (phase V) a été observée dans le système ternaire La-Mg-Zn et cette phase est différente des phases des systèmes ternaires Ce-Mg-Zn et Nd-Mg-Zn. La phase $\tau3$ est supposé exister dans tout les systèmes RE-Mg-Zn a donc également été supposer exister dans le système La-Mg-Zn. Une lacune de démixtion entre LaZn et LaMg a été observée. Cependant, les deux phases ont une fois de plus été modélisées comme des phases solutions solides étendues pour être compatible avec d'autres systèmes ternaires RE-Mg-Zn. Les systèmes Pr-Mg-Zn et Sm-Mg-Zn sont similaires aux systèmes Ce-Mg-Zn et Nd-Mg-Zn. L'optimisation des systèmes Pr-Mg-Zn et Sm-Mg-Zn est

grandement facilitée par l'optimisation simultanée d'autres systèmes RE-Mg-Zn, en particulier les systèmes Ce-Mg-Zn et Nd-Mg-Zn.

Le sixième article (chapitre 9) présente la modélisation thermodynamique des systèmes plus lourds RE-Mg-Zn (Gd-Mg-Zn, Tb-Mg-Zn, Dy-Mg-Zn, Ho-Mg-Zn, Er-MG Zn, Tm-Mg-Zn, Lu-Mg-Zn et Y-Mg-Zn). Les systèmes RE-Mg-Zn sont semblables les uns aux autres, mais différents des systèmes plus légers RE-Mg-Zn. Les systèmes Eu-Mg-Zn et Yb-Mg-Zn ne furent pas optimisés car aucune étude expérimentale ne fut effectuée pour les deux systèmes. En outre, les éléments Eu et Yb sont différents des autres éléments de terres rares; il est donc impossible de proposer des phases dans les systèmes ternaires Eu-Mg-Zn et Yb-Mg-Zn. La périodicité au sein de la phase ordonnée (phase LPSO, notée X dans la présente étude) et la phase icosaédrique (notée phase I) sont supposées exister dans tous les systèmes lourd RE-Mg-Zn. La phase $\tau 3$, une phase commune dans tous les systèmes RE-Mg-Zn, furent également considéré dans les systèmes plus lourd RE-Mg-Zn. Le système Y-Mg-Zn a été étudié par plusieurs auteurs. Toutes les données expérimentales ont été prises en compte dans la présente étude et une amélioration significative a été obtenue pour ce système. Toutes les sections isoplèthes et isothermes disponibles dans la littérature reproduits avec un bon accord.

Des informations détaillées sur le modèle semi-empirique de Miedema sont présentées dans l'annexe 1; Des exemples d'application de la base de données RE-Mg-Zn sont présentés à l'annexe 2; L'annexe 3 présente tous les spectres de diffraction de neutrons mesurés lors de cette étude; Les coefficients de dilatation thermique linéaire de Ta et Mo à haute température sont calculés à partir des spectres ND et figurent à l'annexe 4; enfin les calculs de la projection du liquidus ainsi que des réactions invariantes de tous les systèmes RE-Mg-Zn sont présentés à l'Annexe 5.

TABLE OF CONTENTS

DEDICATION III

ACKNOWLEDGEMENTS IV

RÉSUMÉ VI

ABSTRACT VIII

CONDENSÉ EN FRANÇAIS X

TABLE OF CONTENTS XVII

LIST OF TABLES XXIV

LIST OF FIGURES XXVI

LIST OF SYMBOLS XXXV

LIST OF ABBREVIATIONS XXXVI

LIST OF APPENDICES XXXVII

Chapter 1 INTRODUCTION 1

1.1 The CALPHAD method 6

1.2 Thermodynamic modelling 8

1.2.1 Elements 8

1.2.2 Compounds 8

1.2.3 Terminal solid solutions 9

1.2.4 Compound energy formalism (CEF) 9

1.2.5 Modified Quasichemical Model 10

1.3 In-situ neutron diffraction 14

1.4 Objective of the present project 16

Chapter 2 LITERATURE REVIEW 17

Chapter 3 ORGANIZATION OF THE ARTICLES 28

Chapter 4 ARTICLE 1: CRITICAL ASSESSMENT AND OPTIMIZATION OF PHASE DIAGRAMS AND THERMODYNAMIC PROPERTIES OF RE-ZN SYSTEMS-PART I: SC-ZN, LA-ZN, CE-ZN, PR-ZN, ND-ZN, PM-ZN AND SM-ZN 31

4.1 Introduction 31

4.2 Phase equilibrium and thermodynamic data 33

4.2.1 Sc-Zn system 33

4.2.2 La-Zn system 38

4.2.3 Ce-Zn system 43

4.2.4 Pr-Zn system 45

4.2.5 Nd-Zn system 46

4.2.6 Pm-Zn system 48

4.2.7 Sm-Zn system 48

4.3 Thermodynamic modeling 49

4.3.1 Elements 49

4.3.2 Compounds 49

4.3.3 Terminal solid solutions 49

4.3.4 Liquid solutions 50

4.4 Optimizations 52

4.5 Discussion 57

4.6 Conclusions 61

Acknowledgements 61

References 62

Chapter 5 ARTICLE 2: CRITICAL ASSESSMENT AND OPTIMIZATION OF PHASE DIAGRAMS AND THERMODYNAMIC PROPERTIES OF RE-ZN SYSTEMS-PART II-Y-ZN, EU-ZN, GD-ZN, TB-ZN, DY-ZN, HO-ZN, ER-ZN, TM-ZN, YB-ZN AND LU-ZN 67

5.1 Introduction 67

5.2 Phase equilibrium and thermodynamic data 74

5.2.1 Y-Zn system 74

5.2.2 Eu-Zn system.....79

5.2.3 Gd-Zn system 79

5.2.4 Tb-Zn system.....80

5.2.5 Dy-Zn system 81

5.2.6 Ho-Zn system 82

5.2.7 Er-Zn system 83

5.2.8 Tm-Zn system 84

5.2.9 Yb-Zn system 84

5.2.10 Lu-Zn system.....85

5.3 Thermodynamic modeling 85

5.3.1 Elements 85

5.3.2 Compounds.....85

5.3.3 Terminal solid solutions 86

5.3.4 Liquid solutions.....86

5.4 Optimizations 87

5.5 Discussion 93

5.6 Conclusions 94

Acknowledgements 95

References 96

Chapter 6 ARTICLE 3: THERMODYNAMIC MODELING AND *IN-SITU* NEUTRON DIFFRACTION INVESTIGATION OF THE CE-MG-ZN SYSTEM 100

6.1 Introduction 101

6.2 Phase equilibrium and thermodynamic data 102

6.3 Experimental investigation.....108

6.3.1 Sample #1 ($Ce_{40}Mg_{10}Zn_{50}$).....111

6.3.2 Sample #2 ($Ce_{16}Mg_{40}Zn_{44}$).....112

6.3.3 Sample #3 ($Ce_{4}Mg_{58}Zn_{38}$) 112

6.3.4 Sample #4 ($Ce_{20}Mg_{22}Zn_{58}$).....114

6.4 Thermodynamic optimizations.....115

6.5 Comparison of calculations with experimental data 117

6.6 Discussion 122

6.7 Conclusions 123

Acknowledgements 123

References 124

Chapter 7 ARTICLE 4: THERMODYNAMIC MODELING AND *IN-SITU* NEUTRON DIFFRACTION INVESTIGATION OF THE ND-MG-ZN SYSTEM..... 128

7.1 Introduction 128

7.2 Phase equilibrium and thermodynamic data 130

7.3 Experimental investigation.....138

7.3.1 Sample #1 ($Nd_{15}Mg_{65}Zn_{20}$) 140

7.3.2 Sample #2 ($Nd_{16}Mg_{37}Zn_{47}$) 142

7.3.3 Sample #3 ($Nd_{6}Mg_{41}Zn_{53}$).....143

7.3.4 Sample #4 ($Nd_{20}Mg_{20}Zn_{60}$) 143

7.4 Thermodynamic optimization 143

7.5 Comparison of calculations with experimental data 146

7.6 Discussion 150

7.7 Conclusions 150

Acknowledgements 151

References 152

Chapter 8 ARTICLE 5: THERMODYNAMIC MODELING OF THE LA-MG-ZN, PR-MG-ZN AND SM-MG-ZN SYSTEM 156

8.1 Introduction 156

8.2 Phase equilibrium and thermodynamic data 161

8.2.1 La-Mg-Zn 165

8.2.2 Pr-Mg-Zn 166

8.2.3 Sm-Mg-Zn 166

8.2.4 Ternary phases considered in the present study 167

8.3 Thermodynamic models 168

8.4 Comparison of calculations with experimental data 172

8.4.1 La-Mg-Zn 172

8.4.2 Pr-Mg-Zn 177

8.4.3 Sm-Mg-Zn 179

8.5 Discussion 182

8.6 Conclusions 183

Acknowledgements 184

References 185

Chapter 9 ARTICLE 6: THERMODYNAMIC MODELING OF THE Y-MG-ZN, GD-MG-ZN, TB-MG-ZN, DY-MG-ZN, HO-MG-ZN, ER-MG-ZN, TM-MG-ZN AND LU-MG-ZN SYSTEM 188

9.1 Introduction 188

9.2 Phase equilibrium and thermodynamic data 198

9.2.1 Y-Mg-Zn 203

9.2.2 Gd-Mg-Zn 205

9.2.3 Tb-Mg-Zn 205

9.2.4 Dy-Mg-Zn 205

9.2.5 Ho-Mg-Zn, Er-Mg-Zn, Tm-Mg-Zn and Lu-Mg-Zn 206

9.2.6 Ternary phases considered in the present study 206

9.3 Thermodynamic models 207

9.4 Comparison of calculations with experimental data 213

9.4.1 Y-Mg-Zn 213

9.4.2 Gd-Mg-Zn 222

9.4.3 Tb-Mg-Zn 224

9.4.4 Dy-Mg-Zn 224

9.4.5 Ho-Mg-Zn, Er-Mg-Zn, Tm-Mg-Zn and Lu-Mg-Zn 226

9.5 Discussion 229

9.6 Conclusions 229

Acknowledgements 230

References 231

Chapter 10 GENERAL DISCUSSION 235

CONCLUSION AND FUTURE PERSPECTIVE 238

BIBLIOGRAPHIE 241

APPENDIX 1 – MIEDEMA MODEL 261

APPENDIX 2 – APPLICATION OF THE DATABASE-SCHEIL COOLING SIMULATION 265

APPENDIX 3 – DIFFRACTION PATTERNS OF ALL SAMPLES 268

APPENDIX 4 – COEFFICIENT OF LINEAR EXPANSION OF TA AND MO AT HIGH TEMPERATURES 276

APPENDIX 5 – CALCULATED LIQUIDUS PROJECTIONS AND INVARIANT REACTIONS IN THE OPTIMIZED RE-MG-ZN SYSTEMS 281

LIST OF TABLES

Table 2.1. The investigation status of the 17 RE-Zn systems 17

Table 2.2. Thermodynamic model parameters of the liquid phases of all the optimized RE-Zn systems from the literature (J/g•atom). 19

Table 2.3. Thermodynamic model parameters of the solid compounds of all the optimized RE-Zn systems from the literatures (J/g•atom). 23

Table 4.1 All reported stable and metastable compounds in Sc-Zn, Y-Zn and all RE-Zn systems (For references see Table 1.2 or reference [12]) 35

Table 4.2 Optimized Gibbs energy of formation (J/g•atom) of intermetallic compounds as in Eq(1) and references for the crystal structure. 55

Table 4.3 Optimized model parameters of Eq (3) for the bcc phase and optimized Modified Quasichemical Model parameters of Eq (5) for the liquid phase in Sc-Zn, La-Zn, Ce-Zn, Pr-Zn, Nd-Zn, Pm-Zn and Sm-Zn systems (J/mol).....57

Table 5.1 All reported stable and metastable compounds in Sc-Zn, Y-Zn and all RE-Zn systems (For references see Table 5.2 or reference [12]) 77

Table 5.2 Optimized Gibbs energy of formation (J/g•atom) of intermetallic compounds as in Eq(1) and references for the crystal structure. 90

Table 5.3 Optimized model parameters of Eq (3) for the bcc phase and Optimized Modified Quasichemical Model parameters of Eq (5) for the liquid phase in Y-Zn, Eu-Zn, Gd-Zn, Tb-Zn, Dy-Zn, Ho-Zn, Er-Zn, Tm-Zn, Yb-Zn and Lu-Zn systems (J/mol). 93

Table 6.1Phases with ternary phase fields in the Ce-Mg-Zn system 104

Table 6.2. Sample compositions and transition temperatures measured in NPD experiments....111

Table 6.3. Thermodynamic model parameters optimized in the present work for the Ce-Mg-Zn system.....116

Table 6.4. Tentative calculated invariant reactions, maxima and minima and their temperatures (^{o}C) in the Ce-Mg-Zn system 122

Table 7.1. Phases with ternary phase fields in the Nd-Mg-Zn system.....132

Table 7.2. Sample compositions and transition temperatures measured in NPD experiments....140

Table 7.3. Thermodynamic model parameters optimized in the present work for the Nd-Mg-Zn system.....145

Table 7.4. Tentative Calculated invariant reactions, maxima and minima and their temperatures (^{o}C) in the Nd-Mg-Zn system.....148

Table 8.1. Phases with possible ternary phase fields in the La-Mg-Zn, Pr-Mg-Zn and Sm-Mg-Zn systems 162

Table 8.2. Phases with possible ternary phase fields in RE-Mg-Zn systems as assumed in the present project [14-16] 164

Table 8.3. Thermodynamic model parameters optimized or estimated in the present work for the La-Mg-Zn, Pr-Mg-Zn and Sm-Mg-Zn systems 171

Table 8.4. Tentative calculated invariant reactions, maxima and minima and their temperatures (^{o}C) in the La-Mg-Zn system 177

Table 8.5. Tentative calculated invariant reactions, maxima and minima and their temperatures (^{o}C) in the the Pr-Mg-Zn system 179

Table 8.6. Tentative calculated invariant reactions, maxima and minima and their temperatures (^{o}C) in the the Sm-Mg-Zn system 182

Table 9.1 Phases with ternary phase fields in the Y-Mg-Zn, Gd-Mg-Zn, Tb-Mg-Zn, Dy-Mg-Zn, Ho-Mg-Zn, Er-Mg-Zn, Tm-Mg-Zn and Lu-Mg-Zn systems 200

Table 9.2. Phases with possible ternary phase fields in RE-Mg-Zn systems as assumed in the present project [14, 15, 16].....202

Table 9.3 Thermodynamic model parameters optimized or estimated in the present work for the Y-Mg-Zn, Gd-Mg-Zn, Tb-Mg-Zn, Dy-Mg-Zn, Ho-Mg-Zn, Er-Mg-Zn, Tm-Mg-Zn and Lu-Mg-Zn systems.....210

Table 9.4. Tentative calculated invariant reactions, maxima and minima and their temperatures (^{o}C) in the Y-Mg-Zn system.....222

LIST OF FIGURES

Figure 1.1. Specific strength of various structural materials (Gupta & Sharon, 2011).....1

Figure 1.2. Specific stiffness of various structural materials (Gupta & Sharon, 2011) 2

Figure 1.3 Alloying behavior of Mg 3

Figure 1.4. A schematic diagram of the CALPHAD method (Lukas, Fries, & Sundman, 2007)....7

Figure 1.5. Some "geometric" models for estimating ternary thermodynamic properties from optimized binary data (A. D. Pelton, 2001). 14

Figure 2.1. The calculated enthalpies of formation of RE-Zn systems at 1600 ^{o}C from different authors from the literature. 21

Figure 2.2. The calculated entropies of formation of RE-Zn systems at 1600 ^{o}C from different authors from the literature. 22

Figure 4.1. Calculated Sc-Zn phase diagram and experimental data points [14].....34

Figure 4.2 Calculated La-Zn phase diagram and experimental data points [15-17, 28] 34

Figure 4.3 Calculated Ce-Zn phase diagram and experimental data points [29] 36

Figure 4.4 Calculated Pr-Zn phase diagram and experimental data points [16, 32, 33] 36

Figure 4.5 Calculated Nd-Zn phase diagram and experimental data points [16, 36].....37

Figure 4.6 Calculated Pm-Zn phase diagram 37

Figure 4.7 Calculated Sm-Zn phase diagram and experimental data points [16, 41] 38

Figure 4.8 Lattice constants of RE-Zn compounds (for references, see Table 2 and ref [12]).....39

Figure 4.9 Enthalpies of liquid-liquid mixing of Sc-Zn, Y-Zn and RE-Zn systems at compositions of minimum enthalpy at 1600 ^{o}C 40

Figure 4.10 Emf of alloy concentration cells in the La-Zn system. Lines are calculated from the optimized model parameters. All data are from Kovalevskii et al [23] unless otherwise indicated in the figure [20-22].....41

Figure 4.11Calculated enthalpy of formation of compounds in the La-Zn system with experimental data points and values calculated from DFT [20-26]. 42

Figure 4.12 Heat capacity of La_2Zn_{17} and $LaZn_{13}$ reported by Morishita et al [25, 26] and as calculated from the Neumann-Kopp equation (solid lines) 42

Figure 4.13 Calculated and experimental vapor pressures over liquid Ce-Zn alloys [29].....43

Figure 4.14 Calculated and experimental vapor pressures over two-phase Ce-Zn alloys [29].....44

Figure 4.15 Emf of concentration cells for the formation of $CeZn_{11}$ and $PrZn_{11}$ [22].....44

Figure 4.16 Calculated and experimental vapor pressures over liquid Pr-Zn alloys [34].....45

Figure 4.17 Calculated and experimental vapor pressures over two-phase Pr-Zn alloys [34].....46

Figure 4.18 Calculated and experimental vapor pressures over liquid Nd-Zn alloys [37] 47

Figure 4.19 Calculated and experimental vapor pressures over two-phase Nd-Zn alloys [37] 47

Figure 4.20 Calculated and experimental vapor pressures over liquid Sm-Zn alloys [41].....48

Figure 4.21 Calculated congruent melting points of all compounds in the Sc-Zn, Y-Zn and RE-Zn systems. ■=stable compounds shown on experimental phase diagrams; ▲=stable compounds. Melting point from interpolation or extrapolation; □=metastable compounds. Melting point from interpolation or extrapolation 54

Figure 4.22 Calculated enthalpies of formation of compounds in the Sc-Zn, Y-Zn and RE-Zn systems. 58

Figure 4.23 Calculated enthalpy of liquid-liquid mixing for Sc-Zn, La-Zn, Ce-Zn, Pr-Zn, Nd-Zn, Pm-Zn and Sm-Zn systems at 1600 ^{o}C 59

Figure 4.24 Calculated entropy of liquid-liquid mixing for Sc-Zn, La-Zn, Ce-Zn, Pr-Zn, Nd-Zn, Pm-Zn and Sm-Zn systems at 1600 ^{o}C 59

Figure 4.25 Calculated enthalpy of liquid-liquid mixing in the La-Zn system from different optimizations [27, 28] 60

Figure 4.26 Calculated entropy of liquid-liquid mixing in the La-Zn system from different optimizations [27, 28] 60

Figure 5.1(a) Calculated Y-Zn phase diagram and experimental data points [17, 18] 69

Figure 5.2 Calculated Eu-Zn phase diagram and experimental data points [27] 70

Figure 5.3 Calculated Gd-Zn phase diagram and experimental data points [27, 29].....70

Figure 5.4 Calculated Tb-Zn phase diagram and experimental data points [27, 32] 71

Figure 5.5 Calculated Dy-Zn phase diagram and experimental data points [27, 35].....71

Figure 5.6 Calculated Ho-Zn phase diagram and experimental data points [27, 32].....72

Figure 5.7 Calculated Er-Zn phase diagram and experimental data points [27, 32, 57].....72

Figure 5.8 Calculated Tm-Zn phase diagram and experimental data points [27] 73

Figure 5.9 Calculated Yb-Zn phase diagram and experimental data points [27, 41].....73

Figure 5.10 Calculated Lu-Zn phase diagram and experimental data points [27] 74

Figure 5.11 Lattice constants of RE-Zn compounds (for references, see Table 2 and ref [12]) 76

Figure 5.12 Calculated and experimental vapor pressures over two-phase Y-Zn alloys [17, 18] .78

Figure 5.13 Emf of concentration cells for the formation of YZn_{12} and Y_2Zn_{17} [19, 20] 78

Figure 5.14 Heat capacities of YZn, Y_2Zn_{17} and YZn_{12} as measured [21-23] and as calculated (solid line) from the Neumann-Kopp equation 79

Figure 5.15 Heat capacity of Gd_2Zn_{17} as measured [30] and as calculated (solid line) from the Neumann-Kopp equation 80

Figure 5.16 Heat capacities of TbZn and Tb_2Zn_{17} as measured [22, 23] and as calculated (solid line) from the Neumann-Kopp equation 81

Figure 5.17 Gibbs energy of formation of $DyZn_{12}$ as reported [38] and as calculated from the optimized parameters 82

Figure 5.18 Heat capacities of HoZn and Yb_2Zn_{17} as measured [22, 30] and as calculated (solid line) from the Neumann-Kopp equation 83

Figure 5.19 Gibbs energy of formation of $ErZn_{12}$ as reported [40] and as calculated from the optimized parameters 84

Figure 5.20 Calculated congruent melting points of all compounds in the Sc-Zn, Y-Zn and RE-Zn systems. ■=stable compounds shown on experimental phase diagrams; ▲=stable

compounds. Melting point from interpolation or extrapolation; □=metastable compounds. Melting point from interpolation or extrapolation 88

Figure 5.21 Enthalpies of formation of compounds in the Sc-Zn, Y-Zn and RE-Zn systems.....89

Figure 5.22 Calculated enthalpy of liquid-liquid mixing for Y-Zn, Eu-Zn, Gd-Zn, Tb-Zn, Dy-Zn, Ho-Zn , Er-Zn, Tm-Zn, Yb-Zn and Lu-Zn systems at 1600 ^{o}C 94

Figure 5.23 Calculated entropy of liquid-liquid mixing for Y-Zn, Eu-Zn, Gd-Zn, Tb-Zn, Dy-Zn, Ho-Zn , Er-Zn, Tm-Zn, Yb-Zn and Lu-Zn systems at 1600 ^{o}C 95

Figure 6.1 Calculated optimized isothermal section (mole fraction) of the Ce-Mg-Zn system at 350°C showing data points of Kevorkov and Pekguleryuz [15] which indicate single-phase regions. Compositions of the four samples used in the present ND experiments are also shown 103

Figure 6.2. Calculated optimized isopleth with constant Zn content of 24 wt.% (a) and 34 wt.% (b) in the Ce-Mg-Zn system showing points from Drits *et al* [21]. 105

Figure 6.3. Schematic drawing of the furnace used for the ND experiments. 110

Figure 6.4. Selected NPD patterns for (a) $Ce_{40}Mg_{10}Zn_{50}$, (sample #1), (b) $Ce_{16}Mg_{40}Zn_{44}$, (sample #2), (c) $Ce_{4}Mg_{58}Zn_{38}$, (sample #3) and (d) $Ce_{20}Mg_{22}Zn_{58}$, (sample #4) 113

Figure 6.5. Calculated optimized isopleths of the (a) $Ce_{40}Mg_{60}$-$Ce_{40}Zn_{60}$, (b) $Ce_{16}Mg_{84}$-$Ce_{16}Zn_{84}$, (c) $Ce_{4}Mg_{96}$-$Ce_{4}Zn_{96}$ and (d) $Ce_{20}Mg_{80}$-$Ce_{20}Zn_{80}$ sections showing experimental transition temperatures from samples #1, #2, #3 and #4, respectively 114

Figure 6.6. (a) Reported [20] and (b) calculated optimized isothermal section (mole fraction) of the Ce-Mg-Zn system at 300°C showing experimental data points identified by Chiu *et al* [28] as lying in three-phase regions. 119

Figure 6.7. (a) Reported [14] and (b) calculated optimized isothermal section (mole fraction) of the Ce-Mg-Zn system at 197°C.....120

Figure 6.8. Calculated optimized isopleths of the (a) $Ce_{15}Mg_{85}$-$Mg_{85}Zn_{15}$ and (b) $Ce_{65}Mg_{35}$-$Mg_{35}Zn_{65}$ sections showing data points of Chiu *et al* [28]. ▲ strong heating signal; ▼ strong cooling signal; △ weak heating signal; ▽ weak cooling signal.....121

Figure 6.9. Tentative calculated liquidus projection for Ce-Mg-Zn system (mole fraction).....121

Figure 6.10. Enlargement of part of Fig. 6.9 122

Figure 7.1. Calculated optimized isothermal section of the Nd-Mg-Zn system at 300°C showing the compositions of the four samples in the present ND experiments (mole fraction). 130

Figure 7.2. Calculated optimized isopleths (a) from Mg-10wt.%Nd (A) to Mg-10wt.%Nd-60wt.%Zn (B), (b) from Mg-20wt.%Zn (A) to Mg-20wt.%Zn-30wt.%Nd (B) and (c) from Mg-20wt.%Nd (A) to Mg-30wt.%Zn (B) in the Nd-Mg-Zn system showing points from Drits *et al* [24] 134

Figure 7.3. Reported isothermal section of Nd-Mg-Zn system at 320°C from Xu *et al* [17] (mole fraction). (Note: phase names τ1 to τ7 are those of the authors [17]) 136

Figure 7.4. Reported isothermal section of Nd-Mg-Zn system at 300°C from Mostafa and Medraj [18] (mole fraction). (Note: names of the ternary phases are those used in the present study) 136

Figure 7.5. Selected ND patterns for (a) $Nd_{15}Mg_{65}Zn_{20}$ (sample #1), (b) $Nd_{16}Mg_{37}Zn_{47}$ (sample #2), (c) for $Nd_{6}Mg_{41}Zn_{53}$ (sample #3) and $Nd_{20}Mg_{20}Zn_{60}$ (sample #4) 141

Figure 7.6. Calculated optimized isopleths of the (a) $Nd_{15}Mg_{85}$-$Nd_{15}Zn_{85}$, (b) $Nd_{16}Mg_{84}$-$Nd_{16}Zn_{84}$, (c) $Nd_{6}Mg_{94}$-$Nd_{6}Zn_{94}$ and (d) $Nd_{20}Mg_{80}$-$Nd_{20}Zn_{80}$ sections showing experimental transition temperatures from samples #1, #2, #3 and #4, respectively 142

Figure 7.7. Calculated optimized isothermal section of the Nd-Mg-Zn system at 427°C. The $Nd(Mg,Zn)_{12}$ phase is stable at this temperature according to the calculations. (mole fraction) 147

Figure 7.8. Tentative calculated liquidus projection for Nd-Mg-Zn system (mole fraction)..... 149

Figure 7.9. Enlargement of part of Figure 7.8 149

Figure 8.1. Calculated optimized Mg-Zn phase diagram [7] 158

Figure 8.2. Calculated optimized Mg-La phase diagram [8] 158

Figure 8.3. Calculated optimized La-Zn phase diagram [12] 159

Figure 8.4. Calculated optimized Mg-Pr phase diagram [8] 159

Figure 8.5. Calculated optimized Pr-Zn phase diagram [12] 160

Figure 8.6. Calculated optimized Mg-Sm phase diagram [8] 160

Figure 8.7. Calculated optimized Sm-Zn phase diagram [12] 161

Figure 8.8. Calculated enthalpies of formation for compounds in the Y-Mg-Zn and RE-Mg-Zn systems. Trends are very similar to those established in our previous work on the binary systems [12, 13] (The Eu-Mg-Zn and Yb-Mg-Zn systems are not considered in the present work thus the anomalies cannot be seen from the figure). 172

Figure 8.9. Calculated optimized (above) isothermal section of the La-Mg-Zn system at 300°C and reported (below) isothermal section of the La-Mg-Zn system at 322oC [21] (mole fraction). 174

Figure 8.10. Calculated optimized isopleth from Mg-10wt.% La (A) to Mg-30wt.% Zn (B) in the La-Mg-Zn system showing points from Dobatkina et al [17, 18].....175

Figure 8.11. Calculated optimized isopleth from Mg-30wt.% Zn (A) to Mg-15wt.% La-30wt.% Zn (B) in the La-Mg-Zn system showing points from Dobatkina et al [17, 18].....175

Figure 8.12. Tentative calculated liquidus projection for La-Mg-Zn system (mole fraction) 176

Figure 8.13. Enlargement of part of Fig. 8.12.....176

Figure 8.14. Calculated optimized isothermal section of the Pr-Mg-Zn system at 300°C (mole fraction) 177

Figure 8.15. Tentative calculated liquidus projection of the Pr-Mg-Zn system (mole fraction) .178

Figure 8.16. Enlargement of part of Fig. 8.15.....178

Figure 8.17. Calculated optimized isothermal section of the Sm-Mg-Zn system at 300oC (mole fraction) 180

Figure 8.18. Calculated optimized isopleth from Mg-30wt.% Zn (A) to Mg-30wt.% Sm-30wt.% Zn (B) in the Sm-Mg-Zn system showing points from Drits et al [23] 180

Figure 8.19. Calculated optimized isopleth from Mg-35wt.% Sm (A) to Mg-35wt.% Zn (B) in the Sm-Mg-Zn system showing points from Drits et al [23] 181

Figure 8.20. Tentative calculated liquidus projection for Sm-Mg-Zn system (mole fraction) 181

Figure 8.21. Enlargement of part of Fig. 8.20.....182

Figure 9.1. Calculated optimized Mg-Zn phase diagram [7] 190

Figure 9.2. Calculated optimized Y-Mg phase diagram [9].....190

Figure 9.3 Calculated optimized Y-Zn phase diagram [13].....191

Figure 9.4 Calculated optimized Gd-Mg phase diagram [11].....191

Figure 9.5 Calculated optimized Gd-Zn phase diagram [13].....192

Figure 9.6.Calculated optimized Tb-Mg phase diagram [11] 192

Figure 9.7. Calculated optimized Tb-Zn phase diagram [13] 193

Figure 9.8. Calculated optimized Dy-Mg phase diagram [11].....193

Figure 9.9. Calculated optimized Dy-Zn phase diagram [13].....194

Figure 9.10. Calculated optimized Ho-Mg phase diagram [11].....194

Figure 9.11. Calculated optimized Ho-Zn phase diagram [13].....195

Figure 9.12. Calculated optimized Er-Mg phase diagram [11].....195

Figure 9.13. Calculated optimized Er-Zn phase diagram [13].....196

Figure 9.14. Calculated optimized Tm-Mg phase diagram [11] 196

Figure 9.15. Calculated optimized Tm-Zn phase diagram [13] 197

Figure 9.16. Calculated optimized Lu-Mg phase diagram [11] 197

Figure 9.17. Calculated optimized Lu-Zn phase diagram [13] 198

Figure 9.18. Calculated enthalpies of formation for compounds in the Y-Mg-Zn and RE-Mg-Zn systems. Trends are very similar to those established in our previous work on the binary systems [12, 13] (The Eu-Mg-Zn and Yb-Mg-Zn systems are not considered in the present work thus the anomalies cannot be seen from the figure).....212

Figure 9.19 Calculated optimized isothermal section of the Y-Mg-Zn system at 600°C. ▲three-phase equilibria confirmed by Tsai *et al* [21] (mole fraction). 213

Figure 9.20 Calculated optimized isothermal section of the Y-Mg-Zn system at 500°C. ▲three-phase equilibria confirmed by Tsai *et al* [21] (mole fraction). 214

Figure 9.21 Calculated optimized isothermal section of the Y-Mg-Zn system at 400°C. ▲three-phase equilibria confirmed by Tsai *et al* [21] at 427°C (mole fraction). 214

Figure 9.22 Calculated optimized isothermal section of the Y-Mg-Zn system at 300°C (mole fraction). 215

Figure 9.23 Calculated optimized isopleth between Mg and the X phase showing points from Padezhnova *et al* [22]. 215

Figure 9.24 Calculated optimized isopleth from Mg-18wt.%Y (A) to Mg-18 wt.%Y-28wt.%Zn (B) in the Y-Mg-Zn system showing points from Padezhnova *et al* [23].....216

Figure 9.25 Calculated optimized isopleth from Mg-29wt.%Zn (A) to Mg-18 wt.%Y-29wt.%Zn (B) in the Y-Mg-Zn system showing points from Padezhnova *et al* [23].....216

Figure 9.26 Calculated optimized $Mg_{50}Zn_{50}$-$Y_{10}Mg_{30}Zn_{60}$ isopleth showing points from Langsdorf *et al* [33]. 217

Figure 9.27 Calculated optimized $Mg_{60}Zn_{40}$-$Y_{10}Mg_{30}Zn_{60}$ isopleth showing points from Langsdorf *et al* [33]. 217

Figure 9.28 Calculated optimized $Mg_{80}Zn_{20}$-$Y_{10}Mg_{80}Zn_{10}$ isopleth from the present work compared to that of Gröbner *et al* [53]. Data points are also from ref [52]. (Note that in ref [52] the 18R and 14H phases correspond to the X phase in the present study; the W, H and Z phases correspond to the τ3, YZn_5 and τ5 phases, respectively) 219

Figure 9.29 Calculated optimized Mg-$Y_{10}Mg_{80}Zn_{10}$ isopleth from the present work compared to that reported by Gröbner *et al* [53]. Data points are also from ref [52]. (Note that in ref [52] the 18R and 14H phases correspond to the X phase in the present study and the W phase corresponds to τ3) 220

Figure 9.30 Tentative calculated liquidus projection of the Y-Mg-Zn system (mole fraction) ...221

Figure 9.31 Enlargement of part of Fig. 9.30.....221

Figure 9.32 Calculated isothermal section of the Gd-Mg-Zn system at 400°C (mole fraction) ..223

Figure 9.33 Calculated isothermal section of the Gd-Mg-Zn system at 300°C (mole fraction) ..223

Figure 9.34 The calculated isothermal section of Tb-Mg-Zn system at 300°C (mole fraction) ..224

Figure 9.35 The calculated isothermal section of Dy-Mg-Zn system at 300°C (mole fraction)..225

Figure 9.36 The calculated isothermal section of Dy-Mg-Zn system at 300°C in the Mg-rich region along with experimental data from Rokhlin *et al* [40] (mole fraction). ▲ Data points in a three-phase region; ☐ Data points in a two-phase region.....225

Figure 9.37 Calculated optimized isopleths from Mg-39wt.% Dy (A) to Mg-39wt.% Zn (B) in the Dy-Mg-Zn system showing points from Rokhlin *et al* [40].....226

Figure 9.38 Calculated isothermal section of the Ho-Mg-Zn system at 300°C (mole fraction) ..227

Figure 9.39 Calculated isothermal section of the Er-Mg-Zn system at 300°C (mole fraction) ...227

Figure 9.40 Calculated isothermal section of the Tm-Mg-Zn system at 300°C (mole fraction)..228

Figure 9.41 Calculated isothermal section of the Lu-Mg-Zn system at 300°C (mole fraction)...228

LIST OF SYMBOLS

at.%	Atomic percent
c_p	Molar heat capacity (J/mol-K)
g_i^0	Molar Gibbs energy of component i (J/mol)
Δh^0	Molar enthalpy of formation (J/mol)
n_i	Number of moles of component i in a solution
n_{ij}	Number of moles of i-j pairs in a solution
R	The ideal gas constant
T	Abosolute temperature (K)
wt.%	Weight percent
X_i	Mole fraction of i
X_{ii}	Pair fraction of i-i pair
X_{ij}	Pair fraction of i-j pair
Z_{ii}^i	Coordination number of i, when all the nearest neighbors of an i are i's
Z_{ij}^i	Coordination number of i, when all the nearest neighbors of an i are j's
Δs^0	Molar entropy of formation (J/mol)
ΔS^{config}	Configurational entropy of mixing of a solution (J/K)
Δg_{AB}	Non-configurational Gibbs energy change for the formation of two moles of (A-B) pairs (J/mol)

LIST OF ABBREVIATIONS

BWM	Bragg-Williams Model
CALPHAD	CALculation of PHAse Diagram
CEF	Compound Energy Formalism
DFT	Density Functional Theory
DSC	Differential Scanning Calorimentry
DTA	Differential Thermal Analysis
EDS	Energy Dispersive X-Ray Spectrometry
EMF	Electromotive Force
EPMA	Electron Probe Microanalysis
ICP	Inductively Coupled Plasma
LPSO phase	Long-period Stacking Ordered phase
MQM (MQMPA)	Modified Quasichemical Model in the Pair Approximation
ND	Neutron Diffraction
RE	Rare Earth
SEM	Scanning Electron Microscopy
SRO	Short-Range Order
SGTE	Scientific Group Thermodata Europe
XRD	X-Ray Diffraction

LIST OF APPENDICES

APPENDIX 1 MIEMEMA MODEL 262

APPENDIX 2 APPLICATION OF THE DATABASE-SCHEIL COOLING SIMULATION 266

APPENDIX 3 DIFFRACTION PATTERNS OF ALL SAMPLES 269

APPENDIX 4 COEFFICIENT OF LINEAR EXPANSION OF TA AND MO AT HIGH TEMPERATURES 277

APPENDIX 5 CALCULATED LIQUIDUS PROJECTIONS AND INVARIANT REACTIONS IN THE OPTIMIZED RE-MG-ZN SYSTEMS 282

Chapter 1 **INTRODUCTION**

Magnesium is the eighth most abundant element (Mg, 1.87 wt.%) in the earth's crust (Yaroshevsky, 2006), next to oxygen (O, 47 wt.%), silicon (Si, 29.5 wt.%) , aluminium (Al, 8.05 wt.%), iron (Fe, 4.65 wt.%), calcium (Ca, 2.96 wt.%), sodium (Na, 2.5 wt.%) and potassium (K, 2.5 wt.%). It is more abundant than titanium (Ti, 0.45 wt.%). These nine elements constitute ~99.5 wt.% of the earth's crust. Thanks to their availability, Al, Fe and Mg alloys are the most widely used structural materials (Na and K cannot be used as structural materials, Ti is too expensive).

To decrease growing environmental impact, reduction of emissions becomes more important for human habitation of the planet. As a result, the use of light materials in the transportation sector is generally viewed as becoming of key importance in the future. Of all structural materials mentioned above, Mg has the lowest density (1.738 g/cm^3 for pure Mg, 7.874 g/cm^3 for pure Fe, 2.700 g/cm^3 for pure Al, 4.507 g/cm^3 for pure Ti (Winter, 1993)). Figs. 1-2 show the specific strength and stiffness of various structural materials. Among these, Mg alloys have the highest specific stiffness and the second highest specific strength, inferior only to Ti alloys. Mg alloys also have high damping properties, good casting ability etc.

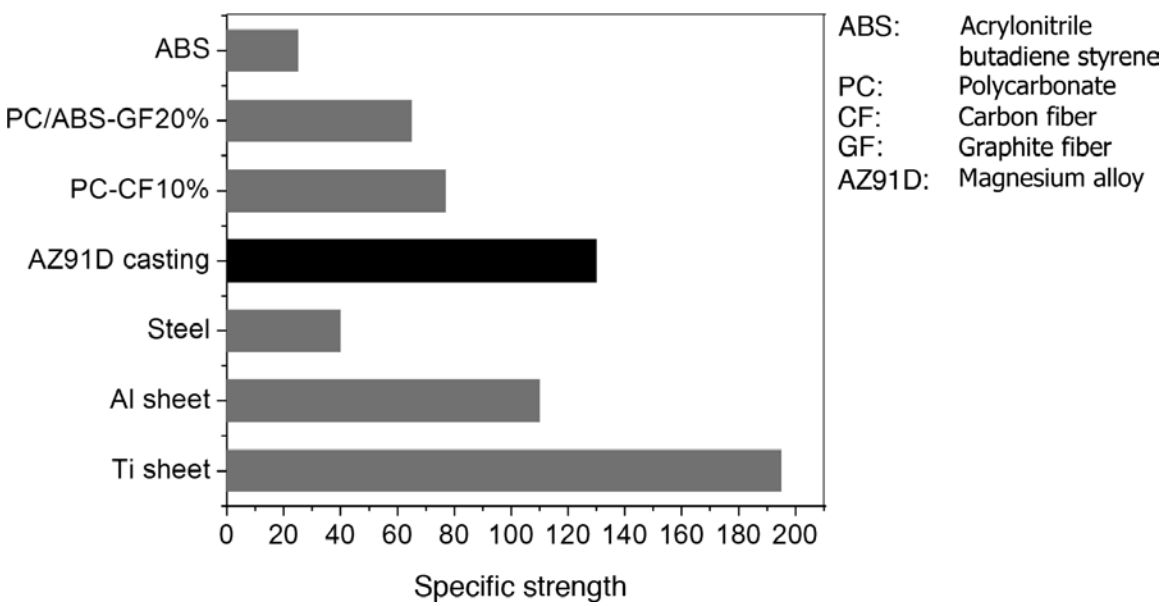

Figure 1.1. Specific strength of various structural materials (Gupta & Sharon, 2011)

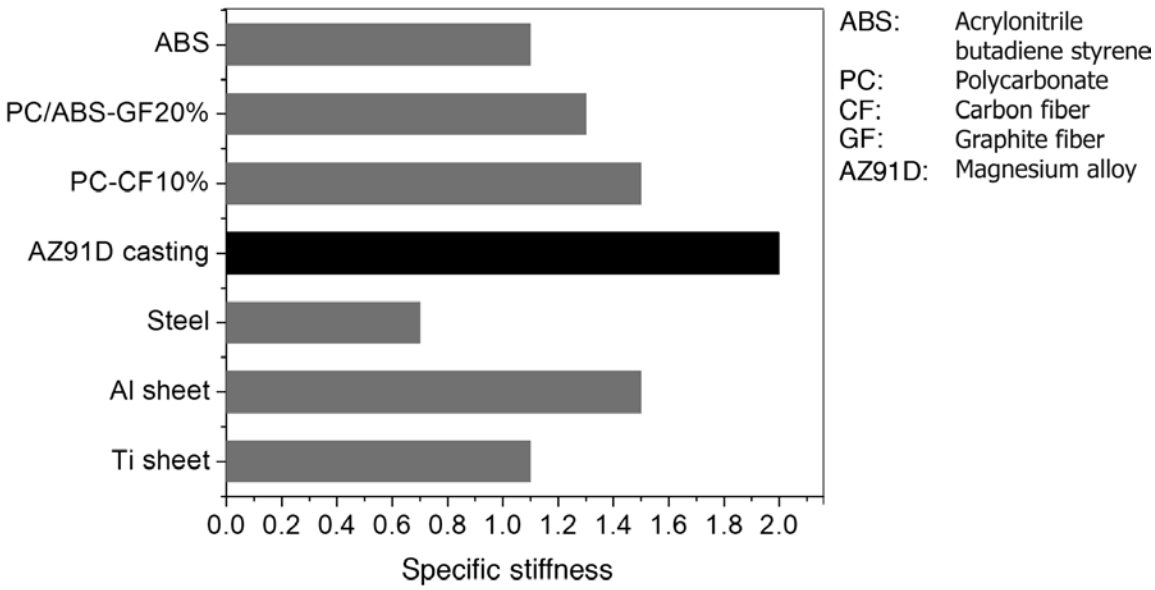

Figure 1.2. Specific stiffness of various structural materials (Gupta & Sharon, 2011)

In the past, the development of magnesium alloys was driven by the potential for lightweight construction materials in military applications. Although magnesium alloys are still used to reduce weight today, the purpose has changed: people are focusing on the more economic use of fuel and lower emissions in a time of growing environmental impact.

Because of its poor mechanical properties, pure Mg must be alloyed with other elements in order to be used as a structural material. Mg alloys can be strengthened by solid solution strengthening and precipitation hardening. According to the Hume-Rothery rules, extensive solid solution cannot be formed if the atomic size of the solvent and solute differ by more than 15%. In addition, the solvent and solute should have similar electronegativities and crystal structures. Moreover, a metal of low valence is more likely to dissolve one with higher valence. The alloying behavior of Mg with respect to atomic size, relative valence and electronegativity is shown in Fig. 3. Near 12-15% size factor, alloying elements in Mg alloys can offer considerable solid solution hardening. These alloying elements are: rare earth elements (RE), Zn, Manganese (Mn), Al etc., among which RE and Zn have hcp structures.

When the Hume-Rothery rules for solid solution formation do not hold, compound formation occurs. The most important second phases in Mg alloys are: $Mg_{17}Al_{12}$, Mg_2Ca, Al_2Ca, $CeMg_{12}$, $NdMg_{12}$, $Al_{11}RE_3$, Al_2RE and Y_5Mg_{24}.

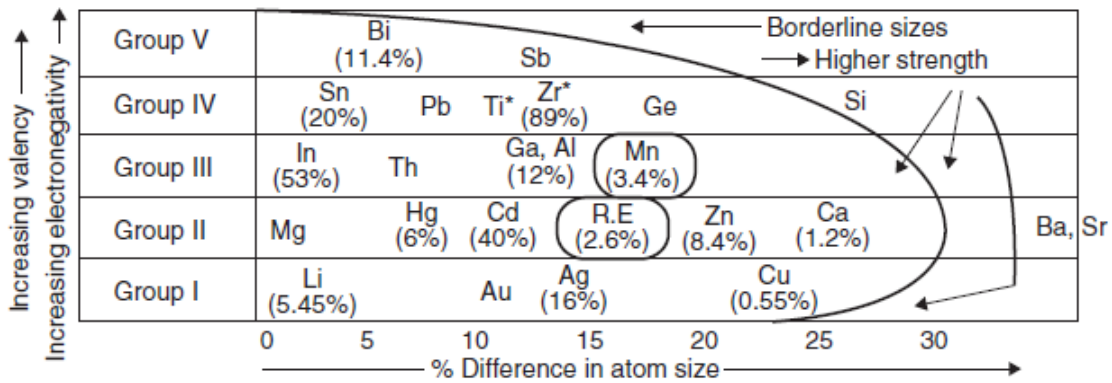

Figure 1.3 Alloying behavior of Mg

The major alloying elements in Mg are: Al, Ca, Li, Mn, RE, Si, silver (Ag), thorium (Th), yttrium (Y), Zn and Zirconium (Zr). Of all the major alloying elements, Al, Zn, Mn, Ca and RE are the most commonly used.

Al is used as an alloying element to increase the hardness and strength of Mg alloys. Al can react with Mg to form $Mg_{17}Al_{12}$ as a strengthening phase. However, $Mg_{17}Al_{12}$ has a body centered cubic (bcc) structure, which is different from the hexagonal close packed (hcp) Mg matrix. As a result, the Mg/$Mg_{17}Al_{12}$ interface is very fragile. $Mg_{17}Al_{12}$ also has very poor strength (Polmear, 1996), and other alloying elements are usually added to improve the mechanical properties of Mg-Al alloys.

Ca is added in magnesium alloys to improve the creep resistance and refine the microstructure. When Ca is added to the AZ series of alloys, it can react with Al to form Al_2Ca, reducing the effect of the relatively unstable $Mg_{17}Al_{12}$ phase. The addition of Ca in AZ91 alloys can reduce the tensile strength and elongation at ambient temperature while increasing the strength at elevated temperature (Qudong et al., 2001). The amount of Ca in Mg alloys cannot exceed 0.3 wt.% or it will reduce the weldability of Mg alloys (Avedesian & Baker, 1999).

Li is the only alloying element that can be used to reduce the density of Mg alloys below that of Mg. The addition of Li also leads to an increase in the ductility but a decrease in the strength (Avedesian & Baker, 1999).

Mn is added to MgAl and MgAlZn alloys to improve their salt water corrosion resistance. e.g. when Mn and RE are added simultaneously in AZ61 alloy, the corrosion resistance can be

improved (Zhu et al., 2013). Experiments also show that Mn can enhance the creep resistance of Mg over a wide temperature range (100-225°C) (Celikin, Kaya, & Pekguleryuz, 2012).

Zr is a very common alloying element. It is used in many alloys (including, but not limited to, Mg alloys) to help refine the grain size. However, one should avoid using Zr in Mg alloys containing Al and Mn, as Zr can form stable compounds with these two alloying elements. The addition of Zr can increase the tensile strength while retaining the ductility of Mg alloys.

Si is one of the cheapest alloying elements. It decreases the castability of Mg alloys but increase the creep resistance.

Ag can be used together with RE elements to improve the high temperature strength and creep resistance of Mg alloys (Avedesian & Baker, 1999).

Th is added in Mg alloys to increase high temperature strength and creep resistance. Th is also very similar to RE elements, as they lie in the same group in the periodic table. However, the use of Th has been phased out due to its radioactive nature.

The addition of RE elements into Mg alloys can increase significantly the high temperature strength and creep resistance, either by solution strengthening or precipitation hardening. RE elements can also weaken the texture of Mg alloys and thus increase their deformability and workability. A possible reason is that the addition of RE changes the stacking fault energy in Mg alloys (Agnew, 2001). The addition of RE can also change the surface composition of the Mg alloy, modifying the driving force for corrosion and oxidation and thus increasing corrosion resistance. RE elements are costly and they are used primarily in high-tech alloys. The most commonly used RE elements are Y, La, Ce, Pr, Nd, Sm and Gd etc. Sc and Y have properties very similar to RE elements and they are generally treated as RE elements (Sc as a lighter-RE element, Y as a heavier-RE element).

Zn is one of the most widely used alloying elements in Mg alloys. The AZ series Mg alloys are the most widely used Mg alloys in which Al and Zn are the major alloying elements. The four criteria of Hume-Rothery rules are satisfied when Zn is added to Mg alloys (the size difference is between 15% and 20%; this may be rather large but the other three criteria are perfectly satisfied). Consequently, solution strengthening can be expected. As shown in Fig. 3, Zn and RE elements (Y, Gd, Tb, Dy, Ho, Er, Tm and Lu etc., which have an hcp structure) are the most effective alloying elements in Mg as far as solution strengthening is concerned. Zn is much

cheaper than RE, making it the most commonly used alloying element offering solution strengthening in Mg alloys.

The mechanical properties of Mg alloys can be significantly improved with the addition of Zn and RE. It is reported that the hot rolled sheet of $Y_3Mg_{94}Zn_3$ exhibited yield strength of 380Mpa and an elongation of 6%.

Nowadays Mg alloys are used mainly in the automobile industry for the purpose of fuel saving via weight reduction. Many components are made of Mg alloys: instrument panel beams, cam covers, steering wheel armatures, steering column supports, seats, transfer cases, and housings and brackets (Luo, 2000). None of these components is used at elevated temperatures. Commonly used Mg alloys in these components are the AZ (Mg-Al-Zn) and AM (Mg-Al-Mn) series. The strengthening phase in these alloys is $Mg_{17}Al_{12}$, which softens above 150°C (P. Zhang, 2005).

To further reduce the weight of vehicles, more Mg alloys should be introduced. Mg alloys to be used at elevated temperatures are in demand (in the powertrain system, engine pistons can operate up to 300°C, engine blocks up to 200°C and automatic transmission cases up to 175°C (Gupta & Sharon, 2011)). Only the Mg alloys containing Ag and RE elements can be used at temperatures exceeding 200°C (Kainer & Kaiser, 2003).

To this end, the RE-containing Mg alloys attract more and more attention. As an ongoing project at the CRCT, a thermodynamic database for Mg-RE-(Al, Zn) is being constructed using the CALPHAD method. While the Mg-RE-Al database has already been built by Liling Jin (Jin, 2012), the thermodynamic database for Mg-Zn-RE is constructed in the present project. This includes thermodynamic optimization of all Zn-RE binary systems and most Mg-Zn-RE ternary systems. The thermodynamic database for the Mg-Si-RE and Mg-Mn-RE systems was constructed by Junghwan Kim at Mcgill University.

Rare earth elements generally refer to the 15 lanthanoids: lanthanum (La), cerium (Ce), praseodymium (Pr), neodymium (Nd), promethium (Pm), samarium (Sm), europium (Eu), gadolinium (Gd), terbium (Tb), dysprosium (Dy), holmium (Ho), erbium (Er), thulium (Tm), ytterbium (Yb) and lutetium (Lu). However, according to IUPAC (Damhus, Hartshorn, & Hutton, 2005), the rare earth elements refer to 15 lanthanoids elements plus scandium (Sc) and Y. The chemical properties of Sc and Y are very similar to those of lanthanoids and it is thus very

reasonable to treat them as rare earth elements. The rare earth elements can be further divided into two groups: the lighter-rare earth elements (La, Ce, Pr, Nd, Pm, Sm and Sc) and the heavier-rare earth elements (Eu, Gd, Tb, Dy, Ho, Er, Tm, Yb, Lu and Y). Elements within the same group have more similar properties. This is evidenced when RE elements are alloyed with other elements: almost the same amount of stable compounds can be found when rare earth elements from the same group are alloyed with the same element. The amount of stable compound is usually different when rare earth elements from different groups are alloyed with the same element. The properties of Eu and Yb are somewhat different from other RE elements due to the half-filled and filled f-shells.

1.1 The CALPHAD method

The phase diagram is one of the most useful tools used in the design of new materials. In the past when computational tools were not available, phase diagrams were constructed only by experiment, which is time-consuming and costly. Hundreds of samples may be needed for the determination of a single isothermal section. Due to the development of computer technology, alloy systems (binary, ternary and multi-component) can be easily optimized with only a few key samples and various phase diagrams are readily available or can be conveniently calculated with different thermodynamic software (Factsage (Bale et al., 2002), Thermo-Calc (Andersson, Helander, Höglund, Shi, & Sundman, 2002), Pandat (Chen et al., 2002) et al) .

The CALPHAD method is shown schematically in Fig. 4. All relevant experimental data are collected and critically evaluated. These experimental data include but are not limited to the following: phase diagram, thermodynamic and crystallographic data. After critical evaluation of the data, proper thermodynamic models are chosen for each of the phases in a specific system. All this information is treated in the optimization process, in which model parameters are assigned and optimized for different phases. A reasonable fit is obtained to all experimental data. A set of self-consistent thermodynamic parameters is created which can be used to describe the system thermodynamically. Thermodynamic descriptions of high-order systems can usually be obtained by extrapolating from low-order systems when experimental data are lacking. More often than not, new parameters are added when experimental data are available for higher-order systems and parameters for lower-order systems are re-adjusted to better describe the higher-order systems.

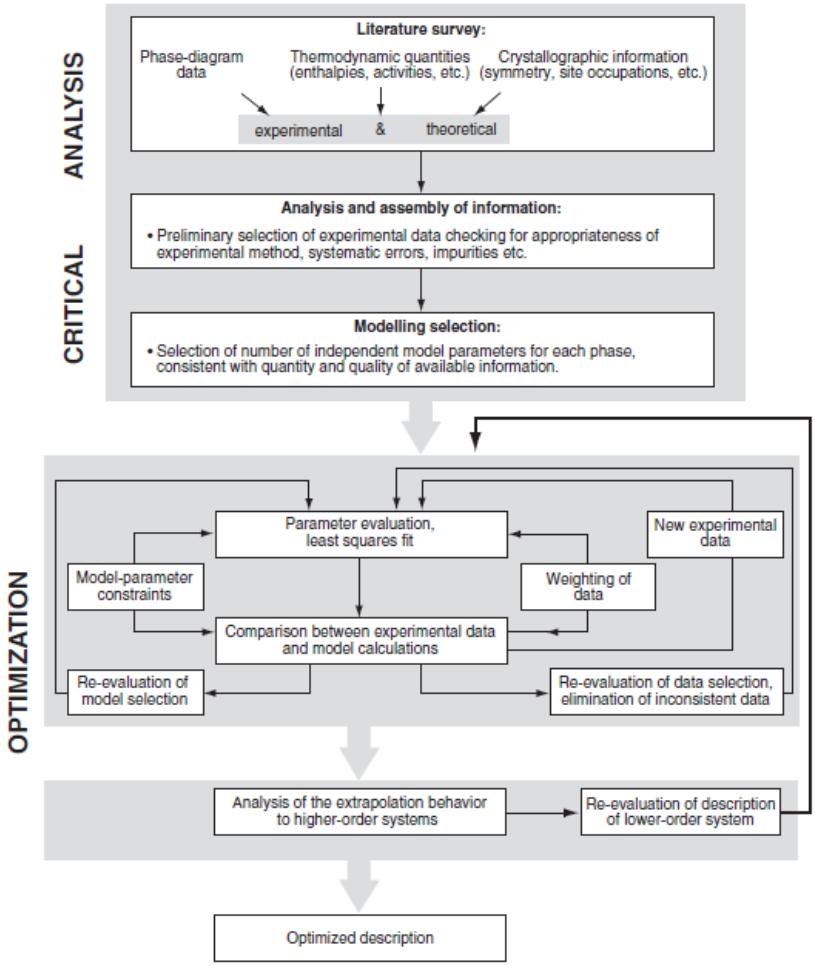

Figure 1.4. A schematic diagram of the CALPHAD method (Lukas, Fries, & Sundman, 2007).

While the general route of a thermodynamic optimization based on the CALPHAD method is schematically shown in Fig.4, the optimization of specific systems may vary. This usually depends on how much information is available for these specific systems. In the present project, as will be mentioned in the succeeding chapters, experimental data are limited and trends/similarities among all systems are utilized to make reasonable predictions of properties of the phases in different systems (i.e. enthalpies of formation, entropies of formation, melting points, etc.). The Miedema Model (Miedema, de Châtel, & de Boer, 1980) is also used in the present project to provide predicted thermodynamic data for the liquid phase in the binary systems. Information on the Miedema model used in the present project is given in Appendix 1.

1.2 Thermodynamic modelling

1.2.1 Elements

The thermodynamic properties of all pure elements are taken from the SGTE-compilation by Dinsdale (A.T, 1991) and described by an equation of the form:

$$G_i(T) - H_i^{SER} = A + BT + CT\ln T + DT^2 + ET^{-1} + FT^3 + IT^7 + JT^{-9} \qquad 1.1$$

where H_i^{SER} is the molar enthalpy of the element *i* at 25 ^{o}C and 1 bar in its standard element reference (SER) state, and *T* is the absolute temperature. The last two terms in Eq. 1.1 are used only outside the ranges of the melting point; $I \cdot T^7$ for a liquid below the melting point and $J \cdot T^{-9}$ for solid phases above the melting point.

The entropy change for the transformation Ce(hcp)→Ce(fcc) was taken from COST (Ansara, Effenberg, & Secretariat, 1998) as 0.56886 J/mol-K, and the enthalpy of transformation was set to 161.1 J/mol in order to reproduce the more recently reported (Gschneidner, Pecharsky, Cho, & Martin, 1996) temperature of transformation of 10 ^{o}C.

1.2.2 Compounds

All binary compounds were assumed to be stoichiometric since solubility data were unavailable. Most of the ternary phases (V, τ2, τ4, τ5, τ6, τ7, I and X) were also assumed to be stoichiometric since only very limited solubility ranges were reported for some of these phases. The Gibbs energies of the compounds (e.g. the binary RE-Zn compounds) were modeled by the equation:

$$g(RE_xZn_{1-x}) = [xg_{RE}^0 + (1-x)g_{Zn}^0] + (\Delta h^0 - T\Delta s^0) \qquad 1.2$$

where $g(RE_xZn_{1-x})$ is the Gibbs energy of the compound per g-atom at temperature *T* (*K*), g_{RE}^0 is the Gibbs energy of the pure RE element at temperature *T* in the state which is stable at 298.15K, and g_{Zn}^0 is the Gibbs energy of pure hcp Zn at *T*.

The enthalpy and entropy of formation, Δh^0 and Δs^0, are assumed to be independent of temperature. That is, the heat capacities of the compounds are all assumed to be given by the Neumann-Kopp equation (Kopp, 1865):

$$C_p = xC_{p(RE)} + (1-x)C_{p(Zn)} \qquad 1.3$$

As will be shown in chapters 4 and 5, the agreement between the measured heat capacities and those calculated from eq. (2-3) is excellent for $LaZn_{13}$, La_2Zn_{17}, YZn, Y_2Zn_{17}, Gd_2Zn_{17}, TbZn, Tb_2Zn_{17}, HoZn and Yb_2Zn_{17}. Hence, in the present study, it is assumed that the Neumann-Kopp equation applies to all stoichiometric compounds, including the ternary compounds.

1.2.3 Terminal solid solutions

Solubility of Zn in the terminal bcc solutions has been reported for the Ce-Zn, Pr-Zn, Nd-Zn and Sm-Zn systems. Zn solubility is also assumed in the Sc-Zn, La-Zn and Pm-Zn systems in which the bcc phase is stable. Furthermore, solubility of Zn and RE in Mg was considered in the thermodynamic descriptions of the respective RE-Mg and Mg-Zn systems. Hence, the hcp (Mg) phase is also considered as a terminal solid solution in the present study. The two terminal solid solutions are modeled as completely disordered phases and their Gibbs energies are described by Redlich-Kister polynomials (Redlich & Kister, 1948). For example, the Gibbs energy of the hcp phase is expressed as:

$$g_{hcp} = x_{RE} g^0_{RE(hcp)} + x_{Mg} g^0_{Mg(hcp)} + x_{Zn} g^0_{Zn(hcp)} + RT(x_{RE} \ln x_{RE} + x_{Mg} \ln x_{Mg} + x_{Zn} \ln x_{Zn})$$
$$+ x_{RE} x_{Mg} L^0_{RE,Mg} + x_{RE} x_{Zn} L^0_{RE,Zn} + x_{Mg} x_{Zn} L^0_{Mg,Zn} + {}^{ex}g^0_{RE,Mg,Zn} \qquad 1.4$$

in which R is the gas constant, x_{RE}, x_{Mg} and x_{Zn} are the mole fractions of RE, Mg and Zn, respectively. The standard element reference (SER) state, i.e. the stable structure of the element at 25°C and 1 bar, is used as the reference state of the Gibbs energy. The parameters denoted as $L^0_{i,j}$ are the interaction parameters from the binary systems. The ternary excess Gibbs energy is expressed as follows:

$$g^0_{RE,Mg,Zn} = x_{RE} x_{Mg} x_{Zn} (x_{RE} L^0_{RE,Mg,Zn} + x_{Mg} L^1_{RE,Mg,Zn} + x_{Zn} L^2_{RE,Mg,Zn}) \qquad 1.5$$

where $L^0_{RE,Mg,Zn}$, $L^1_{RE,Mg,Zn}$ and $L^2_{RE,Mg,Zn}$ are ternary parameters to be optimized in the present work.

1.2.4 Compound energy formalism (CEF)

All solid solution phases in the present project (REZn, $REMg_3$, $LaZn_4$, La_2Mg_{17}, β-La_2Zn_{17}, $REMg_{12}$ and τ3, etc.) are modeled with the Compound Energy Formalisim (CEF) (Hillert, 2001). It should be mentioned that although there could be several sublattices in a solution phase and

different atoms can substitute for each other within different sublatices (as in the case of Laves_C14 and Laves_C15 phases in the Mg-Zn and RE-Mg systems), only Mg and Zn can substitute for each other within one sublattice in all the ternary solid solutions in the present project. The expressions for the Gibbs energies of these solution phases can thus be relatively simple. For example, the Gibbs energy of La(Mg,Zn) (per mole of formula) can be expressed as follows:

$$\begin{aligned} G^{La(Mg,Zn)} = {} & y_{Mg} G^{0,La(Mg,Zn)}_{La:Mg} + y_{Zn} G^{0,La(Mg,Zn)}_{La:Zn} \\ & + RT\left(y_{Mg} ln y_{Mg} + y_{Zn} ln y_{Zn}\right) \\ & + y_{Mg} y_{Zn} (L^{0}_{La:Mg,Zn} \\ & + (y_{Mg} - y_{Zn})\, L^{1}_{La:Mg,Zn}) \end{aligned} \qquad 1.6$$

where y_{Mg} and $y_{Zn}$are the site fractions of Mg and Zn in the second sublattice, $G^{0,La(Mg,Zn)}_{La:Mg}$ and $G^{0,La(Mg,Zn)}_{La:Zn}$ are the Gibbs energies of the end-members (LaMg and LaZn) at temperature T under the convention that the enthalpies of the elements are equal to zero in their stable states at 298.15K, and $L^{0}_{La:Mg,Zn}$ and $L^{1}_{La:Mg,Zn}$ are interaction parameters to be optimized. The Gibbs energies of all other ternary solid solutions can be expressed similarly.

1.2.5 Modified Quasichemical Model

The modified Quasichemical Model in the pair approximation (Pelton, Degterov, Eriksson, Robelin, & Dessureault, 2000) is used in the present project to describe the liquid phases. This model has been used extensively for liquid alloys (Kang, Pelton, Chartrand, Spencer, & Fuerst, 2007; Kang, Pelton, Chartrand, Spencer, & Fuerst, 2007) as well as molten salts (Chartrand & Pelton, 2001a, 2001b; Pelton & Chartrand, 2001), oxides (Jung, Decterov, & Pelton, 2005; Kang, Jung, Decterov, Pelton, & Lee, 2004) and sulfides (Waldner & Pelton, 2004). The following pair-exchange reaction between atoms A and B on neighboring quasi-lattice sites is considered:

$$(A-A)+(B-B)=2(A-B); \Delta g_{AB} \qquad 1.7$$

where (i-j) represents a first-nearest-neighbor (FNN) pair and Δg_{AB} is the non-configurational Gibbs energy change for the formation of two moles of (A-B) pairs. Let n_A and n_B be the number

of moles of A and B atoms, n_{AA}, n_{BB} and n_{AB} be the number of A-A, B-B and A-B pairs, and Z_A and Z_B be the coordination numbers of A and B. The Gibbs energy of the solution can be given as:

$$G = (n_A g_A^0 + n_B g_B^0) - T\Delta S^{config} + (n_{AB}/2)\Delta g_{AB} \qquad 1.8$$

where g_A^0 and g_B^0 are the molar Gibbs energies of the pure elements, and ΔS^{config} is the configurational entropy of mixing given by randomly distributing the (A-A), (B-B) and (A-B) pairs in the one-dimensional Ising approximation:

$$\begin{aligned}\Delta S^{config} &= -R(n_A \ln X_A + n_B \ln X_B) \\ &\quad - R[n_{AA}\ln(X_{AA}/Y_A^2) + n_{BB}\ln(X_{BB}/Y_B^2) \\ &\quad + n_{AB}\ln(X_{AB}/2Y_A Y_B)]\end{aligned} \qquad 1.9$$

where X_A and X_B are the overall mole (or site) fractions of A and B; X_{AA}, X_{BB} and X_{AB} are pair fractions of the (A-A), (B-B) and (A-B) pairs; and Y_A and Y_B are "coordination-equivalent" fractions:

$$X_A = n_A/(n_A + n_B) = 1 - X_B \qquad 1.10$$

$$X_{ij} = n_{ij}/(n_{AA} + n_{BB} + n_{AB}) \qquad \text{(i, j = A or B)} \qquad 1.11$$

$$Y_A = Z_A n_A / Z_A n_A + Z_B n_B) = 1 - Y_B \qquad 1.12$$

The coordination numbers Z_A and Z_B also satisfy the following relationships:

$$Z_A n_A = 2n_{AA} + n_{AB} \qquad 1.13$$

$$Z_B n_B = 2n_{BB} + n_{AB} \qquad 1.14$$

Δg_{AB} in Eqs (7 and 8) can be further expanded as follows:

$$\Delta g_{AB} = \Delta g_{AB}^0 + \sum_{i\geq 1} g_{AB}^{i0} X_{AA}^{i} + \sum_{j\geq 1} g_{AB}^{0j} X_{BB}^{j} \qquad 1.15$$

where Δg_{AB}^0, g_{AB}^{i0} and g_{AB}^{0j} are empirical parameters of the model which may be temperature-dependent. The equilibrium pair distribution is calculated by setting

$$(\partial G / \partial n_{AB})_{n_A, n_B} = 0 \qquad 1.16$$

The model permits Z_A and Z_B to vary with composition as follows:

$$\frac{1}{Z_A} = \frac{1}{Z_{AA}^A}\left(\frac{2n_{AA}}{2n_{AA} + n_{AB}}\right) + \frac{1}{Z_{AB}^A}\left(\frac{n_{AB}}{2n_{AA} + n_{AB}}\right) \qquad 1.17$$

$$\frac{1}{Z_B} = \frac{1}{Z_{BB}^B}\left(\frac{2n_{BB}}{2n_{BB} + n_{AB}}\right) + \frac{1}{Z_{BA}^B}\left(\frac{n_{AB}}{2n_{BB} + n_{AB}}\right) \qquad 1.18$$

In a ternary system (1-2-3), the Gibbs energy of the solution can be given as:

$$G = \sum n_m g_m^0 - T\Delta S^{config} + \sum \sum_{n>m} n_{nm}(\Delta g_{mn} / 2) \qquad 1.19$$

where (m and n =1, 2, 3). g_m^0 is the molar Gibbs energy of the pure element m, Δg_{mn} is the nonconfigurational Gibbs energy change for the formation of two moles of (m-n) pairs, and ΔS^{config} is an approximate expression for the configurational entropy of mixing given by randomly mixing the (m-n) pairs:

$$\begin{aligned} \Delta S^{config} &= -R\sum n_m \ln X_m \\ &\quad - R(\sum n_{mn} \ln(X_{mm} / Y_m^2) + \sum \sum_{m>n} n_{mn} \ln(X_{mn} / 2Y_m Y_n)) \end{aligned} \qquad 1.20$$

where X_m is the overall mole fraction, X_{mm}, X_{mn} are pair fractions, Y_m and Y_n are "coordination-equivalent" fractions. Detailed information on these notations is given by Pelton and Chartrand (Arthur Pelton & Patrice Chartrand, 2001).

Similar to the Δg_{AB} in the binary system, Δg_{mn} for the binary m-n system can be expanded as follows:

$$\Delta g_{mn} = \Delta g_{mn}^0 + \sum_{i+j\geq 1} g_{mn}^{ij} X_{mm}^i X_{nn}^j \qquad 1.21$$

In a symmetrical ternary system (1-2-3), the following equation for Δg_{12} is proposed (Kohler extrapolation):

$$\Delta g_{12} = \Delta g_{12}^{0} + \sum_{(i+j)\geq 1} g_{12}^{ij} \left(\frac{X_{11}}{X_{11}+X_{12}+X_{22}}\right)^{i} \left(\frac{X_{22}}{X_{11}+X_{12}+X_{22}}\right)^{j} + \sum_{\substack{i\geq 0\\ j\geq 0\\ k\geq 1}} g_{12(3)}^{ijk} \left(\frac{X_{11}}{X_{11}+X_{12}+X_{22}}\right)^{i} \left(\frac{X_{22}}{X_{11}+X_{12}+X_{22}}\right)^{j} Y_{3}^{k} \qquad 1.22$$

where $g_{12(3)}^{ijk}$ are the empirical ternary coefficients to be optimized, which give the effect of the presence of component 3 upon the energy Δg_{12} of the (1-2) pair interactions. Similar equations can be proposed for Δg_{13} and Δg_{23}.

For extrapolation into the ternary system, various models can be chosen. The most commonly used models are Kohler (Kohler, 1960), Muggianu (Muggianu, Gambino, & Bros, 1975) and Toop (Toop, 1965) models. The user may also choose other asymmetrical models. Figure 5 shows examples of selected models. The values of Δg_{mn} of a ternary solution at a composition point *p* are estimated from the excess Gibbs energies in the three binary subsystems at points *a*, *b* and *c*. If all three components are chemically similar, the symmetrical model should be chosen for the extrapolation. If two components are chemically similar while the other component is chemically different, either Kohler/Toop (fig. 5b) or Muggianu/Toop (fig. 5d) may be chosen for the extrapolation. In both models, replacing component 2 by 3 has no influence on the excess Gibbs energies of the binary 1-2 and 1-3 systems used for the estimation. Detailed information on extrapolation models is available (Pelton, 2001).

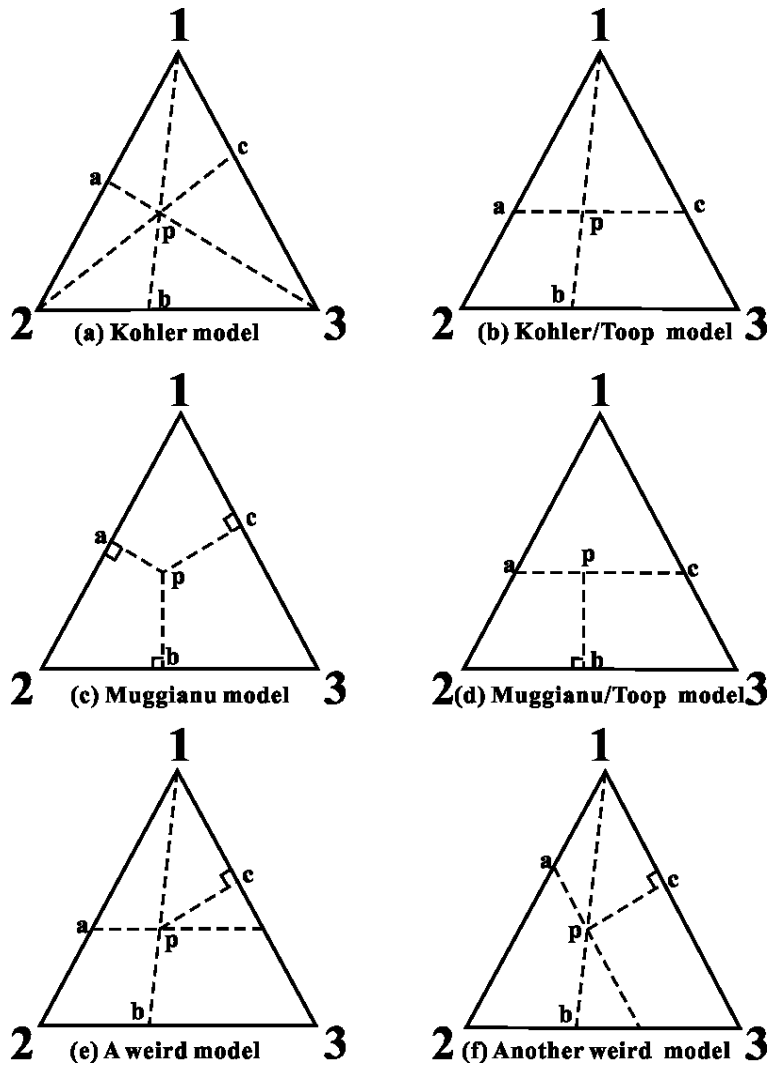

Figure 1.5. Some “geometric” models for estimating ternary thermodynamic properties from optimized binary data (A. D. Pelton, 2001).

1.3 In-situ neutron diffraction

In-situ neutron diffraction (ND) experiments were performed on selected samples in the Ce-Mg-Zn and Nd-Mg-Zn systems to validate these phase diagrams and help refine the model parameters. The two systems were investigated because Ce and Nd are among the most commonly used RE elements in Mg alloys. The Ce-Mg-Zn and Nd-Mg-Zn systems are also typical lighter-RE-Mg-Zn systems. Investigation of the two systems is important for the understanding of other RE-Mg-Zn systems.

Generally, due to the high penetrating power of neutrons, large samples can be investigated

by neutron diffraction, leading to better control of the sample compositions and increased resistance to oxidation. Conventionally, to investigate the phase relationship in a sample at high temperature, the sample should be annealed at the selected temperature and then quenched to retain the phase relationships at high temperature. Reaction can occur during the quenching process. The “frozen in” phase relationships are actually somewhat different from those at high temperature. In an *in-situ* neutron diffraction experiment, the samples can be investigated at a true equilibrium state, providing more accurate experimental information.

The experimental conditions can also be well controlled in an *in-situ* ND experiment. For example, the temperature can be program controlled so that the sample can be investigated at any temperature, for any amount of time. In the present study, all samples are investigated every 5°C so as to obtain the phase transformation temperature as well as the precipitation sequence.

The collected patterns from ND experiments can be analyzed using the Rietveld method (Rietveld, 1969). The lattice constant of the phases can be refined. Quantitative phase analysis can also been performed in a Rietveld analysis with high quality diffraction patterns.

In an in-situ ND experiment, samples can also been investigated in the liquid state. Analysis of the diffraction patterns of the liquid phase can provide information on the short-range ordering in the liquid phase (March, 2012).

Although ND experiments have many advantages, they are not as widely used in material science as X-ray diffraction. The maintenance of a neutron source facility is more expensive than an X-ray diffractometer. Consequently, the beam time is limited. The intensity of the neutron beam is also not as brilliant as the X-ray beam. It takes longer to record a neutron diffraction pattern with peak intensities comparable to that of X-ray patterns.

Neutron diffraction data were acquired using the C2 powder diffractometer of the Canadian Neutron Beam Centre, located at the National Research Universal (NRU) reactor, Canadian Nuclear Laboratories (CNL). Diffraction from the (531) reflection of a silicon single crystal monochromator produced incident neutrons with a nominal wavelength of 0.133 nm. The C2 diffractometer is equipped with an 800-channel detector covering an 80° range in scattering angle 2θ, allowing multiple diffraction peaks to be acquired simultaneously.

Detailed information about the in-situ ND experiments is presented in Chapters 6 and 7.

1.4 Objective of the present project

The main objective of the present project is to construct a thermodynamic database for the RE-Mg-Zn systems (RE=Sc, Y, La, Ce, Pr, Nd, Pm, Sm, Eu, Gd, Tb, Dy, Ho, Er, Tm, Yb and Lu). Thermodynamic descriptions of Mg-Zn and RE-Mg binary sub-systems are available in the Factsage database. Consequently only the RE-Zn and RE-Mg-Zn systems are to be optimized in the present project. The objective can be further divided as follows:

1> Critical review of all experimental data on all RE-Zn and RE-Mg-Zn systems. The missing data are estimated from Miedema Model (Miedema, de Châtel, & de Boer, 1980), first-principal calculation (provided by Aimen Gheribi at CRCT) or directly from the trends among all RE elements.

2> Based on all available experimental data and following the trends/similarities among all RE-Zn systems, perform the systematic optimization of all RE-Zn systems. Obtain a reasonable thermodynamic description of these systems. In particular, model parameters for the metastable or unstable phases are obtained by following the trends.

3> Conduct neutron diffraction experiments on selected samples in the Ce-Mg-Zn and Nd-Mg-Zn systems to obtain the phase transformation behavior in these samples (transition temperatrues and precipitation sequences). The experimental data are used to refine the model parameters in the two systems.

4> Based on the systematically optimized binary systems, together with experimental data from the literature and our experiments, perform a thermodynamic optimization of the Ce-Mg-Zn, Nd-Mg-Zn and Y-Mg-Zn system. The optimization of the three systems are important to the optimization of other RE-Mg-Zn systems where experimental data are lacking.

5> Perform a thermodynamic optimization of all other RE-Mg-Zn systems simultaneouly. The trends are again used in the optimization of the ternary RE-Mg-Zn systems.

6> Construct a thermodynamic database for the RE-Mg-Zn systems.

This research was supported by funding from the Natural Sciences and Engineering Research Council of Canada (NSERC) Magnesium Strategic Research Network. More information on the Network can be found at www.MagNET.ubc.ca.

Chapter 2 **LITERATURE REVIEW**

All 17 RE-Zn binary systems are to be optimized in the present project. A critical review shows that experimental data on the binary RE-Zn systems are limited. The phase diagrams of the Sc-Zn, Y-Zn, La-Zn, Ce-Zn, Pr-Zn, Nd-Zn, Sm-Zn, Gd-Zn, Tb-Zn, Dy-Zn, Ho-Zn, Er-Zn and Yb-Zn are well established, based on DTA measurements by different authors. However, thermodynamic data on the binary RE-Zn systems are very limited. The most important thermodynamic data are the vapor pressure measurement over a series of liquid and solid alloys in the Y-Zn, Ce-Zn, Pr-Zn, Nd-Zn and Sm-Zn systems. Calorimetric data are also available for most of the compounds in the La-Zn system as well as a few compounds in the Y-Zn system. Emf measurements were available for the La-Zn system over the whole composition range. In addition, emf measurements were performed in a few other systems to obtain the enthalpy of formation of the most Zn-rich compounds. All the experimental data are summarized in detail in Chapters 4 and 5. The investigation status of the 17 binary RE-Zn systems is summarized in Table 1.

Table 2.1. The investigation status of the 17 RE-Zn systems

Systems	Phase diagram data	Thermodynamic data	Previous optimization
Sc-Zn	Yes	No	No
Y-Zn	Yes	Yes	Yes
La-Zn	Yes	Yes	Yes
Ce-Zn	Yes	Yes	Yes
Pr-Zn	Yes	Yes	Yes
Nd-Zn	Yes	Yes	Yes
Pm-Zn	No	No	No
Sm-Zn	Yes	Yes	Yes
Eu-Zn	No	No	No
Gd-Zn	Yes	Yes, very limited	Yes
Tb-Zn	Yes	No	No
Dy-Zn	Yes	Yes, very limited	No
Ho-Zn	Yes	Yes, very limited	No
Er-Zn	Yes	Yes, very limited	No
Tm-Zn	No	No	No
Yb-Zn	Yes	No	No
Lu-Zn	No	No	No

Lacking thermodynamic data, it is very difficult to work out a reasonable set of thermodynamic parameters for most of the heavier-RE-Zn as well as Sc-Zn, Pm-Zn and Eu-Zn systems. As a result, no thermodynamic optimization has been carried out on these systems in the literature. For the lighter-RE-Zn as well as Y-Zn systems, optimization was carried out independently for each system by different groups. Since all RE elements have very similar properties, it is better to optimize these systems simultaneously so as to obtain a more reasonable result. The Al-RE systems were optimized this way by Jin et al (Jin, Kang, Chartrand, & Fuerst, 2010, 2011) and in the present work all RE-Zn systems will also be optimized in this manner. The advantages of such an optimization are obvious: thermodynamic descriptions of these systems are more consistent; thermodynamic descriptions of some systems with few or no experimental data can also be obtained by following similarities and trends established among all systems. This approach and its associated advantages will be further discussed in Chapters 4 and 5.

Experimental data on the 17 RE-Mg-Zn ternary systems are quite limited. No thermodynamic data are available for any of the systems. Phase diagram data are also scarce except for the La-Mg-Zn, Ce-Mg-Zn, Nd-Mg-Zn and Y-Mg-Zn systems as summarized in Chapters 6 and 7. However, following the trends established in the binary RE-Zn systems and taking advantage of similarities, it is possible to propose reasonable thermodynamic parameters for all other RE-Mg-Zn systems except for the Pm-Mg-Zn (no thermodynamic description for the Pm-Mg system is available), Sc-Mg-Zn, Eu-Mg-Zn and Yb-Mg-Zn systems (Sc, Eu, and Yb are different from other elements to some extent as will be discussed in succeeding chapters).

So far, the following binary RE-Zn systems have been optimized by different authors: La-Zn (Berche *et al.*, 2012; Qi *et al*., 2010), Ce-Zn (Spencer *et a.l*, 2008; Wang *et al*., 2008), Pr-Zn (Huang *et al*., 2008; Wang, *et al*., 2008), Nd-Zn (Li *et al*., 2008; Liu *et al*., 2009; Qi *et al*., 2008), Sm-Zn (Jia *et al*., 2009; Liu *et al*., 2009), Gd-Zn (Qi *et al*., 2012) and Y-Zn (Liu *et al*., 2008; Shao *et al*., 2006; Spencer *et al*.., 2008),.

The liquid phase was modeled exclusively using the substitutional solution model except for the Ce-Zn and Y-Zn systems from Spencer (Spencer *et al*., 2008), in which the Modified Quasichemical Model was used to describe the liquid phase. All model parameters for the liquid phase are summarized in Table 1.

Table 2.2. Thermodynamic model parameters of the liquid phases of all the optimized RE-Zn systems from the literature (J/g•atom).

Liquid phase (substitutional solution model)				
	${}^{0}L_{RE,Zn}$	${}^{1}L_{RE,Zn}$	${}^{2}L_{RE,Zn}$	Refs.
Y-Zn	-128000+4.2T	56000		(Shao, et al., 2006)
	-120433+18.9T	79694-37.8T	3471+2.88T	(Liu, et al., 2008)
La-Zn	-116372+39.16T	63845-14T	-41912+19.7T	(H. Y. Qi, et al., 2010)
	-107900+9.1T	78100-25T	-37100+17T	(Berche, et al., 2012)
Ce-Zn	-116372+39.3T	70000-19T	-42000+20T	(Wang, et al., 2008)
Pr-Zn	-112894+28T	73584-21.2T	-34066+10.39T	(Wang, et al., 2008)
	-115403+30T	72540-25T	-22030+6.61T	(Huang, et al., 2008)
Nd-Zn	-101982+20T	76183-30T	-31990+18T	(H. Qi, et al., 2008)
	-102649+27.1T	70637-41T		(Li, et al., 2008)
	-112000+27.8T	71411-25.6T	-40932+27T	(Liu, et al., 2009)
Sm-Zn	-139082+8.95T	102515-18.81T	-40836+9T	(Jia, et al., 2009)
	-109032+16.5T	72446-22.7T	-44721+29.6T	(Liu, et al., 2009)
Gd-Zn	-128000+4.2T	56000	-25000	(H. Y. Qi, et al., 2012)

Liquid phase (Modified Quasichemical Model)					
Coordination numbers					
i	j	Z_{ij}^{i}	Z_{ij}^{j}	Gibbs energy of pair exchange reactions	Refs
Y	Zn	4	6	Δg_{YZn}= -28451.2+5.8576T-8284.48X_{YY}+15480.8X_{ZnZn}	(Spencer, et al., 2008)
Ce	Zn	3	6	Δg_{CeZn}= -36400.8+5.8576T-9204.8X_{CeCe}+16736X_{ZnZn}	(Spencer, et al., 2008)

As for the liquid phase described by the substitutional solution model, a total of six parameters were introduced by most authors. The temperature dependent terms differed significantly not only for the same system from different authors (see Table 1) but also for different systems from the same author/group (La-Zn, Nd-Zn and Gd-Zn from Qi et al (H. Qi, et al., 2008; H. Y. Qi, et al., 2012; H. Y. Qi, et al., 2010), Ce-Zn, Pr-Zn, Nd-Zn, Sm-Zn and Y-Zn from Wang et al (Wang, et al., 2008) and Liu et al (Liu, et al., 2009; Liu, et al., 2008)). It should also be mentioned that some of the temperature dependent terms are in the range of 20-40 J/K, which are relatively large and unreasonable. The differences in corresponding temperature independent terms from the same or different systems are not as significant as those in the temperature dependent terms but are still noticeable (Table 1). The parameters of the liquid phase

in the Gd-Zn systems (Qi, *et al*.., 2012) are the same as those of the liquid phase in the Y-Zn system (Shao, *et al*., 2006) except that one additional parameter was added; this could be questioned.

The Ce-Zn and Y-Zn systems were also optimized by Spencer et al (Spencer, et al., 2008) who used the Modified Quasichemical Model to describe the liquid phase. However, different coordination numbers were used for the two systems. Given that Y and Ce are rare earth elements, they have very similar properties. Consequently, it is better to use the same coordination numbers for the liquid phase in these two systems. In addition, the fit to the experimental data in these two systems, e.g. the eutectic reaction of L→YZn+YZn_2, can be improved.

The calculated enthalpies and entropies of mixing at 1600 ^{o}C from different authors are shown in Figs. 1 and 2. While the calculated enthalpies of formation from different authors are more or less the same, the entropies of formation differ significantly. Generally, the entropies of mixing for the liquid phase are positive and have minima at certain compositions where short range ordering occurs. However, most of the entropies of mixing calculated from the parameters in the literature possessed negative values either in a certain range or over the whole composition range; some were very close to ideal mixing (as in the cases of Gd-Zn and Y-Zn systems) in which no short range ordering were considered. Strong tendencies to form solid compounds in all RE-Zn systems were commonly observed. There exist seven or more compound stoichiometries so that short range ordering in the liquid is very probable and cannot be ignored. Consequently, the thermodynamic description of the liquid phase in the La-Zn system from Berche et al (Berche *et al*., 2012), in the Ce-Zn and Y-Zn systems from Spencer et al (Spencer *et al*., 2008), in the Sm-Zn system from Jia et al (Jia, *et al*., 2009) may be considered as better.

All binary compounds in the optimized RE-Zn systems were treated exclusively as stoichiometric compounds and because heat capacity data were lacking, the heat capacities of the compounds were given by the Neumann-Kopp equation (Kopp, 1865). As a result, only two parameters were needed for each binary compound: Δh^0 and Δs^0 (for notation see Section 3 and Chapters 4 and 5). All optimized model parameters for binary compounds are summarized in Table 2.

As can be seen from Table 2, model parameters for the same/similar phases from different authors differ greatly. Normally, when all RE elements are concerned, similarities/trends in

properties can always be observed. e.g. trends in the melting points of RE elements and corresponding RE-Zn compounds, as presented in Chapters 4 and 5. However, no trends can be observed when the optimized enthalpies of formation of the similar RE-Zn binary compounds are considered together. As mentioned above, in most of the optimized binary RE-Zn systems, the authors used only enthalpies of formation derived from vapor pressure or e.m.f data. More reasonable model parameters can be obtained if original experimental data and trends among all RE elements are used in the optimization.

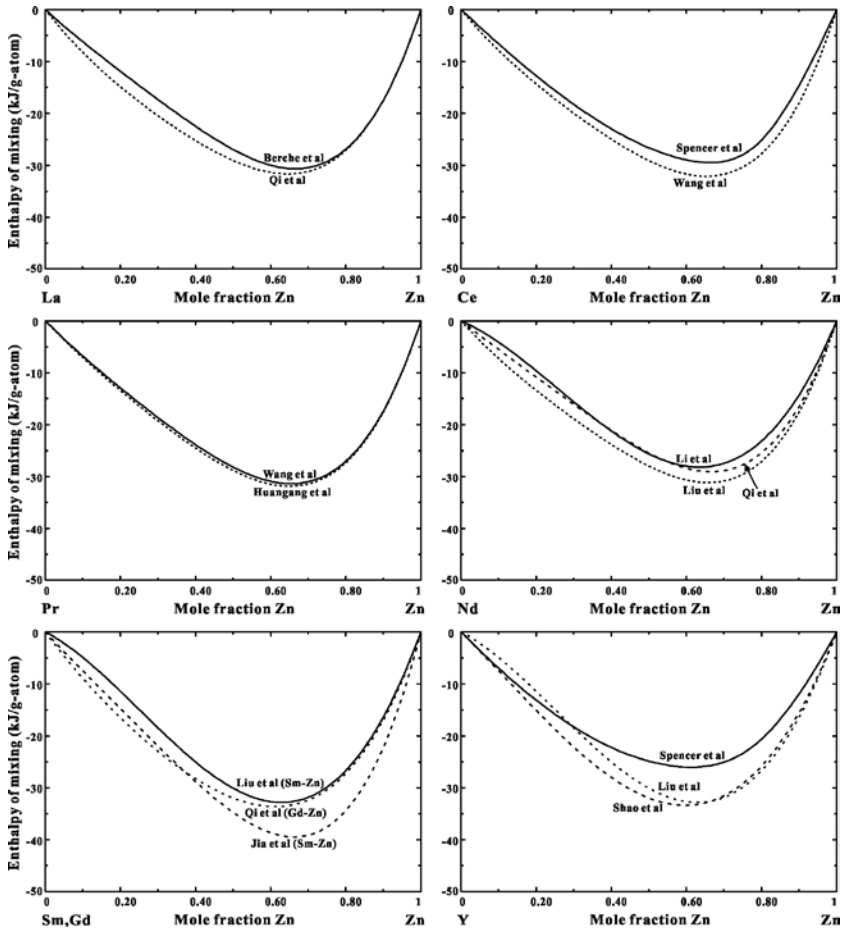

Figure 2.1. The calculated enthalpy of formation of RE-Zn systems at 1600 ^{o}C from different authors from the literature.

It was also found that the enthalpy of formation derived from e.m.f measurements is more negative than that obtained from calorimetry for the La-Zn system (Alexandre Berche, et al., 2012; A. Berche, Marinelli, Mikaelian, Rogez, & Record, 2009). This may be similar in other RE-Zn systems. Systematic optimization of all RE-Zn systems is indicated.

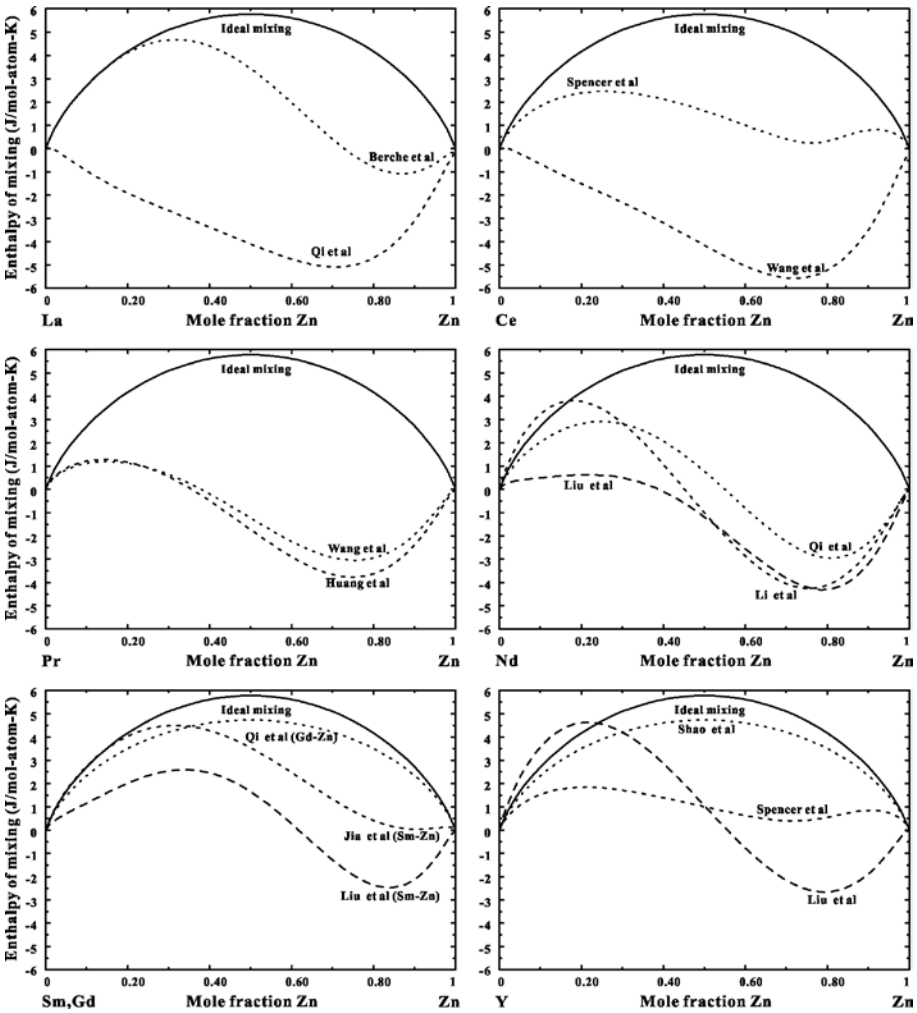

Figure 2.2. The calculated entropy of formation of RE-Zn systems at 1600 ^{o}C from different authors from the literature.

Table 2.3. Thermodynamic model parameters of the solid compounds of all the optimized RE-Zn systems from the literatures (J/g•atom).

Solid phases			
		Gibbs energy of formation	Refs
MZn			
	YZn	-47000+4.75T	(Shao, et al., 2006)
		-45285+8.53T	(Liu, et al., 2008)
		-44005+11.31T	(Spencer, et al., 2008)
	LaZn	-31778+7.5T	(H. Y. Qi, et al., 2010)
		-32800+0.06T	(Alexandre Berche, et al., 2012)
	CeZn	-36525+4.94T	(Spencer, et al., 2008)
		-34040+6.4T	(Wang, et al., 2008)
	PrZn	-32430+2.73T	(Wang, et al., 2008)
		-34221+4.26T	(Huang, et al., 2008)
	NdZn	-31805+2.4T	(H. Qi, et al., 2008)
		-34575+6.35T	(Li, et al., 2008)
		-35460+5.31T	(Liu, et al., 2009)
	SmZn	-41969+0.2T	(Jia, et al., 2009)
		-36494+3.75T	(Liu, et al., 2009)
	GdZn	-53892+10.6T	(H. Y. Qi, et al., 2012)
MZn_2			
	α-YZn_2	-48000+5.02T	(Shao, et al., 2006)
	β-YZn_2	-46000+3.07T	(Shao, et al., 2006)
	α-YZn_2	-51017+13.41T	(Liu, et al., 2008)
	β-YZn_2	-48379+10.83T	(Liu, et al., 2008)
	α-YZn_2	-51789+16.80T	(Spencer, et al., 2008)
	β-YZn_2	-49000+14.08T	(Spencer, et al., 2008)
	$LaZn_2$	-36234+6.3T	(H. Y. Qi, et al., 2010)
		-34900	(Alexandre Berche, et al., 2012)
	$CeZn_2$	-39950+5.09T	(Spencer, et al., 2008)
		-40060+9.22T	(Wang, et al., 2008)
	α-$PrZn_2$	-35867+3.73T	(Wang, et al., 2008)
	β -$PrZn_2$	-35620+3.43T	(Wang, et al., 2008)
	$PrZn_2$	-39219+6.97T	(Huang, et al., 2008)
	$NdZn_2$	-39154+7.28T	(H. Qi, et al., 2008)
		-35732+7.31T	(Li, et al., 2008)

	-39533+7.45T	(Liu, et al., 2009)
$SmZn_2$	-56262+9.07T	(Jia, et al., 2009)
	-41317+6.68T	(Liu, et al., 2009)
$GdZn_2$	-45378+3.0T	(H. Y. Qi, et al., 2012)
MZn_3		
YZn_3	-41500+4.08T	(Shao, et al., 2006)
	-43625+11.48T	(Liu, et al., 2008)
	-44500+14.38T	(Spencer, et al., 2008)
$CeZn_3$	-38988+6.33T	(Spencer, et al., 2008)
	-38474+9.83T	(Wang, et al., 2008)
$PrZn_3$	-34918+4.88T	(Wang, et al., 2008)
	-35518+6.21T	(Huang, et al., 2008)
$NdZn_3$	-37765+8.7T	(H. Qi, et al., 2008)
	-33456+8.0T	(Li, et al., 2008)
	-38065+8.68T	(Liu, et al., 2009)
$SmZn_3$	-51200+8.44T	(Jia, et al., 2009)
	-37619+6.45T	(Liu, et al., 2009)
$GdZn_3$	-39243+2.0T	(H. Y. Qi, et al., 2012)
M_3Zn_{11}		
Y_3Zn_{11}	-38743+3.97T	(Shao, et al., 2006)
	-39857+10.38T	(Liu, et al., 2008)
	-41468+13.68T	(Spencer, et al., 2008)
Ce_3Zn_{11}	-37613+6.29T	(Spencer, et al., 2008)
	-36883+9.286T	(Wang, et al., 2008)
Pr_3Zn_{11}	-34121+5.22T	(Wang, et al., 2008)
	-33932+5.88T	(Huang, et al., 2008)
Nd_3Zn_{11}	-34736+7.15T	(Qi, et al., 2008)
	-31727+7.63T	(Li, et al., 2008)
	-37364+9.14T	(Liu, et al., 2009)
Sm_3Zn_{11}	-49000+8.15T	(Jia, et al., 2009)
	-35943+6.29T	(Liu, et al., 2009)
Gd_3Zn_{11}	-36530+1.8T	(H. Y. Qi, et al., 2012)
MZn_4		
$LaZn_4$	-35610+8.5T	(H. Y. Qi, et al., 2010)
	-34000+3.63T	(Berche, et al., 2012)
$M_{13}Zn_{58}$		
$Y_{13}Zn_{58}$	-36000+3.94T	(Shao, et al., 2006)

	-36555+9.59T	(Liu, et al., 2008)
	-38782+13.3T	(Spencer, et al., 2008)
$Ce_{13}Zn_{58}$	-36745+7.04T	(Spencer, et al., 2008)
	-35353+8.94T	(Wang, et al., 2008)
$Pr_{13}Zn_{58}$	-33304+5.67T	(Wang, et al., 2008)
	-32606+5.89T	(Huang, et al., 2008)
$Nd_{13}Zn_{58}$	-32198+6.7T	(H. Qi, et al., 2008)
	-30195+7.38T	(Li, et al., 2008)
	-35669+8.80T	(Liu, et al., 2009)
$Sm_{13}Zn_{58}$	-46978+8.06T	(Jia, et al., 2009)
	-34289+6.12T	(Liu, et al., 2009)
$Gd_{13}Zn_{58}$	-34222+1.8T	(H. Y. Qi, et al., 2012)
MZn_5		
YZn_5	-34333+3.96T	(Shao, et al., 2006)
	-34840+9.3T	(Liu, et al., 2008)
	-37570+13.27T	(Spencer, et al., 2008)
$LaZn_5$	-34820+9.0T	(H. Y. Qi, et al., 2010)
	-32300+3.98T	(Berche, et al., 2012)
$CeZn_5$	-35617+7.01T	(Spencer, et al., 2008)
	-34492+8.88T	(Wang, et al., 2008)
MZn_7		
$LaZn_7$	-28600+3.3T	(Berche, et al., 2012)
M_3Zn_{22}		
La_3Zn_{22}	-32750+9.5T	(Qi, et al., 2010)
	-28000+3.17T	(Berche, et al., 2012)
Ce_3Zn_{22}	-31168+6.21T	(Spencer, et al., 2008)
	-30196+7.4T	(Wang, et al., 2008)
Pr_3Zn_{22}	-30350+6.49T	(Wang, et al., 2008)
	-30144+7.04T	(Huang, et al., 2008)
Nd_3Zn_{22}	-27400+5.34T	(H. Qi, et al., 2008)
	-26790+7.27T	(Li, et al., 2008)
	-32200+9.08T	(Liu, et al., 2009)
Sm_3Zn_{22}	-43800+11.45T	(Jia, et al., 2009)
	-29316+6.08T	(Liu, et al., 2009)
Gd_3Zn_{22}	-27700+1.9T	(Qi, et al., 2012)
M_2Zn_{17}		
Y_2Zn_{17}	-28000+4.21T	(Shao, et al., 2006)

		-28368+8.25T	(Liu, et al., 2008)
		-27105+8.28T	(Spencer, et al., 2008)
	La_2Zn_{17}	-32163+9.96T	(Qi, et al., 2010)
		-25700+2.61T	(Berche, et al., 2012)
	Ce_2Zn_{17}	-29862+6.37T	(Spencer, et al., 2008)
		-27874+6.53T	(Wang, et al., 2008)
	α-Pr_2Zn_{17}	-29229+6.63T	(Wang, et al., 2008)
	β-Pr_2Zn_{17}	-28898+6.32T	(Wang, et al., 2008)
	α-Pr_2Zn_{17}	-29105+7.21T	(Huang, et al., 2008)
	β-Pr_2Zn_{17}	-28823+6.94T	(Huang, et al., 2008)
	Nd_2Zn_{17}	-26209+5.31T	(Qi, et al., 2008)
		-24503+6.19T	(Li, et al., 2008)
		-30148+8.31T	(Liu, et al., 2009)
	Sm_2Zn_{17}	-42802+12.01T	(Jia, et al., 2009)
		-27886+6.03T	(Liu, et al., 2009)
	Gd_2Zn_{17}	-26146+2.0T	(H. Y. Qi, et al., 2012)
MZn_{11}			
	$LaZn_{11}$	-28263+9.5T	(H. Y. Qi, et al., 2010)
		-21200+1.79T	(Berche, et al., 2012)
	$CeZn_{11}$	-25658+6.14T	(Spencer, et al., 2008)
		-24496+6.5T	(Wang, et al., 2008)
	$PrZn_{11}$	-24688+6.03T	(Wang, et al., 2008)
		-27348+9.21T	(Huang, et al., 2008)
	α-$NdZn_{11}$	-22770+5.28T	(H. Qi, et al., 2008)
	β-$NdZn_{11}$	-22695+5.19T	(H. Qi, et al., 2008)
		-21084+5.72T	(Li, et al., 2008)
		-25333+7.21T	(Liu, et al., 2009)
	$SmZn_{11}$	-33577+8.21T	(Jia, et al., 2009)
		-25375+7.16T	(Liu, et al., 2009)
MZn_{12}			
	YZn_{12}	-23070+4.93T	(Shao, et al., 2006)
		-23129+7.72T	(Liu, et al., 2008)
		-20628+6.1T	(Spencer, et al., 2008)
	$GdZn_{12}$	-20345+2.0T	(H. Y. Qi, et al., 2012)
MZn_{13}			
	$LaZn_3$	-25747+9.24T	(H. Y. Qi, et al., 2010)
		-18760+1.66T	(Berche, et al., 2012)

Generally, ternary systems are estimated from the respective binary sub-systems. Consequently, the binary sub-systems are required for this estimation. So far, only the La-Mg-Zn (Qi, et al., 2010), Ce-Mg-Zn (Chiu, Gröbner, Kozlov, & Schmid-Fetzer, 2010), Nd-Mg-Zn (Qi et al., 2011; C. Zhang, Luo, Peng, Stone, & Chang, 2011), Sm-Mg-Zn (Xia et al., 2014), Gd-Mg-Zn (Qi, et al., 2012) and Y-Mg-Zn (Gröbner et al., 2012; Shao, et al., 2006) systems have been optimized. The RE-Zn binary sub-systems were taken exclusively from those mentioned above. One of the goals of the present project is to obtain a reasonable thermodynamic description of all the RE-Zn systems by systematic optimization.

Chapter 3 **ORGANIZATION OF THE ARTICLES**

The results obtained in the present study are presented in the following chapters. Each chapter is associated with an article that has already been published or submitted to a journal.

Critical assessment and optimization of all the binary RE-Zn systems are presented in Chapters 4 and 5. All the RE-Zn systems have been systematically assessed and optimized to obtain reasonable thermodynamic descriptions.

The first article entitled "Critical Assessment and Optimization of Phase Diagrams and Thermodynamic Properties of RE-Zn Systems-Part I: Sc-Zn, La-Zn, Ce-Zn, Pr-Zn, Nd-Zn, Pm-Zn and Sm-Zn" is presented in Chapter 4. This article has been published in the Journal of Alloys and Compounds (Zhu & Pelton, 2015a). In this article, all the experimental data of the six lighter-RE-Zn systems as well as the Sc-Zn system were collected and critically evaluated. Thermodynamic descriptions of the Sc-Zn, La-Zn, Ce-Zn, Pr-Zn, Nd-Zn and Sm-Zn systems were obtained using the CALPHAD method. No experimental data can be found in the literature for the Pm-Zn system because Pm is a radioactive element. However, following the similarity and trends among all RE-Zn systems, a reasonable thermodynamic description of this system was proposed. The enthalpies of mixing of the liquid phases were estimated from the Miedema Model (Miedema, de Châtel, & de Boer, 1980) and used in the optimization. In particular, the enthalpies of formation of the compound phases in the La-Zn system was calculated by Aimen Gheribi at CRCT using *ab-inition* method; these calculated data were also used in the optimization.

The second article entitled "Critical Assessment and Optimization of Phase Diagrams and Thermodynamic Properties of RE-Zn Systems-Part II-Y-Zn, Eu-Zn, Gd-Zn, Tb-Zn, Dy-Zn, Ho-Zn, Er-Zn, Tm-Zn, Yb-Zn and Lu-Zn" is presented in Chapter 5. This article has been published in the same journal as the first (Zhu & Pelton, 2015b). In this article, all the experimental data of the nine heavier-RE-Zn systems as well as the Y-Zn system were collected and critically evaluated. Although experimental data for Eu-Zn, Tm-Zn and Lu-Zn are very limited, thermodynamic descriptions of the three systems were obtained by following the similarities and trends among all RE-Zn systems. The two articles are directly related to each other because all the binary RE-Zn systems are optimized simultaneously. The Modified Quasichemical Model (MQM), which takes into account Short-Range Ordering (SRO), was used to describe the liquid

phase. It is shown that the MQM can describe satisfactorily the liquid phase in the RE-Zn systems.

Experimental investigation and thermodynamic modeling of the Ce-Mg-Zn and Nd-Mg-Zn as well as thermodynamic modeling of all other RE-Mg-Zn systems (except Sc-Mg-Zn, Pm-Mg-Zn, Eu-Mg-Zn and Yb-Mg-Zn systems) are presented in Chapters 6-9. The four chapters are directly related because all RE-Mg-Zn systems were optimized simultaneously and the optimization was greatly aided by the similarities and trends among all these systems.

Chapter 6 presents the article entitled "Experimental Investigation and Thermodynamic Modeling of the Ce-Mg-Zn system" which has been submitted to Acta Materialia. *In-situ* neutron diffraction (ND) experiments were performed on selected samples to obtain phase transformation temperatures and precipitation sequences. All experimental data from the literature as well as those from the present ND experiments were used in the optimization, and model parameters for all the new ternary phases were obtained.

Chapter 7 presents the article entitled "Experimental Investigation and Thermodynamic Modeling of the Nd-Mg-Zn system" which has been submitted to Acta Materialia. *In-situ* ND experiments were performed on selected samples to obtain transition temperatures and precipitation sequences. All experimental data from the literature as well as those from the present NPD experiments were used in the optimization and model parameters for all the new ternary phases were obtained.

Chapter 8 presents the article entitled "Thermodynamic Modeling of the La-Mg-Zn, Pr-Mg-Zn and Sm-Mg-Zn system" which has been submitted to the Journal of Alloys and Compounds. The similarities and trends established in the optimization of all RE-Zn systems were utilized in the optimization of the Pr-Mg-Zn and Sm-Mg-Zn systems. The Pr-Mg-Zn and Sm-Mg-Zn systems are very similar to the Ce-Mg-Zn and Nd-Mg-Zn systems and most of the ternary phases in the Ce-Mg-Zn and Nd-Mg-Zn systems were assumed in the Pr-Mg-Zn and Sm-Mg-Zn systems. The La-Mg-Zn system has been investigated over the entire composition range, but this system differs significantly from other RE-Mg-Zn systems and thus was modeled separately.

Chapter 9 presents the article entitled "Thermodynamic Modeling of the Y-Mg-Zn, Gd-Mg-Zn, Tb-Mg-Zn, Dy-Mg-Zn, Ho-Mg-Zn, Er-Mg-Zn, Tm-Mg-Zn and Lu-Mg-Zn systems"

which has been submitted to the Journal of Alloys and Compounds. The similarities and trends established in the optimization of all RE-Zn systems were utilized in the optimization of all the RE-Mg-Zn systems. The thermodynamic optimization of the Ho-Mg-Zn, Er-Mg-Zn, Tm-Mg-Zn and Lu-Mg-Zn systems was greatly aided by utilizing the similarities and trends among all RE-Mg-Zn systems as mentioned above.

Chapter 10 is a general discussion of the present study.

Detailed information on the Miedema Model is presented in Appendix 1; examples of applications of the RE-Mg-Zn database are presented in Appendix 2; Appendix 3 presents all the neutron diffraction patterns collected in the present study; the coefficients of linear expansion of Ta and Mo at high temperature are calculated from the ND patterns and shown in Appendix 4; and finally the calculated liquidus projection and invariant reactions of all the RE-Mg-Zn systems are shown in Appendix 5.

Chapter 4 ARTICLE 1: CRITICAL ASSESSMENT AND OPTIMIZATION OF PHASE DIAGRAMS AND THERMODYNAMIC PROPERTIES OF RE-ZN SYSTEMS-PART I: SC-ZN, LA-ZN, CE-ZN, PR-ZN, ND-ZN, PM-ZN AND SM-ZN

Published in Journal of Alloys and Compounds, 641(2015), 249-260

Zhijun Zhu, Arthur D. Pelton*

Centre de Recherche en Calcul Thermochimique, Département de Génie Chimique, Ecole Polytechnique, Montréal, Québec, Canada

*Corresponding author

KEY WORDS

Rare earth systems, Zinc systems, Phase diagrams, Thermodynamic assessment, Thermodynamic optimization

ABSTRACT

All available phase diagram and thermodynamic data for the Sc-Zn, La-Zn, Ce-Zn, Pr-Zn, Nd-Zn, Pm-Zn and Sm-Zn systems have been collected and critically assessed. Optimized model parameters for the thermodynamic properties of all phases have been obtained. Trends in the properties of the rare earth (RE)-Zn systems as one traverses the rare earth series have been exploited for purposes of estimating missing data and for checking existing data for consistency.

4.1 Introduction

Magnesium being the lightest structural metal, Mg-based alloys have many applications. Zinc is already one of the most commonly used alloying elements in Mg (AZ series), and the rare earth (RE) metals have been shown to improve sheet formability by reducing texture [1-4] and to improve creep resistance [5, 6]. For the design of potential new Mg-Zn-RE alloys, information on the phase behavior is essential. However, few studies of the phase diagrams and thermodynamic properties of these systems have been made.

Consequently, we have undertaken a project to better define the phase diagrams of the Mg-Zn-RE ternary systems through the technique of critical thermodynamic assessment and optimization coupled with some limited experimentation.

In a thermodynamic ‘‘optimization’’, adjustable model parameters are calculated using, simultaneously, all available thermodynamic and phase-equilibrium data in order to obtain one set of model equations as functions of temperature and composition. Thermodynamic data, such as activities, can aid in the evaluation of the phase diagrams, and information on phase equilibria can be used to deduce thermodynamic properties. Thus, it is frequently possible to resolve discrepancies in the available data. From the model equations, all of the thermodynamic properties and phase diagrams can be back-calculated, and interpolations and extrapolations can be made in a thermodynamically correct manner. The data are thereby rendered self-consistent and consistent with thermodynamic principles, and the available data are distilled into a small set of model parameters, ideal for computer storage. Generally, in the optimization of a ternary system one begins by optimizing the three binary sub-systems. The binary model parameters are then used to estimate the properties of the ternary phases, and these estimates are then refined by introducing ternary model parameters where required to reproduce available ternary data.

We have already completed thermodynamic optimizations of the Mg-Zn [7] and all Mg-RE binary systems [8-11]. In the present article we report on the optimization of the binary systems formed between Zn and the lighter RE elements (La, Ce, Pr, Nd, Pm, Sm) as well as the Sc-Zn system. In a second article [12] we report on optimizations of the binary systems formed between Zn and the heavier RE elements (Eu to Lu) as well as the Y-Zn system. (The properties of Sc and Y are quite similar to those of the lighter and heavier RE elements respectively.) In subsequent articles we shall report on our optimizations of the ternary Mg-Zn-RE systems as well as on our experimental phase diagram studies of the Mg-Zn-Ce and Mg-Zn-Nd systems.

Complete sets of phase diagram and thermodynamic data are not available for all RE-Zn systems. However, all RE metals have very similar properties, and very definite trends are observed in the properties of the binary RE-Zn systems as one traverses the RE series. These trends may be exploited for purposes of estimating missing data and for checking existing data for consistency. Hence, a great advantage is realized by assessing and optimizing all the RE-Zn systems together.

The phase diagrams of the systems Sc-Zn, La-Zn, Ce-Zn, Pr-Zn, Nd-Zn, Pm-Zn and Sm-Zn are shown in Figs. 1 to 7. The similarities among the figures are obvious. Only the Sc-Zn system, as might be expected, exhibits a somewhat difference appearance, with fewer compounds with lower melting points in Zn-rich alloys. As will be shown in the second article in this series [12], the phase diagrams of the systems of Zn with the heavier RE elements are all also very similar to those in Figs. 1 to 7.

Table 1 provides a list of all compounds, both stable and metastable, which have been observed for all fifteen RE-Zn systems as well as the Sc-Zn and Y-Zn systems. With some exceptions, compounds with the same stoichiometry and crystal structure are found in most systems and, as can be seen in Figs. 1 to 7, compounds with the same stoichiometry have very similar melting points. Fig. 8 shows that the lattice constants of compounds with the same stoichiometry are also very similar for all systems.

No experimental evidence for non-stoichiometry of any compounds has been reported and none has been assumed in the present assessments. Solid solubility of Zn in the terminal bcc phases has been reported in several systems. No solubility of Zn in any other terminal solid phase has been reported, nor has solubility of Sc, Y, or any RE in the terminal hcp-Zn phase has been reported.

For the binary liquid phases, in the absence of experimental data, the Miedema model [13] is frequently used to provide a rough estimate of the enthalpy of mixing from certain physical properties of the pure liquid metals. Calculations with this model indicate that the minimum in the enthalpy of mixing occurs near the mole fraction $X_{Zn} = 0.55$ for all RE-Zn liquids. Enthalpies of mixing calculated at this composition from the Miedema model are shown in Fig. 9. It can be seen that the estimated enthalpies are very similar for all systems and have quite negative values. These values were used as first estimates in the optimizations.

4.2 Phase equilibrium and thermodynamic data

4.2.1 Sc-Zn system

The Sc-Zn system, Fig. 1, was investigated by Palenzona and Manfrinetti [14] using DTA, metallographic analysis, XRD and electron microscopy in the range from 40 to 100 at. % Zn.

Five intermediate phases were identified as shown on Fig. 1. The reported crystallographic data are in good agreement with those published earlier. (See Table 2.)

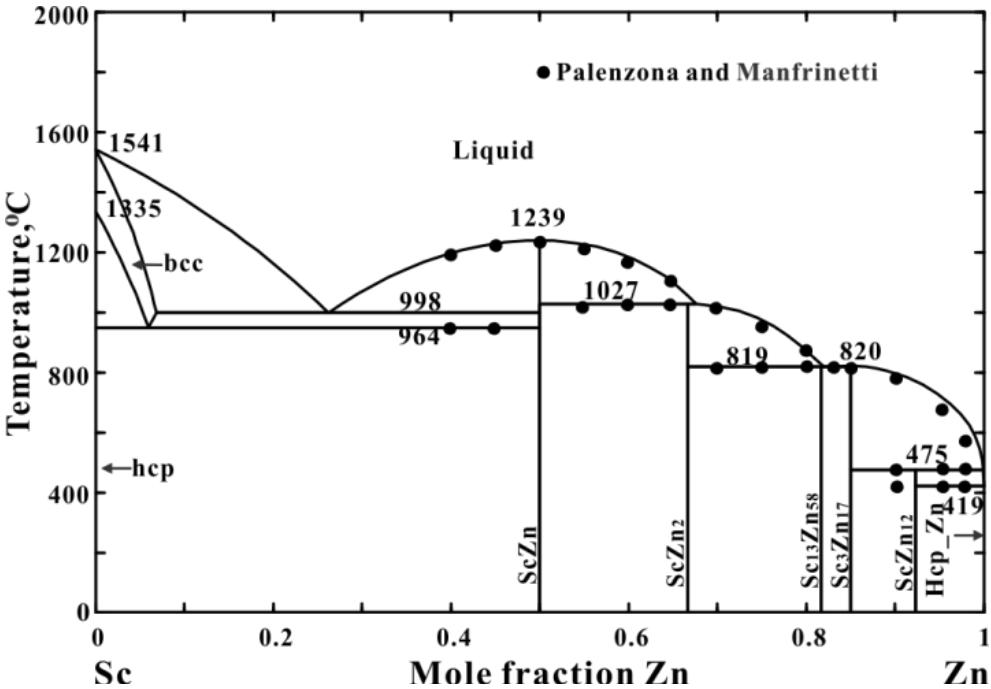

Figure 4.1. Calculated Sc-Zn phase diagram and experimental data points [14]

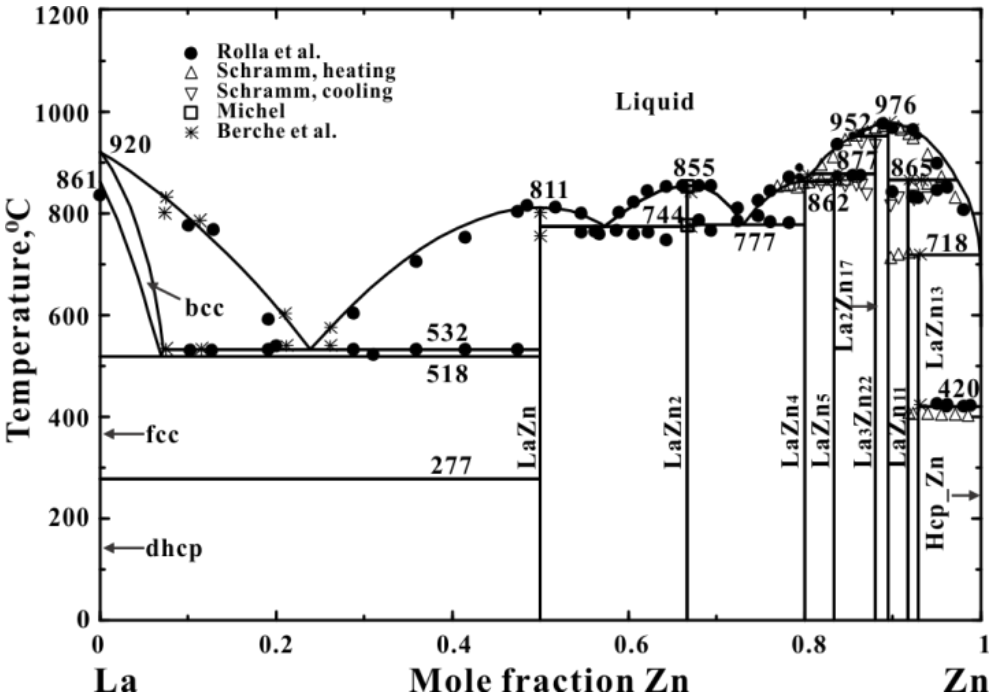

Figure 4.2 Calculated La-Zn phase diagram and experimental data points [15-17, 28]

Table 4.1 All reported stable and metastable compounds in Sc-Zn, Y-Zn and all RE-Zn systems (For references see Table 1.2 or reference [12])

(Prototype-Pearson symbol-space group)	Sc	Y	La	Ce	Pr	Nd	Pm	Sm	Eu	Gd	Tb	Dy	Ho	Er	Tm	Yb	Lu
MZn (CsCl-cP2-Pm$\bar{3}$m)	×	×	×	×	×[1]	×	×	×	×	×	×[1]	×[1]	×	×	×	×	×
MZn_2 ($CeCu_2$-oI12-Imma)	×[2]	×[3]	×	×	×	×	×	×	×	×	×	×	×	×	×	×[3]	×
MZn_3 (YZn_3-oP16-Pmna)		×		×	×	×	×	×		×	×	×	×	×	×		×
M_3Zn_{11} ($Al_{11}La_3$-oI28-Immm)		×		×	×	×	×	×		×	×	×				×	
M_6Zn_{23} ($Mn_{23}Th_6$-cF116-Fm$\bar{3}$m)		●								●	●	●	●[4]	●	●		●
MZn_4 (orthorhombic)			×														
$M_{13}Zn_{58}$ ($Gd_{13}Zn_{58}$-hP142-P6_3mc)	×	×[5]		×	×	×	×	×		×	×	×	×	×	×	×	×
MZn_5 ($CaCu_5$-hP6-P6/mmm)		●	×	×	●	●		●	×	●		●		●			
MZn_5 ($ErZn_5$-hP36-P6_3/mmc)		×											×	×	×		×
M_3Zn_{17} (Ru_3Be_{17}-cI160-Im$\bar{3}$)	×															●	
M_3Zn_{22} (Pu_3Zn_{22}-tI100-I4_1/amd)			×	×	×	×	×	×		×							
M_2Zn_{17} (LT) ($Ni_{17}Th_2$-hP38-P6_3/mmc)		×		×	×	×	×	×		×	×	×	×	×	×	×	×
M_2Zn_{17} (HT) (Th_2Zn_{17}-hR19-R$\bar{3}$m)		×	×	×	×	×	×	×		×	×	×	×	×	×	×	×
MZn_{11} ($BaCd_{11}$-tI48-I4_1/amd)			×	×	×	×	×	×[6]	×							×	
MZn_{12} ($Mn_{12}Th$-tI26-I4/mmm)	×	×				●		●		×	×	×	×	×	×		×
MZn_{13} ($NaZn_{13}$-cF112-Fm$\bar{3}$c)			×						×							●	

×=compounds reported or estimated as stable (for references see table 2)
●=Meta-stable compounds reorted (for references see table 2)
1=Meta-stable (HgMn-tP2-P4/mmm) also reported
2= AlB2-hP3-P6/mmm. Meta-stable ($MgZn_2$-hP12-P6_3/mmc) also has been reported.
3=Also, α form reported, structure unknown
4=reported as Ho_5Zn_{23} [68]
5=reported as Y_2Zn_9 (Y_2Zn_9-hP146-P6_3/mmc) but interpreted here as $Y_{13}Zn_{58}$.
6= $SmZn_{11}$-hP42-P6/mmm

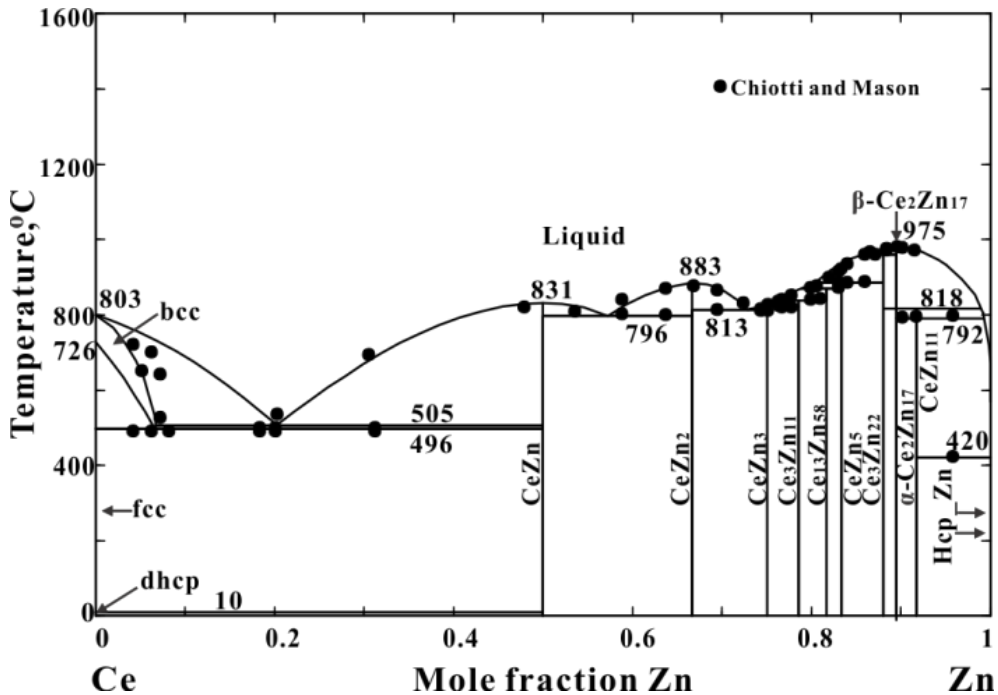

Figure 4.3 Calculated Ce-Zn phase diagram and experimental data points [29]

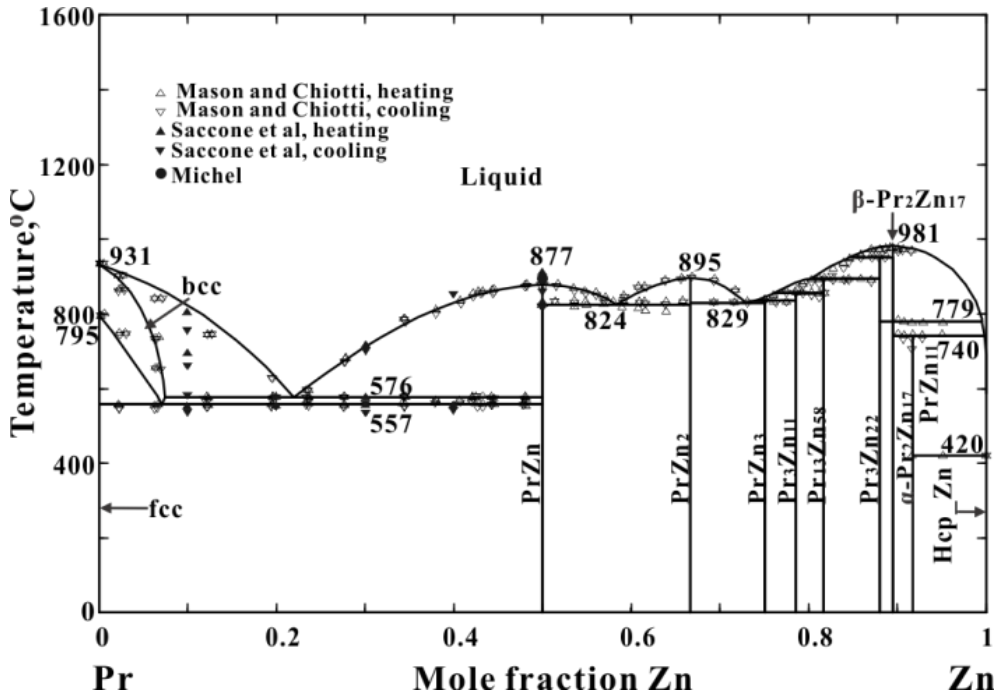

Figure 4.4 Calculated Pr-Zn phase diagram and experimental data points [16, 32, 33]

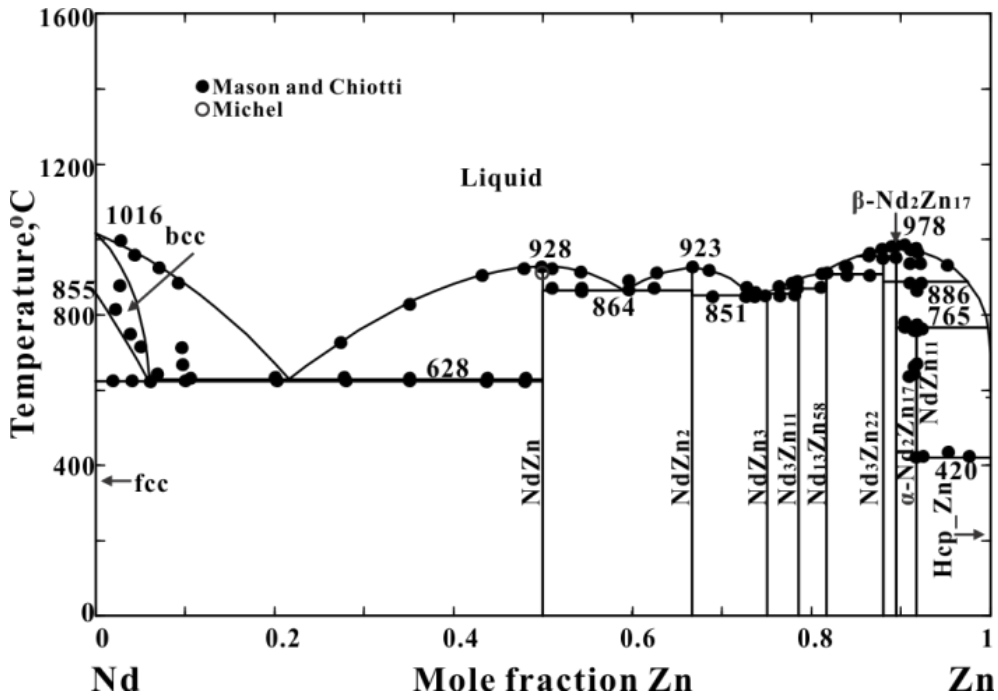

Figure 4.5 Calculated Nd-Zn phase diagram and experimental data points [16, 36]

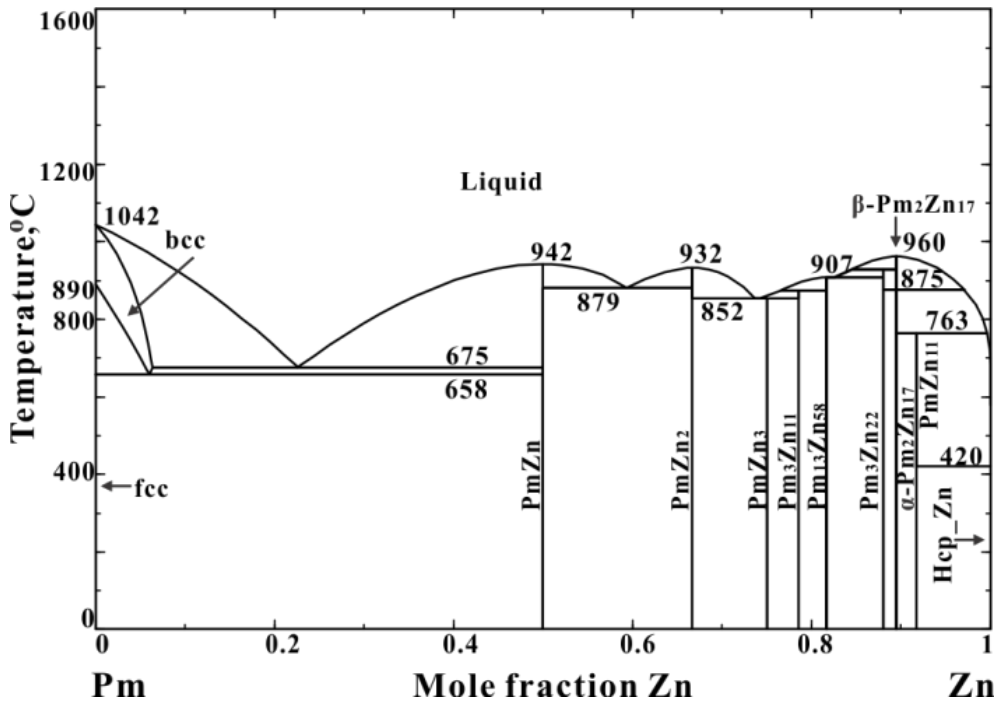

Figure 4.6 Calculated Pm-Zn phase diagram

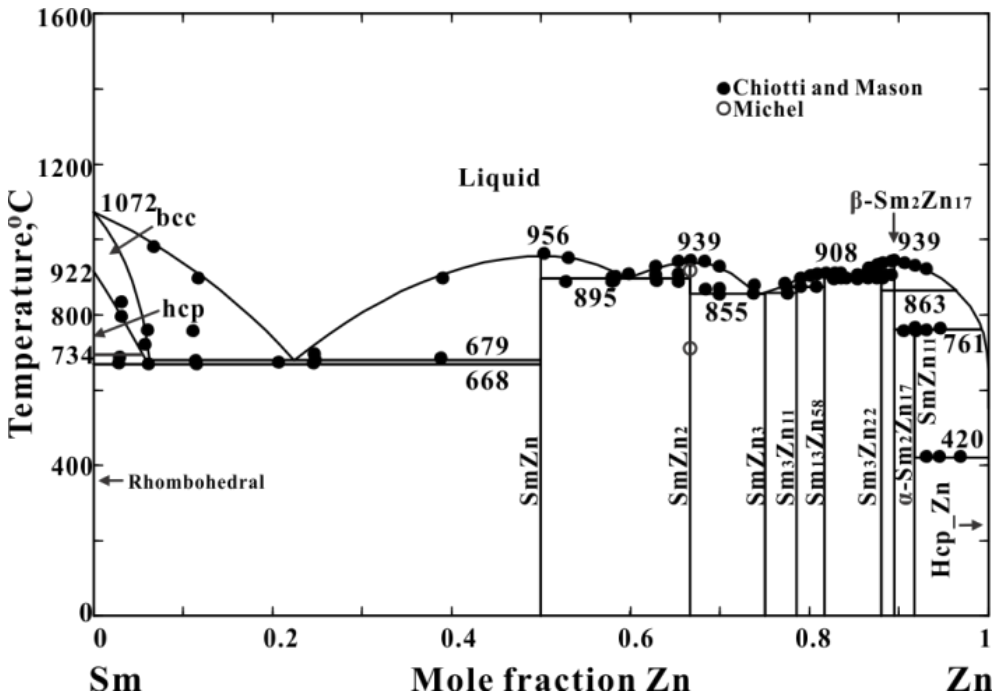

Figure 4.7 Calculated Sm-Zn phase diagram and experimental data points [16, 41]

4.2.2 La-Zn system

The La-Zn system, Fig. 2, was investigated by Rolla et al [15] over the entire composition range by DTA and metallography. Five compounds were reported: LaZn, $LaZn_2$, $LaZn_4$, $LaZn_8$ and $LaZn_{13}$. Michel et al [16] studied the melting behavior of $LaZn_2$ by DTA. Schramm's work [17] reveals more detail in the composition range from 76 to 86 at. % Zn; according to the DTA analysis there could be one or two invariant transitions between 1100 and 1150 K which could be associated with the decomposition of $LaZn_4$ and $LaZn_5$. However, the measured temperatures of the two possible transitions are very close together. More recently, Berche et al [18] reinvestigated the system by XRD, SEM, microprobe analysis and DTA and critically reviewed [19] all the earlier work. Their DTA analysis confirmed the existence of two peritectic transitions associated with $LaZn_4$ and $LaZn_5$. According to the phase diagram proposed by Berche et al [18] , there are eight stable compounds in this system: LaZn, $LaZn_2$, $LaZn_4$, $LaZn_5$, La_3Zn_{22}, La_2Zn_{17}, $LaZn_{11}$ and $LaZn_{13}$, in conformity with the earlier crystallographic studies.

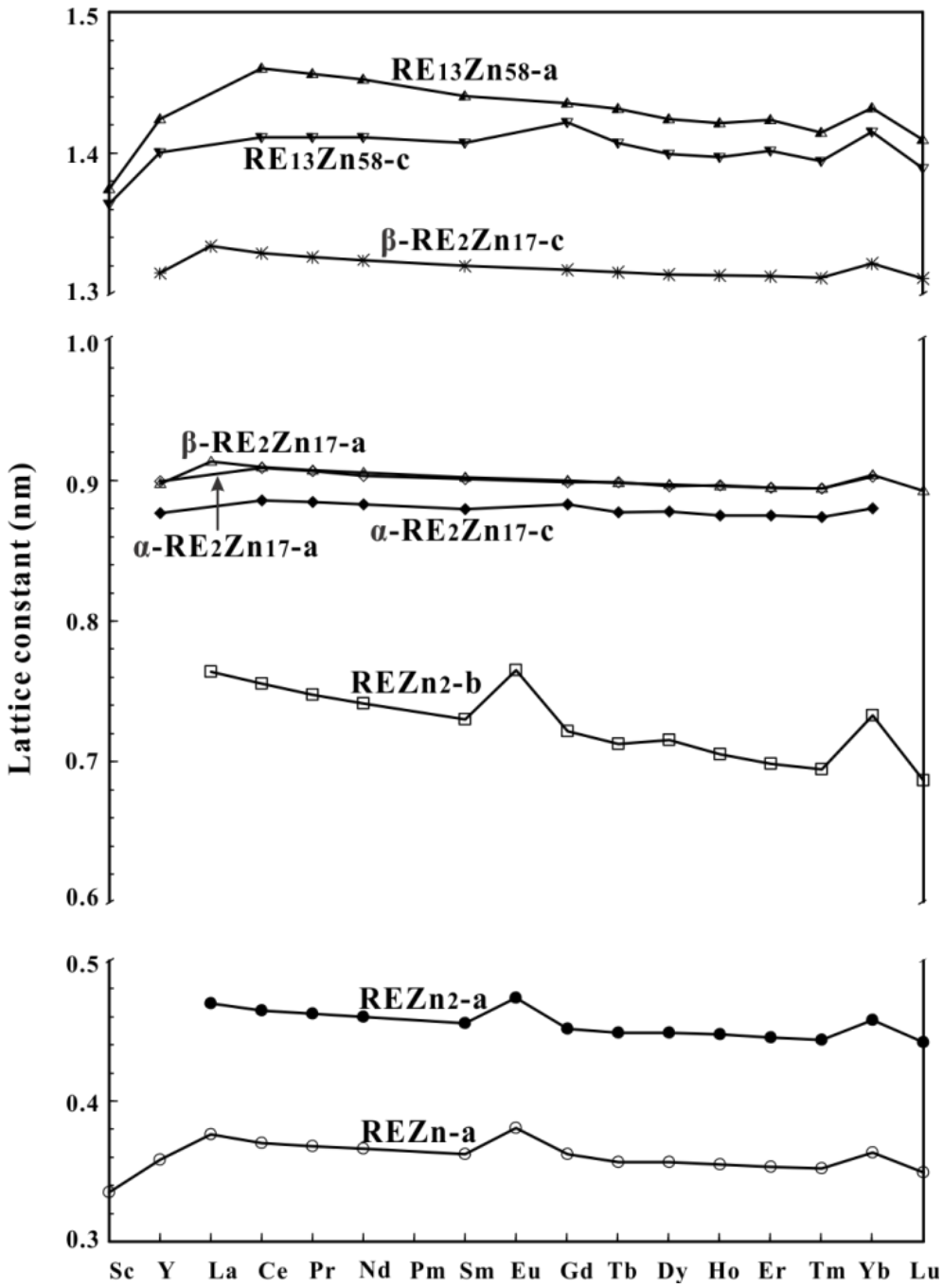

Figure 4.8 Lattice constants of RE-Zn compounds (for references, see Table 2 and ref [12])

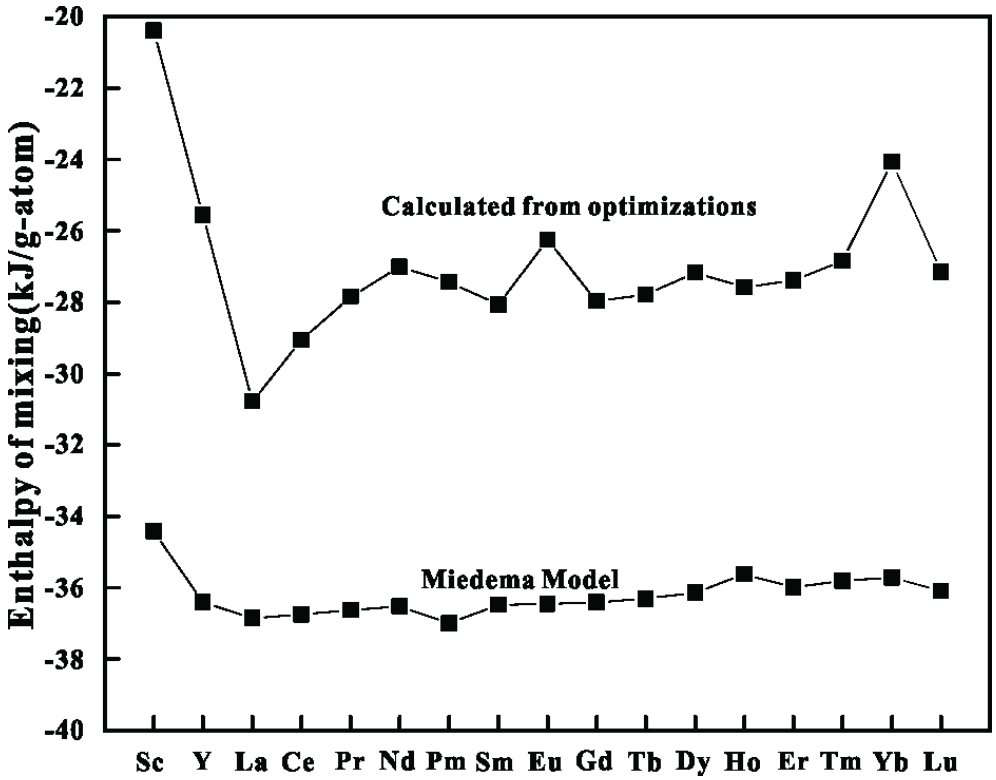

Figure 4.9 Enthalpies of liquid-liquid mixing of Sc-Zn, Y-Zn and RE-Zn systems at compositions of minimum enthalpy at 1600 ^{o}C

Emf measurements with alloy concentration cells were carried out by Lesourd and Plambeck [20], Mullayanov et al [21] and Johnson and Yonco [22] with pure La reference electrodes and working electrodes consisting of a two-phase mixture of $LaZn_{13}$ and liquid Zn. (As can be seen from the phase diagram in Fig. 2, the liquid in equilibrium with $LaZn_{13}$ is nearly pure Zn.) As shown in Fig. 10, the results of the three studies are in good agreement. In interpreting their results, these authors all assumed that the phase in equilibrium with liquid Zn was $LaZn_{11}$, but the XRD results, the phase diagram measurements and the present assessment indicate that $LaZn_{13}$ was the actual solid phase at equilibrium in the experiments.

Kovalevskii et al [23] subsequently performed emf measurements with alloy concentration cells in two-phase regions across the entire composition range with a reference electrode consisting of a two-phase ($LaZn_{13}$ + liquid Zn) mixture. Their results, converted to emf's versus a pure La reference electrode by using the results of the previous authors [20-22] , are plotted in Fig. 10.

Enthalpies of formation were measured by solution calorimetry by Berche et al [24] for eight compounds and by Morishita et al [25, 26] for two compounds. Their results are plotted in Fig. 11. The compound reported by Morishita et al as $LaZn_8$ is shown as La_2Zn_{17} in Fig. 11. Enthalpies of formation calculated from the temperature dependencies of the aforementioned emf measurements [20-23] are also plotted in Fig. 11. As well, enthalpies of formation, calculated by Density Functional Theory (DFT) for several compounds by Berche et al [24] and in the present work, are also plotted in Fig. 11.

Finally, the heat capacities of $LaZn_{13}$ and "$LaZn_8$", measured between 0 and 300 K by Morishita et al [25, 26] by a "thermal relaxation method" are plotted in Fig. 12 where "$LaZn_8$" is shown as La_2Zn_{17}. Third Law integration of these data by the authors gave entropies of formation of $LaZn_{13}$ and La_2Zn_{17} at 298.15 K as -1.80 and -1.32 J/g.atom K respectively.

Previous thermodynamic assessments of the La-Zn system have been reported by Qi et al [27] and Berche et al [28].

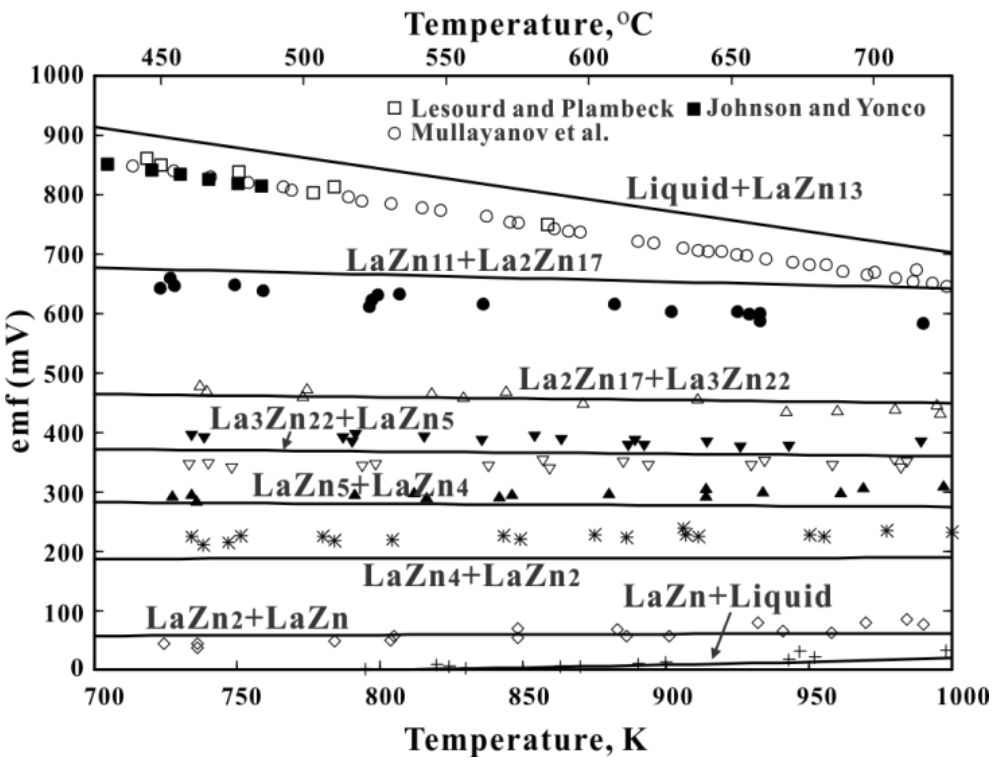

Figure 4.10 Emf of alloy concentration cells in the La-Zn system. Lines are calculated from the optimized model parameters. All data are from Kovalevskii et al [23] unless otherwise indicated in the figure [20-22].

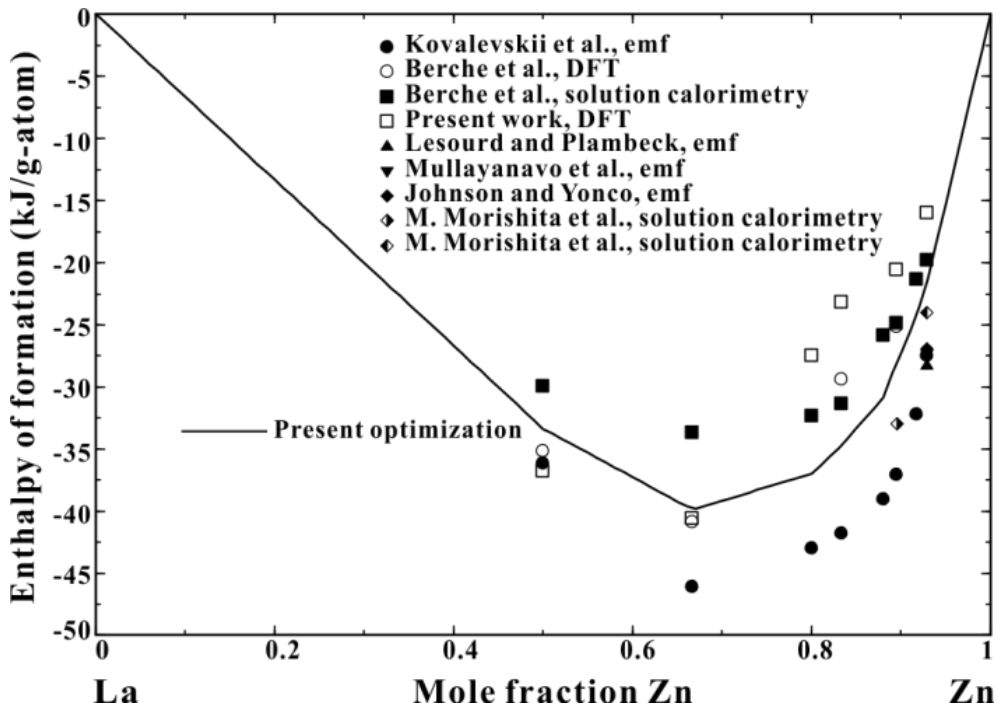

Figure 4.11Calculated enthalpy of formation of compounds in the La-Zn system with experimental data points and values calculated from DFT [20-26].

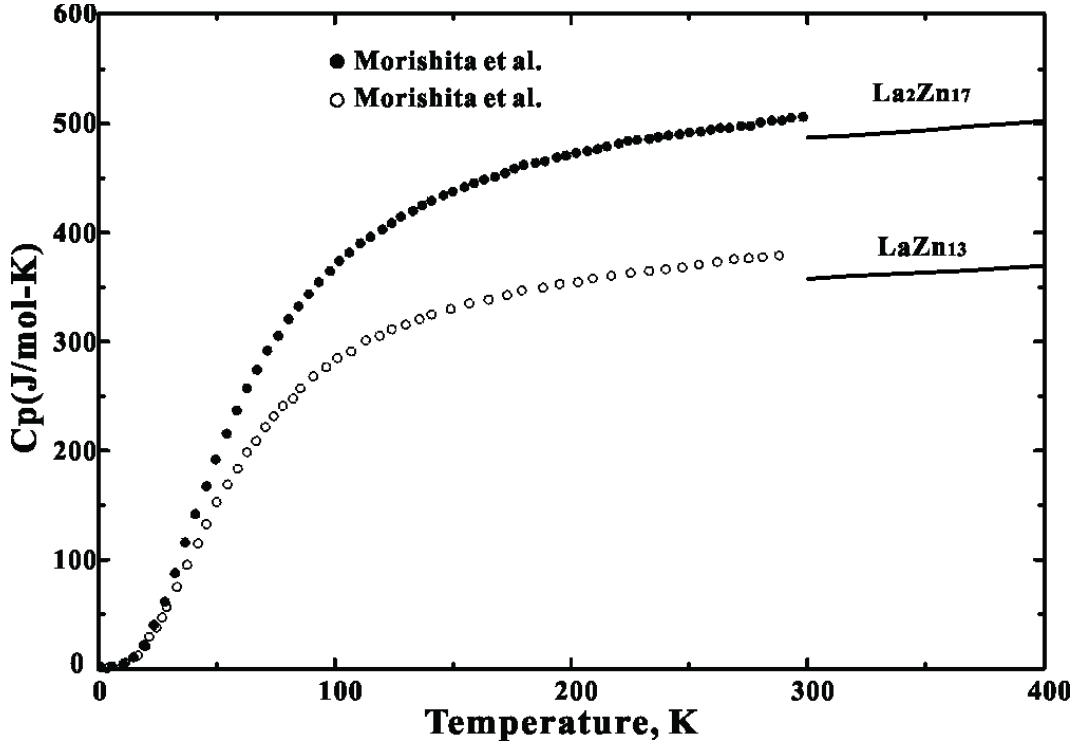

Figure 4.12 Heat capacity of La_2Zn_{17} and $LaZn_{13}$ reported by Morishita et al [25, 26] and as calculated from the Neumann-Kopp equation (solid lines)

4.2.3 Ce-Zn system

The Ce-Zn system, Fig. 3, was investigated by Chiotti and Mason [29] by metallography, thermal analysis, XRD and vapor pressure measurements. The following nine intermediate phases were proposed: CeZn, $CeZn_2$, $CeZn_3$, $CeZn_{3.67}$, $CeZn_{4.5}$, $CeZn_{5.25}$. $CeZn_7$, $CeZn_{8.5}$ and $CeZn_{11}$. These correspond very closely to CeZn, $CeZn_2$, $CeZn_3$, Ce_3Zn_{11}, $Ce_{13}Zn_{58}$, $CeZn_5$, Ce_3Zn_{22}, Ce_2Zn_{17} and $CeZn_{11}$ and have been interpreted as such in the present assessment.

Using the dew point method, Chiotte and Mason [29] measured vapor pressures over a series of Ce-Zn alloys. Results are shown in Figs. 13 & 14.

Johnson and Yonco [22] measured emf's of alloy concentration cells with pure Ce reference electrodes and working electrodes consisting of virtually pure liquid Zn in equilibrium with $CeZn_{11}$. Their results are plotted in Fig. 15.

Previous thermodynamic assessments of the Ce-Zn system have been reported by Spencer et al [30] and Wang et al [31].

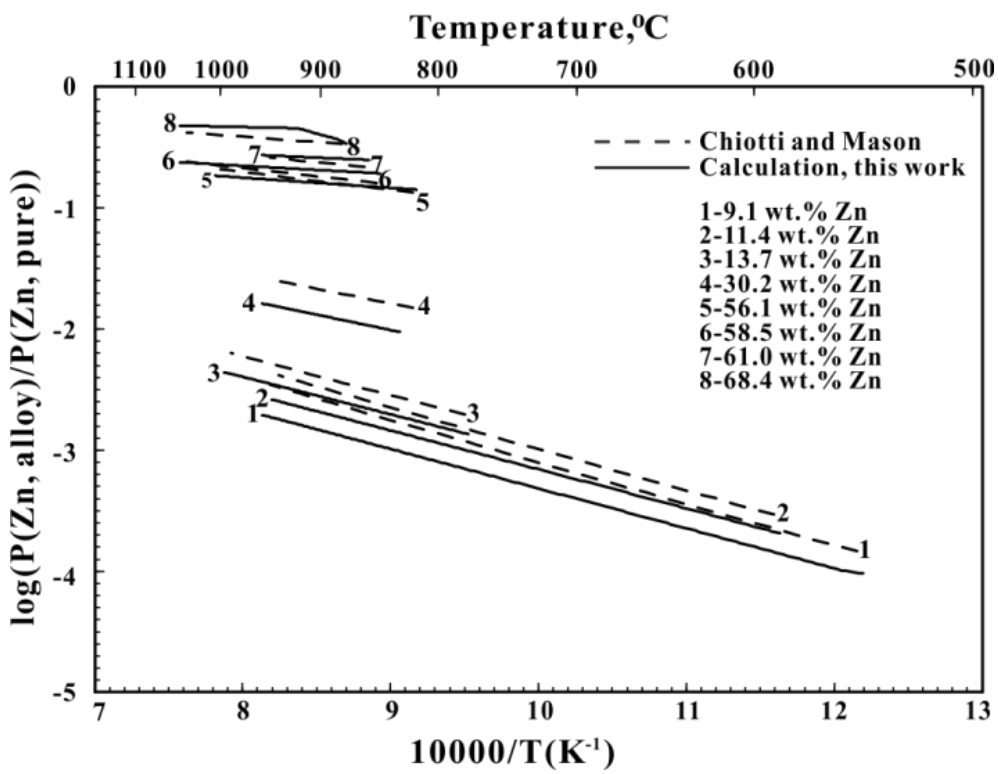

Figure 4.13 Calculated and experimental vapor pressures over liquid Ce-Zn alloys [29]

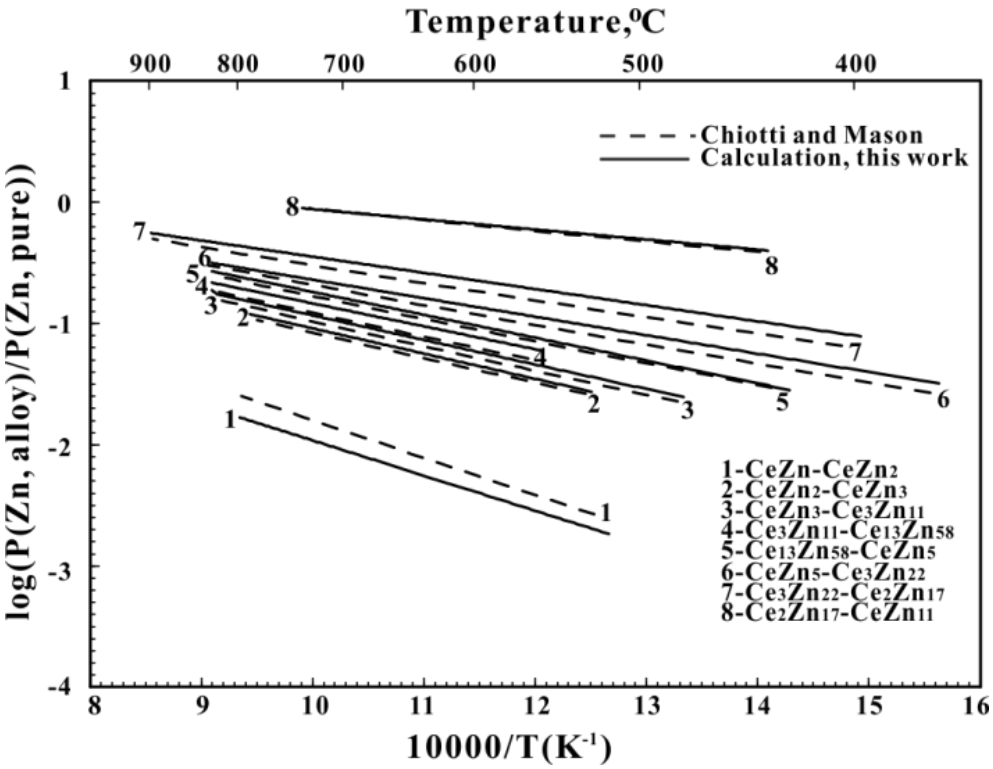

Figure 4.14 Calculated and experimental vapor pressures over two-phase Ce-Zn alloys [29]

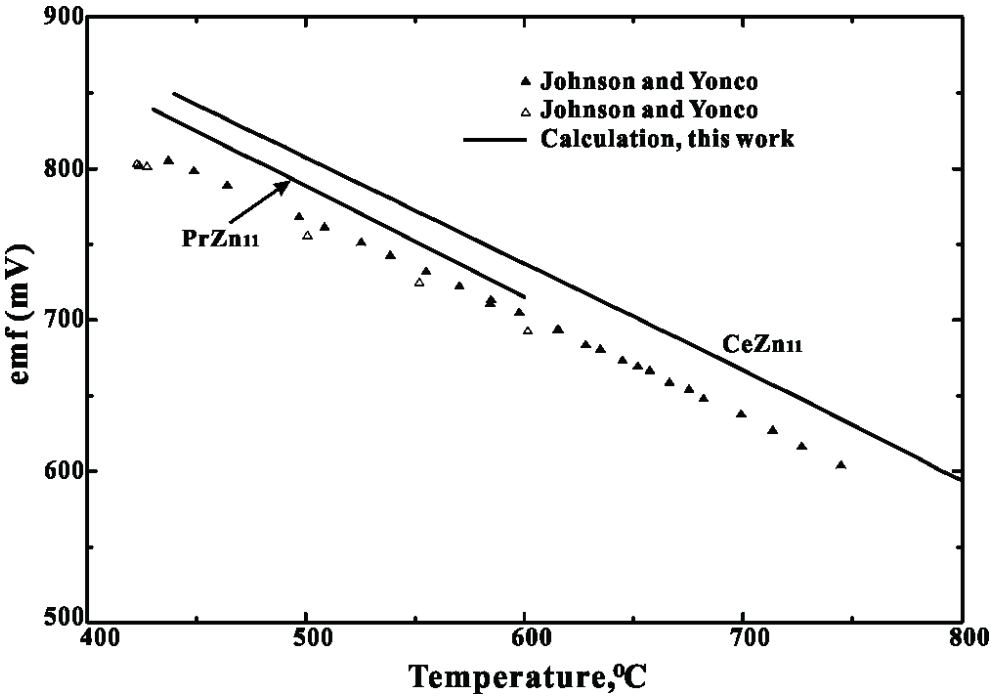

Figure 4.15 Emf of concentration cells for the formation of $CeZn_{11}$ and $PrZn_{11}$ [22]

4.2.4 Pr-Zn system

The Pr-Zn system, Fig. 4, was investigated over the entire composition range by Mason and Chiotti [32] by metallography, thermal analysis and XRD. Eight intermediate compounds were identified: PrZn, $PrZn_2$, $PrZn_3$, Pr_3Zn_{11}, $Pr_{13}Zn_{58}$, Pr_3Zn_{22}, Pr_2Zn_{17} and $PrZn_{11}$. The reported crystal structures of these phases are in good agreement with those reported previously. (See Table 2.) Using XRD, DTA and metallography, Saccone et al [33] investigated the system in the range from 0 to 50 at. % Zn. Their results are in good agreement with those of Mason and Chiotti.

Vapor pressures over a series of Pr-Zn alloys were measured by Chiotti and Mason [34] using the dew point method. Results are shown in Figs. 16 & 17.

Johnson and Yonco [22] measured emf's of alloy concentration cells with pure Pr reference electrodes and working electrodes consisting of virtually pure liquid Zn in equilibrium with $PrZn_{11}$. Their results are plotted in Fig. 15.

Previous thermodynamic assessments of the Pr-Zn system have been reported by Huang et al [35] and Wang et al [31].

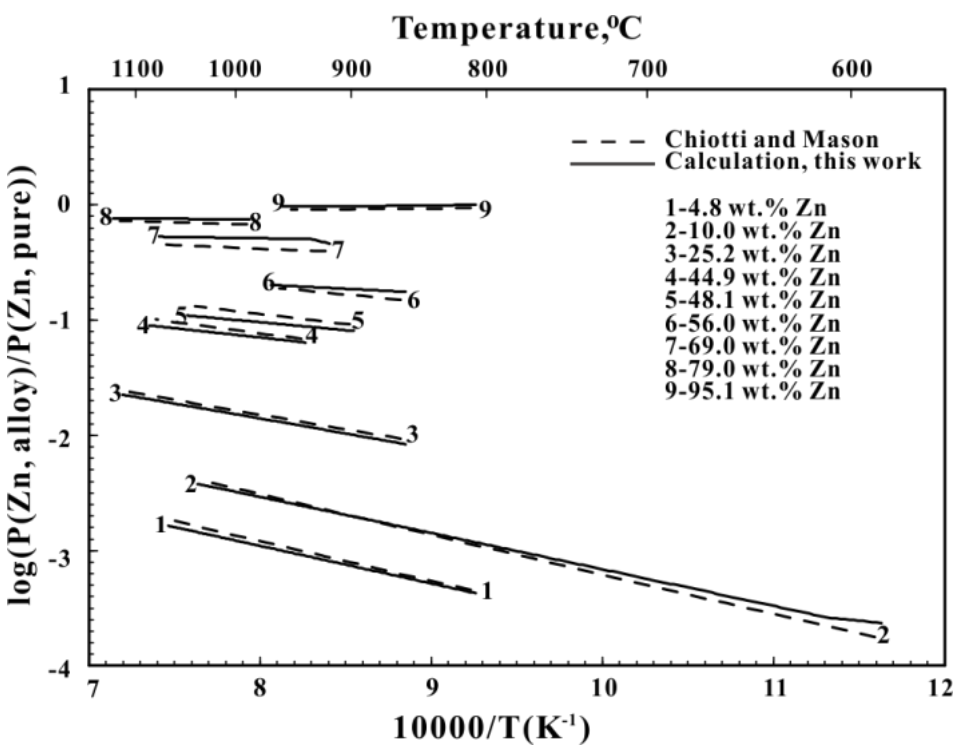

Figure 4.16 Calculated and experimental vapor pressures over liquid Pr-Zn alloys [34]

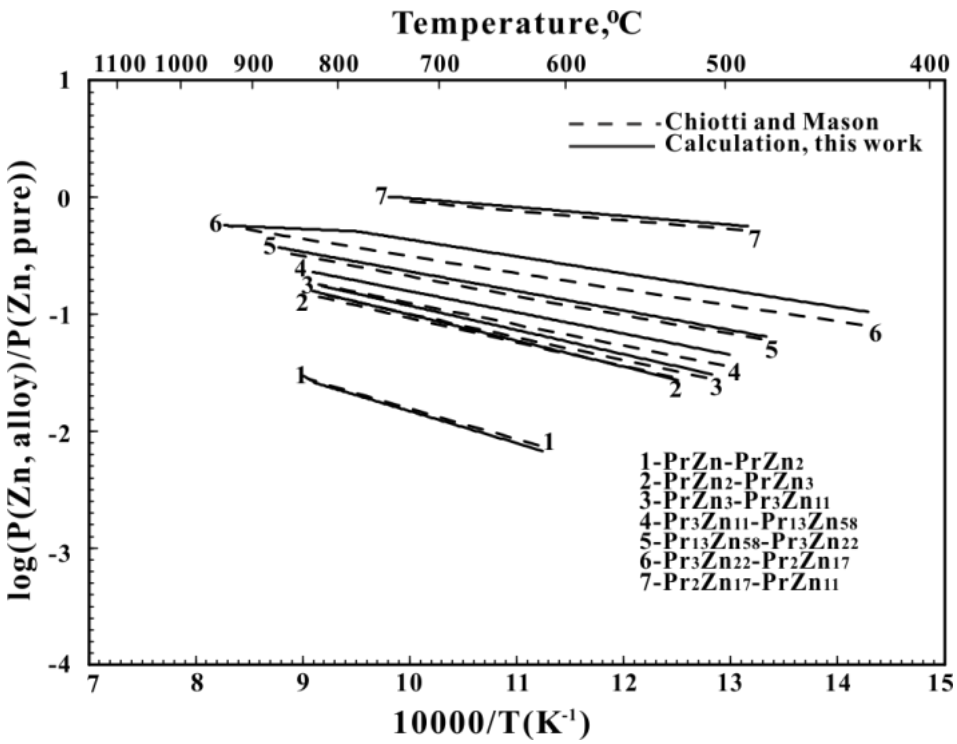

Figure 4.17 Calculated and experimental vapor pressures over two-phase Pr-Zn alloys [34]

4.2.5 Nd-Zn system

The Nd-Zn phase diagram, Fig. 5 , was studied by Mason and Chiotti [36] over the entire composition range using metallographic, thermal and XRD techniques. Eight intermediate compounds were identified: NdZn, $NdZn_2$, $NdZn_3$, Nd_3Zn_{11}, $Nd_{13}Zn_{58}$, Nd_3Zn_{22}, Nd_2Zn_{17} and $NdZn_{12}$. An allotropic transformation between the tetragonal $NdZn_{11}$ structure and a hexagonal $NdZn_{12}$ defect structure was proposed; only $NdZn_{11}$ is considered in the present assessment.

Using the dew point method, Chiotti and Mason [37] measured the zinc vapor pressure over a series of Nd-Zn alloys. Their results are plotted in Figs. 18 & 19.

Previous thermodynamic assessments of the Nd-Zn system have been reported by Li et al [38] , Qi et al [39], and Liu et al [40].

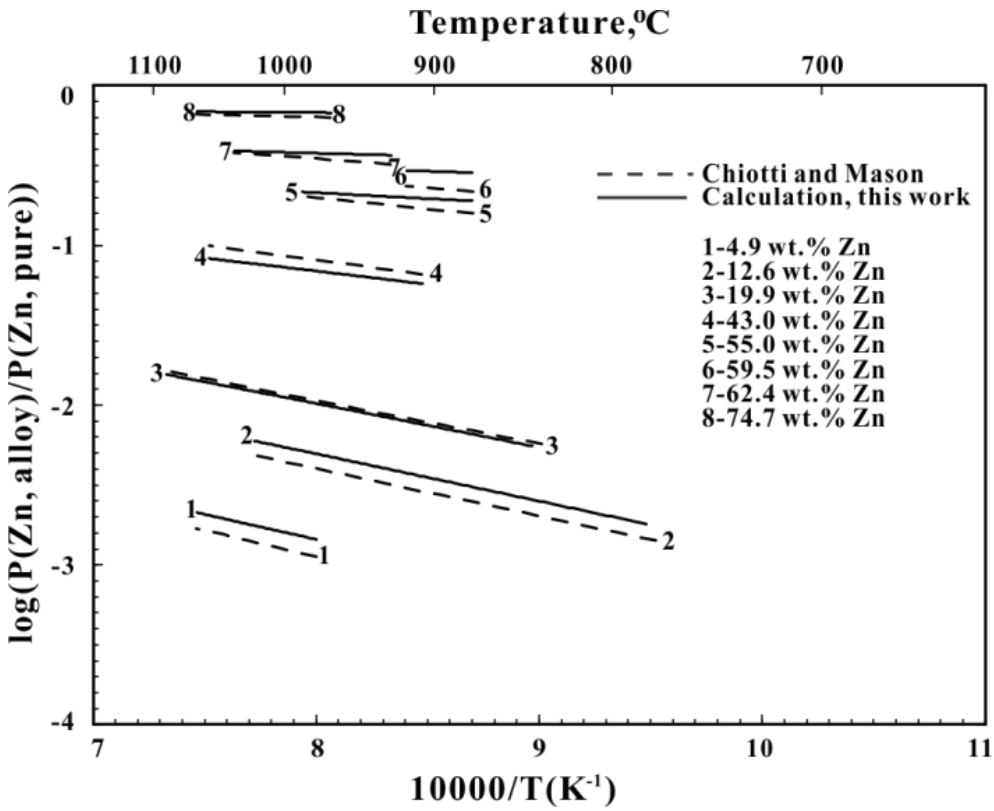

Figure 4.18 Calculated and experimental vapor pressures over liquid Nd-Zn alloys [37]

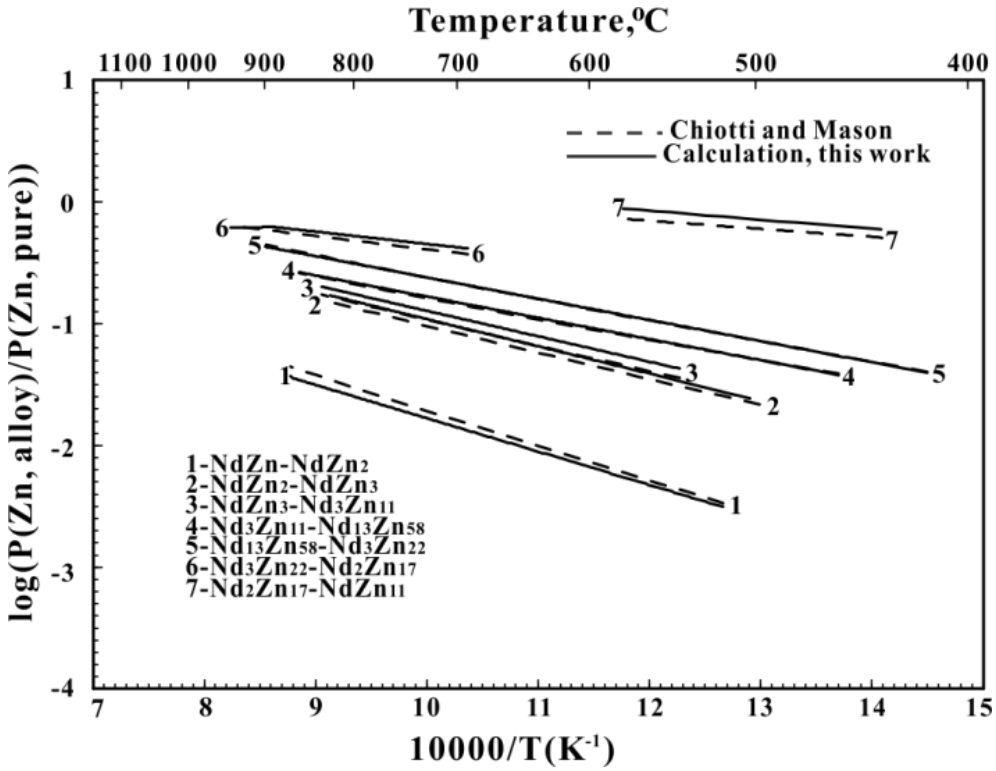

Figure 4.19 Calculated and experimental vapor pressures over two-phase Nd-Zn alloys [37]

4.2.6 Pm-Zn system

No data could be found for this system, undoubtedly because Pm is an unstable element.

4.2.7 Sm-Zn system

The Sm-Zn system, Fig. 7, was systematically investigated by Chiotti and Mason [41]. The phase diagram was studied over the entire composition range by thermal analysis, XRD and metallography. Eight compounds were identified: SmZn, $SmZn_2$, $SmZn_3$, Sm_3Zn_{11}, $SmZn_{4.5}$ (taken in the present assessment as $Sm_{13}Zn_{58}$), $SmZn_{7.5}$ (taken in the present assessment as Sm_3Zn_{22}), Sm_2Zn_{17} and $SmZn_{11}$.

Using the dew point method, Chiotti and Mason [41] measured the zinc vapor pressure over a series of Sm-Zn alloys. Their results are plotted in Fig. 20.

Previous thermodynamic assessments of the Sm-Zn system have been reported by Jia et al [42] and Liu et al [40].

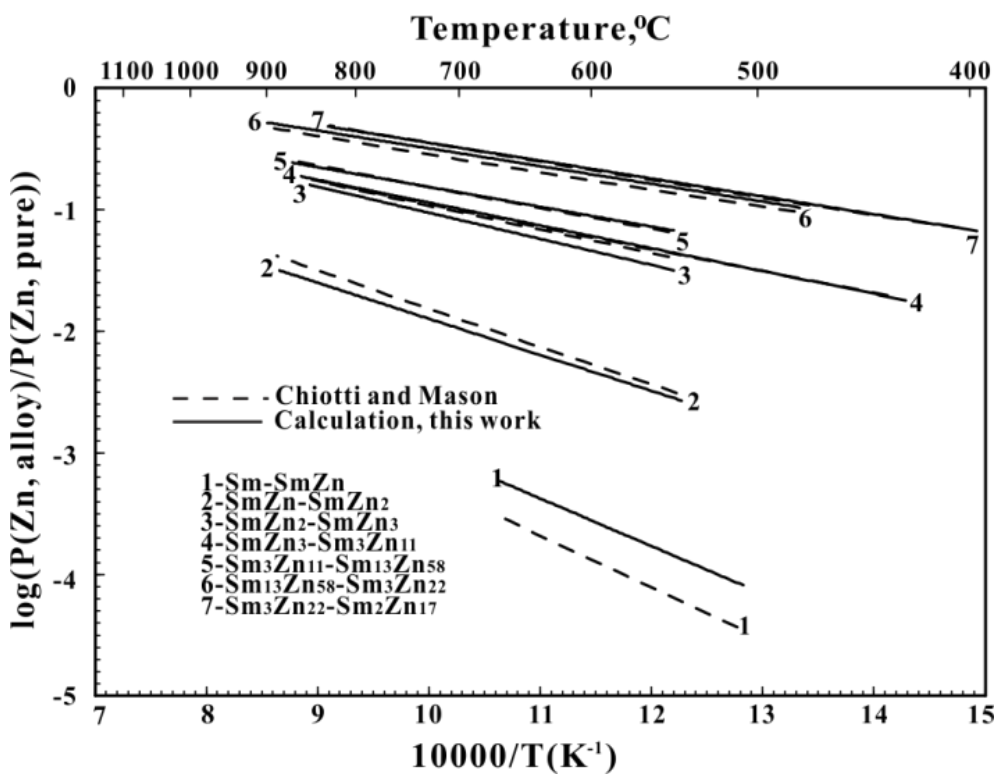

Figure 4.20 Calculated and experimental vapor pressures over liquid Sm-Zn alloys [41]

4.3 Thermodynamic modeling

4.3.1 Elements

The thermodynamic properties of the elements were taken from Dinsdale [70]

4.3.2 Compounds

All compounds were assumed to be stoichiometric since there is no experimental evidence to the contrary and since this assumptions resulted in good reproduction of all the data. The Gibbs energies of all compounds were modeled by the equation:

$$g(RE_xZn_{1-x}) = [xg^0_{RE} + (1-x)g^0_{Zn}] + (\Delta h^0 - T\Delta s^0) \qquad 4.1$$

where $g(RE_xZn_{1-x})$ is the Gibbs energy of the compound per g-atom at temperature T (K), g^0_{RE} is the Gibbs energy of the pure RE element at T in the state which is stable at 298.15K, and g^0_{Zn} is the Gibbs energy of pure hcp Zn at T.

The enthalpy and entropy of formation, Δh^0 and Δs^0, are assumed to be independent of temperature. That is, the heat capacities of the compounds are all assumed to be given by the Neumann-Kopp equation [71]:

$$C_p = xC_{p(RE)} + (1-x)C_{p(Zn)} \qquad 4.2$$

The heat capacities of $LaZn_{13}$ and La_2Zn_{17} as calculated from the Neumann-Kopp equation are shown in Fig. 12. Although there is a slight deviation from the reported values, similar comparisons for the compounds YZn, Y_2Zn_{17}, Gd_2Zn_{17}, TbZn, Tb_2Zn_{17}, HoZn and Yb_2Zn_{17} exhibit excellent agreement between the measured heat capacities and those calculated from Eq. (2) as will be shown in the second article [12]. Hence, in the present assessment it is assumed that Eq. (2) applies for all compounds, including $LaZn_{13}$ and La_2Zn_{17}.

4.3.3 Terminal solid solutions

Clear evidence for solubility of Zn in the terminal bcc solutions can be seen in the measured phase diagrams for the Ce-Zn, Pr-Zn, Nd-Zn and Sm-Zn systems (Figs. 3, 4, 5 & 7), the extent of solubility being about the same for all these systems. Therefore, such solubility was

assumed to occur in the Sc-Zn, La-Zn and Pm-Zn bcc solutions as well. No evidence for solid solubility has been found in any of the other terminal solid solutions and none has been assumed in the current assessment. The molar Gibbs energies of the bcc solutions have been modeled by the equation:

$$g_{bcc} = [xg^0_{Zn(bcc)} + (1-x)g^0_{RE(bcc)}] + RT(x\ln x + (1-x)\ln(1-x)] + x(1-x)L^0_{RE,Zn} \qquad 4.3$$

where x is the atomic fraction of Zn in the solution, $g^0_{Zn(bcc)}$ and $g^0_{RE(bcc)}$ are the Gibbs energies of pure bcc Zn (metastable) and the pure bcc RE element, both taken from the compilation of Dinsdale [70], and $L^0_{RE,Zn}$ is a regular solution parameter assumed to be constant, independent of both temperature and composition.

4.3.4 Liquid solutions

As discussed in Section 2, calculations with the Miedema model indicate negative enthalpies of liquid mixing with minima of the order of -36 kJ/mol. From our experience, such relatively large negative enthalpies are associated with a significant degree of short-range ordering (SRO); that is, the fraction of RE-Zn nearest-neighbor atom pairs is expected to be significantly larger than in a random Bragg-Williams distribution. Taking account of SRO in systems where it is appreciable has been shown to result in better representations of the thermodynamic properties, particularly in dilute composition regions [72, 73], better estimates of entropies of mixing [72-74] and better results when the thermodynamic properties and phase equilibria in ternary and multicomponent systems are estimated from the optimized model parameters of the binary sub-systems [72, 73]. Of the previous optimizations of the RE-Zn systems, only that of Spencer et al [30] took account of SRO.

In the present assessment, the liquid phase was modeled with the Modified Quasichemical Model (MQM) in the pair approximation [74]. This model has been used extensively for liquid alloys [9, 75] as well as molten salts [76-78], oxides [79, 80] and sulfides [81]. The following pair-exchange reaction between atoms A and B on neighboring quasi-lattice sites is considered:

$$(A-A) + (B-B) = 2(A-B); \quad \Delta g_{AB} \qquad 4.4$$

where (i-j) represents a first-nearest-neighbor (FNN) pair. Δg_{AB}, the non-configurational Gibbs energy change for the formation of two moles of (A-B) pairs, is expanded as follows:

$$\Delta g_{AB} = \Delta g^0_{AB} + \sum_{i\geq 1} g^{i0}_{AB} X^i_{AA} + \sum_{j\geq 1} g^{0j}_{AB} X^j_{BB} \qquad 4.5$$

where Δg^0_{AB}, g^{i0}_{AB} and g^{0j}_{AB} are empirical parameters of the model which may be temperature-dependent and X_{AA} and X_{BB} are the fractions of all pairs which are (A-A) or (B-B) pairs respectively. The Gibbs energy of the solution is given by:

$$G = (n_A g^0_A + n_B g^0_B) - T\Delta S^{config} + (n_{AB}/2)\Delta g_{AB} \qquad 4.6$$

where g^0_A and g^0_B are the molar Gibbs energies of the pure elements, n_A and n_B are the numbers of moles of A and B in solution, n_{AB} is the number of moles of (A-B) pairs in solution, and ΔS^{config} is the configurational entropy of mixing given by randomly distributing the (A-A), (B-B) and (A-B) pairs in the one-dimensional Ising approximation. The equilibrium pair distribution is calculated by setting

$$(\partial G / \partial n_{AB})_{n_A, n_B} = 0 \qquad 4.7$$

As Δg_{AB} is made progressively more negative, reaction (4) is shifted progressively to the right and the degree of SRO increases.

A detailed derivation of the MQM for binary systems is given by Pelton et al [74]. A summary of the model is given by Kang et al [10]. When a significant amount of SRO is present, plots of the enthalpy and entropy of liquid mixing, ΔH and ΔS, exhibit minima near the composition of maximum SRO which is the composition where the mole fraction ratio X_B/X_A is given by the ratio of coordination numbers Z_A/Z_B. That is, when Δg_{AB} is very negative, the maximum number of (A-B) pairs will occur near the composition where each A atom is surrounded by Z_A B atoms and each B atom is surrounded by Z_B A atoms. The MQM requires four coordination numbers, Z^A_{AA} and Z^A_{AB} which are the values of Z_A respectively when all nearest-neighbors of an A atom are other A atoms and when all nearest-neighbors of an A atom are B atoms, and Z^B_{BB} and Z^B_{BA} which are defined similarly. For consistency with our earlier optimizations of systems containing Zn, RE elements, Mg and Al, we set Z^i_{ii}= 6 for *i* = Zn, Sc, Y,

and all the RE elements. Our experience with many alloy systems has shown that the best results are often obtained by setting the ratio Z_{BA}^{B} / Z_{AB}^{A} equal to the ratio of valences of the components A and B. In the present assessments we have set $Z_{Zn,RE}^{Zn}$ = 4 and $Z_{Zn,RE}^{RE}$ = 6 for Sc, Y and all RE elements, thereby setting the composition of maximum ordering at a composition where the mole fraction of Zn is approximately 0.6. However, the actual calculated minima in the ΔH and ΔS can deviate somewhat from this value depending upon the parameters of Eq. (5). This choice of coordination numbers consistently yielded the best optimizations in all systems.

The use of the one-dimensional Ising approximation for ΔS^{config} introduces a mathematical approximation which we have found [72] can be partially compensated by selecting values of the coordination numbers which are smaller than their actual physical values. In this regard it should be noted that although the model is sensitive to the ratio of the coordination numbers, it is less sensitive to their absolute values.

4.4 Optimizations

All the data described in Section 2 were considered in the optimizations, taking account of systematic trends across the RE series. The optimized model parameters are given in Tables 1.2 and 1.3. The phase diagrams and thermodynamic properties calculated from the optimized parameters are compared with the experimental data in Figs. 1 to 7 and 10 to 20. In all cases the data are reproduced by the calculations within the experimental error limits. The optimized entropies of formation of $LaZn_{13}$ and La_2Zn_{17} at 298.15 K are -4.51 and -4.82 J/g.atom K respectively (Table 2) which may be compared to the reported [25, 26] values of -1.8 and -1.32 J/g.atom K discussed in Section 2.2. The deviations are somewhat outside the estimated experimental error limits. However, it proved impossible to reproduce simultaneously these data and all the other experimental data (particularly the emf data in Fig. 10).

The melting points and enthalpies of formation of all compounds calculated from the optimized parameters are shown in Figs. 21 and 22. Values for systems with Y and the heavy RE elements taken from the second article in the present series [12] are also shown. In the case of the Pm-Zn system for which no phase diagram data are available, the melting points of the compounds were estimated by interpolation on Fig. 21. The enthalpies of formation of the compounds were estimated by interpolation on Fig. 22, and the entropies of formation of the

compounds were estimated by taking the average of the entropies of formation of the other RE-Zn compounds of the same stoichiometry from Table 2. Model parameters of the liquid phase (Table 3) were then obtained by optimization in order to reproduce the estimated melting points closely. Small adjustments to the enthalpies and entropies of formation were then made in order to reproduce the estimated melting points exactly.

In a number of systems the metastable congruent melting points of metastable compounds were estimated by interpolation or extrapolation in Fig. 21. The enthalpies of formation of the compounds were estimated by interpolation on Fig. 22 and the entropies of formation were estimated by taking the average of the entropies of formation of the other RE-Zn compounds of the same stoichiometry from Table 2. These enthalpies and entropies were then adjusted slightly in order to reproduce the estimated metastable congruent melting points.

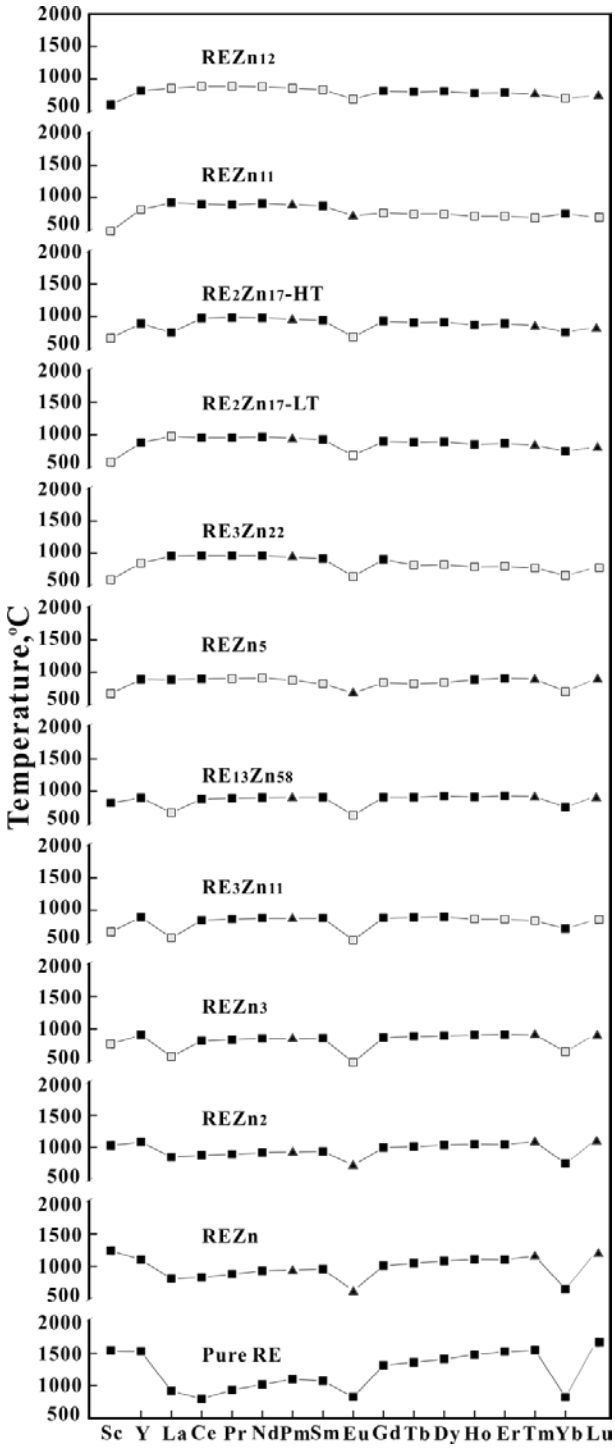

Figure 4.21 Calculated congruent melting points of all compounds in the Sc-Zn, Y-Zn and RE-Zn systems. ■=stable compounds shown on experimental phase diagrams; ▲=stable compounds. Melting point from interpolation or extrapolation; □=metastable compounds. Melting point from interpolation or extrapolation

Table 4.2 Optimized Gibbs energy of formation (J/g•atom) of intermetallic compounds as in Eq(1) and references for the crystal structure.

(Prototype-Pearson symbol-space group)	Gibbs energy of formation	References for crystal structure
MZn (CsCl-cP2-Pm$\bar{3}$m)		
ScZn	-28900+2.64T	[14, 43, 44]
LaZn	-33400+2.27T	[45, 46]
CeZn	-34150+3.54T	[47]
PrZn	-33150+3.28T	[32, 48, 49]
NdZn	-32850+3.36T	[50]
PmZn	-33221+3.45T	
SmZn	-33800+3.56T	[50]
MZn_2 ($CeCu_2$-oI12-Imma)		
[1]$ScZn_2$	-33933+7.3T	[14, 44]
$LaZn_2$	-39900+4.72T	[51, 52]
$CeZn_2$	-38800+4.74T	[53]
$PrZn_2$	-37100+4.4T	[32, 51, 52]
$NdZn_2$	-36900+4.78T	[36, 54]
$PmZn_2$	-37628+5.02T	
$SmZn_2$	-38967+5.59T	[51]
MZn_3 (YZn_3-oP16-Pmna)		
#$ScZn_3$	-29288+8.22T	
#$LaZn_3$	-35821+6.44T	
$CeZn_3$	-37200+5.84T	[29, 55]
$PrZn_3$	-36625+6.46T	[32, 52]
$NdZn_3$	-36525+6.99T	[55]
$PmZn_3$	-36976+6.99T	
$SmZn_3$	-37625+6.85T	[55]
M_3Zn_{11} ($Al_{11}La_3$-oI28-Immm)		
#Sc_3Zn_{11}	-27999+10.05T	
#La_3Zn_{11}	-33976+6.76T	
Ce_3Zn_{11}	-36364+6.45T	[29, 55]
Pr_3Zn_{11}	-36000+7.12T	[32, 52]
Nd_3Zn_{11}	-35964+7.73T	[36, 55]
Pm_3Zn_{11}	-36132+7.43T	
Sm_3Zn_{11}	-36321+6.89T	[55]
MZn_4 (orthorhombic)		
$LaZn_4$	-37040+6.18T	[55]
$M_{13}Zn_{58}$ ($Gd_{13}Zn_{58}$-hP142-P6_3mc)		
$Sc_{13}Zn_{58}$	-25211+5.98T	[14]
#$La_{13}Zn_{58}$	-32902+6.51T	
$Ce_{13}Zn_{58}$	-35254+6.88T	[29]
$Pr_{13}Zn_{58}$	-34732+7.33T	[32]
$Nd_{13}Zn_{58}$	-34507+7.73T	[56]
$Pm_{13}Zn_{58}$	-34501+7.31T	
$Sm_{13}Zn_{58}$	-34493+6.59T	[55]
MZn_5 ($CaCu_5$-hP6-P6/mmm)		
#$ScZn_5$	-24755+8.96T	
$LaZn_5$	-34767+6.18T	[17, 52, 57]
$CeZn_5$	-34667+7.27T	[29]
*$PrZn_5$	-33817+7.52T	[58]
*$NdZn_5$	-33120+7.52T	[58]

#$PmZn_5$	-32981+7.52T	
*$SmZn_5$	-32841+-7.52T	[58]
M_3Zn_{17} (Ru_3Be_{17}-cI160-Im$\bar{3}$)		
Sc_3Zn_{17}	-23250+5.78T	[14, 59, 60]
M_3Zn_{22} (Pu_3Zn_{22}-tI100-I4_1/amd)		
#Sc_3Zn_{22}	-20083+8.65T	
La_3Zn_{22}	-30880+5.86T	[61]
Ce_3Zn_{22}	-31060+6.97T	[61]
Pr_3Zn_{22}	-31240+7.95T	[32]
Nd_3Zn_{22}	-31560+8.76T	[56]
Pm_3Zn_{22}	-30271+7.7T	
Sm_3Zn_{22}	-29680+6.97T	[55]
M_2Zn_{17} (LT) ($Ni_{17}Th_2$-hP38-P6_3/mmc)		
#α-Sc_2Zn_{17}	-17696+7.35T	
#α-La_2Zn_{17}	-28848+7.71T	
α-Ce_2Zn_{17}	-29789+7.4TT	[62]
α-Pr_2Zn_{17}	-29884+8.19T	[32, 52, 62, 63]
α-Nd_2Zn_{17}	-29158+7.94T	[63]
α-Pm_2Zn_{17}	-28936+7.71T	
α-Sm_2Zn_{17}	-28579+7.19T	[63]
M_2Zn_{17} (HT) (Th_2Zn_{17}-hR19-R$\bar{3}$m)		
#β-Sc_2Zn_{17}	-17027+5.06T	
β-La_2Zn_{17}	-28105+4.82T	[64]
β-Pr_2Zn_{17}	-27447+5.87T	[32, 62, 64]
β-Ce_2Zn_{17}	-27263+5.09T	[64]
β-Nd_2Zn_{17}	-26474+5.63T	[64]
β-Pm_2Zn_{17}	-26293+5.41T	
β-Sm_2Zn_{17}	-25947+4.88T	[64]
MZn_{11} ($BaCd_{11}$-tI48-I4_1/amd)		
#$ScZn_{11}$	-14644+7.78T	
$LaZn_{11}$	-24375+4.74T	[22, 62, 65]
$CeZn_{11}$	-25058+6.45T	[29, 65-67]
$PrZn_{11}$	-25142+7.24T	[32, 62, 65]
$NdZn_{11}$	-24167+6.58T	[65, 68]
$PmZn_{11}$	-23971+6.38T	
[2]$SmZn_{11}$	-23667+5.95T	[69]
MZn_{12} ($Mn_{12}Th$-tI26-I4/mmm)		
$ScZn_{12}$	-13231+4.32T	[14, 59]
#$LaZn_{12}$	-22207+4.51T	
#$CeZn_{12}$	-22529+5.15T	
#$PrZn_{12}$	-22400+5.63T	
*$NdZn_{12}$	-22046+5.79T	[36]
#$PmZn_{12}$	-21950+5.79T	
*$SmZn_{12}$	-21853+5.63T	[62]
MZn_{13} ($NaZn_{13}$-cF112-Fm$\bar{3}$c)		
$LaZn_{13}$	-21793+4.51T	[52, 62, 63]

*= Metastable compound that has been observed
#= Assumed to be a metastable compound
[1]= (AlB_2-hP3-P6/mmm)
[2]= ($SmZn_{11}$-hP42-P6/mmm)

Table 4.3 Optimized model parameters of Eq (3) for the bcc phase and optimized Modified Quasichemical Model parameters of Eq (5) for the liquid phase in Sc-Zn, La-Zn, Ce-Zn, Pr-Zn, Nd-Zn, Pm-Zn and Sm-Zn systems (J/mol).

bcc	Liquid (MQM)
$L^0_{Sc,Zn} = -25522$	$\Delta g_{ScZn} = -24267 + 5.8576T - 4184X_{ScSc} - 10042X_{ZnZn}$
$L^0_{La,Zn} = -53556$	$\Delta g_{LaZn} = -32217 + 5.8576T - 2720X_{LaLa} - 23012X_{ZnZn}$
$L^0_{Ce,Zn} = -53136$	$\Delta g_{CeZn} = -31380 + 5.8576T - 1883X_{CeCe} - 19246X_{ZnZn}$
$L^0_{Pr,Zn} = -50208$	$\Delta g_{PrZn} = -30752 + 5.8576T - 1464X_{PrPr} - 16736X_{ZnZn}$
$L^0_{Nd,Zn} = -44350$	$\Delta g_{NdZn} = -30334 + 5.8576T - 418X_{NdNd} - 15062X_{ZnZn}$
$L^0_{Pm,Zn} = -43932$	$\Delta g_{PmZn} = -30334 + 5.8576T - 837X_{PmPm} - 16736X_{ZnZn}$
$L^0_{Sm,Zn} = -44768$	$\Delta g_{SmZn} = -30208 + 5.8576T - 2092X_{SmSm} - 19665X_{ZnZn}$

4.5 Discussion

The systematic trends in the enthalpies of formation of the compounds across the RE series are evident in Fig. 22. (The systems with heavier RE elements as well as the slight deviations seen for Eu and Yb in Fig.22 will be discussed in the second article in the present series [12].) From Table 2 it can be seen that the entropies of formation of all compounds are negative and very similar for all compounds with the same stoichiometry. In general, the enthalpies and entropies of formation for the Sc compounds differ somewhat from the others as is to be expected.

Calculated enthalpies and entropies of liquid mixing are shown in Figs. 23 & 24. The curves are very similar for all systems, with the La-Zn and Ce-Zn systems lying slightly below the others and the Sc-Zn system somewhat above, and with minima between 60 and 66 at. % Zn. Comparison of the optimized values of ΔH at the minimum compositions with the values estimated from the Miedema model is shown in Fig. 9. Comparisons of the optimized enthalpies and entropies of liquid mixing in the La-Zn system with those reported in previous assessments [27, 28] are shown in Figs. 25 & 26. The enthalpies are quite similar, but the optimized entropies are very different due, in large measure, to the fact that the MQM was used only in the present assessment.

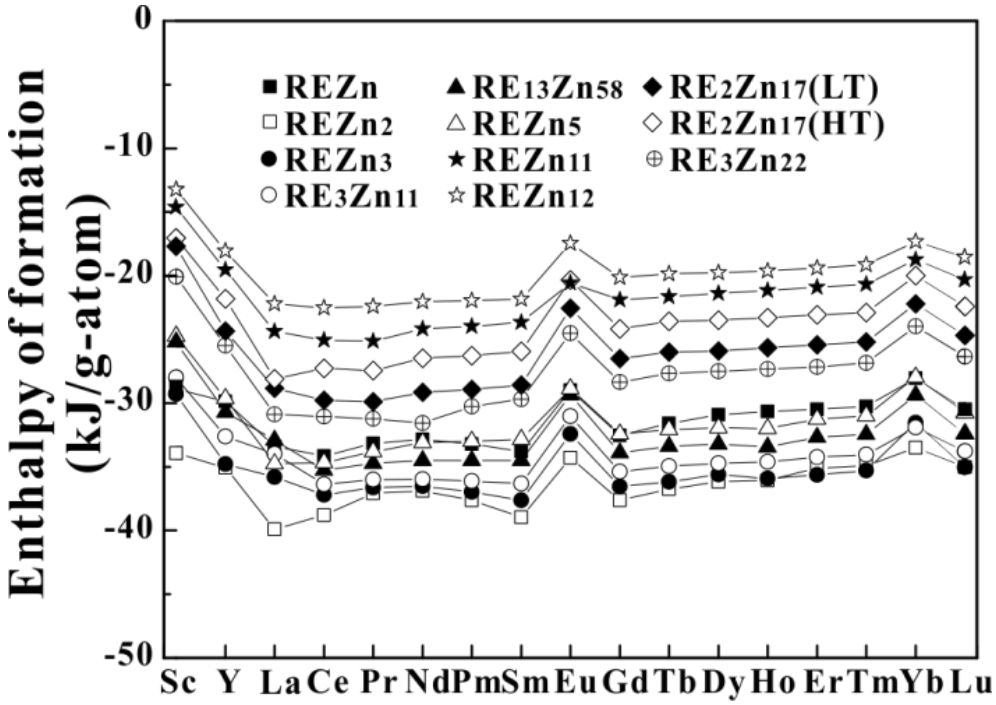

Figure 4.22 Calculated enthalpies of formation of compounds in the Sc-Zn, Y-Zn and RE-Zn systems.

Although, to some extent, the systematic trends in Figs. 22, 23, 24 and Table 2 are the result of *a priori* assumptions by the authors, it would not be possible to assume such trends for the liquid enthalpy, liquid entropy, all solid enthalpies and all solid entropies simultaneously and still reproduce the data unless these assumptions were warranted.

As seen in Table 3, a negative excess non-configurational entropy parameter of -5.8576 J/mol K was required in the expansion for Δg_{AB} in the MQM for the liquid phase in all systems. This is consistent with the optimizations of the Mg-RE [8-11] and Al-RE [82, 83] systems where negative excess non-configurational entropy parameters of approximately the same order were always found to be required.

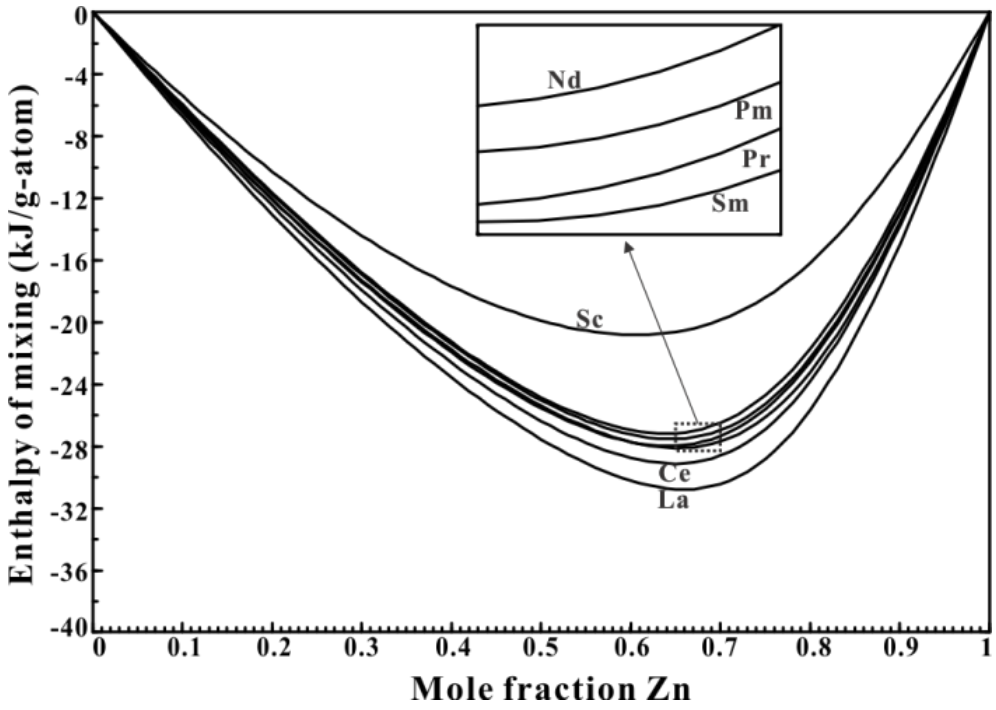

Figure 4.23 Calculated enthalpy of liquid-liquid mixing for Sc-Zn, La-Zn, Ce-Zn, Pr-Zn, Nd-Zn, Pm-Zn and Sm-Zn systems at 1600 ^{o}C

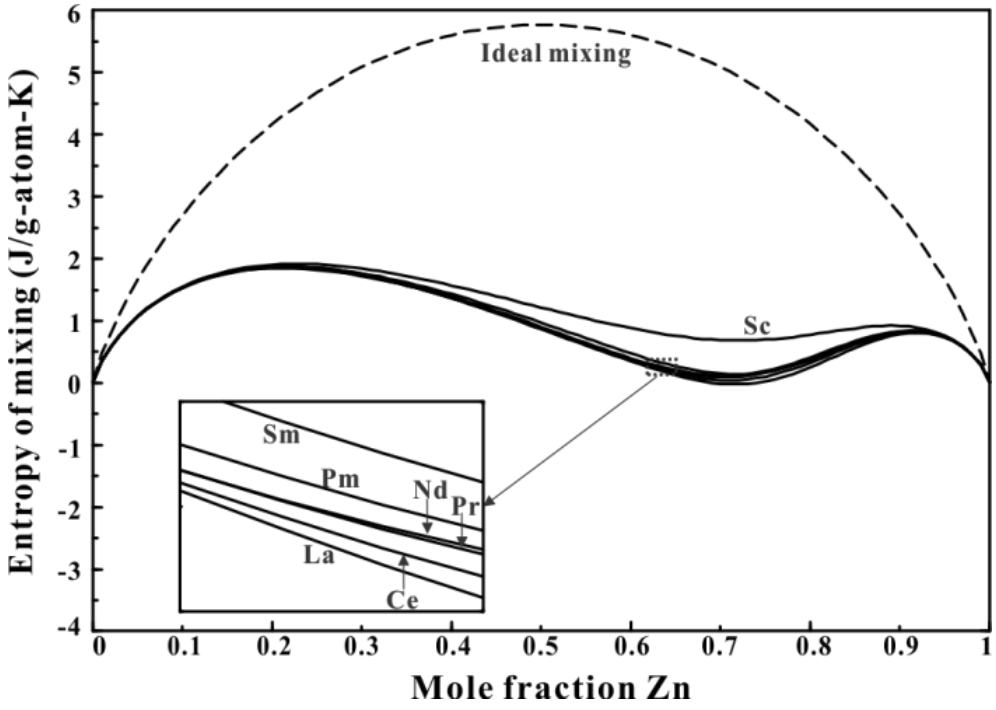

Figure 4.24 Calculated entropy of liquid-liquid mixing for Sc-Zn, La-Zn, Ce-Zn, Pr-Zn, Nd-Zn, Pm-Zn and Sm-Zn systems at 1600 ^{o}C

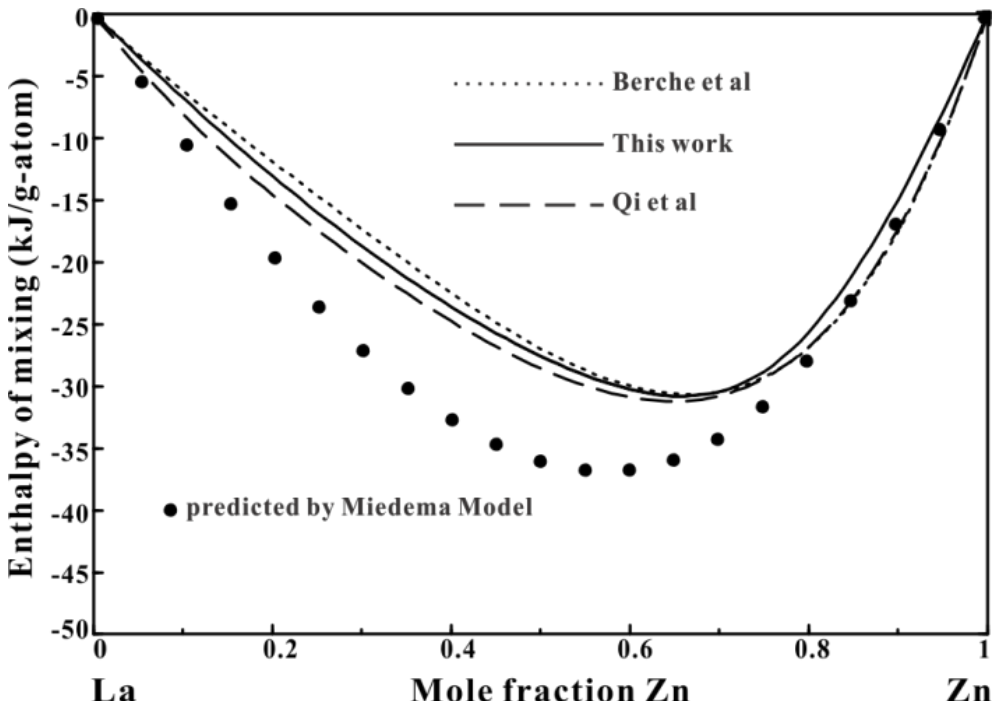

Figure 4.25 Calculated enthalpy of liquid-liquid mixing in the La-Zn system from different optimizations [27, 28]

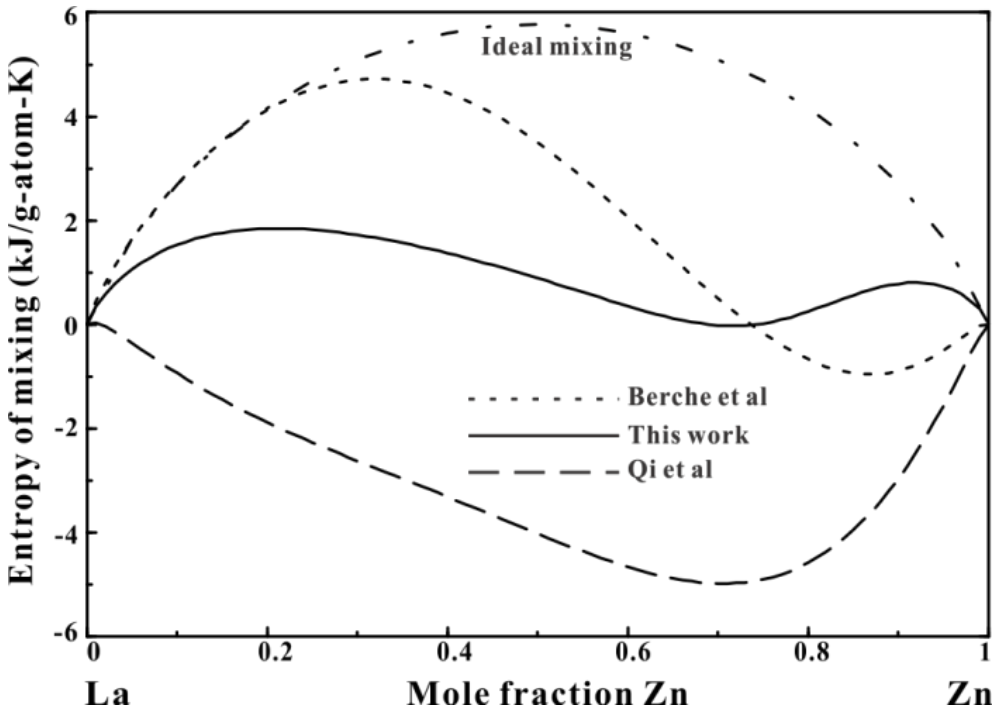

Figure 4.26 Calculated entropy of liquid-liquid mixing in the La-Zn system from different optimizations [27, 28]

4.6 Conclusions

Assessed optimized model parameters have been obtained giving the thermodynamic properties of all phases in the binary systems Sc-Zn, La-Zn, Ce-Zn, Pr-Zn, Nd-Zn, Pm-Zn and Sm-Zn. In a second article [12] we shall report on the optimizations of the binary systems formed between Zn and the heavier RE elements (Eu to Lu) as well as the Y-Zn system. In subsequent articles we shall report on optimizations of all the ternary Mg-Zn-RE systems. These parameters will be included in the FTlite light metals database of the FactSage database computing system [84] which already contains optimized parameters for the solid and liquid phases of a large number of binary and ternary Mg- and Al-containing systems. Through the models, the properties and phase equilibria of multicomponent systems can thus be estimated and calculated.

All calculations in the present work were performed with the FactSage software [84].

Acknowledgements

This research was supported by funding from the Natural Sciences and Engineering Research Council of Canada (NSERC) Magnesium Strategic Research Network. More information on the Network can be found at www.MagNET.ubc.ca.

References

[1] J. Bohlen, M.R. Nürnberg, J.W. Senn, D. Letzig, S.R. Agnew, Acta Mater., 55 (2007) 2101-2112.

[2] R.K. Mishra, A.K. Gupta, P.R. Rao, A.K. Sachdev, A.M. Kumar, A.A. Luo, Scripta Mater., 59 (2008) 562-565.

[3] N. Stanford, M.R. Barnett, Mater. Sci. Eng., A, 496 (2008) 399-408.

[4] K. Hantzsche, J. Bohlen, J. Wendt, K.U. Kainer, S.B. Yi, D. Letzig, Scripta Mater., 63 (2010) 725-730.

[5] B.L. Mordike, T. Ebert, Mater. Sci. Eng., A, 302 (2001) 37-45.

[6] I.P. Moreno, T.K. Nandy, J.W. Jones, J.E. Allison, T.M. Pollock, Scripta Mater., 48 (2003) 1029-1034.

[7] I. Ansara, G. Effenberg, C. Secretariat, COST 507: Definition of thermochemical and thermophysical properties to provide a database for the development of new light alloys, Office for Official Publications of the European Communities, 1998; P. J. Spencer, unpublished work.

[8] Y.-B. Kang, L. Jin, P. Chartrand, A.E. Gheribi, K. Bai, P. Wu, Calphad, 38 (2012) 100-116.

[9] Y.-B. Kang, A. Pelton, P. Chartrand, P. Spencer, C. Fuerst, J. Phase Equilib. Diffus., 28 (2007) 342-354.

[10] Y.-B. Kang, A.D. Pelton, P. Chartrand, C.D. Fuerst, Calphad, 32 (2008) 413-422.

[11] Y.-B.Kang, unpublished work

[12] Z. Zhu, A. Pelton, unpublished work

[13] A.R. Miedema, P.F. de Châtel, F.R. de Boer, Physica B, 100 (1980) 1-28.

[14] A. Palenzona, P. Manfrinetti, J. Alloys Compd., 247 (1997) 195-197.

[15] L. Rolla, A. Iandelli, R. Vogel, G. Canneri, Ric. Sci., 12 (1941) 1216-1226.

[16] D.J. Michel, E. Ryba, P.K. Kejriwal, J. Less-Common Met., 11 (1966) 67-69.

[17] J. Schramm, Z. Metallkd., 33 (1941) 358-360.

[18] A. Berche, P. Benigni, J. Rogez, M.C. Record, Thermochim. Acta, 523 (2011) 70-78.

[19] A. Berche, M.C. Record, J. Rogez, Open Therm. J., 3 (2009) 7-16.

[20] J.B.P.F. Lesourd, J.A. Plambeck, Can. J. Chem., 47 (1969) 3387-3391.

[21] R.K. Mullayanov, V.A. Lebedev, Y.P. Kanashin, I.F. Nichkov, S.P. Raspopin, Zh. Fiz. Khim., 43 (1969) 2776-2779.

[22] I. Johnson, R. Yonco, Metall. Mater. Trans. B, 1 (1970) 905-910.

[23] A.V. Kovalevskii, V.A. Lebedev, I.F. Nichkov, S.P. Raspopin, Izv. Akad. Nauk SSSR, Metal., (1972) 183-187.

[24] A. Berche, F. Marinelli, G. Mikaelian, J. Rogez, M.C. Record, J. Alloys Compd., 475 (2009) 79-85.

[25] M. Morishita, K. Koyama, K. Tsuboki, Z. Metallkd., 95 (2004) 708-712.

[26] M. Morishita, H. Yamamoto, K. Tsuboki, Y. Matsumoto, Mater. Trans., 47 (2006) 1555-1559.

[27] H.Y. Qi, G.X. Huang, R.D. Liu, K. Zhang, L.B. Liu, Z.P. Jin, J. Alloys Compd., 497 (2010) 336-343.

[28] A. Berche, P. Benigni, J. Rogez, M.-C. Record, Calphad, 36 (2012) 65-70.

[29] P. Chiotti, J.T. Mason, Trans. AIME, 233 (1965) 786-795.

[30] P.J. Spencer, A.D. Pelton, Y.-B. Kang, P. Chartrand, C.D. Fuerst, Calphad, 32 (2008) 423-431.

[31] C.P. Wang, X. Chen, X.J. Liu, F.S. Pan, K. Ishida, J. Alloys Compd., 458 (2008) 166-173.

[32] J. Mason, P. Chiotti, Metall. Mater. Trans. B, 1 (1970) 2119-2123.

[33] A. Saccone, A.M. Cardinale, S. Delfino, G. Cacciamani, R. Ferro, J. Alloys Compd., 317-318 (2001) 503-512.

[34] P. Chiotti, J.T. Mason, Metall. Trans., 2 (1971) 967-973.

[35] X.M. Huang, L.B. Liu, L.G. Zhang, B.R. Jia, Z.P. Jin, F. Zheng, J. Alloys Compd., 459 (2008) 191-195.

[36] J.T. Mason, P. Chiotti, Metall. Trans., 3 (1972) 2851-2855.

[37] P. Chiotti, J.T. Mason, Metall. Trans., 4 (1973) 1527-1531.

[38] H. Li, X. Su, Y. Liu, Z. Li, X. Wang, J. Alloys Compd., 457 (2008) 344-347.

[39] H. Qi, Z. Jin, L. Liu, H. Liu, J. Alloys Compd., 458 (2008) 184-188.

[40] X.J. Liu, X. Chen, C.P. Wang, J. Alloys Compd., 468 (2009) 115-121.

[41] P. Chiotti, J.T. Mason, Trans. AIME, 239 (1967) 547-552.

[42] B.R. Jia, L.G. Zhang, G.X. Huang, H.Y. Qi, H. Yang, L.B. Liu, Z.P. Jin, F. Zheng, J. Alloys Compd., 473 (2009) 176-179.

[43] E. Laube, H. Nowotny, Monatsh. Chem., 94 (1963) 162-163.

[44] P.I. Kripyakevich, V.S. Protasov, Y.B. Kuz'ma, Visn. L'viv. Derzh. Univ., Ser. Khim., (1965) 80-82.

[45] A. Iandelli, E. Botti, Gazz. Chim. Ital., 67 (1937) 638-644.

[46] J. Pierre, R.M. Galera, E. Siaud, J. Phys., 46 (1985) 621-626.

[47] Y. Uwatoko, K. Suenaga, G. Oomi, J. Magn. Magn. Mater., 104-107 (1992) 645-646.

[48] A. Iandelli, A. Palenzona, J. Less-Common Met., 9 (1965) 1-6.

[49] P. Morin, J. Pierre, Phys. Status Solidi A, 30 (1975) 549-559.

[50] A. Iandelli, Atti accad. nazl. Lincei, Rend., Classe sci. fis., mat. e, nat., 29 (1960) 62-69.

[51] M.L. Fornasini, F. Merlo, Atti Accad. Naz. Lincei, Rend., Cl. Sci. Fis. Mat. Natur., 43 (1967) 357-363.

[52] E. Veleckis, R.V. Schablaske, I. Johnson, H.M. Feder, Trans. AIME, 239 (1967) 58-63.

[53] D. Debray, M. Sougi, P. Meriel, J. Chem. Phys., 56 (1972) 4325-4328.

[54] D. Debray, M. Sougi, J. Chem. Phys., 58 (1973) 1783-1786.

[55] G. Bruzzone, L. Fornasini Maria, F. Merlo, Journal J. Less-Common Met., 22 (1970) 253-264.

[56] G. Borzone, G. Cacciamani, R. Ferro, J. Charles, J. Hertz, J. Less-Common Met., 128 (1987) 297-312.

[57] H. Nowotny, Z. Metallkd., 34 (1942) 247-253.

[58] M.L. Green, J. Less-Common Met., 32 (1973) 391-394.

[59] P.I. Kripyakevich, V.S. Protasov, Y.B. Kuz'ma, Izv. Akad. Nauk SSSR, Neorg. Mater., 2 (1966) 1574-1580.

[60] R.I. Andrusyak, B.Y. Kotur, V.E. Zavodnik, Kristallografiya, 34 (1989) 996-998.

[61] P.I. Kripyakevich, Y.B. Kuz'ma, N.S. Ugrin, Zh. Strukt. Khim., 8 (1967) 703-705.

[62] A. Iandelli, A. Palenzona, J. Less-Common Met., 12 (1967) 333-343.

[63] Y.B. Kuz'ma, P.I. Kripyakevich, N.S. Ugrin, Izv. Akad. Nauk SSSR, Neorg. Mater., 2 (1966) 630-635.

[64] T. Siegrist, Y. Le Page, J. Less-Common Met., 127 (1987) 189-197.

[65] M.J. Sanderson, N.C. Baenziger, Acta Crystallogr., 6 (1953) 627-631.

[66] G.L. Olcese, Atti Accad. Naz. Lincei, Cl. Sci. Fis., Mat. Nat., Rend., 35 (1963) 48-52.

[67] O. Zelinska, M. Conrad, B. Harbrecht, Z. Krist.-New Cryst. Struct., 219 (2004) 357-358.

[68] Y.B. Kuz'ma, P.I. Kripyakevich, D.P. Frankevich, Izv. Akad. Nauk SSSR, Neorg. Mater., 1 (1965) 1410-1415.

[69] J.T. Mason, K.S. Sree Harsha, P. Chiotti, Acta Crystallogr., Sect. B, 26 (1970) 356-361.

[70] A.T. Dinsdale, Calphad, 15 (1991) 317-425.

[71] H. Kopp, Phil. Trans. R. Soc. Lond., 155 (1865) 71.

[72] A.D. Pelton, Y.-B. Kang, Int. J. Mater. Res., 98 (2007) 907-917.

[73] Y.-B. Kang, A.D. Pelton, Calphad, 34 (2010) 180-188.

[74] A. Pelton, S. Degterov, G. Eriksson, C. Robelin, Y. Dessureault, Metall. Mater. Trans. B, 31 (2000) 651-659.

[75] Y.-B. Kang, A.D. Pelton, P. Chartrand, P. Spencer, C.D. Fuerst, Metall. Mater. Trans. A, 38 (2007) 1231-1243.

[76] A. Pelton, P. Chartrand, Metall. Mater. Trans. A, 32 (2001) 1361-1383.

[77] P. Chartrand, A. Pelton, Metall. Mater. Trans. A, 32 (2001) 1417-1430.

[78] P. Chartrand, A. Pelton, Metall. Mater. Trans. A, 32 (2001) 1385-1396.

[79] Y.-B. Kang, I.-H. Jung, S.A. Decterov, A.D. Pelton, H.-G. Lee, ISIJ Int., 44 (2004) 975-983.

[80] I.-H. Jung, S.A. Decterov, A.D. Pelton, J. Eur. Ceram. Soc, 25 (2005) 313-333.

[81] P. Waldner, A.D. Pelton, Metall. Mater. Trans. B, 35 (2004) 897-907.

[82] L. Jin, Y.-B. Kang, P. Chartrand, C.D. Fuerst, Calphad, 35 (2011) 30-41.

[83] L. Jin, Y.-B. Kang, P. Chartrand, C.D. Fuerst, Calphad, 34 (2010) 456-466.

[84] C.W. Bale, E. Bélisle, P. Chartrand, S.A. Decterov, G. Eriksson, K. Hack, I.H. Jung, Y.B. Kang, J. Melançon, A.D. Pelton, C. Robelin, S. Petersen, Calphad, 33 (2009) 295-311; www.factsage.com

Chapter 5 ARTICLE 2: CRITICAL ASSESSMENT AND OPTIMIZATION OF PHASE DIAGRAMS AND THERMODYNAMIC PROPERTIES OF RE-ZN SYSTEMS-PART II-Y-ZN, EU-ZN, GD-ZN, TB-ZN, DY-ZN, HO-ZN, ER-ZN, TM-ZN, YB-ZN AND LU-ZN

Published in Journal of Alloys and Compounds, 641(2015), 261-271

Zhijun Zhu, Arthur D. Pelton*

Centre de Recherche en Calcul Thermochimique, Département de Génie Chimique, Ecole Polytechnique, Montréal, Québec, Canada

*Corresponding author

KEY WORDS

Rare earth systems, Zinc systems, Phase diagrams, Thermodynamic assessment, Thermodynamic optimization

ABSTRACT

All available phase diagram and thermodynamic data for the Y-Zn, Eu-Zn, Gd-Zn, Tb-Zn, Dy-Zn, Ho-Zn, Er-Zn, Tm-Zn, Yb-Zn and Lu-Zn systems have been collected and critically assessed. Optimized model parameters for the thermodynamic properties of all phases have been obtained. Trends in the properties of the rare earth (RE)-Zn systems as one traverses the rare earth series have been exploited for purposes of estimating missing data and for checking existing data for consistency.

5.1 Introduction

Magnesium being the lightest structural metal, Mg-based alloys have many applications. Zinc is already one of the most commonly used alloying elements in Mg (AZ series), and the rare earth (RE) metals have been shown to improve sheet formability by reducing texture [1-4] and to improve creep resistance [5, 6]. For the design of potential new Mg-Zn-RE alloys, information on the phase behavior is essential. However, few studies of the phase diagrams and thermodynamic properties of these systems have been made.

Consequently, we have undertaken a project to better define the phase diagrams of the Mg-Zn-RE ternary systems through the technique of critical thermodynamic assessment and optimization coupled with some limited experimentation.

We have already completed thermodynamic optimizations of the Mg-Zn [7] and all Mg-RE binary systems [8-11]. In a previous article [12] we reported on the assessment and optimization of the binary systems formed between Zn and the lighter RE elements as well as the Sc-Zn system. In the present article we report on the assessment and optimization of the binary systems formed between Zn and the heavier RE elements (Eu to Lu) as well as the Y-Zn system. (The properties of Sc and Y are quite similar to those of the lighter and heavier RE elements respectively.) In subsequent articles we shall report on our optimizations of the ternary Mg-Zn-RE systems as well as on our experimental phase diagram studies of the Mg-Zn-Ce and Mg-Zn-Nd systems.

Complete sets of phase diagram and thermodynamic data are not available for all RE-Zn systems. However, all RE metals have very similar properties, and very definite trends are observed in the properties of the binary RE-Zn systems as one traverses the RE series. These trends may be exploited for purposes of estimating missing data and for checking existing data for consistency. Hence, a great advantage is realized by assessing and optimizing all the RE-Zn systems together.

The phase diagrams of the systems Y-Zn, Eu-Zn, Gd-Zn, Tb-Zn, Dy-Zn, Ho-Zn, Er-Zn, Tm-Zn, Yb-Zn and Lu-Zn are shown in Figs. 1 to 10. The similarities are obvious. As shown in the previous article [12], the phase diagrams of the systems of Zn with the lighter RE elements are all also very similar.

Table 1 provides a list of all compounds, both stable and metastable, which have been observed for all fifteen RE-Zn systems as well as the Sc-Zn and Y-Zn systems. With some exceptions, compounds with the same stoichiometry and crystal structure are found in most systems and, as can be seen in Figs. 1 to 10, compounds with the same stoichiometry have very similar melting points. Fig. 11 shows that the lattice constants of compounds with the same stoichiometry are also very similar for all systems. Systems with Eu and Yb exhibit anomalies due to their half-filled and filled f-shells respectively.

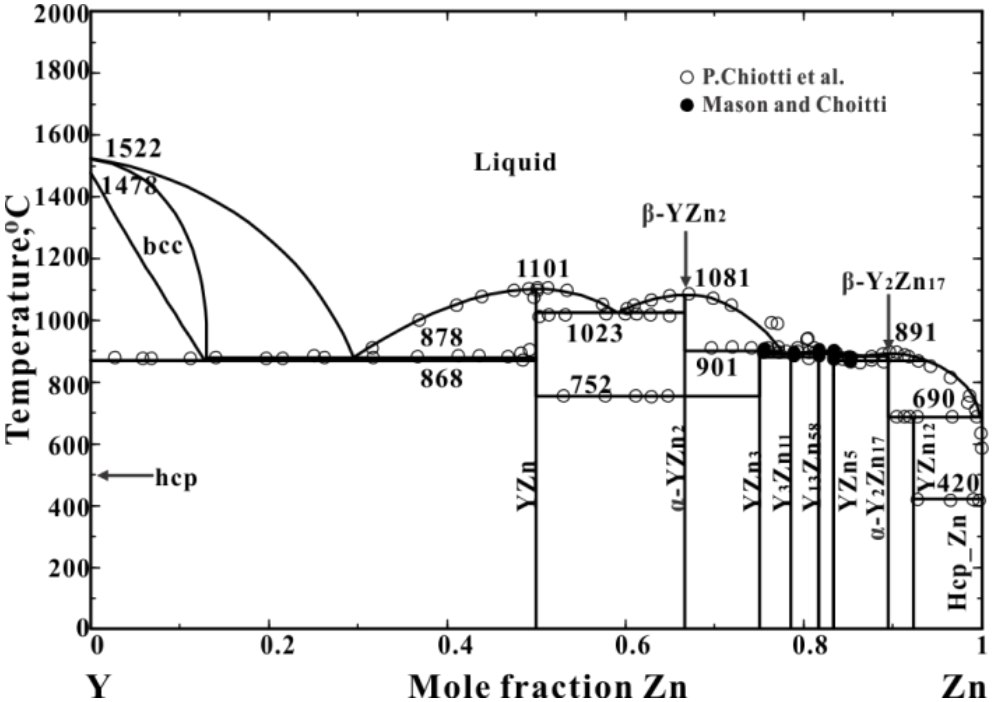

Figure 5.1(a) Calculated Y-Zn phase diagram and experimental data points [17, 18]

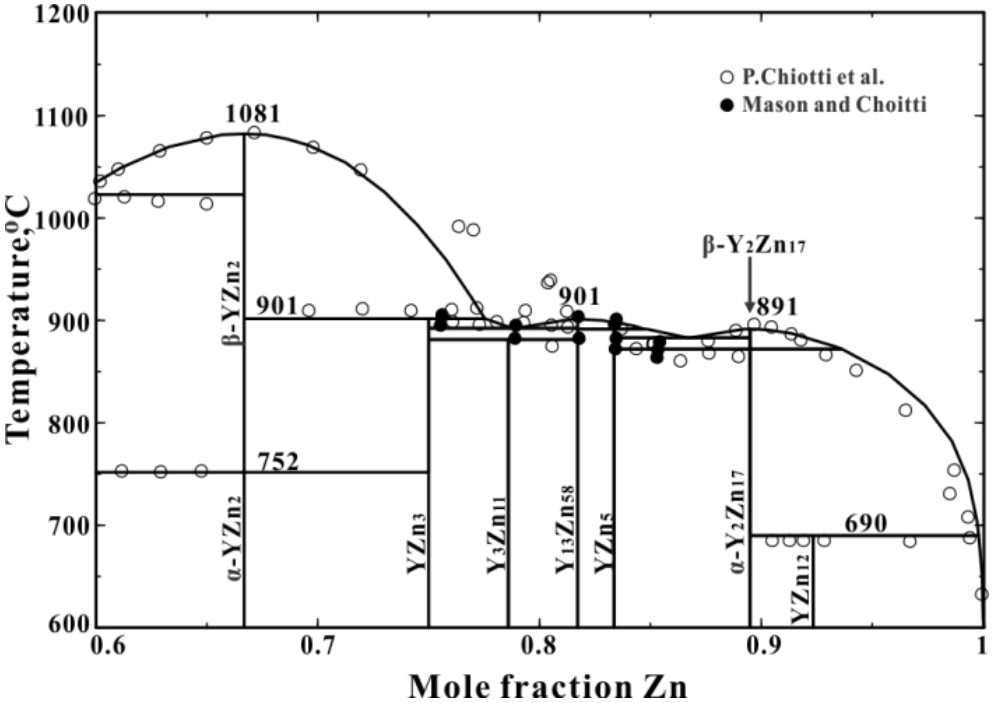

Figure 4.1(b) Calculated Y-Zn phase diagram (enlarged) and experimental data points [17, 18]

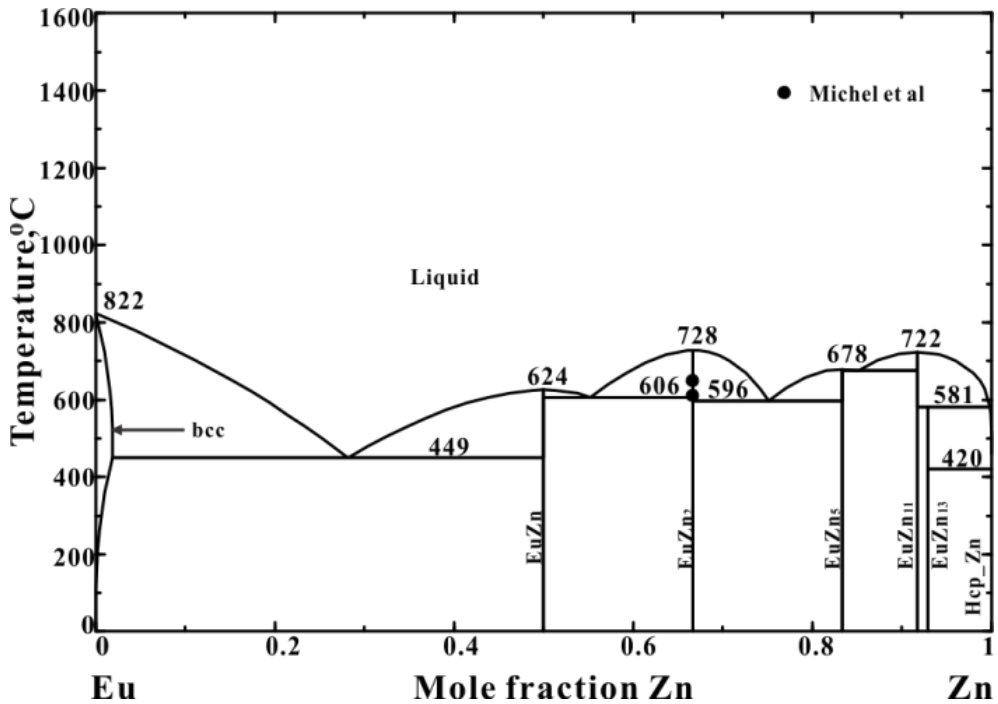

Figure 5.2 Calculated Eu-Zn phase diagram and experimental data points [27]

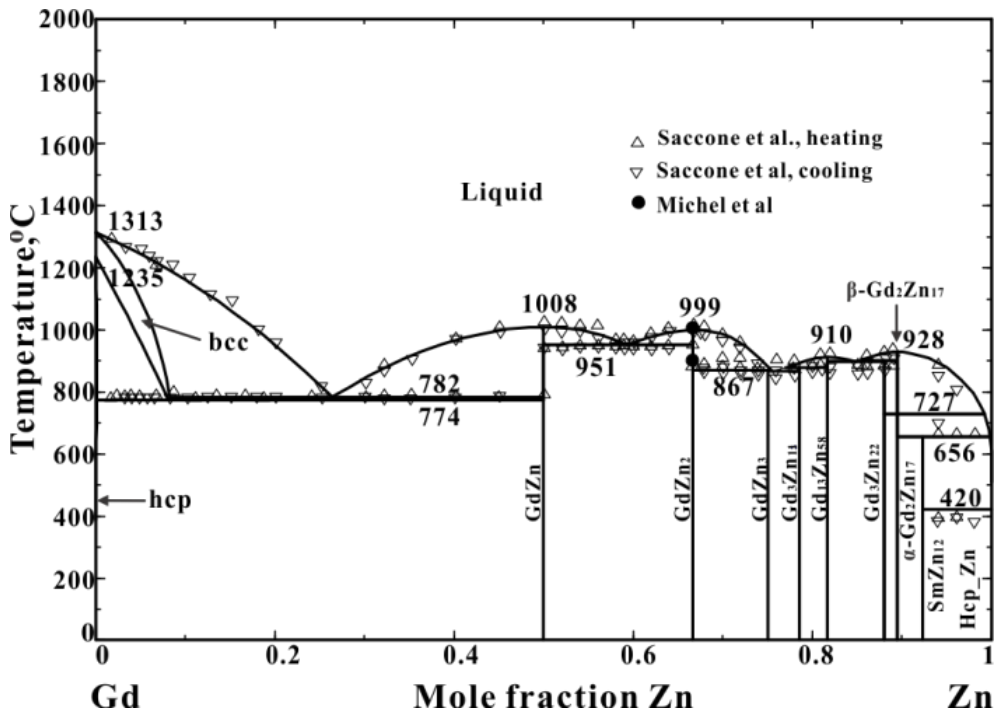

Figure 5.3 Calculated Gd-Zn phase diagram and experimental data points [27, 29]

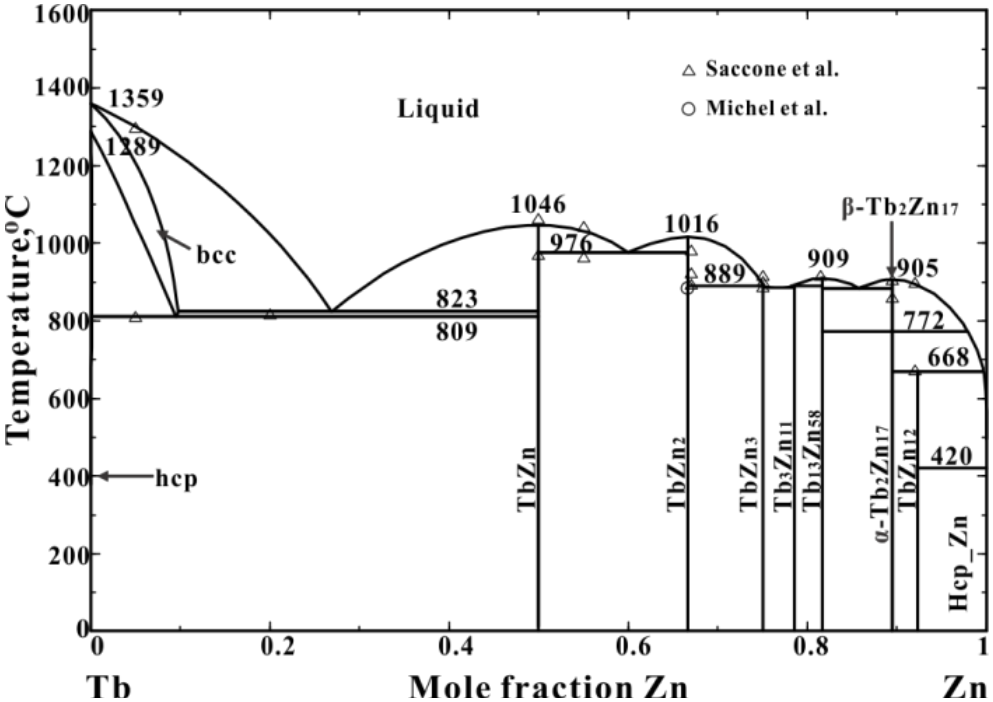

Figure 5.4 Calculated Tb-Zn phase diagram and experimental data points [27, 32]

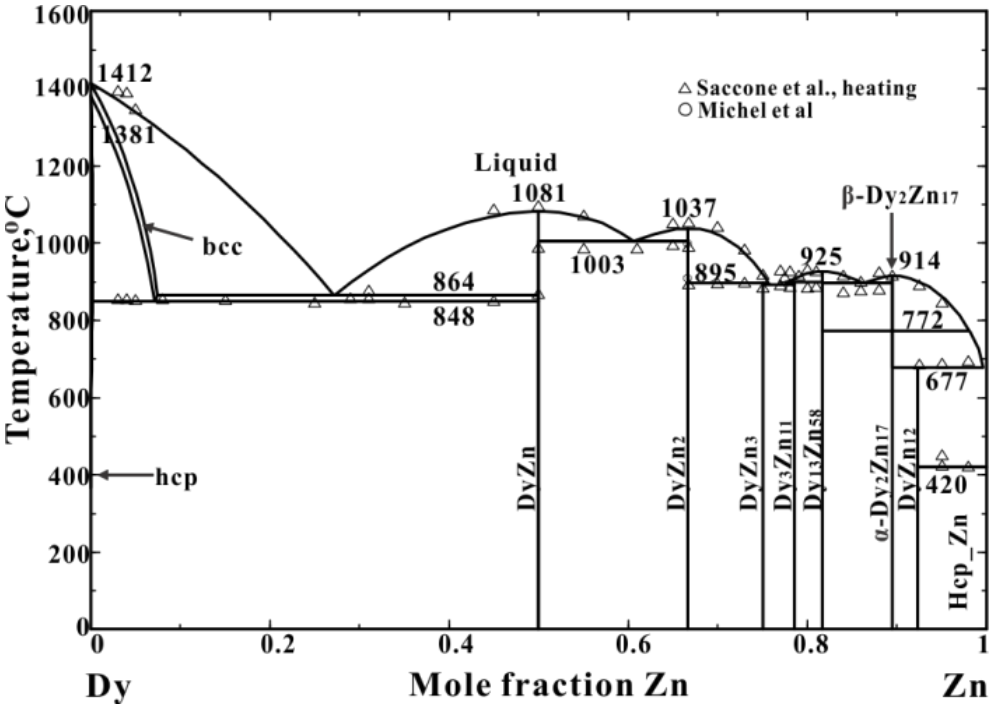

Figure 5.5 Calculated Dy-Zn phase diagram and experimental data points [27, 35]

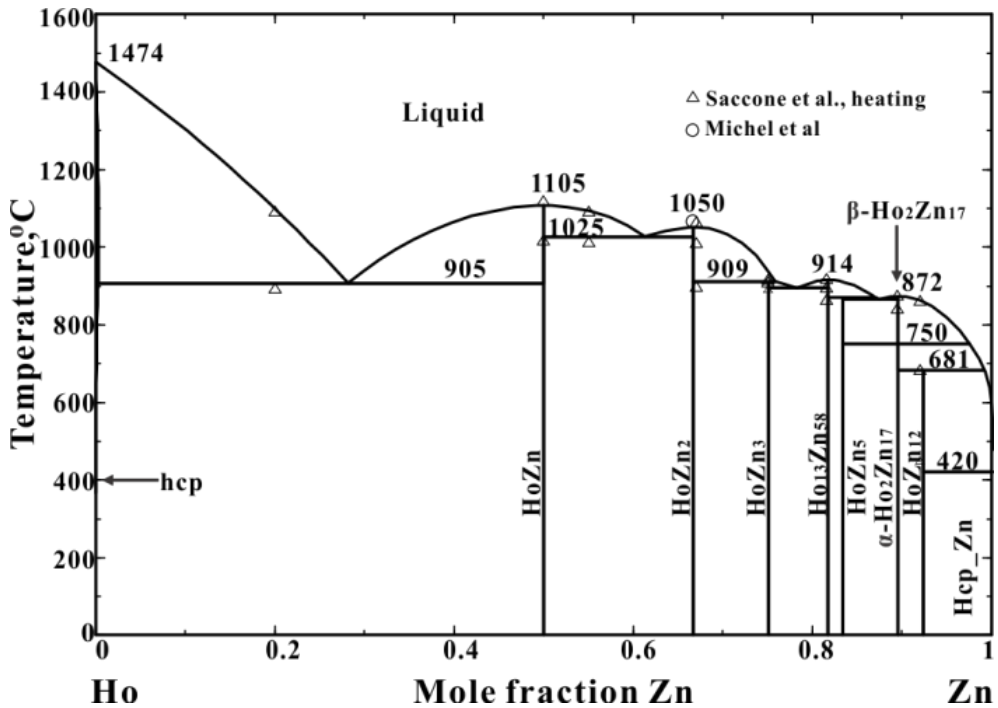

Figure 5.6 Calculated Ho-Zn phase diagram and experimental data points [27, 32]

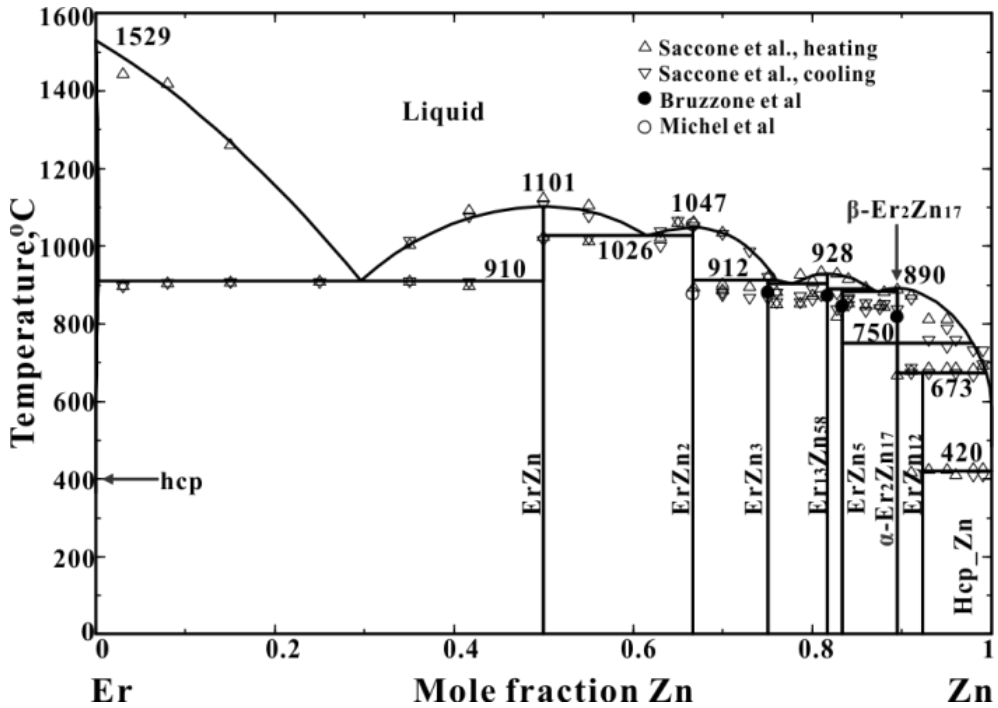

Figure 5.7 Calculated Er-Zn phase diagram and experimental data points [27, 32, 57]

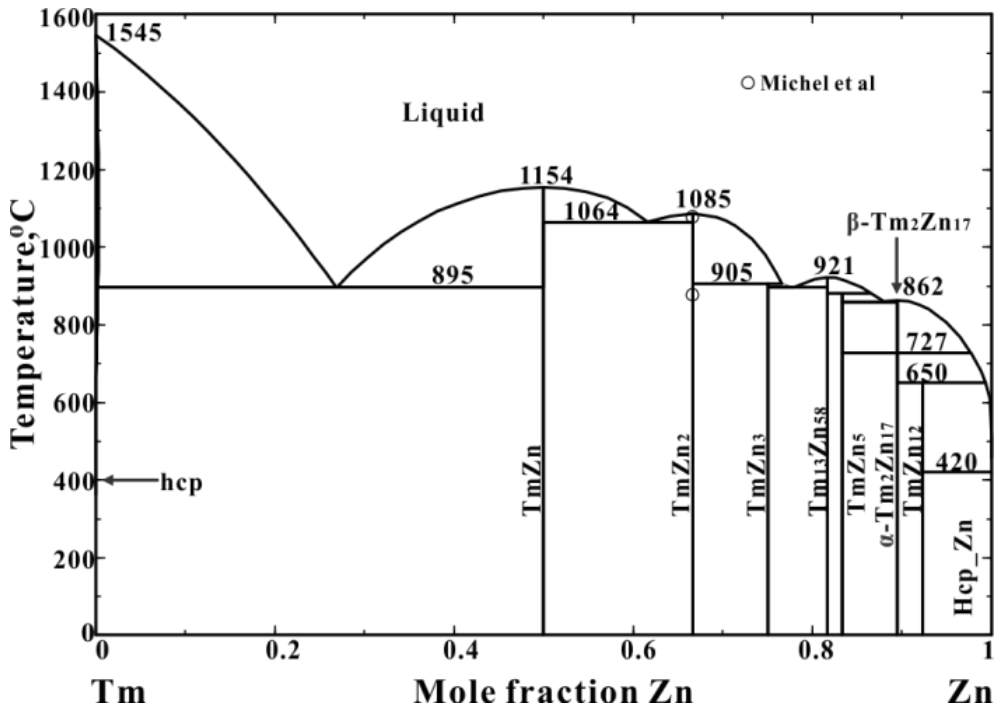

Figure 5.8 Calculated Tm-Zn phase diagram and experimental data points [27]

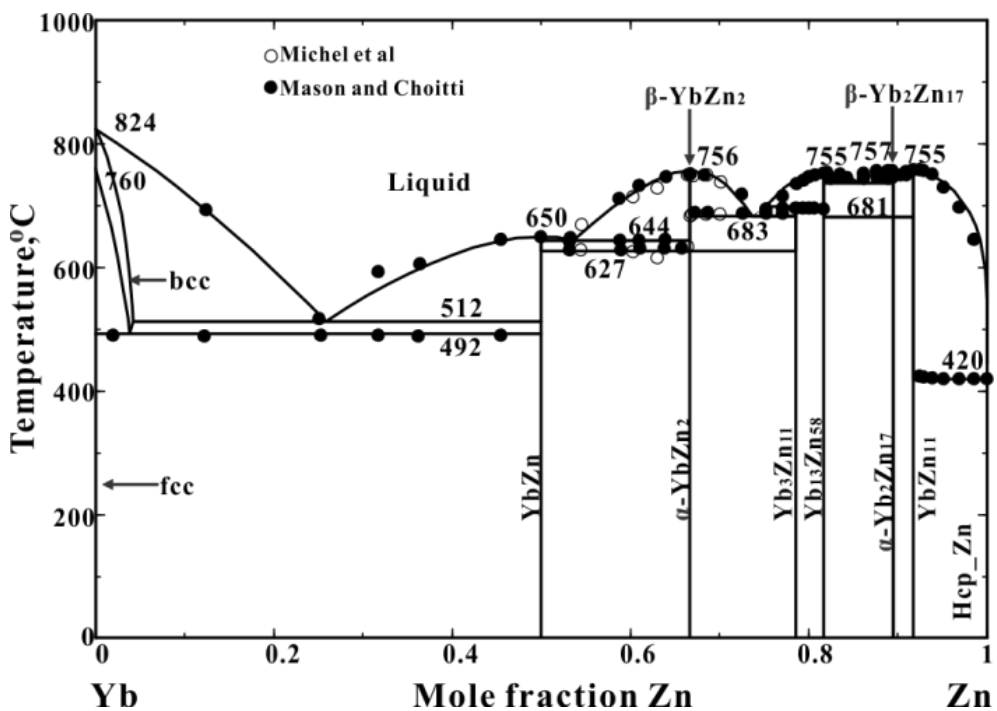

Figure 5.9 Calculated Yb-Zn phase diagram and experimental data points [27, 41]

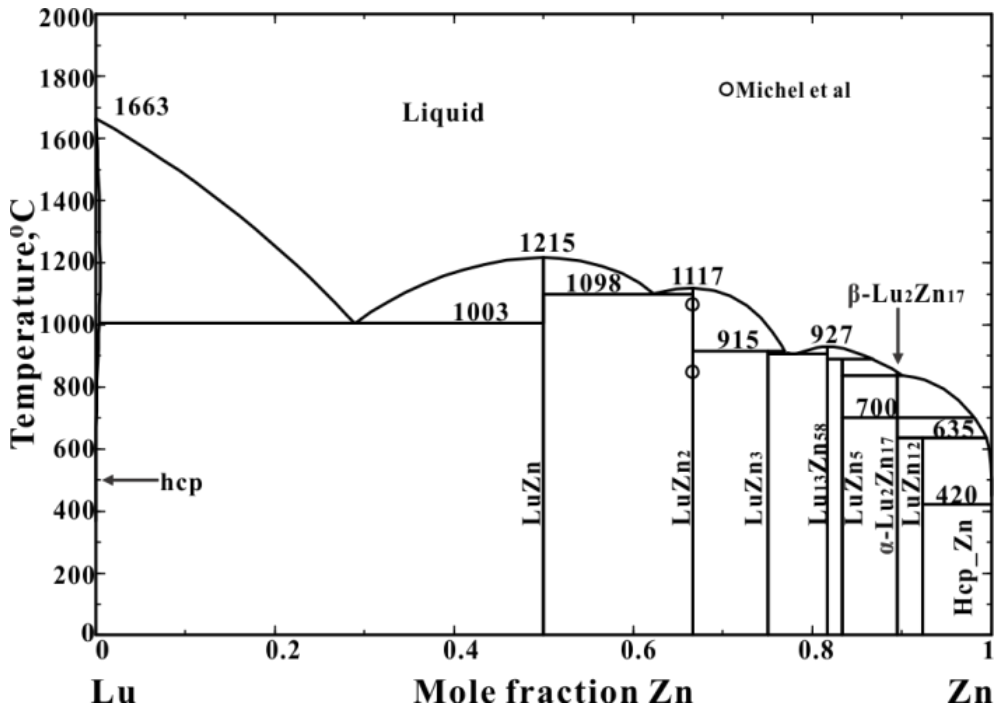

Figure 5.10 Calculated Lu-Zn phase diagram and experimental data points [27]

No experimental evidence for non-stoichiometry of any compounds has been reported and none has been assumed in the present assessments. Solid solubility of Zn in the terminal bcc phases has been reported in several systems of Zn with the lighter RE elements [13-16] with the extent of solubility being about the same for all these systems. Hence, we have assumed such solubility to occur in the bcc terminal solutions in all RE-Zn systems as well as the Sc-Zn and Y-Zn systems. No solubility of Zn in any other terminal solid phase has been reported, nor has solubility of Sc, Y, or any RE in the terminal hcp-Zn phase has been reported.

5.2 Phase equilibrium and thermodynamic data

5.2.1 Y-Zn system

The Y-Zn system, Fig. 1, was investigated by Chiotti et al [17] and later by the same group [18] by thermal analysis, metallography and vapor pressure measurements. Findings from earlier investigators were summarized by Mason and Chiotti [18]. Mason and Chiotti report eight compounds: YZn, YZn_2, YZn_3, Y_3Zn_{11}, $Y_{13}Zn_{58}$, YZn_6, Y_2Zn_{17} and YZn_{12}. To be consistent with the other RE-Zn systems, the reported compound YZn_6 is assumed in the present assessment to actually be YZn_5.

Equilibrium vapor pressures over two-phase Y-Zn mixtures as reported by Chiotti et al [17] and Mason and Chiotti [18] are shown in Fig. 12.

Emf measurements with alloy concentration cells with working electrodes of (liquid + YZn_{12}) and (Liquid+Y_2Zn_{17}) were performed by Hoshino and Plambeck [19] and Butorov et al [20]. Their results are plotted in Fig. 13. Enthalpies of formation of Y_2Zn_{17} and YZn_{12} were measured by solution calorimetry by Morishita et al [21] who reported values of -23.53 and -23.89 J/g-atom respectively. Heat capacities of YZn, Y_2Zn_{17} and YZn_{12} have been measured in the range 0 to 300 K by adiabatic calorimetry [22, 23] and by a “thermal relaxation method” [21]. Results are shown in Fig. 14. Third Law integration of these results by the authors give entropies of formation of YZn, Y_2Zn_{17} and YZn_{12} as -0.46, -3.05 and -0.78 J/g-atom K respectively.

Previous assessments of the Y-Zn system have been reported by Shao et al [24], Liu et al [25] and Spencer et al [26].

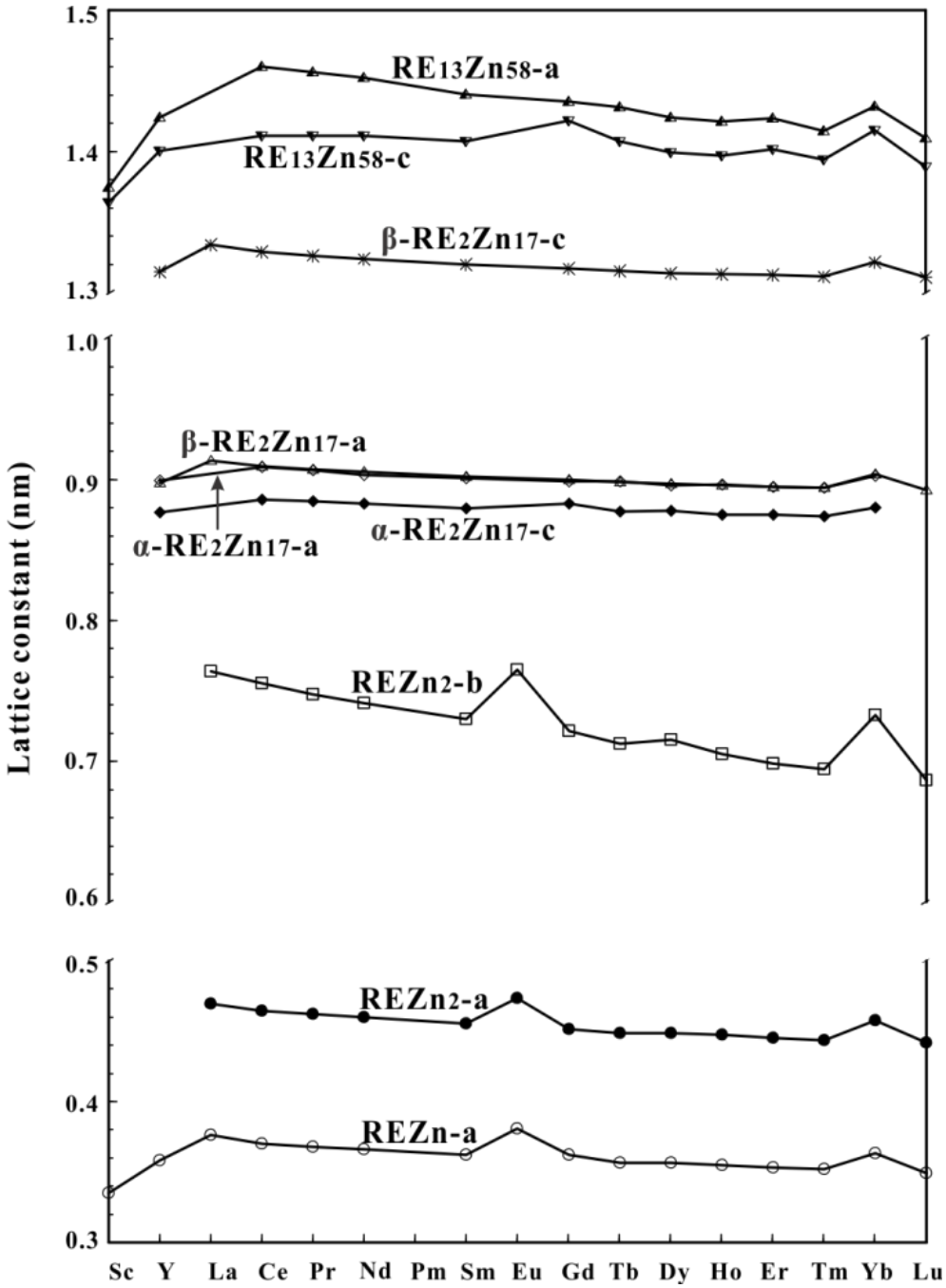

Figure 5.11 Lattice constants of RE-Zn compounds (for references, see Table 2 and ref [12])

Table 5.1 All reported stable and metastable compounds in Sc-Zn, Y-Zn and all RE-Zn systems (For references see Table 5.2 or reference [12])

(Prototype-Pearson symbol-space group)	Sc	Y	La	Ce	Pr	Nd	Pm	Sm	Eu	Gd	Tb	Dy	Ho	Er	Tm	Yb	Lu
MZn (CsCl-cP2-$Pm\bar{3}m$)	×	×	×	×	×[1]	×	×	×	×	×	×[1]	×[1]	×	×	×	×	×
MZn_2 ($CeCu_2$-oI12-Imma)	×[2]	×[3]	×	×	×	×	×	×	×	×	×	×	×	×	×	×[3]	×
MZn_3 (YZn_3-oP16-Pmna)		×		×	×	×	×	×		×	×	×	×	×	×		×
M_3Zn_{11} ($Al_{11}La_3$-oI28-Immm)		×		×	×	×	×	×		×	×	×				×	
M_6Zn_{23} ($Mn_{23}Th_6$-cF116-$Fm\bar{3}m$)		●								●	●	●	●[4]	●	●		●
MZn_4 (orthorhombic)			×														
$M_{13}Zn_{58}$ ($Gd_{13}Zn_{58}$-hP142-$P6_3mc$)	×	×[5]		×	×	×	×	×		×	×	×	×	×	×	×	×
MZn_5 ($CaCu_5$-hP6-P6/mmm)		●	×	×	●	●		●	×	●		●		●			
MZn_5 ($ErZn_5$-hP36-$P6_3$/mmc)		×											×	×	×		×
M_3Zn_{17} (Ru_3Be_{17}-cI160-$Im\bar{3}$)	×															●	
M_3Zn_{22} (Pu_3Zn_{22}-tI100-$I4_1$/amd)			×	×	×	×	×	×		×							
M_2Zn_{17} (LT) ($Ni_{17}Th_2$-hP38-$P6_3$/mmc)		×		×	×	×	×	×		×	×	×	×	×	×	×	×
M_2Zn_{17} (HT) (Th_2Zn_{17}-hR19-$R\bar{3}m$)		×	×	×	×	×	×	×		×	×	×	×	×	×	×	×
MZn_{11} ($BaCd_{11}$-tI48-$I4_1$/amd)			×	×	×	×	×	×[6]	×							×	
MZn_{12} ($Mn_{12}Th$-tI26-I4/mmm)	×	×				●		●		×	×	×	×	×	×		×
MZn_{13} ($NaZn_{13}$-cF112-$Fm\bar{3}c$)			×						×							●	

×=compounds reported or estimated as stable (for references see table 2)
●=Meta-stable compounds reorted (for references see table 2)
1=Meta-stable (HgMn-tP2-P4/mmm) also reported
2= AlB2-hP3-P6/mmm. Meta-stable ($MgZn_2$-hP12-$P6_3$/mmc) also has been reported.
3=Also, α form reported, structure unknown
4=reported as Ho_5Zn_{23} [68]
5=reported as Y_2Zn_9 (Y_2Zn_9-hP146-$P6_3$/mmc) but interpreted here as $Y_{13}Zn_{58}$.
6= $SmZn_{11}$-hP42-P6/mmm

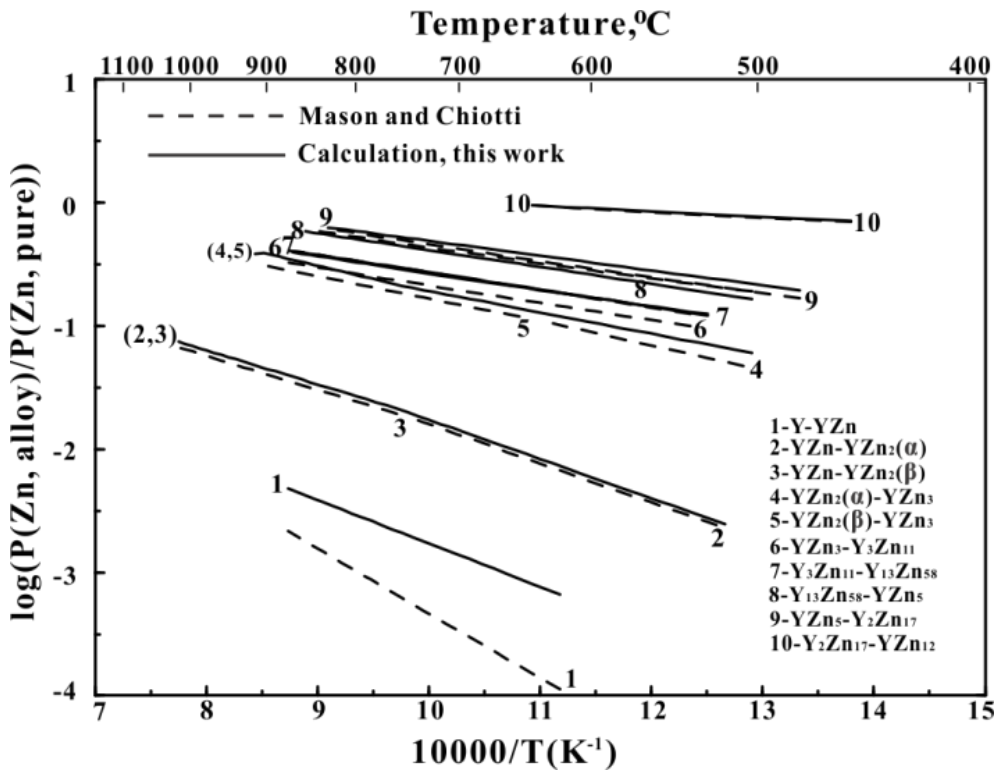

Figure 5.12 Calculated and experimental vapor pressures over two-phase Y-Zn alloys [17, 18]

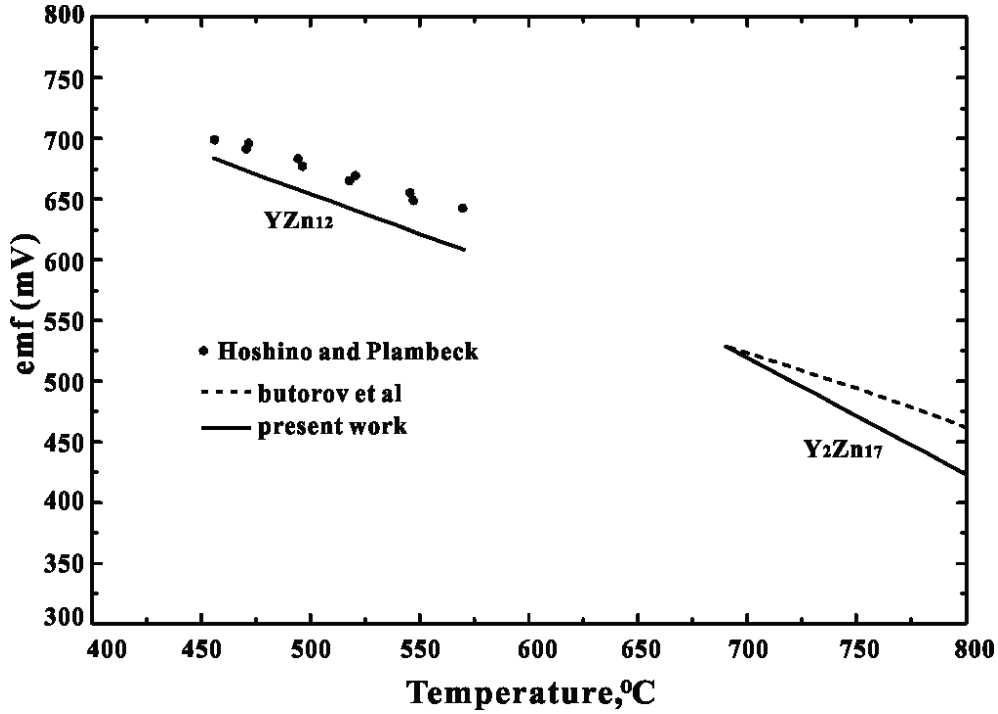

Figure 5.13 Emf of concentration cells for the formation of YZn_{12} and Y_2Zn_{17} [19, 20]

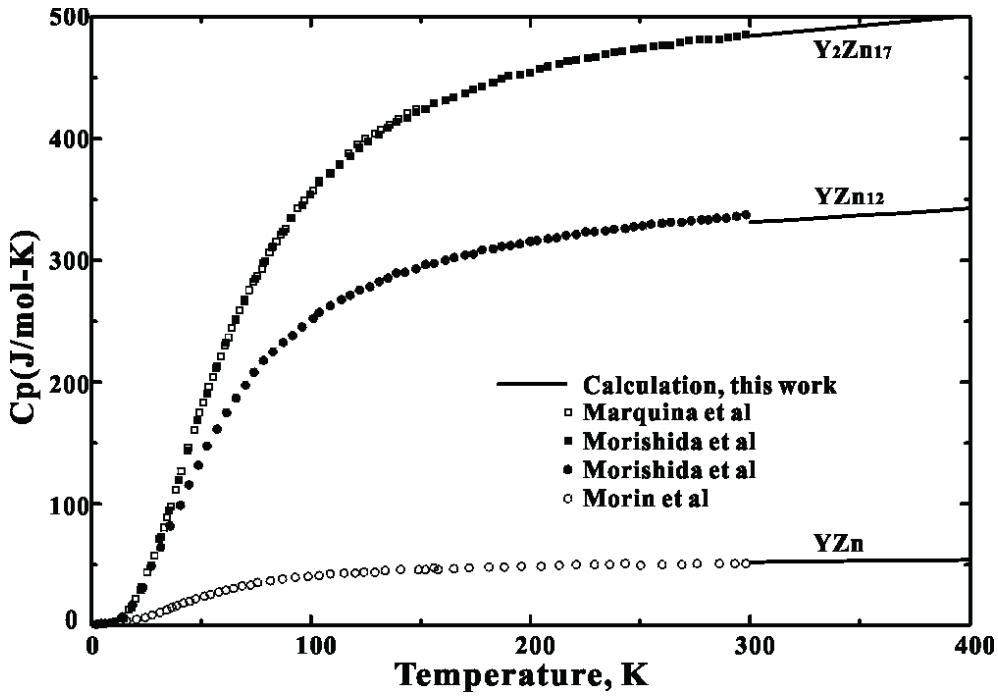

Figure 5.14 Heat capacities of YZn, Y_2Zn_{17} and YZn_{12} as measured [21-23] and as calculated (solid line) from the Neumann-Kopp equation

5.2.2 Eu-Zn system

Five compounds have been reported in this system. (See Table 2.1) The melting behavior of $EuZn_2$ was investigated by DTA by Michel et al [27] whose results are shown on Fig. 2.

5.2.3 Gd-Zn system

The Gd-Zn system, Fig. 3, was first investigated by Saccone et al [28] in the composition range from 0 to 50 at. % Zn by DTA, XRD, metallography and quantitative electron probe microanalysis. An investigation over the entire composition range was later carried out by the same group using DTA, optical microscopy, SEM, EPMA and XRD [29]. Eight intermediate phases were identified: GdZn, $GdZn_2$, $GdZn_3$, Gd_3Zn_{11}, $Gd_{13}Zn_{58}$, Gd_3Zn_{22}, Gd_2Zn_{17} and $GdZn_{12}$. Two forms of Gd_2Zn_{17} were identified. The high temperature form was obtained by annealing at 800°C for 150 h and the low temperature form was observed in samples slowly cooled to room temperature. The transformation temperature is thus below 800°C, but otherwise has not been determined.

The heat capacity of Gd_2Zn_{17} as reported in the temperature range from 0 to 200 K from adiabatic calorimetry by Marquina et al [30] is plotted in Fig. 15. The emf of concentration cells with a (liquid + $GdZn_{12}$) working electrode was reported by Kober et al [31]. The emf was found to be virtually independent of temperature over the range 693 to 1011 K. This behavior is very different from that observed in other RE-Zn systems and so these data have been rejected in the present assessment.

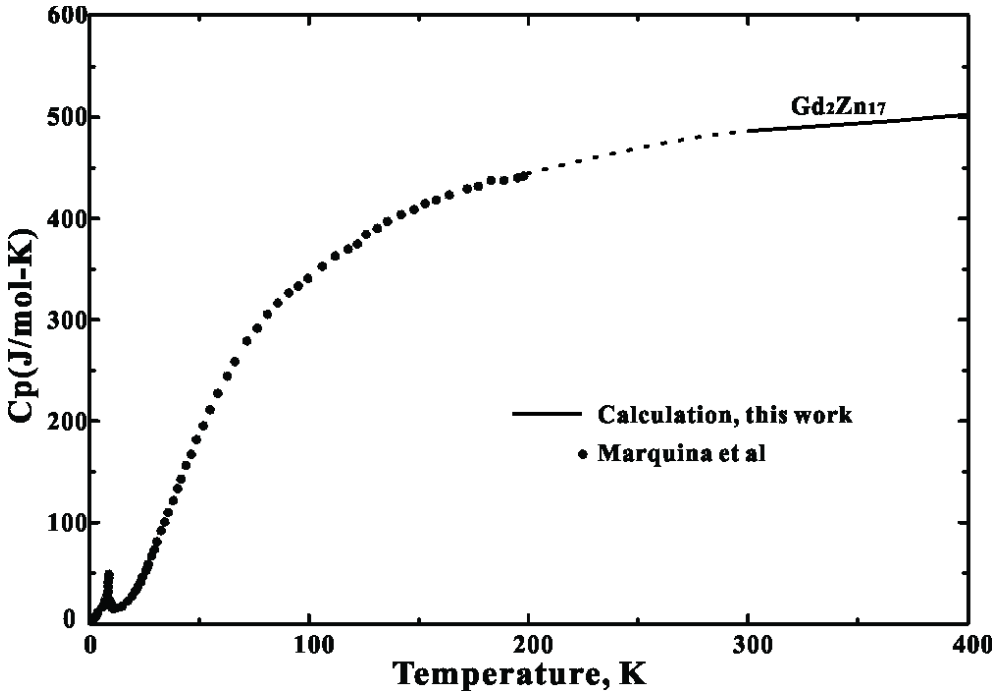

Figure 5.15 Heat capacity of Gd_2Zn_{17} as measured [30] and as calculated (solid line) from the Neumann-Kopp equation

5.2.4 Tb-Zn system

Nine intermetallic phases have been reported in the literature for the Tb-Zn system. (See Table 1.) The phase diagram, Fig. 4, was investigated by Saccone et al [32]. Seven intermetallic phases were proposed, among which TbZn, $TbZn_2$, $Tb_{13}Zn_{58}$ and Tb_2Zn_{17}(LT) were verified by XRD, while $TbZn_3$, Tb_3Zn_{11} and $TbZn_{12}$ were identified by their micrographic appearance. According to Saccone et al, TbZn, $TbZn_2$, $Tb_{13}Zn_{58}$ and Tb_2Zn_{17} melt congruently at 1045°C, 1028°C, 907°C and 915°C respectively while $TbZn_3$ and $TbZn_{12}$ melt peritectically at 900°C and 673°C respectively. Tb_3Zn_{11} was assumed to melt peritectically at a temperature slightly below the liquidus.

Both high- and low-temperature forms of Tb_2Zn_{17} have been reported in the literature. (See Table 1.) Tb_6Zn_{23} has been reported [33], but in the present assessment it is considered to be metastable. Morin et al [34] studied TbZn below room temperature, identifying both a CsCl-type and an HgMn-type structure. Only the CsCl-type structure was observed above room temperature.

The heat capacities of TbZn [22] and Tb_2Zn_{17} [23] have been measured by adiabatic calorimetry below room temperature. Results are plotted in Fig. 16. Third Law integration of these data by the authors gives the entropy of formation of TbZn as -0.32 J/g-atom K.

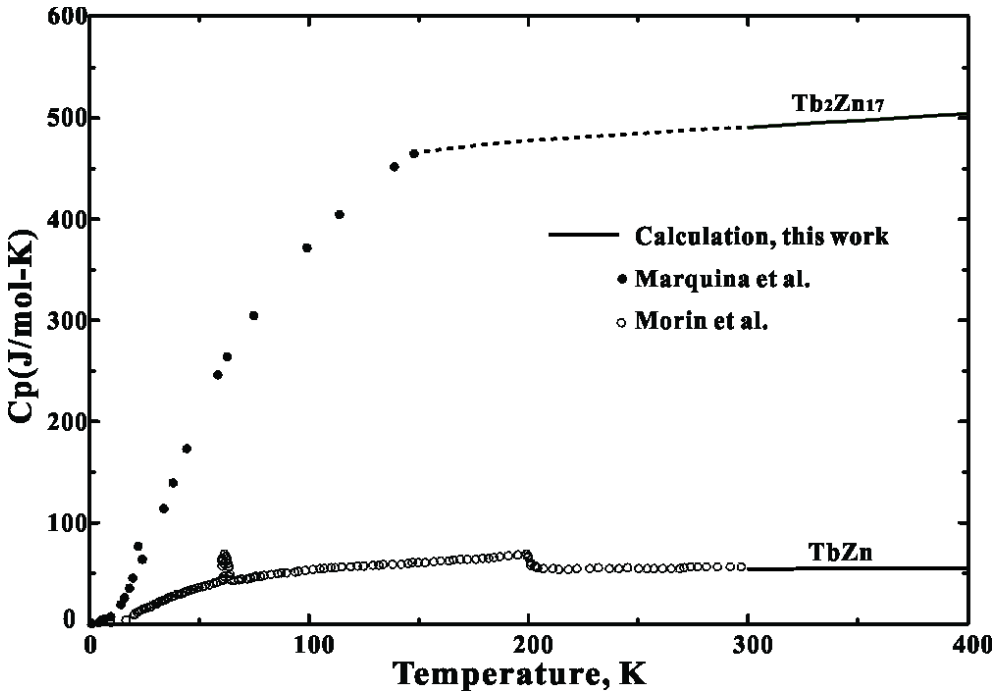

Figure 5.16 Heat capacities of TbZn and Tb_2Zn_{17} as measured [22, 23] and as calculated (solid line) from the Neumann-Kopp equation

5.2.5 Dy-Zn system

The Dy-Zn system, Fig. 5, was investigated by Saccone et al [35] over the entire composition range by DTA, metallography, XRD and EPMA. Seven intermetallic phases were identified by XRD: DyZn, $DyZn_2$, $DyZn_3$, Dy_3Zn_{11}, $Dy_{13}Zn_{58}$, Dy_2Zn_{17} (LT and HT forms) and $DyZn_{12}$. DyZn, $DyZn_2$, $Dy_{13}Zn_{58}$ and Dy_2Zn_{17} were reported to melt congruently at 1095°C, 1050°C, 930°C and 930°C respectively, while $DyZn_3$, Dy_3Zn_{11} and $DyZn_{12}$ were reported to melt peritectically at 895°C, 900°C and 685°C respectively. Although reported in the literature, $DyZn_5$

[36] and Dy_6Zn_{23} [33] were not observed by Saccone et al [35] and are not considered in the present assessment. Also not considered in the assessment is the low temperature form of DyZn which is stable below 139 K according to Morin et al [34]. $Dy_{13}Zn_{58}$ was reported as $Dy_{13}Zn_{57}$ with the space group Pnma by Gomez et al [37]. However, by analogy with the other RE-Zn systems we adopt the formula $Dy_{13}Zn_{58}$.

The emf of alloy concentration cells with (liquid + $DyZn_{12}$) working electrodes was measured by Yamchikov et al [38]. Their results are plotted in Fig. 17.

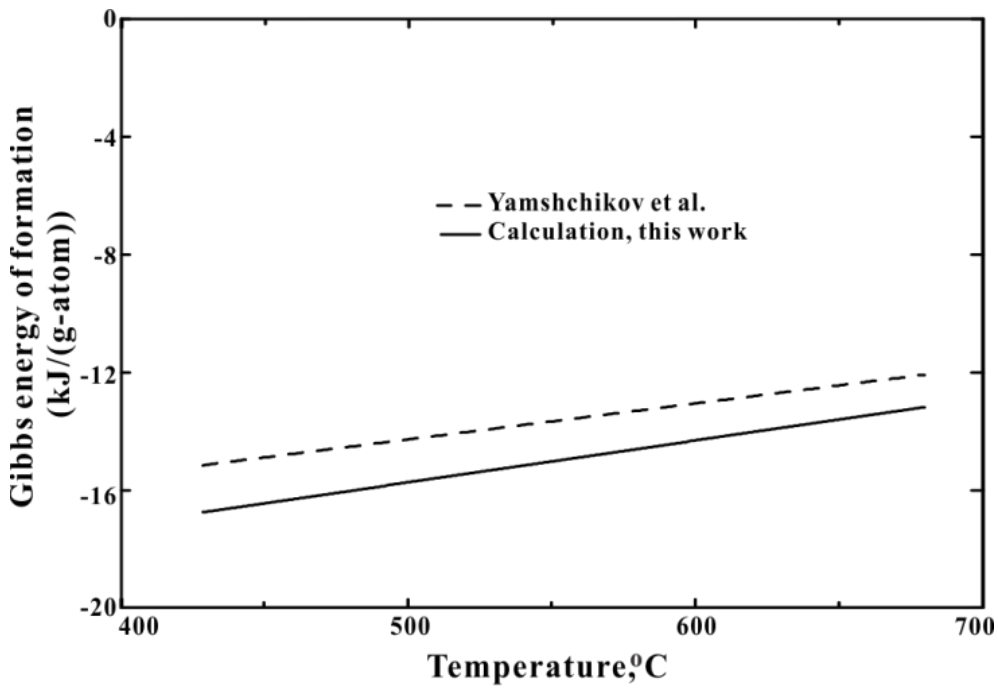

Figure 5.17 Gibbs energy of formation of $DyZn_{12}$ as reported [38] and as calculated from the optimized parameters

5.2.6 Ho-Zn system

The Ho-Zn phase diagram, Fig. 6, was studied in the same way as the Tb-Zn system by Saccone et al [32]. Seven intermetallic phases were proposed, among which HoZn, $HoZn_2$, $Ho_{13}Zn_{58}$ and Ho_2Zn_{17} (LT) were verified by XRD, while $HoZn_3$ and $HoZn_{12}$ were identified by their metallographic appearance. After considering all available information on the Gd-Zn, Dy-Zn and Er-Zn systems, Saccone et al [32] suggested that $HoZn_5$ is also a stable compound. The Ho_6Zn_{23} [39] phase was not observed.

According to Saccone et al [32], HoZn, $HoZn_2$, $Ho_{13}Zn_{58}$ and Ho_2Zn_{17} melt congruently at 1109°C, 1054°C, 924°C and 902°C respectively while $HoZn_3$ and $HoZn_{12}$ melt peritectically at 910°C and 686°C respectively; $HoZn_5$ melts peritectically at either 894°C or 861°C according to the DSC results.

The heat capacity of HoZn, as measured by Morin et al [22] by adiabatic calorimetry between 20 and 300 K, is plotted in Fig. 18. Third Law integration of these data by the authors gives the entropy of formation of HoZn as -1.42 J/g-atom K.

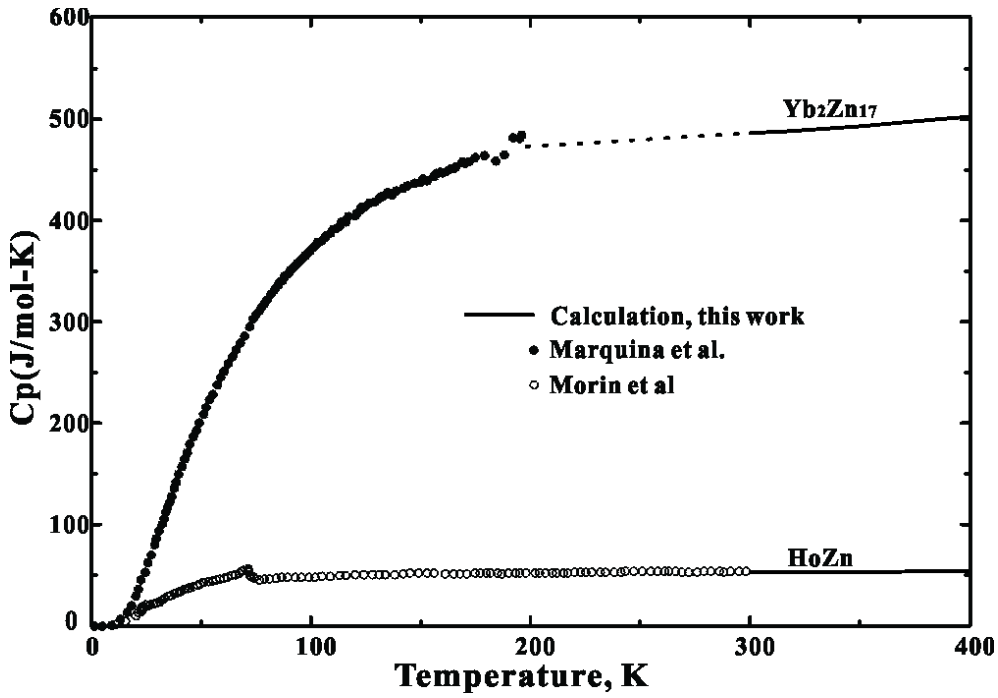

Figure 5.18 Heat capacities of HoZn and Yb_2Zn_{17} as measured [22, 30] and as calculated (solid line) from the Neumann-Kopp equation

5.2.7 Er-Zn system

The Er-Zn system, Fig. 7, was investigated over the entire composition range by Saccone et al [32] using DTA, XRD, optical microscopy, TEM and EPMA. Seven intermetallic phases were identified by XRD: ErZn, $ErZn_2$, $ErZn_3$, $Er_{13}Zn_{58}$, $ErZn_5$, Er_2Zn_{17} (HT and LT forms) and $ErZn_{12}$. The Er_6Zn_{23} phase was not observed. ErZn, $ErZn_2$, $Er_{13}Zn_{58}$ and Er_2Zn_{17} were reported to melt congruently at 1125°C, 1065°C, 940°C and 890°C respectively, while $ErZn_3$ and $ErZn_{12}$ were reported to melt peritectically at 890°C and 685°C respectively. The melting temperature of $ErZn_5$ was not resolved. Both forms of Er_2Zn_{17} were observed; the transformation temperature

was not measured, but lies below 800°C since the HT form was obtained upon quenching after annealing at 800°C for 150 h.

The emf of alloy concentration cells with (liquid + $ErZn_{12}$) working electrodes was measured by Yamchikov et al [40]. Their results are plotted in Fig. 19.

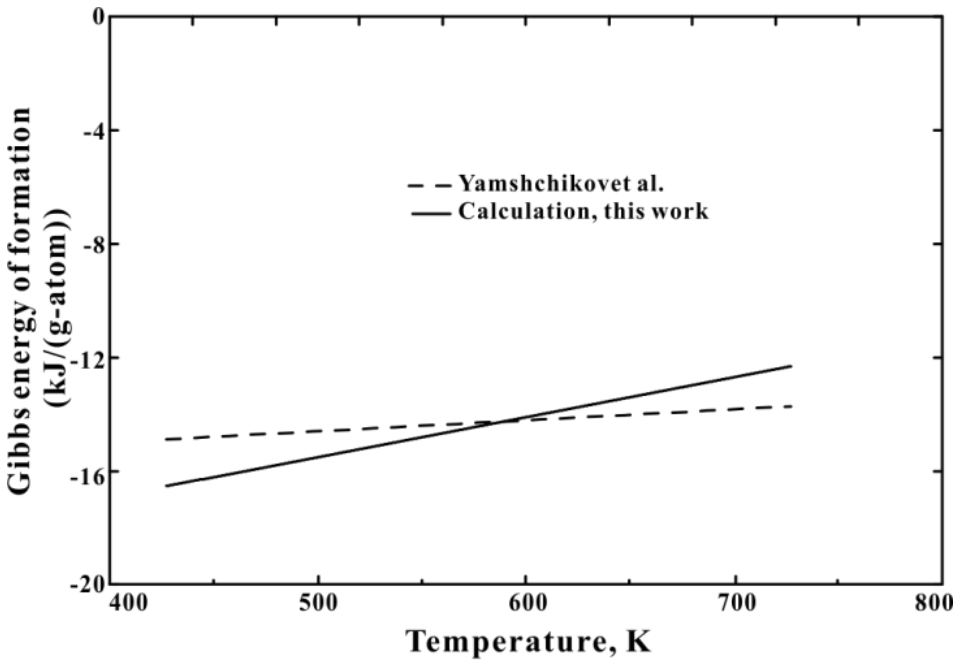

Figure 5.19 Gibbs energy of formation of $ErZn_{12}$ as reported [40] and as calculated from the optimized parameters

5.2.8 Tm-Zn system

Eight compounds have been reported in this system. (See Table 1) In the present assessment, by analogy to other RE-Zn systems, we consider seven of these to be stable as shown on Fig. 8, while Tm_6Zn_{23} is assumed to be metastable. The melting behavior of $TmZn_2$ was studied by DTA by Michel et al [27] whose results are shown on Fig. 8.

5.2.9 Yb-Zn system

Eight intermediate compounds have been reported in the literature as shown in Table 1. Mason and Chiotti [41] investigated the system, Fig. 9, over the entire composition range using DTA, XRD and metallographic analysis. In this study only six intermediate compounds were identified: YbZn, $YbZn_2$, $Yb_{13}Zn_{58}$, Yb_2Zn_{17} and $YbZn_{11}$, melting congruently at 650 °C, 751 °C, 752 °C, 754 °C and 755 °C respectively, and Yb_3Zn_{11} melting peritectically at 695 °C. In the

present assessment, Yb_3Zn_{17} and $YbZn_{13}$ are considered to be metastable. The melting behavior or $YbZn_2$ was studied by Michel et al [27] using DTA; their results are shown on Fig. 9.

The heat capacity of Yb_2Zn_{17}, as measured between 0 and 200 K by Marquina et al [30] is plotted in Fig. 18.

5.2.10 Lu-Zn system

Seven compounds have been reported in this system as shown in Table 1. The melting behavior of $LuZn_2$ was investigated using DTA by Michel et al [27] whose results are shown on Fig. 10.

5.3 Thermodynamic modeling

5.3.1 Elements

The thermodynamic properties of the elements were taken from Dinsdale [42].

5.3.2 Compounds

All compounds were assumed to be stoichiometric since there is no experimental evidence to the contrary and since this assumptions resulted in good reproduction of all the data. The Gibbs energies of all compounds were modeled by the equation:

$$g(RE_xZn_{1-x}) = [xg^0_{RE} + (1-x)g^0_{Zn}] + (\Delta h^0 - T\Delta s^0) \qquad 5.1$$

where $g(RE_xZn_{1-x})$ is the Gibbs energy of the compound per g-atom at temperature T (K), g^0_{RE} is the Gibbs energy of the pure RE element at T in the state which is stable at 298.15K, and g^0_{Zn} is the Gibbs energy of pure hcp Zn at T.

The enthalpy and entropy of formation, Δh^0 and Δs^0, are assumed to be independent of temperature. That is, the heat capacities of the compounds are all assumed to be given by the Neumann-Kopp equation [43]:

$$C_p = xC_{p(RE)} + (1-x)C_{p(Zn)} \qquad 5.2$$

The heat capacities of Y_2Zn_{17}, Gd_2Zn_{17}, TbZn, Tb_2Zn_{17}, HoZn and Yb_2Zn_{17} as calculated from the Neumann-Kopp equation are shown in Figs. 14-16 and 18. Since excellent agreement is

found with the experimental data in all cases, we have assumed that the Neumann-Kopp equation applies for all compounds in the present assessment.

5.3.3 Terminal solid solutions

As discussed in Section 1, solubility of Zn in the terminal bcc solutions has been assumed in all systems. The molar Gibbs energies of the bcc solutions have been modeled by the equation:

$$g_{bcc} = [xg^0_{Zn(bcc)} + (1-x)g^0_{RE(bcc)}] + RT(x\ln x + (1-x)\ln(1-x)] + x(1-x)L^0_{RE,Zn} \qquad 5.3$$

where x is the atomic fraction of Zn in the solution, $g^0_{Zn(bcc)}$ and $g^0_{RE(bcc)}$ are the Gibbs energies of pure bcc Zn (metastable) and the pure bcc RE element, both taken from the compilation of Dinsdale [42], and $L^0_{RE,Zn}$ is a regular solution parameter assumed to be constant, independent of both temperature and composition.

5.3.4 Liquid solutions

As discussed in the previous article [12], the liquid phase was modeled with the Modified Quasichemical Model (MQM) in the pair approximation which takes account of short-range ordering (SRO) among first-nearest-neighbor atoms. The following pair-exchange reaction between atoms A and B on neighboring quasi-lattice sites is considered:

$$(A-A)+(B-B)=2(A-B); \quad \Delta g_{AB} \qquad 5.4$$

where (i-j) represents a first-nearest-neighbor (FNN) pair. Δg_{AB}, the non-configurational Gibbs energy change for the formation of two moles of (A-B) pairs, is expanded as follows:

$$\Delta g_{AB} = \Delta g^0_{AB} + \sum_{i\geq 1} g^{i0}_{AB} X^i_{AA} + \sum_{j\geq 1} g^{0j}_{AB} X^j_{BB} \qquad 5.5$$

where Δg^0_{AB}, g^{i0}_{AB} and g^{0j}_{AB} are empirical parameters of the model which may be temperature-dependent and X_{AA} and X_{BB} are the fractions of all pairs which are (A-A) or (B-B) pairs respectively. As Δg_{AB} is made progressively more negative, reaction (4) is shifted progressively to the right and the degree of SRO increases.

A more complete description of the MQM was given in the previous article [12]. As in the previous article, the "coordination numbers" which are model parameters, were set to $Z^{Zn}_{Zn,RE}$ = 4, $Z^{RE}_{Zn,RE}$ = 6, and $Z^{Zn}_{Zn,Zn}$ = $Z^{RE}_{RE,RE}$ = 6 for all RE elements as well as Sc and Y.

5.4 Optimizations

All the data described in Section 2 were considered in the optimizations, taking account of systematic trends across the RE series. The optimized model parameters are given in Tables 2 and 3. The phase diagrams and thermodynamic properties calculated from the optimized parameters are compared with the experimental data in Figs. 1 to 10 and 12 to 19. In all cases the data are reproduced by the calculations within the experimental error limits. The optimized enthalpies of formation of Y_2Zn_{17}(LT) and YZn_{12} are -24347 and -18062 J/g-atom respectively which may be compared to the reported [21] values of -23530 and -23890 J/g-atom described in Section 2.1. The optimized entropies of formation of YZn, Y_2Zn_{17}, YZn_{12}, TbZn and HoZn at 298.15 K are -1.71, -6.65, -4.33, -2.22 and -1.57 J/g.atom K respectively (Table 2.) which may be compared to the reported [21, 22] values of -0.46, -3.05, -0.78, -0.32 and -1.42 J/g.atom K discussed in Section 2. The deviations are somewhat outside the estimated experimental error limits. However, it proved impossible to reproduce simultaneously these data and all the other experimental data (particularly the emf data in Fig. 12).

The melting points and enthalpies of formation of all compounds calculated from the optimized parameters are shown in Figs. 20 and 21. Values for systems with Sc and the light RE elements taken from the first article in the present series [12] are also shown. In the case of several compounds for which no phase diagram data are available, the melting points of the compounds were estimated by interpolation on Fig. 20. The enthalpies of formation of the compounds were estimated by interpolation on Fig. 21, and the entropies of formation of the compounds were estimated by taking the average of the entropies of formation of the other RE-Zn compounds of the same stoichiometry from Table 2. Model parameters of the liquid phase (Table 3.) were then obtained by optimization in order to reproduce the estimated melting points closely. Small adjustments to the enthalpies and entropies of formation were then made in order to reproduce the estimated melting points exactly.

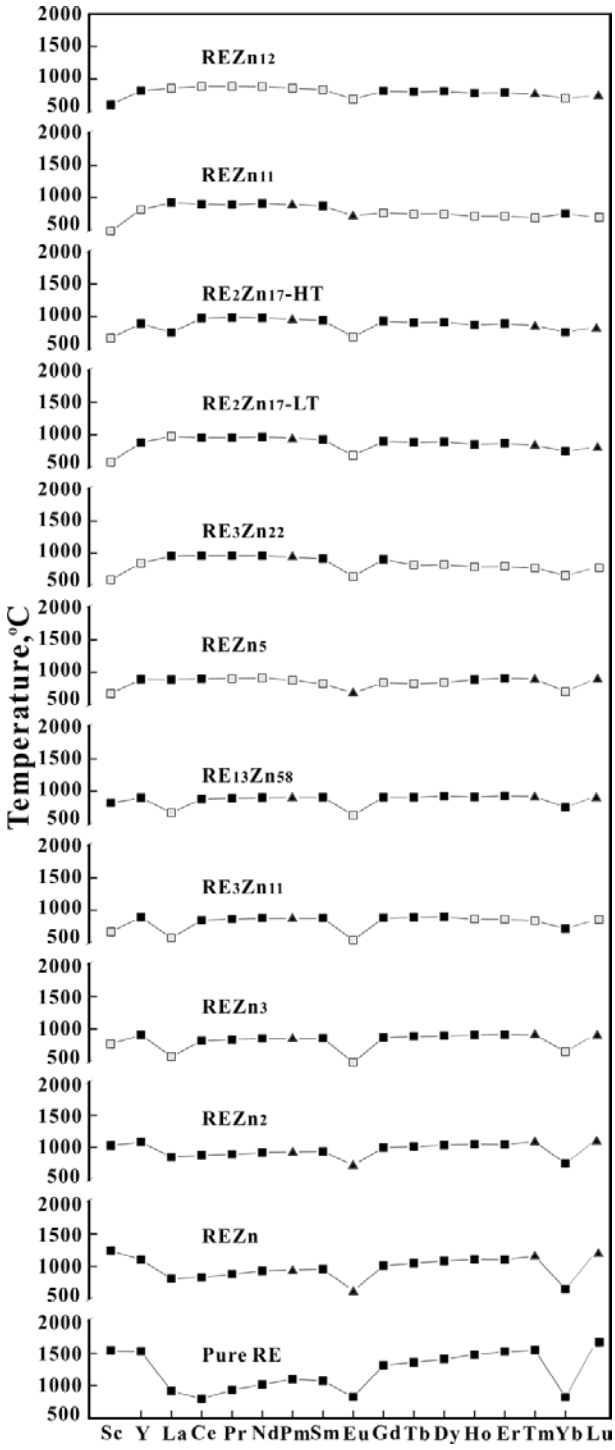

Figure 5.20 Calculated congruent melting points of all compounds in the Sc-Zn, Y-Zn and RE-Zn systems. ■=stable compounds shown on experimental phase diagrams; ▲=stable compounds. Melting point from interpolation or extrapolation; □=metastable compounds. Melting point from interpolation or extrapolation

In a number of cases the congruent melting points of metastable compounds were estimated by interpolation or extrapolation in Fig. 20. The enthalpies of formation of the compounds were estimated by interpolation on Fig. 21 and the entropies of formation were estimated by taking the average of the entropies of formation of the other RE-Zn compounds of the same stoichiometry from Table 2. These enthalpies and entropies were then adjusted slightly in order to reproduce the estimated metastable congruent melting points.

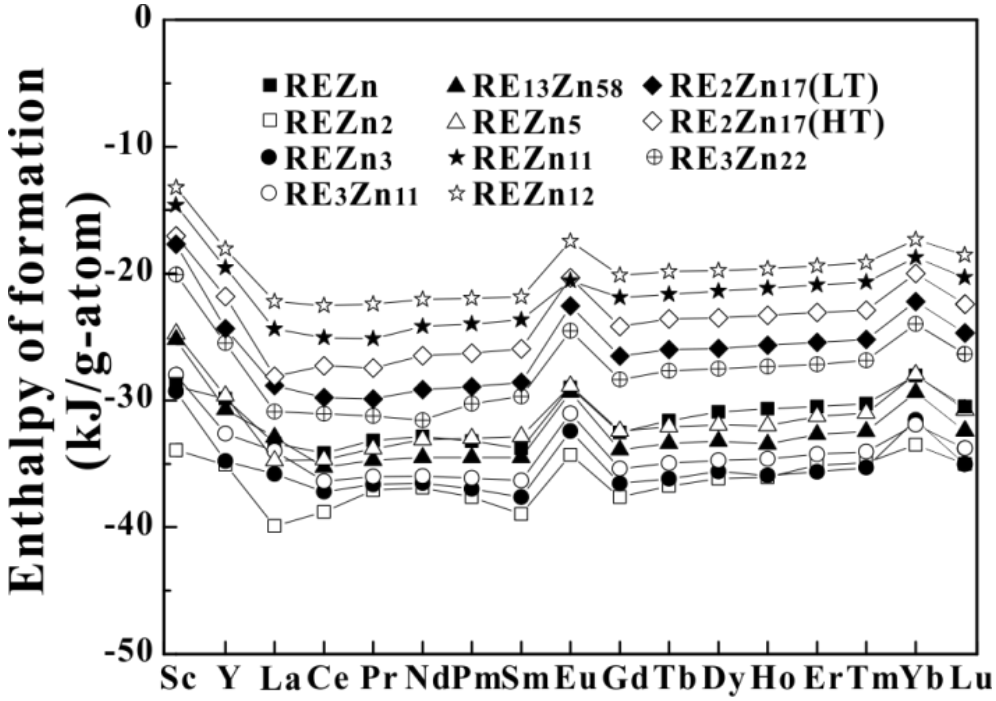

Figure 5.21 Enthalpies of formation of compounds in the Sc-Zn, Y-Zn and RE-Zn systems

Table 5.2 Optimized Gibbs energy of formation (J/g•atom) of intermetallic compounds as in Eq(1) and references for the crystal structure.

(Prototype-Pearson symbol-space group)	Gibbs energy of formation	References for crystal structure
MZn (CsCl-cP2-Pm$\bar{3}$m)		
YZn	-29850+1.71T	[34, 44-46]
EuZn	-28974+3.35T	[47]
GdZn	-32524+2.88T	[48]
TbZn	-31600+2.22T	[34]
DyZn	-30929+2.02T	[34]
HoZn	-30650+1.57T	[34]
ErZn	-30500+1.65T	[32, 34]
TmZn	-30250+1.32T	[44]
YbZn	-28050+4.73T	[49]
LuZn	-30500+1.3T	[50]
MZn_2 (low temperature form, structure unknown)		
α -YZn_2	-37800+6.68T	
α -$YbZn_2$	-35900+8.53T	
MZn_2 ($CeCu_2$-oI12-Imma)		
β -YZn_2	-35067+4.02T	[51]
$EuZn_2$	-34309+5.02T	[47]
$GdZn_2$	-37616+4.46T	[52]
$TbZn_2$	-36733+3.85T	[53]
$DyZn_2$	-36186+3.79T	[52]
$HoZn_2$	-36067+3.43T	[54, 55]
$ErZn_2$	-35100+3.15T	[32, 52]
$TmZn_2$	-34933+2.76T	[52]
β-$YbZn_2$	-33500+5.86T	[56]
$LuZn_2$	-35000+2.74T	[52]
MZn_3 (YZn_3-oP16-Pmna)		
YZn_3	-34775+7.17T	[51]
#$EuZn_3$	-32426+9.41T	
$GdZn_3$	-36537+6.26T	[57]
$TbZn_3$	-36175+5.8T	[57]
$DyZn_3$	-35614+5.75T	[58]
$HoZn_3$	-35925+5.55T	[58]
$ErZn_3$	-35625+5.77T	[32, 59]
$TmZn_3$	-35300+5.48T	[57]
#$YbZn_3$	-32997+8.53T	
$LuZn_3$	-35050+5.46T	[57]
M_3Zn_{11} ($Al_{11}La_3$-oI28-Immm)		
Y_3Zn_{11}	-32635+6.95T	[18, 51, 57]
#Eu_3Zn_{11}	-30988+8.97T	
Gd_3Zn_{11}	-35375+6.45T	[57]
Tb_3Zn_{11}	-34964+6.06T	[57]
Dy_3Zn_{11}	-34727+6.16T	[57]
#Ho_3Zn_{11}	-34604+6.17T	
#Er_3Zn_{11}	-34245+6.43T	
#Tm_3Zn_{11}	-34036+6.43T	
Yb_3Zn_{11}	-31914+7.96T	[41]

#Lu_3Zn_{11}	-33797+6.43T	

$M_{13}Zn_{58}$ ($Gd_{13}Zn_{58}$-hP142-$P6_3mc$)

$Y_{13}Zn_{58}$	-30718+6.72T	[60]
#$Eu_{13}Zn_{58}$	-29347+7.54T	
$Gd_{13}Zn_{58}$	-33898+6.4T	[61]
$Tb_{13}Zn_{58}$	-33380+6.02T	[57]
$Dy_{13}Zn_{58}$	-33222+6.04T	[57]
$Ho_{13}Zn_{58}$	-33437+5.97T	[57]
$Er_{13}Zn_{58}$	-32676+5.53T	[32, 57]
$Tm_{13}Zn_{58}$	-32465+5.38T	[57]
$Yb_{13}Zn_{58}$	-29366+6.51T	[57]
$Lu_{13}Zn_{58}$	-32394+5.7T	[57]

MZn_5 ($ErZn_5$-hP36-$P6_3/mmc$)

YZn_5	-29633+6.82T	[62]
[1]$EuZn_5$	-28870+7.52T	[47]
#$GdZn_5$	-32423+7.17T	[36]
#$TbZn_5$	-32074+7.17T	
#$DyZn_5$	-31935+7.17T	[36]
$HoZn_5$	-31983+6.03T	[62]
$ErZn_5$	-31250+5.55T	[32, 62]
$TmZn_5$	-31000+5.36T	[62]
#$YbZn_5$	-27960+7.17T	
$LuZn_5$	-30733+5.52T	[62]

M_3Zn_{22} (Pu_3Zn_{22}-tI100-$I4_1/amd$)

#Y_3Zn_{22}	-25496+6.97T	
#Eu_3Zn_{22}	-24518+7.81T	
Gd_3Zn_{22}	-28370+6.21T	[57]
#Tb_3Zn_{22}	-27672+6.97T	
#Dy_3Zn_{22}	-27504+6.97T	
#Ho_3Zn_{22}	-27337+6.97T	
#Er_3Zn_{22}	-27170+6.97T	
#Tm_3Zn_{22}	-26835+6.97T	
#Yb_3Zn_{22}	-23990+7.81T	
#Lu_3Zn_{22}	-26333+6.97T	

M_2Zn_{17} (LT) ($Ni_{17}Th_2$-hP38-$P6_3/mmc$)

α-Y_2Zn_{17}	-24347+6.65T	[39]
#α-Eu_2Zn_{17}	-22541+6.69T	
α-Gd_2Zn_{17}	-26500+6.05T	[39]
α-Tb_2Zn_{17}	-26000+5.81T	[39]
α-Dy_2Zn_{17}	-25901+5.84T	[63]
α-Ho_2Zn_{17}	-25658+5.83T	[39]
α-Er_2Zn_{17}	-25421+5.64T	[63]
α-Tm_2Zn_{17}	-25211+5.78T	[39]
α-Yb_2Zn_{17}	-22211+5.81T	[33]
α-Lu_2Zn_{17}	-24674+6.14T	

M_2Zn_{17} (HT) (Th_2Zn_{17}-hR19-$R\bar{3}m$)

β-Y_2Zn_{17}	-21816+4.33T	[64]
#β-Eu_2Zn_{17}	-20330+4.37T	

β-Gd_2Zn_{17}	-24184+3.74T	[64]
β-Tb_2Zn_{17}	-23579+3.49T	[64]
β-Dy_2Zn_{17}	-23480+3.52T	[64]
β-Ho_2Zn_{17}	-23289+3.51T	[64]
β-Er_2Zn_{17}	-23053+3.32T	[64]
β-Tm_2Zn_{17}	-22895+3.46T	[64]
β-Yb_2Zn_{17}	-20000+3.49T	[64]
β-Lu_2Zn_{17}	-22421+3.82T	[64]
MZn_{11} ($BaCd_{11}$-tI48-$I4_1/amd$)		
YZn_{11}	-19552+5.18T	
$EuZn_{11}$	-20571+6.38T	[63]
#$GdZn_{11}$	-21888+6.22T	
$TbZn_{11}$	-21644+-6.22T	
#$DyZn_{11}$	-21400+6.22T	
#$HoZn_{11}$	-21156+6.22T	
#$ErZn_{11}$	-20912+-6.22T	
#$TmZn_{11}$	-20668+6.22T	
$YbZn_{11}$	-18750+4.48T	[39]
#$LuZn_{11}$	-20319+6.22T	
MZn_{12} ($Mn_{12}Th$-tI26-$I4/mmm$)		
YZn_{12}	-18062+4.33T	[65]
#$EuZn_{12}$	-17476+4.51T	
$GdZn_{12}$	-20134+4.51T	[66]
$TbZn_{12}$	-19846+4.37T	[63]
$DyZn_{12}$	-19766+4.36T	[39]
$HoZn_{12}$	-19615+4.35T	[66]
$ErZn_{12}$	-19408+4.21T	[39]
$TmZn_{12}$	-19154+4.27T	[63]
#$YbZn_{12}$	-17315+4.51T	
$LuZn_{12}$	-18538+4.35T	[33]
MZn_{13} ($NaZn_{13}$-cF112-$Fm\bar{3}c$)		
$EuZn_{13}$	-18335+6T	[33]

[1]= reported as ($CaCu_5$-hP6-$P6/mmm$)

#= assumed to be a metastable compound

Table 5.3 Optimized model parameters of Eq (3) for the bcc phase and Optimized Modified Quasichemical Model parameters of Eq (5) for the liquid phase in Y-Zn, Eu-Zn, Gd-Zn, Tb-Zn, Dy-Zn, Ho-Zn, Er-Zn, Tm-Zn, Yb-Zn and Lu-Zn systems (J/mol).

bcc	Liquid (MQM)
$L^0_{Y,Zn} = -47698$	$\Delta g_{YZn} = -29957 + 5.8576T - 6276X_{YY} - 10460X_{ZnZn}$
$L^0_{Eu,Zn} = -31380$	$\Delta g_{EuZn} = -29288 + 5.8576T - 837X_{EuEu} - 15899X_{ZnZn}$
$L^0_{Gd,Zn} = -44350$	$\Delta g_{GdZn} = -29957 + 5.8576T - 2929X_{GdGd} - 20083X_{ZnZn}$
$L^0_{Tb,Zn} = -45606$	$\Delta g_{TbZn} = -29539 + 5.8576T - 2929X_{TbTb} - 20920X_{ZnZn}$
$L^0_{Dy,Zn} = -38074$	$\Delta g_{DyZn} = -28870 + 5.8576T - 2929X_{DyDy} - 20920X_{ZnZn}$
	$\Delta g_{HoZn} = -28451 + 5.8576T - 5439X_{HoHo} - 23849X_{ZnZn}$
	$\Delta g_{ErZn} = -28033 + 5.8576T - 8787X_{ErEr} - 23849X_{ZnZn}$
	$\Delta g_{TmZn} = -27405 + 5.8576T - 6694X_{TmTm} - 24267X_{ZnZn}$
$L^0_{Yb,Zn} = -31380$	$\Delta g_{YbZn} = -26778 + 5.8576T - 1255X_{YbYb} - 16736X_{ZnZn}$
	$\Delta g_{LuZn} = -28786 + 5.8576T - 4184X_{LuLu} - 20920X_{ZnZn}$

5.5 Discussion

The systematic trends in the enthalpies of formation of the compounds across the RE series are evident in Fig. 21. From Table 2 it can be seen that the entropies of formation of all compounds are negative and very similar for all compounds with the same stoichiometry.

Calculated enthalpies and entropies of liquid mixing are shown in Figs. 22 & 23. The curves are very similar for all systems, with the curves for the enthalpies of the Y-Zn, Eu-Zn and Yb-Zn systems lying somewhat above the others, and with minima between 60 and 66 at. % Zn.

As seen in Table 3, a negative excess non-configurational entropy parameter of -5.8576 J/mol K was required in the expansion for Δg_{AB} in the MQM for the liquid phase in all systems. This is consistent with the optimizations of the Mg-RE [8-11] and Al-RE [67, 68] systems where negative excess non-configurational entropy parameters of approximately the same order were always found to be required.

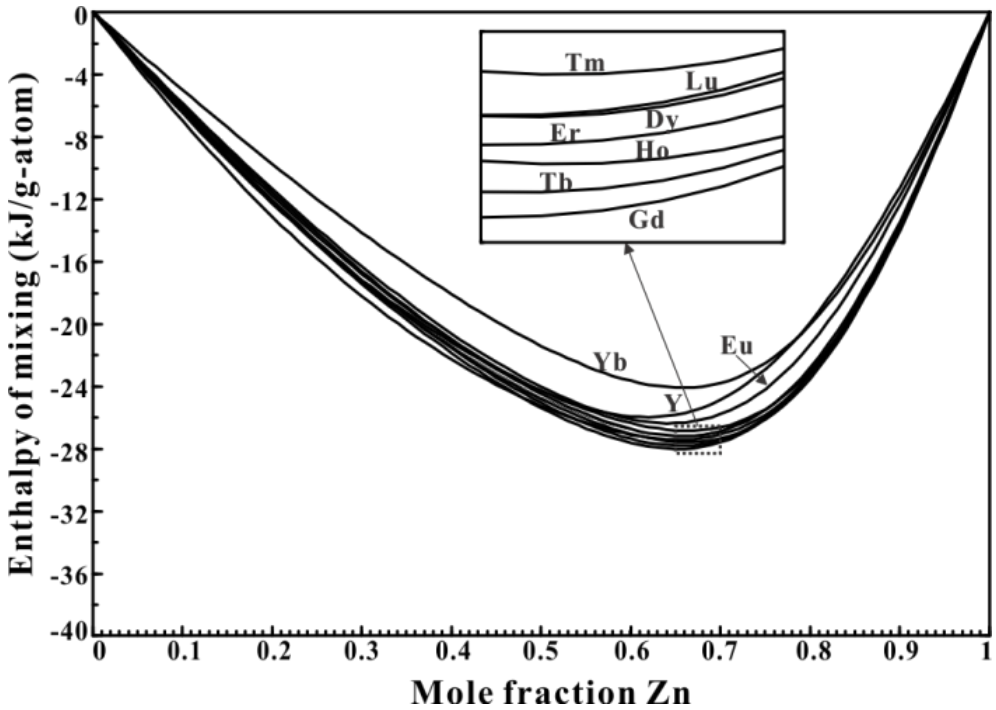

Figure 5.22 Calculated enthalpy of liquid-liquid mixing for Y-Zn, Eu-Zn, Gd-Zn, Tb-Zn, Dy-Zn, Ho-Zn , Er-Zn, Tm-Zn, Yb-Zn and Lu-Zn systems at 1600 ^{o}C

5.6 Conclusions

Assessed optimized model parameters have been obtained giving the thermodynamic properties of all phases in the binary systems Y-Zn, Eu-Zn, Gd-Zn, Tb-Zn, Dy-Zn, Ho-Zn, Er-Zn, Tm-Zn, Yb-Zn and Lu-Zn. In a previous article [12] we reported on the optimizations of the binary systems formed between Zn and the lighter RE elements as well as the Sc-Zn system. In subsequent articles we shall report on optimizations of all the ternary Mg-Zn-RE systems. These parameters will be included in the FTlite light metals database of the FactSage database computing system [69] which already contains optimized parameters for the solid and liquid phases of a large number of binary and ternary Mg- and Al-containing systems. Through the models, the properties and phase equilibria of multicomponent systems can thus be estimated and calculated.

All calculations in the present work were performed with the FactSage software [69].

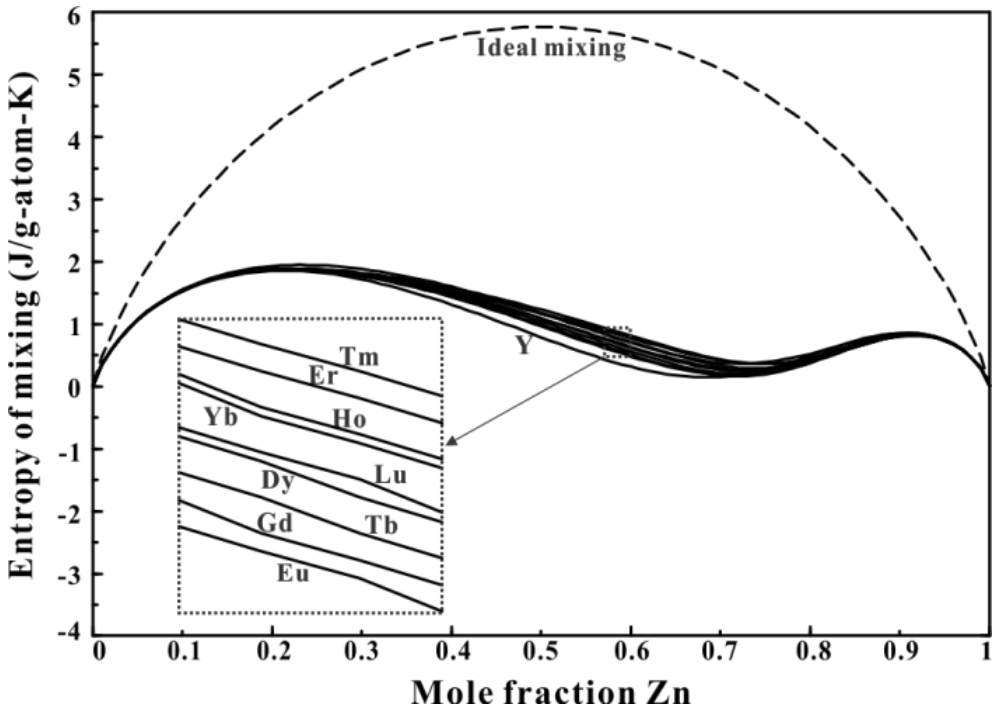

Figure 5.23 Calculated entropy of liquid-liquid mixing for Y-Zn, Eu-Zn, Gd-Zn, Tb-Zn, Dy-Zn, Ho-Zn , Er-Zn, Tm-Zn, Yb-Zn and Lu-Zn systems at 1600 ^{o}C

Acknowledgements

This research was supported by funding from the Natural Sciences and Engineering Research Council of Canada (NSERC) Magnesium Strategic Research Network. More information on the Network can be found at www.MagNET.ubc.ca.

References

[1] J. Bohlen, M.R. Nürnberg, J.W. Senn, D. Letzig, S.R. Agnew, Acta Mater., 55 (2007) 2101-2112.

[2] R.K. Mishra, A.K. Gupta, P.R. Rao, A.K. Sachdev, A.M. Kumar, A.A. Luo, Scripta Mater., 59 (2008) 562-565.

[3] N. Stanford, M.R. Barnett, Mat. Sci. Eng., A-Struct., 496 (2008) 399-408.

[4] K. Hantzsche, J. Bohlen, J. Wendt, K.U. Kainer, S.B. Yi, D. Letzig, Scripta Mater., 63 (2010) 725-730.

[5] B.L. Mordike, T. Ebert, Mat. Sci. Eng., A-Struct., 302 (2001) 37-45.

[6] I.P. Moreno, T.K. Nandy, J.W. Jones, J.E. Allison, T.M. Pollock, Scripta Mater., 48 (2003) 1029-1034.

[7] I. Ansara, G. Effenberg, C. Secretariat, COST 507: Definition of thermochemical and thermophysical properties to provide a database for the development of new light alloys, Office for Official Publications of the European Communities, 1998; P. Spencer, unpublished work

[8] Y.-B. Kang, L. Jin, P. Chartrand, A.E. Gheribi, K. Bai, P. Wu, Calphad, 38 (2012) 100-116.

[9] Y.-B. Kang, A. Pelton, P. Chartrand, P. Spencer, C. Fuerst, J. Phase Equilib. Diff., 28 (2007) 342-354.

[10] Y.-B. Kang, A.D. Pelton, P. Chartrand, C.D. Fuerst, Calphad, 32 (2008) 413-422.

[11] Y.-B.Kang, unpublished work

[12] Z. Zhu, A. Pelton, unpublished work

[13] P. Chiotti, J.T. Mason, Trans. AIME., 239 (1967) 547-552.

[14] P. Chiotti, J.T. Mason, Trans. AIME., 233 (1965) 786-795.

[15] J. Mason, P. Chiotti, Metall. Mater. Trans. B., 1 (1970) 2119-2123.

[16] J.T. Mason, P. Chiotti, Metall. Trans., 3 (1972) 2851-2855.

[17] P. Chiotti, J.T. Mason, K.J. Gill, Trans. AIME., 227 (1963) 910-916.

[18] J.T. Mason, P. Chiotti, Metall. Trans. A., 7 (1976) 287-291.

[19] Y. Hoshino, J.A. Plambeck, Can. J. Chemistry, 48 (1970) 685-687.

[20] V.P. Butorov, I.F. Nichkov, E.A. Novikov, S.P. Raspopin, Izv. Vyssh. Ucheb. Zaved., Tsvet. Met., 16 (1973) 96-102.

[21] M. Morishita, H. Yamamoto, K. Tsuboki, T. Horike, Int. J. Mater. Res., 98 (2007) 10-15.

[22] P. Morin, J. Pierre, J. Chaussy, Phys. Status Solidi A., 24 (1974) 425-432.

[23] C. Marquina, N. H. Kim-Ngan, K. Bakker, R. J. Radwanski, T. H. Jacobs, K. H. J. Buschow, J. J. M. Franse, M. R. Ibarra, J. Phys-Condens Mat., 5 (1993) 2009.

[24] G. Shao, V. Varsani, Z. Fan, Calphad, 30 (2006) 286-295.

[25] X.J. Liu, M.Z. Wen, C.P. Wang, F.S. Pan, J. Alloys Compd., 452 (2008) 283-290.

[26] P.J. Spencer, A.D. Pelton, Y.-B. Kang, P. Chartrand, C.D. Fuerst, Calphad, 32 (2008) 423-431.

[27] D.J. Michel, E. Ryba, P.K. Kejriwal, J. Less-Common Met., 11 (1966) 67-69.

[28] A. Saccone, A.M. Cardinale, S. Delfino, G. Cacciamani, R. Ferro, J. Alloys Compd., 317-318 (2001) 503-512.

[29] A. Saccone, A.M. Cardinale, S. Delfino, R. Ferro, Z. Metallkd., 92 (2001) 959-965.

[30] C. Marquina, N.T.H. Kim-Ngan, K.H.J. Buschow, J.J.M. Franse, M.R. Ibarra, J. Magn. Magn. Mater., 157-158 (1996) 403-404.

[31] V.I. Kober, I.F. Nichkov, S.P. Raspopin, V.M. Kuz'minykh, Splavy Redk. Met. Osobymi Fiz. Svoistvami Redkozem. Blagorodn. Met., (1983) 132-135.

[32] A. Saccone, A.M. Cardinale, S. Delfino, R. Ferro, Z. Metallkd., 96 (2005) 1369-1379.

[33] Y.B. Kuz'ma, P.I. Kripyakevich, N.S. Ugrin, Izv. Akad. Nauk SSSR, Neorg. Mater., 2 (1966) 630-635.

[34] P. Morin, J. Laforest, J. Pierre, J.S. Shah, C. R. Acad. Sci., Ser. B, 277 (1973) 353-354.

[35] A. Saccone, A. Cardinale, S. Delfino, R. Ferro, Metall. Mater. Trans. A., 34 (2003) 743-750.

[36] M.L. Green, J. Less-Common Met., 32 (1973) 391-394.

[37] C.P. Gomez, S. Lidin, Solid State Sci., 4 (2002) 901-906.

[38] L.F. Yamshchikov, F.N. Sattarov, H.I. Moskalenko, Izv. Vyssh. Uchebn. Zaved., Tsvetn. Metall., (1988) 123.

[39] Y.B. Kuz'ma, P.I. Kripyakevich, D.P. Frankevich, Izv. Akad. Nauk SSSR, Neorg. Mater., 1 (1965) 1410-1415.

[40] L.F. Yamshchikov, V.A. Lebedev, I.F. Nichkov, S.P. Raspopin, Russ. Metall., (1985) 218-222.

[41] J.T. Mason, P. Chiotti, Trans. AIME., 242 (1968) 1167-1171.

[42] A.T. Dinsdale, Calphad, 15 (1991) 317-425.

[43] H. Kopp, Phil. Trans. R. Soc. Lond., 155 (1865) 71.

[44] C.C. Chao, H.L. Luo, P. Duwez, J. Appl. Phys., 35 (1964) 257-258.

[45] C.-C. Chao, PhD thesis, California Institute of Technology, United States -- California, 1965, pp. 96.

[46] G. Bruzzone, A.F. Ruggiero, Atti Accad. Nazl. Lincei, Rend. Sci. Fis., Mat. Nat., 33 (1962) 312-314.

[47] A. Iandelli, A. Palenzona, Atti Accad. Naz. Lincei, Cl. Sci. Fis., Mat. Nat., Rend., 37 (1964) 165-168.

[48] U. Koebler, W. Kinzel, W. Zinn, J. Magn. Magn. Mater., 25 (1981) 124-134.

[49] C.C. Chao, P. Duwez, J. Appl. Phys., 37 (1966) 2631-2632.

[50] A. Iandelli, A. Palenzona, J. Less-Common Met., 9 (1965) 1-6.

[51] K.S.S. Harsha, PhD thesis, The Pennsylvania State University, United States -- Pennsylvania, 1964, pp. 132.

[52] M.L. Fornasini, F. Merlo, Atti Accad. Naz. Lincei, Rend., Cl. Sci. Fis. Mat. Natur., 43 (1967) 357-363.

[53] D. Debray, M. Sougi, P. Meriel, J. Chem. Phys., 56 (1972) 4325-4328.

[54] D. Debray, M. Sougi, J. Chem. Phys., 57 (1972) 2156-2159.

[55] D.J. Michel, E. Ryba, J. Less-Common Met., 14 (1968) 367-369.

[56] D.J. Michel, E. Ryba, Acta Crystallogr., 19 (1965) 687-688.

[57] G. Bruzzone, L. Fornasini Maria, F. Merlo, J. Less-Common Met., 22 (1970) 253-264.

[58] D.J. Michel, E. Ryba, Acta Crystall. B-Stru., 24 (1968) 1267-1269.

[59] D.J. Michel, E. Ryba, Scripta Metall., 3 (1969) 683-685.

[60] D.T. Cromer, A.C. Larson, Acta Crystallogr. B., 28 (1972) 1016-1022.

[61] F. Wang, Acta Crystallogr., 22 (1967) 579-584.

[62] M.L. Fornasini, J. Less-Common Met., 25 (1971) 329-332.

[63] A. Iandelli, A. Palenzona, J. Less-Common Met., 12 (1967) 333-343.

[64] T. Siegrist, Y. Le Page, J. Less-Common Met., 127 (1987) 189-197.

[65] J.B. Kusma, E. Laube, Monatsh. Chem., *96* (1965) 1496-1502.

[66] E. Laube, Monatsh. Chem., 97 (1966) 722-732.

[67] L. Jin, Y.-B. Kang, P. Chartrand, C.D. Fuerst, Calphad, 35 (2011) 30-41.

[68] L. Jin, Y.-B. Kang, P. Chartrand, C.D. Fuerst, Calphad, 34 (2010) 456-466.

[69] C.W. Bale, E. Bélisle, P. Chartrand, S.A. Decterov, G. Eriksson, K. Hack, I.H. Jung, Y.B. Kang, J. Melançon, A.D. Pelton, C. Robelin, S. Petersen, Calphad, 33 (2009) 295-311; www.factsage.com

Chapter 6 ARTICLE 3: THERMODYNAMIC MODELING AND *IN-SITU* NEUTRON DIFFRACTION INVESTIGATION OF THE CE-MG-ZN SYSTEM

Submitted to Acta Materialia

Zhijun Zhu[a], Michael Gharghouri[b], Mamoun Medraj[c], Soo Yeol Lee[d] and Arthur D. Pelton[a*],

[a]Centre de Recherche en Calcul Thermochimique, Département de Génie Chimique, Ecole Polytechnique, Montréal, Québec, Canada

[b]Canadian Neutron Beam Centre, Chalk River, Ontario, Canada

[c]Department of Mechanical Engineering, Concordia University, Montréal, Québec, Canada

[d]Department of Materials Science and Engineering, Chungnam National University, Daejeon 305-764, Korea

*Corresponding author

KEY WORDS

Ce-Mg-Zn system, Phase diagram, *In-situ* neutron diffraction, Thermodynamic assessment, Thermodynamic optimization

ABSTRACT

All available phase diagram data for the Ce-Mg-Zn system were critically assessed. *In-situ* neutron diffraction (ND) experiments were performed on selected samples to identify phases and transition temperatures. A critical thermodynamic evaluation and optimization of the Ce-Mg-Zn system was carried out and model parameters for the thermodynamic properties of all phases were obtained. The phase transformation behavior of selected samples was well resolved from the ND experiments and experimental data were used to refine the thermodynamic model parameters.

6.1 Introduction

Magnesium being the lightest structural metal, Mg-based alloys have many applications. Zinc is one of the most commonly used alloying elements in Mg (AZ series), and the rare earth (RE) metals have been shown to improve creep resistance [1, 2] and sheet formability (by reducing texture [3-6]).

Information on phase behavior is essential for the design of new RE-Mg-Zn alloys. However, few studies of the phase diagrams and thermodynamic properties of these systems have been made. The present study was thus undertaken to better define the phase diagrams of the RE-Mg-Zn ternary systems through the technique of critical thermodynamic assessment and optimization coupled with limited experimentation.

In a thermodynamic optimization, adjustable model parameters are calculated using all available thermodynamic and phase-equilibrium data in order to obtain one set of model equations as functions of temperature and composition. Thermodynamic data, such as activities, can aid in the evaluation of the phase diagrams, and information on phase equilibria can be used to deduce thermodynamic properties. With this technique, it is frequently possible to resolve discrepancies in the available data. From the model equations, all of the thermodynamic properties and phase diagrams can be back-calculated, and interpolations and extrapolations can be made in a thermodynamically correct manner. The thermodynamic properties and phase diagrams are thereby rendered self-consistent and consistent with thermodynamic principles, and the available data are distilled into a small set of model parameters, ideal for computer storage. Generally, in the optimization of a ternary system one begins by optimizing the three binary sub-systems. The binary model parameters are then used to estimate the properties of the ternary phases, and these estimates are then refined by introducing ternary model parameters where required to reproduce available ternary data.

Thermodynamic evaluations and optimizations have already been reported for the binary Mg-Zn system [7], all binary Mg-RE systems [8-11] and all binary RE-Zn systems (as well as Sc-Zn and Y-Zn) [12, 13]. In the present article we report on our evaluation, optimization and experimental phase diagram study of the Ce-Mg-Zn system. In subsequent articles we shall report on our evaluations and optimizations of other RE-Mg-Zn systems as well as on our evaluation,

optimization and experimental phase diagram study of the Nd-Mg-Zn system. As expected, all RE-Mg-Zn systems are very similar. The present work on the Ce-Mg-Zn system was greatly aided by our simultaneous assessments of all the other RE-Mg-Zn systems.

6.2 Phase equilibrium and thermodynamic data

The Ce-Mg-Zn system has been investigated by several authors. Different ternary phase names were used by different authors. Phases with ternary phase fields considered in the present optimization are summarized in Table 1. All these phases can also be seen in the calculated isothermal section at 350°C shown in Fig. 1. Our nomenclature for the ternary phases τ1 to τ7 is in agreement with that of Pavlyuk *et al* [14]. The same nomenclature will be adopted for similar phases in other RE-Mg-Zn systems in our future reports. The phase Ce(Mg,Zn) in Table 1 is a solid solution of CeMg and CeZn. The $CeMg_3$ and $CeMg_{12}$ phases are solid solutions with limited solubility of Zn. Although Pavlyuk *et al* [14] and Mostafa and Medraj [20] suggested some solubility of Mg in $CeZn_3$, Ce_3Zn_{11}, $CeZn_5$, α-Ce_2Zn_{17} and $CeZn_{11}$, we have assumed that these and all other binary phases do not extend into the ternary system. The prototypes, Pearson symbols and space groups of all binary phases were given previously [7, 8, 12]. Although Ce_2Mg_{17} and α-Ce_2Zn_{17} have the same structure, they are treated as separate phases in the present study.

The Ce-Mg-Zn system was first investigated by Korol'kov and Sal'dau [16] by thermal analysis (TA). An invariant equilibrium at 341-343°C was reported at a composition of 50-47.5 Zn-2.5 Ce (wt.%). Later, an isothermal section at 300°C was established by Mel'nik *et al* [17] using X-ray diffraction (XRD) analysis. A total of 150 samples were studied, most of which were located in the region bounded by Mg, $MgZn_2$, CeZn and CeMg. Four ternary compounds were identified and their formulae were proposed as follows: $CeMg_7Zn_{12}$, ~$CeMg_3Zn_5$, $Ce_2Mg_3Zn_3$, and ~$Ce(Mg_{0.50\text{-}0.85}Zn_{0.5\text{-}0.15})_9$. Some of the binary and ternary compounds were reported to have limited ternary homogeneity ranges (see Table 1), while CeMg and CeZn were found to form a continuous solid solution. Kolitsch *et al* [18] reviewed all the experimental work on the Ce-Mg-Zn system up to the year 2000. The isothermal section at 300°C proposed by Mel'nik *et al* [17] was redrawn by Kolitsch *et al* [18] to make it consistent with the accepted Mg-Zn binary phase

diagram [19]. The four ternary compounds were denoted τ1, τ3, τ4, τ2 respectively by Kolitsch *et al* [18]; these are the phases called τ5, τ4, τ3 and $CeMg_{12}$, respectively, in the present work.

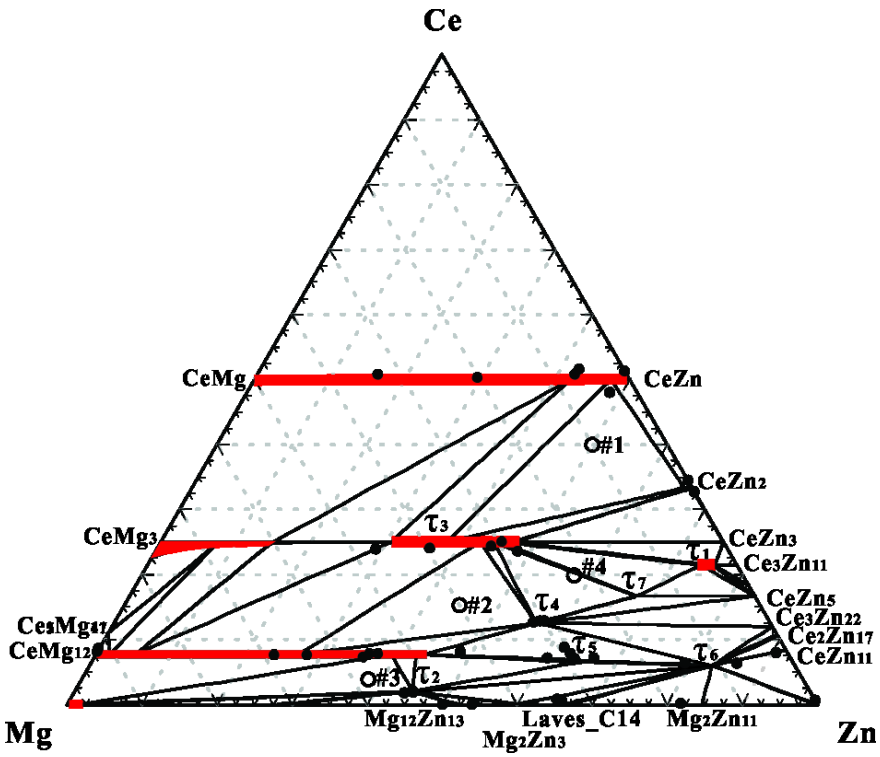

Figure 6.1 Calculated optimized isothermal section (mole fraction) of the Ce-Mg-Zn system at 350°C showing data points of Kevorkov and Pekguleryuz [15] which indicate single-phase regions. Compositions of the four samples used in the present ND experiments are also shown

By means of XRD, TA and scanning electron microscopy (SEM), two isopleths were established by Drits *et al* [21] in the Mg-rich region, as shown in Figs. 2. Two ternary phases were also identified: $Ce(Mg_{0.9\text{-}0.5}Zn_{0.1\text{-}0.5})_{10.1}$ (believed to correspond to the $CeMg_{12}$ solid solution in the present work) and $CeMg_7Zn_{12}$ (believed to correspond to τ5 in the present work).

Table 6.1Phases with ternary phase fields in the Ce-Mg-Zn system

Phase name	Prototype-Pearson symbol-Space group	Thermodynamic model*	
Ce(Mg,Zn)	CsCl-cP2-Pm$\bar{3}$m [14]	Ce(Mg,Zn)	CeMg and CeZn form continuous solution [14, 15, 17, 20]
$CeMg_3$	BiF_3-cF16-Fm$\bar{3}$m [14]	$Ce(Mg,Zn)_3$	Reported Zn solubility 30 at.% at 300°C [17] Reported Zn solubility 36 at.% at 350°C [15] Reported Zn solubility 40 at.% at 197°C [14] Reported Zn solubility 28.4 at.% at 300°C [20]
$CeMg_{12}$	$Mn_{12}Th$-tI26-I4/mmm [14]	$Ce(Mg,Zn)_{12}$	Reported as ~$Ce(Mg_{0.50\text{-}0.85}Zn_{0.5\text{-}0.15})_9$ [17] τ2 in ref [18] with Zn content up to 45 at.% Reported as phase 1, with Zn content 0-48.49 at.% at 350 ^{o}C[15], $Ce(Mg_{0.9\text{-}0.5}Zn_{0.1\text{-}0.5})_{10.1}$ in ref [21] Reported as $Ce(Mg_{0.9\text{-}0.5}Zn_{0.1\text{-}0.5})_{10.1}$ [22] Reported Zn solubility 44.5 at.% at 197 ^{o}C [14] Reported Zn solubility 43.6 at.% at 350 and 400°C [23, 24] Reported Zn solubility 39.4 at.% at 300 ^{o}C [20]
τ1	$Al_{11}La_3$-oI28-Immm [25]	$Ce_3Zn_9(Mg,Zn)_2$	Reported as τ1 with Zn content 64.3-69 at.% [14] Reported as τ1 ($Ce_6Mg_3Zn_{19}$) [20]
τ2	unknown	$Ce_2Mg_{53}Zn_{45}$	Assumed stoichiometric in present study Phase 2 in ref [15], τ2 in ref [14] Reported as τ2 ($CeMg_{29}Zn_{25}$) [20]
τ3	$MnCu_2Al$-cF16-Fm$\bar{3}$m [14, 26]	$CeMg(Mg,Zn)_2$	Reported as τ3 in ref [14] with Zn content 38-50 at.% Phase 3 in ref [15] with proposed Zn content 45-50 at.% Phase 3 in ref [17] with Zn content 35-45 at.% Reported as τ3 in ref [18] Reported as τ3 in ref [20] with Zn content 35-52 at.%
τ4	$TbCu_7$-hP8-P6/mmm [14]	$Ce_2Mg_5Zn_9$	Assumed stoichiometric in present study Phase 2 in ref [17], τ3 in ref [18] Phase 4 in ref [15] , τ4 in ref [14] and [20]
τ5	$Ce_3Mg_{13}Zn_{30}$-hP92-$P6_3$/mmc [14]	$Ce_3Mg_{13}Zn_{30}$	Assumed stoichiometric in present study. Phase 1 in ref [17], τ1 in ref [18], phase 5 in ref [15], τ5 in ref [14] and [20], $CeMg_7Zn_{12}$ in ref [21]
τ6	unknown	$Ce_6Mg_{11}Zn_{83}$	Assumed stoichiometric in present study Phase 6 in ref [15] ,τ6 in ref [14] and [20]
τ7	$Ce_{20}Mg_{19}Zn_{81}$-cF480-F$\bar{4}$3m [27]	$Ce_{20}Mg_{19}Zn_{81}$	Assumed stoichiometric in present study, τ6 in ref [14] Reported as τ7 [20]

*Elements within brackets substitute on the same sublattice.

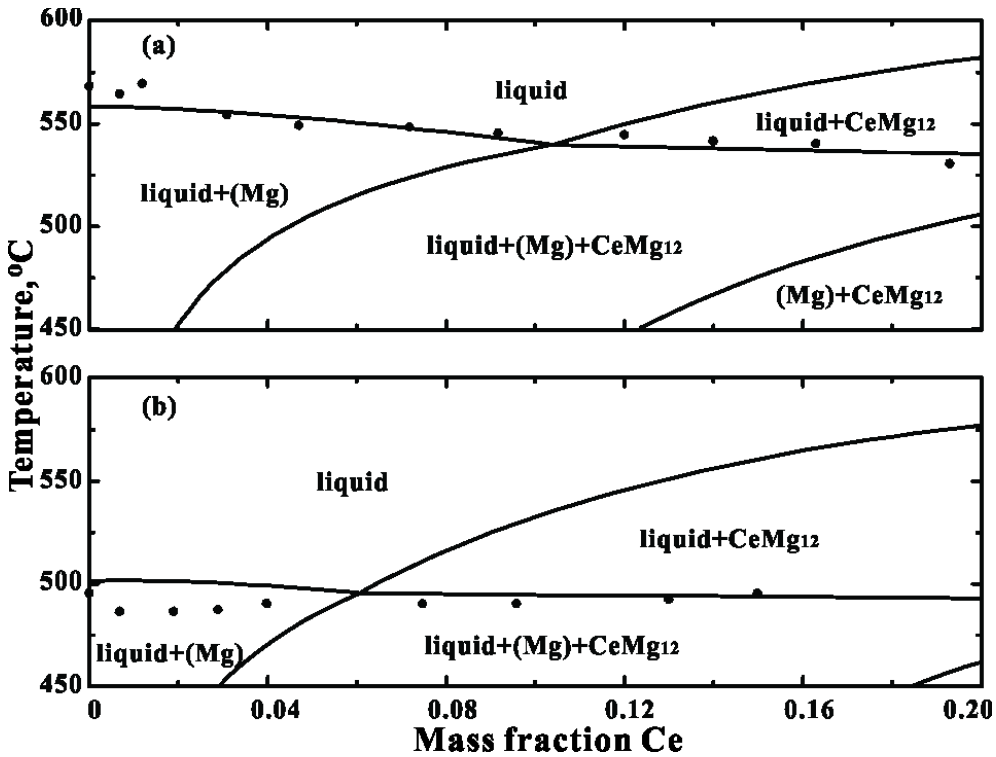

Figure 6.2. Calculated optimized isopleth with constant Zn content of 24 wt.% (a) and 34 wt.% (b) in the Ce-Mg-Zn system showing points from Drits *et al* [21].

A ternary phase with constant Ce content of ~7.7 at.% was reported by Huang *et al* [23, 24] based on their analysis of equilibrium alloys at 350°C and 400°C. This phase is treated as $CeMg_{12}$ in the present study.

Using diffusion couple techniques, Kevorkov and Pekguleryuz [15] investigated the Ce-Mg-Zn phase diagram at 350°C. Their points are shown in Fig.1. These points all represent single-phase compositions [15]. Solubilities in binary and ternary solid solutions were determined by energy dispersive spectroscopy (EDS) and electron probe microanalysis (EPMA). Two new ternary compounds, called τ2 and τ6 in the present work, were reported. τ2 was denoted as ~$Ce_2Mg_{53}Zn_{45}$ while τ6 was reported to be a solid solution with constant Ce content of ~6 at.% and Mg content of ~7.5-14.5 at.%. Due to its limited solubility and unknown crystal structure, τ6 is assumed to be a stoichiometric phase in the present work as shown in Table 1. The $Ce(Mg_{0.9-0.5}Zn_{0.1-0.5})_{10.1}$ phase reported in ref [22] was shown to be part of the $CeMg_{12}$ solution which can dissolve Zn up to 48.49 at.% according to the EDS measurements.

The Ce-Mg-Zn system was later investigated by Chiu *et al* [28]. Ten samples were prepared and studied by Differential Scanning Calorimetry (DSC). However, only data from Mg-

rich samples were interpreted by the authors. Some of the tie-triangles were experimentally validated but no details of the experiments were given. Their results will be shown later in Section 5.

An isothermal section at 197°C was later constructed by Pavlyuk *et al* [14] using XRD, wavelength dispersive spectrometry (WDS) and EPMA. Their diagram will be shown later in Section 5. A total of 53 samples were prepared covering the entire ternary composition range. All ternary compounds reported by Kevorkov and Pekguleryuz [15] were confirmed. In addition, two new compounds were identified: $Ce_3(Zn_{0.863}Mg_{0.137})_{11}$ and $Ce_{20}Mg_{19}Zn_{81}$ (τ1 and τ7 in the present work). Although $Ce_3(Zn_{0.863}Mg_{0.137})_{11}$ and Ce_3Zn_{11} have the same structural prototype, Pavlyuk *et al* [14] treated them as two separate phases. They argued that the lattice parameters of these two phases differ significantly and a sample consisting of these two phases at equilibrium was observed.

The isothermal section at 300°C was recently investigated by Mostafa and Medraj [20] over the entire composition range using diffusion couples. Their reported isothermal section [20] is shown later in Fig. 6(a). All the ternary phases reported by Pavlyuk *et al* [14] were confirmed. In addition, the ternary solution phase proposed by Huang *et al* [23, 24] was also reported, but its crystal structure was not resolved.

Based on the available experimental data from the literature, the following phases with ternary phase fields are considered in the present work (see Fig.1 and Table 1):

<u>Ce(Mg,Zn)</u>: The CeMg and CeZn binary phases both have the CsCl structure and in all reported isothermal sections [14, 15, 17, 20] they form a continuous solution. The reported lattice constant of CeMg at room temperature is 0.3898 nm [29] and that of CeZn is 0.3696 nm [30], while that of the Ce(Mg,Zn) solution is 0.3730 nm at 40 at.%Zn and 0.384 nm at 10 at.%Zn [14]. The Ce content is constant at 50 at.%. Consequently, the model Ce(Mg,Zn) was chosen in the present optimization, in which Mg and Zn substitute on one sublattice while Ce occupies a second sublattice.

<u>$CeMg_3$</u>: Zn can substitute for Mg in $CeMg_3$ [14, 15, 17, 20]. Consequently, the model $Ce(Mg,Zn)_3$ is used. The phase has the same structure as $CeMg_3$. The solubility of Zn in $CeMg_3$ as reported by different authors is summarized in Table 1. The lattice constant of binary $CeMg_3$

was reported to be 0.7443 nm [31], decreasing with increasing Zn content to 0.7077 nm at 40 at.%Zn [14] which is due to the smaller atomic radius of Zn compared to Mg.

<u>$CeMg_{12}$</u>: A ternary phase with approximately the same mole fraction of Ce (~$Ce(Mg_{0.50-0.85}Zn_{0.5-0.15})_9$ [17], $Ce(Mg_{0.9-0.5}Zn_{0.1-0.5})_{10.1}$ [21], a ternary phase with ~7.7 at.% Ce [23, 24] and τ8 in ref [20]) was reported by several investigators who treated the ternary phase and $CeMg_{12}$ as separate phases. However, other investigators reported [14, 15, 28] that the ternary phase is actually continuous with $CeMg_{12}$ (see Fig.1). This point is still a subject of controversy. In the present work we have found that one continuous phase with the model $Ce(Mg,Zn)_{12}$ is most consistent with all the data.

<u>τ1</u>: The structural prototype of both τ1 and the Ce_3Zn_{11} binary phase is $Al_{11}La_3$. However, Pavlyuk *et al* [14] showed that they have been observed to coexist and their lattice constants differ significantly; the lattice constant of τ1, when extrapolated to the binary composition of Ce_3Zn_{11}, does not coincide with that of Ce_3Zn_{11}. Hence, in the present work, we treat them as two separate phases. In the $Al_{11}La_3$ prototype there are 6 distinct sites: 2*a*, 2*c*, 4*g*, 4*j* and two 8*l* sites [32], the 2*a* and 4*g* sites being occupied by La. The crystal structure of τ1 was resolved by Pavlyuk *et al* from single crystal data [25]: the 2*a* and 4*g* sites are occupied solely by Ce (Ce does not enter the other sites, thereby giving a constant Ce mole fraction); the two 8*l* sites are occupied solely by Zn and the 2*c* and 4*j* sites can be occupied by Mg and Zn. However, since the lowest Zn content reported by Pavlyuk *et al* [14] was 64.2 at.%, which is the case when the 2*c* and the two 8*l* sites are fully occupied by Zn and the 4*j* sites are fully occupied by Mg, the model $Ce_2Zn_2Ce_4(Mg,Zn)_4Zn_8Zn_8$ (simplified to $Ce_3Zn_9(Mg,Zn)_2$) seems more reasonable for τ1.

<u>τ2</u>: This phase was reported as phase 2 by Kevorkov and Pekguleryuz [15], as τ2 by Pavlyuk *et al* [14], and as τ2 ($CeMg_{29}Zn_{25}$) by Mostafa and Medraj [20]. The crystal structure remains unknown. EDS measurement [15] gave a composition of $Ce_{1.82}Mg_{53.14}Zn_{45.04}$ in good agreement with EPMA measurements [14] which gave a composition of $Ce_{1.8}Mg_{53.1}Zn_{45.1}$. No solubility information on this phase can be found. Consequently, it is treated in the present work as a stoichiometric compound, with the suggested formula $Ce_2Mg_{53}Zn_{45}$.

<u>τ3</u>: The τ3 phase was first reported by Mel'nik *et al* [17] with a lattice constant of 0.7064 nm. The prototype was reported to be either $MgLi_2Ag$ or $AlMnCu_2$. The crystal structure was

later resolved by Pavluyk *et al* [14, 26]; the prototype was determined from single crystal X-ray diffraction measurements to be $AlMnCu_2$ with a lattice constant ranging from 0.7035 to 0.7036 nm depending on the Zn content. Given that the maximum Zn content of this phase is reported as 50 at.% [14, 15], 45 at.% [17], or 52 at.% [20] the model $CeMg(Mg,Zn)_2$ is used in the present work.

τ4, τ5, τ6 and τ7: Although some limited solubility is reported for these four phases [14, 15, 17, 20], they are treated in the present work as stoichiometric phases, with suggested stoichiometries $Ce_2Mg_5Zn_9$, $Ce_3Mg_{13}Zn_{30}$, $Ce_6Mg_{11}Zn_{83}$, and $Ce_{20}Mg_{19}Zn_{81}$, respectively, based on the reported compositions. The crystal structures of τ4 and τ5 were obtained by Pavlyuk *et al* [14] from XRD powder diffraction data while that of τ7 was resolved from single crystal data [27]. The crystal structure of τ6 remains unknown.

It may be noted that phases similar to all the ternary phases shown in Table 1 have been observed in several other RE-Mg-Zn systems with the exception of the τ1, τ2, τ6 and τ7 phases. However, investigations have not been carried out in the composition regions where these four phases appear in any system other than the Ce-Mg-Zn and Nd-Mg-Zn systems (τ1, τ2, and τ7 were reported in the Nd-Mg-Zn system [33]).

6.3 Experimental investigation

In-situ neutron diffraction (ND) was used in the present work to investigate the phase transformation behavior in order to validate and refine the thermodynamic modelling.

Neutron diffraction data were acquired using the C2 powder diffractometer of the Canadian Neutron Beam Centre, located at the National Research Universal (NRU) reactor, Canadian Nuclear Laboratories (CNL). Diffraction from the (531) reflection of a silicon single crystal monochromator produced incident neutrons with a nominal wavelength of 0.133 nm. The C2 diffractometer is equipped with an 800-channel detector covering an 80° range in scattering angle 2θ, allowing multiple diffraction peaks to be acquired simultaneously.

The four sample compositions shown in Fig. 1 and Table 1 were selected based on preliminary optimizations of the isothermal phase diagram at 300°C. Sample compositions

corresponding to three-phase regions were chosen as they were expected to exhibit the greatest number of transitions, thereby providing the most information.

All samples were prepared from Ce (99.9 wt.%, STREM Chemicals Inc., Newburyport, MA, USA), Mg (99.8 wt.%, CANMET Materials Technology Laboratory , Ottawa, ON, Canada) and Zn (99.9 wt.%, Alfa Aesar, Haverhill, MA, USA) in an induction furnace under an Ar atmosphere. Crucibles were made from 0.15 mm thick Ta foil with a purity of 99.5 wt. %. All samples were melted three times to improve homogeneity. ICP tests (Inductively Coupled Plasma mass spectrometry) showed that Zn losses of 5 wt.% by vaporization occurred during melting. Consequently, an excess of 5 wt.% Zn was added before melting.

Figure 3 shows the furnace used for the NPD experiments. Two infrared lamps were used to heat the samples. Crucibles were made of 304 stainless steel for samples #1, #2 and #3. For sample #4, a Ta crucible was required because of the high melting point. The use of a Ta crucible also simplified the analysis of the diffraction patterns since Ta has fewer diffraction peaks than stainless steel. Stainless steel, however, is less expensive. An eccentrically loaded motor was attached to the top of the furnace to vibrate the sample in order to weaken preferred orientation and to avoid super-cooling that occurred during preliminary tests performed without vibrating the sample. All the ND experiments were carried out under a flowing Ar atmosphere.

In an *in-situ* ND experiment, diffraction patterns are acquired as a function of temperature as a specimen is heated or cooled. Each crystallographic phase in the specimen produces a distinct set of diffraction peaks, with the intensity of each diffraction peak proportional to the quantity of the corresponding phase in the specimen. During cooling or heating, a transition temperature is thus the temperature at which the diffraction peaks for a given phase first appear or completely disappear. Due to limitations in the sensitivity of the technique, diffraction peaks for new phases are typically not detectable until the temperature is somewhat below or above the equilibrium transition temperature. In order to quantify the offset associated with the sensitivity of the method, heating and cooling ND measurements on pure Mg were carried out. The apparent melting temperature of pure Mg was determined to be 640°C upon heating and 635°C upon cooling. The accepted melting temperature of pure Mg is 650°C [34]. Hence, all reported

temperatures shown in the present report have been corrected by 15°C because only *in-situ* data collected during cooling were analyzed.

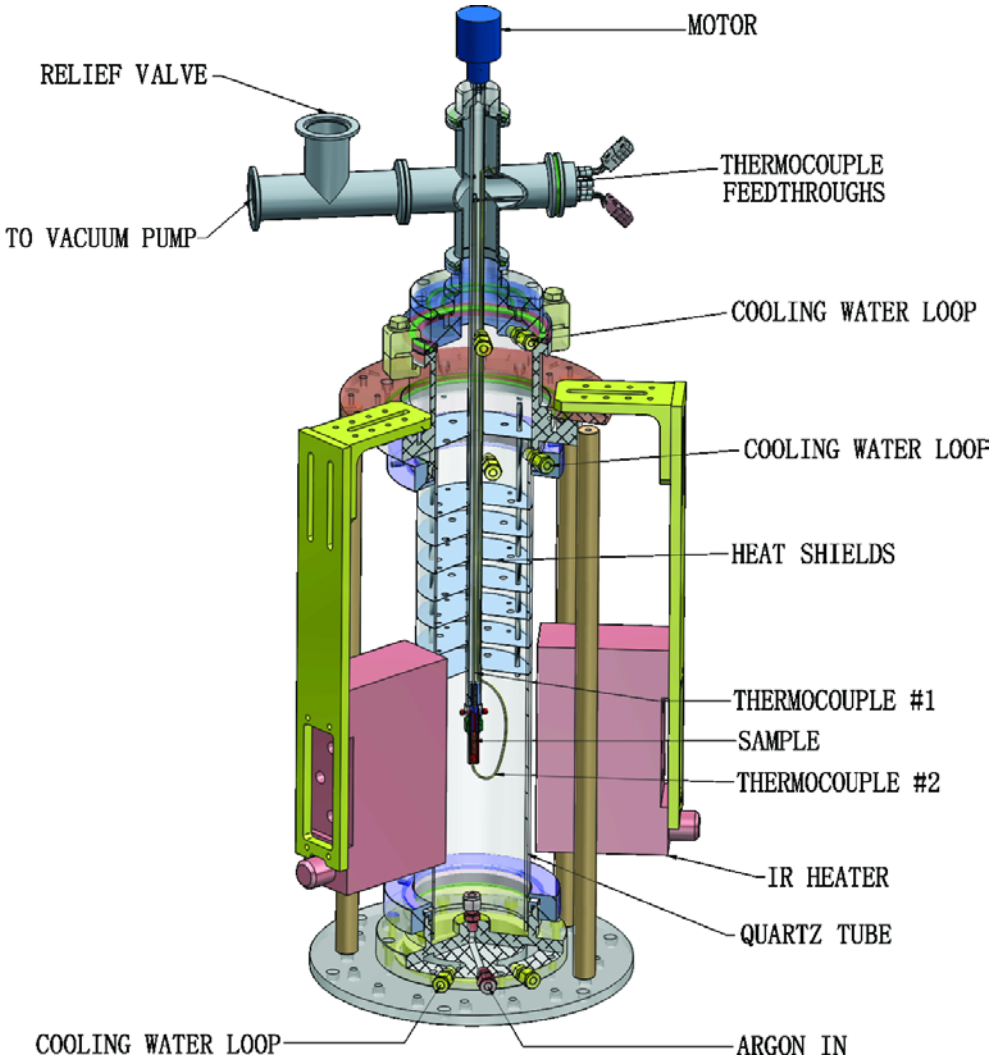

Figure 6.3. Schematic drawing of the furnace used for the ND experiments.

Several samples were prepared for preliminary tests. ICP measurements were performed on these samples before and after the ND experiments. It was found that the change in composition during the ND experiments was very limited, typically less than 2 at.% for any component.

XRD was also performed to identify the phases present in the as-cast alloys. The information obtained from XRD was used as a starting point to index the subsequent ND results. Rietveld analysis was performed on the ND patterns as well as the XRD patterns using the

GSAS/EXPGUI software [35]. Transition temperatures obtained from the ND experiments are summarized in Table 2.

Table 6.2. Sample compositions and transition temperatures measured in NPD experiments

Sample No.	Composition (at.%)	Transition temperatures (±2.5°C)	Phase first appearing below this temperature
#1	$Ce_{40}Mg_{10}Zn_{50}$	735°C	$CeZn_2$
		720°C	Ce(Mg,Zn)
		665°C	τ3
#2	$Ce_{16}Mg_{40}Zn_{44}$	700 °C	τ3
		615 °C	τ1
		550 °C	$CeMg_{12}$
#3	$Ce_4Mg_{58}Zn_{38}$	555 °C	$CeMg_{12}$
		455 °C	τ6?
		365 °C	(Mg), hcp
#4	$Ce_{20}Mg_{22}Zn_{58}$	730 °C	τ1
		710 °C	τ3

? Possible phase

In the ND experiments it was found from initial tests that the intensity of the diffraction peaks for newly precipitated phases stabilized very quickly (within 3 minutes) as the temperature changed. Consequently, in later experiments, diffraction patterns were recorded at intervals of 5°C, with an acquisition time of 3 minutes at each temperature. In this way, relatively accurate transformation temperatures could be obtained within a reasonable amount of beam time.

6.3.1 Sample #1 ($Ce_{40}Mg_{10}Zn_{50}$)

Figure 4(a) shows ND patterns for sample #1 obtained upon cooling. Although patterns were acquired every 5°C, only a few selected patterns are shown. A hump around 2θ = 30° due to the liquid phase is visible at 765°C. All other peaks above background at this temperature correspond to the crucible or the thermocouples, indicating that the sample was entirely in the liquid state at 765°C. Patterns for 735°C, 720°C and 665°C were obtained just after the appearance of a new phase. Analysis of the patterns shows that $CeZn_2$ is the first phase to appear upon cooling at 735°C, followed by Ce(Mg,Zn) at 720°C and τ3 at 665°C. The diffraction peaks corresponding to these precipitating phases are weak but discernible, despite the short acquisition

time (3 minutes). The pattern at 645°C shows no new peaks compared with those observed at 665°C. The derived transition temperatures for sample #1 are shown on Fig. 5(a).

The room temperature lattice constant of the Ce(Mg,Zn) phase was 0.3712 nm which is closer to that of CeZn (0.3696 nm [30]) than that of CeMg (0.3898 nm [29]), consistent with the phase relationships in Fig. 1.

6.3.2 Sample #2 ($Ce_{16}Mg_{40}Zn_{44}$)

ND patterns at selected temperatures for sample #2 are shown in Fig. 4(b). The primary phase for this sample is τ3, which forms at 700°C. τ1 appears at 615°C and $CeMg_{12}$ is first detected at 550°C. At 370°C, no new peaks other than those at 550°C were are observed. τ3 and τ1 have their strongest diffraction peak at 2θ = ~30°, making the analysis difficult. Furthermore, diffraction peaks from the sample are much weaker than those from the crucible and thermocouple, further complicating the analysis. The measured transition temperatures for sample #2 are shown on Fig. 5(b).

6.3.3 Sample #3 ($Ce_{4}Mg_{58}Zn_{38}$)

ND patterns at selected temperatures for sample #3 are shown in Fig. 4(c). The first phase that appears upon cooling is $CeMg_{12}$ which forms at 555°C. At 505°C, no additional peaks are observed. At 455°C, a weak diffraction peak appears on the shoulder of the strong stainless steel peak at a scattering angle of ~37°. The diffraction peak could not be indexed, but we believe it to correspond to τ6, which would be consistent with our thermodynamic analysis. Peaks from the hcp (Mg) phase are first observed at 365°C. The measured transition temperatures for sample #3 are shown on Fig. 5(c).

The lattice constants of $CeMg_{12}$ measured for sample #3 (a = b = 0.9592 nm; c = 0.5608 nm) are smaller than those measured in sample #2 (a = b = 0.9791 nm; c = 0.5616 nm). Since the atomic size of Zn is smaller than that of Mg, this result indicates a higher content of Zn in sample #3 than in sample #2 in agreement with the phase relationships in Fig. 1.

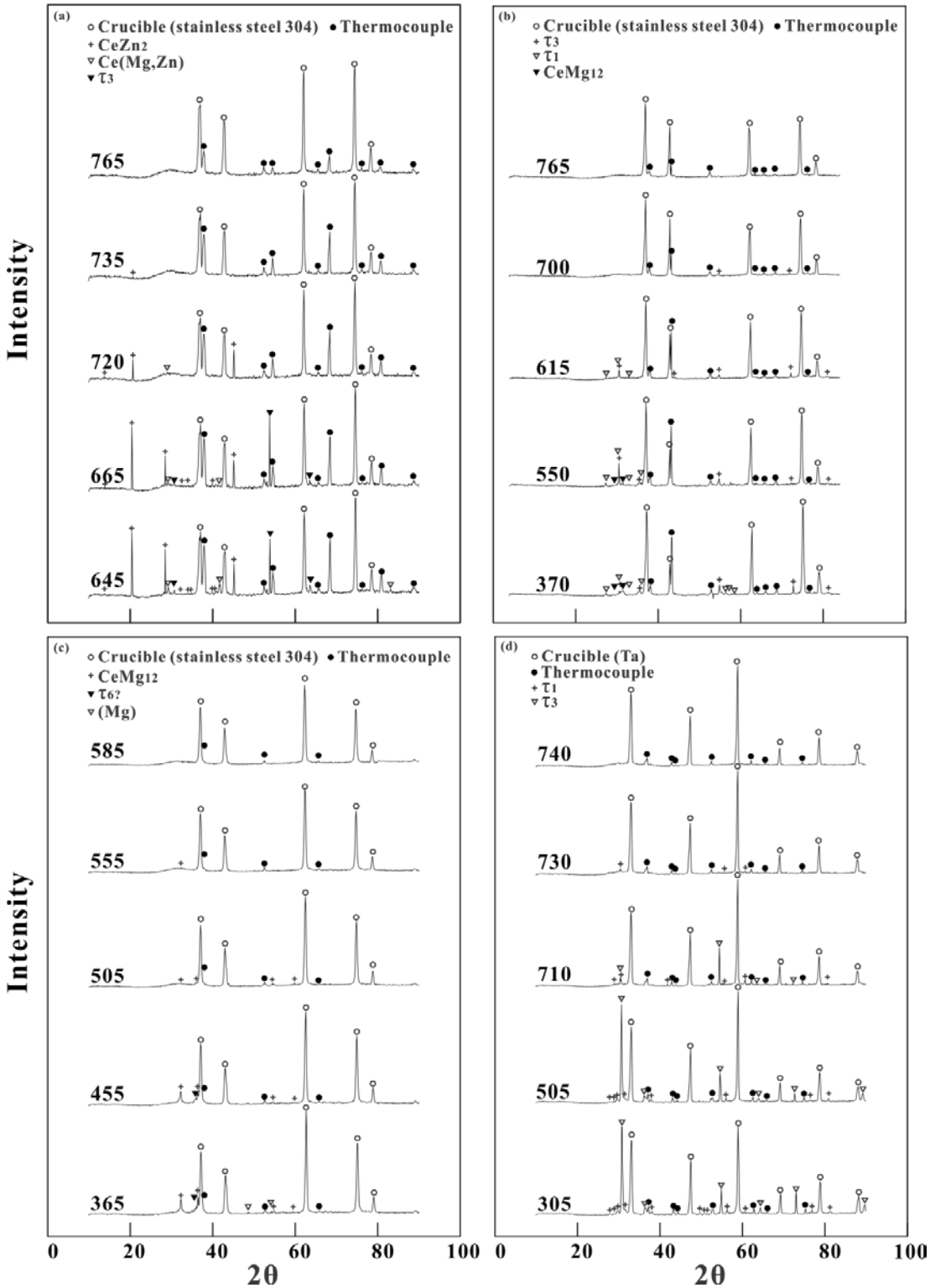

Figure 6.4. Selected NPD patterns for (a) $Ce_{40}Mg_{10}Zn_{50}$, (sample #1), (b) $Ce_{16}Mg_{40}Zn_{44}$, (sample #2), (c) $Ce_{4}Mg_{58}Zn_{38}$, (sample #3) and (d) $Ce_{20}Mg_{22}Zn_{58}$, (sample #4)

6.3.4 Sample #4 ($Ce_{20}Mg_{22}Zn_{58}$)

Figure 4(d) shows selected ND patterns for $Ce_{20}Mg_{22}Zn_{58}$. Analysis of the patterns shows that only two phases were observed to form during cooling with τ1 forming below 730°C and τ3 below 710°C. The τ3 peak at 2θ = ~30° is very strong, indicating preferred orientation. The measured transition temperatures for sample #4 are shown in Fig. 5(d).

Our refined values for the lattice constants of the τ3 phase for samples #1, 2 and 4 were nearly identical (0.7049(0), 0.7049(8) and 0.7048(5) nm respectively), indicating that the compositions of this phase are very similar in the three samples, in agreement with the phase relationships shown in Fig. 1.

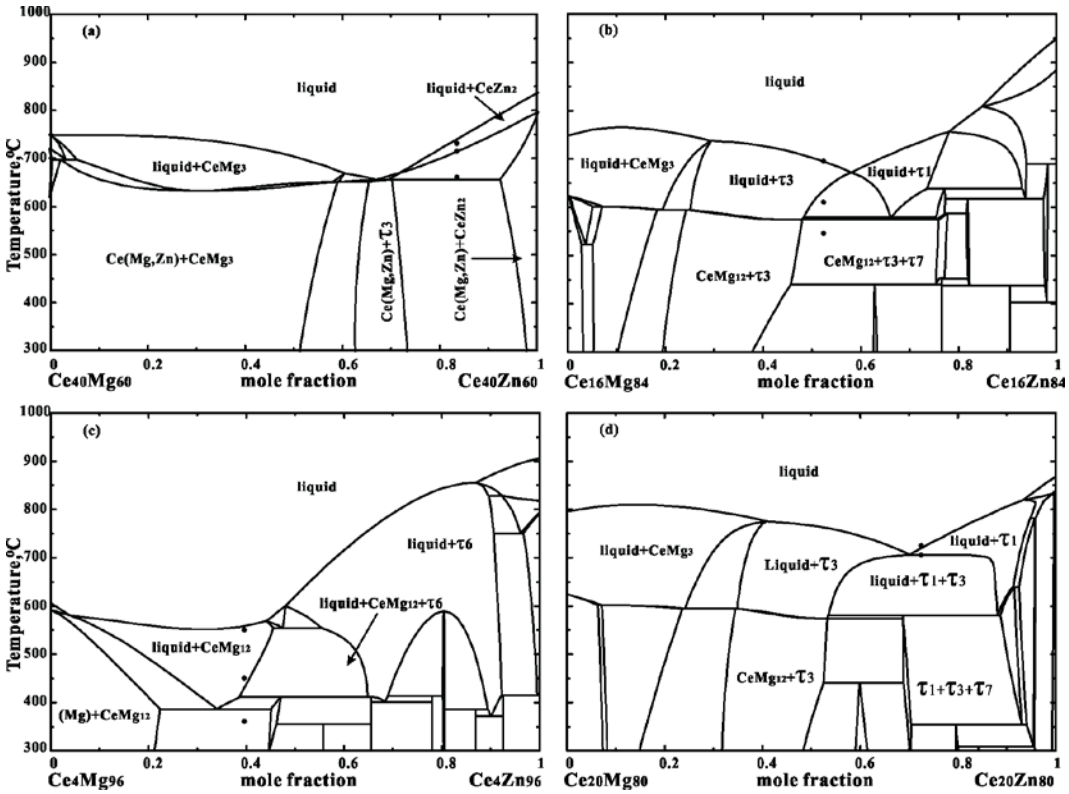

Figure 6.5. Calculated optimized isopleths of the (a) $Ce_{40}Mg_{60}$-$Ce_{40}Zn_{60}$, (b) $Ce_{16}Mg_{84}$-$Ce_{16}Zn_{84}$, (c) Ce_4Mg_{96}-Ce_4Zn_{96} and (d) $Ce_{20}Mg_{80}$-$Ce_{20}Zn_{80}$ sections showing experimental transition temperatures from samples #1, #2, #3 and #4, respectively

6.4 Thermodynamic optimizations

Thermodynamic data for the pure elements were given previously [7, 8, 12]. The optimized thermodynamic model parameters of the three binary sub-systems were taken from Ansara *et al* [7] (Mg-Zn), Kang *et al* [8] (Ce-Mg) and Zhu and Pelton [12] (Ce-Zn).

For the three binary sub-systems, the Modified Quasichemical Model (MQM) [36, 37], which takes account of short-range ordering, was used to model the liquid phase. Consequently, the MQM is used to model the liquid phase in the ternary system. For details of the model, see references [12, 13, 36, 37]. The symmetric (Kohler-like) model [37] was used to estimate the properties of the ternary liquid phase from the optimized binary model parameters. No additional ternary model parameters were introduced.

In the optimization of the Mg-Zn binary system, Ansara *et al* [7] did not use the MQM for the liquid phase. Consequently, the liquid phase was remodelled using the MQM, keeping the same parameters as Ansara *et al* [7] for all other Mg-Zn binary phases. The "coordination numbers", which are MQM model parameters, were set to

$$Z^{Mg}_{Mg,Zn} = Z^{Zn}_{Mg,Zn} = Z^{Mg}_{Mg,Mg} = Z^{Zn}_{Zn,Zn} = 6 \qquad 6.1$$

and the MQM model parameters were introduced as

$$\Delta g_{MgZn} = -6778 + 3.138T + (-1966 + 2.008)X_{MgMg}$$
$$+(-3975 + 1.6736)X_{ZnZn} \text{ (J/g-atom)} \qquad 6.2$$

The binary Bcc_A2, Fcc_A1 and Hcp_A3 solutions are described by a substitutional solution model as discussed previously [12].

As shown in Table 1, Mg and Zn can substitute for each other on one sublattice in some phases (τ1, τ3, Ce(Mg,Zn), $CeMg_3$, $CeMg_{12}$). These phases are modeled with the Compound Energy Formalisim (CEF) [38]. For example, the Gibbs energy of Ce(Mg,Zn) (per mole of formula) can be expressed as follows:

$$G^{Ce(Mg,Zn)} = y_{Mg}G^{0,Ce(Mg,Zn)}_{Ce:Mg} + y_{Zn}G^{0,Ce(Mg,Zn)}_{Ce:Zn} + RT\left(y_{Mg}lny_{Mg} + y_{Zn}lny_{Zn}\right)$$
$$+y_{Mg}y_{Zn}(L^{0}_{Ce:Mg,Zn} + (y_{Mg} - y_{Zn})\,L^{1}_{Ce:Mg,Zn}) \qquad 6.3$$

where y_{Mg} and $y_{Zn}$are the site fractions of Mg and Zn in the second sublattice, $G_{Ce:Mg}^{0,Ce(Mg,Zn)}$ and $G_{Ce:Zn}^{0,Ce(Mg,Zn)}$ are the Gibbs energies of the end-members (CeMg and CeZn) at temperature T under the convention that the enthalpies of the elements are equal to zero in their stable states at 298.15K, and $L_{Ce:Mg,Zn}^{0}$ and $L_{Ce:Mg,Zn}^{1}$ are interaction parameters to be optimized. The Gibbs energies of τ1, τ3, $CeMg_3$ and $CeMg_{12}$ can be expressed similarly.

The τ2, τ4, τ5, τ6 and τ7 phases are treated as stoichiometric compounds.

Table 6.3. Thermodynamic model parameters optimized in the present work for the Ce-Mg-Zn system

Phase name	Model	Parameters (J/g-atom)
Ce(Mg,Zn)	Ce(Mg,Zn)	Ideal mixing
$CeMg_3$	$Ce(Mg,Zn)_3$	$G_{Ce:Zn}^{0,CeMg_3} = -34204 + 5.23T$
		$L_{Ce:Mg,Zn}^{0,CeMg_3} = -4184$
		$L_{Ce:Mg,Zn}^{1,CeMg_3} = -2092$
$CeMg_{12}$	$Ce(Mg,Zn)_{12}$	$L_{Ce:Mg,Zn}^{0,CeMg_{12}} = -2248$
τ1	$Ce_3Zn_9(Mg,Zn)_2$	$G_{Ce:Zn:Mg}^{0,\tau1} = -31380 + 2.99T$
		$G_{Ce:Zn:Zn}^{0,\tau1} = -36334 + 6.45T$
τ2	$Ce_2Mg_{53}Zn_{45}$	$G_{Ce:Mg:Zn}^{0,\tau2} = -10547 + 0.92T$
τ3	$Ce(Mg,Zn)_2Mg$	$G_{Ce:Mg:Mg}^{0,\tau3} = -19000 + 6.63T$
		$G_{Ce:Zn:Mg}^{0,\tau3} = -34037 + 6.28T$
		$L_{Ce:Mg,Zn:Mg}^{0,\tau3} = 1046$
		$L_{Ce:Mg,Zn:Mg}^{1,\tau3} = 4184$
τ4	$Ce_2Mg_5Zn_9$	$G_{Ce:Mg:Zn}^{0,\tau4} = -25724 + 5.23T$
τ5	$Ce_3Mg_{13}Zn_{30}$	$G_{Ce:Mg:Zn}^{0,\tau5} = -20465 + 3.94T$
τ6	$Ce_6Mg_{11}Zn_{83}$	$G_{Ce:Mg:Zn}^{0,\tau6} = -23389 + 4.89T$
τ7	$Ce_{20}Mg_{19}Zn_{81}$	$G_{Ce:Mg:Zn}^{0,\tau7} = -30193 + 4.20T$

No thermodynamic properties for the ternary compounds could be found in the literature. To obtain initial estimates of the enthalpies and entropies of formation of the ternary compounds, three lines passing through the compound on the ternary Gibbs triangle were drawn parallel to the three edges of the triangle. The six intersection points of these lines with the edges defined six "binary compounds" whose enthalpies and entropies were then averaged to give the initial estimates. Thereafter, these values were adjusted to best reproduce the available data.

All model parameters optimized in the present work are listed in Table 3. All other model parameters (apart from the MQM parameters for liquid Mg-Zn shown in Section 4) have been given previously [7, 8, 12]. Very few model parameters are required. The enthalpies of formation of all compounds have reasonable values. The entropies of formation are all small and negative.

6.5 Comparison of calculations with experimental data

The calculated isothermal section at 350°C, including the experimental data from Kevorkov and Pekguleryuz [15], is shown in Fig. 1. All compositions identified as lying in single-phase regions are reproduced as such. Reported compositions [15] corresponding to the single-phase regions of $\tau 2$, $\tau 4$, $\tau 5$ and $\tau 6$ are not reproduced exactly since these four ternary phases were treated as stoichiometric compounds in the present work.

Figure 6(b) shows the calculated isothermal section at 300°C along with points which Chiu *et al* [28] identified as lying in three-phase regions. All these tie-triangles were reproduced in the present work. The region containing the data point corresponding to the highest Mg content was mistakenly interpreted as a three-phase region in ref [28]. The more recently reported isothermal section at 300°C from Mostafa and Medraj [20] is shown in Fig. 6(a). As expected, the reported solubility ranges of some of the ternary phases are not reproduced because we treated these phases as stoichiometric compounds. The proposed phase relationships in the Zn-rich region were also not all reproduced.

In the optimizations, more weight was given to the experimental data from the present ND experiments because these experiments were performed at higher temperatures and in the presence of the liquid phase; hence, equilibrium is more likely to be attained.

Reported [14] and calculated isothermal sections at 197°C are shown in Fig. 7. The

solubility of Zn in the $CeMg_{12}$ phase is calculated as ~8 at.%, which is much less than that reported in ref [14] (44.5 at.%). Furthermore, the τ7 phase is not stable at 197°C according to the calculations. It was not possible to reproduce all the experimental data from the present ND experiments while simultaneously reproducing the reported large Zn solubility in $CeMg_{12}$ and maintaining τ7 stable at 197°C. The samples of Pavlyuk *et al* [14] were annealed at 197°C for four weeks which may have been insufficient to reach equilibrium at such a low temperature. That their system was not completely at equilibrium is supported by their observation of $Mg_{51}Zn_{20}$, which is metastable [7]. As mentioned above, more weight was given to the current high temperature ND results in the optimization.

Calculated Zn solubilities in $CeMg_3$ are less than those reported at 350°C, 300°C and 197°C. The ND results proved incompatible with the higher solubilities and, again, more weight was given to the ND results, which are more likely to correspond to true equilibrium conditions due to the presence of the liquid phase.

Two calculated isopleths with constant Zn contents of 24 and 34 wt.% are shown in Fig. 2 along with experimental TA data from Drits *et al* [21]. The experimental points [21] at low Ce contents cannot be reproduced since they are in disagreement with the accepted liquidus in the Mg-Zn binary system.

Figures 8 shows calculated optimized isopleths along with the DTA data of Chiu *et al* [28]. The data are reasonably well reproduced.

Chiu *et al* [28] proposed a thermodynamic optimization of the system. However, they focused mainly on Mg-rich compositions and included only three ternary compounds. Their optimization reproduced the data shown in Fig. 8(a) reasonably well, but not the data in Fig. 8(b).

Calculated isopleths are shown in Fig. 5 along with experimental data from the present ND experiments. Calculated transition temperatures and precipitation sequences are in good agreement with the experiments. The higher transition temperatures (especially the liquidus temperatures) are considered more reliable than the lower transition temperatures because of kinetic constraints on attaining equilibrium at low temperature.

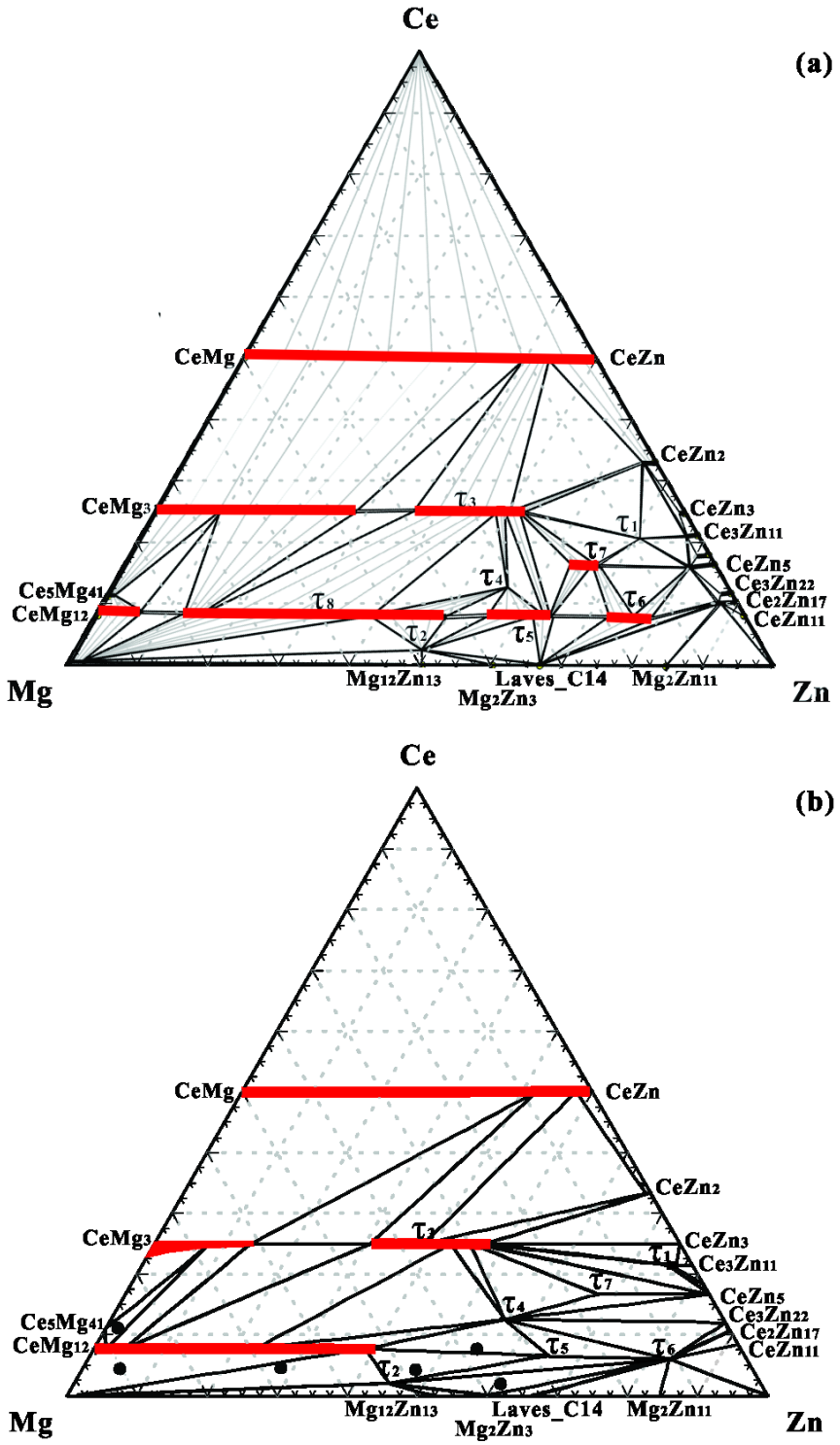

Figure 6.6. (a) Reported [20] and (b) calculated optimized isothermal section (mole fraction) of the Ce-Mg-Zn system at 300°C showing experimental data points identified by Chiu *et al* [28] as lying in three-phase regions.

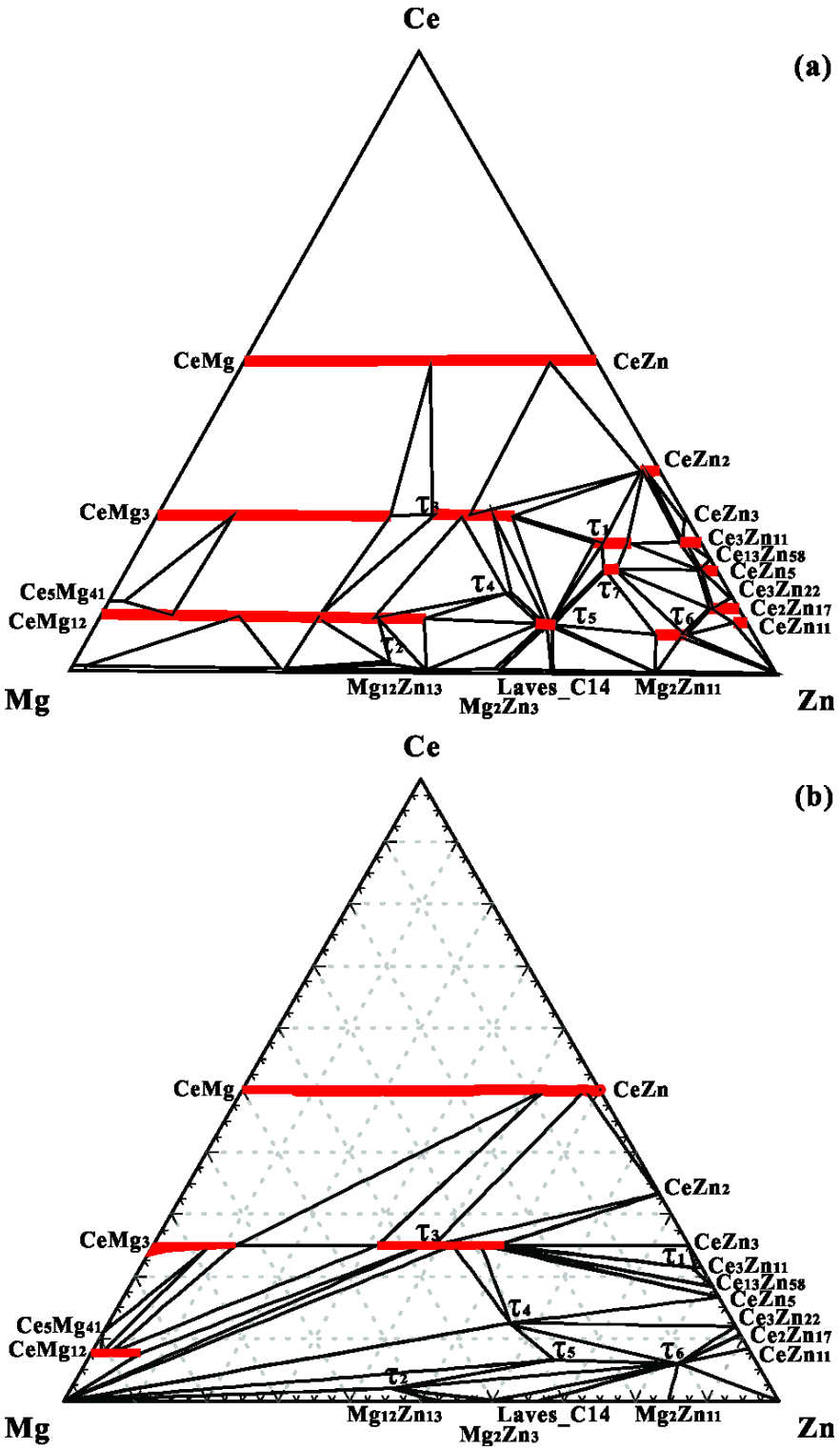

Figure 6.7. (a) Reported [14] and (b) calculated optimized isothermal section (mole fraction) of the Ce-Mg-Zn system at 197°C

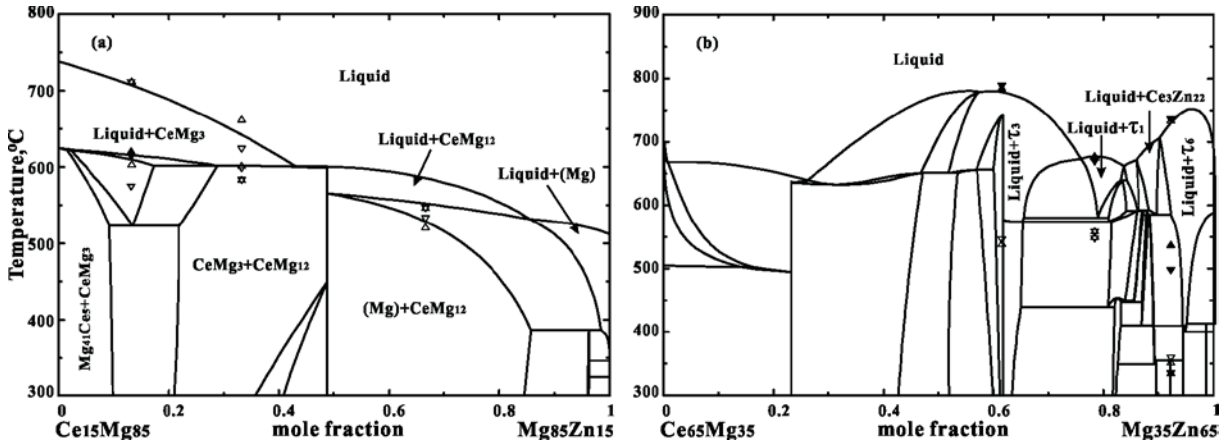

Figure 6.8. Calculated optimized isopleths of the (a) $Ce_{15}Mg_{85}$-$Mg_{85}Zn_{15}$ and (b) $Ce_{65}Mg_{35}$-$Mg_{35}Zn_{65}$ sections showing data points of Chiu *et al* [28]. ▲ strong heating signal; ▼ strong cooling signal; △ weak heating signal; ▽ weak cooling signal.

A tentative calculated liquidus projection for the Ce-Mg-Zn system is shown in Figs. 9-10 and a tentative list of the calculated temperatures of invariant reactions, maxima and minima is given in Table 4.

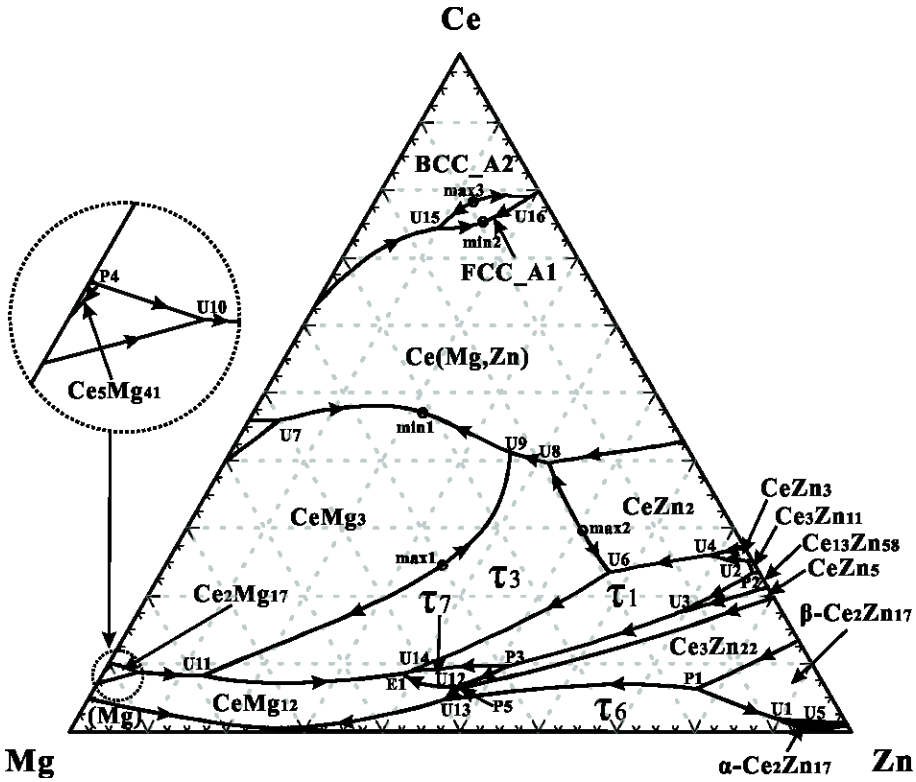

Figure 6.9. Tentative calculated liquidus projection for Ce-Mg-Zn system (mole fraction)

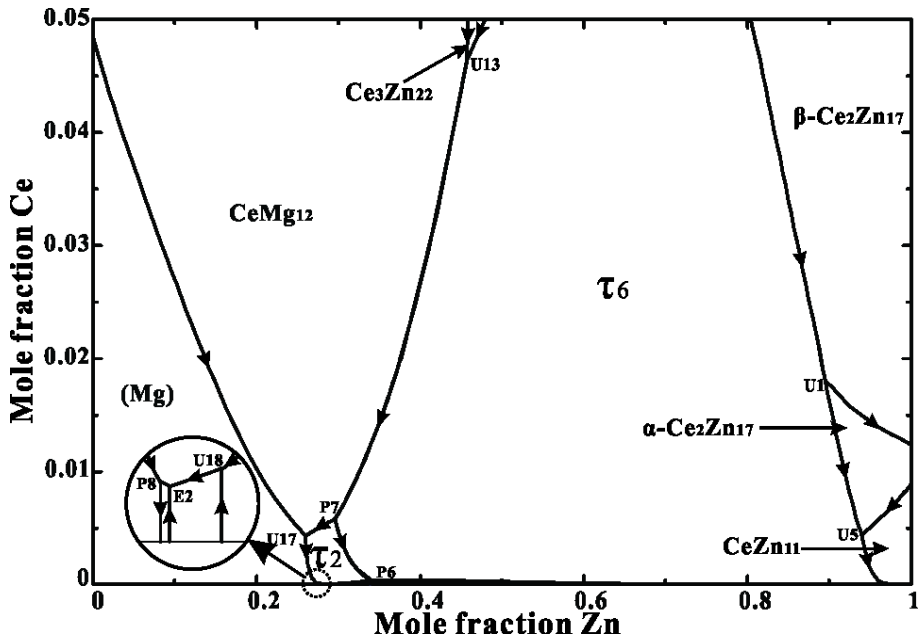

Figure 6.10. Enlargement of part of Fig. 6.9

As mentioned in Section 2, an invariant equilibrium at 341-343°C was reported by Korol'kov and Sal'dau [16], which could correspond to U18, P8 or E2, the most likely being E2 because eutectic reactions are the most easily detected by thermal analysis.

Table 6.4. Tentative calculated invariant reactions, maxima and minima and their temperatures (^{o}C) in the Ce-Mg-Zn system

P1	849	P2	833	U1	818	U2	816	U3	781	U4	775	U5	751
U6	709	U7	697	U8	656	U9	650	P3	639	P4	622	U10	601
U11	594	P5	592	U12	591	U13	584	U14	580	E1	574	U15	502
U16	498	P6	413	P7	410	U17	386	U18	351	P8	346	E2	346
max1	~782	max2	~743	max3	~533	min1	~632	min2	~484				

6.6 Discussion

In the optimization, greater weight was accorded to the ND data from the present investigation, firstly because the ND data were obtained in situ at equilibrium at higher temperatures, and secondly because, due to the high penetrating power of neutrons, large samples (10 to 20 g) could be used, thereby leading to better control of composition and increased resistance to oxidation.

In subsequent articles we shall report on thermodynamic modeling and ND experiments in the Nd-Mg-Zn system as well as thermodynamic optimizations of most other ternary RE-Mg-Zn systems. The model parameters will be included in the FTlite light metals database of the FactSage database computing system [39] which already contains optimized model parameters for the solid and liquid phases of a large number of binary and ternary Mg- and Al-containing systems. Through the models, the properties and phase equilibria of multicomponent systems can thus be estimated and calculated.

All calculations in the present work were performed with the FactSage software [39].

6.7 Conclusions

All available phase diagram data for the Ce-Mg-Zn system were critically assessed. *In-situ* neutron diffraction (ND) experiments were performed on selected samples to identify phases and transition temperatures. A critical thermodynamic evaluation and optimization of the Ce-Mg-Zn system was carried out and model parameters for the thermodynamic properties of all phases were obtained. The phase transformation behavior of selected samples were well resolved from the ND experiments and experimental data were used to refine the thermodynamic model parameters.

All optimized model parameters from the present work are summarized in Table 3. Binary parameters were reported in previous articles [7, 8, 12]. Very few model parameters are required, and all parameters have thermodynamically reasonable values. In particular, no additional ternary parameters were required in the MQM model for the liquid phase.

Acknowledgements

This research was supported by funding from the Natural Sciences and Engineering Research Council of Canada (NSERC) Magnesium Strategic Research Network. More information on the Network can be found at www.MagNET.ubc.ca. The authors would like to thank Dr. Dmytro Kevorkov and Dr. Ahmad Mostafa for helping prepare the samples.

References

[1] B.L. Mordike, T. Ebert, Magnesium: Properties — applications — potential, Mat. Sci. Eng. A-Struct, 302 (2001) 37-45.

[2] I.P. Moreno, T.K. Nandy, J.W. Jones, J.E. Allison, T.M. Pollock, Microstructural stability and creep of rare-earth containing magnesium alloys, Scripta Mater., 48 (2003) 1029-1034.

[3] J. Bohlen, M.R. Nürnberg, J.W. Senn, D. Letzig, S.R. Agnew, The texture and anisotropy of magnesium-zinc-rare earth alloy sheets, Acta Mater., 55 (2007) 2101-2112.

[4] R.K. Mishra, A.K. Gupta, P.R. Rao, A.K. Sachdev, A.M. Kumar, A.A. Luo, Influence of cerium on the texture and ductility of magnesium extrusions, Scripta Mater., 59 (2008) 562-565.

[5] N. Stanford, M.R. Barnett, The origin of “rare earth” texture development in extruded Mg-based alloys and its effect on tensile ductility, Mat. Sci. Eng. A-Struct, 496 (2008) 399-408.

[6] K. Hantzsche, J. Bohlen, J. Wendt, K.U. Kainer, S.B. Yi, D. Letzig, Effect of rare earth additions on microstructure and texture development of magnesium alloy sheets, Scripta Mater., 63 (2010) 725-730.

[7] I. Ansara, A. T. Dinsdale, M. H. Rand, COST 507: Definition of thermochemical and thermophysical properties to provide a database for the development of new light alloys, Thermochemical database for light metal alloys, Vol. 2, Office for Official Publications of the European Communities, Luxembourg,1998; P. Spencer, unpublished work

[8] Y.-B. Kang, L. Jin, P. Chartrand, A.E. Gheribi, K. Bai, P. Wu, Thermodynamic evaluations and optimizations of binary Mg-light Rare Earth (La, Ce, Pr, Nd, Sm) systems, CALPHAD, 38 (2012) 100-116.

[9] Y.-B. Kang, A. Pelton, P. Chartrand, P. Spencer, C. Fuerst, Critical Evaluation and Thermodynamic Optimization of the Binary Systems in the Mg-Ce-Mn-Y System, J. Phase Equilib. Diff., 28 (2007) 342-354.

[10] Y.-B. Kang, A.D. Pelton, P. Chartrand, C.D. Fuerst, Critical evaluation and thermodynamic optimization of the Al–Ce, Al–Y, Al–Sc and Mg–Sc binary systems, CALPHAD, 32 (2008) 413-422.

[11] L. Jin, PhD Thesis, Ecole Polytechnique, Montreal (Canada), 2012, pp. 407

[12] Z. Zhu, A. Pelton, Critical assessment and optimization of phase diagrams and thermodynamic properties of RE–Zn systems-part I: Sc–Zn, La–Zn, Ce–Zn, Pr–Zn, Nd–Zn, Pm–Zn and Sm–Zn, J. Alloys Compd. 641 (2015) 249-260

[13] Z. Zhu, A. Pelton, Critical assessment and optimization of phase diagrams and thermodynamic properties of RE–Zn systems-Part II: Y–Zn, Eu–Zn, Gd–Zn, Tb–Zn, Dy–Zn, Ho–Zn, Er–Zn, Tm–Zn, Yb–Zn and Lu–Zn, J. Alloys Compd, 641 (2015) 261-271

[14] V. Pavlyuk, B. Marciniak, E. Różycka-Sokołowska, The isothermal section of the phase diagram of Ce–Mg–Zn ternary system at 470 K, Intermetallics, 20 (2012) 8-15.

[15] D. Kevorkov, M. Pekguleryuz, Experimental study of the Ce-Mg-Zn phase diagram at 350 °C via diffusion couple techniques, J. Alloys Compd., 478 (2009) 427-436.

[16] A.M. Korol'kov, P.Y. Sal'dau, Solubility of zinc and cerium in magnesium in the solid state, Izv. Sekt. Fiz.-Khim. Anal., Inst. Obshch. Neorg. Khim., Akad. Nauk SSSR, 16 (1946) 295-306.

[17] E.V. Mel’nik, M.F. Kostina, Ya.P. Yarmlyuk, O.F. Zmii, Study of magnesium-zinc-cerium and magnesium-zinc-calcium ternary systems, Magnievye Splavy, Mater.Vses. Soveshch. Issled., Razrab. Primen. Magnievyhk Splavov, (1978) 95-99.

[18] U. Kolitsch, P. Bellen, S. Kaesche, D. Macciò, N. Bochvar, Y. Liberov, P. Rogl, G. Effenberg, G. Petzow, Ternary Alloys–A Comprehensive Compendium of Evaluated Constitutional Data and Phase Diagrams, Stuttgart, Germany: Weinheim: VCH Verlagsgesellschaft, MSI GmbH; 17 (2000) 168–76.

[19] R. Agarwal, S.G. Fries, H.L. Lukas, G. Petzow, F. Sommen, T.G. Chart, G. Effenberg, Assessment of the Mg-Zn system, Z Metallkd, 83 (1992) 216-223.

[20] A. Mostafa, M. Medraj, Phase Equilibria of the Ce-Mg-Zn Ternary System at 300 °C, Metals, 4 (2014) 168-195.

[21] M.E. Drits, E.I. Drozdova, I.G. Korol'kova, V.V. Kinzhibalo, A.T. Tyvanchuk, Investigation of polythermal sections of the Mg-Zn-Ce system in the Mg-rich region, Russ Metall-Metall-U, (1989) 195-197.

[22] M.E. Drits, E.I. Drozdova, I.G. Korol'kova, V.V. Kinzhibalo, A.T. Tyvanchuk, Polythermal sections of the magnesium-zinc-cerium system in the magnesium-rich region, Izv. Akad. Nauk SSSR, Met., (1989) 198-200.

[23] M.-I. Huang, H.-X. Li, H. Ding, Y.-P. Ren, G.-W. Qin, S.-M. Hao, Partial phase relationships of Mg-Zn-Ce system at 350 °C, T. Nonferr Metal Soc., 19 (2009) 681-685.

[24] M.-L. Huang, H.-X. Li, H. Ding, L. Bao, X.-B. Ma, S.-M. Hao, Intermetallics and phase relations of Mg-Zn-Ce alloys at 400 °C, T. Nonferr Metal Soc., 22 (2012) 539-545.

[25] V. Pavlyuk, E. Rozycka-Sokolowska, B. Marciniak, The new ternary phases of $La_3(Zn_{0.874}Mg_{0.126})_{11}$ and $Ce_3(Zn_{0.863}Mg_{0.137})_{11}$, Acta Crystallogr C, 66 (2010) i25-i28.

[26] V. Pavlyuk, P. Solokha, G. Dmytriv, B. Marciniak, V. Paul-Boncour, The Heusler-type alloy $MgZn_2Ce$, Acta Crystallogr E, 63 (2007) i161-i161.

[27] V. Pavlyuk, P. Solokha, O. Zelinska, V. Paul-Boncour, A. Nowik-Zajac, $Ce_{20}Mg_{19}Zn_{81}$: A new structure type with a giant cubic cell, Acta Crystallogr C, 64 (2008) i50-i52.

[28] C.-N. Chiu, J. Gröbner, A. Kozlov, R. Schmid-Fetzer, Experimental study and thermodynamic assessment of ternary Mg-Zn-Ce phase relations focused on Mg-rich alloys, Intermetallics, 18 (2010) 399-405.

[29] H. Nowotny, The crystal structures of Ni_5Ce, Ni_5La, Ni_5Ca, Cu_5La, Cu_5Ca, Zn_5La, Zn_5Ca, MgCe, MgLa and MgSr, Z Metallkd., 34 (1942) 247-253.

[30] Y. Uwatoko, K. Suenaga, G. Oomi, X-ray diffraction study of the structural change in cerium-zinc (CeZn) under high pressure, J. Magn. Magn. Mater., 104-107 (1992) 645-646.

[31] G. Berger, A. Weiss, Ternary intermetallic phases with Heusler-phase-type structure in the system Ag-Mg-RE (RE≡ La, Ce, Pr, Nd, Sm), J. Less-common Met., 142 (1988) 109-121.

[32] A.H. Gomes de Mesquita, K.H.J. Buschow, The crystal structure of so-called α-$LaAl_4$ (La_3Al_{11}), Acta Crystallogr, 22 (1967) 497-501.

[33] H. Xu, J. Fan, H.-L. Chen, R. Schmid-Fetzer, F. Zhang, Y. Wang, Q. Gao, T. Zhou, Experimental determination of the phase equilibria of the Mg–Nd–Zn system at 320 °C, J. Alloys Compd., 603 (2014) 100-110.

[34] W. M. Haynes, ed., CRC Handbook of Chemistry and Physics, 95th Edition (Internet Version 2015), CRC Press/Taylor and Francis, Boca Raton, FL.

[35] B. Toby, EXPGUI, A graphical user interface for GSAS, J. Appl. Crystallogr., 34 (2001) 210-213.

[36] A. Pelton, S. Degterov, G. Eriksson, C. Robelin, Y. Dessureault, The modified quasichemical model I—Binary solutions, Metall. Mater. Trans. B, 31 (2000) 651-659.

[37] A. Pelton, P. Chartrand, The modified quasi-chemical model: Part II. Multicomponent solutions, Metall. Mater. Trans. A, 32 (2001) 1355-1360.

[38] M. Hillert, The compound energy formalism, J. Alloys Compd., 320 (2001) 161-176.

[39] C.W. Bale, E. Bélisle, P. Chartrand, S.A. Decterov, G. Eriksson, K. Hack, I. H. Jung, Y.B. Kang, J. Melançon, A.D. Pelton, C. Robelin, S. Petersen, FactSage thermochemical software and databases — recent developments, CALPHAD, 33 (2009) 295-311; www.factsage.com

Chapter 7 ARTICLE 4: THERMODYNAMIC MODELING AND *IN-SITU* NEUTRON DIFFRACTION INVESTIGATION OF THE ND-MG-ZN SYSTEM

Submitted to Acta Materialia

Zhijun Zhu[a], Michael Gharghouri[b] and Arthur D. Pelton[a*],

[a]Centre de Recherche en Calcul Thermochimique, Département de Génie Chimique, Ecole Polytechnique, Montréal, Québec, Canada

[b]Canadian Neutron Beam Centre, Chalk River, Ontario, Canada

*Corresponding author

KEY WORDS

Nd-Mg-Zn system, Phase diagram, Thermodynamic assessment, Thermodynamic optimization, *In-situ* neutron diffraction

ABSTRACT

All available phase diagram data for the Nd-Mg-Zn system were critically assessed. *In-situ* neutron diffraction (ND) experiments were performed on selected samples to identify phases and transition temperatures. A critical thermodynamic evaluation and optimization of the Nd-Mg-Zn system was carried out and model parameters for the thermodynamic properties of all phases were obtained. The phase transformation behavior of selected samples was well resolved from the ND experiments and experimental data were used to refine the thermodynamic model parameters.

7.1 Introduction

Magnesium being the lightest structural metal, Mg-based alloys have many applications. Zinc is one of the most commonly used alloying elements in Mg (AZ series), and the rare earth (RE) metals have been shown to improve creep resistance [1, 2] and sheet formability (by reducing texture [3-6]).

Information on phase behavior is essential for the design of new RE-Mg-Zn alloys. However, few studies of the phase diagrams and thermodynamic properties of these systems have been made. The present study was thus undertaken to better define the phase diagrams of the RE-Mg-Zn ternary systems through the technique of critical thermodynamic assessment and optimization coupled with limited experimentation.

In a thermodynamic optimization, adjustable model parameters are calculated using all available thermodynamic and phase-equilibrium data in order to obtain one set of model equations as functions of temperature and composition. Thermodynamic data, such as activities, can aid in the evaluation of the phase diagrams, and information on phase equilibria can be used to deduce thermodynamic properties. With this technique, it is frequently possible to resolve discrepancies in the available data. From the model equations, all of the thermodynamic properties and phase diagrams can be back-calculated, and interpolations and extrapolations can be made in a thermodynamically correct manner. The thermodynamic properties and phase diagrams are thereby rendered self-consistent and consistent with thermodynamic principles, and the available data are distilled into a small set of model parameters, ideal for computer storage. Generally, in the optimization of a ternary system one begins by optimizing the three binary sub-systems. The binary model parameters are then used to estimate the properties of the ternary phases, and these estimates are then refined by introducing ternary model parameters where required to reproduce available ternary data.

Thermodynamic evaluations and optimizations have already been reported for the binary Mg-Zn system [7], all binary Mg-RE systems [8-11] and all binary RE-Zn systems (including Sc-Zn and Y-Zn) [12, 13]. An evaluation, optimization and experimental phase diagram study of the Ce-Mg-Zn system has been reported previously [14]. In the present article we report on our evaluation, optimization and experimental phase diagram study of the Nd-Mg-Zn system. In subsequent articles we shall report on our evaluations and optimizations of other ternary RE-Mg-Zn systems [15, 16]. As expected, all RE-Mg-Zn systems are very similar. The present work on the Nd-Mg-Zn system was greatly aided by our simultaneous assessments of all the other RE-Mg-Zn systems.

7.2 Phase equilibrium and thermodynamic data

The Nd-Mg-Zn system has been investigated by several research groups, who used different designations for the ternary phases. Phases with ternary phase fields considered in the present optimization are summarized in Table 1. The nomenclature employed in our previous report on the Ce-Mg-Zn system [14] is used again here. Consequently, τ2, τ3, τ4, τ5 and τ7 are found in the Nd-Mg-Zn system while τ1 and τ6 are not. These two phases may be stable in the Nd-Mg-Zn system given that Ce and Nd have very similar properties. However, the existence of τ1 is in doubt and no detailed experimental investigation has been made in the composition range where τ6 might be found. Furthermore, neither τ1 nor τ6 has been reported in any RE-Mg-Zn system other than Ce-Mg-Zn [14]. Hence, they are not assumed in the Nd-Mg-Zn system. All phases shown in Table 1 (except $Nd(Mg,Zn)_{12}$ which is not stable at 300°C according to our calculations) can also be seen in the calculated isothermal section at 300°C shown in Fig. 1.

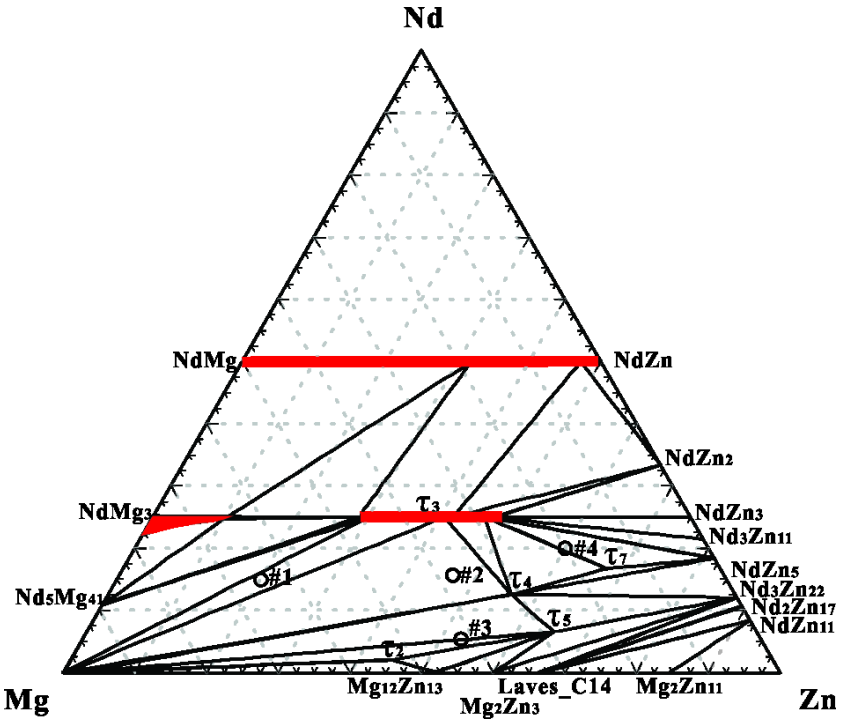

Figure 7.1. Calculated optimized isothermal section of the Nd-Mg-Zn system at 300°C showing the compositions of the four samples in the present ND experiments (mole fraction).

The ternary compounds τ2, τ4, τ5 and τ7 are assumed to have the same stoichiometries as the corresponding phases in the Ce-Mg-Zn system [14] since the latter have been well studied. As

mentioned previously [14], limited ternary homogeneity ranges were reported for τ4, τ5 and τ7 in the Ce-Mg-Zn system. For lack of evidence to the contrary, these phases are all assumed to be stoichiometric compounds in the Nd-Mg-Zn system.

The phase Nd(Mg,Zn) in Table 1 is a solid solution of NdMg and NdZn. The phase $NdMg_3$ is a solution with limited solubility of Zn. $NdMg_{12}$ and $NdZn_{12}$ (both of the $Mn_{12}Th$ structural prototype) are metastable in their respective binary systems; however, their solution has been reported to be stable in the ternary composition region according to several investigators as summarized in Table 1. Although some limited solubility of Mg in $NdZn_2$, $NdZn_3$, Nd_3Zn_{11}, $Nd_{13}Zn_{58}$, α-Nd_2Zn_{17} and Nd_3Zn_{22} and of Zn in Nd_5Mg_{41} has been reported [17, 18], as will be discussed later in this section, it is likely that the samples were not at equilibrium; hence, we have assumed that these and all other binary phases do not extend into the ternary system. The prototypes, Pearson symbols and space groups of all binary phases were given previously [7, 8, 12].

Using thermal, micro-structural and micro-hardness analysis, Drits *et al* [24] investigated the Nd-Mg-Zn system in the Mg-rich region. Five isopleths were investigated but only the three shown in Fig. 2 were reported. Three ternary compounds (X, Y and Z) were proposed but their compositions were not given. Four invariant reactions were also reported:

$$L \leftrightarrow (Mg) + Nd_5Mg_{41} + X \text{ at } 520 \pm 3^{o}C \qquad 7.1$$

$$L + X \leftrightarrow (Mg) + Y \text{ at } 473 \pm 3^{o}C \qquad 7.2$$

$$L + Y \leftrightarrow (Mg) + Z \text{ at } 440 \pm 3^{o}C \qquad 7.3$$

$$L \leftrightarrow (Mg) + Mg_{51}Zn_{20} + Z \text{ at } 336 \pm 3^{o}C \qquad 7.4$$

Table 7.1. Phases with ternary phase fields in the Nd-Mg-Zn system

Phase name	Prototype-Pearson symbol-Space group	thermodynamic model	
Nd(Mg,Zn)	CsCl-cP2-Pm$\bar{3}$m [19-21]	Nd(Mg,Zn)	NdMg and NdZn form continuous solution [17, 19]
$NdMg_3$	BiF_3-cF16-Fm$\bar{3}$m [19]	$Nd(Mg,Zn)_3$	Reported Zn Solubility 40 at.% at 297°C [19] Reported Zn solubility 50 at.% at 320°C [17] Reported Zn solubility 30 at.% at 300°C [18]
$Nd(Mg,Zn)_{12}$	$Mn_{12}Th$-tI26-I4/mmm [19]	$Nd(Mg,Zn)_{12}$	Reported as $NdMg_6Zn_3$ in ref [19], as $Nd(Mg,Zn)_{11.5}$ in ref [22] with Zn content 26.9-41.3 at.% Reported as T- $Nd(Mg,Zn)_{12}$ and τ1 in ref [17] and T in ref [18]
[1]τ1	[2]$Al_{11}La_3$-oI28-Immm		
τ2	unknown	$Nd_2Mg_{53}Zn_{45}$	Assumed stoichiometric in present study. Reported as τ4 in ref [18]
τ3	MnCu_2Al-cF16-Fm$\bar{3}$m [19, 23]	$NdMg(Mg,Zn)_2$	Reported as X in refs [24-28], Reported as B ($Nd_3Mg_8Zn_{11}$) in ref [19] Reported as τ3 in ref [18] and T' in ref [17].
τ4	[2]TbCu_7-hP8-P6/mmm	$Nd_2Mg_5Zn_9$	Assumed stoichiometric in present study. Reported as τ2 in ref [17], τ1 in ref [18] Reported as D ($Nd_2Mg_7Zn_{11}$) in ref [19]
τ5	[2]$Ce_3Mg_{13}Zn_{30}$-hP92-P6_3/mmc	$Nd_3Mg_{13}Zn_{30}$	Assumed stoichiometric in present study. Reported as C ($NdMg_7Zn_{12}$) in ref [19], τ5 in ref [18]
[1]τ6	unknown		
τ7	[2]$Ce_{20}Mg_{19}Zn_{81}$-cF480-F$\bar{4}$3m	$Nd_{20}Mg_{19}Zn_{81}$	Assumed stoichiometric in present study. Reported as τ6 in ref [18]

Elements within brackets substitute on the same sublattice

[1] Possible stable phase not considered in the present work. τ1 was modeled as $Ce_3Zn_9(Mg,Zn)_2$ and τ6 was modeled as $Ce_6Mg_{11}Zn_{83}$ in the Ce-Mg-Zn system. Please refer to ref [14] for details.

[2]Crystal structure of these phases are proposed based on crystallographic information from similar phases in the Ce-Mg-Zn system [14]

Three partial isothermal sections (200°C, 250°C and 300°C) in the Mg-rich region were established by the same group using micro-structural analysis [25]. However, the compositions and crystal structures of the three ternary compounds were still not resolved. Four partial isothermal sections (200 ^{o}C, 300 ^{o}C, 400 ^{o}C and 500 ^{o}C) in the Mg-rich region, as well as the compositions of the three ternary compounds, were later proposed by the same group [27, 28]. The three ternary compounds were proposed as $MgNd_4Zn_5$, $Mg_6Nd_2Zn_7$ and $Mg_2Nd_2Zn_9$ according to X-ray spectral analysis. However, the compositions were determined from samples containing yttrium, thereby casting doubt on the results. None of these isothermal sections have been considered in the present study because only very limited composition ranges were examined.

The Nd-Mg-Zn system was later investigated by Kinzhibalo *et al* [19] over the entire composition range by X-ray diffraction (XRD). An isothermal section at 297°C was established and four ternary compounds were reported: $NdMg_6Zn_3$, $Nd_3Mg_8Zn_{11}$, $Nd_2Mg_7Zn_{11}$ and $NdMg_7Zn_{12}$. $Nd_3Mg_8Zn_{11}$ was reported to have the $AlMnCu_2$ structural prototype, the same as that of τ3 in the Ce-Mg-Zn system, and it is thus denoted τ3 in the present study; $NdMg_6Zn_3$ is treated as part of the $Nd(Mg,Zn)_{12}$ solution; $Nd_2Mg_7Zn_{11}$ and $NdMg_7Zn_{12}$ are denoted τ4 and τ5 respectively in the present work. NdMg and NdZn were reported to form a continuous solution while Zn was reported to substitute for Mg in $NdMg_3$ up to 40 at. %.

Using scanning electron microscopy (SEM), XRD, electron probe microanalysis (EPMA) and transmission electron microscopy (TEM), Huang *et al* [22] investigated the isothermal section at 400°C in the Mg-rich region. A ternary compound with a suggested formula of $Nd(Mg,Zn)_{11.5}$ was proposed. The Zn content of this compound ranged from 26.9 at.% to 41.3 at.% and the crystal structure was reported as C-centered orthorhombic. This phase is considered as the $Nd(Mg,Zn)_{12}$ solution in the present work.

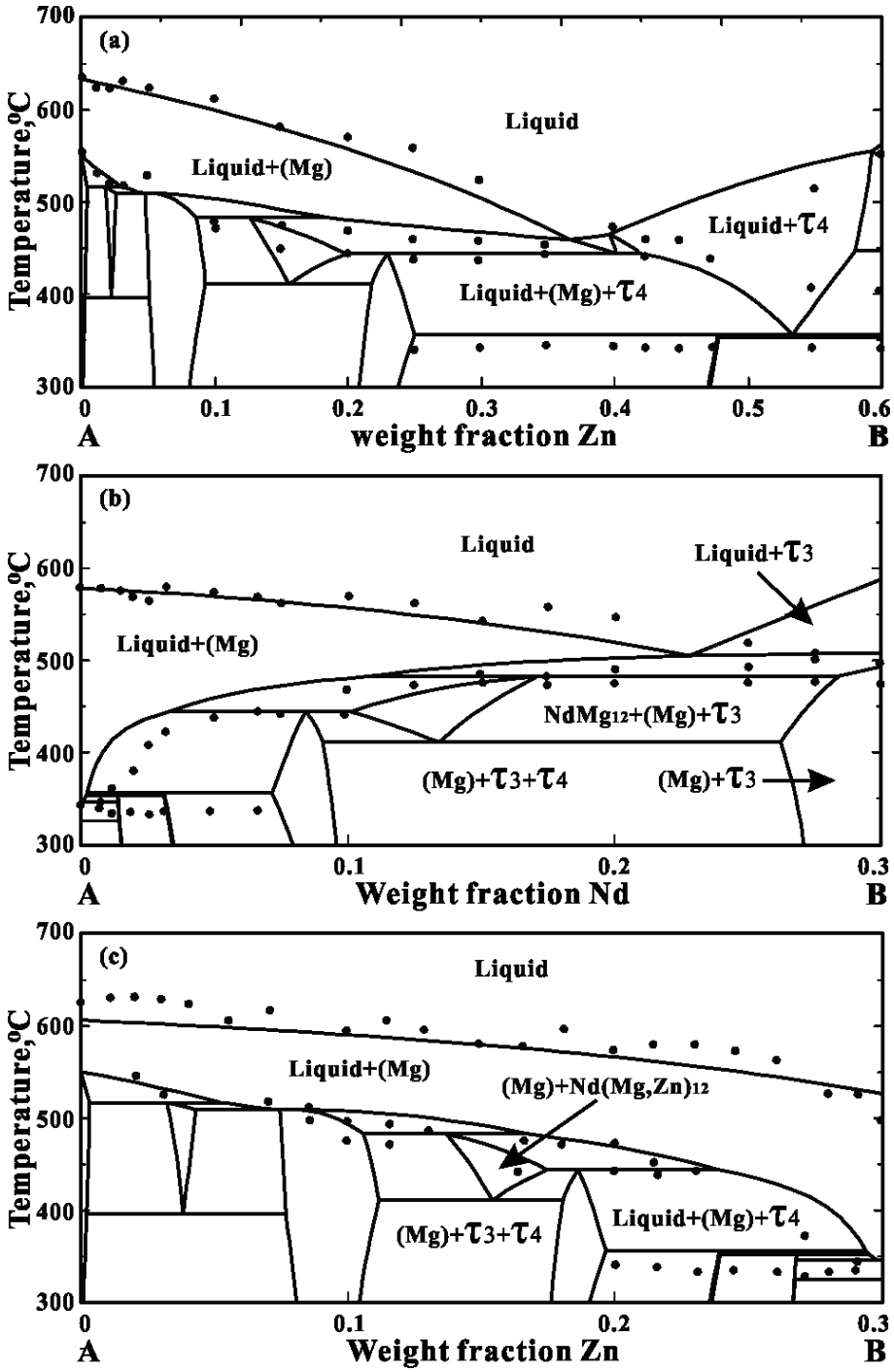

Figure 7.2. Calculated optimized isopleths (a) from Mg-10wt.%Nd (A) to Mg-10wt.%Nd-60wt.%Zn (B), (b) from Mg-20wt.%Zn (A) to Mg-20wt.%Zn-30wt.%Nd (B) and (c) from Mg-20wt.%Nd (A) to Mg-30wt.%Zn (B) in the Nd-Mg-Zn system showing points from Drits *et al* [24]

Based on diffusion couples and equilibrium alloys, Xu *et al* [17] investigated the Nd-Mg-Zn system at 320°C (Fig. 3) by XRD and EPMA techniques. The alloys were annealed at 320°C for 100 days. Two ternary phases, $Ce(Mg,Zn)_{12}$ and τ5 (reported as τ1 and τ2 in ref [17]), were identified in the diffusion couple. The reported $Nd(Mg,Zn)_{12}$ phase is in agreement with that reported by Kinzhibalo *et al* [19] and the reported composition of τ5 is very close to that of τ5 in the Ce-Mg-Zn system [29]. The structure of τ5 was reported as hexagonal while the space group and prototype were not given. The lattice constants of τ5 were given as a = 1.47 nm and c = 0.87 nm which are very close to the reported lattice constants of τ5 in the Ce-Mg-Zn system [29] (a = 1.4981(2) nm and c = 0.8688(9) nm). Extensive discussion was provided by Xu *et al* [17] on the 34 selected samples. Many of the samples contained more than three phases according to XRD and EPMA analysis, which led the authors to conclude that equilibrium had not been reached even after annealing for 100 days at 320°C. Consequently, the additional phases reported by Xu *et al* [17] are not considered in the present study.

Using diffusion couples and equilibrium alloys, Mostafa and Medraj [18] investigated the Nd-Mg-Zn system at 300°C by means of wavelength-dispersive X-ray spectroscopy (WDS), XRD and metallographic techniques. Their reported isothermal section at 300°C is shown in Fig.4. The ternary phases τ2, τ3, τ4, τ5 and τ7 were detected in the diffusion couples. All these phases have corresponding phases in the Ce-Mg-Zn system although the reported compositions may differ to some extent. The selected samples were annealed at 300°C for 45 days. This length of time may have been insufficient for the samples to reach equilibrium, given that samples annealed at 320°C for 100 days were not at equilibrium according to Xu *et al* [17], as described above.

Based on the available experimental data from the literature, the following phases with ternary phase fields are considered in the present optimization (See Fig. 1 and Table 1):

Nd(Mg,Zn): The NdMg and NdZn binary phases both have the CsCl structure and in all reported isothermal sections [17-19] they form a continuous solution. The Nd content is constant at 50 at.%. Consequently, the model Nd(Mg,Zn) was chosen in the present optimization (That is, Mg and Zn substitute on one sublattice while Nd occupies a second lattice). The lattice constant

of NdMg has been reported as 0.3789 nm [19] or 0.3869 nm [21], while that of NdZn has been reported as 0.3653 nm [19] or 0.3657 nm [20].

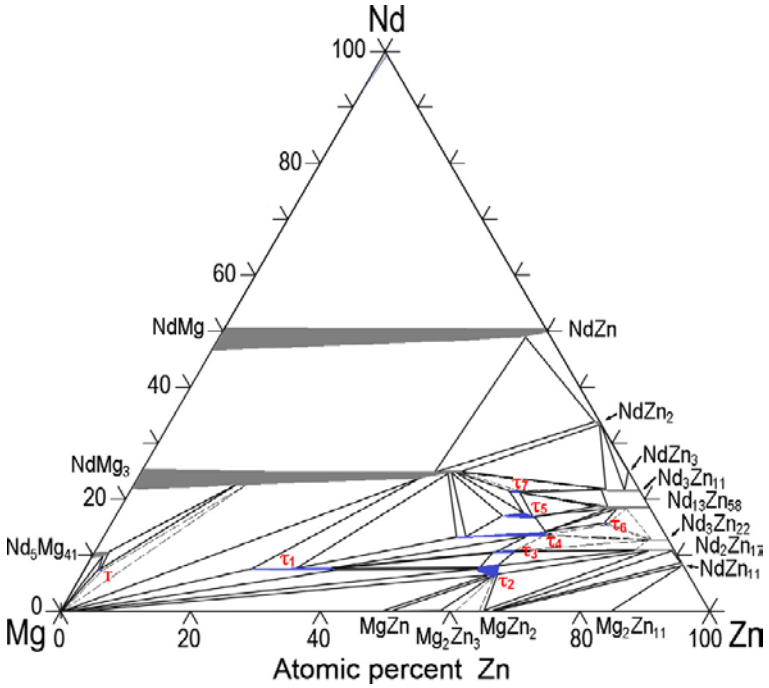

Figure 7.3. Reported isothermal section of Nd-Mg-Zn system at 320°C from Xu *et al* [17] (mole fraction). (Note: phase names τ1 to τ7 are those of the authors [17])

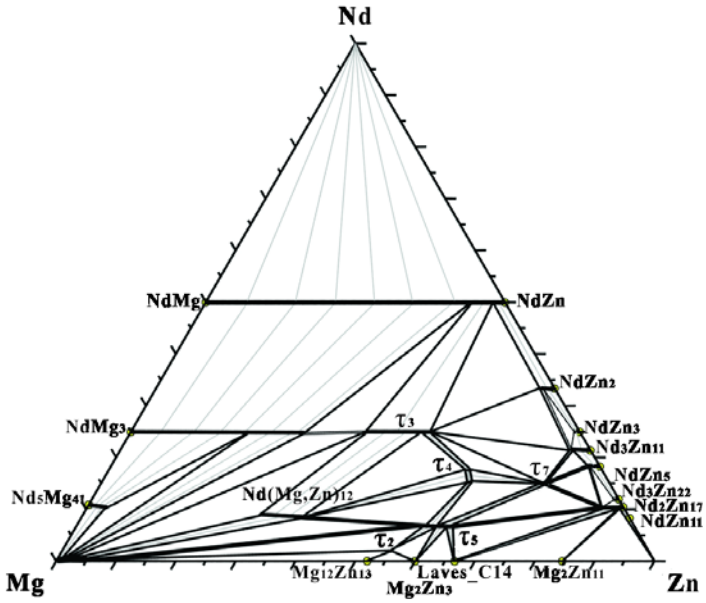

Figure 7.4. Reported isothermal section of Nd-Mg-Zn system at 300°C from Mostafa and Medraj [18] (mole fraction). (Note: names of the ternary phases are those used in the present study)

$NdMg_3$: Zn can substitute for Mg in $NdMg_3$ [17-19]. Consequently, the model $Nd(Mg,Zn)_3$ is used. Zn solubilities in $NdMg_3$ reported by different authors are summarized in Table 1. $NdMg_3$ and τ3 are treated as one continuous phase in ref [17]; the reported solubility limit of 50 at.% of Zn should thus be considered as the maximum Zn content of the τ3 phase. The reported lattice constant for $NdMg_3$ is 0.7413 nm [21]. The lattice constant of $NdMg_3$ is expected to decrease when Mg is substituted by Zn since the atomic size of Zn is smaller than that of Mg [30]. The lattice constant of $NdMg_3$ decreases from ~0.74 nm to ~0.725 nm as the Zn content increases from 0 to 20 at.% according to Xu *et al* [17].

$Nd(Mg,Zn)_{12}$: The $NdMg_{12}$ and $NdZn_{12}$ binary phases both have $Mn_{12}Th$ structure. Both phases are metastable in the respective binary systems [7, 12]. However, a stable solution with the model $Nd(Mg,Zn)_{12}$ can exist over a range of composition in the ternary system.

τ2: The τ2 phase has been reported in the Ce-Mg-Zn system by several authors [29, 31] and a similar phase denoted τ4 by the authors was reported by Mostafa and Medraj [18] in the Nd-Mg-Zn system. Although the reported composition differs somewhat from that of τ2 in the Ce-Mg-Zn system, the same stoichiometry as in the Ce-Mg-Zn system has been assumed in the present study.

τ3: This phase was first reported by Mel'nik *et al* [23] with the formula $Nd_2Mg_3Zn_3$. The prototype was given as $AlMnCu_2$ and the lattice constant was reported as 0.6967 nm. According to Xu *et al* [17] the lattice constants of $NdMg_3$ and τ3 (reported as T') are different when extrapolated to the same Zn content. Given that the existence of τ3 as a separate phase is well established in the Ce-Mg-Zn [29, 32], Y-Mg-Zn[33-35] and Gd-Mg-Zn [36] systems, $NdMg_3$ and τ3 are considered as separate phases in the present work. The two phases were also proposed as being separate phases by Mostafa and Medraj [18], although no crystallographic data were provided.

τ4, τ5 and τ7: Although some limited solubility has been reported for these three phases [17, 18], they are treated in the present work as stoichiometric phases, with suggested stoichiometries $Nd_2Mg_5Zn_9$, $Nd_3Mg_{13}Zn_{30}$ and $Nd_{20}Mg_{19}Zn_{81}$, respectively, in accordance with the corresponding phases in the Ce-Mg-Zn system.

A phase (denoted τ6 in ref [17]) with the approximate composition of the τ1 phase ($Ce_3Zn_9(Mg,Zn)_2$) in the Ce-Mg-Zn system [14] was reported by Xu *et al* [17]. However, according to the authors, the sample may not have been at equilibrium. Furthermore, as described later, the existence of this phase is not supported by our own experimental work. Consequently, this phase is not considered in the present work. However, it is shown in Table 1 as possibly being stable.

It should be noted here that a phase analogous to the τ6 ($Ce_6Mg_{11}Zn_{83}$) phase of in the Ce-Mg-Zn system [14] could exist in the Nd-Mg-Zn system. However, no investigation in any of the other RE-Mg-Zn systems has been carried out in the composition region where this phase could appear. Hence, it has not been considered in the present study.

7.3 Experimental investigation

In-situ neutron diffraction (ND) was used in the present work to investigate the phase transformation behavior in the Nd-Mg-Zn system in order to validate and refine the thermodynamic modelling.

Neutron diffraction data were acquired using the C2 powder diffractometer of the Canadian Neutron Beam Centre, located at the National Research Universal (NRU) reactor, Canadian Nuclear Laboratories (CNL). Diffraction from the (531) reflection of a silicon single crystal monochromator produced incident neutrons with a nominal wavelength of 0.133 nm. The C2 diffractometer is equipped with an 800-channel detector covering an 80° range in scattering angle 2θ, allowing multiple diffraction peaks to be acquired simultaneously.

The four sample compositions shown in Fig.1 and Table 1 were selected based on preliminary optimizations of the isothermal phase diagram at 300°C. Sample compositions corresponding to three-phase regions were chosen as they were expected to exhibit the greatest number of transitions, thereby providing the most information.

All samples were prepared from Nd (99.9 wt.%, STREM Chemicals Inc., Newburyport, MA, USA), Mg (99.8 wt.%, CANMET Materials Technology Laboratory, Ottawa, ON, Canada) and Zn (99.9 wt.%, Alfa Aesar, Haverhill, MA, USA) in an induction furnace under an Ar atmosphere. Crucibles were made from 0.15 mm thick Ta foil with a purity of 99.5 wt. %. All

samples were melted three times to improve homogeneity. ICP tests (Inductively coupled plasma mass spectrometry) showed that Zn loss of 5 wt.% by vaporization occurred during melting. Consequently, an excess of 5 wt.% Zn was added before melting.

Detailed information on the furnace has already been discussed in our previous paper on Ce-Mg-Zn system [14] and thus will not be provided here. A graphite crucible was used for sample #1 and Mo crucibles were used for samples #2, 3 and 4. Graphite is less expensive and easier to machine than Mo, but gives rise to several diffraction peaks which can interfere with the sample peaks.

In an *in-situ* ND experiment, diffraction patterns are acquired as a function of temperature as a specimen is heated or cooled. Each crystallographic phase in the specimen produces a distinct set of diffraction peaks, with the intensity of each peak proportional to the quantity of the corresponding phase in the specimen. During cooling or heating, a transition temperature is thus identified as the temperature at which the diffraction peaks for a given phase first appear or completely disappear. Due to limitations in the sensitivity of the technique, diffraction peaks for new phases are typically not detectable until the temperature is somewhat below or above the equilibrium transition temperature. In order to quantify the uncertainty associated with the sensitivity of the method, heating and cooling NPD measurements on pure Mg were carried out. The melting temperature of pure Mg was determined to be 640°C upon heating and 635°C upon cooling. The accepted melting temperature of pure Mg is 650°C [37]. Hence, all reported temperatures shown in the present report have been corrected by 15°C. Only *in-situ* cooling experiments were performed on alloy samples.

In the ND experiments it was found from preliminary tests on Ce-Mg-Zn samples that the intensity of the diffraction peaks for newly precipitated phases stabilized very quickly (within 3 minutes) as the temperature changed. Consequently, in later experiments, diffraction patterns were recorded at intervals of 5°C, with an acquisition time of 3 minutes at each temperature. In this way, relatively accurate transformation temperatures could be obtained within a reasonable amount of beam time.

Table 7.2. Sample compositions and transition temperatures measured in NPD experiments

Sample No.	Composition (at.%)	Transition temperatures (±2.5°C)	Phase first appearing below this temperature
1	$Nd_{15}Mg_{65}Zn_{20}$	715°C	τ3
		505°C	(Mg)
2	$Nd_{16}Mg_{37}Zn_{47}$	730 °C	τ3
		645 °C	τ7?
		505 °C	$Nd(Mg,Zn)_{12}$
3	$Nd_{6}Mg_{41}Zn_{53}$	660 °C	α-Nd_2Zn_{17}
		595 °C	τ4?
		445 °C	τ5?
		330 °C	*
4	$Nd_{20}Mg_{20}Zn_{60}$	740 °C	Nd_3Zn_{11}
		725°C	τ3
		685 °C	τ7

* The hump related to the liquid phase disappeared at this temperature

? Possible phase

All patterns were analyzed using the GSAS/EXPGUI software [38]. Transition temperatures obtained from the ND experiments are summarized in Table 2.

7.3.1 Sample #1 ($Nd_{15}Mg_{65}Zn_{20}$)

Figure 5(a) shows ND patterns for sample #1 obtained upon cooling. Although patterns were acquired every 5 °C, only a few selected patterns are shown. A hump around $2\theta = 30^{o}$ due to the liquid phase is visible at 755°C. All other peaks above the background at this temperature were indexed as being from the crucible or the thermocouple. Hence, the sample at 755°C was entirely liquid. Patterns shown at 715°C and 505°C were obtained just after the appearance of a new phase. Analysis of the patterns shows that τ3 is the first phase to appear upon cooling at 715°C, followed by hcp (Mg) at 505 °C. The measured transition temperatures for sample #1 are shown on Fig. 6(a).

The lattice constant of τ3 is refined to be 0.7013(3) nm, which is in good agreement with the reported values (~0.695-0.720 nm, depending on the Zn content) from Xu *et al* [17].

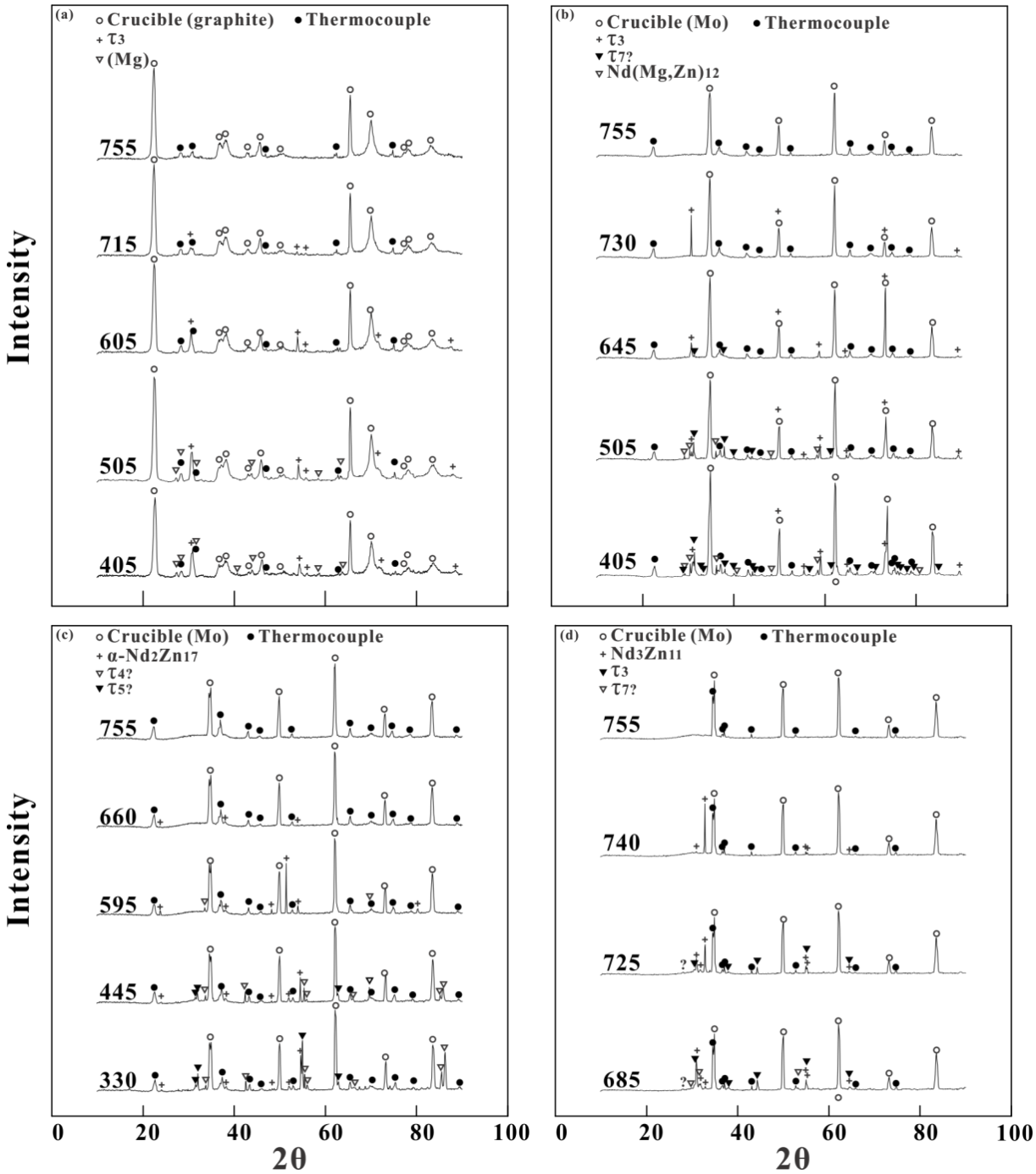

Figure 7.5. Selected ND patterns for (a) $Nd_{15}Mg_{65}Zn_{20}$ (sample #1), (b) $Nd_{16}Mg_{37}Zn_{47}$ (sample #2), (c) for $Nd_6Mg_{41}Zn_{53}$ (sample #3) and $Nd_{20}Mg_{20}Zn_{60}$ (sample #4)

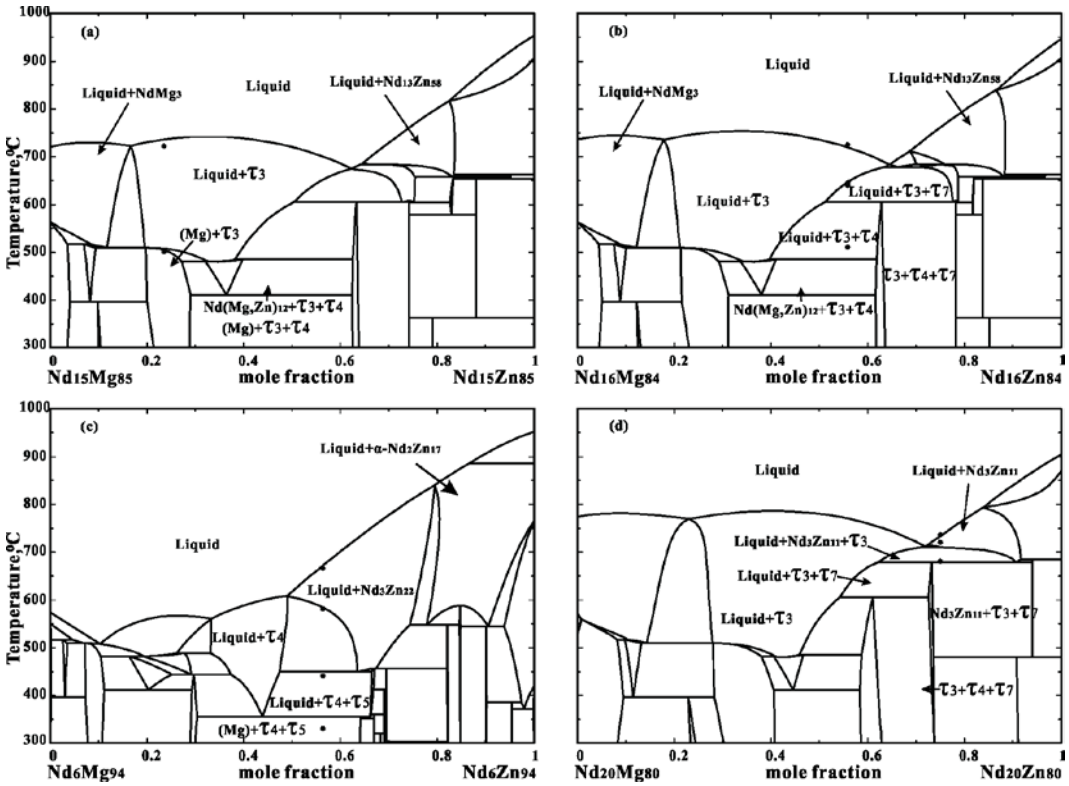

Figure 7.6. Calculated optimized isopleths of the (a) $Nd_{15}Mg_{85}$-$Nd_{15}Zn_{85}$, (b) $Nd_{16}Mg_{84}$-$Nd_{16}Zn_{84}$, (c) Nd_6Mg_{94}-Nd_6Zn_{94} and (d) $Nd_{20}Mg_{80}$-$Nd_{20}Zn_{80}$ sections showing experimental transition temperatures from samples #1, #2, #3 and #4, respectively

7.3.2 Sample #2 ($Nd_{16}Mg_{37}Zn_{47}$)

ND patterns at selected temperatures for sample #2 are shown in Fig. 5(b). τ3 is the primary phase which forms at 730 ^{o}C upon cooling while τ7 (possible phase, not indexed) and $Nd(Mg,Zn)_{12}$ form at 645 ^{o}C and 505 ^{o}C, respectively. Peaks from τ3 are very easy to recognize since τ3 has a simple cubic structure. However, the crystal structures of τ7 and $Nd(Mg,Zn)_{12}$ are more complex, resulting in many peaks. The measured transition temperatures for sample #2 are shown on Fig. 6(b).

The lattice constant of τ3 was refined to be 0.6986(2) nm, which is less than that of τ3 in sample #1. From Fig. 1 it can be seen that the Zn content of τ3 is highest in sample #4, followed by sample #2 and then #1. As Mg is replaced by Zn, the lattice constant is expected to decrease because Zn has a smaller atomic radius [30]. Hence, the lattice constant of τ3 in sample #2 is

expected to be less than in sample #1 as observed. The lattice constant of τ3 in sample #4 can thus be expected to be even smaller, as is in fact confirmed in this work (see below).

7.3.3 Sample #3 ($Nd_6Mg_{41}Zn_{53}$)

Figure 5(c) shows ND patterns for sample #3 at selected temperatures. The primary phase for this sample is α-Nd_2Zn_{17}, which forms at 660°C. A second phase forms at 595°C and a third at 445 ^{o}C. These two phases cannot be indexed as any of the binary phases which could occur. Hence, they could be two ternary phases. Unfortunately, the low peak intensities make it impossible to determine the crystal structures of these two ternary phases. However, it is believed they are most likely the τ4 and τ5 phases as this is consistent with the thermodynamic analysis. The hump related to the liquid phase disappeared at 330°C. Some new peaks appeared at this temperature which could be contributed to (Mg). However, they could not be indexed because the intensities were too low. The measured transition temperatures from sample #3 are shown in Fig. 6(c).

7.3.4 Sample #4 ($Nd_{20}Mg_{20}Zn_{60}$)

Figure 5(d) shows selected ND patterns for sample #4. At least four phases are observed during the cooling process: Nd_3Zn_{11} forms at 740°C; τ3 forms at 725°C: τ7 (possible phase, not indexed) forms at 685°C and at the same temperature the peaks for Nd_3Zn_{11} disappears. As can be seen in Fig. 6(d), our optimization predicts that Nd_3Zn_{11} may actually persist below 685°C, but in very small, and hence undetectable, amounts, since the overall sample composition lies very close to the 2-phase (τ3+τ7) field.

The refined lattice constant for τ3 is 0.6973(1) nm, which, as expected, is less than that for τ3 in samples #1 and #2, in agreement with the phase relationships in Fig. 1, as discussed in Section 3.2.

7.4 Thermodynamic optimization

Thermodynamic data for the pure elements were given previously [12]. The thermodynamic parameters of the three binary sub-systems are taken from Ansara *et al* [7] (Mg-Zn), Kang *et al* [8] (Nd-Mg) and Zhu and Pelton [12] (Nd-Zn).

For the three binary sub-systems, the Modified Quasichemical Model (MQM) [39, 40], which takes account of short-range ordering, was used to model the liquid phase. Consequently, the MQM is used to model the liquid phase in the ternary system. For details of the model, see references [12, 13, 39, 40]. The symmetric (Kohler-like) model [40] was used to estimate the properties of the ternary liquid phase from the optimized binary model parameters. No additional ternary model parameters were introduced.

In the optimization of the Mg-Zn binary system, Ansara *et al* [7] did not use the MQM for the liquid phase. Consequently, the liquid phase was remodelled using the MQM, keeping the same parameters as Ansara *et al* [7] for all other binary phases. The "coordination numbers", which are MQM model parameters, were set to

$$Z^{Mg}_{Mg,Zn} = Z^{Zn}_{Mg,Zn} = Z^{Mg}_{Mg,Mg} = Z^{Zn}_{Zn,Zn} = 6 \qquad 7.5$$

and the MQM model parameters were introduced as

$$\Delta g_{MgZn} = -6778 + 3.138T + (-1966 + 2.008)X_{MgMg} + (-3975 + 1.6736)X_{ZnZn} \text{ (J/g-atom)} \qquad 7.6$$

The binary Bcc_A2, Fcc_A1 and Hcp_A3 solutions are described by a substitutional solution model as discussed previously [12].

As shown in Table 1, Mg and Zn can substitute for each other on one sublattice in some phases (τ3, Nd(Mg,Zn), $NdMg_3$ and $Nd(Mg,Zn)_{12}$). These phases are modeled with the Compound Energy Formalisim (CEF) [41]. For example, the Gibbs energy of Nd(Mg,Zn) (per mole formula) can be expressed as follows:

$$G^{Nd(Mg,Zn)} = y_{Mg}G^{0,Nd(Mg,Zn)}_{Nd:Mg} + y_{Zn}G^{0,Nd(Mg,Zn)}_{Nd:Zn} + RT\left(y_{Mg}lny_{Mg} + y_{Zn}lny_{Zn}\right) + y_{Mg}y_{Zn}(L^{0}_{Nd:Mg,Zn} + (y_{Mg} - y_{Zn})\,L^{1}_{Nd:Mg,Zn}) \qquad 7.7$$

where y_{Mg} and $y_{Zn}$are the site fractions of Mg and Zn in the second sublattice, $G^{0,Nd(Mg,Zn)}_{Nd:Mg}$ and $G^{0,Nd(Mg,Zn)}_{Nd:Zn}$ are the Gibbs energies of the end-members (NdMg and NdZn) at temperature T under the convention that the enthalpies of the elements are in their stable states at 298.15K and $L^{0}_{Nd:Mg,Zn}$ and $L^{1}_{Nd:Mg,Zn}$ are interaction parameters to be optimized. The Gibbs energies of τ3, $NdMg_3$ and $Nd(Mg,Zn)_{12}$ can be expressed similarly.

The τ2, τ4, τ5 and τ7 phases are treated as stoichiometric compounds.

No thermodynamic properties for the ternary compounds could be found in the literature. To obtain initial estimates of the enthalpies and entropies of formation of the ternary compounds, three lines passing through the compound on the ternary Gibbs triangle were drawn parallel to the three edges of the triangle. The six intersection points of these lines with the edges defined six "binary compounds" whose enthalpies and entropies were then averaged to give the initial estimates. Thereafter, these values were adjusted to best reproduce the available data.

All model parameters optimized in the present work are listed in Table 3. All other model parameters (apart from the MQM parameters for liquid Mg-Zn given in section 4) have been given previously [7, 8, 12]. Very few model parameters are required. The enthalpies of formation of all compounds have reasonable values. The entropies of formation are all small and negative as expected.

Table 7.3. Thermodynamic model parameters optimized in the present work for the Nd-Mg-Zn system

Phase name	Model	Parameters (J/mol-atom)
Nd(Mg,Zn)	Nd(Mg,Zn)	Ideal mixing
$NdMg_3$	$Nd(Mg,Zn)_3$	$G^0_{Nd:Zn} = -32655 + 6.28T$
		$L^0_{Nd:Mg,Zn} = -4184$
		$L^1_{Nd:Mg,Zn} = -2092$
$NdMg_{12}$	$Nd(Mg,Zn)_{12}$	$L^0_{Nd:Mg,Zn} = -2736$
τ2	$Nd_2Mg_{53}Zn_{45}$	$G^0_{Nd:Mg:Zn} = -9836 + 0.92T$
τ3	$Nd(Mg,Zn)_2Mg$	$G^0_{Nd:Mg:Mg} = -18375 + 6.63T$
		$G^0_{Nd:Zn:Mg} = -33158 + 6.28T$
		$L^0_{Nd:Mg,Zn:Mg} = 1046$
		$L^1_{Nd:Mg,Zn:Mg} = 4184$
τ4	$Nd_2Mg_5Zn_9$	$G^0_{Nd:Mg:Zn} = -25601 + 5.23T$
τ5	$Nd_3Mg_{13}Zn_{30}$	$G^0_{Nd:Mg:Zn} = -19738 + 3.94T$
τ7	$Nd_{20}Mg_{19}Zn_{81}$	$G^0_{Nd:Mg:Zn} = -29946 + 5.25$

7.5 Comparison of calculations with experimental data

The Nd-Mg-Zn system was optimized by Qi *et al* [42] and Zhang *et al* [43]. However, only a few of the ternary compounds were considered in their optimizations.

The calculated 300°C isothermal section of the Nd-Mg-Zn system is shown in Fig. 1. Although both $NdMg_{12}$ and $NdZn_{12}$ end-members are not stable in the respective binary systems, the $Nd(Mg,Zn)_{12}$ phase is a stable phase in the isothermal section at 300°C according to several authors [17-19]. However, in the current optimization, it is impossible to reproduce other data, particularly most data points in Figs. 2(c) and 6(b) apart from the liquidus points, if we assume that this phase is stable at 300°C. According to our calculation, this phase is only stable in the temperature range ~413-488°C. Our calculations in the Sm-Mg-Zn system [15] show that the $Sm(Mg,Zn)_{12}$ phase is not stable at any temperature, in agreement with the results of Xia *et al* [44]. That is, the $RE(Mg,Zn)_{12}$ phase becomes less stable going along the RE series from Ce-Mg-Zn to Sm-Mg-Zn. The calculated Nd-Mg-Zn isothermal section at 300°C (Fig. 1) does not agree exactly with the reported sections (Figs. 3 and 4). As expected, the reported small solubility ranges of some of the ternary phases are not reproduced because we treated these phases as stoichiometric compounds. Some of the reported compatibility triangles in Figs. 3 and 4 are also not reproduced as it proved impossible to fit all the reported isothermal sections as well as our ND data simultaneously. The trends identified above, and our ND data, are favored in the optimization since the two reported isothermal sections shown in Figs. 3 and 4 may not represent complete equilibrium as has been discussed in Section 2. Figure 7 shows the calculated isothermal section at 427°C. In this section $Nd(Mg,Zn)_{12}$ is a stable phase.

In general, in our optimizations more weight was given to the experimental data from the present ND experiments because these experiments provided data at higher temperatures, at which liquid was present, making it more likely that equilibrium was reached. Furthermore, large samples (10 to 20 g) were used in the present ND experiments, leading to better control of composition and increased resistance to oxidation.

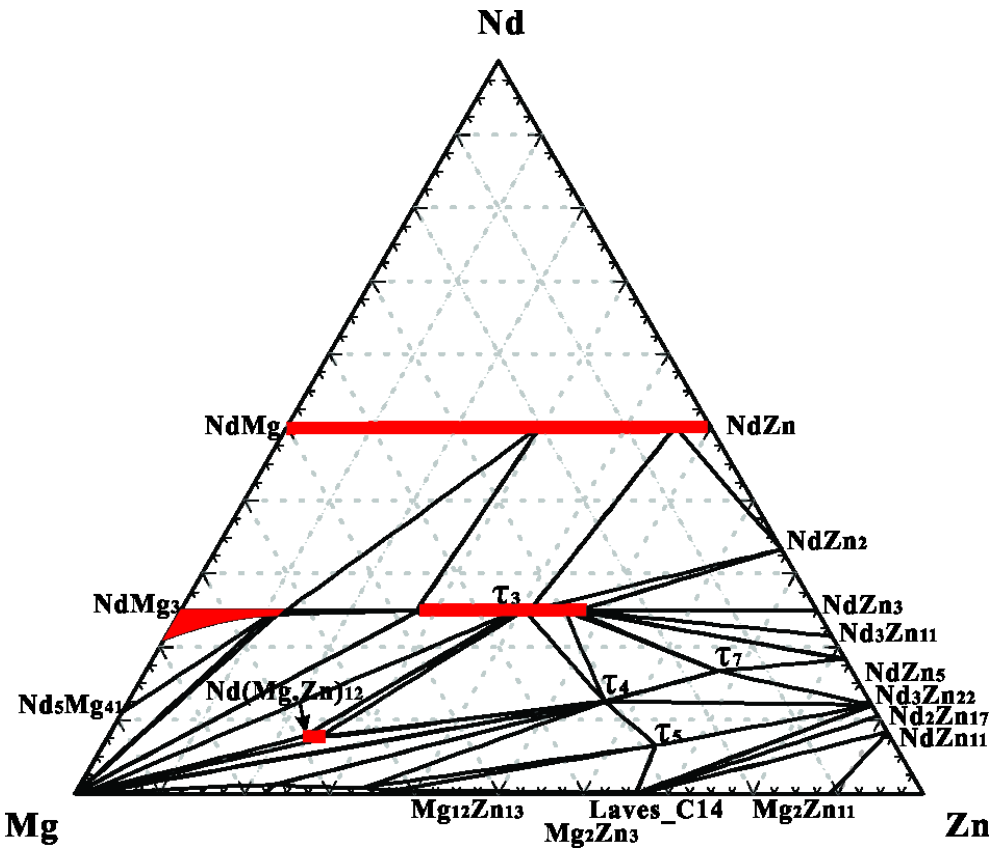

Figure 7.7. Calculated optimized isothermal section of the Nd-Mg-Zn system at 427°C. The $Nd(Mg,Zn)_{12}$ phase is stable at this temperature according to the calculations. (mole fraction)

Calculated Zn solubilities in $NdMg_3$ are less than those reported. However, the higher reported solubilities proved inconsistent with the current ND results . Again, more weight was given to the high temperature ND results which are more likely to correspond to equilibrium due to the presence of the liquid phase.

Figs. 2 shows three calculated isopleths along with experimental TA data from Drits *et al* [24]. Most of the data points are well accounted for in the present optimization.

Only one isopleth (the same as Fig. 2(c)) was calculated in the optimization of Qi *et al* [42] and their fit to the experimental data points is not good. The same isopleth was also calculated in the optimization of Zhang *et al* [43] who could only reproduce the data points for the liquidus.

Calculated isopleths are shown in Fig. 6 along with experimental data from the present ND experiments. Calculated transition temperatures and precipitation sequences are in good

agreement with the experiments. The higher transition temperatures (especially the liquidus temperatures) are considered more reliable than the lower transition temperatures because of kinetic constraints on attaining equilibrium at low temperature.

No ternary MQM parameters were required for the liquid phase, yet all the liquidus data points from the literature (see Fig. 2) and the present ND experiments (see Fig. 6) are well reproduced.

A tentative calculated liquidus projection for the Nd-Mg-Zn system is shown in Figs. 8-9 and a tentative list of the calculated temperatures of invariant reactions, maxima and minima is given in Table 4. As discussed in Section 2, two additional ternary phases, τ1 and τ6, might be stable, but were not considered for lack of evidence. If these phases actually are stable, then the liquidus surface will contain a τ1 field and a τ6 field in the Zn-rich region as in the Ce-Mg-Zn system (see Figs 9 and 10 of ref [14]).

Table 7.4. Tentative Calculated invariant reactions, maxima and minima and their temperatures (^{o}C) in the Nd-Mg-Zn system

P1	886	U1	755	E1	735	U2	727	E2	722	U3	716	P2	694
U4	688	U5	665	P3	612	U6	610	U7	548	U8	544	U9	516
U10	509	P4	488	U11	482	P5	456	U12	449	U13	443	U14	413
P6	359	U15	355	U16	351	U17	350	U18	345	E3	345	max1	~788
max2	~766	max3	~741	max4	~588								

Four invariant reactions were reported by Drits *et al* [24] (Eqs 1-4). These most likely correspond to the following invariant reactions from the present calculations:

U9: $L + Nd_5Mg_{41} \leftrightarrow (Mg) + NdMg_3$ at 516°C 7.8

U11: $L + \tau3 \leftrightarrow (Mg) + Nd(Mg,Zn)_{12}$ at 482°C 7.9

U13: $L + Nd(Mg,Zn)_{12} \leftrightarrow (Mg) + \tau4$ at 443°C 7.10

E3: $L \leftrightarrow \tau2 + (Mg) + Mg_{51}Zn_{20}$ at 345°C 7.11

The invariant reactions are not identical to those proposed by Drits *et al* [24], but the temperatures are in very good agreement.

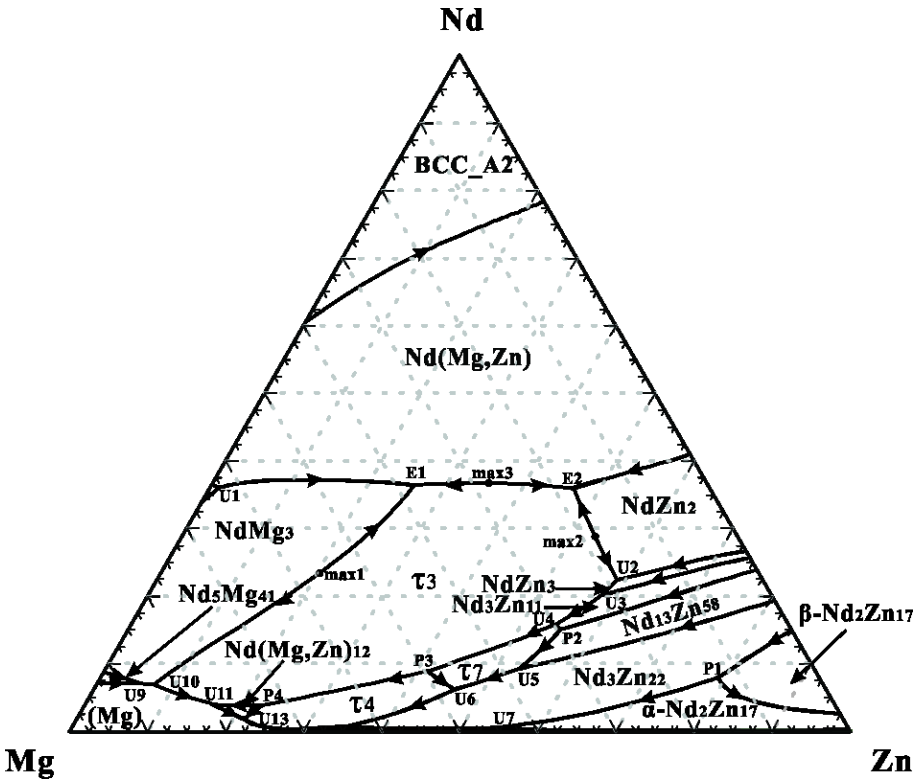

Figure 7.8. Tentative calculated liquidus projection for Nd-Mg-Zn system (mole fraction)

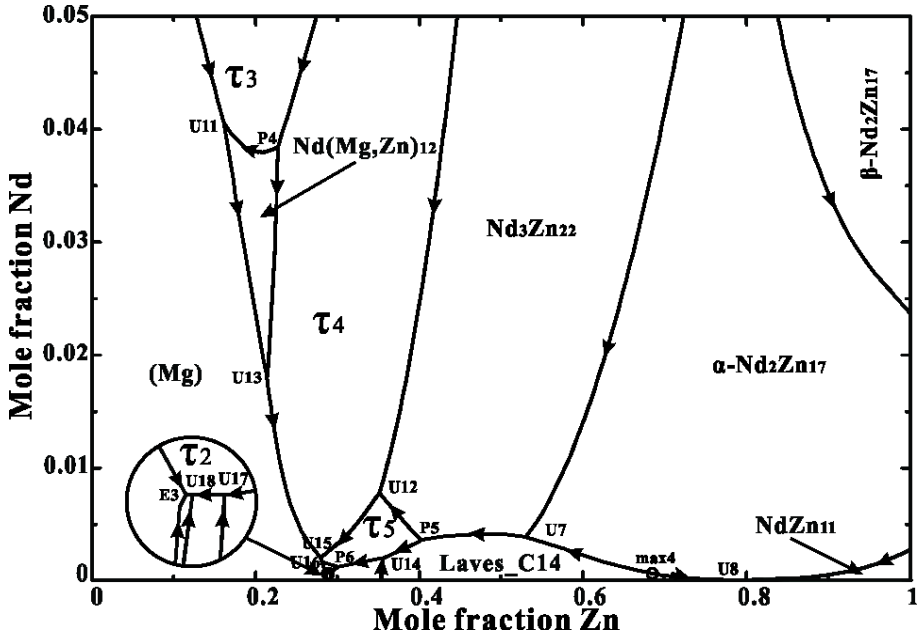

Figure 7.9. Enlargement of part of Figure 7.8

7.6 Discussion

In the optimization, greater weight was accorded to the ND data from the present investigation, firstly because the ND data were obtained in situ at equilibrium at higher temperatures, and secondly because, due to the high penetrating power of neutrons, large samples (10 to 20 g) could be used, thereby leading to better control of composition and increased resistance to oxidation.

The τ1 and τ6 phases are not considered in the present optimization. The presence of these two possible phases would affect the phase relationships in the composition ranges where the two phases could be stable. Future ND could be carried out to verify whether these two phases are stable.

Thermodynamic modeling and ND experiments in the Ce-Mg-Zn system have been reported in a previous article [14]. In subsequent articles we shall report on thermodynamic optimizations of most other ternary RE-Mg-Zn systems. The model parameters will be included in the FTlite light metals database of the FactSage database computing system [45] which already contains optimized model parameters for the solid and liquid phases of a large number of binary and ternary Mg- and Al-containing systems. Through the models, the properties and phase equilibria of multicomponent systems can thus be estimated and calculated.

All calculations in the present work were performed with the FactSage software [45].

7.7 Conclusions

All available phase diagram data for the Nd-Mg-Zn system were critically assessed. *In-situ* neutron diffraction (ND) experiments were performed on selected samples to identify phases and transition temperatures. A critical thermodynamic evaluation and optimization of the Nd-Mg-Zn system was carried out and model parameters for the thermodynamic properties of all phases were obtained. The phase transformation behavior of selected samples was well resolved from the ND experiments and experimental data were used to refine the thermodynamic model parameters.

All optimized model parameters from the present work are summarized in Table 3. Binary parameters were reported in previous articles [7, 8, 12]. Very few model parameters are required, and all parameters have thermodynamically reasonable values. In particular, no additional ternary parameters were required in the MQM model for the liquid phase.

Acknowledgements

This research was supported by funding from the Natural Sciences and Engineering Research Council of Canada (NSERC) Magnesium Strategic Research Network. More information on the Network can be found at www.MagNET.ubc.ca. The authors would like to thank Prof. Mamoun Medraj for allowing us to use the facilities of theTMG laboratory at Concordia University for preparing all the samples. The authors would also like to thank Dr. Dmytro Kevorkov and Dr. Ahmad Mostafa for helping prepare the samples.

References

[1] B.L. Mordike, T. Ebert, Magnesium: Properties — applications — potential, Mat. Sci. Eng. A-Struct, 302 (2001) 37-45.

[2] I.P. Moreno, T.K. Nandy, J.W. Jones, J.E. Allison, T.M. Pollock, Microstructural stability and creep of rare-earth containing magnesium alloys, Scripta Mater., 48 (2003) 1029-1034.

[3] J. Bohlen, M.R. Nürnberg, J.W. Senn, D. Letzig, S.R. Agnew, The texture and anisotropy of magnesium-zinc-rare earth alloy sheets, Acta Mater., 55 (2007) 2101-2112.

[4] R.K. Mishra, A.K. Gupta, P.R. Rao, A.K. Sachdev, A.M. Kumar, A.A. Luo, Influence of cerium on the texture and ductility of magnesium extrusions, Scripta Mater., 59 (2008) 562-565.

[5] N. Stanford, M.R. Barnett, The origin of “rare earth” texture development in extruded Mg-based alloys and its effect on tensile ductility, Mat. Sci. Eng. A-Struct, 496 (2008) 399-408.

[6] K. Hantzsche, J. Bohlen, J. Wendt, K.U. Kainer, S.B. Yi, D. Letzig, Effect of rare earth additions on microstructure and texture development of magnesium alloy sheets, Scripta Mater., 63 (2010) 725-730.

[7] I. Ansara, A. T. Dinsdale, M. H. Rand, COST 507: Definition of thermochemical and thermophysical properties to provide a database for the development of new light alloys, Thermochemical database for light metal alloys, Vol. 2, Office for Official Publications of the European Communities, Luxembourg,1998; P. Spencer, unpublished work

[8] Y.-B. Kang, L. Jin, P. Chartrand, A.E. Gheribi, K. Bai, P. Wu, Thermodynamic evaluations and optimizations of binary Mg-light Rare Earth (La, Ce, Pr, Nd, Sm) systems, CALPHAD, 38 (2012) 100-116.

[9] Y.-B. Kang, A. Pelton, P. Chartrand, P. Spencer, C. Fuerst, Critical Evaluation and Thermodynamic Optimization of the Binary Systems in the Mg-Ce-Mn-Y System, J. Phase Equilib. Diff., 28 (2007) 342-354.

[10] Y.-B. Kang, A.D. Pelton, P. Chartrand, C.D. Fuerst, Critical evaluation and thermodynamic optimization of the Al–Ce, Al–Y, Al–Sc and Mg–Sc binary systems, CALPHAD, 32 (2008) 413-422.

[11] L. Jin, PhD Thesis, Ecole Polytechnique, Montreal (Canada), 2012, pp. 407

[12] Z. Zhu, A. Pelton, Critical assessment and optimization of phase diagrams and thermodynamic properties of RE–Zn systems-part I: Sc–Zn, La–Zn, Ce–Zn, Pr–Zn, Nd–Zn, Pm–Zn and Sm–Zn, J. Alloys Compd. 641 (2015) 249-260

[13] Z. Zhu, A. Pelton, Critical assessment and optimization of phase diagrams and thermodynamic properties of RE–Zn systems-Part II: Y–Zn, Eu–Zn, Gd–Zn, Tb–Zn, Dy–Zn, Ho–Zn, Er–Zn, Tm–Zn, Yb–Zn and Lu–Zn, J. Alloys Compd, 641 (2015) 261-271

[14] Z. Zhu, M.A. Gharghouri, M. Medraj, S.Y. Lee, A.D. Pelton, Thermodynamic Modeling and In-situ Neutron Diffraction Investigation of the Ce-Mg-Zn system, submitted for publication.

[15] Z. Zhu, A. Pelton, Thermodynamic Modeling of the La-Mg-Zn, Pr-Mg-Zn and Sm-Mg-Zn system, submitted for publication.

[16] Z. Zhu, A. Pelton, Thermodynamic Modeling of the Y-Mg-Zn, Gd-Mg-Zn, Tb-Mg-Zn, Dy-Mg-Zn, Ho-Mg-Zn, Er-Mg-Zn, Tm-Mg-Zn and Lu-Mg-Zn systems, submitted for publication.

[17] H. Xu, J. Fan, H.-L. Chen, R. Schmid-Fetzer, F. Zhang, Y. Wang, Q. Gao, T. Zhou, Experimental determination of the phase equilibria of the Mg–Nd–Zn system at 320 °C, J. Alloys Compd., 603 (2014) 100-110.

[18] A. Mostafa, M. Medraj, Experimental Investigation of the Mg-Nd-Zn Isothermal Section at 300 °C Metals, 5 (2015) 84-101.

[19] V. Kinzhibalo, A. Tyvanchuk, E. Melnik, Stable and Metastable Phase Equilibria in Metallic Systems, Nauka Mosc. USSR (1985) 70-74.

[20] A. Iandelli, Intermetallic and metalloid gadolinium compounds, Atti accad. nazl. Lincei, Rend., Classe sci. fis., mat. e, nat., 29 (1960) 62-69

[21] S. Delfino, A. Saccone, R. Ferro, Phase relationships in the neodymium-magnesium alloy system, Metall. Trans. A, 21 (1990) 2109-2114.

[22] M.L. Huang, H.X. Li, H. Ding, Z.Y. Tang, R.B. Mei, H.T. Zhou, R.P. Ren, S.M. Hao, A ternary linear compound T2 and its phase equilibrium relationships in Mg-Zn-Nd system at 400 °C, J. Alloys Compd, 489 (2010) 620-625.

[23] E.V. Mel'nik, V.V. Kinzhibalo, E.M. Padezhnova, T.V. Dobatkina, New ternary compounds with face-centered lattice in the Mg-Zn-RE systems, Tezizy Dokl. Vses. Konf. Kristallokhim. Intermet. Soeden., (1978).

[24] M.E. Drits, E.M. Padezhnova, N.V. Miklina, Phase diagram of the magnesium-neodymium-zinc system in the magnesium-rich phase, Izv. Vyssh. Ucheb. Zaved., Tsvet. Met., 14 (1971) 104-107.

[25] M.E. Drits, E.M. Padezhnova, N.V. Miklina, Solubility of neodymium and zinc in solid magnesium, Tekhnol. Legk. Splavov. Nauch.-Tekh. Byul. Vses. Inst. Legk. Splavov, 1 (1971) 32-35.

[26] M.E. Drits, E.M. Padezhnova, N.V. Miklina, An investigation of the mutual solubility of neodymium and zinc in solid magnesium, Izv. Akad. Nauk SSSR, Met., (1974) 225-229.

[27] M.E. Drits, E.M. Padezhnova, N.V. Miklina, Phase equilibriums in magnesium-neodymium-yttrium-zinc alloys, Izv. Akad. Nauk SSSR, Met., (1974) 218-222.

[28] M.E. Drits, E.M. Padezhanova, N.V. Miklina, Combined solubility of neodymium and zinc in solid magnesium, Izv. Akad. Nauk SSSR, Met., (1974) 225-229.

[29] V. Pavlyuk, B. Marciniak, E. Różycka-Sokołowska, The isothermal section of the phase diagram of Ce–Mg–Zn ternary system at 470 K , Intermetallics, 20 (2012) 8-15.

[30] L. Pauling, Atomic Radii and Interatomic Distances in Metals, J. Am. Chem. Soc., 69 (1947) 542-553.

[31] D. Kevorkov, M. Pekguleryuz, Experimental study of the Ce-Mg-Zn phase diagram at 350 °C via diffusion couple techniques , J. Alloys Compd, 478 (2009) 427-436.

[32] V. Pavlyuk, P. Solokha, G. Dmytriv, B. Marciniak, V. Paul-Boncour, The Heusler-type alloy $MgZn_2Ce$, Acta Crystallogr E, 63 (2007) i161-i161.

[33] T. Horiuchi, H. Ikee, A. Hamaya, S. Minamoto, S. Nomoto, S. Miura, in: 7th International Conference on Processing and Manufacturing of Advanced Materials, THERMEC'2011, August 1, 2011 - August 5, 2011, Trans Tech Publications Ltd, Quebec City, QC, Canada, 2012, pp. 1170-1175.

[34] G. Shao, V. Varsani, Z. Fan, Thermodynamic modelling of the Y-Zn and Mg-Zn-Y systems, Calphad, 30 (2006) 286-295.

[35] A.-P. Tsai, Y. Murakami, A. Niikura, The Zn-Mg-Y phase diagram involving quasicrystals, Philos. Mag. A, 80 (2000) 1043-1054.

[36] H.Y. Qi, G.X. Huang, H. Bo, G.L. Xu, L.B. Liu, Z.P. Jin, Experimental investigation and thermodynamic assessment of the Mg-Zn-Gd system focused on Mg-rich corner, J. Mater. Sci., 47 (2012) 1319-1330.

[37] W. M. Haynes, ed., CRC Handbook of Chemistry and Physics, 95th Edition (Internet Version 2015), CRC Press/Taylor and Francis, Boca Raton, FL.

[38] B. Toby, EXPGUI, a graphical user interface for GSAS, J. Appl. Crystallogr., 34 (2001) 210-213.

[39] A. Pelton, S. Degterov, G. Eriksson, C. Robelin, Y. Dessureault, The modified quasichemical model I—Binary solutions, Metall. Mater. Trans. B, 31 (2000) 651-659.

[40] A. Pelton, P. Chartrand, The modified quasi-chemical model: Part II. Multicomponent solutions, Metall. Mater. Trans. A, 32 (2001) 1355-1360.

[41] M. Hillert, The compound energy formalism, J. Alloys Compd., 320 (2001) 161-176.

[42] H.Y. Qi, G.X. Huang, H. Bo, G.L. Xu, L.B. Liu, Z.P. Jin, Thermodynamic description of the Mg-Nd-Zn ternary system, J. Alloys Compd, 509 (2011) 3274-3281.

[43] C. Zhang, A.A. Luo, L. Peng, D.S. Stone, Y.A. Chang, Thermodynamic modeling and experimental investigation of the magnesium–neodymium–zinc alloys, Intermetallics, 19 (2011) 1720-1726.

[44] X. Xia, A. Sanaty-Zadeh, C. Zhang, A.A. Luo, X. Zeng, Y. Austin Chang, D.S. Stone, Thermodynamic modeling and experimental investigation of the magnesium–zinc–samarium alloys, J. Alloys Compd, 593 (2014) 71-78.

[45] C.W. Bale, E. Bélisle, P. Chartrand, S.A. Decterov, G. Eriksson, K. Hack, I.H. Jung, Y.B. Kang, J. Melançon, A.D. Pelton, C. Robelin, S. Petersen, FactSage thermochemical software and databases — recent developments, Calphad, 33 (2009) 295-311; www.factsage.com

Chapter 8 ARTICLE 5: THERMODYNAMIC MODELING OF THE LA-MG-ZN, PR-MG-ZN AND SM-MG-ZN SYSTEM

Submitted to Journal of Alloys and Compounds

Zhijun Zhu, Arthur D. Pelton*

Centre de Recherche en Calcul Thermochimique, Département de Génie Chimique, Ecole Polytechnique, Montréal, Québec, Canada

*Corresponding author

KEY WORDS

Rare earth systems, Magnesium systems, Zinc systems, Phase diagram, Thermodynamic assessment

ABSTRACT

All available phase diagram data for the La-Mg-Zn, Pr-Mg-Zn and Sm-Mg-Zn systems have been collected and critically assessed. Critical thermodynamic evaluations and optimizations of the La-Mg-Zn, Pr-Mg-Zn and Sm-Mg-Zn systems were carried out and model parameters for the thermodynamic properties of all phases have been obtained.

8.1 Introduction

Magnesium being the lightest structural metal, Mg-based alloys have many applications. Zinc is one of the most commonly used alloying elements in Mg (AZ series), and the rare earth (RE) metals have been shown to improve creep resistance [1, 2] and sheet formability (by reducing texture [3-6]).

Information on phase behavior is essential for the design of new RE-Mg-Zn alloys. However, few studies of the phase diagrams and thermodynamic properties of these systems have been made. The present study was thus undertaken to better define the phase diagrams of the RE-Mg-Zn ternary systems through the technique of critical thermodynamic assessment and optimization coupled with limited experimentation.

In a thermodynamic optimization, adjustable model parameters are calculated using all available thermodynamic and phase-equilibrium data in order to obtain one set of model equations as functions of temperature and composition. Thermodynamic data, such as activities, can aid in the evaluation of the phase diagrams, and information on phase equilibria can be used to deduce thermodynamic properties. With this technique, it is frequently possible to resolve discrepancies in the available data. From the model equations, all of the thermodynamic properties and phase diagrams can be back-calculated, and interpolations and extrapolations can be made in a thermodynamically correct manner. The thermodynamic properties and phase diagrams are thereby rendered self-consistent and consistent with thermodynamic principles, and the available data are distilled into a small set of model parameters, ideal for computer storage. Generally, in the optimization of a ternary system one begins by optimizing the three binary sub-systems. The binary model parameters are then used to estimate the properties of the ternary phases, and these estimates are then refined by introducing ternary model parameters where required to reproduce available ternary data.

Thermodynamic evaluations and optimizations have already been reported for the binary Mg-Zn system [7], all binary Mg-RE systems [8-11] and all binary RE-Zn systems (including Sc-Zn and Y-Zn) [12, 13]. Evaluations, optimizations and experimental phase diagram studies of the Ce-Mg-Zn and Nd-Mg-Zn systems have been reported in our previous articles [14, 15]. In the present article we report on our evaluations and optimizations of the La-Mg-Zn, Pr-Mg-Zn and Sm-Mg-Zn systems. In a subsequent article we shall report on our evaluations and optimizations of other ternary heavier-RE-Mg-Zn systems [16]. As expected, all RE-Mg-Zn systems are very similar. The present work on the La-Mg-Zn, Pr-Mg-Zn and Sm-Mg-Zn systems was greatly aided by our simultaneous assessments of the other RE-Mg-Zn systems.

Figs. 1-7 show the seven binary sub-systems of the La-Mg-Zn, Pr-Mg-Zn and Sm-Mg-Zn systems [7, 8, 12].

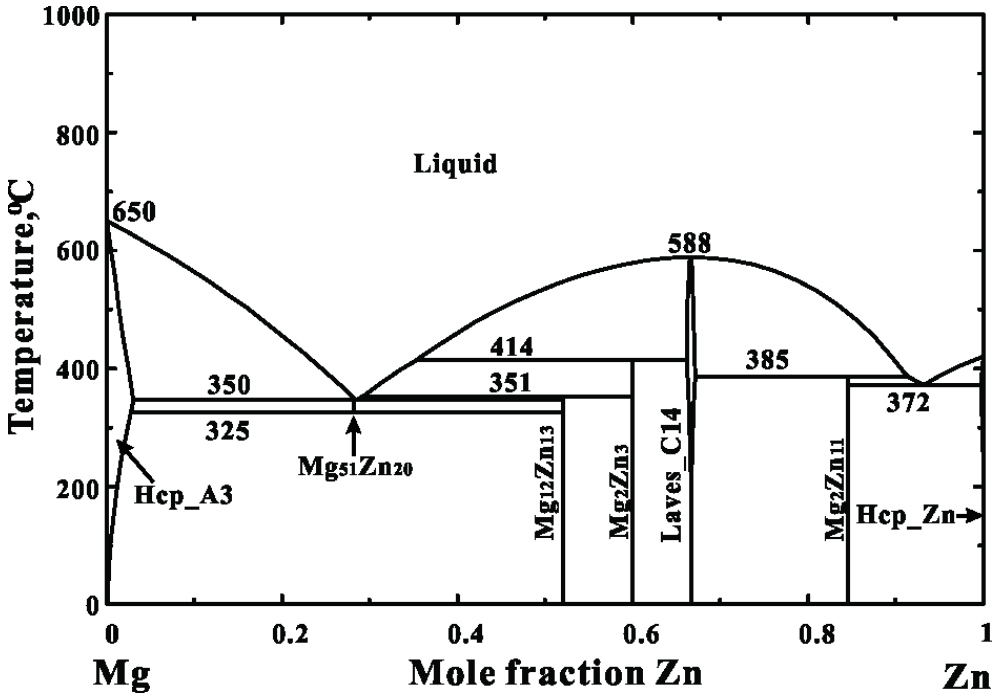

Figure 8.1. Calculated optimized Mg-Zn phase diagram [7]

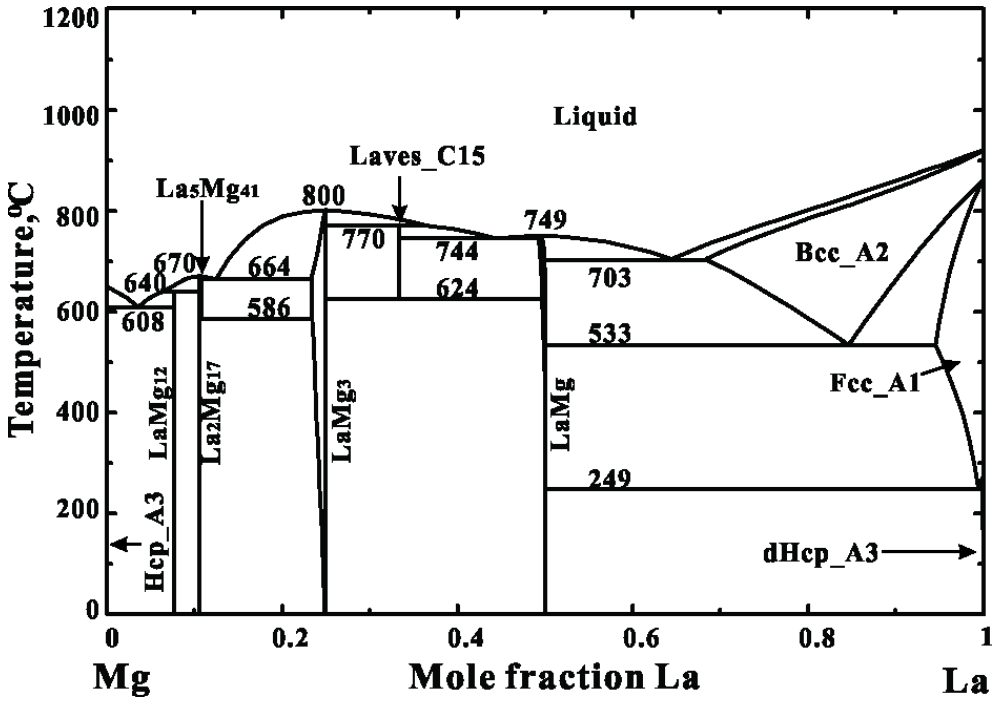

Figure 8.2. Calculated optimized Mg-La phase diagram [8]

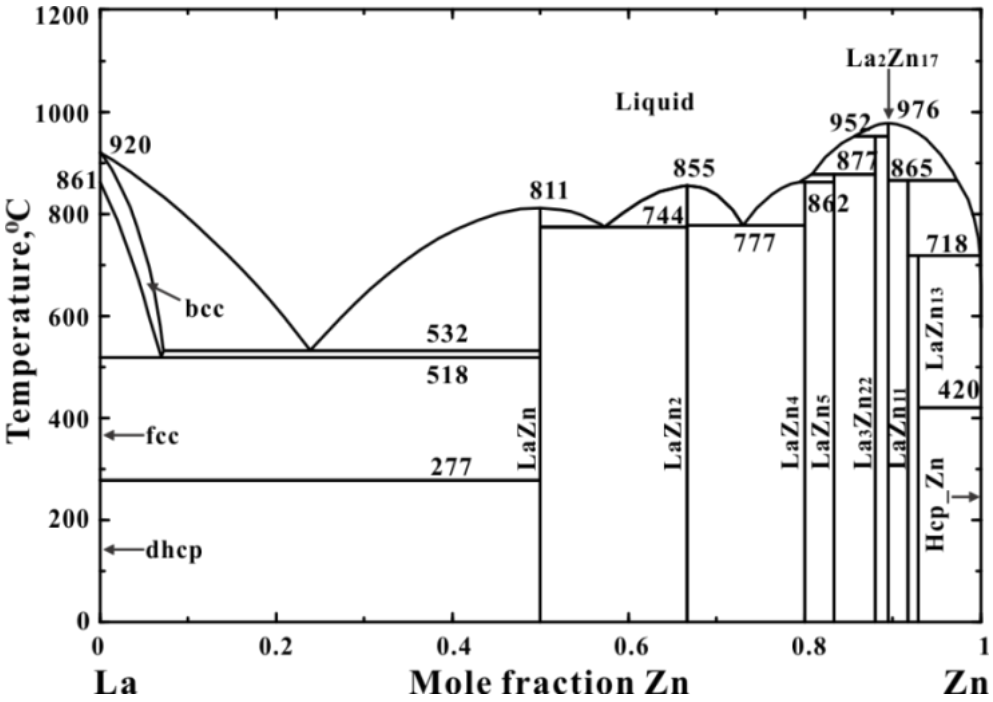

Figure 8.3. Calculated optimized La-Zn phase diagram [12]

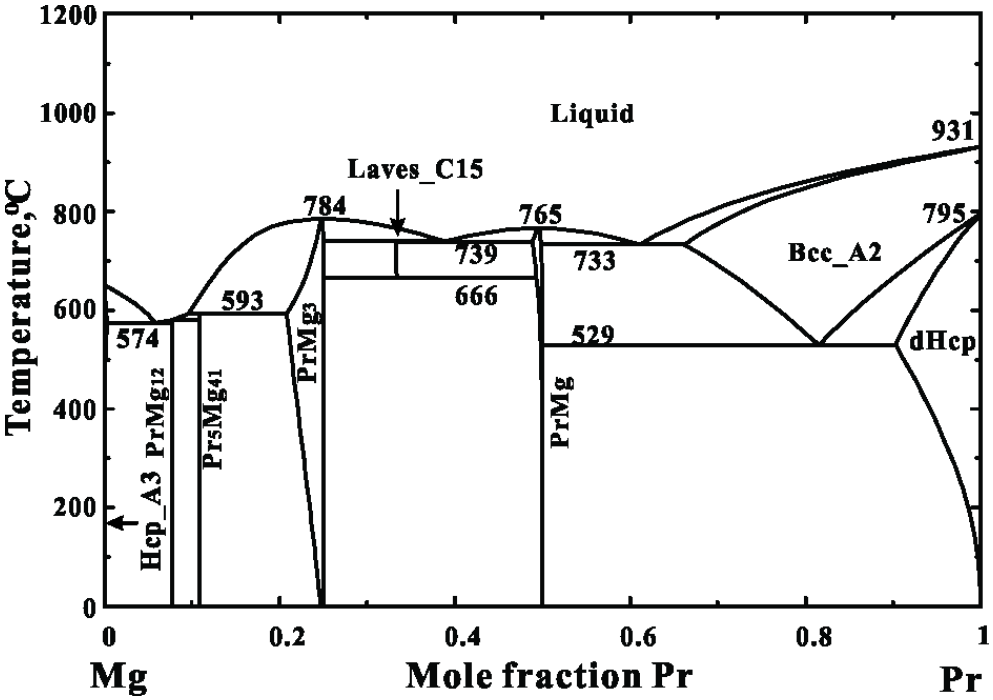

Figure 8.4. Calculated optimized Mg-Pr phase diagram [8]

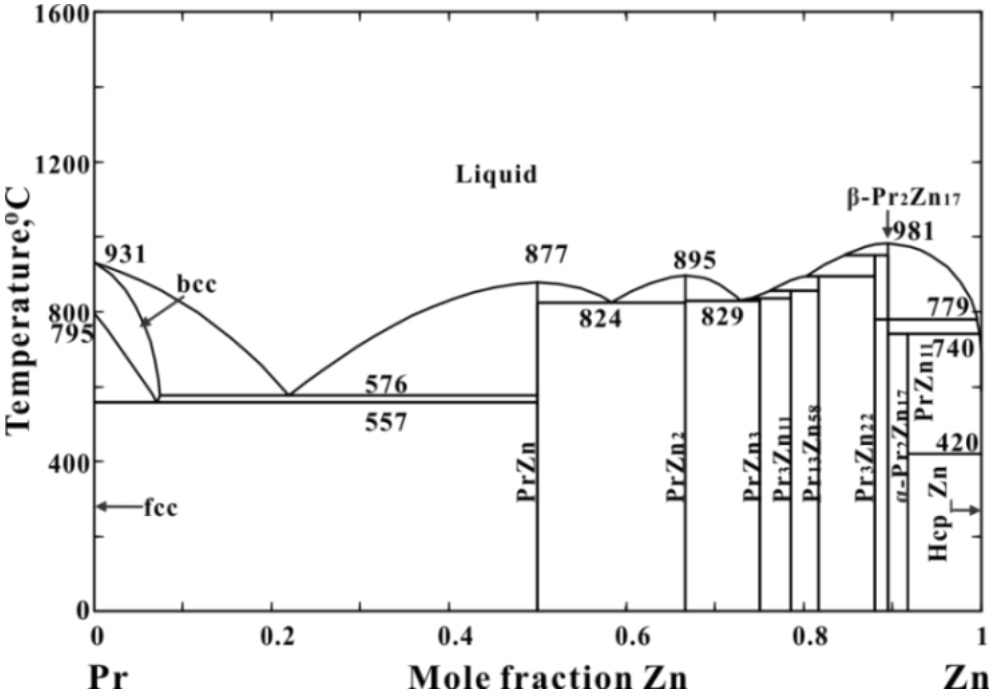

Figure 8.5. Calculated optimized Pr-Zn phase diagram [12]

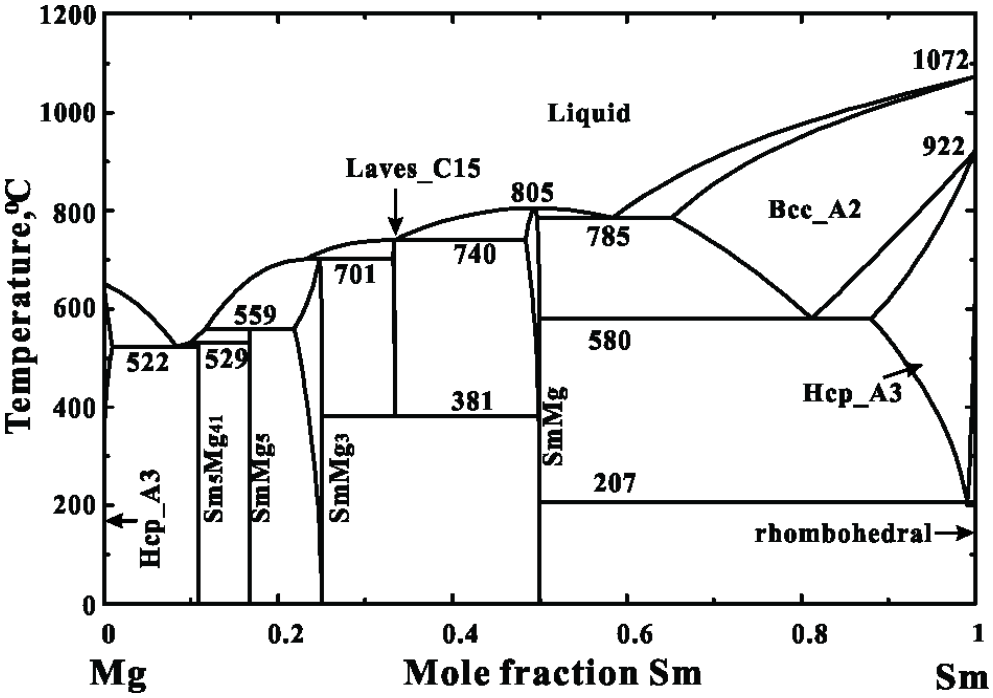

Figure 8.6. Calculated optimized Mg-Sm phase diagram [8]

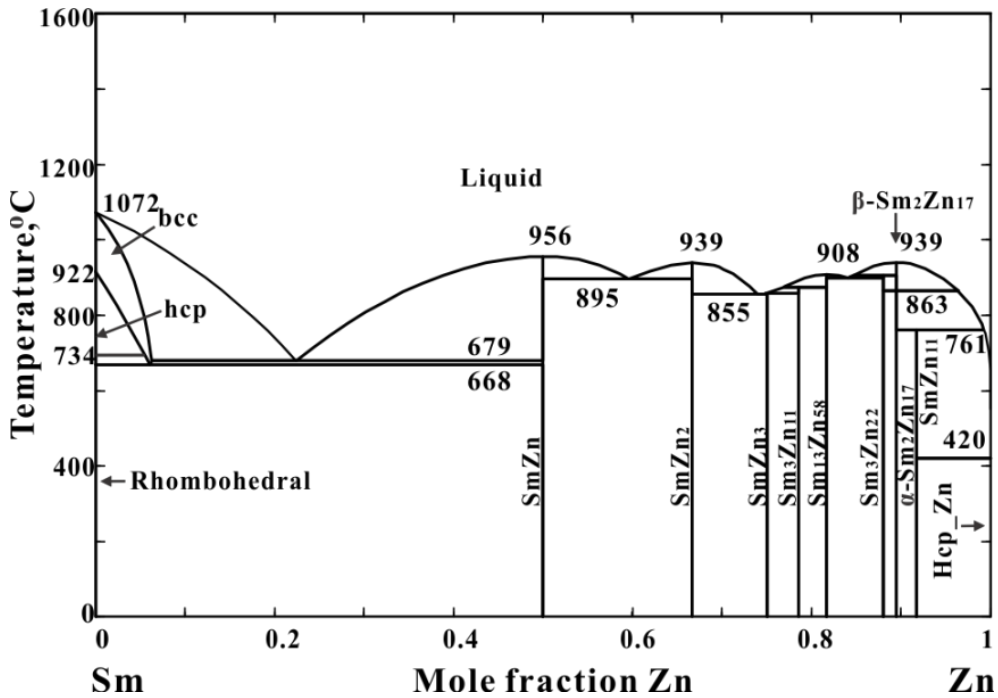

Figure 8.7. Calculated optimized Sm-Zn phase diagram [12]

8.2 Phase equilibrium and thermodynamic data

The La-Mg-Zn, Pr-Mg-Zn and Sm-Mg-Zn systems have been investigated by several authors. Different ternary phase names were used by different authors. Phases with ternary phase fields considered in the present optimization are summarized in Table 1. All these phases (except the metastable ones) can also be seen in the calculated isothermal sections at 300°C shown in Figs. 8, 13 and 16.

The same nomenclature as described in our previous report on the Ce-Mg-Zn system [14] is used here. The La-Mg-Zn system has been investigated over the entire composition range. None of the phases corresponding to phases τ1 to τ7 as considered in the Ce-Mg-Zn system [14] have been observed. However, although τ3 was not reported in the La-Mg-Zn system as a phase separate from $LaMg_3$, it is nevertheless assumed in the present study because it is a common phase observed in many other RE-Mg-Zn systems.

Table 8.1. Phases with possible ternary phase fields in the La-Mg-Zn, Pr-Mg-Zn and Sm-Mg-Zn systems

Phase name	Prototype-Pearson symbol-Space group	Thermodynamic model*	
La(Mg,Zn)	CsCl-cP2-$Pm\bar{3}m$	La(Mg,Zn)	LaMg and LaZn form a continuous solution [25] LaMg and LaZn do not form a continuous solution. Zn can dissolve in LaMg up to 1 at.% and Mg can dissolve in LaZn up to 7 at.% [21]
$LaMg_3$	BiF_3-cF16-$Fm\bar{3}m$	$La(Mg,Zn)_3$	Reported Zn solubility 42 at.% at 300°C [25] Reported Zn solubility 45 at.% at 322°C [21]
τ3	$Mn\mathit{Cu}_2\mathit{Al}$-cF16-$Fm\bar{3}m$	$LaMg(Mg,Zn)_2$	Assumed in the present work as a phase separate from $LaMg_3$
La_2Mg_{17}	$Ni_{17}Th_2$-hP38-$P6_3/mmc$	$La_2(Mg,Zn)_{17}$	La_2Mg_{17} and La_2Zn_{17} form continuous solution [25] Reported Zn solubility 52 at.% at 322°C [21]
β-La_2Zn_{17}	Th_2Zn_{17}-hR19-$R\bar{3}m$	$La_2(Mg,Zn)_{17}$	Reported Mg solubility 23.5 at.% at 322°C [21]
$LaMg_{12}$	$Mn_{12}Th$-tI26-$I4/mmm$	$La(Mg,Zn)_{12}$	Reported as a ternary phase with La content of ~8 at.% in ref [19, 20]
$LaZn_4$	orthorhombic	$La(Mg,Zn)_4$	Reported Mg solubility 22 at.% at 322°C [21]
V	unknown	$La_5Mg_{42}Zn_{53}$	Reported as V in ref [21, 25]
Pr(Mg,Zn)	CsCl-cP2-$Pm\bar{3}m$	Pr(Mg,Zn)	PrMg and PrZn form a continuous solution [22]
$PrMg_3$	BiF_3-cF16-$Fm\bar{3}m$	$Pr(Mg,Zn)_3$	Reported Zn solubility 42 at.% at 300°C [22]
$PrMg_{12}$	$Mn_{12}Th$-tI26-$I4/mmm$	$Pr(Mg,Zn)_{12}$	Reported [22] as separate phases: $PrMg_{12}$ with Zn solubility of 6 at.% at 300°C and $PrMg_6Zn_3$
[1]τ1	[2]$Al_{11}La_3$-oI28-Immm		
[1]τ2	unknown		
τ3	$Mn\mathit{Cu}_2\mathit{Al}$-cF16-$Fm\bar{3}m$	$PrMg(Mg,Zn)_2$	Reported as $Pr_3Mg_8Zn_{11}$ [22]
τ4	[2]$Tb\mathit{Cu}_7$-hP8-$P6/mmm$	$Pr_2Mg_5Zn_9$	Assumed stoichiometric in present study Reported as $Pr_2Mg_7Zn_{11}$ [22]
τ5	[2]$Ce_3Mg_{13}Zn_{30}$-hP92-$P6_3/mmc$	$Pr_3Mg_{13}Zn_{30}$	Assumed stoichiometric in present study Reported as $PrMg_7Zn_{12}$ [22]
[1]τ6	unknown		
[1]τ7	[2]$Ce_{20}Mg_{19}Zn_{81}$-cF480-$F\bar{4}3m$		

Sm(Mg,Zn)	CsCl-cP2-Pm$\bar{3}$m	Sm(Mg,Zn)	Assumed continuous solution in present study
$SmMg_3$	BiF_3-cF16-Fm$\bar{3}$m	$Sm(Mg,Zn)_3$	Assumed same Zn solubilities as other $REMg_3$ phases
$SmMg_{12}$	$Mn_{12}Th$-tI26-I4/mmm	$Sm(Mg,Zn)_{12}$	Assumed in present work
[1]τ1	[2]$Al_{11}La_3$-oI28-Immm		
[1]τ2	unknown		
τ3	MnCu_2Al-cF16-Fm$\bar{3}$m	$SmMg(Mg,Zn)_2$	Reported as X phase [23]
τ4	[2]TbCu_7-hP8-P6/mmm	$Sm_2Mg_5Zn_9$	Assumed stoichiometric in present study Reported as Y phase [23]
τ5	[2]$Ce_3Mg_{13}Zn_{30}$-hP92-P6_3/mmc	$Sm_3Mg_{13}Zn_{30}$	Assumed stoichiometric in present study Reported as Z phase [23]
[1]τ6	unknown		
[1]τ7	[2]$Ce_{20}Mg_{19}Zn_{81}$-cF480-F$\bar{4}$3m		

*Elements within brackets substitute on the same sublattice.

[1] Possible stable phase but not considered in the present work. τ1, τ2, τ6 and τ7 were modeled as $Ce_3Zn_9(Mg,Zn)_2$, $Ce_2Mg_{53}Zn_{45}$, $Ce_6Mg_{11}Zn_{83}$ and $Ce_{20}Mg_{19}Zn_{81}$, respectively, in the Ce-Mg-Zn system. Please refer to ref [14] for details.

[2]Crystal structures of these phases are proposed based on structures of similar phases in the Ce-Mg-Zn system [14]

Table 8.2. Phases with possible ternary phase fields in RE-Mg-Zn systems as assumed in the present project [14-16]

	Thermodynamic model	Y	La	Ce	Pr	Nd	(Pm)	Sm	(Eu)	Gd	Tb	Dy	Ho	Er	Tm	(Yb)	Lu
RE(Mg,Zn)	RE(Mg,Zn)	×	×	×	×	×		×		×	×	×	×	×	×		×
$REMg_3$	$RE(Mg,Zn)_3$	○	×	×	×	×		×		×	×	×	⦿	⦿	⦿		⦿
RE_2Mg_{17}	$RE_2(Mg,Zn)_{17}$	○	×	□	○	○		○		○	○	○	○	○	○		○
α-RE_2Zn_{17}	$RE_2(Mg,Zn)_{17}$	×	□	□	□	□		□		□	□	□	□	□	□		□
β-RE_2Zn_{17}	$RE_2(Mg,Zn)_{17}$	□	×	□	□	□		□		□	□	□	□	□	□		□
$REMg_{12}$	$RE(Mg,Zn)_{12}$	○	×	×	×	×		⦿		○	○	○	○	○	○		○
$REZn_4$	$RE(Mg,Zn)_4$	○	×	○	○	○		○		○	○	○	○	○	○		○
$\tau1$	$RE_3Zn_9(Mg,Zn)_2$	○	○	×	●	●		●		○	○	○	○	○	○		○
$\tau2$	$RE_2Mg_{53}Zn_{45}$	○	○	×	●	×		●		○	○	○	○	○	○		○
$\tau3$	$REMg(Mg,Zn)_2$	×	×	×	×	×		×		×	×	×	×	×	×		×
$\tau4$	$RE_2Mg_5Zn_9$	○	○	×	×	×		×		○	○	○	○	○	○		○
$\tau5$	$RE_3Mg_{13}Zn_{30}$	×	○	×	×	×		×		○	○	○	○	○	○		○
$\tau6$	$RE_6Mg_{11}Zn_{83}$	○	○	×	●	●		●		○	○	○	○	○	○		○
$\tau7$	$RE_{20}Mg_{19}Zn_{81}$	○	○	×	●	×		●		○	○	○	○	○	○		○
V phase	$RE_5Mg_{42}Zn_{53}$	○	×	○	○	○		○		○	○	○	○	○	○		○
H phase	$RE_{15}Mg_{15}Zn_{70}$	×	○	○	○	○		○		○	○	○	○	○	○		○
X phase	$RE_2Mg_{12}Zn$	×	○	○	○	○		○		×	×	×	×	×	×		×
I phase	$REMg_3Zn_6$	×	○	○	○	○		○		×	×	×	×	×	×		×
Decagonal phase		●	○	○	○	○		○		○	○	●	●	●	●		●

× stable phases considered in the present project (verified or assumed); ○ phases considered unstable; ⦿ phases considered metastable. Parameters have been assigned; □ binary phases assumed to have no ternary phase fields; ●possible stable phases not considered in the present project. No parameters have been ass

Phases corresponding to τ3, τ4 and τ5 were reported in the Pr-Mg-Zn and Sm-Mg-Zn systems, as will be discussed in section 2.2 and 2.3. Consequently, they are considered in the present study. Phases corresponding to τ1, τ2, τ6 and τ7 have not been reported. As mentioned previously [14, 15], these phases could very well be stable in the Pr-Mg-Zn and Sm-Mg-Zn systems. However, no investigations have been carried out in the composition ranges where they might be found. Consequently, τ1, τ2, τ6 and τ7 are not assumed in the present study in the Pr-Mg-Zn and Sm-Mg-Zn systems.

The phase La(Mg,Zn), Pr(Mg,Zn) and Sm(Mg,Zn) in Table 1 are solid solutions of LaMg and LaZn, PrMg and PrZn and SmMg and SmZn, respectively. The phases $LaMg_3$, $PrMg_3$, $SmMg_3$, La_2Mg_{17}, $LaMg_{12}$ and $PrMg_{12}$ are solutions with limited solubility of Zn. The phases $LaZn_4$ and La_2Zn_{17} are solutions with limited solubility of Mg. The metastable binary $SmMg_{12}$ and $SmZn_{12}$ phases were considered and their thermodynamic parameters were estimated in previous work [8, 12]. These two phases have the same crystal structure and thus are assumed to form a possible solution phase in the present study. As will be discussed in Section 4.3, the present calculations suggest that this phase is metastable. All other binary phases are assumed not to extend into the ternary systems. The prototypes, Pearson symbols and space groups of all binary phases were given previously [7, 8, 12].

Possible ternary phases in RE-Mg-Zn systems, both stable and metastable, as assumed in the present project [14-16], are summarized in Table 2.

8.2.1 La-Mg-Zn

The La-Mg-Zn system was first investigated by Dobatkina et al [17, 18] by differential thermal analysis (DTA), electron probe microanalysis (EPMA), X-ray diffraction analysis (XRD) and micro-structural analysis. An isothermal section at 300°C and two isopleths (shown later in Figs. 9 and 10) were constructed. The $LaZn_5$, La_3Zn_{22}, $LaZn_{13}$ and $LaMg_{12}$ phases were not reported. According to Dobatkina et al [17, 18], LaMg and LaZn form a continuous solution; Zn can substitute for Mg up to 42 at.% in the $LaMg_3$ phase, and La_2Mg_{17} forms a continuous solid solution with La_2Zn_{17}. Only one ternary compound, reported as V, was identified.

Partial isothermal sections at 350 ^{o}C and 400 ^{o}C in the Mg-rich region were proposed by Huang et al [19, 20] based on their experimental results from scanning electron microscopy

(SEM), EPMA and XRD. A ternary compound with constant La content of ~8 at.% was reported. This ternary phase is considered as $La(Mg,Zn)_{12}$ in the present study.

Later, the La-Mg-Zn system was experimentally re-investigated by Berche et al [21] by means of XRD and EPMA (see Fig.8). Twenty-six samples were synthesized and the system was investigated over the entire composition range at 322°C. The ternary V phase proposed by Dobatkina et al [17, 18] was confirmed. Zn was reported to dissolve in the $LaMg_3$ phase by substituting for Mg up to 42 at.%, in good agreement with Dobatkina et al [17, 18]. However, in contrast with Dobatkina et al [17, 18], LaMg and LaZn were not reported to form a continuous solution; solubilities of only 1 at.% Zn in LaMg and 7 at.% Mg in LaZn were observed. Furthermore, La_2Mg_{17} and β-La_2Zn_{17} also were not observed to form a continuous solution; solubilities of 52 at.% Zn in La_2Mg_{17} and 34 at.% Mg in β-La_2Zn_{17} were reported. At least 22 at.% Mg was observed to dissolve in $LaZn_4$ according to EPMA analysis.

8.2.2 Pr-Mg-Zn

An isothermal section at 297°C was established over the entire composition range by Kinzhibalo et al [22] by means of XRD analysis. According to the authors, PrZn and PrMg form a continuous solution and Zn can dissolve in $PrMg_3$ up to 40 at.%. Four ternary phases were reported; $Pr_3Mg_8Zn_{11}$, $Pr_2Mg_7Zn_{11}$, $PrMg_7Zn_{12}$ and $PrMg_6Zn_3$. It should be noted that four ternary phases with the same stoichiometries were reported by the same authors in the Nd-Mg-Zn system [22]. These phases were denoted τ3, τ4, τ5 and $Nd(Mg,Zn)_{12}$ in our previous paper on the Nd-Mg-Zn system [15]. The same notation is used in the present study. Consequently, the $PrMg_6Zn_3$ phase is treated as part of the $PrMg_{12}$ solution.

8.2.3 Sm-Mg-Zn

The phase diagram of the Sm-Mg-Zn system was investigated in the Mg-rich region (up to 40 wt.% Sm and 45 wt.% Zn) by Drits et al [23] using DTA, XRD, EPMA, microhardness measurements and metallographic analysis. An isothermal section at 300°C and three isopleths were reported (two of which are shown later in Figs. 17-18). Three ternary phases were reported: τ3, τ4 and τ5 (reported as X, Y and Z, respectively). The τ3 phase and τ5 phase have fcc and hexagonal lattices according to the XRD analysis.

The Sm-Mg-Zn system was later investigated by Xia et al [24] in the Mg-rich region. Three partial isothermal sections in the Mg-rich region (at 350°C, 400°C and 450°C) were presented. The only ternary compound reported was τ5.

8.2.4 Ternary phases considered in the present study

Based on the available experimental data from the literature, the following ternary phases are considered in the present optimizations. All these ternary phases can be found in Table 1.

RE(Mg,Zn): The REMg and REZn binary phases both have the CsCl structure and in some reported isothermal sections they form a continuous solution [22, 25]. Although Berche et al [21] reported that LaMg and LaZn do not form a continuous solution, in the present study we treat them as one continuous solution phase because REMg and REZn were reported to form continuous solutions in all other RE-Mg-Zn systems where measurement are available [22, 26-28]. Furthermore, good agreement with experimental data was obtained in our optimizations of all other systems [14-16] assuming ideal mixing behavior (see section 3). It is unlikely that the La(Mg,Zn) phase would then uniquely deviate greatly from ideal behavior. The RE content is constant at 50 at.%. Consequently, the model RE(Mg,Zn) was chosen in the present optimization (That is, Mg and Zn substitute on one sublattice while RE occupies a second lattice).

$REMg_3$: Zn can substitute for Mg in $REMg_3$ [22, 28, 29]. Consequently, the model $RE(Mg,Zn)_3$ is used. Zn solubility in $REMg_3$ reported by different authors are summarized in Table 1. It should be mentioned here that τ3 is assumed to be a separate stable phase in all RE-Mg-Zn systems. Maximum Zn solubilities reported in $REMg_3$ by authors [17, 18, 21, 22] who assumed one continuous solution should thus be considered as the maximum Zn solubility in τ3.

La_2Mg_{17}: A large solubility of Zn (52 at.%) in La_2Mg_{17} was reported for this phase while the La content remains constant [21]. Consequently, the model $La_2(Mg,Zn)_{17}$ is used.

β-La_2Zn_{17}: A Mg solubility of 22.5 at.% in La_2Zn_{17} was reported while the La content remains constant [21]. Consequently, the model $La_2(Mg,Zn)_{17}$ is used. Although the same model is used for La_2Mg_{17} and La_2Zn_{17}, they are different phases because they have different crystal structures as shown in Table 1.

<u>$REMg_{12}$</u>: The $REMg_{12}$ and $REZn_{12}$ binary phases both have the $Mn_{12}Th$ structure. The model $RE(Mg,Zn)_{12}$ is used to describe the solution phases.

<u>τ3</u>: The existence of τ3 as a phase separate from $REMg_3$ is well established in the Ce-Mg-Zn [26, 30], Nd-Mg-Zn [28, 31], Y-Mg-Zn [32-34] and Gd-Mg-Zn [35] systems. This phase was not reported in the La-Mg-Zn system, most probably because no detailed experiments were carried out to verify its existence. Since this phase has been observed in several lighter- and heavier-RE-Mg-Zn systems, it is assumed in all RE-Mg-Zn systems.

<u>τ4 and τ5</u>: These two phases are treated in the present work as stoichiometric phases with suggested stoichiometries $RE_2Mg_5Zn_9$ and $RE_3Mg_{13}Zn_{30}$ based upon results in the Ce-Mg-Zn system. No crystallographic data have been reported. We assume that their crystal structures are the same as in the Ce-Mg-Zn system [14]. Detailed information can be found in Table 1.

It should be noted that τ1, τ2, τ4, τ5, τ6 and τ7 are not considered in the La-Mg-Zn system because they have not been observed. τ1, τ2, τ6 and τ7 are not considered in the Pr-Mg-Zn and Sm-Mg-Zn systems because no investigation has been carried out in the composition region where these phases would appear. However, their existence as stable phases in these systems is a possibility.

8.3 Thermodynamic models

Thermodynamic data for the pure elements were given previously [7, 8, 12]. The optimized thermodynamic model parameters of the seven binary sub-binary systems were taken from Ansara et al [7] (Mg-Zn), Kang et al [8] (La-Mg, Pr-Mg and Sm-Mg) and Zhu and Pelton [12] (La-Zn, Pr-Zn and Sm-Zn).

For the seven binary sub-systems, the Modified Quasichemical Model (MQM) [36, 37], which takes account of short-range ordering, was used to model the liquid phase. Consequently, the MQM is used to model the liquid phase in the ternary systems. For details of the model, see references [12, 13, 36, 37]. The symmetric (Kohler-like) model [37] was used to estimate the properties of the ternary liquid phases from the optimized binary model parameters. No additional ternary model parameters were introduced in the Pr-Mg-Zn and Sm-Mg-Zn systems. One ternary parameter was required in the La-Mg-Zn system.

In the optimization of the Mg-Zn binary system, Ansara et al [7] did not use the MQM for the liquid phase. Consequently, the liquid phase was remodelled using the MQM, keeping the same parameters as Ansara et al [7] for all other phases. The "coordination numbers", which are MQM model parameters, were set to

$$Z^{Mg}_{Mg,Zn} = Z^{Zn}_{Mg,Zn} = Z^{Mg}_{Mg,Mg} = Z^{Zn}_{Zn,Zn} = 6 \qquad 8.1$$

and the new MQM model parameters were introduced as

$$\Delta g_{MgZn} = -6778 + 3.138T + (-1966 + 2.008)X_{MgMg}$$
$$+(-3975 + 1.6736)X_{ZnZn} \text{ (J/g-atom)} \qquad 8.2$$

The binary Bcc_A2, Fcc_A1 and Hcp_A3 solutions are described by a substitutional solution model as discussed previously [12].

As shown in Table 1, Mg and Zn can substitute for each other on one sublattice in some phases (τ3, La(Mg,Zn), Pr(Mg,Zn), Sm(Mg,Zn), $LaMg_3$, $PrMg_3$, $SmMg_3$, $LaZn_4$, La_2Mg_{17}, β-La_2Zn_{17}, $LaMg_{12}$, $PrMg_{12}$ and $Sm(Mg,Zn)_{12}$). These phases are modeled with the Compound Energy Formalisim (CEF) [38]. For example, the Gibbs energy of La(Mg,Zn) (per mole formula) can be expressed as follows:

$$G^{La(Mg,Zn)} = y_{Mg}G^{0,La(Mg,Zn)}_{La:Mg} + y_{Zn}G^{0,La(Mg,Zn)}_{La:Zn}$$
$$+RT\left(y_{Mg}lny_{Mg} + y_{Zn}lny_{Zn}\right)$$
$$+y_{Mg}y_{Zn}(L^{0}_{La:Mg,Zn}$$
$$+(y_{Mg} - y_{Zn})\, L^{1}_{La:Mg,Zn}) \qquad 8.3$$

where y_{Mg} and $y_{Zn}$are the site fractions of Mg and Zn in the second sublattice, $G^{0,La(Mg,Zn)}_{La:Mg}$ and $G^{0,La(Mg,Zn)}_{La:Zn}$ are the Gibbs energies of the end-members (LaMg and LaZn) at temperature T under the convention that the enthalpies of the elements are equal to zero in their stable states at 298.15K, and $L^{0}_{La:Mg,Zn}$ and $L^{1}_{La:Mg,Zn}$ are interaction parameters to be optimized. The Gibbs energies of τ3, Pr(Mg,Zn), Sm(Mg,Zn), $LaMg_3$, $PrMg_3$, $SmMg_3$, $LaZn_4$, La_2Mg_{17}, La_2Zn_{17}, $LaMg_{12}$, $PrMg_{12}$ and $Sm(Mg,Zn)_{12}$ can be expressed similarly.

The V, τ4 and τ5 phases are treated as stoichiometric compounds.

No thermodynamic properties for the ternary compounds could be found in the literature. To obtain initial estimates of the enthalpies and entropies of formation of the ternary compounds, three lines passing through the compound on the ternary Gibbs triangle were drawn parallel to the three edges of the triangle. The six intersection points of these lines with the edges defined six "binary compounds" whose enthalpies and entropies were then averaged to give the initial estimates. Thereafter, these values were adjusted to best reproduce the available data.

All model parameters optimized in the present work are listed in Table 3. All other model parameters (apart from the MQM parameters for liquid Mg-Zn given in Equations (1, 2)) have been given previously [7, 8, 12]. Very few model parameters are required. The enthalpies of formation of all compounds have reasonable values. The entropies of formation are all small and negative as expected.

Experimental data for the Pr-Mg-Zn system are limited. Thermodynamic parameters for the ternary phases in this system are estimated in the present project. The interaction parameters of the solution phases are set to be the same as those of the corresponding phases in other RE-Mg-Zn systems. The enthalpies of formation of the ternary compounds and end-members are estimated based on the trends established in our previous reports on the binary RE-Zn systems [12, 13]. The trends in the ternary RE-Mg-Zn systems as well as Y-Mg-Zn system are shown in Fig. 8.

As expected, these trends resemble those established earlier in the binary systems [12, 13]. The entropies of formation of similar phases are set to the same value.

Table 8.3. Thermodynamic model parameters optimized or estimated in the present work for the La-Mg-Zn, Pr-Mg-Zn and Sm-Mg-Zn systems

Phase name	Model	Parameters (J/mol-atom)
La-Mg-Zn liquid	MQM	* $q_{La,Zn,(Mg)}$ =-8368
Pr-Mg-Zn liquid	MQM	no ternary parameters
Sm-Mg-Zn liquid	MQM	no ternary parameters
La(Mg,Zn)	La(Mg,Zn)	ideal mixing
Pr(Mg,Zn)	Pr(Mg,Zn)	ideal mixing
Sm(Mg,Zn)	Sm(Mg,Zn)	ideal mixing
$LaMg_3$	$La(Mg,Zn)_3$	$G^{0,LaMg_3}_{La:Zn} = -35564 + 6.28T$
		$L^{0,LaMg_3}_{La:Mg,Zn} = -4184$
		$L^{1,LaMg_3}_{La:Mg,Zn} = -2092$
$PrMg_3$	$Pr(Mg,Zn)_3$	$G^{0,PrMg_3}_{Pr:Zn} = -33472 + 6.45T$
		$L^{0,PrMg_3}_{Pr:Mg,Zn} = -4184$
		$L^{1,PrMg_3}_{Pr:Mg,Zn} = -2092$
$SmMg_3$	$Sm(Mg,Zn)_3$	$G^{0,SmMg_3}_{Sm:Zn} = -32008 + 6.28T$
		$L^{0,SmMg_3}_{Sm:Mg,Zn} = -4184$
		$L^{1,SmMg_3}_{Sm:Mg,Zn} = -2092$
$LaMg_{12}$	$La(Mg,Zn)_{12}$	ideal mixing
$PrMg_{12}$	$Pr(Mg,Zn)_{12}$	$L^{0,PrMg_{12}}_{Pr:Mg,Zn} = -2253$
$SmMg_{12}$	$Sm(Mg,Zn)_{12}$	$L^{0,SmMg_{12}}_{Sm:Mg,Zn} = -2253$
La_2Mg_{17}	$La_2(Mg,Zn)_{17}$	$L^{0,La_2Mg_{17}}_{La:Mg,Zn} = -3523$
La_2Zn_{17}	$La_2(Mg,Zn)_{17}$	$G^{0,La_2Mg_{17}}_{La:Mg} = -7311 + 0.71T$
		$L^{1,La_2Mg_{17}}_{La:Mg,Zn} = -3303$
$LaZn_4$	$La(Mg,Zn)_4$	$G^{0,LaZn_4}_{La:Mg} = -12552 + 4.18T$
		$L^{0,LaZn_4}_{La:Mg,Zn} = -1674$
V	$La_5Mg_{42}Zn_{53}$	$G^{0,V}_{La:Mg:Zn} = -16280 + 2.3T$
τ3	$La(Mg,Zn)_2Mg$	$G^{0,\tau3}_{La:Mg:Mg} = -18900 + 6.20T$
		$G^{0,\tau3}_{La:Zn:Mg} = -35041 + 5.23T$
		$L^{0,\tau3}_{La:Mg,Zn:Mg} = 1046$
		$L^{1,\tau3}_{La:Mg,Zn:Mg} = 4184$
	$Pr(Mg,Zn)_2Mg$	$G^{0,\tau3}_{Pr:Mg:Mg} = -18500 + 6.63T$
		$G^{0,\tau3}_{Pr:Zn:Mg} = -33681 + 6.28T$
		$L^{0,\tau3}_{Pr:Mg,Zn:Mg} = 1046$
		$L^{1,\tau3}_{Pr:Mg,Zn:Mg} = 4184$
	$Sm(Mg,Zn)_2Mg$	$G^{0,\tau3}_{Sm:Mg:Mg} = -16875 + 6.63T$
		$G^{0,\tau3}_{Sm:Zn:Mg} = -32845 + 6.28T$
		$L^{0,\tau3}_{Sm:Mg,Zn:Mg} = 1046$
		$L^{1,\tau3}_{Sm:Mg,Zn:Mg} = 4184$
τ4	$Pr_2Mg_5Zn_9$	$G^{0,\tau4}_{Pr:Mg:Zn} = -25653 + 5.23T$
	$Sm_2Mg_5Zn_9$	$G^{0,\tau4}_{Sm:Mg:Zn} = -25384 + 5.82T$
τ5	$Pr_3Mg_{13}Zn_{30}$	$G^{0,\tau5}_{Pr:Mg:Zn} = -20192 + 3.94T$
	$Sm_3Mg_{13}Zn_{30}$	$G^{0,\tau5}_{Sm:Mg:Zn} = -19555 + 3.94T$

* for notation see refs [36, 37]

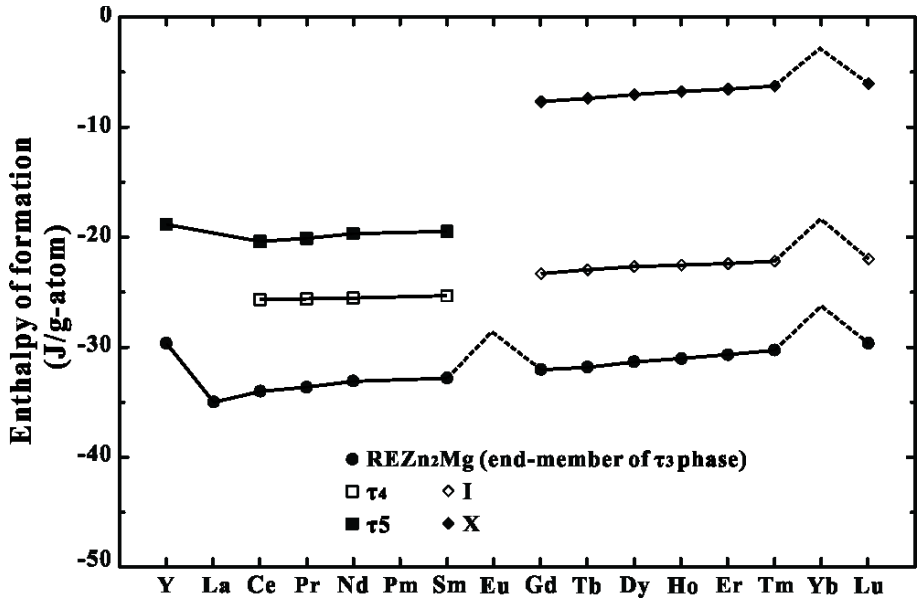

Figure 8.8. Calculated enthalpies of formation for compounds in the Y-Mg-Zn and RE-Mg-Zn systems. Trends are very similar to those established in our previous work on the binary systems [12, 13] (The Eu-Mg-Zn and Yb-Mg-Zn systems are not considered in the present work thus the anomalies cannot be seen from the figure).

8.4 Comparison of calculations with experimental data

8.4.1 La-Mg-Zn

The calculated isothermal section of the La-Mg-Zn at 300°C is shown in Fig. 9. It is in good agreement with the experimental section from Berche et al [21] except that τ3 is added as a phase separate from $LaMg_3$ and the La(Mg,Zn) phase is considered to be continuous to be in accordance with other RE-Mg-Zn systems. Furthermore, it was found during the optimization that in order to reproduce the miscibility gap in La(Mg,Zn) reported by Berche et al [21], a very positive interaction parameter is needed for the La(Mg,Zn) phase and very negative parameters are required for the $LaMg_3$ and τ3 phases. However, if this is done, most of the phase relationships are changed significantly and the isopleths shown in Figs. 10 and 11 can no longer be reproduced.

The same interaction parameters were assumed for $LaMg_3$ and τ3 as those for the corresponding phases in the Ce-Mg-Zn and Nd-Mg-Zn systems [14, 15]. The solubilities of Mg

in $LaZn_4$ and β-La_2Zn_{17} and of Zn in La_2Mg_{17} are reproduced well in the present calculations.

It should be mentioned here that Qi et al [39] optimized this system based on experimental data from Dobatkina [17, 18]. However, their calculated isothermal section at 300°C is not in accordance with the La-Mg and La-Zn binary phase diagrams: the stable $LaZn_5$, La_3Zn_{22}, $LaZn_{13}$ and $LaMg_{12}$ phases are missing. Also $LaMg_{12}$ is missing in one of their calculated isopleths. In their optimization the La_2Mg_{17} and La_2Zn_{17} solutions are modeled as one continuous solution phase even though the binary phases have different structures.

Two isopleths are calculated and compared to experimental data [17, 18], as shown in Figs. 10 and 11. The data points close to the La-Mg binary system in Fig. 9 cannot be reproduced since they are in disagreement with the accepted liquidus in the La-Mg binary system.

No solubility of Zn in $LaMg_{12}$ has been reported. Since significant solubility of Zn in $CeMg_{12}$, $PrMg_{12}$ (and a ternary $Nd(Mg,Zn)_{12}$ phase) have been observed, appreciable solubility of Zn in $LaMg_{12}$ is a distinct possibility. However, attempts to introduce this solubility into the optimization resulted in isopleths (Fig. 10 and 11) which did not agree with the experimental data.

A tentative calculated liquidus projection for the La-Mg-Zn system is shown in Figs. 12-13 and a tentative list of the calculated temperatures of invariant reactions, maxima and minima is given in Table 4.

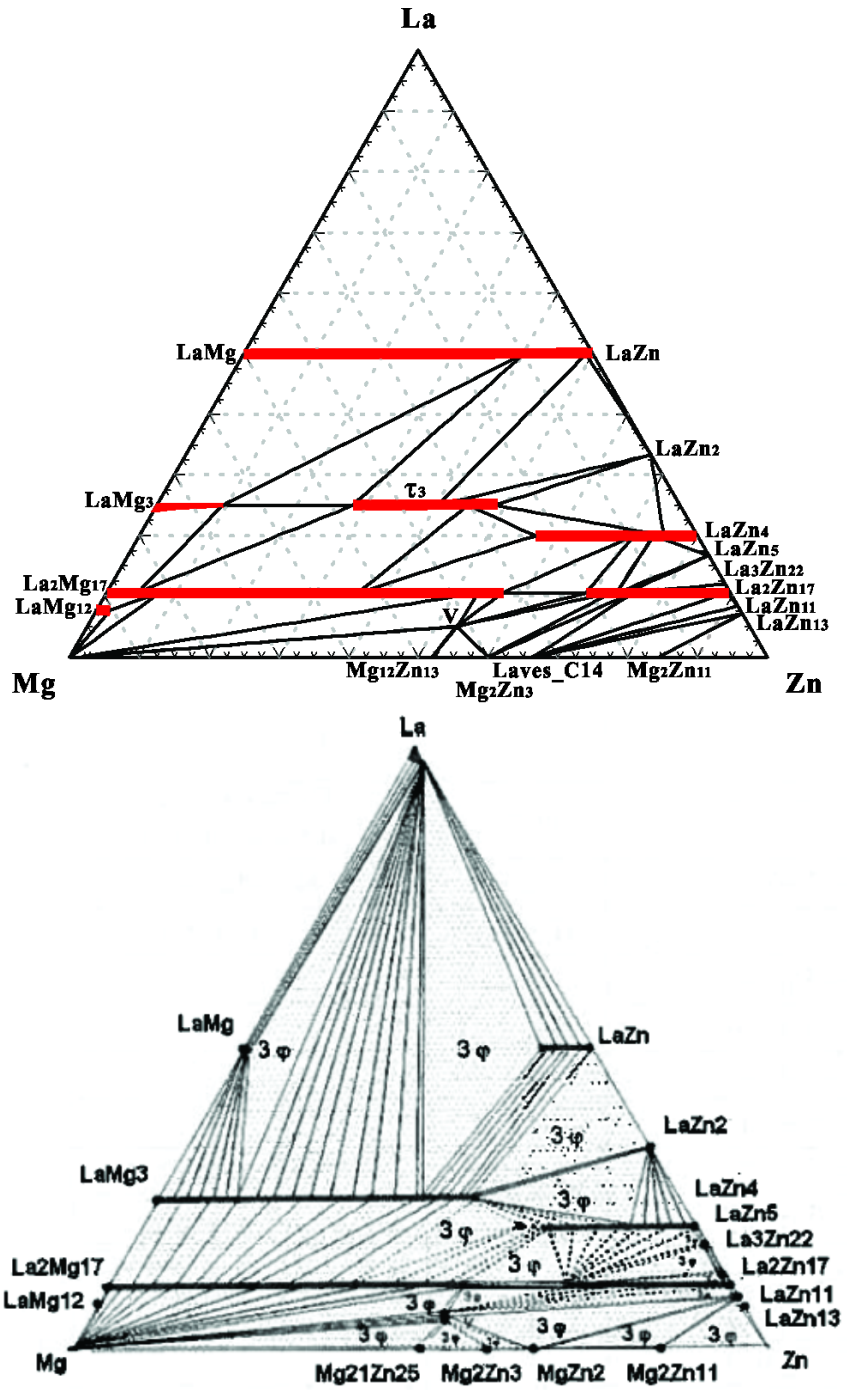

Figure 8.9. Calculated optimized (above) isothermal section of the La-Mg-Zn system at 300°C and reported (below) isothermal section of the La-Mg-Zn system at 322oC [21] (mole fraction).

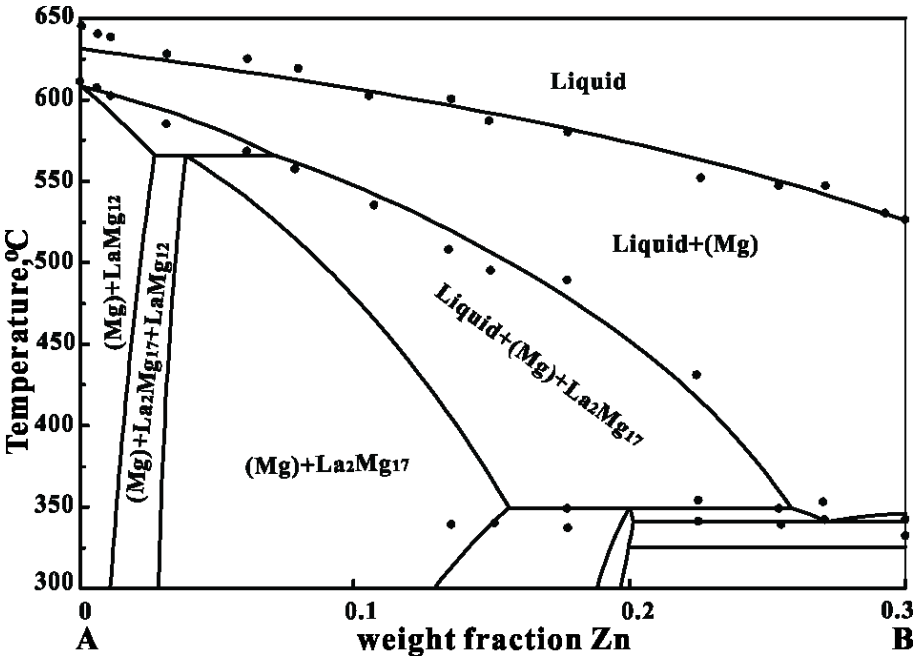

Figure 8.10. Calculated optimized isopleth from Mg-10wt.% La (A) to Mg-30wt.% Zn (B) in the La-Mg-Zn system showing points from Dobatkina et al [17, 18]

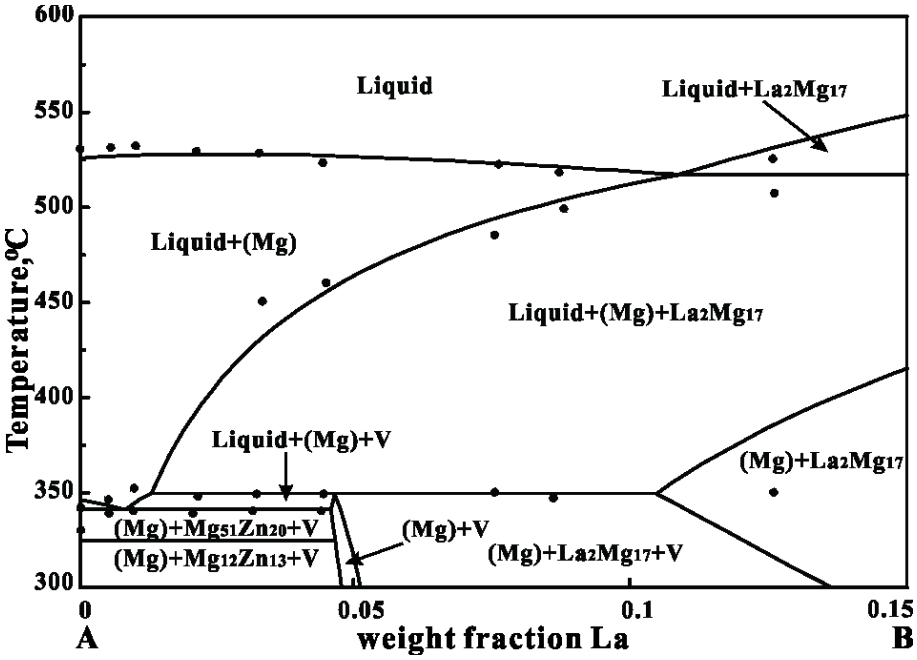

Figure 8.11. Calculated optimized isopleth from Mg-30wt.% Zn (A) to Mg-15wt.% La-30wt.% Zn (B) in the La-Mg-Zn system showing points from Dobatkina et al [17, 18]

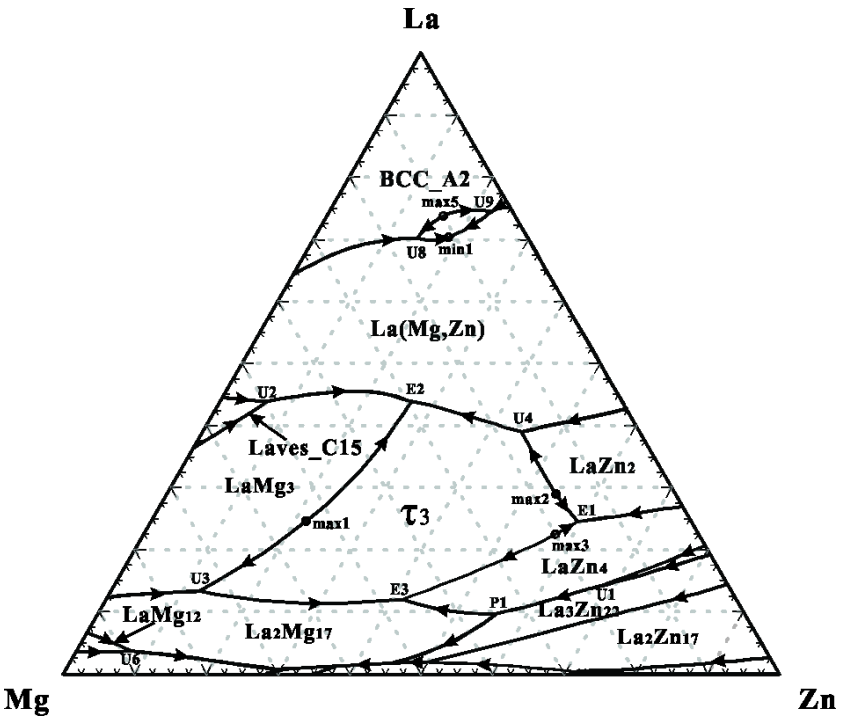

Figure 8.12. Tentative calculated liquidus projection for La-Mg-Zn system (mole fraction)

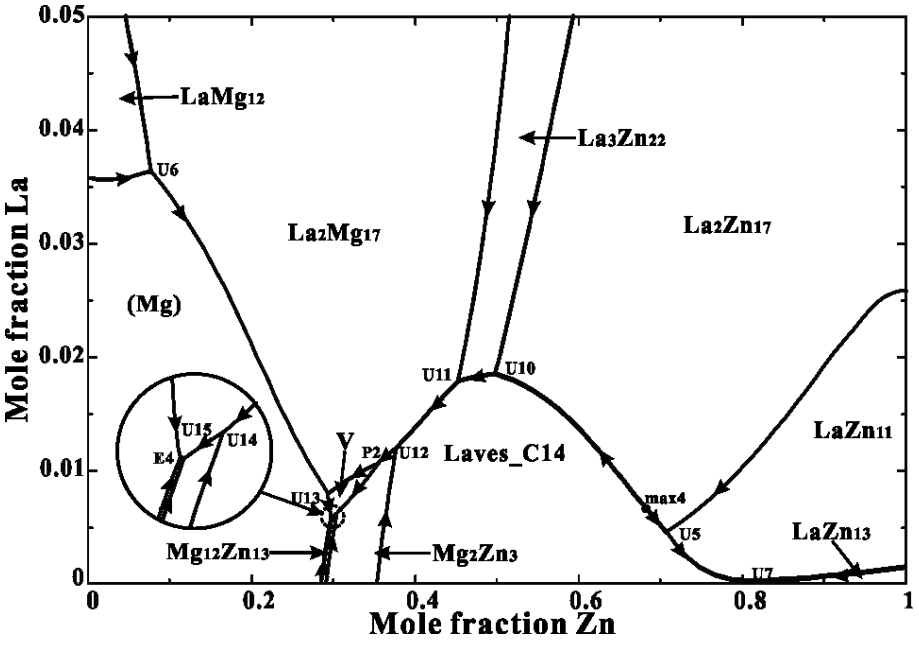

Figure 8.13. Enlargement of part of Fig. 8.12

Table 8.4. Tentative calculated invariant reactions, maxima and minima and their temperatures (^{o}C) in the La-Mg-Zn system

U1	742	U2	701	E1	691	U3	638	U4	634	P1	625	E2	602
E3	591	U5	582	U6	566	U7	536	U8	517	U9	517	U10	501
U11	464	U12	402	P2	385	U13	350	U14	345	U15	340	E4	340
max1	~750	max2	~719	max3	~696	max4	~584	max5	~559	min1	~493		

8.4.2 Pr-Mg-Zn

The calculated isothermal section of the Pr-Mg-Zn system at 300°C is shown in Fig. 14. The same interaction parameters were assumed for the $PrMg_3$, $PrMg_{12}$ and τ3 phases as for the corresponding phases in the Ce-Mg-Zn and Nd-Mg-Zn systems [14, 15]. The calculated Zn solubility in $PrMg_{12}$ is less than in $CeMg_{12}$.

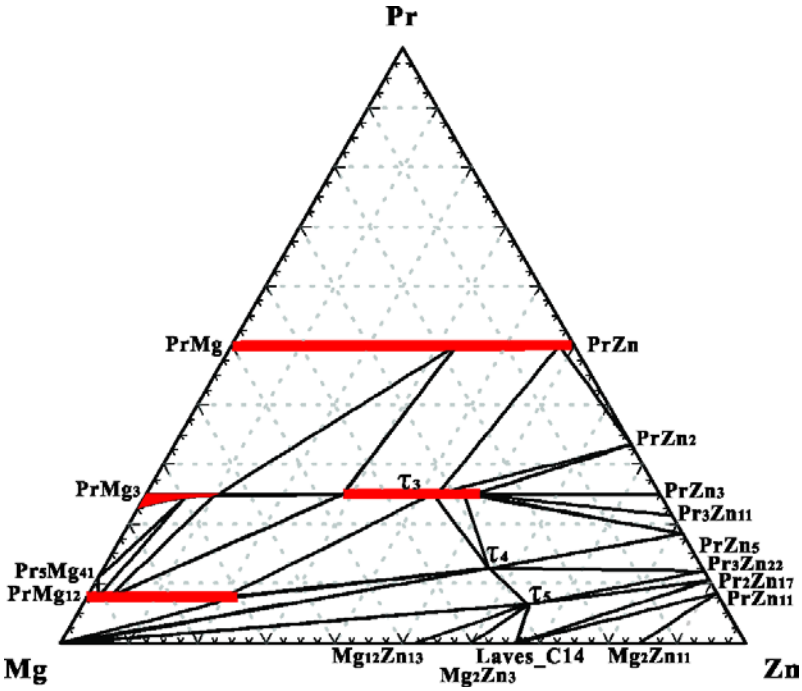

Figure 8.14. Calculated optimized isothermal section of the Pr-Mg-Zn system at 300°C (mole fraction)

A tentative calculated liquidus projection for the Pr-Mg-Zn system is shown in Figs. 15-16 and a tentative list of the calculated temperatures of invariant reactions, maxima and minima is given in Table 5.

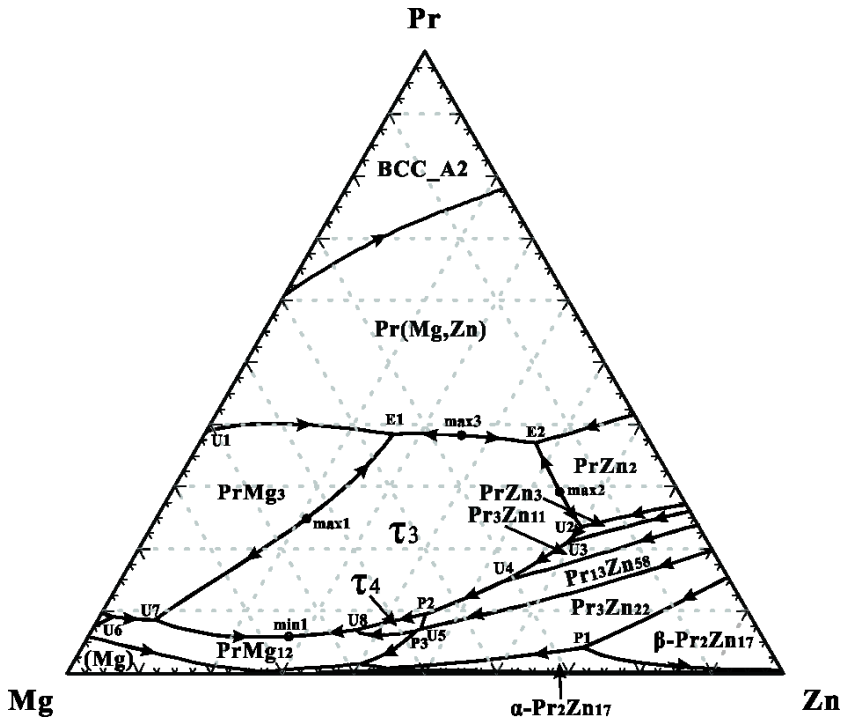

Figure 8.15. Tentative calculated liquidus projection of the Pr-Mg-Zn system (mole fraction)

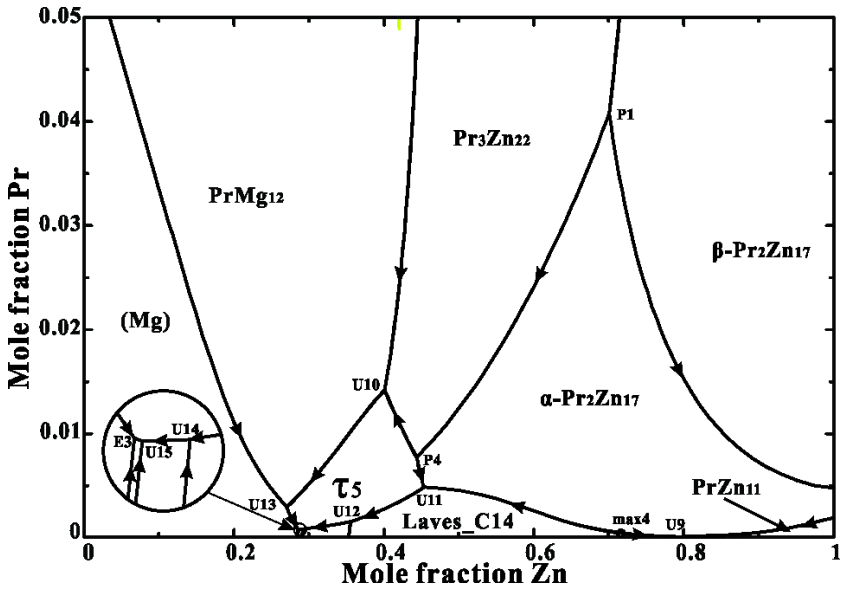

Figure 8.16. Enlargement of part of Fig. 8.15

Table 8.5. Tentative calculated invariant reactions, maxima and minima and their temperatures (^{o}C) in the the Pr-Mg-Zn system

P1	779	U1	737	U2	717	E1	711	U3	708	E2	698	U4	666
P2	602	U5	594	P3	590	U6	576	U7	575	U8	569	U9	547
P4	509	U10	508	U11	497	U12	413	U13	369	U14	351	U15	346
E3	346	max1	~783	max2	~753	max3	~715	max4	~592	min1	~562		

8.4.3 Sm-Mg-Zn

The calculated isothermal section of the Sm-Mg-Zn system at 300°C is shown in Fig. 17. The X, Y and Z phases reported by Drits et al [23] are interpreted here as τ3, τ4 and τ5. The τ4 phase was not observed by Xia et al [24]. The same interaction parameters were assumed for the $SmMg_3$, $SmMg_{12}$ and τ3 phases as for the corresponding phases in the Ce-Mg-Zn and Nd-Mg-Zn systems [14, 15].

The $SmMg_{12}$ phase is not stable according to our calculations. As mentioned in our previous paper [15] on the Nd-Mg-Zn system, the $NdMg_{12}$ phase is not stable in the Nd-Mg binary system but it is stabilized in the ternary Nd-Mg-Zn system when the same interaction parameter as for $CeMg_{12}$ is used [15]. However, the $SmMg_{12}$ phase cannot be stabilized with the same interaction parameter and the existence of this phase in the ternary Sm-Mg-Zn has never been evidenced. The $REMg_{12}$ phase becomes less and less stable as one progresses from Ce to Sm. We conclude here that this phase will not be stable in the heavier-RE-Mg-Zn systems.

Calculated isopleths are shown in Figs. 18 and 19 along with experimental data [23]. Most of the data can be well fitted except for some of the liquidus data close to the binary Mg-Zn and Sm-Mg systems. These data cannot be reproduced since they are in disagreement with the accepted liquiduses in the Mg-Zn and Sm-Mg binary systems. Another isopleth of Mg-30wt.% Sm to Mg-30wt.% Sm-30wt.% Zn from the same authors [23] cannot be reproduced because it contradicts the binary phase diagrams.

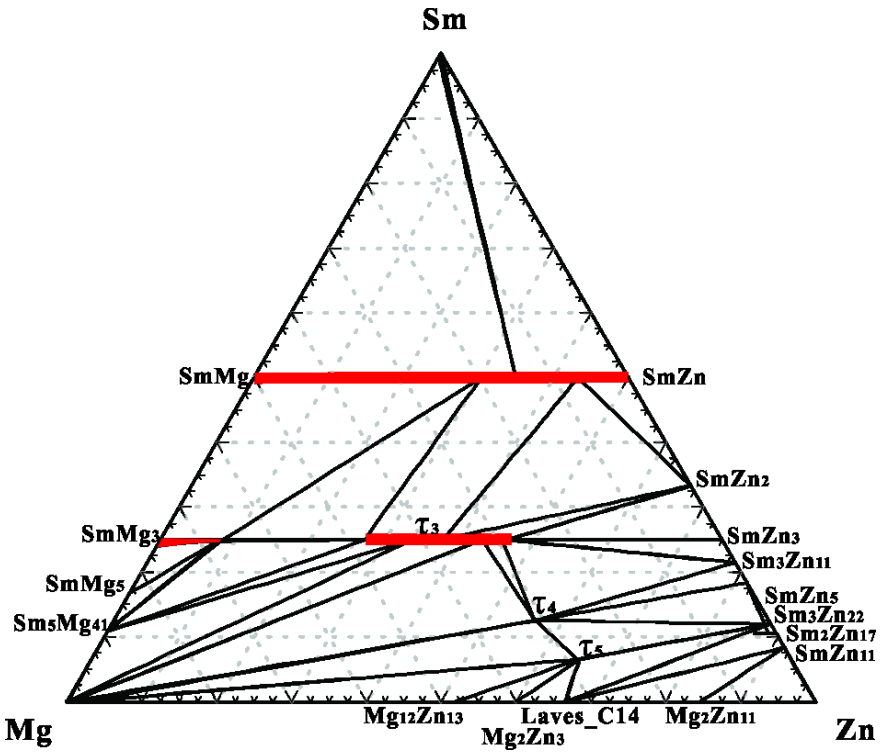

Figure 8.17. Calculated optimized isothermal section of the Sm-Mg-Zn system at 300oC (mole fraction)

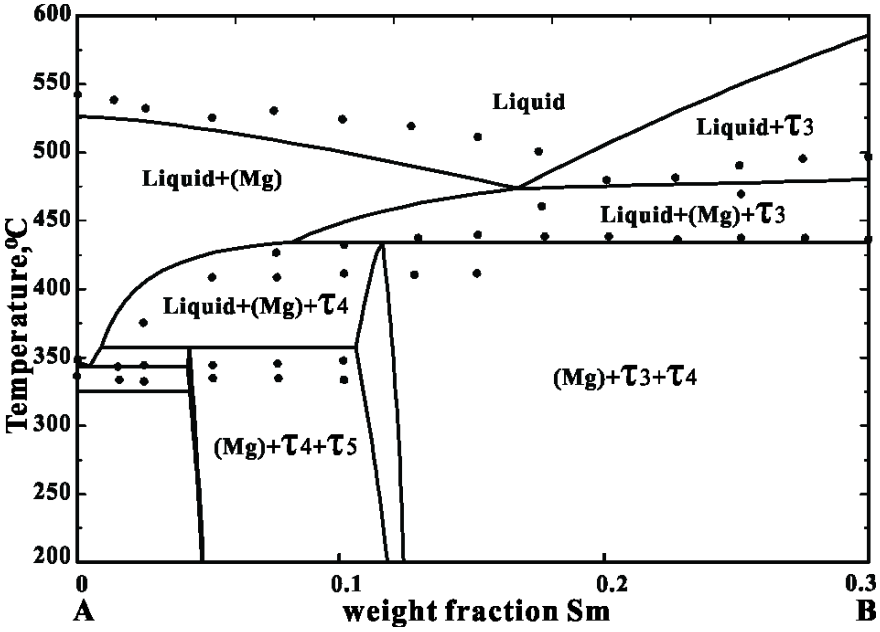

Figure 8.18. Calculated optimized isopleth from Mg-30wt.% Zn (A) to Mg-30wt.% Sm-30wt.% Zn (B) in the Sm-Mg-Zn system showing points from Drits et al [23]

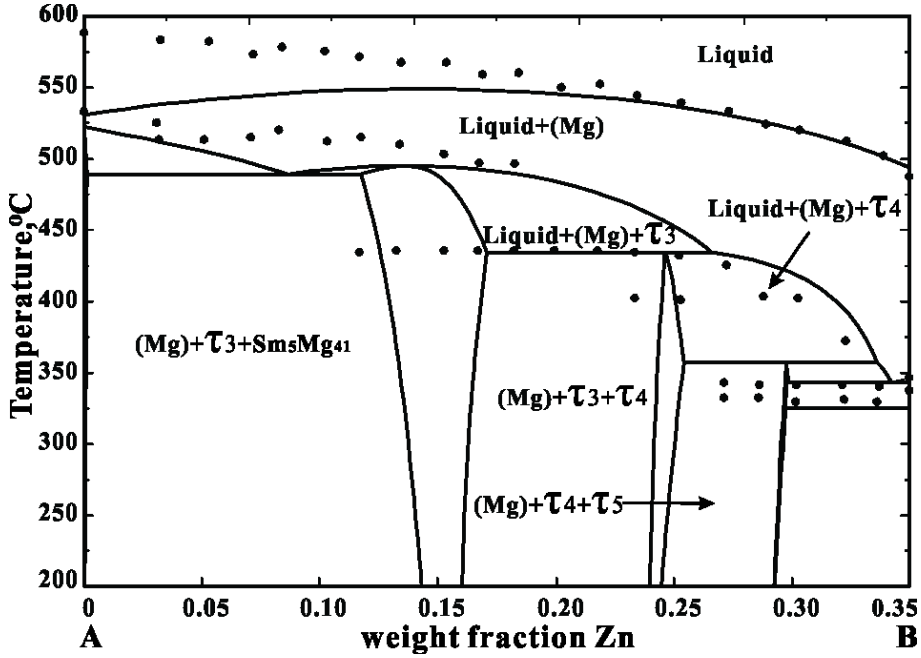

Figure 8.19. Calculated optimized isopleth from Mg-35wt.% Sm (A) to Mg-35wt.% Zn (B) in the Sm-Mg-Zn system showing points from Drits et al [23]

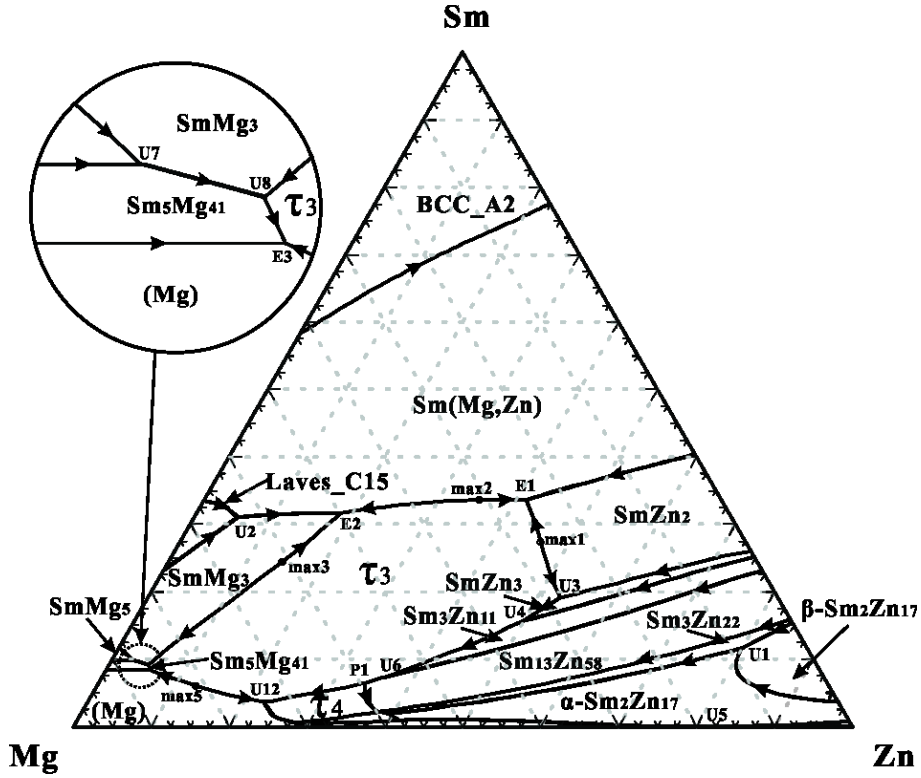

Figure 8.20. Tentative calculated liquidus projection for Sm-Mg-Zn system (mole fraction)

A tentative calculated liquidus projection for the Sm-Mg-Zn system is shown in Figs. 20-21 and a tentative list of the calculated temperatures of invariant reactions, maxima and minima is given in Table 6.

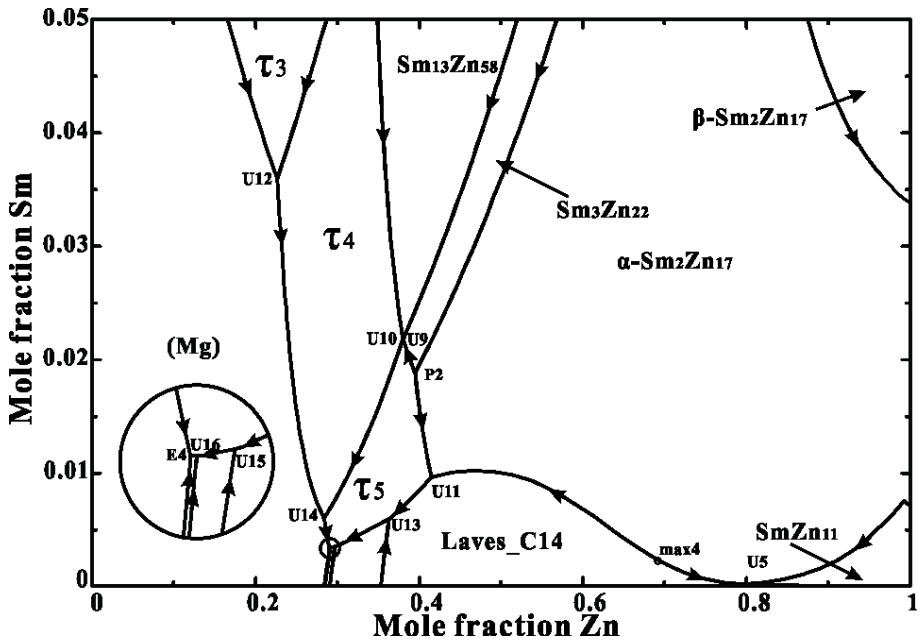

Figure 8.21. Enlargement of part of Fig. 8.20

Table 8.6. Tentative calculated invariant reactions, maxima and minima and their temperatures (^{o}C) in the the Sm-Mg-Zn system

U1	863	E1	712	U2	695	E2	693	U3	685	U4	655	U5	543
U6	529	U7	515	P1	510	U8	498	E3	489	P2	464	U9	458
U10	458	U11	453	U12	434	U13	410	U14	357	U15	349	U16	343
E4	343	max1	~742	max2	~716	max3	~708	max4	~587	max5	~496		

8.5 Discussion

As mentioned in our previous papers on the binary RE-Zn systems [12, 13], the phase diagrams of all RE-Zn systems are very similar. This is also the case for all the RE-Mg-Zn ternary systems. The calculated isothermal sections at 300°C shown in Figs. 9, 14 and 17 are very similar as are the calculated liquidus projections shown in Figs. 12, 15 and 20. These isothermal

sections and liquidus projections are also very similar to those published earlier for the Ce-Mg-Zn and Nd-Mg-Zn systems [14, 15]

In our previous articles on the binary RE-Zn systems [12, 13], trends among all RE-Zn systems were established and utilized during the optimization. The trends are introduced in the optimization of all RE-Mg-Zn systems (See Fig. 8).

Entropies of formation of all compounds with the same stoichiometry are negative and very similar. The same interaction parameters are used for corresponding solution phases in different ternary systems except for the La-Mg-Zn system.

8.6 Conclusions

All optimized thermodynamic parameters for La-Mg-Zn, Pr-Mg-Zn and Sm-Mg-Zn systems in the present work are summarized in Table 3. Binary parameters were reported in previous articles [7, 8, 12]. Very few model parameters are required, and all parameters have thermodynamically reasonable values. In particular, no additional ternary parameters were required in the MQM model for the liquid phase in the Pr-Mg-Zn and Sm-Mg-Zn system and only one ternary parameter was required in the MQM model for the liquid phase in the La-Mg-Zn system.

Assessed optimized model parameters for the La-Mg-Zn, Pr-Mg-Zn and Sm-Mg-Zn systems have been obtained by considering experimental data from the literature. Previous articles [8-13] reported on the optimizations of all RE-Zn and RE-Mg binary systems as well as an evaluation, optimization and experimental phase diagram study of the Ce-Mg-Zn and Nd-Mg-Zn systems [14, 15]. In subsequent articles we shall report on evaluations and optimizations of other ternary heavier-RE-Mg-Zn systems. The model parameters will be included in the FTlite light metals database of the FactSage database computing system [40] which already contains optimized model parameters for the solid and liquid phases of a large number of binary and ternary Mg- and Al-containing systems. Through the models, the properties and phase equilibria of multicomponent systems can thus be estimated and calculated. All calculations in the present work were performed with the FactSage software [40]

Acknowledgements

This research was supported by funding from the Natural Sciences and Engineering Research Council of Canada (NSERC) Magnesium Strategic Research Network. More information on the Network can be found at www.MagNET.ubc.ca.

References

[1] B.L. Mordike, T. Ebert, Mat. Sci. Eng. A-Struct, 302 (2001) 37-45.

[2] I.P. Moreno, T.K. Nandy, J.W. Jones, J.E. Allison, T.M. Pollock, Scripta Mater., 48 (2003) 1029-1034.

[3] J. Bohlen, M.R. Nürnberg, J.W. Senn, D. Letzig, S.R. Agnew, Acta Mater., 55 (2007) 2101-2112.

[4] R.K. Mishra, A.K. Gupta, P.R. Rao, A.K. Sachdev, A.M. Kumar, A.A. Luo, Scripta Mater., 59 (2008) 562-565.

[5] N. Stanford, M.R. Barnett, Mat. Sci. Eng. A-Struct, 496 (2008) 399-408.

[6] K. Hantzsche, J. Bohlen, J. Wendt, K.U. Kainer, S.B. Yi, D. Letzig, Scripta Mater., 63 (2010) 725-730.

[7] I. Ansara, A. T. Dinsdale, M. H. Rand, COST 507: Definition of thermochemical and thermophysical properties to provide a database for the development of new light alloys, Thermochemical database for light metal alloys, Vol. 2, Office for Official Publications of the European Communities, Luxembourg,1998; P. Spencer, unpublished work

[8] Y.-B. Kang, L. Jin, P. Chartrand, A.E. Gheribi, K. Bai, P. Wu, CALPHAD, 38 (2012) 100-116.

[9] Y.-B. Kang, A. Pelton, P. Chartrand, P. Spencer, C. Fuerst, J. Phase Equilib. Diff., 28 (2007) 342-354.

[10] Y.-B. Kang, A.D. Pelton, P. Chartrand, C.D. Fuerst, CALPHAD, 32 (2008) 413-422.

[11] L. Jin, PhD Thesis, Ecole Polytechnique, Montreal (Canada), 2012, pp. 407

[12] Z. Zhu, A. Pelton, J. Alloys Compd. 641 (2015) 249-260

[13] Z. Zhu, A. Pelton, J. Alloys Compd, 641 (2015) 261-271

[14] Z. Zhu, M. Gharghouri, M. Medraj, S.Y. Lee, A. D. Pelton, submitted for publication

[15] Z. Zhu, A. Pelton, submitted for publication.

[16] Z. Zhu, A. Pelton, submitted for publication.

[17] T.V. Dobatkina, E.V. Melnik, A.T. Tyvanchuk, E.V. Muratova, Stable and Metastable Phase Equilibria in Metallic Systems, Nauka Mosc. USSR (1985) 75-79.

[18] T.V. Dobatkina, E.V. Muratova, E.I. Drozdova, Izv. Akad. Nauk SSSR, Met., (1987) 205-207.

[19] M.L. Huang, H.X. Li, H. Ding, Y.P. Ren, S.M. Hao, Acta Metall. Sin., 21 (2008) 329-335.

[20] M.L. Huang, H.X. Li, Y.P. Ren, H. Ding, S.M. Hao, H. Chen, T. Nonferr. Metal. Soc., 17 (2007) S8-S11.

[21] A. Berche, M.C. Record, J. Rogez, Arch. Metall. Mater., 53 (2008) 1141-1148.

[22] V. Kinzhibalo, A. Tyvanchuk, E. Melnik, Nauka, Stable and Metastable Phase Equilibria in Metallic Systems, Nauka Mosc. USSR (1985) 70-74.

[23] M.E. Drits, L.L. Rokhlin, N.P. Abrukina, V.V. Kinzhibalo, A.T. Tyvanchuk, Russ. Metall-Metall-U, (1985) 183-189.

[24] X. Xia, A. Sanaty-Zadeh, C. Zhang, A.A. Luo, X. Zeng, Y. Austin Chang, D.S. Stone, J. Alloys Compd., 593 (2014) 71-78.

[25] T.V. Dobatkina, E.V. Muratova, E.I. Drozdova, Russ. Metall-Metall-U, (1987) 205-208.

[26] V. Pavlyuk, B. Marciniak, E. Różycka-Sokołowska, Intermetallics, 20 (2012) 8-15.

[27] E.V. Melnik, M.F. Kostina, Ya.P. Yarmlyuk, O.F. Zmii, Magnievye Splavy, Mater.Vses. Soveshch. Issled., Razrab. Primen. Magnievyhk Splavov, (1978) 95-99.

[28] H. Xu, J. Fan, H.-L. Chen, R. Schmid-Fetzer, F. Zhang, Y. Wang, Q. Gao, T. Zhou, J. Alloys Compd., 603 (2014) 100-110.

[29] A. Mostafa, M. Medraj, Metals, 5 (2015) 84-101.

[30] V. Pavlyuk, P. Solokha, G. Dmytriv, B. Marciniak, V. Paul-Boncour, Acta Crystallogr. E, 63 (2007) i161-i161.

[31] E.V. Melnik, V.V. Kinzhibalo, E.M. Padezhnova, T.V. Dobatkina, Tezizy Dokl. Vses. Konf. Kristallokhim. Intermet. Soeden., (1978) 73c.

[32] T. Horiuchi, H. Ikee, A. Hamaya, S. Minamoto, S. Nomoto, S. Miura, in: 7th International Conference on Processing and Manufacturing of Advanced Materials, THERMEC'2011, August 1, 2011 - August 5, 2011, Trans Tech Publications Ltd, Quebec City, QC, Canada, 2012, pp. 1170-1175.

[33] G. Shao, V. Varsani, Z. Fan, Calphad, 30 (2006) 286-295.

[34] A.-P. Tsai, Y. Murakami, A. Niikura, Philos. Mag. A, 80 (2000) 1043-1054.

[35] H.Y. Qi, G.X. Huang, H. Bo, G.L. Xu, L.B. Liu, Z.P. Jin, J. Mater. Sci., 47 (2012) 1319-1330.

[36] A. Pelton, S. Degterov, G. Eriksson, C. Robelin, Y. Dessureault, Metall. Mater. Trans. B, 31 (2000) 651-659.

[37] A. Pelton, P. Chartrand, Metall. Mater. Trans. A, 32 (2001) 1355-1360.

[38] M. Hillert, J. Alloys Compd., 320 (2001) 161-176.

[39] H.Y. Qi, G.X. Huang, R.D. Liu, K. Zhang, L.B. Liu, Z.P. Jin, J. Alloys Compd., 497 (2010) 336-343.

[40] C.W. Bale, E. Bélisle, P. Chartrand, S.A. Decterov, G. Eriksson, K. Hack, I.H. Jung, Y.B. Kang, J. Melançon, A.D. Pelton, C. Robelin, S. Petersen, Calphad, 33 (2009) 295-311; www.factsage.com

Chapter 9 ARTICLE 6: THERMODYNAMIC MODELING OF THE Y-MG-ZN, GD-MG-ZN, TB-MG-ZN, DY-MG-ZN, HO-MG-ZN, ER-MG-ZN, TM-MG-ZN AND LU-MG-ZN SYSTEM

Submitted to Journal of Alloys and Compounds

Zhijun Zhu, Arthur D. Pelton*

Centre de Recherche en Calcul Thermochimique, Département de Génie Chimique, Ecole Polytechnique, Montréal, Québec, Canada

*Corresponding author

KEY WORDS

Rare earth systems, Magnesium systems, Zinc systems, Phase diagram, Thermodynamic assessment

ABSTRACT

All available phase diagram data for the Y-Mg-Zn, Gd-Mg-Zn, Tb-Mg-Zn, Dy-Mg-Zn, Ho-Mg-Zn, Er-Mg-Zn, Tm-Mg-Zn and Lu-Mg-Zn systems have been collected and critically assessed. Critical thermodynamic evaluations and optimizations of these heavier-RE-Mg-Zn systems were carried out and model parameters for the thermodynamic properties of all phases have been obtained.

9.1 Introduction

Magnesium being the lightest structural metal, Mg-based alloys have many applications. Zinc is one of the most commonly used alloying elements in Mg (AZ series), and the rare earth (RE) metals have been shown to improve creep resistance [1, 2] and sheet formability (by reducing texture [3-6]).

Information on phase behavior is essential for the design of new RE-Mg-Zn alloys. However, few studies of the phase diagrams and thermodynamic properties of these systems have been made. The present study was thus undertaken to better define the phase diagrams of the RE-Mg-Zn ternary systems through the technique of critical thermodynamic assessment and optimization.

In a thermodynamic optimization, adjustable model parameters are calculated using all available thermodynamic and phase-equilibrium data in order to obtain one set of model equations as functions of temperature and composition. Thermodynamic data, such as activities, can aid in the evaluation of the phase diagrams, and information on phase equilibria can be used to deduce thermodynamic properties. With this technique, it is frequently possible to resolve discrepancies in the available data. From the model equations, all of the thermodynamic properties and phase diagrams can be back-calculated, and interpolations and extrapolations can be made in a thermodynamically correct manner. The thermodynamic properties and phase diagrams are thereby rendered self-consistent and consistent with thermodynamic principles, and the available data are distilled into a small set of model parameters, ideal for computer storage. Generally, in the optimization of a ternary system one begins by optimizing the three binary sub-systems. The binary model parameters are then used to estimate the properties of the ternary phases, and these estimates are then refined by introducing ternary model parameters where required to reproduce available ternary data.

Thermodynamic evaluations and optimizations have already been reported for the binary Mg-Zn system [7], all binary Mg-RE systems [8-11] and all binary RE-Zn systems (including Sc-Zn and Y-Zn) [12, 13]. Evaluations, optimizations and experimental phase diagram studies of the Ce-Mg-Zn and Nd-Mg-Zn systems have been reported in our previous articles [14, 15]. Evaluations and optimizations of the La-Mg-Zn, Pr-Mg-Zn and Sm-Mg-Zn system have also been reported previously [16]. In the present article we report on our evaluations and optimizations of the ternary heavier-RE-Mg-Zn systems as well as the Y-Mg-Zn system. As expected, all RE-Mg-Zn systems are very similar. The present work was greatly aided by our simultaneous assessments of all the other RE-Mg-Zn systems.

Due to a complete lack of data in the literature, and to the fact that these systems are expected to exhibit anomalies because of the half-filled and filled f-shells in Eu and Yb respectively, we have not included the Eu-Mg-Zn and Yb-Mg-Zn systems.

Figs. 1-17 show the 17 binary sub-systems of the Y-Mg-Zn, Gd-Mg-Zn, Tb-Mg-Zn, Dy-Mg-Zn, Ho-Mg-Zn, Er-Mg-Zn, Tm-Mg-Zn and Lu-Mg-Zn systems [7, 9, 11, 13].

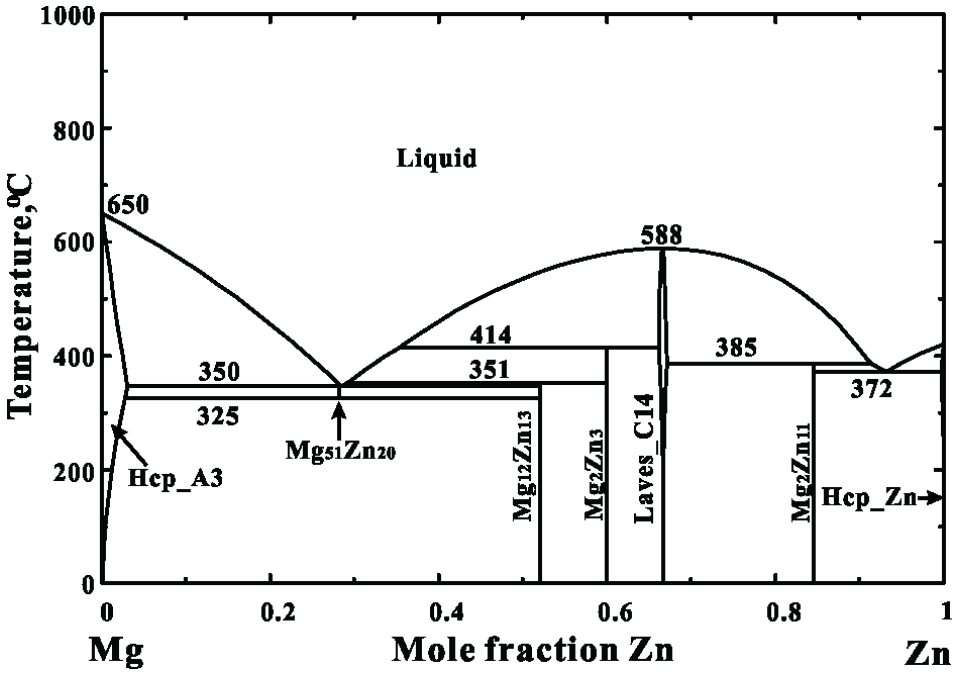

Figure 9.1. Calculated optimized Mg-Zn phase diagram [7]

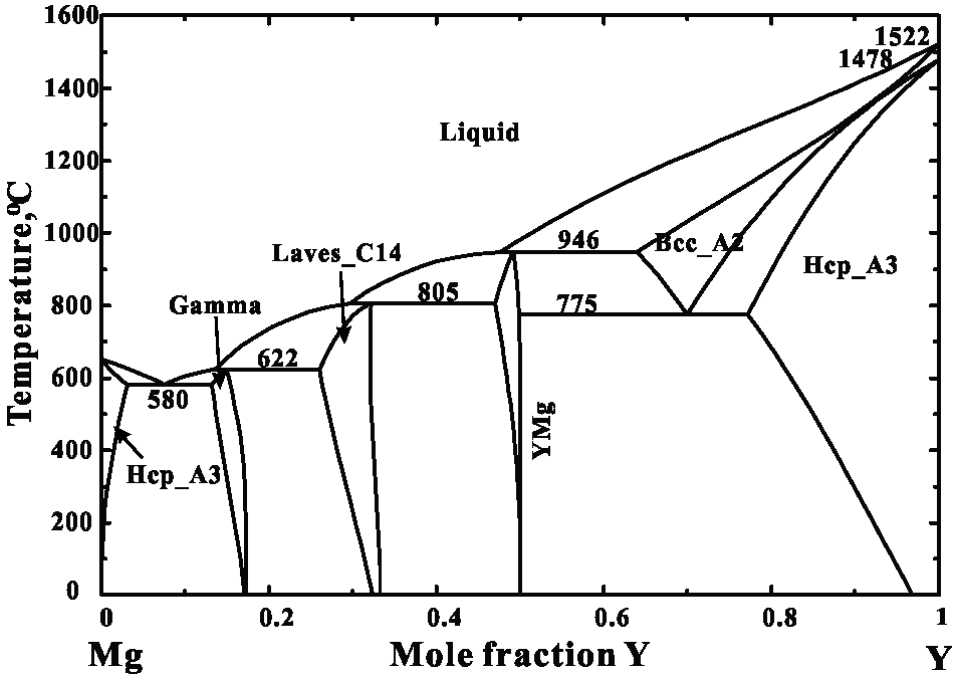

Figure 9.2. Calculated optimized Y-Mg phase diagram [9]

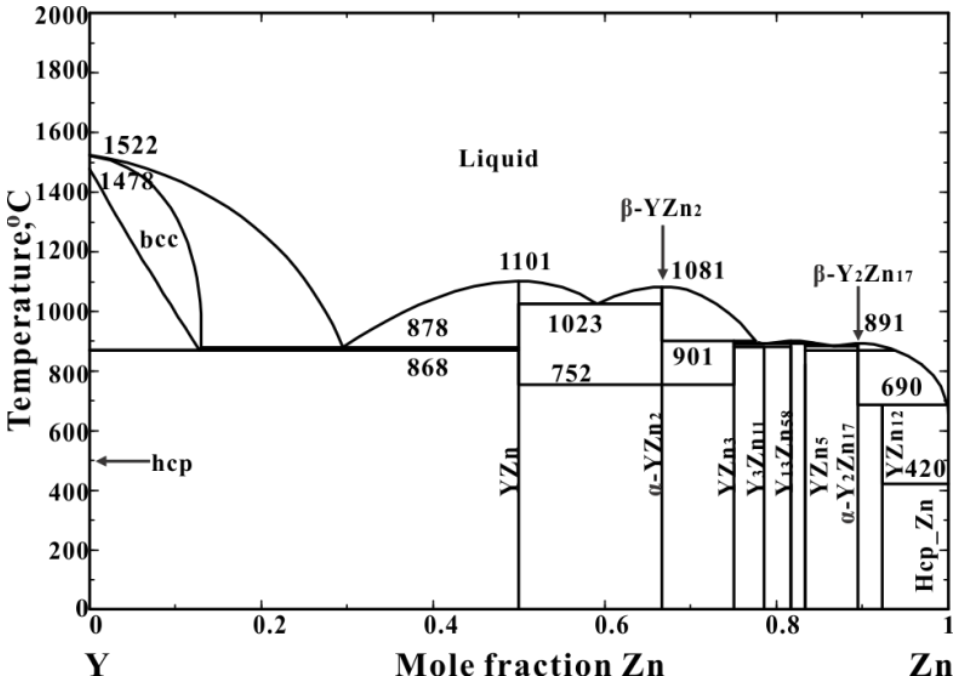

Figure 9.3 Calculated optimized Y-Zn phase diagram [13]

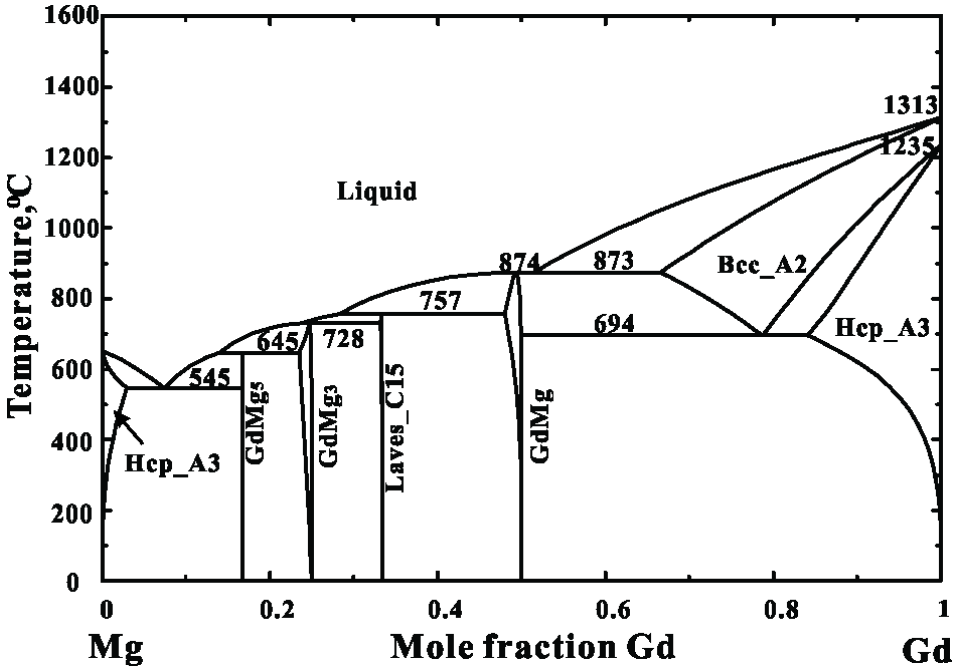

Figure 9.4 Calculated optimized Gd-Mg phase diagram [11]

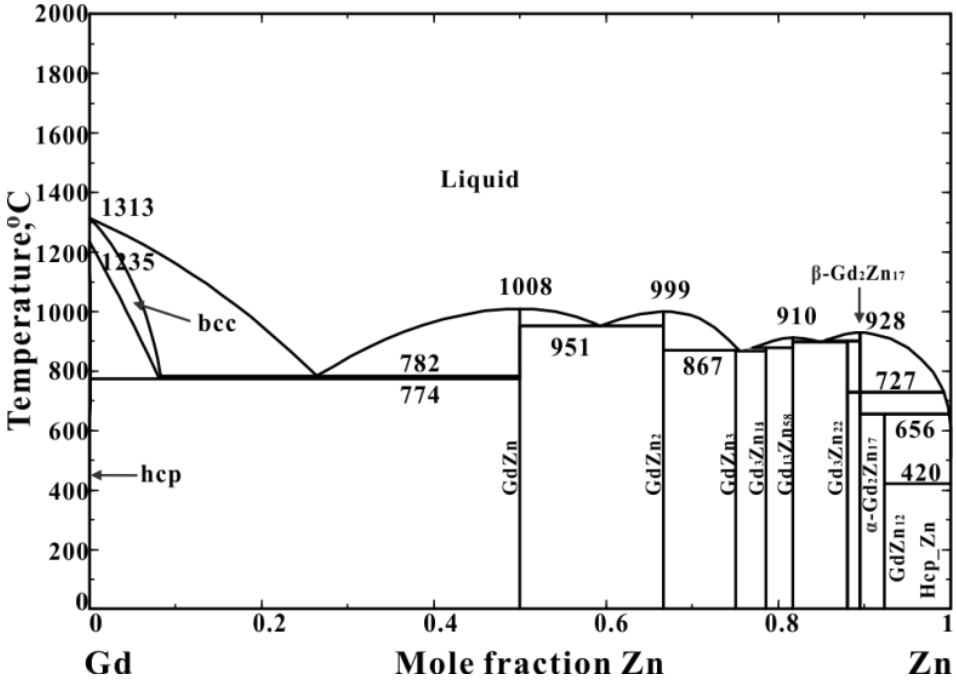

Figure 9.5 Calculated optimized Gd-Zn phase diagram [13]

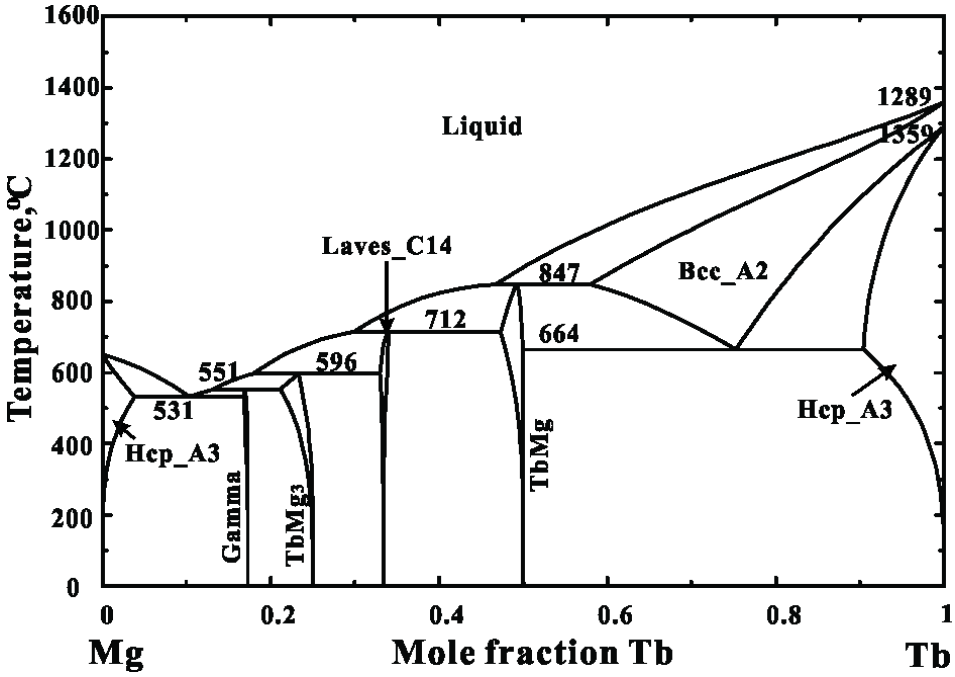

Figure 9.6.Calculated optimized Tb-Mg phase diagram [11]

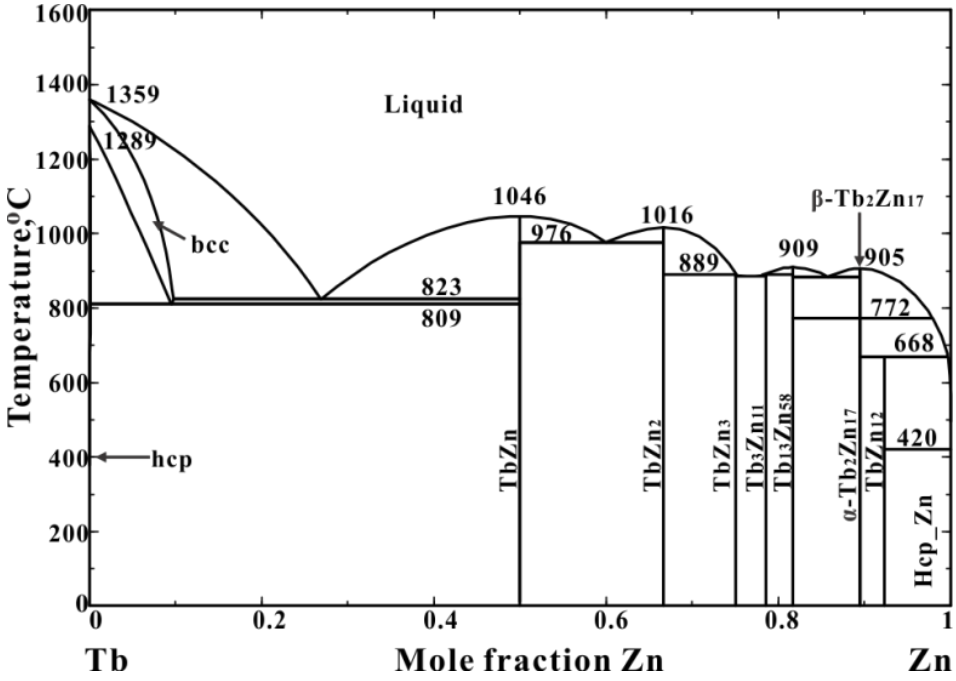

Figure 9.7. Calculated optimized Tb-Zn phase diagram [13]

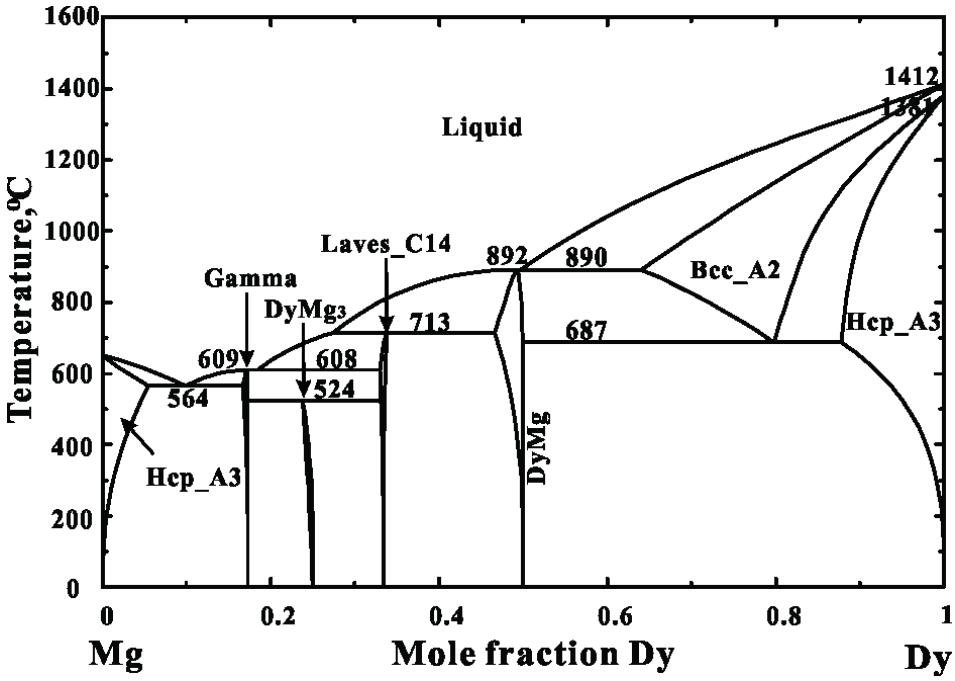

Figure 9.8. Calculated optimized Dy-Mg phase diagram [11]

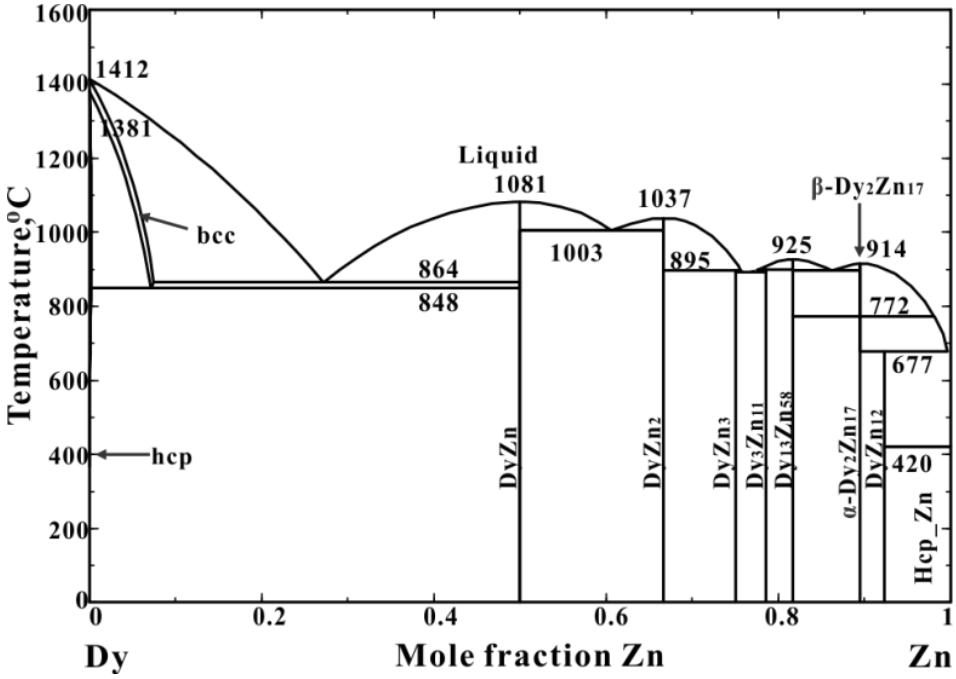

Figure 9.9. Calculated optimized Dy-Zn phase diagram [13]

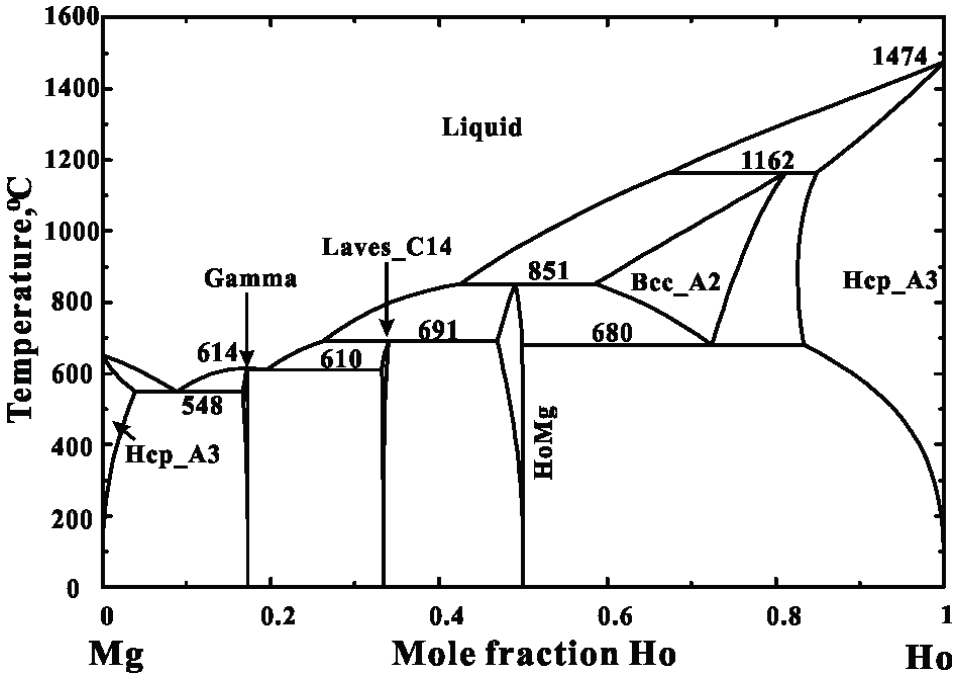

Figure 9.10. Calculated optimized Ho-Mg phase diagram [11]

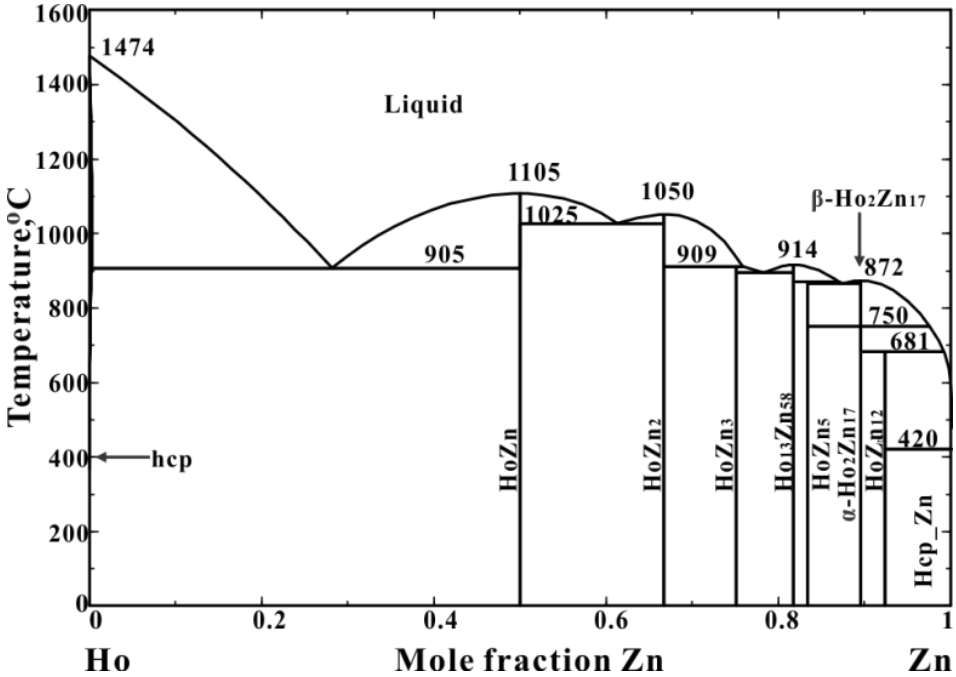

Figure 9.11. Calculated optimized Ho-Zn phase diagram [13]

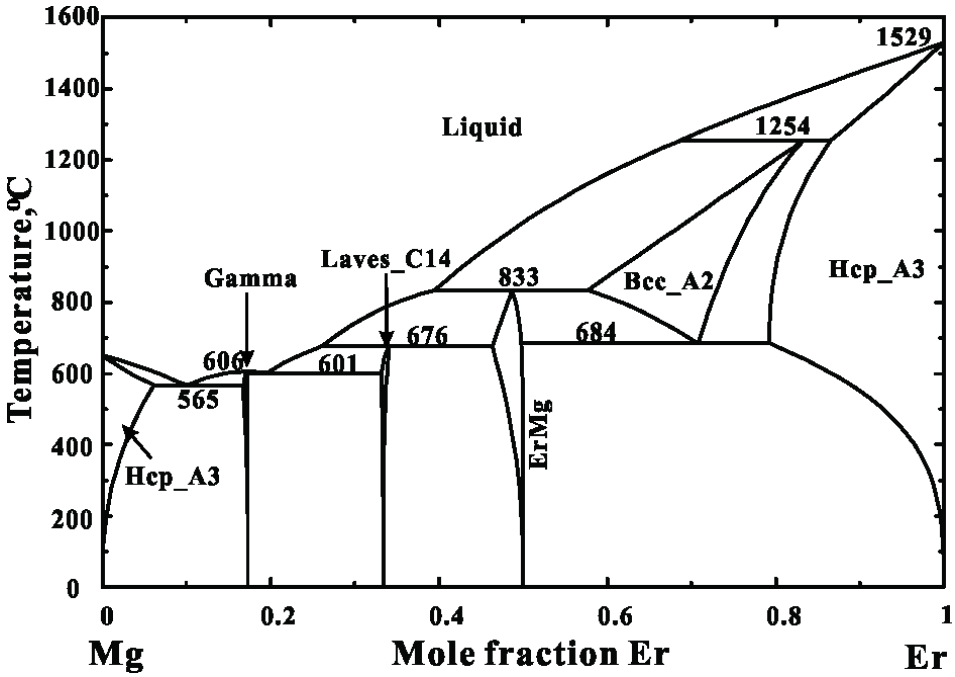

Figure 9.12. Calculated optimized Er-Mg phase diagram [11]

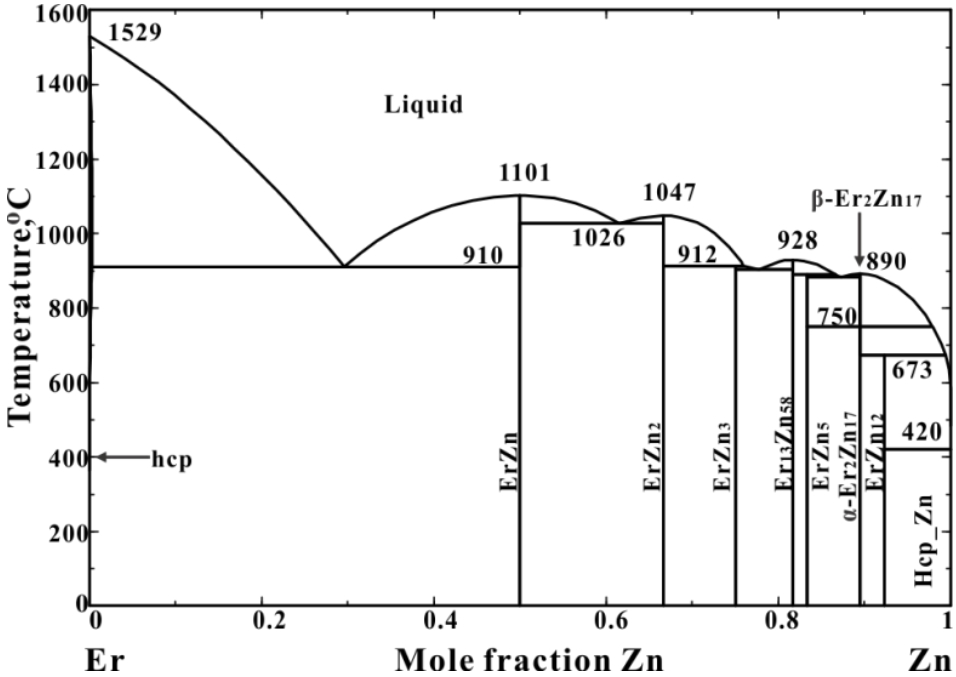

Figure 9.13. Calculated optimized Er-Zn phase diagram [13]

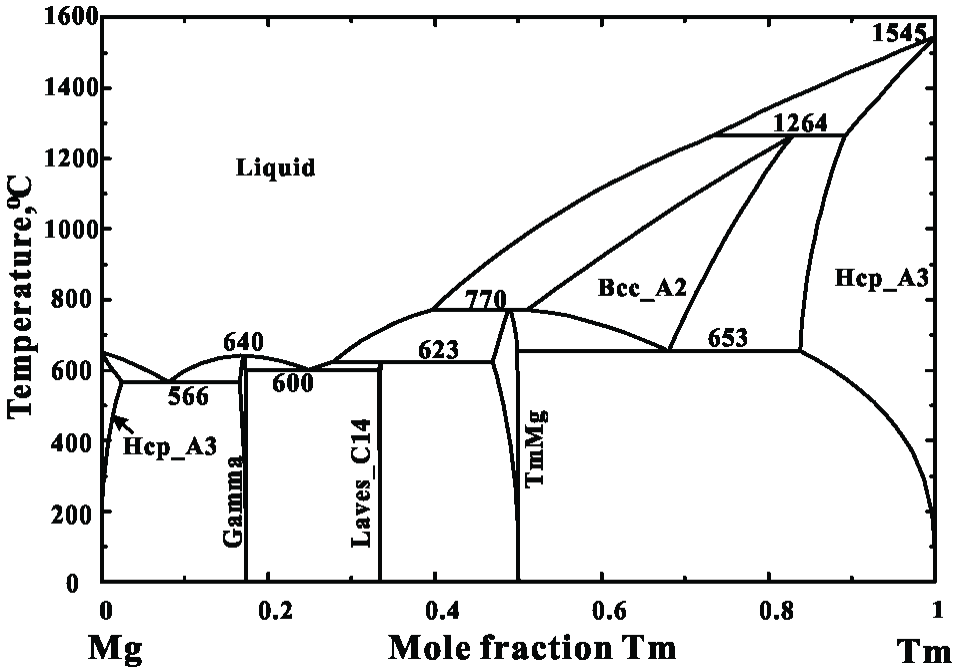

Figure 9.14. Calculated optimized Tm-Mg phase diagram [11]

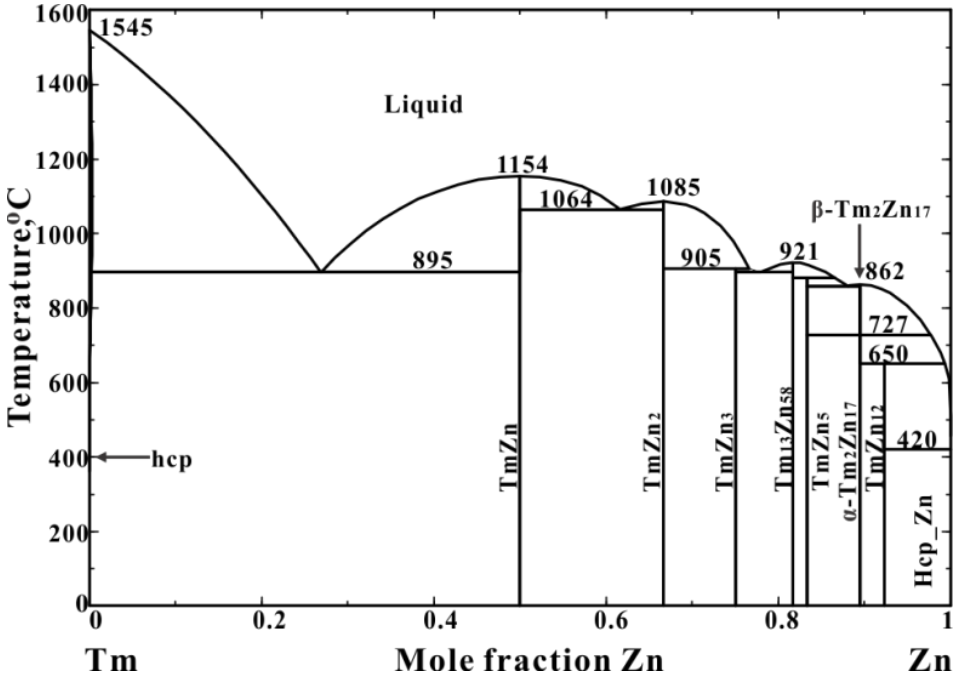

Figure 9.15. Calculated optimized Tm-Zn phase diagram [13]

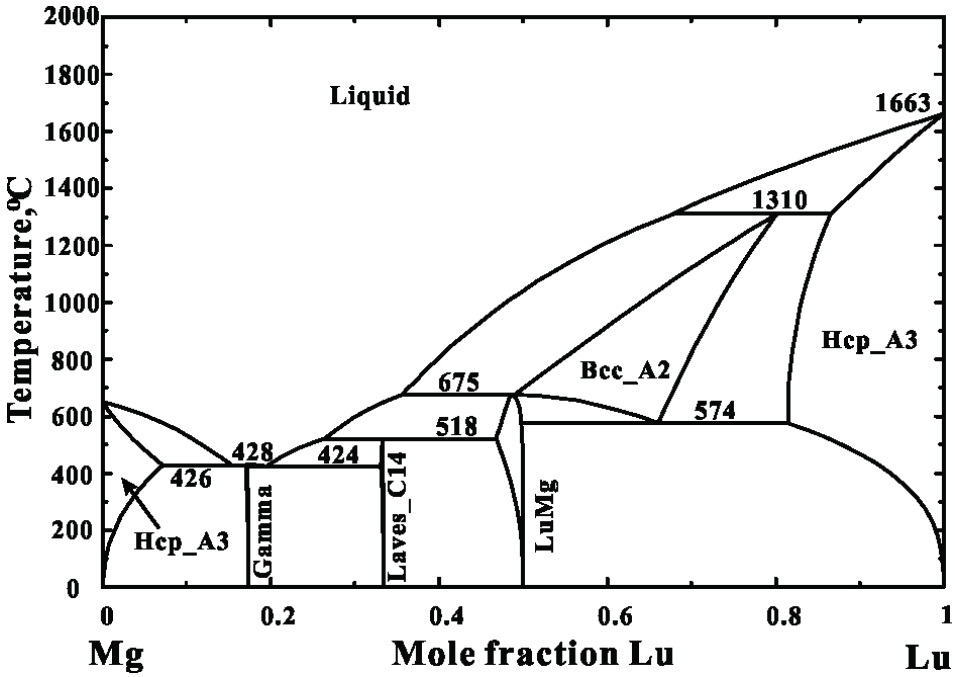

Figure 9.16. Calculated optimized Lu-Mg phase diagram [11]

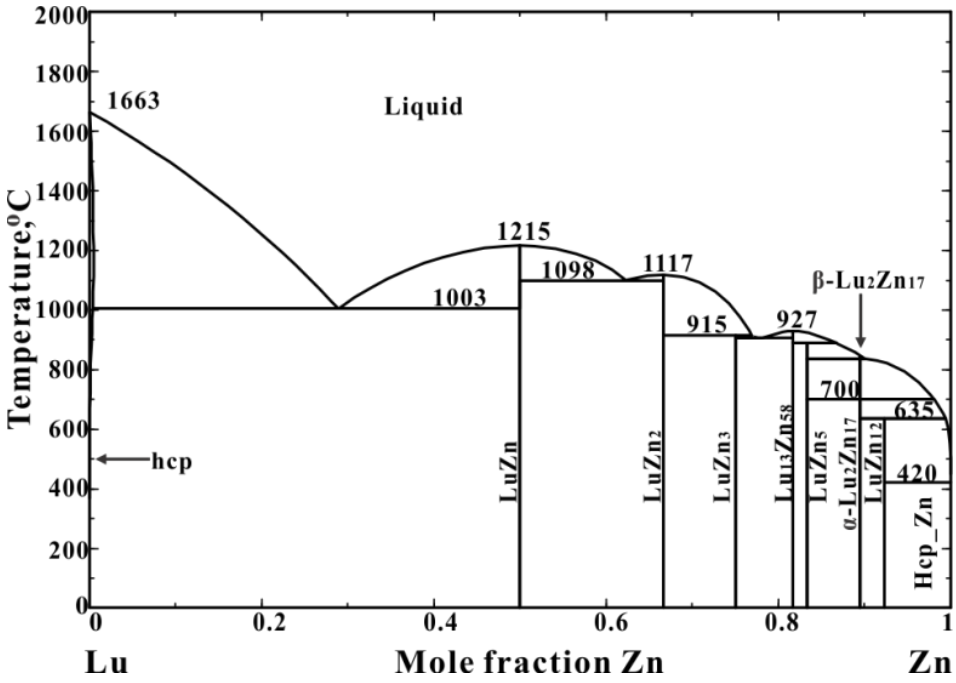

Figure 9.17. Calculated optimized Lu-Zn phase diagram [13]

9.2 Phase equilibrium and thermodynamic data

The Y-Mg-Zn, Gd-Mg-Zn, Tb-Mg-Zn, Dy-Mg-Zn, Ho-Mg-Zn, Er-Mg-Zn, Tm-Mg-Zn and Lu-Mg-Zn systems have been investigated by several authors. Different ternary phase names were used by different authors. Phases with ternary phase fields considered in the present optimization are summarized in Table 1. All these phases (except the metastable ones) can also be seen in the calculated isothermal sections at 300°C shown in Figs.22, 32, 34, 35 and 38-41. As shown in Table 1, the ternary phase τ3 is considered in all heavier-RE-Mg-Zn systems and τ5 is considered only in the Y-Mg-Zn system in the present study. The same nomenclature is used for τ3 and τ5 as in our previous paper on the Ce-Mg-Zn system [14]. The X and I phases have only been identified in heavier-RE-Mg-Zn systems. It should be mentioned that although the τ5 and I phases have very similar compositions they are different phases (τ5 has an hcp structure while I has an icosahedral structure). τ5 is unique to the lighter-RE-Mg-Zn systems while I is unique to the heavier-RE-Mg-Zn systems. Exceptionally, both phases are stable in the Y-Mg-Zn system. The phases RE(Mg,Zn) in Table 1 are solid solutions of REMg and REZn. The phases $GdMg_3$, $TbMg_3$ and $DyMg_3$ are solutions with limited solubility of Zn. The phases YMg_3, $HoMg_3$, $ErMg_3$,

$TmMg_3$ and $LuMg_3$ are metastable phases in their respective binary RE-Mg systems. The $REMg_{12}$ phase was not reported in any of the heavier-RE-Mg-Zn systems and in a previous paper [16] we concluded that this phase will not be a stable phase in the heavier-RE-Mg-Zn systems. Hence, it is not considered in the present study. All other binary phases are assumed not to extend into the ternary systems because no solubilities have been reported. The prototypes, Pearson symbols and space groups of all binary phases were given previously [7, 8, 13].

A decagonal phase, denoted as $Dy_2Mg_{40}Zn_{58}$, has been reported [17-19]. Experiments were performed on alloys in other RE-Mg-Zn systems (except Pm) by the same authors to verify the existence of the decagonal phase. The existence of the decagonal phase was confirmed in the Y-Mg-Zn, Ho-Mg-Zn, Er-Mg-Zn, Tm-Mg-Zn and Lu-Mg-Zn systems in addition to the Dy-Mg-Zn system. This phase is not considered in the present project because no detailed information can be found in the literature.

Possible ternary phases in all RE-Mg-Zn systems, both stable and metastable in the present project, are summarized in Table 2 [20-48].

Table 9.1 Phases with ternary phase fields in the Y-Mg-Zn, Gd-Mg-Zn, Tb-Mg-Zn, Dy-Mg-Zn, Ho-Mg-Zn, Er-Mg-Zn, Tm-Mg-Zn and Lu-Mg-Zn systems

Phase name	Prototype-Pearson symbol-Space group	Thermodynamic model*	
Y(Mg,Zn)	CsCl-cP2-Pm$\bar{3}$m	Y(Mg,Zn)	Assumed continuous solution
YMg_3	BiF_3-cF16-Fm$\bar{3}$m	$Y(Mg,Zn)_3$	Metastable phase
α-Y_2Zn_{17}	$Ni_{17}Th_2$-hP38-$P6_3/mmc$	$Y_2(Mg,Zn)_{17}$	Reported Mg content of 3 at.% [20]
τ3	MnCu_2Al-cF16-Fm$\bar{3}$m [21]	$YMg(Mg,Zn)_2$	Reported as W ($Y_2Mg_3Zn_3$) [22, 23]
			Reported as W [21, 24]
τ5	$Ce_3Mg_{13}Zn_{30}$-hP92-$P6_3/mmc$ [21]	$Y_3Mg_{13}Zn_{30}$	Assumed stoichiometric in present study
			Reported as Z phase [22, 23]
			Reported as $Y_7Mg_{28}Zn_{65}$ [21]
			Reported as $Y_{6.86}Mg_{27.92}Zn_{65.22}$ [25]
X	LPSO	$YMg_{12}Zn$	Assumed stoichiometric in present study
			Reported as X [23, 24]
			Reported as 10H, 14H and 18R [26-31]
I	Fm53(icosahedral) [21]	YMg_3Zn_6	Assumed stoichiometric in present study
			Reported as icosahedral phase [20, 32, 33]
			Reported as I phase [21]
H	Hexagonal [21]	$Y_{15}Mg_{15}Zn_{70}$	Assumed stoichiometric in present study
		Reported as H ($Y_{15}Mg_{15}Zn_{70}$) [21]	
Gd(Mg,Zn)	CsCl-cP2-Pm$\bar{3}$m	Gd(Mg,Zn)	Assumed continuous solution
$GdMg_3$	BiF_3-cF16-Fm$\bar{3}$m	$Gd(Mg,Zn)_3$	
τ3	MnCu_2Al-cF16-Fm$\bar{3}$m	$GdMg(Mg,Zn)_2$	Reported Zn content 35-49 at.% [34]
X	LPSO	$GdMg_{12}Zn$	Assumed stoichiometric in present study
			Reported as 14H phase [28, 34, 35]
I	Quasicrystal (Icosahedral)	$GdMg_3Zn_6$	Assumed stoichiometric in present study
			Reported as I phase [34, 36-38]
Tb(Mg,Zn)	CsCl-cP2-Pm$\bar{3}$m	Tb(Mg,Zn)	Assumed continuous solution
$TbMg_3$	BiF_3-cF16-Fm$\bar{3}$m	$Tb(Mg,Zn)_3$	
τ3	MnCu_2Al-cF16-Fm$\bar{3}$m	$TbMg(Mg,Zn)_2$	Assumed in present study
X	LPSO	$TbMg_{12}Zn$	Assumed stoichiometric in present study
			Reported as X [28]
I	Quasicrystal (Icosahedral)	$TbMg_3Zn_6$	Assumed stoichiometric in present study
		Reported as I phase [36, 37, 39]	
Dy(Mg,Zn)	CsCl-cP2-Pm$\bar{3}$m	Dy(Mg,Zn)	Assumed continuous solution
$DyMg_3$	BiF_3-cF16-Fm$\bar{3}$m	$Dy(Mg,Zn)_3$	Metastable phase

τ3	MnCu_2Al-cF16-Fm$\bar{3}$m	DyMg(Mg,Zn)$_2$	Reported as Y phase [40]
X	LPSO	DyMg$_{12}$Zn	Assumed stoichiometric in present study
			Reported as X [40]
I	Quasicrystal (Icosahedral)	DyMg$_3$Zn$_6$	Assumed stoichiometric in present study
			Reported as Z phase [40]
			Reported as an icosahedral phase [41]
Ho(Mg,Zn)	CsCl-cP2-Pm$\bar{3}$m	Ho(Mg,Zn)	Assumed continuous solution
HoMg$_3$	BiF$_3$-cF16-Fm$\bar{3}$m	Ho(Mg,Zn)$_3$	Metastable phase
τ3	MnCu_2Al-cF16-Fm$\bar{3}$m	HoMg(Mg,Zn)$_2$	Assumed in present study
X	LPSO	HoMg$_{12}$Zn	Assumed stoichiometric in present study
			Reported as LPSO phase [28]
I	Quasicrystal (Icosahedral)	ErMg$_3$Zn$_6$	Assumed stoichiometric in present study
			Reported as an icosahedral phase [37, 42-45]
Er(Mg,Zn)	CsCl-cP2-Pm$\bar{3}$m	Er(Mg,Zn)	Assumed continuous solution
ErMg$_3$	BiF$_3$-cF16-Fm$\bar{3}$m	Er(Mg,Zn)$_3$	Metastable phase
τ3	MnCu_2Al-cF16-Fm$\bar{3}$m	ErMg(Mg,Zn)$_2$	Assumed in present study
X	LPSO	ErMg$_{12}$Zn	Assumed stoichiometric in present study
			Reported as LPSO phase [28]
I	Quasicrystal (Icosahedral)	ErMg$_3$Zn$_6$	Assumed stoichiometric in present study
			Reported as an icosahedral phase [46-48]
Tm(Mg,Zn)	CsCl-cP2-Pm$\bar{3}$m	Tm(Mg,Zn)	Assumed continuous solution
TmMg$_3$	BiF$_3$-cF16-Fm$\bar{3}$m	Tm(Mg,Zn)$_3$	Metastable phase
τ3	MnCu_2Al-cF16-Fm$\bar{3}$m	TmMg(Mg,Zn)$_2$	Assumed in present study
X	LPSO	TmMg$_{12}$Zn	Assumed stoichiometric in present study
			Reported as LPSO phase [28]
I	Quasicrystal (Icosahedral)	LuMg$_3$Zn$_6$	Assumed stoichiometric in present study
Lu(Mg,Zn)	CsCl-cP2-Pm$\bar{3}$m	Lu(Mg,Zn)	Assumed continuous solution
LuMg$_3$	BiF$_3$-cF16-Fm$\bar{3}$m	Lu(Mg,Zn)$_3$	Metastable phase
τ3	MnCu_2Al-cF16-Fm$\bar{3}$m	LuMg(Mg,Zn)$_2$	Assumed in present study
X	LPSO	LuMg$_{12}$Zn	Assumed stoichiometric in present study
I	Quasicrystal (Icosahedral)	LuMg$_3$Zn$_6$	Assumed stoichiometric in present study

*Elements within brackets substitute on the same sublattice.

Table 9.2. Phases with possible ternary phase fields in RE-Mg-Zn systems as assumed in the present project [14, 15, 16]

	Thermodynamic model	Y	La	Ce	Pr	Nd	(Pm)	Sm	(Eu)	Gd	Tb	Dy	Ho	Er	Tm	(Yb)	Lu
RE(Mg,Zn)	RE(Mg,Zn)	×	×	×	×	×		×		×	×	×	×	×	×		×
$REMg_3$	$RE(Mg,Zn)_3$	○	×	×	×	×		×		×	×	×	⦿	⦿	⦿		⦿
RE_2Mg_{17}	$RE_2(Mg,Zn)_{17}$	○	×	□	○	○		○		○	○	○	○	○	○		○
α-RE_2Zn_{17}	$RE_2(Mg,Zn)_{17}$	×	□	□	□	□		□		□	□	□	□	□	□		□
β-RE_2Zn_{17}	$RE_2(Mg,Zn)_{17}$	□	×	□	□	□		□		□	□	□	□	□	□		□
$REMg_{12}$	$RE(Mg,Zn)_{12}$	○	×	×	×	×		⦿		○	○	○	○	○	○		○
$REZn_4$	$RE(Mg,Zn)_4$	○	×	○	○	○		○		○	○	○	○	○	○		○
$\tau1$	$RE_3Zn_9(Mg,Zn)_2$	○	○	×	●	●		●		○	○	○	○	○	○		○
$\tau2$	$RE_2Mg_{53}Zn_{45}$	○	○	×	●	×		●		○	○	○	○	○	○		○
$\tau3$	$REMg(Mg,Zn)_2$	×	×	×	×	×		×		×	×	×	×	×	×		×
$\tau4$	$RE_2Mg_5Zn_9$	○	○	×	×	×		×		○	○	○	○	○	○		○
$\tau5$	$RE_3Mg_{13}Zn_{30}$	×	○	×	×	×		×		○	○	○	○	○	○		○
$\tau6$	$RE_6Mg_{11}Zn_{83}$	○	○	×	●	●		●		○	○	○	○	○	○		○
$\tau7$	$RE_{20}Mg_{19}Zn_{81}$	○	○	×	●	×		●		○	○	○	○	○	○		○
V phase	$RE_5Mg_{42}Zn_{53}$	○	×	○	○	○		○		○	○	○	○	○	○		○
H phase	$RE_{15}Mg_{15}Zn_{70}$	×	○	○	○	○		○		○	○	○	○	○	○		○
X phase	$RE_2Mg_{12}Zn$	×	○	○	○	○		○		×	×	×	×	×	×		×
I phase	$REMg_3Zn_6$	×	○	○	○	○		○		×	×	×	×	×	×		×
Decagonal phase		●	○	○	○	○		○		○	○	●	●	●	●		●

× stable phases considered in the present project (verified or assumed); ○ phases considered unstable; ⦿ phases considered metastable. Parameters have been assigned; □ binary phases assumed to have no ternary phase fields; ●possible stable phases not considered in the present project. No parameters have been ass

9.2.1 Y-Mg-Zn

Based on micrographic analysis, Drits *et al* [49] proposed two ternary phases in the Y-Mg-Zn system. However, neither compositions nor crystal structures were reported. Two isopleths in the Mg-rich region (18 wt.% Y and 29 wt.% Zn) were given by Padezhnova *et al* [23] based on differential thermal analysis (DTA). Three ternary phases (denoted in the present work as X, τ3 and τ5, reported as X, W and Z, respectively) were reported in their work. τ3 has an fcc lattice with parameter a = 0.685± 0.001nm according to the X-ray analysis (XRD). Also reported in their work were four invariant equilibria:

$$liquid \leftrightarrow (Mg) + Mg_{24}Y_5 + X \text{ at } 533\ ^{o}\text{C} \qquad 9.1$$

$$liquid \leftrightarrow (Mg) + X + \tau 3 \text{ at } 527\ ^{o}\text{C} \qquad 9.2$$

$$liquid \leftrightarrow (Mg) + Mg_7Zn_3 + \tau 5 \text{ at } 340\ ^{o}\text{C} \qquad 9.3$$

$$liquid + W \leftrightarrow (Mg) + \tau 5 \text{ at } 448\ ^{o}\text{C} \qquad 9.4$$

Subsequently, the solubility of Y and Zn in Mg as well as phase relationships in the Mg-rich region were studied by Dobatkina by microscopic examination, XRD and resistivity measurements [50]. Phase relationships of compositions up to 70 at.% Zn and 50 at.% Y were later examined by Padezhnova by DTA, XRD, microstructural analysis and electron probe microanalysis (EPMA) [22]. Compositions of the three ternary phases were determined by EPMA and their formulae were suggested to be $YMg_{12}Zn$ (X), YMg_3Zn_6 (τ5) and $Y_2Mg_3Zn_3$ (τ3). The crystal structure of $Y_2Mg_3Zn_3$ was determined to be cubic, of the $AlMnCu_2$ prototype and space group Fm3m. An isothermal section at 300°C and an isopleth which corresponds to the quasibinary Mg-X section were presented.

Later, a quasicrystal was obtained by Langsdorf *et al* [32] using the Bridgman technique, with a nearly constant Zn content of 65 at.%, with Mg and Y contents ranging from 30 to 24 at.% and from 6.5 to 9 at.%, respectively. The existence of the quasicrystal phase was confirmed by Tsai *et al* [20] using XRD, EPMA and DTA measurements and its stoichiometric composition was determined to be close to YMg_3Zn_6. During the solidification of an $Y_{10}Mg_{30}Zn_{60}$ melt, an $Y(Zn,Mg)_5$ phase crystallized as primary phase at about 687°C followed by an invariant reaction at about 547 ^{o}C. This quasicrystaline phase is denoted I in the present study.

The X phase is a long-period stacking ordered phase (LPSO) in the Mg-rich region. Neutron diffraction experiments showed that the LPSO phase has the 18R structure with space group $P3_212$ with a = 1.1182(0) nm and c = 4.7032(5) nm [51]. However, a small amount of another LPSO phase with the 14H structure was also detected in this experiment. Several LPSO structures have been reported in the literature: 10H, 14H and 18R [26-31, 52]. Some of these phases could be metastable. According to Itoi *et al* [27], the 18R phase transforms to 14H phase after annealing at 500°C for 5 hours. Given the fact that the LPSO phase is complex and transformation among the forms may be very slow, it is very hard to deduce which form/forms could be stable. In the present work, all forms of LPSO phases are treated as the X phase.

Using scanning electron microscopy (SEM), wavelength dispersive X-ray spectroscopy (WDS), XRD and transmission electron microscopy (TEM), Tsai *et al* [21] determined three isothermal sections at 423°C, 500 ^{o}C and 600 ^{o}C in the region of 30-70 at. % Zn, 20-60 at.% Mg and 0-20 at.% Y. Four ternary phases were identified: τ3, τ5, I and H (reported as W, Z, I and H, respectively). Crystal structure information for these ternary phases is shown in Table 1. An isothermal section at 300 ^{o}C was studied by Horiuchi *et al* [24] based on investigation of five samples with compositions close to the Mg-Zn binary system. The τ3, τ5, I, H and X phases (reported as W, Z, I, H and X, respectively) were proposed in the isothermal section. DTA measurement on $Y_{11.9}Mg_{50.7}Zn_{37.4}$ gave two signals: one at 656°C corresponding to the liquidus and another at 450°C, which may correspond to an invariant reaction.

A later investigation by Li *et al* [53] suggested that the H phase was actually a YZn_5 phase in which Zn was substituted by Mg up to 25 at.%. In the present work, however, the H phase is modeled separately because the lattice constants of the H phase (a = 0.776 nm, c = 0.92 nm) differ significantly from those of YZn_5 (a = 0.519 nm, c = 0.438 nm) according to Tasi *et al* [21].

Using DTA, SEM, EDX and XRD analysis, Langsdorf *et al* [33] investigated the liquidus surface in the vicinity of the I phase. Two isopleths were reported where only the liquiduses were shown: $Mg_{60}Zn_{40}$-$Y_{10}Mg_{30}Zn_{60}$ and $Mg_{50}Zn_{50}$-$Y_{10}Mg_{30}Zn_{60}$.

Seven samples were later prepared by Grobner et al [52] and DSC measurements were performed in the temperature range from 300°C to 900°C.

9.2.2 Gd-Mg-Zn

Three ternary phases have been reported in the Gd-Mg-Zn system: the I phase, the W phase and the X phase. The I phase has been reported by several authors [36-38]. This is an icosahedral phase with a formula of ~$GdMg_3Zn_6$. The W phase has the same structure as $Y_2Mg_3Zn_3$ according to XRD analysis [54]. The X phase was reported as a 14H LPSO phase [28, 35] as in the Y-Mg-Zn system.

The partial isothermal section of Gd-Mg-Zn system at 400°C was for the first time investigated by Qi *et al* [34] by means of XRD, SEM equipped with energy dispersive X-ray spectroscopy (EDS) and EPMA. All the three ternary compounds reported in refs [36-38] were confirmed. Based on the experimental data, the Gd-Mg-Zn system was thermodynamically optimized by the same authors.

9.2.3 Tb-Mg-Zn

Research on Tb-Mg-Zn system is limited to the report of two ternary compounds: the I phase [36, 37, 39] and the X phase [28].

9.2.4 Dy-Mg-Zn

The Mg-rich region of the Dy-Mg-Zn system was investigated by Rokhlin *et al* [40] using DTA and XRD analysis. Three ternary phases were reported but their structures were not given: X, Y, and Z (denoted X, τ3 and I in the present study). A partial isothermal section in the Mg-rich region at 300°C and an isopleth (Mg-39 wt.% Dy to Mg-39.wt% Zn) were reported. Four invariant equilibria were also reported:

$$L \leftrightarrow \alpha + X + Y \text{ at } 537^o\text{C} \qquad 9.5$$

$$L \leftrightarrow (Mg) + Gamma + X \text{ at } 531^o\text{C} \qquad 9.6$$

$$L + \tau 3 \leftrightarrow (Mg) + Z \text{ at } 437^o\text{C} \qquad 9.7$$

$$L \leftrightarrow (Mg) + Mg_{51}Zn_{20} + Z \text{ at } 340^o\text{C.} \qquad 9.8$$

The Z phase was found by Luo *et al* [41] to be an icosahedral phase with the same structure as $GdMg_3Zn_6$. This structure differs from that of the τ5 phase (which has a similar composition) in the lighter-RE-Mg-Zn systems.

In this work, the Y and Z phases are denoted τ3 and I, respectively, to be in accordance with our notation for all RE-Mg-Zn systems.

9.2.5 Ho-Mg-Zn, Er-Mg-Zn, Tm-Mg-Zn and Lu-Mg-Zn

Neither phase diagram nor thermodynamic data are available for these four systems. The LPSO phase (the X phase) was reported in the Ho-Mg-Zn, Er-Mg-Zn and Tm-Mg-Zn systems [28]; the icosahedral phase was reported by several authors for the Ho-Mg-Zn [37, 42-45] and Er-Mg-Zn systems [46-48].

9.2.6 Ternary phases considered in the present study

Based on the available experimental data, the following ternary phases are considered in the present optimization. All these ternary phases can be found in Table 1.

<u>RE(Mg,Zn)</u>: As with the RE(Mg,Zn) phases in all lighter-RE-Mg-Zn systems [14-16], the REMg and REZn binary phases all have the CsCl structure and they are assumed in the present study to form continuous solutions. The RE content is constant at 50 at.%. Consequently, the model RE(Mg,Zn) was chosen in the present optimization (That is, Mg and Zn substitute on one sublattice while RE occupies a second lattice).

<u>$REMg_3$</u>: $GdMg_3$, $TbMg_3$ and $DyMg_3$ are stable binary phases while $HoMg_3$, $ErMg_3$, $TmMg_3$, $LuMg_3$ and YMg_3 are not. Solubilities of Zn in the stable $REMg_3$ phases have not been reported. Since all $REMg_3$ phases have the same structure, the model $RE(Mg,Zn)_3$, which was used for the $REMg_3$ phases in the lighter-RE-Mg-Zn systems in our previous reports [14-16], is also used in the present study.

<u>α-Y_2Zn_{17}</u>: Mg can substitute for Zn up to 3 at.% Mg in α-Y_2Zn_{17} [21]. Consequently, the α-Y_2Zn_{17} solution phase is modeled as $Y_2(Mg,Zn)_{17}$. Thermodynamic parameters of the unstable Y_2Mg_{17} end-member of the α-Y_2Zn_{17} phase have been estimated previously [11].

τ3: The existence of τ3 is well established in the Ce-Mg-Zn [55, 56], Nd-Mg-Zn [57, 58], Y-Mg-Zn [21, 24, 59] and Gd-Mg-Zn [34] systems. This phase was not reported in most of the heavier-RE-Mg-Zn systems considered in the present study, most probably because no detailed experiments were carried out to verify its existence. Since this phase is evidenced in several lighter-RE-Mg-Zn and heavier-RE-Mg-Zn systems, it is assumed to be stable in all RE-Mg-Zn systems.

τ5: The τ5 phase was only reported in the Y-Mg-Zn system and the reported crystal structure [21] was the same as that of τ5 in Ce-Mg-Zn system. It should be mentioned here that the compositions of τ5 and I are very close but the two phases coexist in the Y-Mg-Zn system.

X, I and H: The X phase is an LPSO phase (several forms have been reported in the literature, as summarized in section 2) and the I phase is an icosahedral phase. The two phases have been observed in most of the heavier-RE-Mg-Zn systems. The H phase has been reported only in the Y-Mg-Zn system. Only limited solubility was reported for these phases in the Y-Mg-Zn system and they are treated as stoichiometric phases in the present study, with suggested stoichiometries $REMgZn_{12}$, $REMg_3Zn_6$ and $Y_{15}Mg_{15}Zn_{70}$, respectively.

Ternary phases similar to the τ1, τ2, τ4, τ5, τ6 and τ7 phases observed in the lighter-RE-Mg-Zn systems [14-16] have not been reported in any of the heavier-RE-Mg-Zn systems (except for τ5 in the Y-Mg-Zn system). Consequently, these phases are not considered in the present study except for τ5 in the Y-Mg-Zn system.

9.3 Thermodynamic models

Thermodynamic data for the pure elements were given previously [7, 9, 11, 13]. The thermodynamic parameters of the binary sub-systems are taken from Ansara *et al* [7] (Mg-Zn), Kang et al [9, 11] (Y-Mg, Gd-Mg, Tb-Mg, Dy-Mg, Ho-Mg, Er-Mg, Tm-Mg and Lu-Mg) and Zhu and Pelton [13] (Y-Zn, Gd-Zn, Tb-Zn, Dy-Zn, Ho-Zn, Er-Zn, Tm-Zn and Lu-Zn).

For the binary sub-systems, the Modified Quasichemical Model (MQM) [60, 61], which takes account of short-range ordering, was used to model the liquid phase. Consequently, the MQM is used to model the liquid phase in the ternary system. For details of the model, see references [12, 13, 60, 61]. The symmetric (Kohler-like) model [63] was used to estimate the

properties of the ternary liquid phases from the optimized binary model parameters. No additional ternary model parameters were introduced.

In the optimization of the Mg-Zn binary system, Ansara *et al* [7] did not use the MQM for the liquid phase. Consequently, the liquid phase was remodelled using the MQM, keeping the same parameters as Ansara *et al* [7] for all other phases. The "coordination numbers", which are MQM model parameters, were set to

$$Z^{Mg}_{Mg,Zn} = Z^{Zn}_{Mg,Zn} = Z^{Mg}_{Mg,Mg} = Z^{Zn}_{Zn,Zn} = 6 \qquad 9.9$$

and the new MQM model parameters were introduced as

$$\Delta g_{MgZn} = -6778 + 3.138T + (-1966 + 2.008)X_{MgMg}$$
$$+(-3975 + 1.6736)X_{ZnZn} \text{ (J/g-atom)} \qquad 9.10$$

The binary Bcc_A2, Fcc_A1 and Hcp_A3 solutions are described by a substitutional solution model as discussed previously [13].

As shown in Table 1, Mg and Zn can substitute for each other on one sublattice in some phases (τ3, RE(Mg,Zn), $REMg_3$ and α-RE_2Zn_{17}). These phases are modeled with the Compound Energy Formalisim (CEF) [62]. For example, the Gibbs energy of Y(Mg,Zn) (per mole formula) can be expressed as follows:

$$G^{Y(Mg,Zn)} = y_{Mg}G^{0,Y(Mg,Zn)}_{Y:Mg} + y_{Zn}G^{0,Y(Mg,Zn)}_{Y:Zn}$$
$$+RT\left(y_{Mg}lny_{Mg} + y_{Zn}lny_{Zn}\right)$$
$$+y_{Mg}y_{Zn}(L^{0}_{Y:Mg,Zn}$$
$$+(y_{Mg} - y_{Zn})\, L^{1}_{Y:Mg,Zn}) \qquad 9.11$$

where y_{Mg} and $y_{Zn}$are the site fractions of Mg and Zn in the second sublattice, $G^{0,Y(Mg,Zn)}_{Y:Mg}$ and $G^{0,Y(Mg,Zn)}_{Y:Zn}$ are the Gibbs energies of the end-members (YMg and YZn) at temperature T under the convention that the enthalpies of the elements are equal to zero in their stable states at 298.15K, and $L^{0}_{Y:Mg,Zn}$ and $L^{1}_{Y:Mg,Zn}$ are interaction parameters to be optimized. The Gibbs energies of other solid solution phases can be expressed similarly.

The X, I, H and τ5 phases are treated as stoichiometric compounds.

No thermodynamic properties for the ternary compounds can be found in the literature. To obtain initial estimates of the enthalpies and entropies of formation of the ternary compounds, three lines passing through the compound on the ternary Gibbs triangle were drawn parallel to the three edges of the triangle. The six intersection points of these lines with the edges defined six "binary compounds" whose enthalpies and entropies were then averaged to give the initial estimates. Thereafter, these values were adjusted to best reproduce the available data.

All model parameters optimized in the present work are listed in Table 3. All other model parameters (apart from the MQM parameters for liquid Mg-Zn given in section Eqs (9, 10)) have been given previously [7, 9, 11, 13]. Very few model parameters are required. The enthalpies of formation of all compounds have reasonable values. The entropies of formation are all small and negative as expected.

As mentioned in Section 2, neither phase diagram data nor thermodynamic data are available for the Tb-Mg-Zn, Ho-Mg-Zn, Er-Mg-Zn, Tm-Mg-Zn and Lu-Mg-Zn systems. Thermodynamic parameters for the ternary phases in these systems are estimated in the present project. The interaction parameters of the solution phases are set to be the same as those of the corresponding phases in other RE-Mg-Zn systems. The enthalpies of formation of the ternary compounds and end-members are estimated based on the trends established in our previous reports on the binary RE-Zn systems [12, 13]. The trends in the ternary RE-Mg-Zn systems as well as the Y-Mg-Zn system are shown in Fig. 18. As expected, these trends resemble those established earlier in the binary systems [12, 13]. The entropies of formation of similar phases are set to the same value.

Table 9.3 Thermodynamic model parameters optimized or estimated in the present work for the Y-Mg-Zn, Gd-Mg-Zn, Tb-Mg-Zn, Dy-Mg-Zn, Ho-Mg-Zn, Er-Mg-Zn, Tm-Mg-Zn and Lu-Mg-Zn systems

Phase name	Model	Parameters(J/mol-atom)
RE(Mg,Zn)	RE(Mg,Zn)	Ideal mixing
YMg_3	$Y(Mg,Zn)_3$	$G^{0,YMg_3}_{Y:Zn} = -34518 + 7.17$
		$L^{0,YMg_3}_{Y:Mg,Zn} = -4184$
		$L^{1,YMg_3}_{Y:Mg,Zn} = -2092$
$GdMg_3$	$Gd(Mg,Zn)_3$	$G^{0,GdMg_3}_{Gd:Zn} = -31380 + 6.26T$
		$L^{0,GdMg_3}_{Gd:Mg,Zn} = -4184$
		$L^{1,GdMg_3}_{Gd:Mg,Zn} = -2092$
$TbMg_3$	$Tb(Mg,Zn)_3$	$G^{0,TbMg_3}_{Tb:Zn} = -30857 + 5.8T$
		$L^{0,TbMg_3}_{Tb:Mg,Zn} = -4184$
		$L^{1,TbMg_3}_{Tb:Mg,Zn} = -2092$
$DyMg_3$	$Dy(Mg,Zn)_3$	$G^{0,DyMg_3}_{Dy:Zn} = -30334 + 5.75T$
		$L^{0,DyMg_3}_{Dy:Mg,Zn} = -4184$
		$L^{1,DyMg_3}_{Dy:Mg,Zn} = -2092$
$HoMg_3$	$Ho(Mg,Zn)_3$	$G^{0,HoMg_3}_{Ho:Zn} = -29811 + 5.55T$
		$L^{0,HoMg_3}_{Ho:Mg,Zn} = -4184$
		$L^{1,HoMg_3}_{Ho:Mg,Zn} = -2092$
$ErMg_3$	$Er(Mg,Zn)_3$	$G^{0,ErMg_3}_{Er:Zn} = -29288 + 5.77T$
		$L^{0,ErMg_3}_{Er:Mg,Zn} = -4184$
		$L^{1,ErMg_3}_{Er:Mg,Zn} = -2092$
$TmMg_3$	$Tm(Mg,Zn)_3$	$G^{0,TmMg_3}_{Tm:Zn} = -28765 + 5.48T$
		$L^{0,TmMg_3}_{Tm:Mg,Zn} = -4184$
		$L^{1,TmMg_3}_{Tm:Mg,Zn} = -2092$
$LuMg_3$	$Lu(Mg,Zn)_3$	$G^{0,LuMg_3}_{Lu:Zn} = -28242 + 5.46T$
		$L^{0,LuMg_3}_{Lu:Mg,Zn} = -4184$
		$L^{1,LuMg_3}_{Lu:Mg,Zn} = -2092$
α-Y_2Zn_{17}	$Y_2(Mg,Zn)_{17}$	$G^{0,\alpha-Y_2Zn_{17}}_{Y:Mg} = -4624 + 2.64T$ [11]
		Ideal mixing
$\tau3$	$Y(Mg,Zn)_2Mg$	$G^{0,\tau3}_{Y:Mg:Mg} = -8577 + 6.63T$
		$G^{0,\tau3}_{Y:Zn:Mg} = -28400 + 6.28T$
		$L^{0,\tau3}_{Y:Mg,Zn:Mg} = 1046$
		$L^{1,\tau3}_{Y:Mg,Zn:Mg} = 4184$
	$Gd(Mg,Zn)_2Mg$	$G^{0,\tau3}_{Gd:Mg:Mg} = -13785 + 3.67T$

		$G^{0,\tau3}_{Gd:Zn:Mg} = -32112 + 6.28T$
		$L^{0,\tau3}_{Gd:Mg,Zn:Mg} = 1046$
		$L^{1,\tau3}_{Gd:Mg,Zn:Mg} = 4184$
	$Tb(Mg,Zn)_2Mg$	$G^{0,\tau3}_{Tb:Mg:Mg} = -12448 + 4.82T$
		$G^{0,\tau3}_{Tb:Zn:Mg} = -31903 + 5.23T$
		$L^{0,\tau3}_{Tb:Mg,Zn:Mg} = 1046$
		$L^{1,\tau3}_{Tb:Mg,Zn:Mg} = 4184$
	$Dy(Mg,Zn)_2Mg$	$G^{0,\tau3}_{DY:Mg:Mg} = -10983 + 3.11T$
		$G^{0,\tau3}_{Dy:Zn:Mg} = -31380 + 6.28T$
		$L^{0,\tau3}_{Dy:Mg,Zn:Mg} = 1046$
		$L^{1,\tau3}_{Dy:Mg,Zn:Mg} = 4184$
	$Ho(Mg,Zn)_2Mg$	$G^{0,\tau3}_{Ho:Mg:Mg} = -8920 + 3.11T$
		$G^{0,\tau3}_{Ho:Zn:Mg} = -31066 + 6.28T$
		$L^{0,\tau3}_{Ho:Mg,Zn:Mg} = 1046$
		$L^{1,\tau3}_{Ho:Mg,Zn:Mg} = 4184$
	$Er(Mg,Zn)_2Mg$	$G^{0,\tau3}_{Er:Mg:Mg} = -7392 + 3.11T$
		$G^{0,\tau3}_{Er:Zn:Mg} = -30753 + 6.28T$
		$L^{0,\tau3}_{Er:Mg,Zn:Mg} = 1046$
		$L^{1,\tau3}_{Er:Mg,Zn:Mg} = 4184$
	$Tm(Mg,Zn)_2Mg$	$G^{0,\tau3}_{Tm:Mg:Mg} = -6346 + 3.11T$
		$G^{0,\tau3}_{Tm:Zn:Mg} = -30334 + 6.28T$
		$L^{0,\tau3}_{Tm:Mg,Zn:Mg} = 1046$
		$L^{1,\tau3}_{Tm:Mg,Zn:Mg} = 4184$
	$Lu(Mg,Zn)_2Mg$	$G^{0,\tau3}_{Lu:Mg:Mg} = -5300 + 3.11T$
		$G^{0,\tau3}_{Lu:Zn:Mg} = -29707 + 6.28T$
		$L^{0,\tau3}_{Lu:Mg,Zn:Mg} = 1046$
		$L^{1,\tau3}_{Lu:Mg,Zn:Mg} = 4184$
H	$Y_{15}Mg_{15}Zn_{70}$	$G^{0,H}_{Y:Mg:Zn} = -27800 + 6.02T$
I	YMg_3Zn_6	$G^{0,I}_{Y:Mg:Zn} = -22395 + 4.67T$
	$GdMg_3Zn_6$	$G^{0,I}_{Gd:Mg:Zn} = -23315 + 4.67T$
	$TbMg_3Zn_6$	$G^{0,I}_{Tb:Mg:Zn} = -23022 + 4.67T$
	$DyMg_3Zn_6$	$G^{0,I}_{Dy:Mg:Zn} = -22729 + 4.67T$
	$HoMg_3Zn_6$	$G^{0,I}_{Ho:Mg:Zn} = -22562 + 4.67T$
	$ErMg_3Zn_6$	$G^{0,I}_{Er:Mg:Zn} = -22395 + 4.67T$
	$TmMg_3Zn_6$	$G^{0,I}_{Tm:Mg:Zn} = -22227 + 4.67T$

	$LuMg_3Zn_6$	$G^{0,X}_{Lu:Mg:Zn} = -21976 + 4.67T$
X	$YMg_{12}Zn$	$G^{0,X}_{Y:Mg:Zn} = -6905 + 1.39T$
	$GdMg_{12}Zn$	$G^{0,X}_{Gd:Mg:Zn} = -7532 + 1.39T$
	$TbMg_{12}Zn$	$G^{0,X}_{Tb:Mg:Zn} = -7377 + 1.39T$
	$DyMg_{12}Zn$	$G^{0,X}_{Dy:Mg:Zn} = -7018 + 1.39T$
	$HoMg_{12}Zn$	$G^{0,X}_{Ho:Mg:Zn} = -6779 + 1.39T$
	$ErMg_{12}Zn$	$G^{0,X}_{Er:Mg:Zn} = -6540 + 1.39T$
	$TmMg_{12}Zn$	$G^{0,X}_{Tm:Mg:Zn} = -6301 + 1.39T$
	$LuMg_{12}Zn$	$G^{0,X}_{Lu:Mg:Zn} = -6062 + 1.39T$

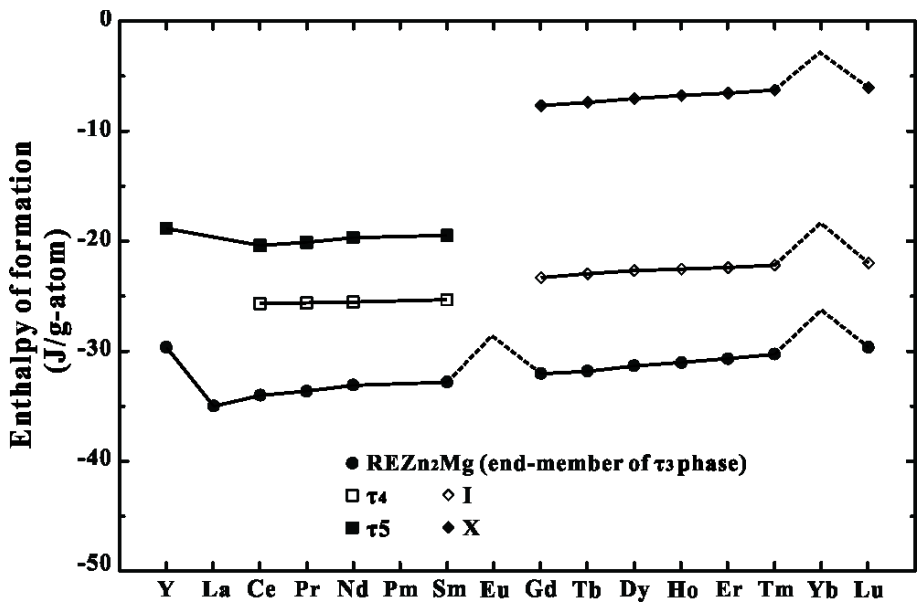

Figure 9.18. Calculated enthalpies of formation for compounds in the Y-Mg-Zn and RE-Mg-Zn systems. Trends are very similar to those established in our previous work on the binary systems [12, 13] (The Eu-Mg-Zn and Yb-Mg-Zn systems are not considered in the present work thus the anomalies cannot be seen from the figure).

9.4 Comparison of calculations with experimental data

9.4.1 Y-Mg-Zn

Calculated isothermal sections of the Y-Mg-Zn system at 600°C, 500°C and 400°C are shown in Figs. 19-21. The phase relationship are in good agreement with those reported by Tsai *et al* [21]. The calculated isothermal section at 300 °C is shown in Fig. 22.

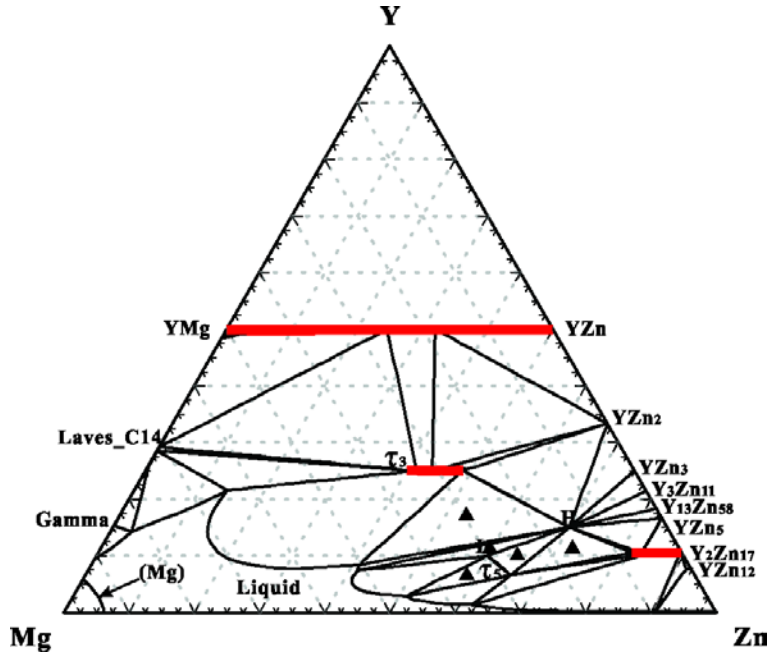

Figure 9.19 Calculated optimized isothermal section of the Y-Mg-Zn system at 600°C. ▲three-phase equilibria confirmed by Tsai *et al* [21] (mole fraction).

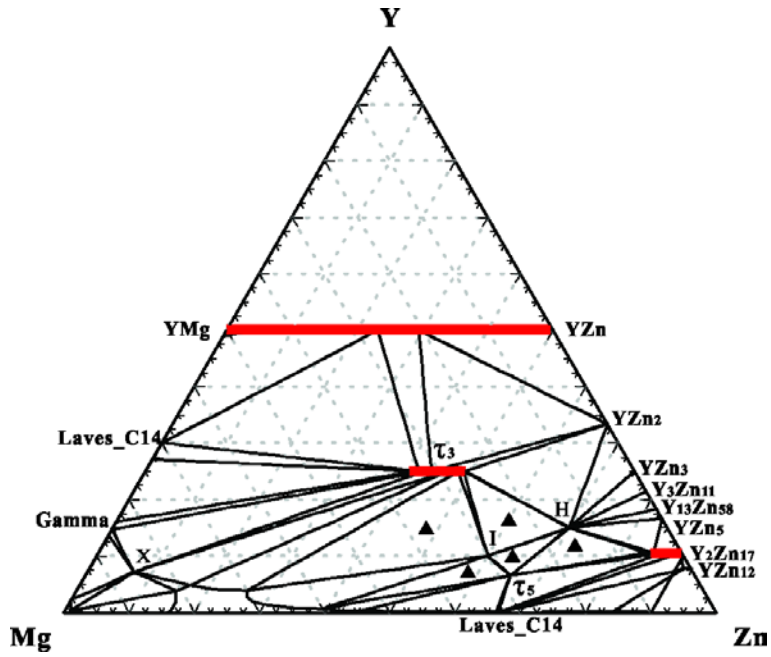

Figure 9.20 Calculated optimized isothermal section of the Y-Mg-Zn system at 500°C. ▲three-phase equilibria confirmed by Tsai *et al* [21] (mole fraction).

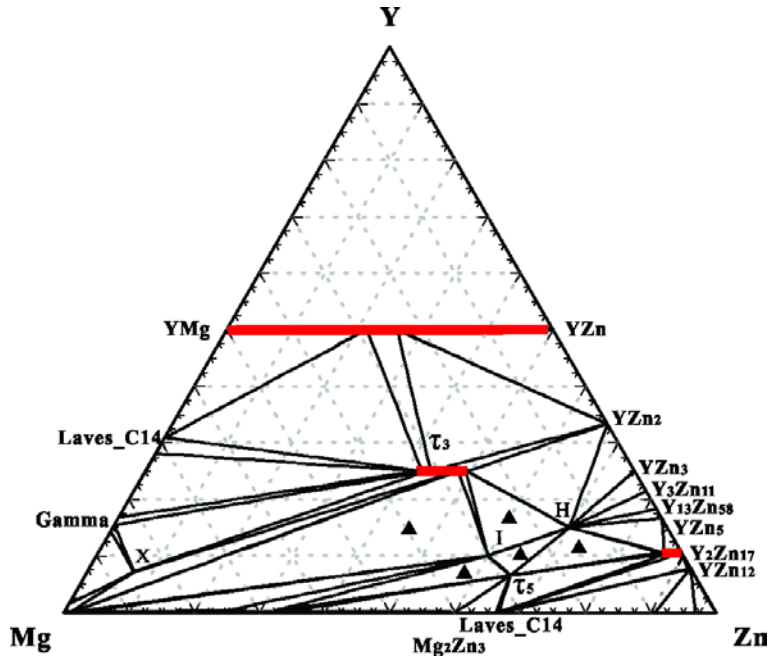

Figure 9.21 Calculated optimized isothermal section of the Y-Mg-Zn system at 400°C. ▲three-phase equilibria confirmed by Tsai *et al* [21] at 427°C (mole fraction).

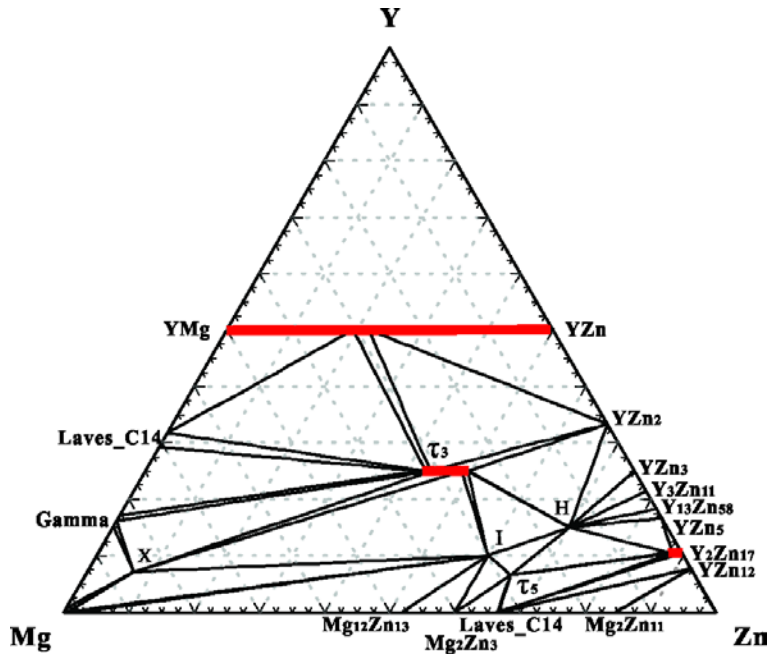

Figure 9.22 Calculated optimized isothermal section of the Y-Mg-Zn system at 300°C (mole fraction).

Figure 23 shows the calculated Mg-X section along with experimental data from Padezhnova *et al* [22]. The Liquid+(Mg)+X region was not shown in ref [22].

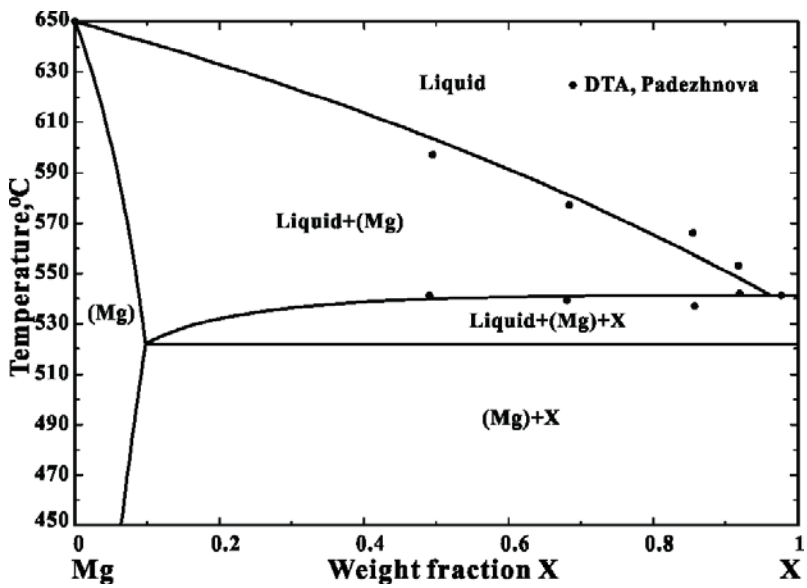

Figure 9.23 Calculated optimized isopleth between Mg and the X phase showing points from Padezhnova *et al* [22].

Two calculated isopleths in the Mg-rich region (18 wt.% Y and 29 wt.% Zn) are shown in Figs. 24 and 25.

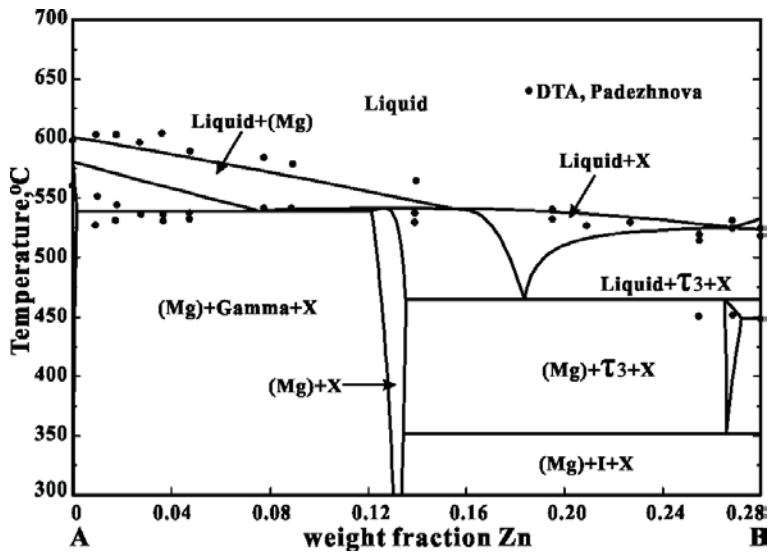

Figure 9.24 Calculated optimized isopleth from Mg-18wt.%Y (A) to Mg-18 wt.%Y-28wt.%Zn (B) in the Y-Mg-Zn system showing points from Padezhnova *et al* [23]

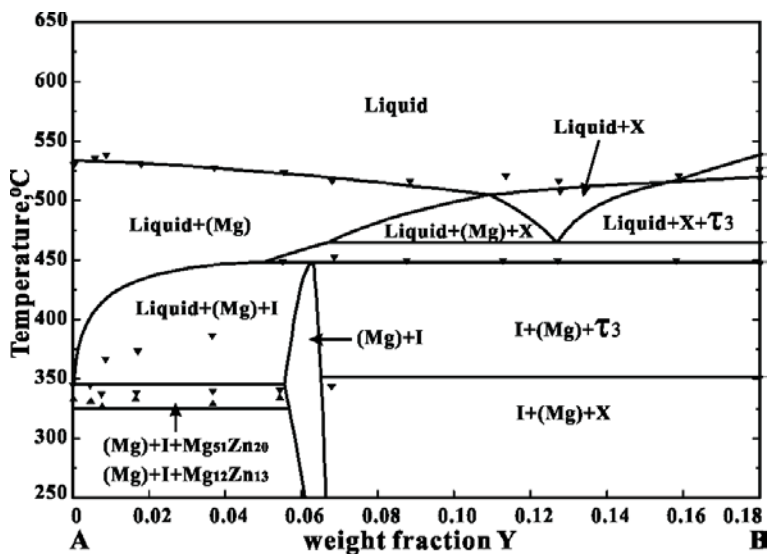

Figure 9.25 Calculated optimized isopleth from Mg-29wt.%Zn (A) to Mg-18 wt.%Y-29wt.%Zn (B) in the Y-Mg-Zn system showing points from Padezhnova *et al* [23]

The two isopleths reported by Langsdorf *et al* [33] were also calculated and are compared with the measurements in Figs 26 and 27.

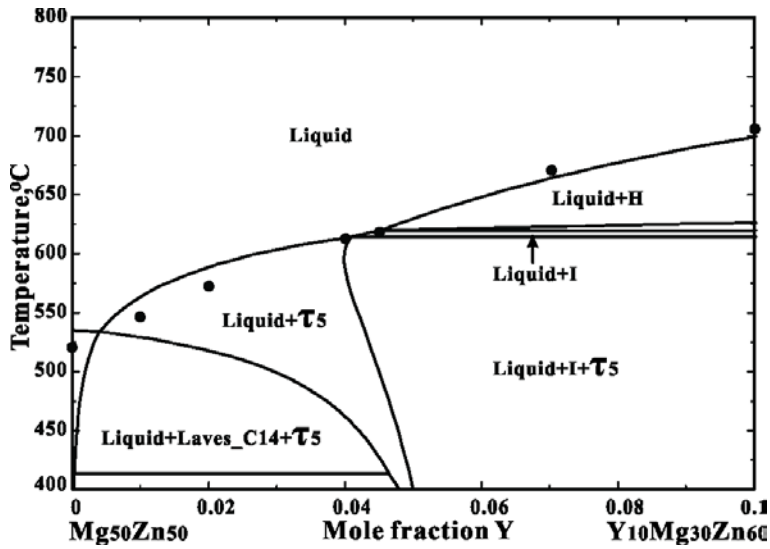

Figure 9.26 Calculated optimized $Mg_{50}Zn_{50}$-$Y_{10}Mg_{30}Zn_{60}$ isopleth showing points from Langsdorf *et al* [33].

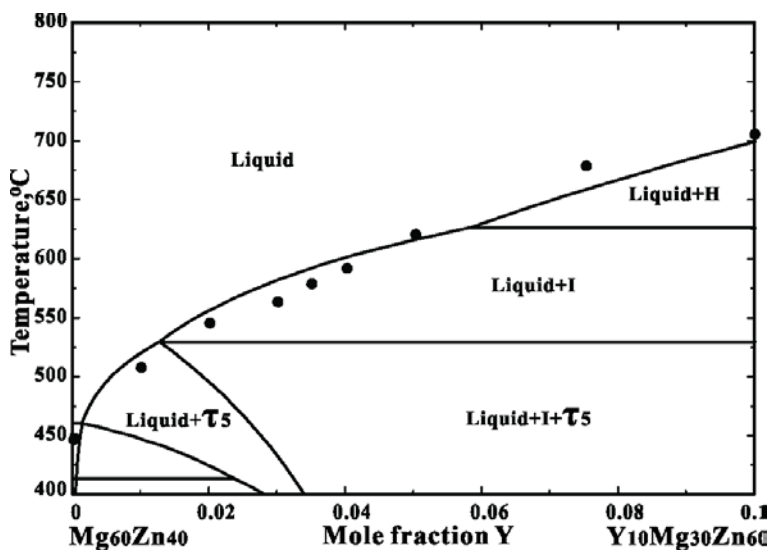

Figure 9.27 Calculated optimized $Mg_{60}Zn_{40}$-$Y_{10}Mg_{30}Zn_{60}$ isopleth showing points from Langsdorf *et al* [33].

The liquidus temperature at $Y_{10}Mg_{30}Zn_{60}$ is calculated as 698.8°C, in satisfactory agreement with the reported value of 687°C [32].

The DTA measurements on a sample with composition $Y_{11.9}Mg_{50.7}Zn_{37.4}$ reported by Horiuchi *et al* [24] are also reproduced. According to our calculations, the liquidus temperature is 661°C, which is close to the reported value of 656°C. Our calculations give another three

transition temperatures: 547°C, 448°C and 352°C, while Horiuchi *et al* [24] reported one additional peak at 450°C.

Two additional calculated isopleths are shown and compared to the DSC data from Gröbner *et al* [52] in Figs.28 and 29.

The Y-Mg-Zn system was also optimized by Gröbner *et al* [52]. Their calculated isopleths are also shown in Figs. 28 and 29. As can be seen, their interpretation of the data is much different than ours.

In the optimization by Shao *et al* [59], the data points from Padezhnova et al [22] (see Fig. 23) were interpreted differently. The Figs. 28 and 29 can not be reproduced with the thermodynamic parameters from Shao *et al* [59].

Figs. 24-27 were also not be reproduced by early optimizations [52, 59].

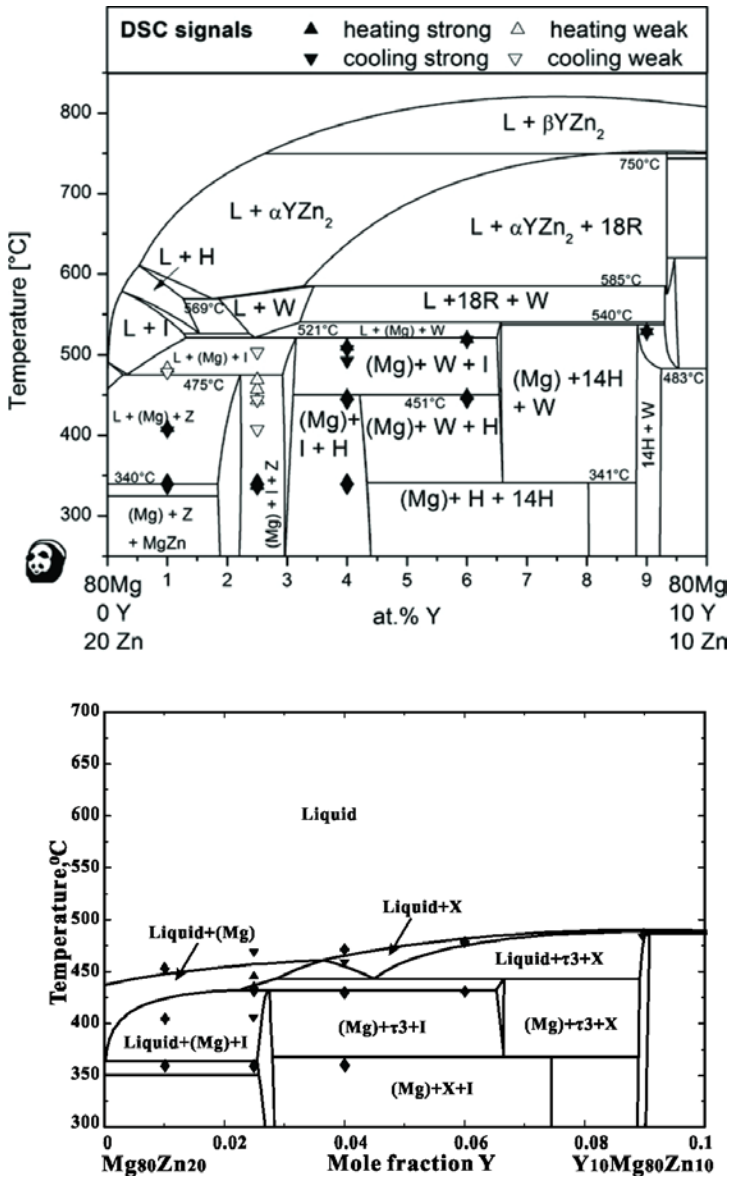

Figure 9.28 Calculated optimized $Mg_{80}Zn_{20}$-$Y_{10}Mg_{80}Zn_{10}$ isopleth from the present work compared to that of Gröbner *et al* [53]. Data points are also from ref [52]. (Note that in ref [52] the 18R and 14H phases correspond to the X phase in the present study; the W, H and Z phases correspond to the τ3, YZn_5 and τ5 phases, respectively)

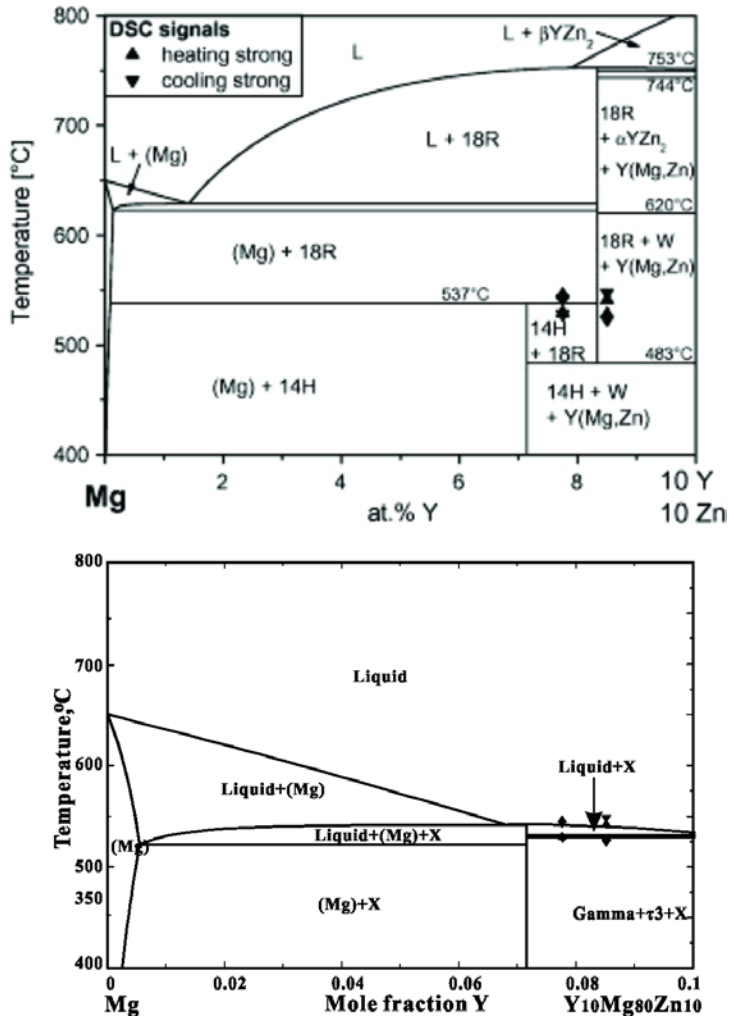

Figure 9.29 Calculated optimized Mg-$Y_{10}Mg_{80}Zn_{10}$ isopleth from the present work compared to that reported by Gröbner *et al* [53]. Data points are also from ref [52]. (Note that in ref [52] the 18R and 14H phases correspond to the X phase in the present study and the W phase corresponds to τ3)

A tentative calculated liquidus projection for the Y-Mg-Zn system is shown in Figs. 30-31 and a tentative list of the calculated temperatures of invariant reactions, maxima and minima is given in Table 4.

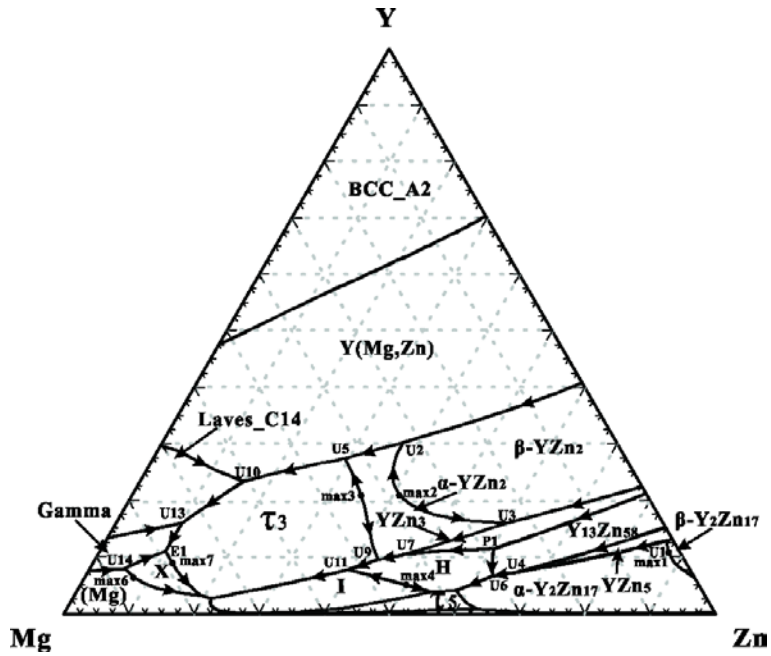

Figure 9.30 Tentative calculated liquidus projection of the Y-Mg-Zn system (mole fraction)

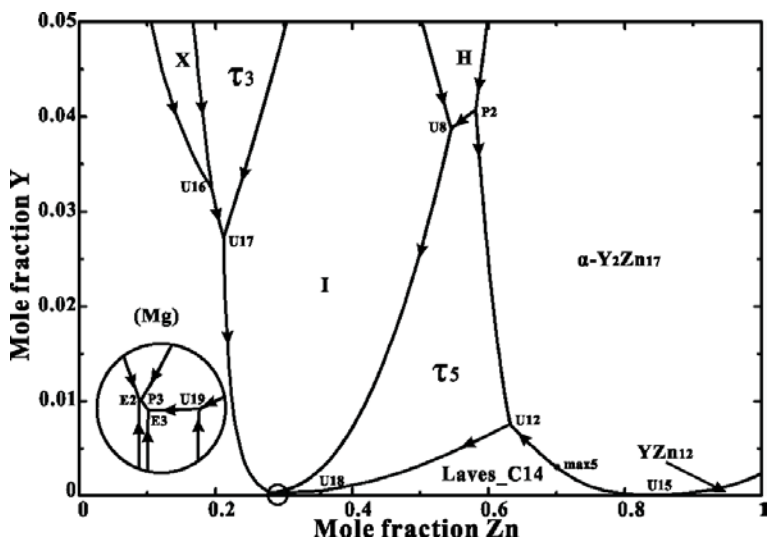

Figure 9.31 Enlargement of part of Fig. 9.30

Table 9.4. Tentative calculated invariant reactions, maxima and minima and their temperatures (^{o}C) in the Y-Mg-Zn system

U1	877	U2	752	U3	752	P1	704	U4	703	U5	683	U6	677
U7	636	P2	629	U8	618	U9	615	U10	608	U11	590	U12	581
U13	555	U14	539	E1	529	U15	505	U16	464	U17	448	U18	413
U19	351	P3	346	E2	346	E3	346	max1	~880	max2	~752	max3	~716
max4	~628	max5	~585	max6	~585	max7	~534						

Four invariant reactions were reported by Padezhnova *et al* [23] (Eqs 1-4). These most likely correspond to the following invariant reactions from the present calculations:

$$\text{U14:}\quad liquid + (Mg) \leftrightarrow Gamma + X \quad (539^{o}\text{C}) \qquad 9.12$$

$$\text{E1:}\ liquid \leftrightarrow X + Gamma + \tau 3 \quad (529^{o}\text{C}) \qquad 9.13$$

$$\text{E2:}\ liquid \leftrightarrow (Mg) + Mg_{51}Zn_{20} + I \quad (346^{o}\text{C}) \qquad 9.14$$

$$\text{U17:}\quad liquid + \tau 3 \leftrightarrow (Mg) + I \quad (448^{o}\text{C}) \qquad 9.15$$

9.4.2 Gd-Mg-Zn

Figure 32 and 33 show the calculated isothermal sections of the Gd-Mg-Zn system at 400°C and 300°C. The phase relationships at 400°C are in good agreement with those proposed by Qi *et al* [34] in their optimization. However, the experimental data [34] cannot be well accounted for, neither in the optimization of Qi *et al* [34] nor in the present optimization. Since all the experimental data are from compositions in the Mg-rich region, an uncertainty of a few atomic percent of Gd or Zn (which is normal in EPMA) can shift the sample to a different phase region.

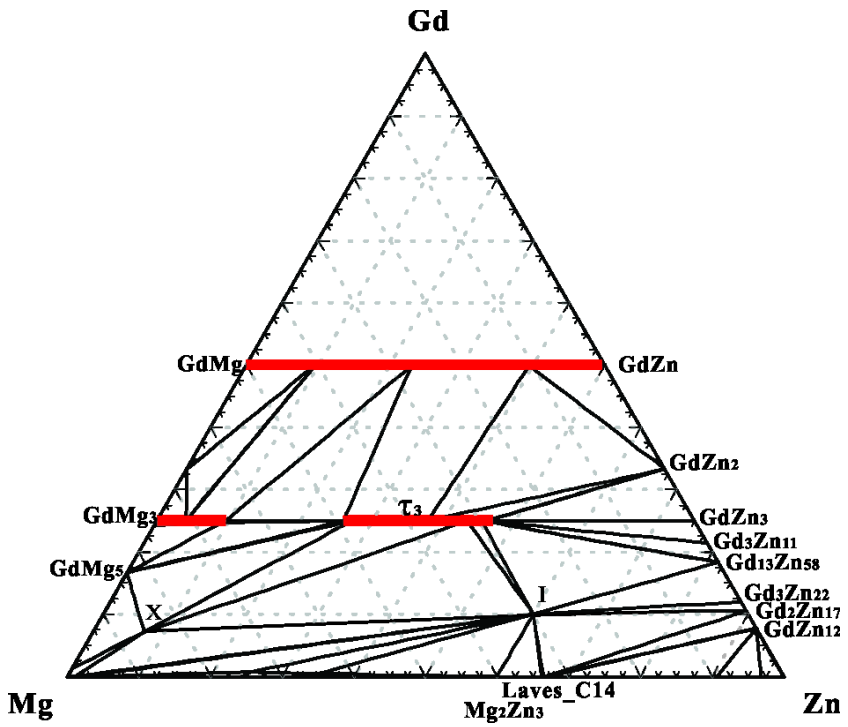

Figure 9.32 Calculated isothermal section of the Gd-Mg-Zn system at 400°C (mole fraction)

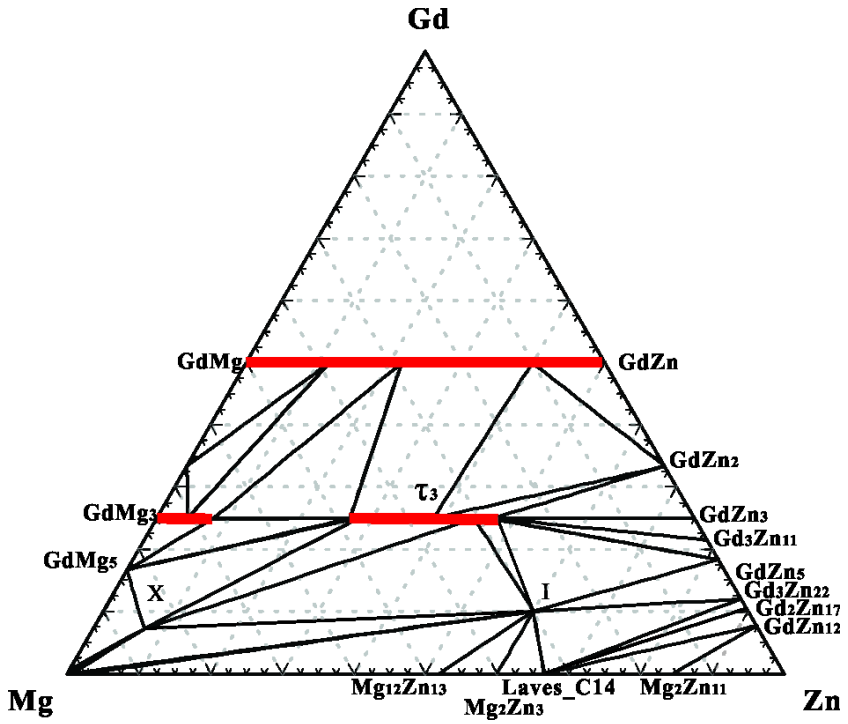

Figure 9.33 Calculated isothermal section of the Gd-Mg-Zn system at 300°C (mole fraction)

9.4.3 Tb-Mg-Zn

No phase diagram data are available in the literature for the Tb-Mg-Zn system. The I phase and X phase have been observed. The τ3 phase is assumed based on the similarity among all RE-Mg-Zn systems. All thermodynamic parameters are estimated, as mentioned in Section 3.

The calculated isothermal section of the Tb-Mg-Zn system at 300°C shown in Fig. 34 is very similar to those of other RE-Mg-Zn systems.

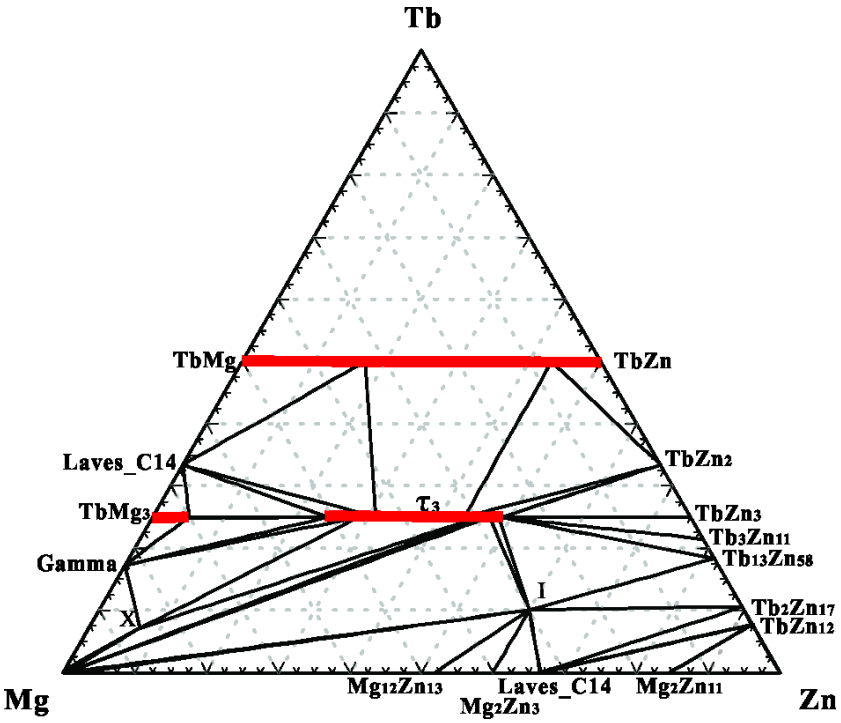

Figure 9.34 The calculated isothermal section of Tb-Mg-Zn system at 300°C (mole fraction)

9.4.4 Dy-Mg-Zn

The calculated isothermal section of the Dy-Mg-Zn system at 300°C is shown in Fig. 35. Figure 36 presents the isothermal section in the Mg-rich region together with experimental data from Rokhlin *et al* [40]. The calculated isopleth from Mg-39 wt.%Dy to Mg-39.wt% Zn is shown in Fig. 37 along with the points of Rokhlin *et al* [40].

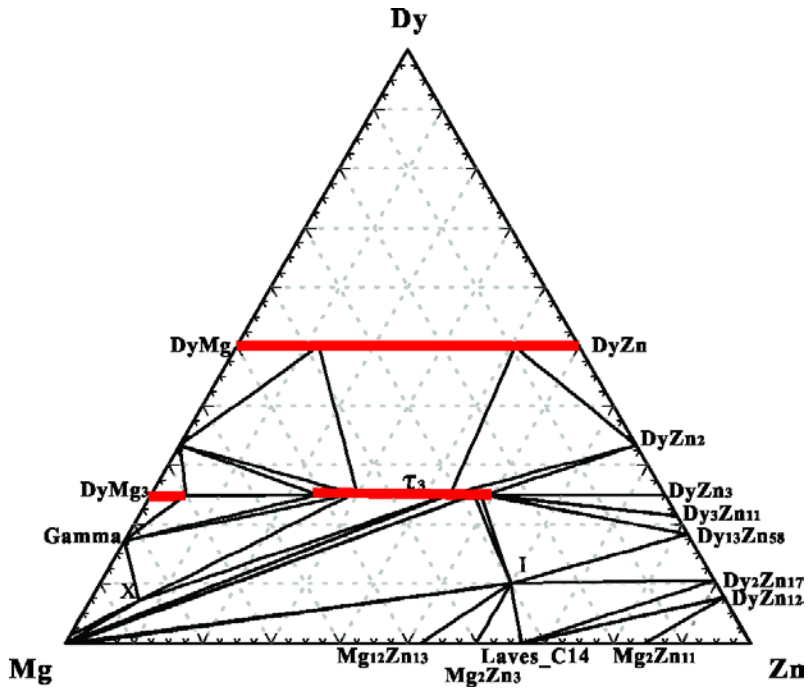

Figure 9.35 The calculated isothermal section of Dy-Mg-Zn system at 300°C (mole fraction)

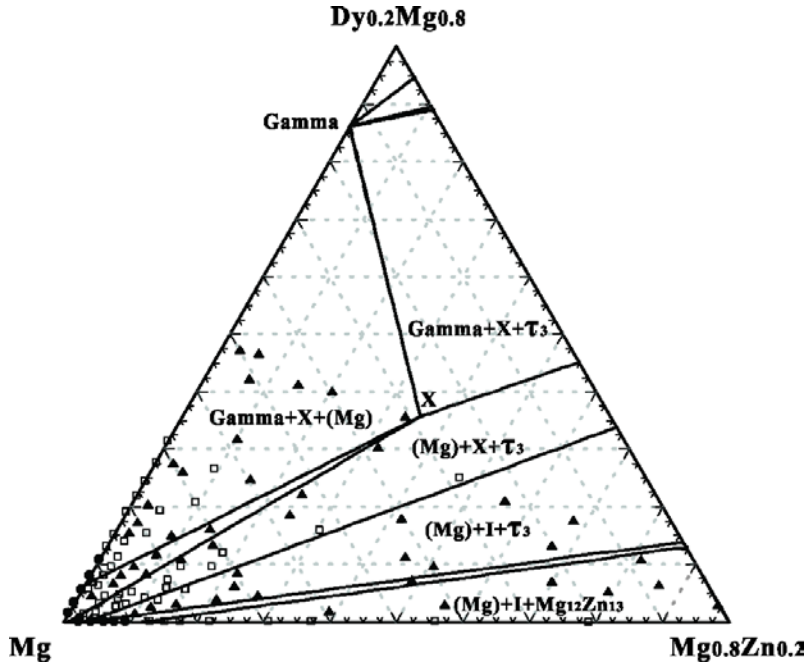

Figure 9.36 The calculated isothermal section of Dy-Mg-Zn system at 300°C in the Mg-rich region along with experimental data from Rokhlin *et al* [40] (mole fraction). ▲ Data points in a three-phase region; □ Data points in a two-phase region

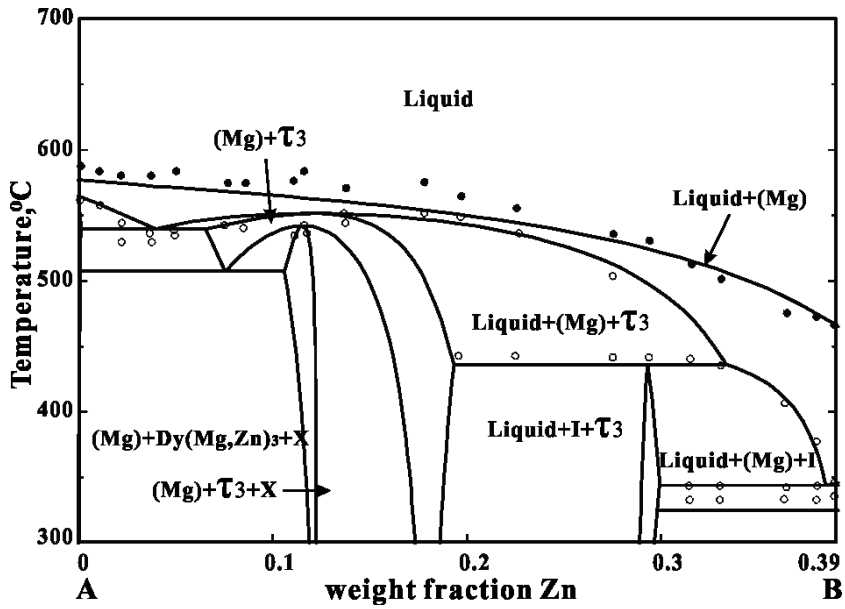

Figure 9.37 Calculated optimized isopleths from Mg-39wt.% Dy (A) to Mg-39wt.% Zn (B) in the Dy-Mg-Zn system showing points from Rokhlin *et al* [40].

Four invariant reactions were reported by Rokhlin *et al* [40] (Eqs 5-8). These most likely correspond to the following invariant reactions from the present calculations:

$$liquid + DyMg_3 \leftrightarrow Gamma + \tau 3 \quad (577^{o}\text{C}) \qquad 9.16$$

$$liquid \leftrightarrow (Mg) + Gamma + \tau 3 \quad (539^{o}\text{C}) \qquad 9.17$$

$$liquid + \tau 3 \leftrightarrow (Mg) + I \quad (436^{o}\text{C}) \qquad 9.18$$

$$liquid \leftrightarrow Mg_{51}Zn_{20} + Mg_{12}Zn_{13} + I \quad (344^{o}\text{C}) \qquad 9.19$$

9.4.5 Ho-Mg-Zn, Er-Mg-Zn, Tm-Mg-Zn and Lu-Mg-Zn

Since no phase diagram data are available for these four systems, all thermodynamic parameters are estimated, as mentioned in Section 3. Figs. 38-41 show the calculated isothermal sections at 300°C for the Ho-Mg-Zn, Er-Mg-Zn, Tm-Mg-Zn and Lu-Mg-Zn systems.

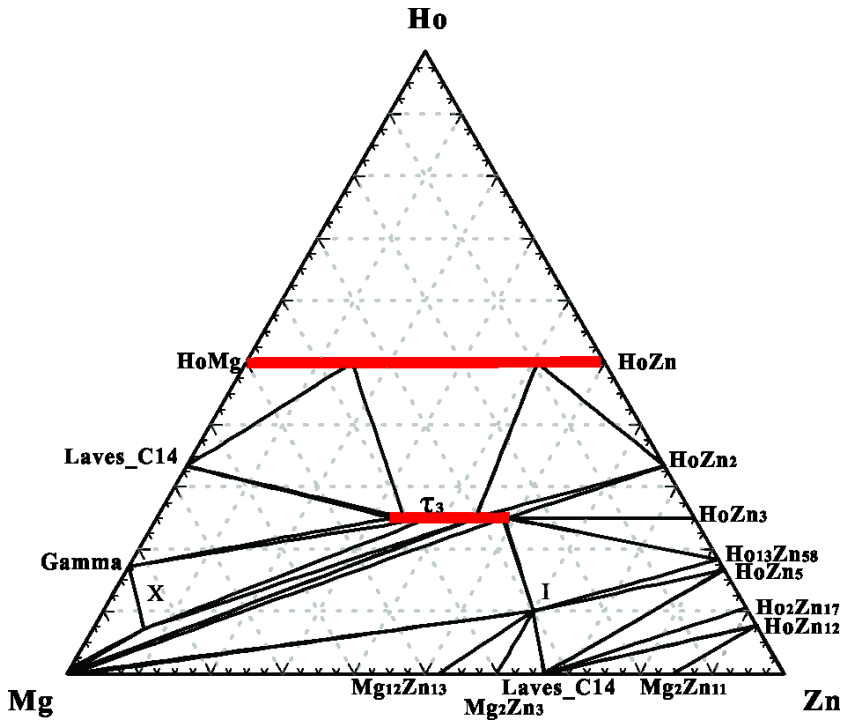

Figure 9.38 Calculated isothermal section of the Ho-Mg-Zn system at 300°C (mole fraction)

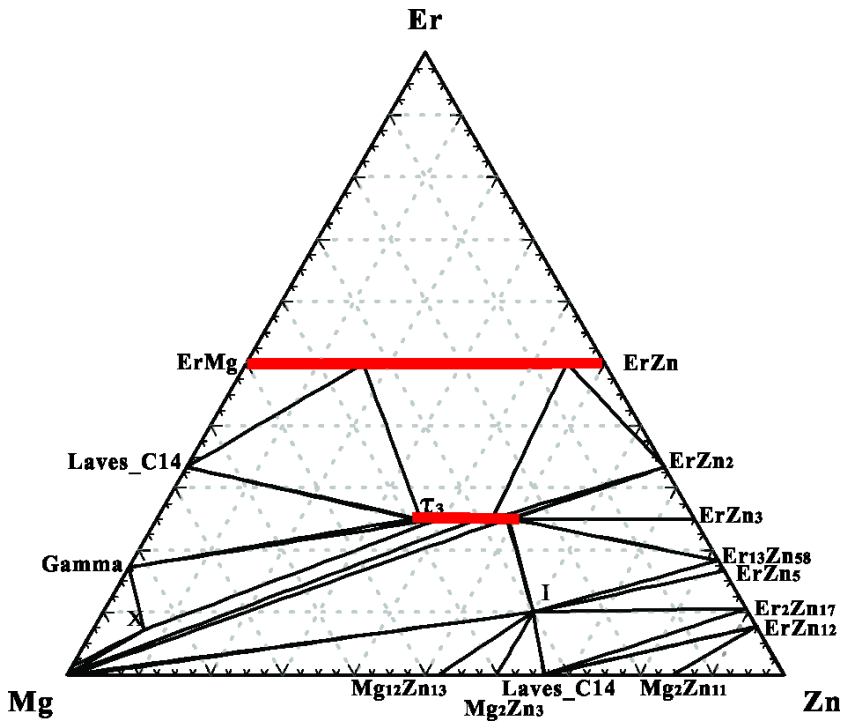

Figure 9.39 Calculated isothermal section of the Er-Mg-Zn system at 300°C (mole fraction)

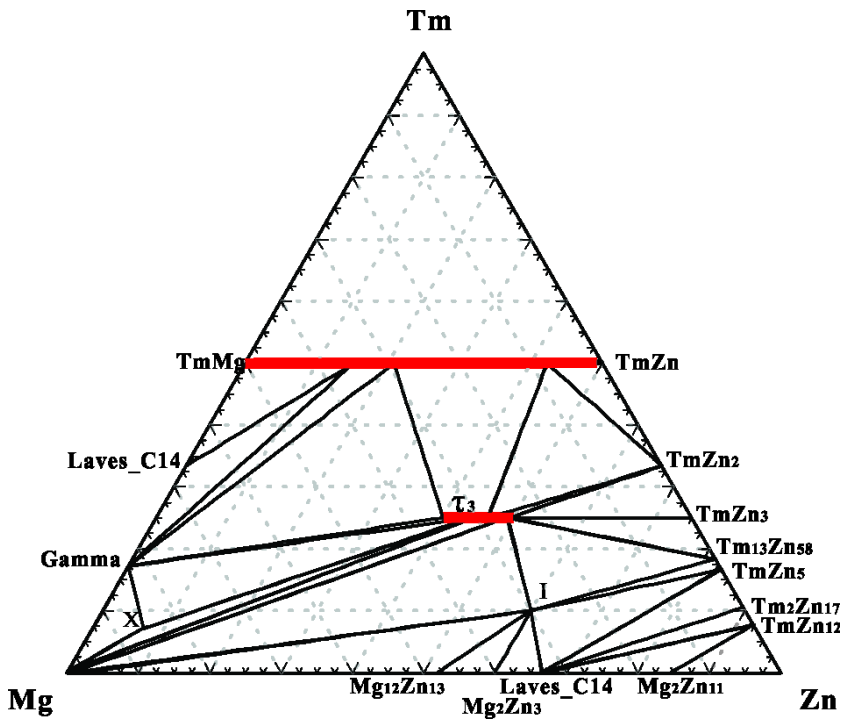

Figure 9.40 Calculated isothermal section of the Tm-Mg-Zn system at 300°C (mole fraction)

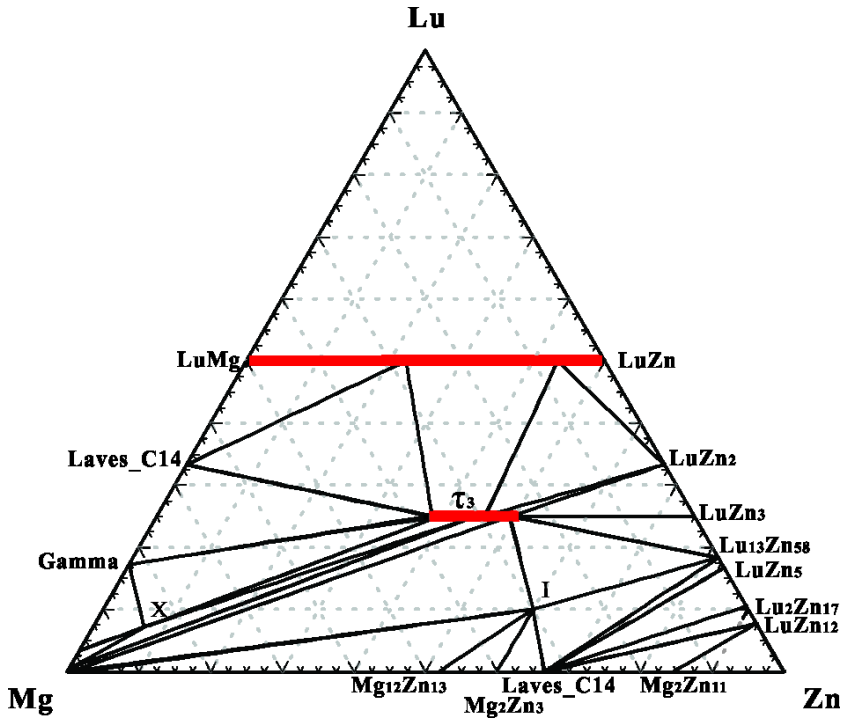

Figure 9.41 Calculated isothermal section of the Lu-Mg-Zn system at 300°C (mole fraction)

9.5 Discussion

As mentioned in our previous papers on the binary RE-Zn systems [12, 13], the phase diagrams of all RE-Zn systems are very similar. This is also the case for all the RE-Mg-Zn ternary systems. The calculated isothermal sections at 300°C are very similar. These isothermal sections are also very similar to those published earlier for the lighter-RE-Mg-Zn systems [14-16]

In our previous articles on the binary RE-Zn systems [12, 13], trends among all RE-Zn systems were established and utilized during the optimization. The trends are introduced in the optimization of all RE-Mg-Zn systems (See Fig. 18).

Entropies of formation of all compounds with the same stoichiometry are negative and very similar. The same interaction parameters are used for corresponding solution phases in different ternary systems.

9.6 Conclusions

All optimized thermodynamic parameters for the Y-Mg-Zn, Gd-Mg-Zn, Tb-Mg-Zn, Dy-Mg-Zn, Ho-Mg-Zn, Er-Mg-Zn, Tm-Mg-Zn and Lu-Mg-Zn systems in the present work are summarized in Table 3. Binary parameters were reported in previous articles [7, 9, 11, 13]. Very few model parameters are required, and all parameters have thermodynamically reasonable values. In particular, no additional ternary parameters were required in the MQM model for the liquid phase.

Assessed optimized model parameters for the Y-Mg-Zn, Gd-Mg-Zn, Tb-Mg-Zn, Dy-Mg-Zn, Ho-Mg-Zn, Er-Mg-Zn, Tm-Mg-Zn and Lu-Mg-Zn systems have been obtained by considering experimental data from the literature. Previous articles [8-13] reported on the optimizations of all RE-Zn and RE-Mg binary systems. Also reported in our previous articles [14-16] are the experimental investigation and thermodynamic optimization of the Ce-Mg-Zn and Nd-Mg-Zn systems as well as optimization of the La-Mg-Zn, Pr-Mg-Zn and Sm-Mg-Zn systems. The model parameters will be included in the FTlite light metals database of the FactSage database computing system [63] which already contains optimized model parameters for the solid and liquid phases of a large number of binary and ternary Mg- and Al-containing systems.

Through the models, the properties and phase equilibria of multicomponent systems can thus be estimated and calculated. All calculations in the present work are performed with the FactSage software [63].

Acknowledgements

This research was supported by funding from the Natural Sciences and Engineering Research Council of Canada (NSERC) Magnesium Strategic Research Network. More information on the Network can be found at www.MagNET.ubc.ca.

References

[1] B.L. Mordike, T. Ebert, Mat. Sci. Eng. A-Struct, 302 (2001) 37-45.

[2] I.P. Moreno, T.K. Nandy, J.W. Jones, J.E. Allison, T.M. Pollock, Scripta Mater., 48 (2003) 1029-1034.

[3] J. Bohlen, M.R. Nürnberg, J.W. Senn, D. Letzig, S.R. Agnew, Acta Mater., 55 (2007) 2101-2112.

[4] R.K. Mishra, A.K. Gupta, P.R. Rao, A.K. Sachdev, A.M. Kumar, A.A. Luo, Scripta Mater., 59 (2008) 562-565.

[5] N. Stanford, M.R. Barnett, Mat. Sci. Eng. A-Struct, 496 (2008) 399-408.

[6] K. Hantzsche, J. Bohlen, J. Wendt, K.U. Kainer, S.B. Yi, D. Letzig, Scripta Mater., 63 (2010) 725-730.

[7] I. Ansara, A. T. Dinsdale, M. H. Rand, COST 507: Definition of thermochemical and thermophysical properties to provide a database for the development of new light alloys, Thermochemical database for light metal alloys, Vol. 2, Office for Official Publications of the European Communities, Luxembourg,1998; P. Spencer, unpublished work

[8] Y.-B. Kang, L. Jin, P. Chartrand, A.E. Gheribi, K. Bai, P. Wu, CALPHAD, 38 (2012) 100-116.

[9] Y.-B. Kang, A. Pelton, P. Chartrand, P. Spencer, C. Fuerst, J. Phase Equilib. Diff., 28 (2007) 342-354.

[10] Y.-B. Kang, A.D. Pelton, P. Chartrand, C.D. Fuerst, CALPHAD, 32 (2008) 413-422.

[11] L. Jin, PhD Thesis, Ecole Polytechnique, Montreal (Canada), 2012, pp. 407

[12] Z. Zhu, A. Pelton, J. Alloys Compd. 641 (2015) 249-260

[13] Z. Zhu, A. Pelton, J. Alloys Compd, 641 (2015) 261-271

[14] Z. Zhu, M. Gharghouri, M. Medraj, D. Kevorkov, A. D. Pelton, submitted for publication.

[15] Z. Zhu, A. Pelton, submitted for publication.

[16] Z. Zhu, A. Pelton, submitted for publication.

[17] T.J. Sato, E. Abe, A.P. Tsai, Mat. Sci. Eng. A-struct, 304-306 (2001) 867-870.

[18] T.J. Sato, E. Abe, A.P. Tsai, Phil. Mag. Lett., 77 (1998) 213-219.

[19] E. Abe, A.P. Tsai, Acta Crystallogr. B, 56 (2000) 915-917.

[20] A.P. Tsai, A. Niikura, A. Inoue, T. Masumoto, J. Mater. Res., 12 (1997) 1468-1471.

[21] A.-P. Tsai, Y. Murakami, A. Niikura, Philos. Mag. A, 80 (2000) 1043-1054.

[22] E.M. Padezhnova, E.V. Mel'nik, R.A. Milievskii, T.V. Dobatkina, V.V. Kinzhibalo, Izv. Akad. Nauk SSSR, Met., (1982) 204-208.

[23] E.M. Padezhnova, E.V. Mel'nik, T.V. Dobatkina, Izv. Akad. Nauk SSSR, Met., (1979) 217-221.

[24] T. Horiuchi, H. Ikee, A. Hamaya, S. Minamoto, S. Nomoto, S. Miura, in: 7th International Conference on Processing and Manufacturing of Advanced Materials, THERMEC'2011, August 1, 2011 - August 5, 2011, Trans Tech Publications Ltd, Quebec City, QC, Canada, 2012, pp. 1170-1175.

[25] H. Takakura, A. Sato, A. Yamamoto, A.P. Tsai, Phil. Mag. Lett., 78 (1998) 263-270.

[26] M. Matsuda, S. Ii, Y. Kawamura, Y. Ikuhara, M. Nishida, Mat. Sci. Eng. A-struct, 393 (2005) 269-274.

[27] T. Itoi, T. Seimiya, Y. Kawamura, M. Hirohashi, Scripta Mater., 51 (2004) 107-111.

[28] Y. Kawamura, M. Yamasaki, Mater. Trans., 48 (2007) 2986-2992.

[29] Y. Kawamura, S. Yoshimoto, in: 2005 TMS Annual Meeting, February 13, 2005 - February 17, 2005, Minerals, Metals and Materials Society, San Francisco, CA, United states, 2005, pp. 499-502.

[30] E. Abe, A. Ono, T. Itoi, M. Yamasaki, Y. Kawamura, Phil. Mag. Lett., 91 (2011) 690-696.

[31] H. Okuda, T. Horiuchi, T. Tsukamoto, S. Ochiai, M. Yamasaki, Y. Kawamura, Scripta Mater., 68 (2013) 575-578.

[32] A. Langsdorf, W. Assmus, G.J. Babonas, A. Reza, Liet. Fiz. Z., 37 (1997) 40-45.

[33] A. Langsdorf, C. Seuring, F. Ritter, W. Assmus, Cryst. Res. Technol., 32 (1997) 1067-1072.

[34] H.Y. Qi, G.X. Huang, H. Bo, G.L. Xu, L.B. Liu, Z.P. Jin, J. Mater. Sci., 47 (2012) 1319-1330.

[35] M. Yamasaki, T. Anan, S. Yoshimoto, Y. Kawamura, Scripta Mater., 53 (2005) 799-803.

[36] Y. Hatton, A. Nikura, A.P. Tsai, A. Inoue, T. Masumoto, K. Fukamichi, H. Aruga-Katon, T. Goto, J. Phys-Condens Mat., 7 (1995) 2313-2313.

[37] A.P. Tsai, A. Niikura, A. Inoue, T. Masumoto, Y. Nishida, K. Tsuda, M. Tanaka, Phil. Mag. Lett., 70 (1994) 169-175.

[38] X. Wang, W. Du, Z. Wang, K. Liu, S. Li, J. Rare Earth., 30 (2012) 503-506.

[39] A. Niikura, A.-P. Tsai, A. Inoue, T. Masumoto, Jpn. J. Appl. Phys. 2, 33 (1994) L1538-L1541.

[40] L.L. Rokhlin, N.I. Nikitina, Izv. Akad. nauk SSSR, Met., (1992) 213-219.

[41] L. Zhiping, Z. Shaoqing, J. Mater. Sci. Lett., 12 (1993) 1490-1492.

[42] E. Uhrig, S. Bruhne, R. Sterzel, L. Schropfer, W. Assmus, Phil. Mag. Lett., 83 (2003) 265-272.

[43] T. Ishimasa, T. Shimizu, Jpn. J. Appl. Phys. 1, 39 (2000) 1235-1240.

[44] T.J. Sato, H. Takakura, A.P. Tsai, K. Shibata, K. Ohoyama, K.H. Andersen, J. Phys. Chem. Solids, 60 (1999) 1257-1259.

[45] T. Shimizu, T. Ishimasa, Jpn. J. Appl. Phys. 1, 37 (1998) 5691-5696.

[46] R. Sterzel, W. Assmus, A. Kounis, G. Miehe, H. Fuess, Phil. Mag. Lett., 80 (2000) 239-247.

[47] R. Sterzel, C. Gross, A. Kounis, G. Miehe, H. Fuess, S. Reutzel, D. Holland-Moritz, W. Assmus, Phil. Mag. Lett., 82 (2002) 443-450.

[48] A. Kounis, G. Miehe, H. Fuess, Mat. Sci. Eng. A-struct, 294-296 (2000) 323-326.

[49] M.E. Drits, E.M. Padezhnova, N.V. Miklina, Izv. Akad. Nauk SSSR, Met., (1974) 218-222.

[50] T.V. Dobatkina, Izv. Akad. Nauk SSSR, Met., (1979) 211-214.

[51] W. Gong, K. Aizawa, S. Harjo, J. Abe, T. Iwahashi, T. Kamiyama, in, Japan Institute of Metals (JIM), 1-14-32 Ichibancho, Aoba-ku, Sendai, 980-8544, Japan, 2013, pp. 974-976.

[52] J. Gröbner, A. Kozlov, X.Y. Fang, J. Geng, J.F. Nie, R. Schmid-Fetzer, Acta Mater., 60 (2012) 5948-5962.

[53] M.R. Li, K.H. Kuo, J. Alloys Compd., 432 (2007) 81-89.

[54] J. Yang, L. Wang, L. Wang, H. Zhang, J. Alloys Compd., 459 (2008) 274-280.

[55] V. Pavlyuk, P. Solokha, G. Dmytriv, B. Marciniak, V. Paul-Boncour, Acta Crystallogr. E, 63 (2007) i161-i161.

[56] V. Pavlyuk, B. Marciniak, E. Różycka-Sokołowska, Intermetallics, 20 (2012) 8-15.

[57] E.V. Melnik, V.V. Kinzhibalo, E.M. Padezhnova, T.V. Dobatkina, Tezizy Dokl. Vses. Konf. Kristallokhim. Intermet. Soeden., (1978) 73c.

[58] H. Xu, J. Fan, H.-L. Chen, R. Schmid-Fetzer, F. Zhang, Y. Wang, Q. Gao, T. Zhou, J. Alloys Compd., 603 (2014) 100-110.

[59] G. Shao, V. Varsani, Z. Fan, Calphad, 30 (2006) 286-295.

[60] A. Pelton, S. Degterov, G. Eriksson, C. Robelin, Y. Dessureault, Metall. Mater. Trans. B, 31 (2000) 651-659.

[61] A. Pelton, P. Chartrand, Metall. Mater. Trans. A, 32 (2001) 1355-1360.

[62] M. Hillert, J. Alloys Compd., 320 (2001) 161-176.

[63]] C.W. Bale, E. Bélisle, P. Chartrand, S.A. Decterov, G. Eriksson, K. Hack, I.H. Jung, Y.B. Kang, J. Melançon, A.D. Pelton, C. Robelin, S. Petersen, Calphad, 33 (2009) 295-311; www.factsage.com

Chapter 10 **GENERAL DISCUSSION**

In this thesis the thermodynamic descriptions for all RE-Zn systems (RE=Sc, Y, La, Ce, Pr, Nd, Pm, Sm, Eu, Gd, Tb, Dy, Ho, Er, Tm, Yb and Lu) as well as RE-Mg-Zn systems (excluding Sc, Pm, Eu and Yb) are obtained.

Significant improvements are achieved on the thermodynamic descriptions of all binary systems that have been optimized previously (Y-Zn, La-Zn, Ce-Zn, Pr-Zn, Nd-Zn, Sm-Zn and Gd-Zn system). As pointed out in the Introduction of this thesis, the calculated entropies of mixing for the optimized binary systems from the literature are generally not reasonable because the calculated entropies of mixing for the liquid phases possess negative values in some of the composition range in almost all the optimized binary systems. We also mentioned that the temperature dependent parameters for the liquid phase for some optimized systems are relatively large. It should also be noted that there exist many binary compounds in each individual binary RE-Zn system (at least five, e.g. the Sc-Zn system), and the minima of enthalpies of liquid mixing are less than -36 kJ/mol according to predictions from the Miedema Model. According to our experience, there should be a significant degree of short-range ordering (SRO) in the liquid phase. However, the short-range ordering was not considered in most of the previous optimizations.

Due to the limited experimental data on the RE-Zn systems, the following assumptions are proposed and utilized in the optimization of all binary RE-Zn and ternary RE-Mg-Zn systems:

1) Similarity: all RE elements are presumed to have similar alloying behavior. Based on this assumption, the maximum ordering for all RE-Zn liquid phases is set at the same Zn mole fraction, which is approximately 0.6. Upon examination of all available experimental RE-Zn phase diagrams, we found that the REZn and $REZn_2$ compounds are the most stable phases in all systems (These two phases, rather than RE_2Zn_{17}, are chosen as the most stable phases. This is because RE_2Zn_{17} is less stable in the heavier-RE-Zn systems and REZn and $REZn_2$ are relatively stable in all RE-Zn systems). As a result, it is natural to put the maximum ordering at a composition between these two phases. Calculation from the Miedema Model also suggests that the minimum occurs around a Zn mole fraction of ~0.55. Consequently, the coordination numbers are set as $Z^{Zn}_{Zn,\mathrm{R}E} = 4$ and $Z^{RE}_{Zn,\mathrm{R}E} = 6$.

Entropy is a measure of the degree of disorder. Due to behavioral similarities, when RE elements are alloyed with Zn, the change of entropies is assumed to be the same; the non-configurational entropy parameter was set exclusively at -5.8576 J/mol K in the expansion for Δg_{AB} in the MQM for the liquid phase in all systems. The entropy of formation for compounds with the same stoichiometry in all systems are set to the same values (slight adjustments are made in order to reproduce all experimental data or estimated melting points for all compounds when no experimental data are available).

Similar compounds are assumed for the Pm-Zn system with respect to all other RE-Zn systems (especially lighter-RE-Zn systems, e.g. Nd-Zn and Sm-Zn systems, the adjacent RE-Zn systems of Pm-Zn). No experimental data can be found in the literature for Pm-Zn, undoubtedly because Pm is a radioactive and unstable element. As a result, no compounds in the Pm-Zn system were reported. Given that all compounds in the Nd-Zn system have their corresponding compounds in Sm-Zn system and vice versa, it is reasonable to assume similar compounds in the Pm-Zn system.

2) Trends: Trends in the properties of RE elements and compounds containing RE elements and the same alloying elements can always be observed. Trends have already been observed in the melting points of RE elements and compounds with the same stoichiometry in RE-Zn systems; lattice constants of compounds with the same stoichiometry in RE-Zn systems, etc. The trend lines are linear when Sc, Y, Eu and Yb are singled out. These trends are exploited for the purpose of estimating missing data and for checking existing data for consistency.

   The enthalpy terms for the liquid phase and compounds with the same stoichiometry in all RE-Zn and RE-Mg-Zn systems are optimized in such a way that these values, when plotted together, follow the trends as mentioned above for the melting points and lattice constants. In practice, all available thermodynamic data are used in the optimization-model parameters are assigned to different phases following the trends when thermodynamic data are lacking while reasonable fits to the available experimental data are retained.

In cases where phase diagram data are unavailable, the melting points of all possible phases, stable or metastable, are proposed based on the trends.

Based on these assumptions, all RE-Zn and RE-Mg-Zn systems are critically optimized. The results of the optimization suggest that all these assumptions work well; satisfactory thermodynamic descriptions of all RE-Zn and RE-Mg-Zn systems are obtained and similar trends in different properties are established. All these trends are similar to those already established (trend in the melting points of pure RE, for example). The thermodynamic database can thus be considered self-consistent.

In the optimization of the Ce-Mg-Zn and Nd-Mg-Zn systems, greater weight was accorded to the ND data from the present investigation. The primary reason was that the ND data were obtained in situ at equilibrium at higher temperatures. Also due to the high penetrating power of neutrons, large samples (10 to 20 g) could be used, thereby leading to better control of composition and increased resistance to oxidation.

Thermodynamic modeling of all the RE-Zn systems has been reported. The results of thermodynamic modeling of all the RE-Mg-Zn systems as well as ND experiments in the Ce-Mg-Zn and Nd-Mg-Zn system have been submitted for publication. The model parameters will be included in the FTlite light metals database of the FactSage database computing system (Bale et al., 2009), which already contains optimized model parameters for the solid and liquid phases of a large number of binary and ternary Mg- and Al-containing systems. Through the models, the properties and phase equilibria of multicomponent systems can thus be estimated and calculated.

The RE-Mg-Zn thermodynamic database constructed in the present project is by far the most complete and reliable one, not only because some of the systems have been optimized here for the first time but also because significant improvements have been achieved for systems which have already been optimized. The fit to experimental data and the predictability of phase relations with the current database is much better. As an example, the solidification of two alloys in the Y-Mg-Zn system is simulated and compared to the simulation from the previous database (see appendix 2). Our prediction is satisfactory.

All calculations in the present work were performed with the FactSage software (Bale et al., 2009).

CONCLUSION AND FUTURE PERSPECTIVE

In this thesis the optimization of all RE-Zn systems (RE=Sc, Y, La, Ce, Pr, Nd, Pm, Sm, Eu, Gd, Tb, Dy, Ho, Er, Tm, Yb and Lu) and most of the ternary RE-Mg-Zn systems (RE= Y, La, Ce, Pr, Nd, Sm, Gd, Tb, Dy, Ho, Er, Tm and Lu) as well as experimental work on Ce-Mg-Zn and Nd-Mg-Zn systems is presented. A thermodynamic database for the RE-Mg-Zn systems is established. The following goals are achieved in the present project:

1) Thermodynamic descriptions of all RE-Zn systems (Sc-Zn, Y-Zn, La-Zn, Ce-Zn, Pr-Zn, Nd-Zn, Sm-Zn, Gd-Zn, Tb-Zn, Dy-Zn, Ho-Zn, Er-Zn and Yb-Zn) are obtained using the CALPHAD method. Critical assessment and optimization of all the binary RE-Zn systems are presented in Chapters 2 and 3. Systematic optimization has, for the first time, been performed on these binary systems in which similarities and trends among all these systems are considered. Significant improvements have been achieved on the thermodynamic description of these systems compared to those available in the literature. Reasonable thermodynamic parameters for all phases with no experimental data were obtained by following the trends and similarities among all systems. Similarly, reasonable thermodynamic parameters for metastable phases were obtained in the present work. The thermodynamic parameters for metastable phases were not proposed in previous optimizations, but these parameters are important when higher-order systems are concerned. Two papers on the optimization of all the binary systems have been published.

2) Neutron diffraction (ND) experiments were carried out on selected samples in the Ce-Mg-Zn and Nd-Mg-Zn systems. The transition temperatures and precipitation sequences of the selected samples are well resolved from the ND experiments. Taking into account all experimental data (from the literature and the present NPD experiments) the two systems were critically assessed and optimized. All confirmed stable ternary compounds were considered in the present optimization. The thermodynamic description covers the whole composition range; this is an improvement over earlier optimizations where only the Mg-rich corner was investigated. As for the Ce-Mg-Zn system, all experimental data that were not well explained by early investigators are well accounted for in the present work. Two

papers on experimental and optimization studies on the Ce-Mg-Zn and Nd-Mg-Zn systems have been submitted for publication.

3) Thermodynamic descriptions of the Y-Mg-Zn, La-Mg-Zn, Pr-Mg-Zn, Sm-Mg-Zn, Gd-Mg-Zn, Tb-Mg-Zn, Dy-Mg-Zn, Ho-Mg-Zn, Er-Mg-Zn, Tm-Mg-Zn and Lu-Mg-Zn systems are obtained. The trends and similarities observed among all the RE-Zn binary systems are applied to the ternary systems. Similar ternary compounds were assumed in all lighter-RE-Mg-Zn systems (except La-Mg-Zn system) and heavier-RE-Mg-Zn systems. The Sc-Mg-Zn, Pm-Mg-Zn, Eu-Mg-Zn and Yb-Mg-Zn systems were not optimized in the present project. Two papers have been submitted for publication (one on the lighter-RE-Mg-Zn systems and another on the heavy-RE-Mg-Zn systems).

Experimental investigations of RE-Zn and RE-Mg-Zn systems are limited. By taking advantage of trends and similarities among all these systems a thermodynamic database was obtained; future work on these systems is still indicated as follows:

1) The transformation between low temperature and high temperature forms of $REZn_2$ and RE_2Zn_{17} is reported for some of the systems (all the systems except La-Zn for RE_2Zn_{17}). However, detailed information on the transformation is lacking. Although for RE_2Zn_{17} the transformation temperatures in all systems are proposed, they are predictions. These predictions are the results of following the trends of enthalpies for both forms. They cannot be treated as actual transformation temperatures. These calculated transformation temperatures are very sensitive to the difference in Gibbs energies of the two forms and thus might be quite different from the true behavior.

2) Experimental investigation of the Eu-Zn system is still needed. The melting points and enthalpies of formation of the compounds are proposed following the trend in melting points of RE elements. However, unlike other RE elements, Eu does not lie on the trend line and the predicted melting temperatures for the compounds in Eu-Zn system may be in error. No similar problem for the Pm-Zn, Tm-Zn and Lu-Zn systems is envisaged.

3) Crystal structures of the ternary compounds should be resolved in the future. One of the goals of the ND experiments was to work out the crystal structures of the possible ternary compounds in the Ce-Mg-Zn and Nd-Mg-Zn systems. However, this goal has not been

fulfilled because of the extremely low intensities of the peaks from the ternary compounds.

4) Experimental investigation for most of the ternary systems to search for new ternary compounds is still required. Similar compounds in different systems can reasonably be assumed, but this may not be the case for new compounds. Investigation of the the Sc-Mg-Zn, Eu-Mg-Zn and Yb-Mg-Zn systems is particularly required because these systems are quite different from other RE-Mg-Zn systems. Prediction of ternary compounds in the three systems is not possible.

BIBLIOGRAPHIE

A.T, D. (1991). SGTE data for pure elements. *Calphad, 15*(4), 317-425.

Abe, E., Ono, A., Itoi, T., Yamasaki, M., & Kawamura, Y. (2011). Polytypes of long-period stacking structures synchronized with chemical order in a dilute Mg-Zn-Y alloy. *Phil. Mag. Lett., 91*(10), 690-696.

Abe, E., & Tsai, A. P. (2000). Orthorhombic τ-Zn–Mg–Dy phase related to a Frank-Kasper type decagonal quasicrystal. *Acta Crystallogr. B, 56*(5), 915-917.

Agarwal, R., Fries, S. G., Lukas, H. L., Petzow, G., Sommen, F., Chart, T. G., et al. (1992). Assessment of the Mg-Zn system. *Z. Metallkd., 83*(4), 216-223.

S.R. Agnew , M.H. Yoo , C.N. Tome , (2001). Application of texture simulation to understanding mechanical behavior of Mg and solid solution alloys containing Li or Y , *Acta Mater.* , 49 , 4277-4242.

Andersson, J. O., Helander, T., Höglund, L., Shi, P., & Sundman, B. (2002). Thermo-Calc & DICTRA, computational tools for materials science. *Calphad, 26*(2), 273-312.

Andrusyak, R. I., Kotur, B. Y., & Zavodnik, V. E. (1989). Crystal structure of scandium-zinc (Sc_3Zn_{17}). *Kristallografiya, 34*(4), 996-998.

Ansara, I., Effenberg, G., & Secretariat, C. (1998). *COST 507: Definition of thermochemical and thermophysical properties to provide a database for the development of new light alloys*: Office for Official Publications of the European Communities.

Avedesian, M. M., & Baker, H. (1999). *Magnesium and magnesium alloys*: ASM international.

Bale, C. W., Bélisle, E., Chartrand, P., Decterov, S. A., Eriksson, G., Hack, K., et al. (2009). FactSage thermochemical software and databases — recent developments. *Calphad, 33*(2), 295-311.

Bale, C. W., Chartrand, P., Degterov, S. A., Eriksson, G., Hack, K., Ben Mahfoud, R., et al. (2002). FactSage thermochemical software and databases. *Calphad, 26*(2), 189-228.

Berche, A., Benigni, P., Rogez, J., & Record, M.-C. (2012). Thermodynamic assessment of the La-Zn system. *Calphad, 36*, 65-70.

Berche, A., Benigni, P., Rogez, J., & Record, M. C. (2011). New experimental investigation of the lanthanum zinc phase diagram. *Thermochim. Aata, 523*(1–2), 70-78.

Berche, A., Marinelli, F., Mikaelian, G., Rogez, J., & Record, M. C. (2009). Enthalpies of formation of the La-Zn compounds between 298 K and 910 K: Experimental and theoretical investigations. *J. Alloy. Compd., 475*(1-2), 79-85.

Berche, A., Record, M. C., & Rogez, J. (2008). Triangulation of the La-Mg-Zn System. *Arch. Metall. Mater., 53*(4), 1141-1148.

Berche, A., Record, M. C., & Rogez, J. (2009). Critical review of the La-Zn system. *Open Thermodyn. J., 3*, 7-16.

Berger, G., & Weiss, A. (1988). Ternary intermetallic phases with Heusler-phase-type structure in the system Ag-Mg-RE (RE= La, Ce, Pr, Nd, Sm). *J. Less-Common Met., 142*, 109-121.

Bohlen, J., Nürnberg, M. R., Senn, J. W., Letzig, D., & Agnew, S. R. (2007). The texture and anisotropy of magnesium–zinc–rare earth alloy sheets. *Acta Mater., 55*(6), 2101-2112.

Borzone, G., Cacciamani, G., Ferro, R., Charles, J., & Hertz, J. (1987). A contribution to the study of the alloying behavior of the rare earths with zinc. *J. Less-Common Met., 128*, 297-312.

Bruzzone, G., Fornasini Maria, L., & Merlo, F. (1970). Rare-earth intermediate phases with zinc. *J. Less-Common Metals, 22*(3), 253-264.

Bruzzone, G., & Ruggiero, A. F. (1962). The structure of some intermetallic compounds of yttrium. I. -Compounds with Cu, Ag, Au, Zn, Cd, and Hg. *Atti Accad. Nazl. Lincei, Rend. Sci. Fis., Mat. Nat., 33*, 312-314.

Butorov, V. P., Nichkov, I. F., Novikov, E. A., & Raspopin, S. P. (1973). Reaction of yttrium with zinc. *Izv. Vyssh. Ucheb. Zaved., Tsvet. Met., 16*, 96-102.

Celikin, M., Kaya, A. A., & Pekguleryuz, M. (2012). Effect of manganese on the creep behavior of magnesium and the role of α-Mn precipitation during creep. *Mat. Sci. Eng. A-STRUCT., 534*(0), 129-141.

Chao, C.-C. (1965). *A study of cscl type intermediate phases involving rare-earth elements.* Unpublished, California Institute of Technology, United States -- California.

Chao, C. C., & Duwez, P. (1966). New CsCl-type intermediate phases in binary alloys involving rare-earth elements. *J. Appl. Phys., 37*(7), 2631-2632.

Chao, C. C., Luo, H. L., & Duwez, P. (1964). CsCl-type compounds in binary alloys of rare-earth metals with zinc and copper. *J. Appl. Phys., 35*, 257-258.

Chartrand, P., & Pelton, A. (2001a). Thermodynamic evaluation and optimization of the Li, Na, K, Mg, Ca//F, Cl reciprocal system using the modified quasi-chemical model. *Metall. Mater. Trans. A, 32*(6), 1417-1430.

Chartrand, P., & Pelton, A. (2001b). Thermodynamic evaluation and optimization of the LiF-NaF-KF-MgF2-CaF2 system using the modified quasi-chemical model. *Metall. Mater. Trans. A, 32*(6), 1385-1396.

Chen, S.-L., Daniel, S., Zhang, F., Chang, Y., Yan, X.-Y., Xie, F.-Y., et al. (2002). The PANDAT software package and its applications. *Calphad, 26*(2), 175-188.

Chiotti, P. (1972). New integration of the Gibbs-Duhem equation and thermodynamics of Pr-Zn alloys. *Metall. Mater. Trans. B, 3*(11), 2911-2916.

Chiotti, P., & Mason, J. T. (1965). Phase relations and thermodynamic properties for the cerium-zinc system. *Trans. Am. Inst. Min., Metall. Pet. Eng., 233*(4), 786-795.

Chiotti, P., & Mason, J. T. (1967). Phase relations and thermodynamic properties for samarium-zinc system. *Trans. AIME, 239*(4), 547-552.

Chiotti, P., & Mason, J. T. (1971). Thermodynamic properties of pr-zn alloys. *Metall. Trans., 2*, 967-973.

Chiotti, P., & Mason, J. T. (1973). Thermodynamic properties of nd-zn alloys. *Metall. Trans., 4*, 1527-1531.

Chiotti, P., Mason, J. T., & Gill, K. J. (1963). Phase diagram and thermodynamic properties of yttrium-zinc system. *Trans. AIME, 227*(4), 910-916.

Chiu, C.-n., Gröbner, J., Kozlov, A., & Schmid-Fetzer, R. (2010). Experimental study and thermodynamic assessment of ternary Mg-Zn-Ce phase relations focused on Mg-rich alloys. *Intermetallics, 18*(4), 399-405.

Cromer, D. T., & Larson, A. C. (1972). On the structures of Y2Zn~9, Gd2Zn~9 and related compounds. *Acta Crystallogr. B, 28*(4), 1016-1022.

Damhus, T., Hartshorn, R. M., & Hutton, A. T. (2005). *Nomenclature of inorganic chemistry: IUPAC recommendations 2005*: Royal Society of Chemistry.

Debray, D., & Sougi, M. (1972). Magnetic structure of $HoZn_2$. *J. Chem. Phys., 57*(5), 2156-2159.

Debray, D., & Sougi, M. (1973). Magnetic structure of neodymium-zinc ($NdZn_2$). *J. Chem. Phys., 58*(5), 1783-1786.

Debray, D., Sougi, M., & Meriel, P. (1972). Magnetic structures of $CeZn_2$ and $TbZn_2$. *J. Chem. Phys., 56*(9), 4325-4328.

Delfino, S., Saccone, A., & Ferro, R. (1990). Phase relationships in the neodymium-magnesium alloy system. *Metall. Trans. A, 21*(8), 2109-2114.

Dobatkina, T. V. (1979). Solubility of yttrium and zinc in solid magnesium. *Izv. Akad. Nauk SSSR, Met.*, 211-214.

Dobatkina, T. V., Melnik, E. V., Tyvanchuk, A. T., & Muratova, E. V. (1985). Stable and Metastable Phase Equilibriain Metallic Systems (Eng. Trans.). 75-79.

Dobatkina, T. V., Muratova, E. V., & Drozdova, E. I. (1987a). Crystallization of magnesium alloys in the system Mg-La-Zn. *Russ. metall. Metally*(1), 205-208.

Dobatkina, T. V., Muratova, E. V., & Drozdova, E. I. (1987b). Nature of crystallization of magnesium alloys of the magnesium-lanthanum-zinc system. *Izv. Akad. Nauk SSSR, Met.*, 205-207.

Drits, M. E., Drozdova, E. I., Korol'kova, I. G., Kinzhibalo, V. V., & Tyvanchuk, A. T. (1989a). Investigation of polythermal sections of the Mg-Zn-Ce system in the Mg-rich region. *Russ. metall. Metally*, 195-197.

Drits, M. E., Drozdova, E. I., Korol'kova, I. G., Kinzhibalo, V. V., & Tyvanchuk, A. T. (1989b). Polythermal sections of the magnesium-zinc-cerium system in the magnesium-rich region. *Izv. Akad. Nauk SSSR, Met.*, 198-200.

Drits, M. E., Padezhanova, E. M., & Miklina, N. V. (1974). An investigation of the mutual solubility of neodymium and zinc in solid magnesium. *Izv. Akad.Nauk SSSR, Metally*, 225-229.

Drits, M. E., Padezhnova, E. M., & Miklina, N. V. (1971a). Phase diagram of the magnesium-neodymium-zinc system in the magnesium-rich phase. *Izv. Vyssh. Ucheb. Zaved., Tsvet. Met., 14*, 104-107.

Drits, M. E., Padezhnova, E. M., & Miklina, N. V. (1971b). Solubility of neodymium and zinc in solid magnesium. *Tekhnol. Legk. Splavov. Nauch.-Tekh. Byul. Vses. Inst. Legk. Splavov., 1*, 32-35.

Drits, M. E., Padezhnova, E. M., & Miklina, N. V. (1974a). Combined solubility of neodymium and zinc in solid magnesium. *Izv. Akad. Nauk SSSR, Metal.*, 225-229.

Drits, M. E., Padezhnova, E. M., & Miklina, N. V. (1974b). Phase equilibriums in magnesium-neodymium-yttrium-zinc alloys. *Izv. Akad. Nauk SSSR, Met.*, 218-222.

Drits, M. E., Rokhlin, L. L., Abrukina, N. P., Kinzhibalo, V. V., & Tyvanchuk, A. T. (1985). PHASE EQUILIBRIA IN THE MG-SM-ZN SYSTEM. *Russ. metall. Metally*, 183-189.

Farzadfar, S. A., Sanjari, M., Jung, I. H., Essadiqi, E., & Yue, S. (2012). Experimental and calculated phases in two as-cast and annealed Mg-Zn-Y alloys. *Mater. Charact.*, 63, 9-16.

Ferro, R., & Saccone, A. (2008). *Intermetallic chemistry*: Elsevier.

Fornasini, M. L. (1971). Crystal structure of (Ho-, Er-, Tm, Lu-, Y-)Zn_5 and $ThCd_5$ intermetallic compounds. *J. Less-Common Metals, 25*(3), 329-332.

Fornasini, M. L., & Merlo, F. (1967). Compounds of the formula MX_2 formed by the reaction of rare earths with zinc. *Atti Accad. Naz. Lincei, Rend., Cl. Sci. Fis. Mat. Natur., 43*(5), 357-363.

Gomes de Mesquita, A. H., & Buschow, K. H. J. (1967). The crystal structure of so-called α-$LaAl_4$ (La_3Al_{11}). *Acta Crystallogr., 22*(4), 497-501.

Gomez, C. P., & Lidin, S. (2002). Structure of Dy13Zn57 a binary quasicrystal approximant. *Solid State Sci., 4*, 901-906.

Gong, W., Aizawa, K., Harjo, S., Abe, J., Iwahashi, T., & Kamiyama, T. (2013). *Neutron diffraction on LPSO structure in Mg-Zn-Y alloys*, *Mater. Trans.*, *54*(6), 974-976.

Green, M. L. (1973). Lattice parameters of compounds of the type rare earth-zinc ($REZn_5$) having the calcium-copper ($CaCu_5$) structure. *J. Less-Common Metals, 32*(3), 391-394.

Gröbner, J., Kozlov, A., Fang, X. Y., Geng, J., Nie, J. F., & Schmid-Fetzer, R. (2012). Phase equilibria and transformations in ternary Mg-rich Mg–Y–Zn alloys. *Acta Mater., 60*(17), 5948-5962.

Gschneidner, K., Pecharsky, V., Cho, J., & Martin, S. (1996). The β to γ transformation in cerium—A twenty year study. *Scripta Mater., 34*(11), 1717-1722.

Gupta, M., & Sharon, N. M. L. (2011). *Magnesium, magnesium alloys, and magnesium composites*: John Wiley & Sons.

Hantzsche, K., Bohlen, J., Wendt, J., Kainer, K. U., Yi, S. B., & Letzig, D. (2010). Effect of rare earth additions on microstructure and texture development of magnesium alloy sheets. *Scripta Mater., 63*(7), 725-730.

Harsha, K. S. S. (1964). *The crystal structures of intermetallic compounds in the yttrium - zinc system.* Ph.D. thesis, The Pennsylvania State University, United States -- Pennsylvania.

Hatton, Y., Nikura, A., Tsai, A. P., Inoue, A., Masumoto, T., Fukamichi, K., et al. (1995). Spin-glass behaviour of icosahedral Mg-Gd-Zn and Mg-Tb-Zn quasi-crystals. *J Phys-Condens. Mat., 7*, 2313-2313.

Haynes, W. M. (2015). *CRC Handbook of Chemistry and Physics* (96th Edition (Internet Version 2016) ed.): CRC Press/Taylor and Francis, Boca Raton, FL.

Hidnert, P. (1929). Thermal expansion of molybdenum. *J. Res. Nat. Bur. Standards, 2*, 887.

Hillert, M. (2001). The compound energy formalism. *J. Alloy. Compd., 320*(2), 161-176.

Horiuchi, T., Ikee, H., Hamaya, A., Minamoto, S., Nomoto, S., & Miura, S. (2012). *Experimental study on phase diagram in the vicinity of X or W phase in the Mg-Zn-Y ternary system.* Paper presented at the 7th International Conference on Processing and Manufacturing of Advanced Materials, THERMEC'2011, August 1, 2011 - August 5, 2011, Quebec City, QC, Canada.

Hoshino, Y., & Plambeck, J. A. (1970). Electrochemical studies of yttrium and yttrium-zinc alloys in fused LiCl-KCl eutectic. *Can. J. Chem., 48*, 685-687.

Huang, M.-l., Li, H.-x., Ding, H., Bao, L., Ma, X.-b., & Hao, S.-m. (2012). Intermetallics and phase relations of Mg-Zn-Ce alloys at 400 °C. *T. Nonferr. Metal. Soc.*, *22*(3), 539-545.

Huang, M.-l., Li, H.-x., Ding, H., Ren, Y.-p., Qin, G.-w., & Hao, S.-m. (2009). Partial phase relationships of Mg-Zn-Ce system at 350 C. *T. Nonferr. Metal. Soc. , 19*, 681-685.

Huang, M. L., Li, H. X., Ding, H., Ren, Y. P., & Hao, S. M. (2008). Isothermal Section Of Mg-Zn-La System in Mg Rich Corner at 350C. *Acta Metall. Sin.(English Letters), 21*, 329-335.

Huang, M. L., Li, H. X., Ding, H., Tang, Z. Y., Mei, R. B., Zhou, H. T., et al. (2010). A ternary linear compound T2 and its phase equilibrium relationships in Mg-Zn-Nd system at 400 ^{o}C. *J. Alloy. Compd.*, *489*, 620-625.

Huang, M. L., Li, H. X., Ren, Y. P., Ding, H., Hao, S. M., & Chen, H. (2007). Isothermal section of Mg-Zn-La system in Mg-rich corner at 400 ^{o}C. *T. Nonferr. Metal. Soc.*, *17*, S8-S11.

Huang, X. M., Liu, L. B., Zhang, L. G., Jia, B. R., Jin, Z. P., & Zheng, F. (2008). Thermodynamic assessment of the Pr-Zn binary system. *J. Alloy. Compd.*, *459*, 191-195.

Iandelli, A. (1960). Intermetallic and metalloid gadolinium compounds. *Atti accad. nazl. Lincei, Rend., Classe sci. fis., mat. e, nat.*, *29*, 62-69.

Iandelli, A. (1960). Intermetallic compounds of the rare earth metals. *Phys. Chem. Met. Solutions Intermet. Compd., Symp.*, *1*, 376-385.

Iandelli, A., & Botti, E. (1937). The crystal structure of some intermetallic compounds of the rare earths. *Gazz. Chim. Ital.*, *67*, 638-644.

Iandelli, A., & Palenzona, A. (1964). Intermetallic compounds of europium with zinc, cadmium, and mercury. *Atti Accad. Naz. Lincei, Cl. Sci. Fis., Mat. Nat., Rend.*, *37*(3-4), 165-168.

Iandelli, A., & Palenzona, A. (1965). Atomic size of rare earths in intermetallic compounds. MX compounds of cesium chloride type. *J. Less-Common Met.*, *9*(1), 1-6.

Iandelli, A., & Palenzona, A. (1967). Zinc-rich phases of the rare-earth-zinc alloys. *J. Less-Common Met.*, *12*(5), 333-343.

Ishimasa, T., & Shimizu, T. (2000). Microdomain structure in the disordered Zn-Mg-Ho icosahedral phase. *Jpn. J. Appl. Phys. 1*, *39*, 1235-1240.

Itoi, T., Seimiya, T., Kawamura, Y., & Hirohashi, M. (2004). Long period stacking structures observed in Mg97Zn 1Y2 alloy. *Scripta Mater., 51*(2), 107-111.

Jia, B. R., Zhang, L. G., Huang, G. X., Qi, H. Y., Yang, H., Liu, L. B., et al. (2009). Thermodynamic assessment of the Sm-Zn binary system. *J. Alloy. Compd., 473*, 176-179.

Jin, L. (2012). *Thermodynamic Modeling of Aluminum-Magnesium-Rare Eearth Systems.* Ph. D. thesis, École Polytechnique de Montréal.

Jin, L., Kang, Y.-B., Chartrand, P., & Fuerst, C. D. (2010). Thermodynamic evaluation and optimization of Al–Gd, Al–Tb, Al–Dy, Al–Ho and Al–Er systems using a Modified Quasichemical Model for the liquid. *Calphad, 34*(4), 456-466.

Jin, L., Kang, Y.-B., Chartrand, P., & Fuerst, C. D. (2011). Thermodynamic evaluation and optimization of Al–La, Al–Ce, Al–Pr, Al–Nd and Al–Sm systems using the Modified Quasichemical Model for liquids. *Calphad, 35*(1), 30-41.

Johnson, I., & Yonco, R. (1970). Thermodynamics of cadmium- and zinc-rich alloys in the Cd−La, Cd−Ce, Cd−Pr, Zn−La, Zn−Ce and Zn−Pr systems. *Metall. Mater. Trans. B, 1*(4), 905-910.

Jung, I.-H., Decterov, S. A., & Pelton, A. D. (2005). Critical thermodynamic evaluation and optimization of the CaO–MgO–SiO2 system. *J. Eur. Ceram. Soc., 25*(4), 313-333.

Kainer, K. U., & Kaiser, F. (2003). Magnesium alloys and technology.

Kang, Y.-B., Jin, L., Chartrand, P., Gheribi, A. E., Bai, K., & Wu, P. (2012). Thermodynamic evaluations and optimizations of binary Mg-light Rare Earth (La, Ce, Pr, Nd, Sm) systems. *Calphad, 38*(0), 100-116.

Kang, Y.-B., Jung, I.-H., Decterov, S. A., Pelton, A. D., & Lee, H.-G. (2004). Phase equilibria and thermodynamic properties of the $CaO-MnO-Al_2O_3-SiO_2$ system by critical evaluation, modeling and experiment. *ISIJ Int., 44*(6), 975-983.

Kang, Y.-B., Pelton, A., Chartrand, P., Spencer, P., & Fuerst, C. (2007a). Critical Evaluation and Thermodynamic Optimization of the Binary Systems in the Mg-Ce-Mn-Y System. *J. Phase Equilib. Diff., 28*(4), 342-354.

Kang, Y.-B., Pelton, A. D., Chartrand, P., & Fuerst, C. D. (2008). Critical evaluation and thermodynamic optimization of the Al–Ce, Al–Y, Al–Sc and Mg–Sc binary systems. *Calphad, 32*(2), 413-422.

Kang, Y.-B., Pelton, A. D., Chartrand, P., Spencer, P., & Fuerst, C. D. (2007b). Thermodynamic Database Development of the Mg-Ce-Mn-Y System for Mg Alloy Design. *Metall. Mater. Trans. A, 38*(6), 1231-1243.

Kawamura, Y., & Yamasaki, M. (2007). Formation and mechanical properties of Mg97Zn1RE 2 alloys with long-period stacking ordered structure. *Mater. Trans., 48*(11), 2986-2992.

Kawamura, Y., & Yoshimoto, S. (2005). *High strength Mg-Zn-Y alloys with LPSO structure.* Paper presented at the 2005 TMS Annual Meeting, February 13, 2005 - February 17, 2005, San Francisco, CA, United states.

Kevorkov, D., & Pekguleryuz, M. (2009). Experimental study of the Ce-Mg-Zn phase diagram at 350 °C via diffusion couple techniques. *J. Alloy. Compd., 478*(1-2), 427-436.

Kinzhibalo, V., Tyvanchuk, A., & Melnik, E. (1985). A Study of the Ternary Systems Mg--Zn--Pr and Mg--Zn--Nd. *Nauka, Stable and Metastable Phase Equilibria in Metallic Systems*, 70-74.

Kober, V. I., Nichkov, I. F., Raspopin, S. P., & Kuz'minykh, V. M. (1983). Thermodynamic properties of alloys of gadolinium with low-melting metals. *Splavy Redk. Met. Osobymi Fiz. Svoistvami Redkozem. Blagorodn. Met.*, 132-135.

Koebler, U., Kinzel, W., & Zinn, W. (1981). Magnetic phase diagram of gadolinium-silver-zinc ($GdAg_{1-x}Zn_x$). *J. Magn. Magn. Mater., 25*(2), 124-134.

Kohler, F. (1960). Zur Berechnung der thermodynamischen Daten eines ternären Systems aus den zugehörigen binären Systemen. *Monatsh. Chem. Verw. TL., 91*(4), 738-740.

U. Kolitsch, P. Bellen, S. Kaesche, D. Macciò, N. Bochvar, Y. Liberov, P. Rogl, G. Effenberg, G. Petzow, (2000) Ternary Alloys–A Comprehensive Compendium of Evaluated Constitutional Data and Phase Diagrams, Stuttgart, Germany: Weinheim: VCH Verlagsgesellschaft, MSI GmbH; 17, 168–76.

Kopp, H. (1865). On the specific heat of solid bodies. *Phil. Trans. R. Soc. Lond., 155*, 71.

Korol'kov, A. M., & Sal'dau, P. Y. (1946). Solubility of zinc and cerium in magnesium in the solid state. *Izv. Sekt. Fiz.-Khim. Anal., Inst. Obshch. Neorg. Khim., Akad. Nauk SSSR, 16*, 295-306.

Kounis, A., Miehe, G., & Fuess, H. (2000). Investigation of icosahedral phases in the Zn-Mg-(Y, Er) system by high resolution transmission electron microscopy. *Mater. Sci. Eng. A, 294*, 323-326.

Kovalevskii, A. V., Lebedev, V. A., Nichkov, I. F., & Raspopin, S. P. (1972). Thermodynamic properties and phase composition of lanthanum-zinc alloys. *Izv. Akad. Nauk SSSR, Metal.*, 183-187.

Kripyakevich, P. I., Kuz'ma, Y. B., & Ugrin, N. S. (1967). Crystalline structure of Ce_3Zn_{22}, La_3Zn_{22}, and Pr_3Zn_{22} compounds. *Zh. Strukt. Khim., 8*(4), 703-705.

Kripyakevich, P. I., Protasov, V. S., & Kuz'ma, Y. B. (1965). Crystalline structure of scandium zinc. *Visn. L'viv. Derzh. Univ., Ser. Khim.*(8), 80-82.

Kripyakevich, P. I., Protasov, V. S., & Kuz'ma, Y. B. (1966). Crystal structures of the compounds in the scandium-zinc system. *Izv. Akad. Nauk SSSR, Neorg. Mater., 2*(9), 1574-1580.

Kusma, J. B., & Laube, E. (1965). Crystal structures of YAg_2, YAu_2, and YZn_{12}. *Monatsh. Chem., 96*(5), 1496-1502.

Kuz'ma, Y. B., Kripyakevich, P. I., & Frankevich, D. P. (1965). Compounds of the rare earth metals with zinc and their crystal structures. *Izv. Akad. Nauk SSSR, Neorg. Mater., 1*(9), 1410-1415.

Kuz'ma, Y. B., Kripyakevich, P. I., & Ugrin, N. S. (1966). New compounds of rare earth metals with zinc and their crystal structure. *Izv. Akad. Nauk SSSR, Neorg. Mater., 2*(4), 630-635.

Langsdorf, A., Assmus, W., Babonas, G. J., & Reza, A. (1997). Structural and optical properties of Bridgman-grown Zn-Mg-Y quasicrystals. *Liet. Fiz. Z., 37*, 40-45.

Langsdorf, A., Seuring, C., Ritter, F., & Assmus, W. (1997). Zn-Mg-(Y, RE) quasicrystals. Growth experiments and phase diagrams. [10.1002/crat.2170320808]. *Cryst. Res. Technol., 32*, 1067-1072.

Laube, E. (1966). Structures of new rare earth metal compounds. *Monatsh. Chem., 97*(3), 722-732.

Laube, E., & Nowotny, H. (1963). Crystal types of ScZn and ScCd. *Monatsh. Chem., 94*, 162-163.

Lesourd, J. B. P. F., & Plambeck, J. A. (1969). Electrochemical studies of lanthanum and lanthanum-zinc alloys in fused LiCl-KCl eutectic. *Can. J. Chem., 47*(18), 3387-3391.

Li, H., Su, X., Liu, Y., Li, Z., & Wang, X. (2008). Thermodynamic assessment of the Nd-Zn system. *J. Alloy. Compd., 457*, 344-347.

Li, M. R., & Kuo, K. H. (2007). Intermetallic phases and phase reactions in Zn–Mg (<40 at.%)–Y (<20 at.%) region. *J. Alloy. Compd., 432*(1–2), 81-89.

Liu, X. J., Chen, X., & Wang, C. P. (2009). Thermodynamic assessments of the Sm-Zn and Nd-Zn systems. *J. Alloy. Compd., 468*, 115-121.

Liu, X. J., Wen, M. Z., Wang, C. P., & Pan, F. S. (2008). Thermodynamic assessment of the Zn-Y and Al-Zn-Y systems. *J. Alloy. Compd., 452*, 283-290.

Lukas, H. L., Fries, S. G., & Sundman, B. (2007). *Computational thermodynamics: the Calphad method* (Vol. 131): Cambridge university press Cambridge.

Luo, A. A. (2000). Materials comparison and potential applications of magnesium in automobiles. *Essential Readings in Magnesium Technology*, 25-34.

March, N. H., Tosi, M. P., & March, N. H. (2002). *Introduction to liquid state physics* (pp. 21-23). Singapore: World Scientific.

Marquina, C., & et al. (1993). Specific heats of R_2Zn_{17} intermetallic compounds. *J. Phys-Condens. Mat., 5*(13), 2009.

Marquina, C., Kim-Ngan, N. T. H., Buschow, K. H. J., Franse, J. J. M., & Ibarra, M. R. (1996). Specific heat of Gd_2Zn17 and Yb_2Zn17 intermetallic compounds. *J. Magn. Magn. Mater., 157-158*, 403-404.

Mason, J., & Chiotti, P. (1970). Phase relations and crystallographic data for the Pr-Zn system. *Metall. Mater. Trans. B, 1*(8), 2119-2123.

Mason, J. T., & Chiotti, P. (1968). Ytterbium-zinc phase diagram. *Trans. AIME, 242*(6), 1167-1171.

Mason, J. T., & Chiotti, P. (1972). Nd-Zn PHASE DIAGRAM. *Metall. Trans., 3*, 2851-2855.

Mason, J. T., & Chiotti, P. (1976). Phase diagram and thermodynamic properties of the yttrium-zinc system. *Metall. Trans. A , 7*, 287-291.

Mason, J. T., Sree Harsha, K. S., & Chiotti, P. (1970). The crystal structure of a samarium-zinc compound with approximate composition $SmZn_{11}$. *Acta Crystallogr. B, 26*(4), 356-361.

Matsuda, M., Ii, S., Kawamura, Y., Ikuhara, Y., & Nishida, M. (2005). Variation of long-period stacking order structures in rapidly solidified $Mg_{97}Zn_1Y_2$ alloy. *Mater. Sci. Eng. A, 393*(1-2), 269-274.

Mel'nik, E.V. Kinzhibalo, V.V. Padezhnova, E.M. Dobatkina, T.V. (1978). New ternary compounds with face-centered lattice in the Mg-Zn-RE systems, Tezizy Dokl. Vses. Konf. Kristallokhim. Intermet. Soeden.,

Michel, D. J., & Ryba, E. (1965). The crystal structure of $YbZn_2$. *Acta Crystallogr., 19*(4), 687-688.

Michel, D. J., & Ryba, E. (1968). Crystal structure of $HoZn_3$. *Acta Crystallogr., Sect. B, 24*(Pt. 9), 1267-1269.

Michel, D. J., & Ryba, E. (1968). The high-temperature lattice parameters of $HoZn_2$. *J. Less-Common Metals, 14*(3), 367-369.

Michel, D. J., & Ryba, E. (1969). Intermetallic compounds in the erbium-zinc system. *Scr. Met., 3*(9), 683-685.

Michel, D. J., Ryba, E., & Kejriwal, P. K. (1966). Melting points of $REZn_2$ intermetallic compounds. *J. Less-Common Met., 11*, 67-69.

Miedema, A. R., de Châtel, P. F., & de Boer, F. R. (1980). Cohesion in alloys — fundamentals of a semi-empirical model. *Physica B+C, 100*(1), 1-28.

Mishra, R. K., Gupta, A. K., Rao, P. R., Sachdev, A. K., Kumar, A. M., & Luo, A. A. (2008). Influence of cerium on the texture and ductility of magnesium extrusions. *Scripta Mater., 59*(5), 562-565.

Mordike, B. L., & Ebert, T. (2001). Magnesium: Properties — applications — potential. *Mat. Sci. Eng. A-STRUCT., 302*(1), 37-45.

Moreno, I. P., Nandy, T. K., Jones, J. W., Allison, J. E., & Pollock, T. M. (2003). Microstructural stability and creep of rare-earth containing magnesium alloys. *Scripta Mater., 48*(8), 1029-1034.

Morin, P., Laforest, J., Pierre, J., & Shah, J. S. (1973). Thermal variation of parameters and magnetostriction in equiatomic rare earth metal-zinc compounds. *C. R. Acad. Sci., Ser. B, 277*(14), 353-354.

Morin, P., & Pierre, J. (1975). Magnetic properties, magnetic structure, and crystal field in praseodymium-zinc and neodymium-zinc. *Phys. Status Solidi A, 30*(2), 549-559.

Morin, P., Pierre, J., & Chaussy, J. (1974). Specific Heat in TbZn and HoZn Compounds. *physica status solidi (a), 24*(2), 425-432.

Morishita, M., Koyama, K., & Tsuboki, K. (2004). Calorimetric study of Zn13La. *Z. Metallkd.*, 708-712.

Morishita, M., Yamamoto, H., Tsuboki, K., & Horike, T. (2007). Standard Gibbs energy of formation of $Zn_{17}Y_2$ and $Zn_{12}Y$ determined by solution calorimetry and measurement of heat capacity from near zero Kelvin. *Int. J. Mater. Res., 98*, 10-15.

Morishita, M., Yamamoto, H., Tsuboki, K., & Matsumoto, Y. (2006). Standard Gibbs energy of formation of Zn8La determined by solution calorimetry and measurement of heat capacity from near absolute zero kelvin. *Mater.Trans., 47*, 1555-1559.

Mostafa, A., & Medraj, M. (2014). Phase equilibria of the Ce-Mg-Zn ternary system at 300 ^{o}C. *Metals, 4*(2), 168-195.

Mostafa, A., & Medraj, M. (2015). Experimental Investigation of the Mg-Nd-Zn Isothermal Section at 300 ^{o}C. *Metals, 5*(1), 84-101.

Muggianu, Y. M., Gambino, M., & Bros, J. P. (1975). Enthalpies of formation of liquid bismuth-gallium-tin alloys at 723K. Choice of an analytical representation of integral and partial thermodynamic functions of mixing. *J. Chim. Phys. Pcb., 72*(1), 83-88.

Mullayanov, R. K., Lebedev, V. A., Kanashin, Y. P., Nichkov, I. F., & Raspopin, S. P. (1969). Thermodynamics of a lanthanum-zinc system. *Zh. Fiz. Khim., 43*, 2776-2779.

Niikura, A., Tsai, A.-P., Inoue, A., & Masumoto, T. (1994). New class of amorphous and icosahedral phases in Zn-Mg-Rare-Earth metal alloys. *Jpn. J. Appl. Physi, 2, 33*, L1538-L1541.

Nowotny, H. (1942). The crystal structures of Ni5Ce, Ni5La, Ni5Ca, Cu5La, Cu5Ca, Zn5La, Zn5Ca, MgCe, MgLa and MgSr. *Z. Metallkd., 34*, 247-253.

Okuda, H., Horiuchi, T., Tsukamoto, T., Ochiai, S., Yamasaki, M., & Kawamura, Y. (2013). Evolution of long-period stacking ordered structures on annealing as-cast $Mg_{85}Y_9Zn_6$ alloy ingot observed by synchrotron radiation small-angle scattering. *Scripta Mater., 68*(8), 575-578.

Olcese, G. L. (1963). Magnetic behavior of cerium in intermetallic compounds. II. The Ce-Zn, Ce-Cd, and Ce-Hg systems. *Atti Accad. Naz. Lincei, Cl. Sci. Fis., Mat. Nat., Rend., 35*(1-2), 48-52.

Padezhnova, E. M., Mel'nik, E. V., & Dobatkina, T. V. (1979). Study of phase equilibriums in the magnesium-yttrium-zinc system. *Izv. Akad. Nauk SSSR, Met.* 217-221.

Padezhnova, E. M., Mel'nik, E. V., Milievskii, R. A., Dobatkina, T. V., & Kinzhibalo, V. V. (1982). Magnesium-zinc-yttrium system. *Izv. Akad. Nauk SSSR, Met.*, 204-208.

Palenzona, A., & Manfrinetti, P. (1997). The phase diagram of the Sc-Zn system. *J. Alloy. Compd., 247*(1-2), 195-197.

Pauling, L. (1947). Atomic Radii and Interatomic Distances in Metals. *J. Am. Chem. Soc., 69*(3), 542-553.

Pavlyuk, V., Marciniak, B., & Różycka-Sokołowska, E. (2012). The isothermal section of the phase diagram of Ce–Mg–Zn ternary system at 470 K. *Intermetallics, 20*(1), 8-15.

Pavlyuk, V., Rozycka-Sokolowska, E., & Marciniak, B. (2010). The new ternary phases of $La_3(_{Zn0.874}Mg_{0.126})_{11}$ and $Ce_3(Zn_{0.863}Mg_{0.137})_{11}$. *Acta Crystallogr. C, 66*(3), i25-i28.

Pavlyuk, V., Solokha, P., Dmytriv, G., Marciniak, B., & Paul-Boncour, V. (2007). The Heusler-type alloy $MgZn_2Ce$. *Acta Crystallogr. E, 63*(7), i161-i161.

Pavlyuk, V., Solokha, P., Zelinska, O., Paul-Boncour, V., & Nowik-Zajac, A. (2008). Ce20Mg19Zn81: A new structure type with a giant cubic cell. *Acta Crystallogr. C, 64*(7), i50-i52.

Pelton, A., & Chartrand, P. (2001). The modified quasi-chemical model: Part II. Multicomponent solutions. *Metall. Mater. Trans. A, 32*(6), 1355-1360.

Pelton, A., & Chartrand, P. (2001). Thermodynamic evaluation and optimization of the LiCl-NaCl-KCl-RbCl-CsCl-$MgCl_2$-$CaCl_2$ system using the modified quasi-chemical model. *Metall. Mater. Trans. A, 32*(6), 1361-1383.

Pelton, A., Degterov, S., Eriksson, G., Robelin, C., & Dessureault, Y. (2000). The modified quasichemical model I—Binary solutions. *Metall. Mater. Trans. B, 31*(4), 651-659.

Pelton, A. D. (2001). A general "geometric" thermodynamic model for multicomponent solutions. *Calphad, 25*(2), 319-328.

Pelton, A. D., & Kang, Y.-B. (2007). Modeling short-range ordering in solutions. *Int. J. Mater. Res., 98*(10), 907-917.

Pierre, J., Galera, R. M., & Siaud, E. (1985). Evidence for Kondo-type behavior in $Ce_xR_{1-x}M$ compounds with R = La, Y and M = Mg, Zn. *J. Phys. (Les Ulis, Fr.), 46*(4), 621-626.

Polmear, I. (1996). Recent developments in light alloys. *JIM, Mater. Trans., 37*(1), 12-31.

Qi, H., Jin, Z., Liu, L., & Liu, H. (2008). Thermodynamic assessment of the Nd-Zn binary system. *J. Alloy. Compd., 458*, 184-188.

Qi, H. Y., Huang, G. X., Bo, H., Xu, G. L., Liu, L. B., & Jin, Z. P. (2011). Thermodynamic description of the Mg-Nd-Zn ternary system. *J. Alloy. Compd., 509*, 3274-3281.

Qi, H. Y., Huang, G. X., Bo, H., Xu, G. L., Liu, L. B., & Jin, Z. P. (2012). Experimental investigation and thermodynamic assessment of the Mg-Zn-Gd system focused on Mg-rich corner. *J. Mater. Sci., 47*(3), 1319-1330.

Qi, H. Y., Huang, G. X., Liu, R. D., Zhang, K., Liu, L. B., & Jin, Z. P. (2010). Thermodynamic optimization of La-Zn and La-Mg-Zn systems. *J. Alloy. Compd., 497*, 336-343.

Qudong, W., Wenzhou, C., Xiaoqin, Z., Yizhen, L., Wenjiang, D., Yanping, Z., et al. (2001). Effects of Ca addition on the microstructure and mechanical properties of AZ91magnesium alloy. *J.Mater. Sci., 36*(12), 3035-3040.

Redlich, O., & Kister, A. T. (1948). Algebraic Representation of Thermodynamic Properties and the Classification of Solutions. *Ind. Eng. Chem., 40*(2), 345-348.

Rietveld, H. (1969). A profile refinement method for nuclear and magnetic structures. J. Appl. Crystallogr., 2(2), 65-71.

Rokhlin, L. L., & Nikitina, N. I. (1992). Phase equilibria in the Mg-Dy-Zn system. *Izv. Akad. nauk SSSR. Metally*, 213-219.

Rolla, L., Iandelli, A., Vogel, R., & Canneri, G. (1941). Metals and alloys of the rare earths. I. The system lanthanum-zinc. *Ricerca sci., 12*, 1216-1226.

Saccone, A., Cardinale, A., Delfino, S., & Ferro, R. (2003). The Dy−Zn phase diagram. *Metall. Mater. Trans. A, 34*(13), 743-750.

Saccone, A., Cardinale, A. M., Delfino, S., Cacciamani, G., & Ferro, R. (2001). Effect of Cu and Zn on the melting and transformation temperatures of Pr and Gd. *J. Alloy. Compd., 317-318*, 503-512.

Saccone, A., Cardinale, A. M., Delfino, S., & Ferro, R. (2001). Phase relationships of the Gd-Zn system. *Z. Metallkd.* 92(8), 959-965.

Saccone, A., Cardinale, A. M., Delfino, S., & Ferro, R. (2005). Binary phase diagrams of the rare earth metals with zinc: The Tb-Zn, Ho-Zn and Er-Zn systems. *Z. Metallkd, 96*, 1369-1379.

Sanderson, M. J., & Baenziger, N. C. (1953). The crystal structure of $BaCd_{11}$. *Acta Crystallogr., 6*(7), 627-631.

Sato, T. J., Abe, E., & Tsai, A. P. (1998). Composition and stability of decagonal quasicrystals in the Zn-Mg-rare-earth systems. *Phil. Mag. Lett., 77*(4), 213-219.

Sato, T. J., Abe, E., & Tsai, A. P. (2001). Decagonal quasicrystals in the Zn-Mg-R alloys (R=rare-earth and Y). *Mat. Sci. Eng. A-Struct., 304-306*, 867-870.

Sato, T. J., Takakura, H., Tsai, A. P., Shibata, K., Ohoyama, K., & Andersen, K. H. (1999). Neutron scattering study of the Zn-Mg-Ho icosahedral quasicrystal. J. Phys. Chem. Solids, *60*(8), 1257-1259.

Schramm, J. (1941). The systems zinc-cerium and zinc-lanthanum. *Z. Metallkd., 33*, 358-360.

Shao, G., Varsani, V., & Fan, Z. (2006). Thermodynamic modelling of the Y-Zn and Mg-Zn-Y systems. *Calphad, 30*(3), 286-295.

Shimizu, T., & Ishimasa, T. (1998). Formation of F- and P-type icosahedral quasicrystals in the Zn-Mg-Ho alloy system. *Jpn. J. Appl. Phys. 1, 37*, 5691-5696.

Siegrist, T., & Le Page, Y. (1987). Crystal chemistry of some Th_2Zn_{17}-type rare-earth-zinc phases. *J. Less-Common Met., 127*, 189-197.

Spencer, P. (2007). *Database and Software for Mg Alloy Design (report to GM Canada by A. D. Pelton, P. Spencer, P. Chartrand, C. Bale, G. Eriksson, C. Aliravci, A. Shukla).* Montreal: Ecole Polytechnique.

Spencer, P. J., Pelton, A. D., Kang, Y.-B., Chartrand, P., & Fuerst, C. D. (2008). Thermodynamic assessment of the Ca-Zn, Sr-Zn, Y-Zn and Ce-Zn systems. *Calphad, 32*, 423-431.

Stanford, N., & Barnett, M. R. (2008). The origin of “rare earth” texture development in extruded Mg-based alloys and its effect on tensile ductility. *Mat. Sci. Eng. A-STRUCT., 496*(1–2), 399-408.

Sterzel, R., Assmus, W., Kounis, A., Miehe, G., & Fuess, H. (2000). A cubic approximant in the Zn-Mg-Er alloy. *Phil. Mag. Lett., 80*, 239-247.

Sterzel, R., Gross, C., Kounis, A., Miehe, G., Fuess, H., Reutzel, S., et al. (2002). A new well-ordered simple icosahedral quasicrystalline phase in the Zn-Mg-Er system. *Phil. Mag. Lett., 82*, 443-450.

Takakura, H., Sato, A., Yamamoto, A., & Tsai, A. P. (1998). Crystal structure of a hexagonal phase and its relation to a quasicrystalline phase in Zn-Mg-Y alloy. *Phil. Mag. Lett., 78*(3), 263-270.

Toby, B. (2001). EXPGUI, a graphical user interface for GSAS. *J. Appl. Crystallogr., 34*(2), 210-213.

Toop, G. W. (1965). Predicting ternary activities using binary data. *Trans. AIME, 233*(5), 850-855.

Tsai, A.-P., Murakami, Y., & Niikura, A. (2000). The Zn-Mg-Y phase diagram involving quasicrystals. *Philos.Mag. A*, 1043-1054.

Tsai, A. P., Niikura, A., Inoue, A., & Masumoto, T. (1997). Stoichiometric icosahedral phase in the Zn-Mg-Y system. *J. Mater. Res., 12,* 468-1471.

Tsai, A. P., Niikura, A., Inoue, A., Masumoto, T., Nishida, Y., Tsuda, K., et al. (1994). Highly ordered structure of icosahedral quasicrystals in Zn-Mg-RE (RE = rare earth metals) systems. *Phil. Mag. Lett., 70*(3), 169-175.

Uhrig, E., Bruhne, S., Sterzel, R., Schropfer, L., & Assmus, W. (2003). Growth of simple icosahedral single quasicrystals in the Zn-Mg-Ho system. *Phil. Mag. Lett., 83,* 265-272.

Uwatoko, Y., Suenaga, K., & Oomi, G. (1992). X-ray diffraction study of the structural change in cerium-zinc (CeZn) under high pressure. *J. Magn. Magn. Mater., 104-107*(Proc. Int. Conf. Magn., 1991, Pt. 1), 645-646.

Veleckis, E., Schablaske, R. V., Johnson, I., & Feder, H. M. (1967). Intermetallic phases in the systems of zinc with lanthanum, cerium, praseodymium, neodymium, and yttrium. *Trans. Metall. Soc. AIME, 239*(1), 58-63.

Waldner, P., & Pelton, A. D. (2004). Critical thermodynamic assessment and modeling of the Fe-Ni-S system. *Metall. Mater. Trans. B, 35*(5), 897-907.

Wang, C. P., Chen, X., Liu, X. J., Pan, F. S., & Ishida, K. (2008). Thermodynamic modeling of the Ce-Zn and Pr-Zn systems. *J. Alloy. Compd., 458,* 166-173.

Wang, F. (1967). The crystal structure of $Gd_{13}Zn_{58}$. *Acta Crystallographica, 22*(4), 579-584.

Wang, X., Du, W., Wang, Z., Liu, K., & Li, S. (2012). Stable icosahedral phase in $Mg_{44}Zn_{44}Gd_{12}$ alloy. *J. Rare Earths, 30*(5), 503-506.

Winter, M. (1993). Web elements. from www.webelements.com

Xia, X., Sanaty-Zadeh, A., Zhang, C., Luo, A. A., Zeng, X., Austin Chang, Y., et al. (2014). Thermodynamic modeling and experimental investigation of the magnesium–zinc–samarium alloys. *J. Alloy. Compd., 593*(0), 71-78.

Xu, H., Fan, J., Chen, H.-L., Schmid-Fetzer, R., Zhang, F., Wang, Y., et al. (2014). Experimental determination of the phase equilibria of the Mg–Nd–Zn system at 320 °C. *J. Alloy. Compd., 603*, 100-110.

Yamasaki, M., Anan, T., Yoshimoto, S., & Kawamura, Y. (2005). Mechanical properties of warm-extruded Mg-Zn-Gd alloy with coherent 14H long periodic stacking ordered structure precipitate. *Scripta Mater., 53*(7), 799-803.

Yamshchikov, L. F., Lebedev, V. A., Nichkov, I. F., & Raspopin, S. P. (1985). Thermodynamic properties of erbium-zinc alloys. *Russ. metall.*, 218-222.

Yamshchikov, L. F., Sattarov, F. N., & Moskalenko, H. I. (1988). Thermodynamic properties of dysprosium-zinc melts. *Izv. Vyssh. Uchebn. Zaved., Tsvetn. Metall.* 6, 123.

Yang, J., Wang, L., Wang, L., & Zhang, H. (2008). Microstructures and mechanical properties of the Mg–4.5Zn–xGd (x = 0, 2, 3 and 5) alloys. *J. Alloy. Compd., 459*(1–2), 274-280.

Yaroshevsky, A. A. (2006). Abundances of chemical elements in the Earth's crust. *Geochemistry International, 44*(1), 48-55.

Zelinska, O., Conrad, M., & Harbrecht, B. (2004). Refinement of the crystal structure of cerium zinc (1 : 11), $CeZn_{11}$. *Z. Krist-New Cryst. St., 219*(4), 357-358.

Zhang, C., Luo, A. A., Peng, L., Stone, D. S., & Chang, Y. A. (2011). Thermodynamic modeling and experimental investigation of the magnesium–neodymium–zinc alloys. *Intermetallics, 19*(11), 1720-1726.

Zhang, P. (2005). Creep behavior of the die-cast Mg–Al alloy AS21. *Scripta Mater., 52*(4), 277-282.

Zhiping, L., & Shaoqing, Z. (1993). Comment on the so-called Z-phase in magnesium alloys containing zinc and rare-earth elements. *J. Mater. Sci. Lett.*, *12*, 1490-1492.

Zhu, S., Liu, Z., Qu, R., Wang, L., Li, Q., & Guan, S. (2013). Effect of rare earth and Mn elements on the corrosion behavior of extruded AZ61 system in 3.5 wt% NaCl solution and salt spray test. *J. Magn. Alloy.*, *1*(3), 249-255.

Zhu, Z., & Pelton, A. D. (2015a). Critical assessment and optimization of phase diagrams and thermodynamic properties of RE–Zn systems-part I: Sc–Zn, La–Zn, Ce–Zn, Pr–Zn, Nd–Zn, Pm–Zn and Sm–Zn. *J. Alloy. Compd.*, *641*(0), 249-260.

Zhu, Z., & Pelton, A. D. (2015b). Critical assessment and optimization of phase diagrams and thermodynamic properties of RE–Zn systems – Part II – Y–Zn, Eu–Zn, Gd–Zn, Tb–Zn, Dy–Zn, Ho–Zn, Er–Zn, Tm–Zn, Yb–Zn and Lu–Zn. *J. Alloy. Compd.*, *641*(0), 261-271.

Zhu, Z., & Pelton, A. D. (2015c). Thermodynamic Modeling of the La-Mg-Zn, Pr-Mg-Zn and Sm-Mg-Zn system. *Submitted for publication*

Zhu, Z., & Pelton, A. D. (2015d). Thermodynamic Modeling of the Y-Mg-Zn, Gd-Mg-Zn, Tb-Mg-Zn, Dy-Mg-Zn, Ho-Mg-Zn, Er-Mg-Zn, Tm-Mg-Zn and Lu-Mg-Zn system. *Submitted for publication*

Zhu, Z. , Gharghouri, M.A., Medraj, M., Lee, S.Y., Pelton, A.D. (2015). Thermodynamic modeling and in-situ neutron diffraction INVESTIGATION OF the Ce-Mg-Zn system. *Submitted for publication*

Zhu, Z. , Gharghouri, M.A., Pelton, A.D. (2015). Thermodynamic modeling and in-situ neutron diffraction INVESTIGATION OF the Nd-Mg-Zn system. *Submitted for publication*

APPENDIX 1 – MIEDEMA MODEL

According to the Miedema Model (Miedema, de Châtel, & de Boer, 1980), the enthalpy of mixing of a binary liquid phase can be expressed as follows for systems containing transition metals and non-transition metals:

$$\Delta H = \frac{2Pf(c^s)(c_A V_A^{2/3} + c_B V_B^{2/3})}{\left(n_{WS}^A\right)^{-1/3} + \left(n_{WS}^B\right)^{-1/3}} \times \left[-(\phi_A - \phi_B)^2 + \frac{Q}{P}\left(\Delta n_{WS}^{1/3}\right)^2 - \frac{R}{P} \right] \qquad \text{(A1-1)}$$

where P, Q and R are empirical constants, $f(c^s)$ is a concentration term, c_i, V_i, ϕ_i and n_{WS}^i are the mole fraction, mole volume, chemical potential and electronic density at the Winger-Seitz cell boundary of component i. $f(c^s)$ can be expressed as

$$f(c^s) = c_A^S c_B^S . \qquad \text{(A1-2)}$$

The enthalpy of formation for the intermetallic phases can also be expressed using the same equation except that R will take different values and $f(c^s)$ has a different form. For intermetallic phases, $f(c^s)$ is expressed as

$$f(c^s) = c_A^S c_B^S \left[1 + 8(c_A^S c_B^S)^2 \right] \qquad \text{(A1-3)}$$

The values of P, $\frac{Q}{P}$ and $\frac{R}{P}$ are taken or calculated from the data from Miedema *et al* (Miedema, de Châtel, & de Boer, 1980) as 12.3, 9.4 $V^2/(d.u.)^{2/3}$ and $0.7154V^2$. Values for other parameters are taken from Ferro and Saccone (Ferro & Saccone, 2008), as shown in Table A1.1.

The calculated enthalpies of mixing of the liquid phase for all the RE-Zn systems are shown in Table A1.2. The calculations are in good agreement with the enthalpies of mixing of the liquid phase derived from vapor pressure data. As an example, the calculated enthalpy of mixing of the liquid phase in the Sm-Zn system is shown in Fig. A1.1 with experimental data and calculated data points from the Miedema Model.

The calculated enthalpy of formation of the solid phases differs from the experimental data and thus was not used in the present work. it will not be presented here.

Table A1.1 Miedema Model. The values of the model parameters Φ*, $n_{WS}^{1/3}$ and $V^{2/3}$

H 5.20 1.50 1.42															
Li 2.85 0.98 5.53	Be 5.05 1.67 2.88					El Φ* $n_{ws}^{1/3}$ $V^{2/3}$						B 5.30 1.75 2.80	C 6.24 1.77 2.20	N 6.86 1.65 2.56	O
Na 2.70 0.82 8.27	Mg 3.45 1.17 5.81											Al 4.20 1.39 4.64	Si 4.70 1.50 4.20	P 5.55 1.65 4.15	S
K 2.25 0.65 12.77	Ca 2.55 0.91 8.82	Sc 3.25 1.27 6.09	Ti 3.80 1.52 4.82	V 4.25 1.64 4.12	Cr 4.65 1.73 3.74	Mn 4.45 1.61 3.78	Fe 4.93 1.77 3.69	Co 5.10 1.75 3.55	Ni 5.20 1.75 3.52	Cu 4.45 1.47 3.70	Zn 4.10 1.32 4.38	Ga 4.10 1.31 5.19	Ge 4.55 1.37 4.60	As 4.80 1.44 5.20	Se
Rb 2.10 0.60 14.65	Sr 2.40 0.84 10.48	Y 3.20 1.21 7.34	Zr 3.45 1.41 5.81	Nb 4.05 1.64 4.89	Mo 4.65 1.77 4.45	Tc 5.30 1.81 4.21	Ru 5.40 1.83 4.06	Rh 5.40 1.76 4.10	Pd 5.45 1.67 4.29	Ag 4.35 1.36 4.72	Cd 4.05 1.24 5.53	In 3.90 1.17 6.28	Sn 4.15 1.24 6.43	Sb 4.40 1.26 6.60	Te
Cs 1.95 0.55 16.86	Ba 2.32 0.81 11.32	La 3.17 1.18 7.98	Hf 3.60 1.45 5.65	Ta 4.05 1.63 4.89	W 4.80 1.81 4.50	Re 5.20 1.85 4.28	Os 5.40 1.85 4.15	Ir 5.55 1.83 4.17	Pt 5.65 1.78 4.36	Au 5.15 1.57 4.70	Hg 4.20 1.24 5.83	Tl 3.90 1.12 6.67	Pb 4.10 1.15 6.94	Bi 4.15 1.16 7.20	Po
	Ce^{3+} 3.18 1.19 7.76	Pr 3.19 1.20 7.56	Nd 3.19 1.20 7.51	Pm 3.19 1.21 7.43	Sm 3.20 1.21 7.37	Eu^{3+} 3.20 1.21 7.36	Gd 3.20 1.21 7.34	Tb 3.21 1.22 7.20	Dy 3.21 1.22 7.12	Ho 3.22 1.22 7.06	Er 3.22 1.23 6.98	Tm 3.22 1.23 6.90	Yb^{3+} 3.22 1.23 6.86	Lu 3.22 1.24 6.81	
	Th 3.30 1.28 7.32	Pa 3.60	U 3.90 1.51 5.57	Np 3.85	Pu 3.80 1.44 5.26						Ce^{4+} 3.25 1.34 6.36		Eu^{2+} 2.50 0.88 9.43	Yb^{2+} 2.58 0.92 8.52	

Table A1.2 Calculated enthalpy of mixing for the liquid phase at different composition for all the RE-Zn systems from the Miedema Model (kJ/mol-atom)

	0	0.1	0.2	0.3	0.4	0.5	0.6	0.7	0.8	0.9	1
Sc	0	-9.17	-16.79	-22.71	-26.78	-28.8	-28.59	-25.89	-20.44	-11.93	0
Y	0	-9.04	-16.78	-23.03	-27.59	-30.19	-30.53	-28.21	-22.77	-13.62	0
La	0	-8.87	-16.55	-22.85	-27.56	-30.38	-30.97	-28.88	-23.56	-14.26	0
Ce	0	-8.94	-16.65	-22.95	-27.61	-30.36	-30.86	-28.7	-23.33	-14.06	0
Pr	0	-9	-16.73	-23.01	-27.63	-30.32	-30.74	-28.5	-23.09	-13.87	0
Nd	0	-8.99	-16.71	-22.98	-27.58	-30.24	-30.65	-28.39	-22.98	-13.79	0
Pm	0	-9.16	-17.02	-23.39	-28.04	-30.72	-31.09	-28.77	-23.26	-13.94	0
Sm	0	-9.04	-16.79	-23.05	-27.62	-30.24	-30.58	-28.28	-22.84	-13.67	0
Eu	0	-9.04	-16.79	-23.05	-27.61	-30.22	-30.56	-28.26	-22.82	-13.65	0
Gd	0	-9.04	-16.78	-23.03	-27.59	-30.19	-30.53	-28.21	-22.77	-13.62	0
Tb	0	-9.08	-16.83	-23.07	-27.59	-30.14	-30.42	-28.05	-22.59	-13.48	0
Dy	0	-9.08	-16.81	-23.02	-27.5	-30.01	-30.25	-27.87	-22.41	-13.35	0
Ho	0	-8.96	-16.58	-22.69	-27.09	-29.54	-29.75	-27.38	-22	-13.09	0
Er	0	-9.1	-16.83	-23.02	-27.46	-29.92	-30.1	-27.66	-22.19	-13.18	0
Tm	0	-9.1	-16.81	-22.97	-27.37	-29.78	-29.93	-27.47	-22.01	-13.06	0
Yb	0	-9.09	-16.79	-22.94	-27.32	-29.72	-29.84	-27.38	-21.92	-12.99	0
Lu	0	-9.23	-17.04	-23.26	-27.69	-30.09	-30.2	-27.68	-22.14	-13.11	0

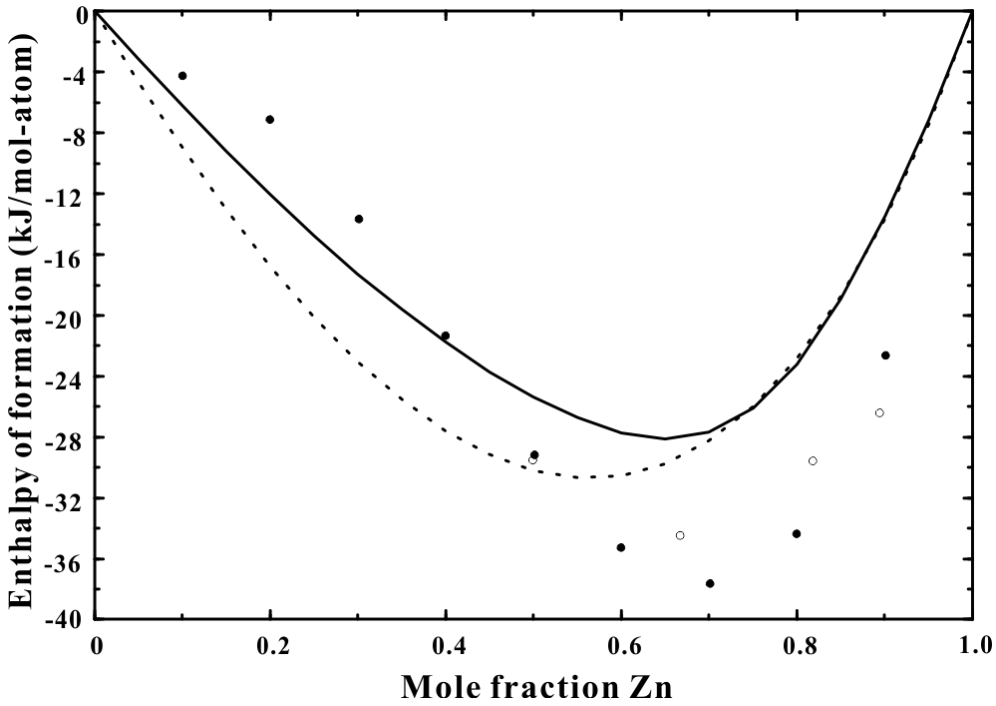

Figure A1.1 The calculated enthalpy of mixing of the liquid phase for the Sm-Zn system at 1600°C compared to calculation from the Miedema Model (dashed line) along with data points from Chiotti et al (Chiotti & Mason, 1967).

The calculated enthalpy of formation of the solid phases is far away from the experimental data and thus was not used in the present work and also will not be presented here.

APPENDIX 2 – APPLICATION OF THE DATABASE-SCHEIL COOLING SIMULATION

As an example of the application of the current thermodynamic database, the solidification of two samples (Mg-6Zn-1.2Y and Mg-5Zn-2Y) were analyzed and compared to experimental data. The two samples were analyzed previously by Farzadfar *et al* (Farzadfar, Sanjari, Jung, Essadiqi, & Yue, 2012). They concluded that the as-cast microstructure of the two alloys is close to the equilibrium state rather than to the Scheil cooling assumption. More often than not, Scheil cooling provides more realistic estimations for the as-cast alloy. Calculations based on the current thermodynamic database is provided here for comparison with the experimental data.

The amount of all possible phases predicted by the Scheil cooling calculation for the two alloys is presented in Figs. A2.1 and A2.2. Using the same density data as Farzadfar *et al* (Farzadfar, Sanjari, Jung, Essadiqi, & Yue, 2012), the volume fractions of different precipitates in the two samples are calculated. The calculated results are shown in Table A2.1 with experimental data and calculation from Farzadfar *et al* (Farzadfar, et al., 2012).

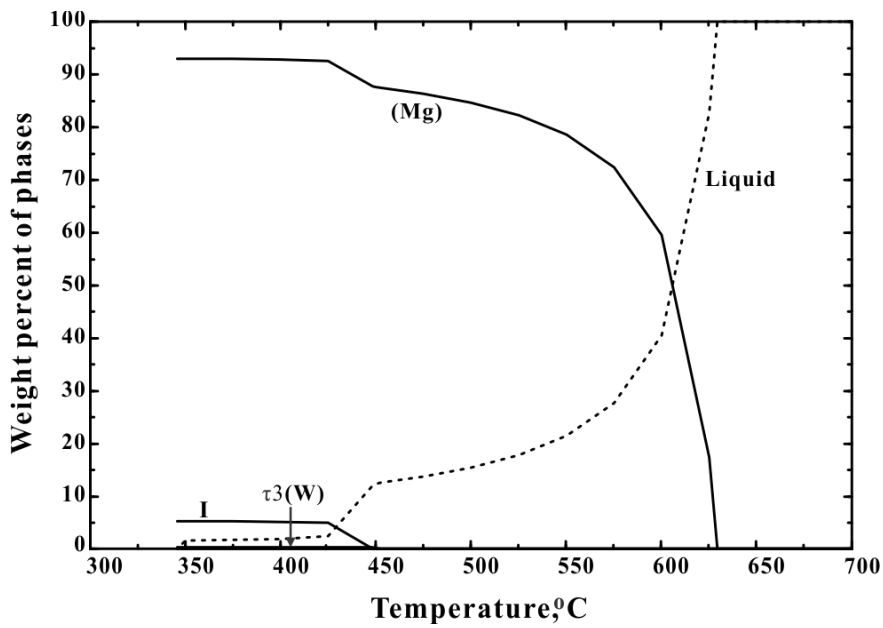

Figure A2.1 The calculated phase amount using Scheil cooling assumption for Mg-6Zn-1.2Y

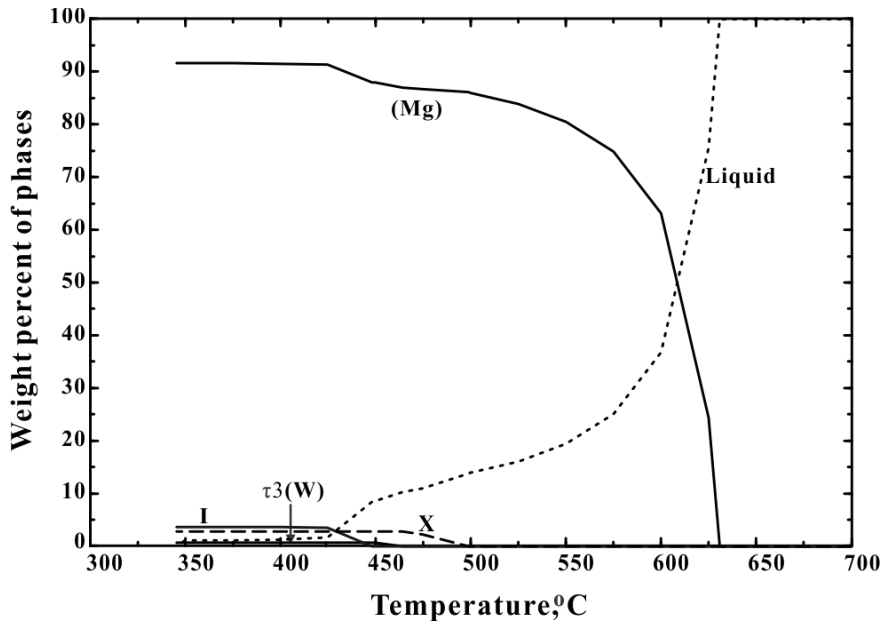

Figure A2.2 The calculated phase amount using Scheil cooling assumption for Mg-5Zn-2Y

Table A2.1 Calculated and experimental volume percent of precipitates in the as cast alloy

As cast alloy	method	(Mg)	I	W (τ3)	Mg_7Zn_3	X	Z (τ5)	
Mg-6Zn-1.2Y	Scheil	95.31	0.14	1.25	3.3	0	0	
		97.91	1.91	0.18	0	0	0	*
	Equilibrium	97.07	2.46	0	0	0	0.47	
		97.81	0.73	1.46	0	0	0	*
	Experimental	97.5	2.5	0	0	0	0	
Mg-5Zn-2Y	Scheil	96.7	0.05	2.07	1.18	0	0	
		95.22	1.32	0.58	0	2.88	0	*
	Equilibrium	96.87	0.63	2.5	0	0	0	
		95.96	1.30	0	0	2.74	0	*
	Experimental	97.6	1.37	1.03	0	0	0	

*This work

The density of X phase is considered as the same of Mg here.

As can be seen from the Table, Scheil cooling predictions from the present calculation are closer to the experimental results, which is as expected. The X phase is a long period stacking ordered phase which has a complex structure. Given that the amount of this phase is small and

that the structure of this phase is very complex (the limited total scattering for this phase are distributed over many peaks), it may not be detected by XRD and thus was not reported by Farzadfar *et al* (Farzadfar, et al., 2012).

We may conclude that Scheil cooling calculations from the present database apply to the above mentioned as-cast alloy.

APPENDIX 3 – DIFFRACTION PATTERNS OF ALL SAMPLES

$Ce_{40}Mg_{10}Zn_{50}$

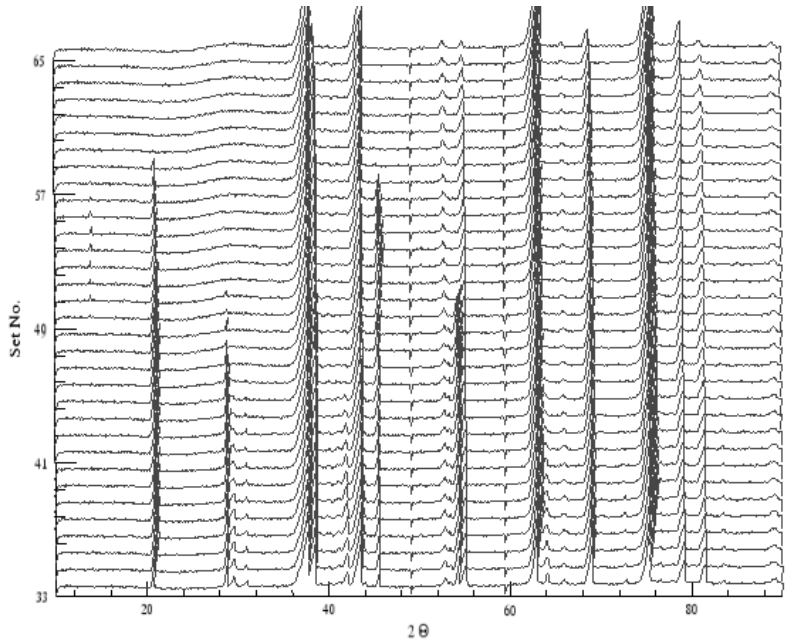

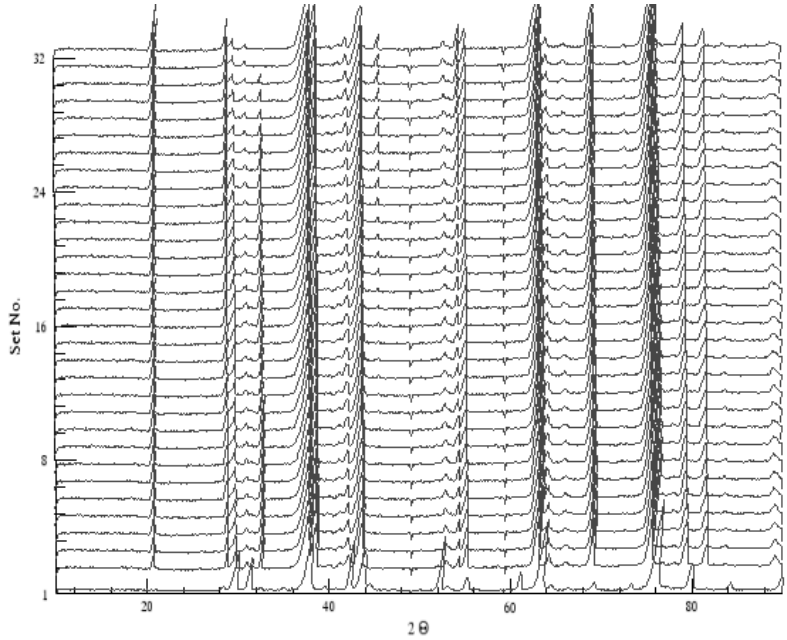

Figure A3.1 NPD diffraction patterns for $Ce_{40}Mg_{10}Zn_{50}$ from 760-445°C (every 5°C) along with the one collected at room temperature

$Ce_{16}Mg_{40}Zn_{44}$

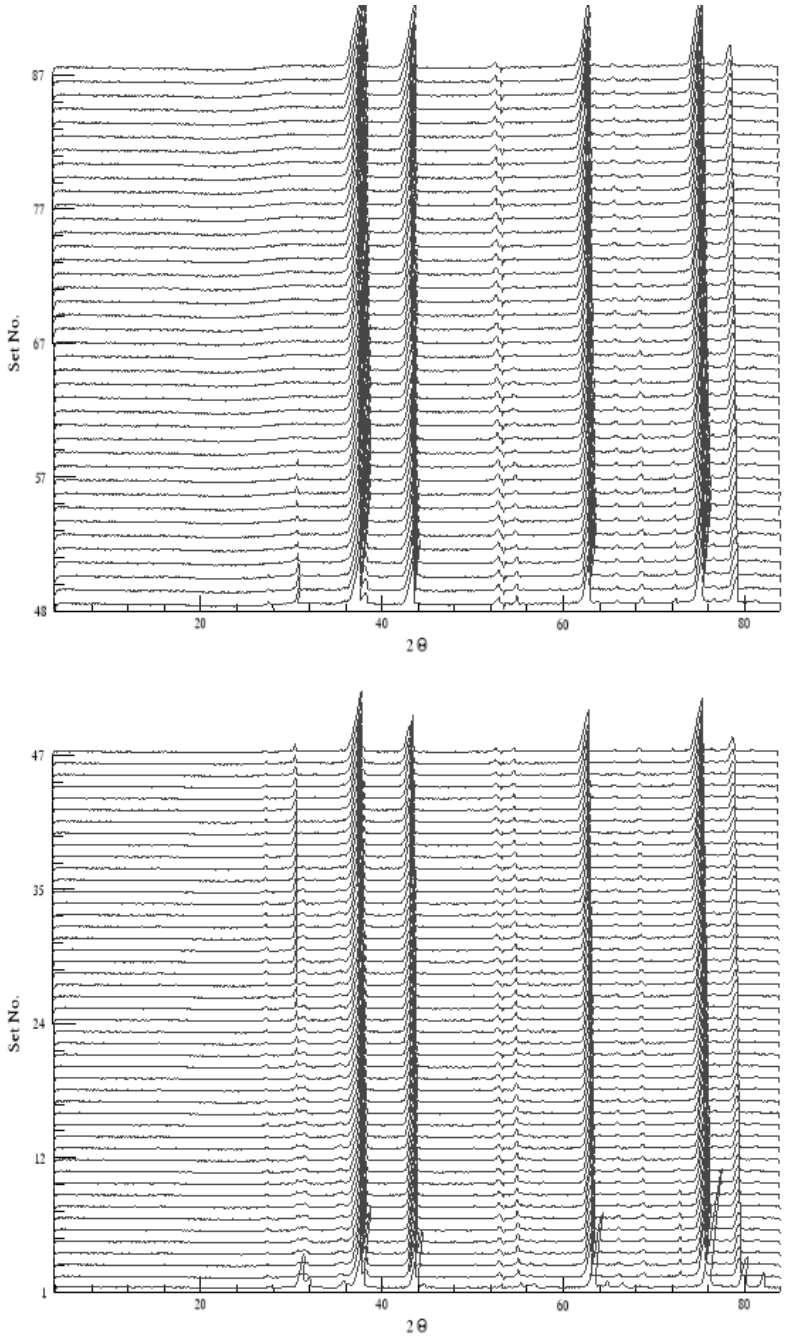

Figure A3.2 NPD diffraction patterns for $Ce_{16}Mg_{40}Zn_{44}$ from 795-365°C (every 5°C) along with the one collected at room temperature

$Ce_4Mg_{58}Zn_{38}$

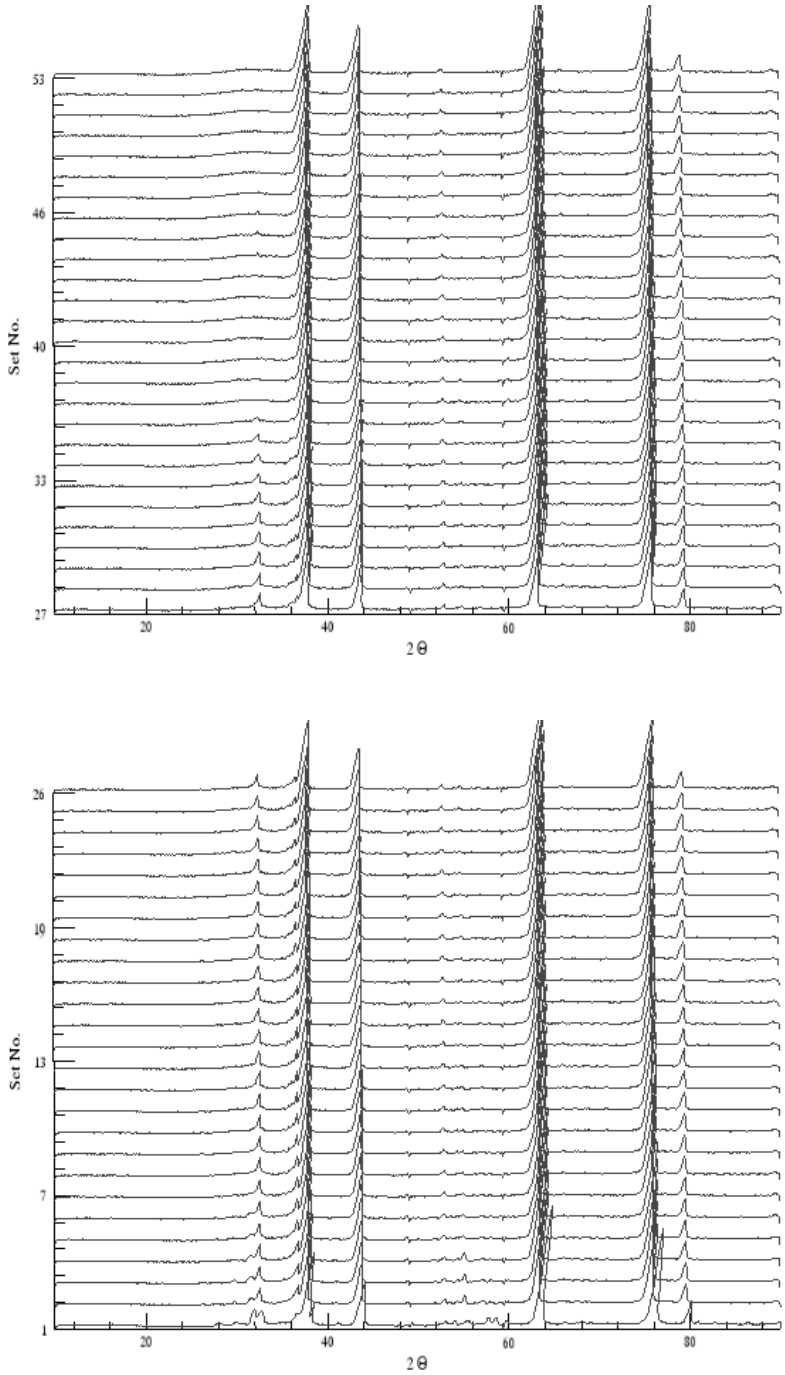

Figure A3.3 NPD diffraction patterns for $Ce_4Mg_{58}Zn_{38}$ from 580-325°C (every 5°C) along with the one collected at room temperature

$Ce_{20}Mg_{22}Zn_{58}$

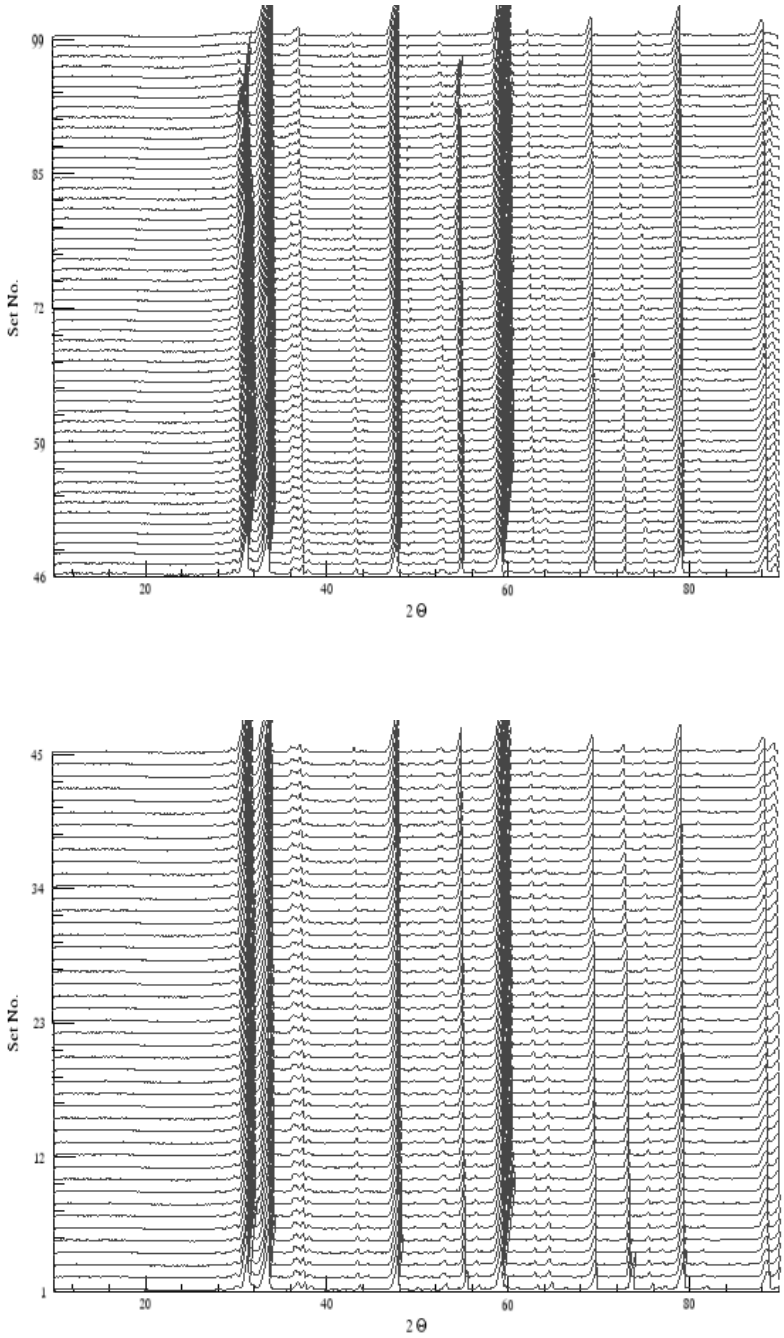

Figure A3.4 NPD diffraction patterns for $Ce_{20}Mg_{22}Zn_{58}$ from 735-250°C (every 5°C) along with the one collected at room temperature

$Nd_{15}Mg_{65}Zn_{20}$

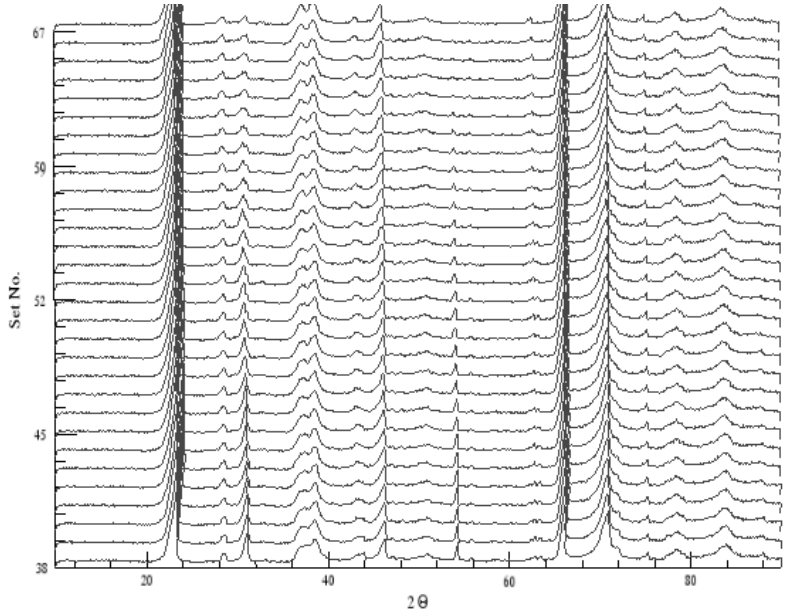

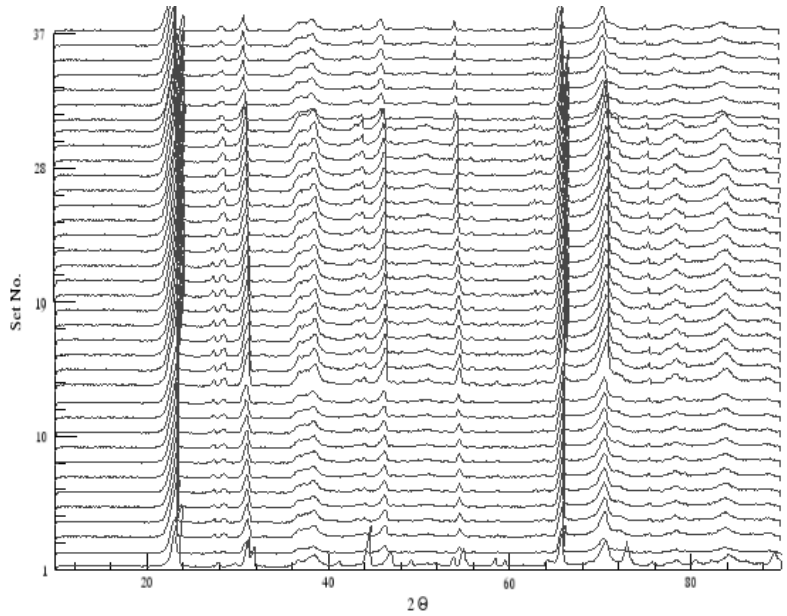

Figure A3.5 NPD diffraction patterns for $Nd_{15}Mg_{65}Zn_{20}$ from 750-400°C (every 5°C) along with the one collected at room temperature

$Nd_{16}Mg_{37}Zn_{47}$

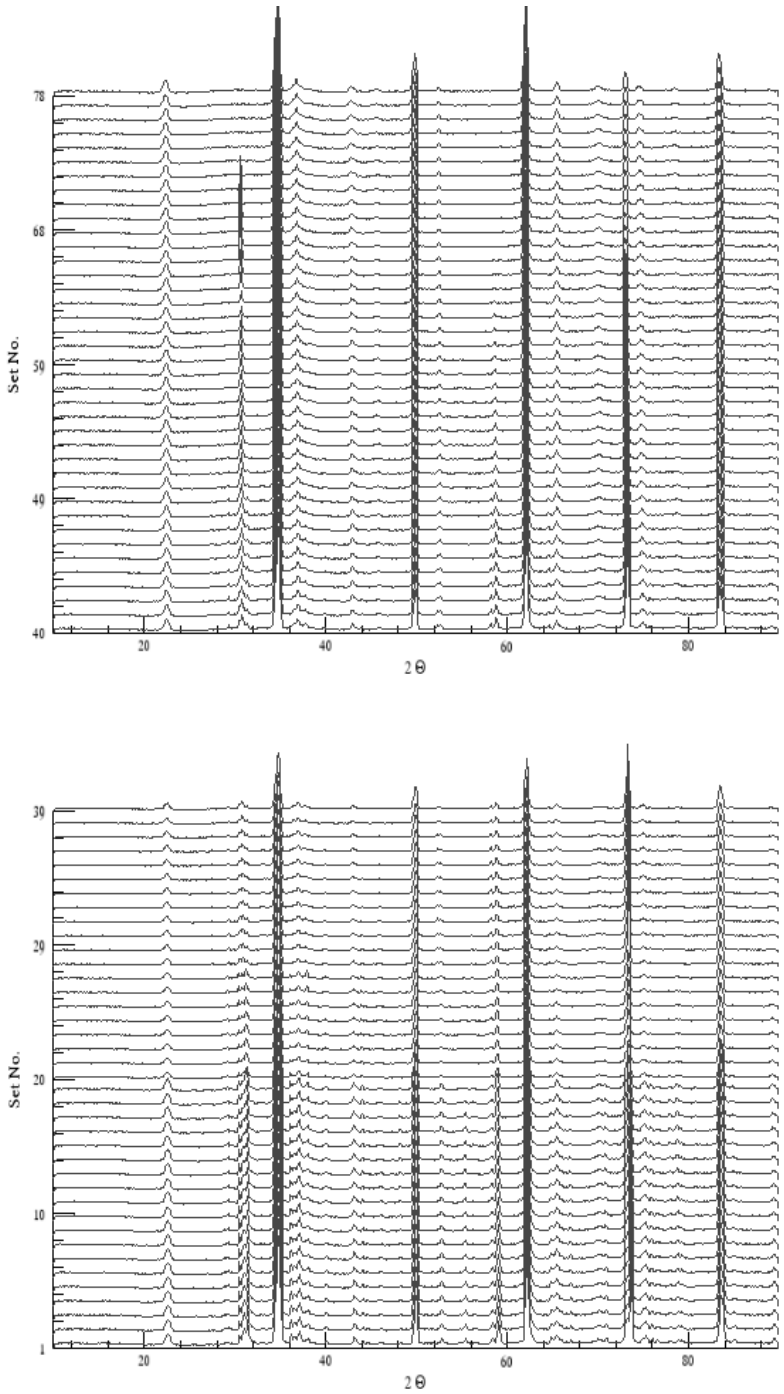

Figure A3.6 NPD diffraction patterns for $Nd_{16}Mg_{37}Zn_{47}$ from 770-380°C (every 5°C)

$Nd_6Mg_{41}Zn_{53}$

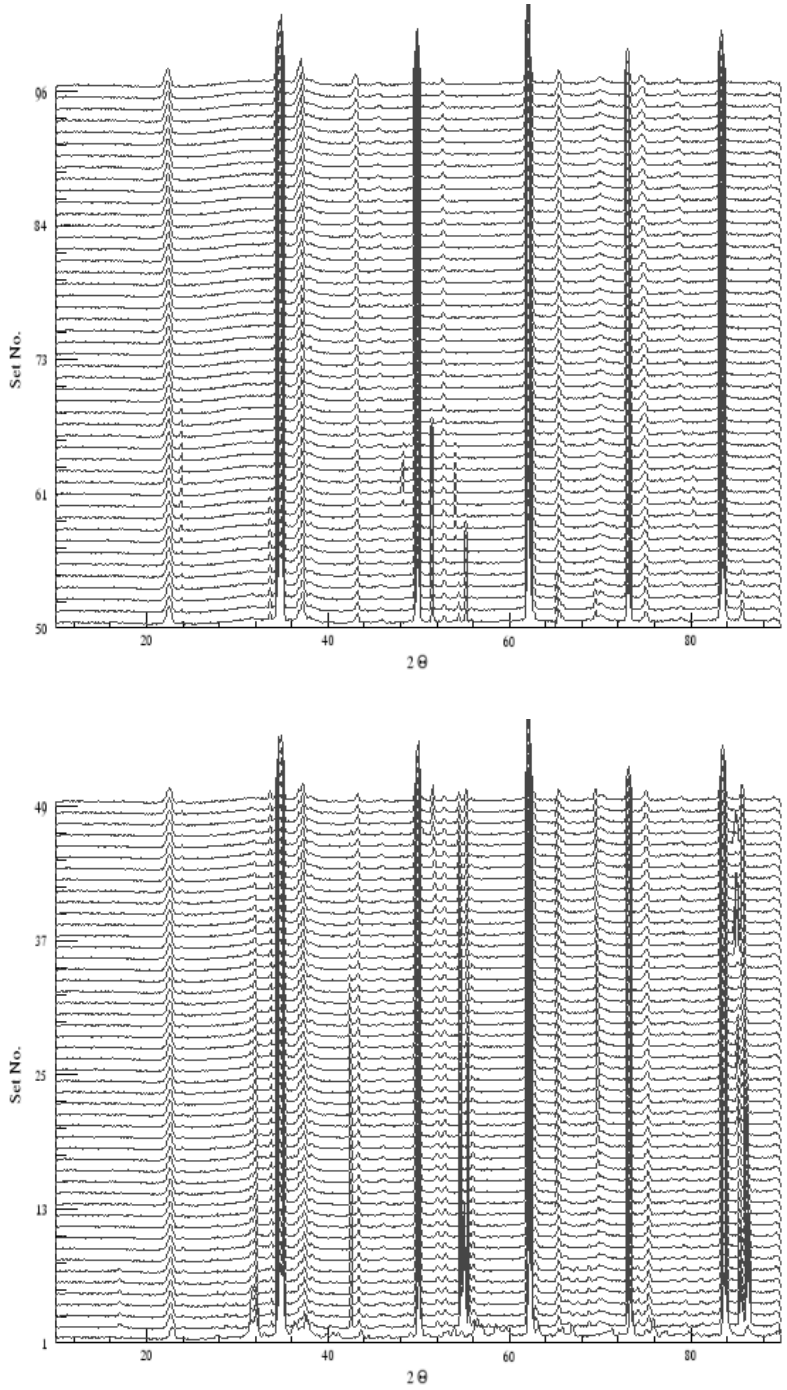

Figure A3.7 NPD diffraction patterns for $Nd_6Mg_{41}Zn_{53}$ from 770-300°C (every 5°C) along with the one collected at room temperature

$Nd_{20}Mg_{20}Zn_{60}$

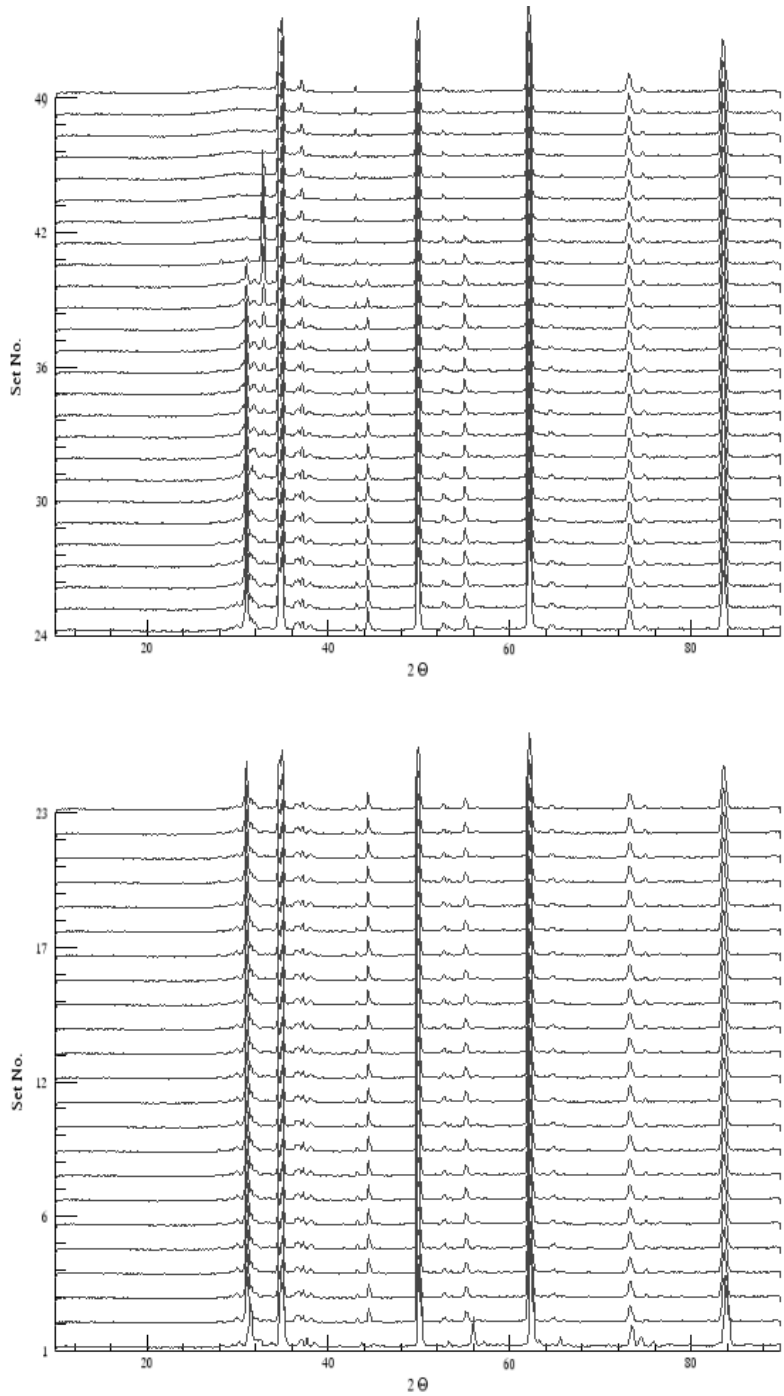

Figure A3.8 NPD diffraction patterns for $Nd_{20}Mg_{20}Zn_{60}$ from 765-530°C (every 5°C) along with the one collected at room temperature

APPENDIX 4 – COEFFICIENT OF LINEAR EXPANSION OF TA AND MO AT HIGH TEMPERATURES

In our neutron powder diffraction experiments, diffraction data were collected every 5° C from 300°C or 500°C to more than 700°C for different samples. Although lattice constants are usually not refined for the new phases from the sample due to the limited number of peaks and their low intensities, the lattice constant for the crucibles can be refined because peaks from the crucibles were usually very strong, especially for the Ta and Mo crucibles.

When the lattice constants at different temperatures are known, the expansion coefficients can be computed. So far, very few experiments have been carried out to measure the expansion coefficients of Ta and Mo and no report on the thermal expansion coefficients in the temperature range of 500-800 ^{o}C can be found in the literature.

The linear expansion in one dimension (length) is expressed as:

$$\Delta L = \alpha L_0 \Delta T \qquad \text{(A4-1)}$$

where ΔL is the change in length, α is the thermal expansion coefficient at a selected temperature, L_0 is the length of the object at the selected temperature and ΔT is the change in temperature.

Tantalum

The coefficient of linear expansion for Tantalum at 25 ^{o}C was reported as 6.3×10^{-6} K^{-1} (Haynes, 2015). The lattice constant of Ta refined from the present experiment are shown in Table A4.1 and Fig A4.1. Linear fitting of the experimental data in the temperature range 250-735 ^{o}C gives the following expression for the lattice constant:

$$L = a + bT = 3.30744 + 2.18017\times10^{-5}T \qquad \text{(A4-2)}$$

The thermal expansivity at any temperature can be expressed as:

$$\alpha = \frac{\Delta L}{L\bullet\Delta T} = \frac{b\bullet\Delta T}{L\bullet\Delta T} = \frac{b}{a+bT} \qquad \text{(A4-3)}$$

Table A4.1. Refined lattice constant for Ta (crucible for sample $Ce_{20}Mg_{22}Zn_{58}$) in the temperature range of 250-735°C (every 5°C)

T-C	lattice constant (nm)	T-C	lattice constant (nm)	T-C	lattice constant (nm)
735	3.32358	730	3.323529	725	3.323302
720	3.32321	715	3.323186	710	3.323163
705	3.323014	700	3.322864	695	3.322518
690	3.322513	685	3.322452	680	3.322299
675	3.322246	670	3.32223	665	3.322129
660	3.321866	655	3.321935	650	3.321814
645	3.321625	640	3.32151	635	3.321502
630	3.321398	625	3.321346	620	3.321195
615	3.321202	610	3.321104	605	3.321073
600	3.32087	595	3.320909	590	3.320829
585	3.320796	580	3.320774	575	3.320657
570	3.320606	565	3.320335	560	3.320043
555	3.320038	550	3.319899	545	3.319787
540	3.319621	535	3.319539	530	3.319386
525	3.319333	520	3.319216	515	3.319132
510	3.319004	505	3.318942	500	3.318804
495	3.318707	490	3.318523	485	3.318425
480	3.31828	475	3.318249	470	3.31817
465	3.317953	460	3.317924	455	3.317813
450	3.317583	445	3.317546	440	3.317495
435	3.317293	430	3.317152	425	3.317069
420	3.316907	415	3.316775	410	3.316722
405	3.316531	400	3.316428	395	3.316406
390	3.316217	385	3.316203	380	3.316110
375	3.316016	370	3.315926	365	3.315714
360	3.315585	355	3.315569	350	3.315413
345	3.315269	340	3.315167	335	3.314963
330	3.314860	325	3.314710	320	3.314637
315	3.314551	310	3.314465	305	3.314317
300	3.314261	295	3.314058	290	3.313928
285	3.313701	280	3.313658	275	3.313546
270	3.313357	265	3.313285	260	3.313203
255	3.313096	250	3.312900	20	3.307548

The average coefficient of linear expansion for tantalum in the temperature range of 250-735 ^{o}C can be calculated as 6.58×10^{-6} K^{-1}; this value is very close to the reported value at room temperature.

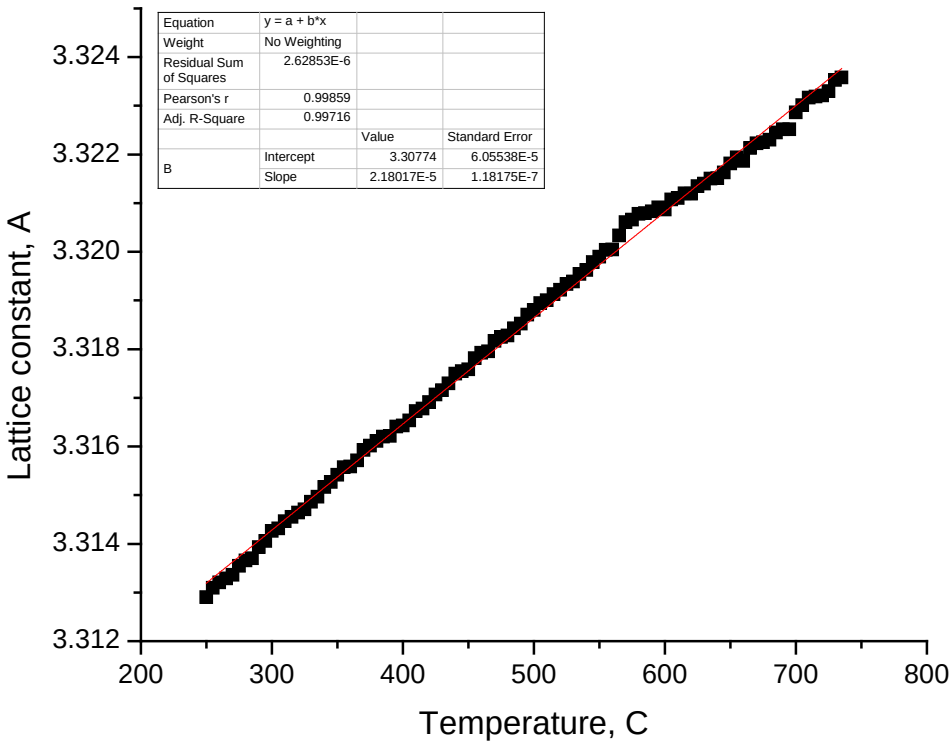

Figure A4.1 Refined lattice constant of Ta at different temperatures

Molybdenum

The coefficient of linear expansion for Mo at 25°C was reported as 4.8×10^{-6} K^{-1} (Haynes, 2015). The lattice constant of Mo refined from present experiments are shown in Table A4.2 and fig A4.2. Linear fitting of the experimental data in the temperature range 530-765 ^{o}C gives the following expression for the lattice constant:

$$L = a + bT = 3.14476 + 2.10448\times10^{-5}T \qquad \text{(A4-4)}$$

The thermal expansivity at any temperature can be expressed by Eq (A4-3)

Table A4.2 Refined lattice constant for Mo (crucible for sample $Nd_{20}Mg_{20}Zn_{60}$) at in the temperature range of 530-765°C (every 5°C)

T-C	lattice constant (nm)	T-C	lattice constant (nm)	T-C	lattice constant (nm)
765	3.160992	760	3.160789	755	3.160637
750	3.160596	745	3.160475	740	3.160369
735	3.160340	730	3.160146	725	3.160081
720	3.159866	715	3.159755	710	3.159552
705	3.159559	700	3.159455	695	3.159357
690	3.159253	685	3.159148	680	3.159045
675	3.158934	670	3.158893	665	3.158789
660	3.158578	655	3.158564	650	3.158383
645	3.158353	640	3.158250	635	3.158018
630	3.157980	625	3.157898	620	3.157833
615	3.157683	610	3.157560	605	3.157432
600	3.157356	595	3.157294	590	3.157123
585	3.156997	580	3.156968	575	3.156855
570	3.156747	565	3.156658	560	3.156459
555	3.156443	550	3.156373	545	3.156278
540	3.156242	535	3.156107	530	3.156023
20	3.148133				

The average coefficient of linear expansion for Mo in the temperature range 530-765 °C can be calculated as 6.67×10^{-6} K^{-1}; this value is significantly larger than that at room temperature. However, the coefficient of linear expansion for Mo at higher temperature is larger than that at room temperature. According to Hidnert (Hidnert, 1929), the coefficient of linear expansion for Mo ranges from 5.7 to 7.4×10^{-6} K^{-1} in the temperature range 400-500 °C for different Mo samples. Values of the coefficient of linear expansion at lower temperatures were also reported, which are less than those at higher temperatures. In our experiment, the temperature range is even higher. Consequently, the value obtained in the present work is reasonable.

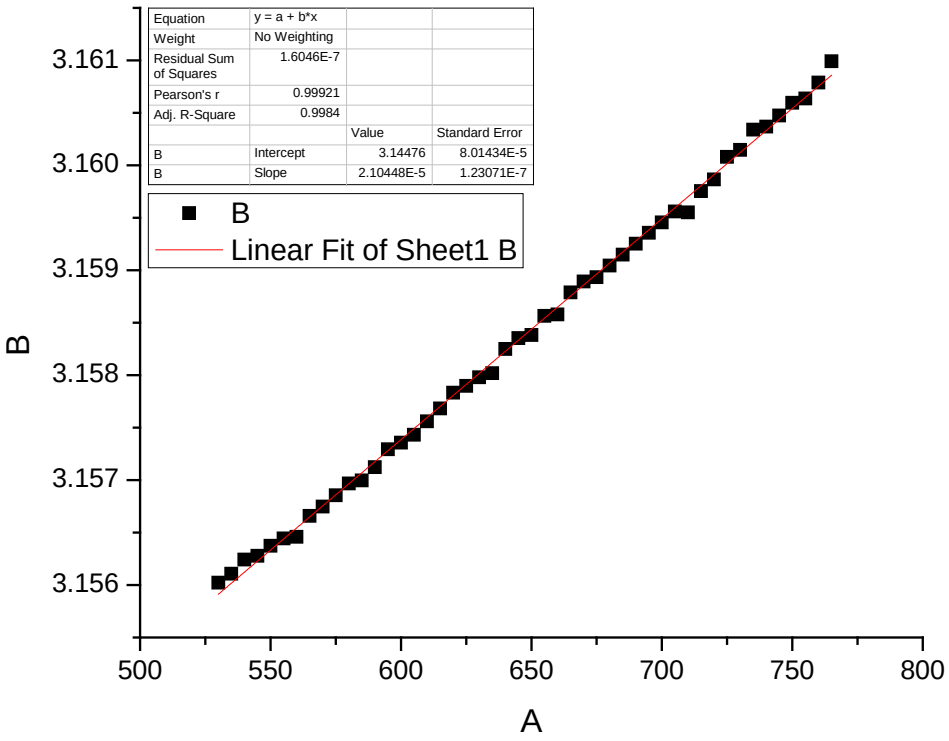

Figure A4.2 Refined lattice constant of Mo at different temperatures

APPENDIX 5 – CALCULATED LIQUIDUS PROJECTIONS AND INVARIANT REACTIONS IN THE OPTIMIZED RE-MG-ZN SYSTEMS

La-Mg-Zn system

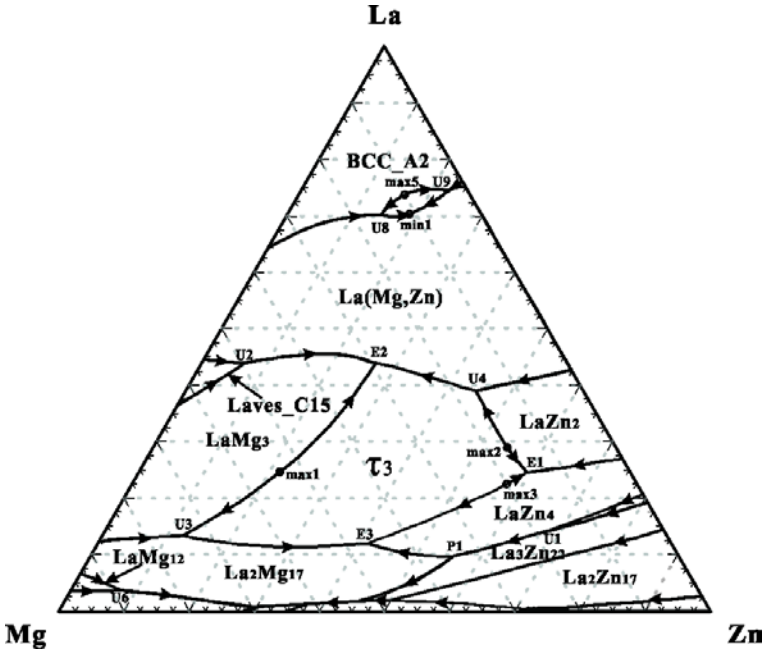

Figure A5.1 Tentative calculated liquidus projection for La-Mg-Zn system (mole fraction)

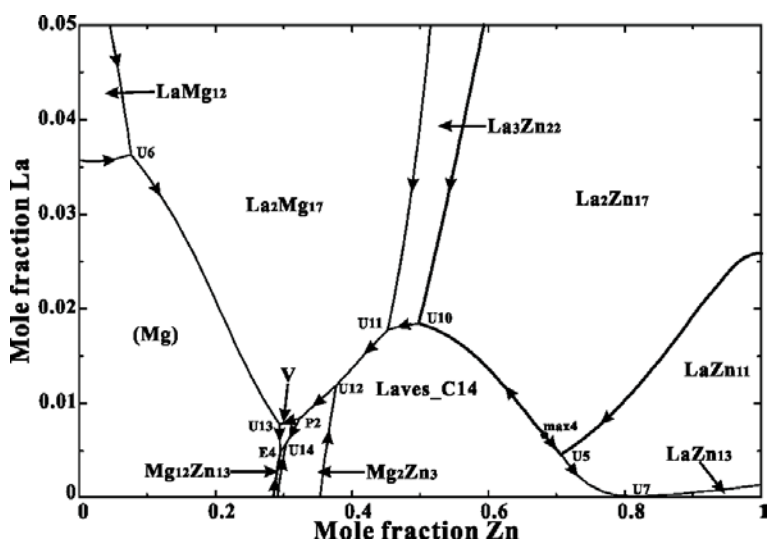

Figure A5.2 Enlargement of part of Fig. A5.1

Table A5.1 Tentative calculated invariant reactions, maxima and minima in the La-Mg-Zn system

Type	**Temperature (^{o}C)**	**Reaction**
U1	742	$L + LaZn_5 \rightarrow LaZn_4 + La_3Zn_{22}$
U2	701	$L + Laves_C15 \rightarrow La(Mg, Zn) + LaMg_3$
E1	691	$L \rightarrow LaZn_2 + LaZn_4 + \tau 3$
U3	638	$L + LaMg_3 \rightarrow La_2Mg_{17} + \tau 3$
U4	634	$L + LaZn_2 \rightarrow La(Mg, Zn) + \tau 3$
P1	625	$L + LaZn_4 + La_3Zn_{22} \rightarrow La_2Mg_{17}$
E2	602	$L \rightarrow La(Mg, Zn) + LaMg_3 + \tau 3$
E3	591	$L \rightarrow \tau 3 + LaZn_4 + La_2Mg_{17}$
U5	582	$L + La_2Zn_{17} \rightarrow Laves_C14 + LaZn_{11}$
U6	566	$L + LaMg_{12} \rightarrow (Mg) + La_2Mg_{17}$
U7	536	$L + LaZn_{11} \rightarrow Laves_C14 + LaZn_{13}$
U8	517	$L + Bcc_A2 \rightarrow La(Mg, Zn) + Fcc_A1$
U9	517	$L + Bcc_A2 \rightarrow La(Mg, Zn) + Fcc_A1$
U10	501	$L + La_2Zn_{17} \rightarrow La_3Zn_{22} + Laves_C14$
U11	464	$L + La_3Zn_{22} \rightarrow La_2Mg_{17} + Laves_C14$
U12	402	$L + Laves_C14 \rightarrow La_2Mg_{17} + Mg_2Zn_3$
P2	385	$L + La_2Mg_{17} + Mg_2Zn_3 \rightarrow V$
U13	350	$L + La_2Mg_{17} \rightarrow V + (Mg)$
U14	345	$L + Mg_2Zn_3 \rightarrow V + Mg_{12}Zn_{13}$
U15	340	$L + Mg_{12}Zn_{13} \rightarrow V + Mg_{51}Zn_{20}$
E4	340	$L \rightarrow (Mg) + V + Mg_{51}Zn_{20}$
max1	~750	$L \rightarrow LaMg_3 + \tau 3$
max2	~719	$L \rightarrow LaZn_2 + \tau 3$
max3	~696	$L \rightarrow LaZn_4 + \tau 3$
max4	~584	$L \rightarrow Laves_C14 + La_2Zn_{17}$
max5	~559	$L \rightarrow Bcc_A2 + Fcc_A1$
min1	~493	$L \rightarrow Bcc_A2 + Fcc_A1$

Ce-Mg-Zn system

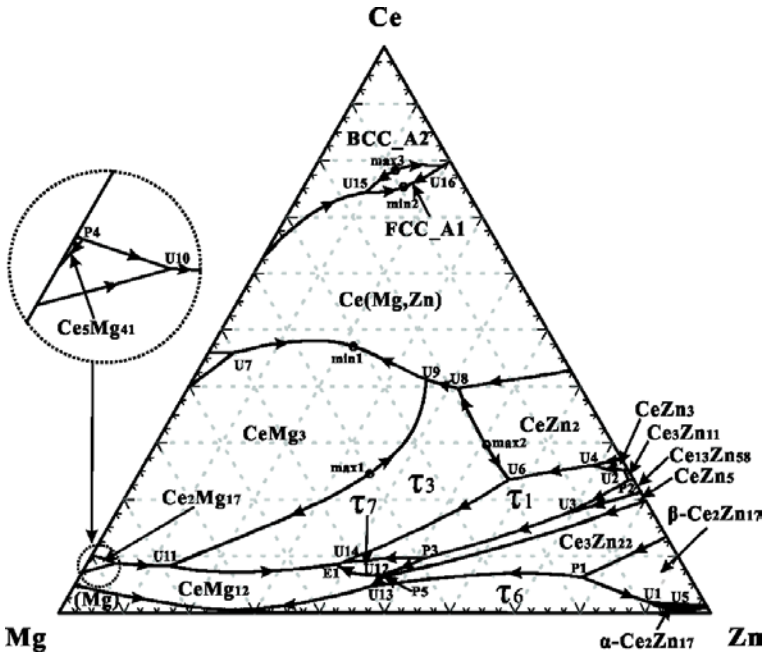

Figure A5.3 Tentative calculated liquidus projection for Ce-Mg-Zn system (mole fraction)

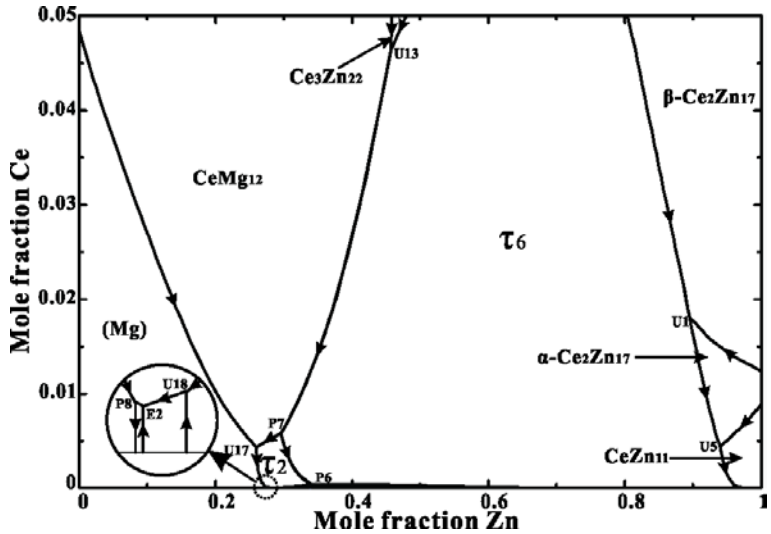

Figure A5.4 Enlargement of part of Fig. A5.3

Table A5.2 Tentative calculated invariant reactions, maxima and minima in the Ce-Mg-Zn system

Type	**Temperature (^{o}C)**	**Reaction**
P1	849	$L + Ce_3Zn_{22} \rightarrow \beta - Ce_2Zn_{17} + \tau 6$
P2	833	$L + Ce_3Zn_{11} + Ce_{13}Zn_{58} \rightarrow \tau 1$
U1	818	$L + \beta - Ce_2Zn_{17} \rightarrow \alpha - Ce_2Zn_{17} + \tau 6$
U2	816	$L + Ce_3Zn_{11} \rightarrow CeZn_3 + \tau 1$
U3	781	$L + Ce_{13}Zn_{58} \rightarrow CeZn_5 + \tau 1$
U4	775	$L + CeZn_3 \rightarrow CeZn_2 + \tau 1$
U5	751	$L + \alpha - Ce_2Zn_{17} \rightarrow CeZn_{11} + \tau 6$
U6	709	$L + CeZn_2 \rightarrow \tau 1 + \tau 3$
U7	697	$L + Laves_C15 \rightarrow CeMg_3 + Ce(Mg, Zn)$
U8	656	$L + CeZn_2 \rightarrow Ce(Mg, Zn) + \tau 3$
U9	550	$L + \tau 3 \rightarrow Ce(Mg, Zn) + CeMg_3$
P3	639	$L + \tau 1 + CeZn_5 \rightarrow \tau 7$
P4	622	$L + CeMg_3 + Ce_5Mg_{41} \rightarrow Ce_2Mg_{17}$
U10	601	$L + Ce_2Mg_{17} \rightarrow CeMg_{12} + CeMg_3$
U11	594	$L + CeMg_3 \rightarrow CeMg_{12} + \tau 3$
P5	592	$L + Ce_3Zn_{22} \rightarrow CeMg_{12} + CeZn_5$
U12	591	$L + CeZn_5 \rightarrow CeMg_{12} + \tau 7$
U13	584	$L + Ce_3Zn_{22} \rightarrow CeMg_{12} + \tau 6$
U14	580	$L + \tau 1 \rightarrow \tau 3 + \tau 7$
E1	574	$L \rightarrow \tau 3 + \tau 7 + CeMg_{12}$
U15	502	$L + Bcc_B2 \rightarrow Ce(Mg, Zn) + Fcc_A1$
U16	498	$L + Bcc_B2 \rightarrow Ce(Mg, Zn) + Fcc_A1$
P6	416	$L + \tau 2 + \tau 6 \rightarrow Laves_C15$
P7	410	$L + CeMg_{12} + \tau 6 \rightarrow \tau 2$
U17	386	$L + CeMg_{12} \rightarrow \tau 2 + (Mg)$
U18	351	$L + Mg_2Zn_3 \rightarrow \tau 2 + Mg_{12}Zn_{13}$
P8	346	$L + \tau 2 + (Mg) \rightarrow Mg_{51}Zn_{20}$
E2	346	$L \rightarrow Mg_{51}Zn_{20} + \tau 2 + Mg_{12}Zn_{13}$
max1	~782	$L \rightarrow CeMg_3 + \tau 3$
max2	~743	$L \rightarrow CeZn_2 + \tau 3$
max3	~533	$L \rightarrow Bcc_B2 + Fcc_A1$
min1	~632	$L \rightarrow Ce(Mg, Zn) + CeMg_3$
min2	~484	$L \rightarrow Bcc_B2 + Fcc_A1$

Pr-Mg-Zn system

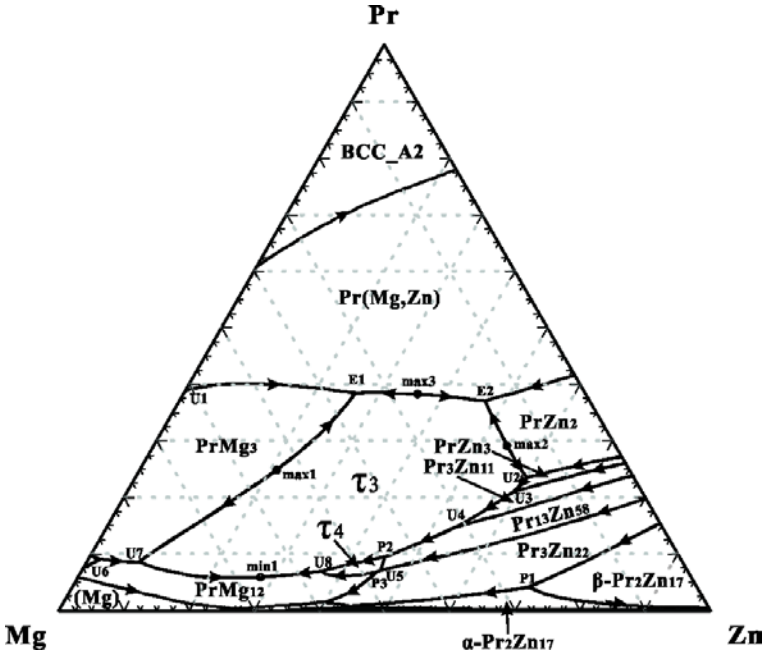

Figure A5.5 Tentative calculated liquidus projection for Pr-Mg-Zn system (mole fraction)

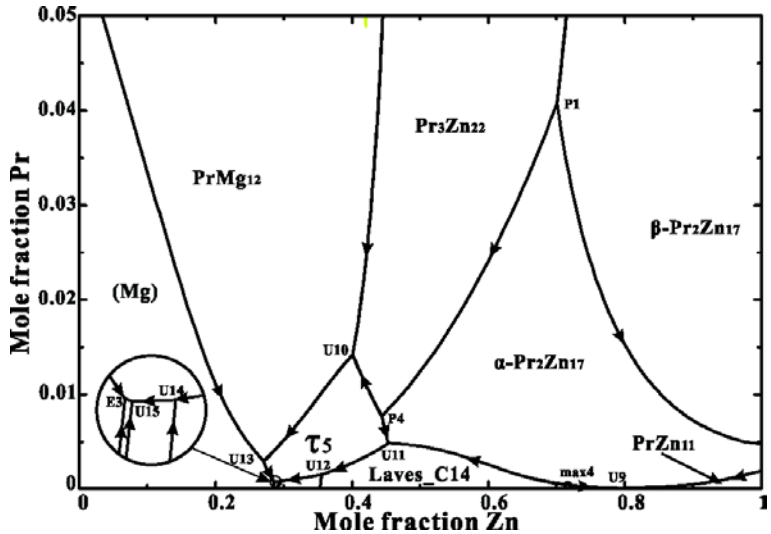

Figure A5.6 Enlargement of part of Fig. A5.5

Table A5.3 Tentative calculated invariant reactions, maxima and minima in the Pr-Mg-Zn system

Type	**Temperature (^{o}C)**	**Reaction**
P1	779	$L + Pr_3 Zn_{22} + \beta\text{-}Pr_2 Zn_{17} \rightarrow \alpha\text{-}Pr_2 Zn_{17}$
U1	737	$L + Laves_C15 \rightarrow Pr\,Mg_3 + Pr(Mg,Zn)$
U2	717	$L + Pr\,Zn_2 \rightarrow Pr\,Zn_3 + \tau 3$
E1	711	$L \rightarrow Pr(Mg,Zn) + Pr\,Mg_3 + \tau 3$
U3	708	$L + Pr\,Zn_3 \rightarrow Pr_3 Zn_{11} + \tau 3$
E2	698	$L \rightarrow Pr(Mg,Zn) + Pr\,Zn_2 + \tau 3$
U4	666	$L + Pr_3 Zn_{11} \rightarrow Pr_{13} Zn_{58} + \tau 3$
P2	602	$L + Pr_{13} Zn_{58} + \tau 3 \rightarrow \tau 4$
U5	594	$L + Pr_{13} Zn_{58} \rightarrow Pr_3 Zn_{22} + \tau 4$
P3	590	$L + Pr_3 Zn_{22} + \tau 4 \rightarrow Pr\,Mg_{12}$
U6	576	$L + Pr_5 Mg_{41} \rightarrow Pr\,Mg_3 + Pr\,Mg_{12}$
U7	575	$L + Pr\,Mg_3 \rightarrow + Pr\,Mg_{12} + \tau 3$
U8	569	$L + \tau 4 \rightarrow + Pr\,Mg_{12} + \tau 3$
U9	547	$L + \alpha\text{-}Pr_2 Zn_{17} \rightarrow Pr\,Zn_{11} + Laves_C14$
P4	509	$L + \alpha\text{-}Pr_2 Zn_{17} + Pr_3 Zn_{22} \rightarrow \tau 5$
U10	508	$L + Pr_3 Zn_{22} \rightarrow Pr\,Mg_{12} + \tau 5$
U11	497	$L + \alpha\text{-}Pr_2 Zn_{17} \rightarrow Laves_C14 + \tau 5$
U12	413	$L + Laves_C14 \rightarrow Mg_2 Zn_3 + \tau 5$
U13	369	$L + Pr\,Mg_{12} \rightarrow (Mg) + \tau 5$
U14	351	$L + Mg_2 Zn_3 \rightarrow Mg_{12} Zn_{13} + \tau 5$
U15	346	$L + Mg_{12} Zn_{13} \rightarrow Mg_{51} Zn_{20} + \tau 5$
E3	346	$L \rightarrow Mg_{51} Zn_{20} + \tau 5 + (Mg)$
max1	~783	$L \rightarrow Pr\,Mg_3 + \tau 3$
max2	~753	$L \rightarrow Pr\,Zn_2 + \tau 3$
max3	~715	$L \rightarrow Pr(Mg,Zn) + \tau 3$
max4	~592	$L \rightarrow Laves_C14 + \alpha - Pr_2 Zn_{17}$
min1	~562	$L \rightarrow Pr\,Mg_{12} + \tau 3$

Nd-Mg-Zn system

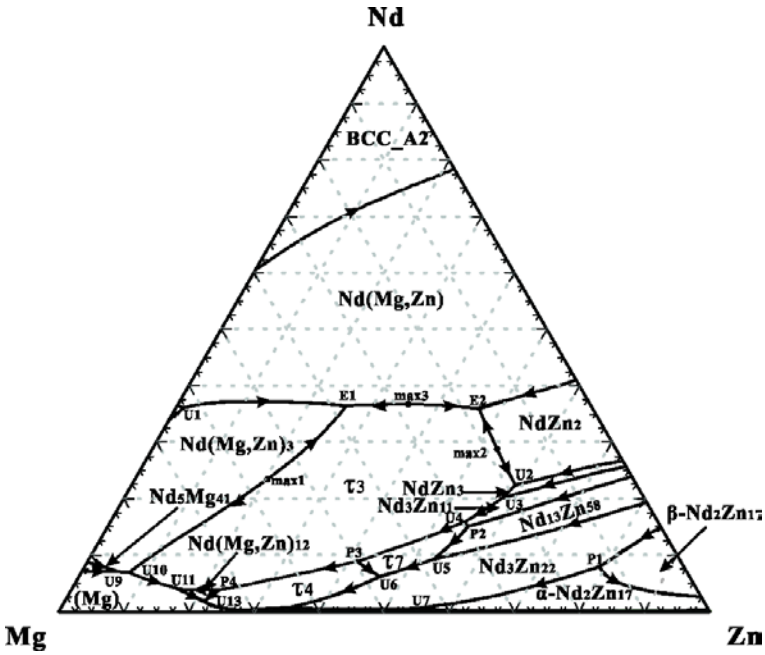

Figure A5.7 Tentative calculated liquidus projection for Nd-Mg-Zn system (mole fraction)

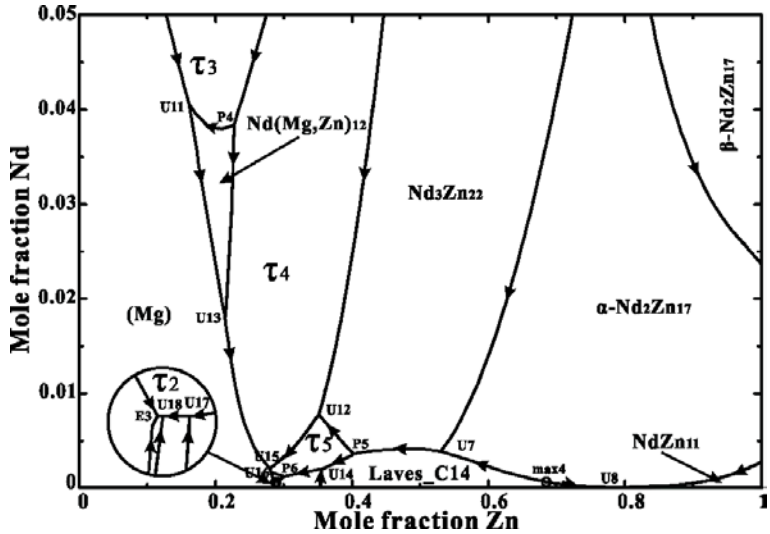

Figure A5.8 Enlargement of part of Fig. A5.7

Table A5.4 Tentative calculated invariant reactions, maxima and minima in the Nd-Mg-Zn system

Type	**Temperature (^{o}C)**	**Reaction**
P1	886	$L + Nd_3Zn_{22} + \beta - Nd_2Zn_{17} \rightarrow \alpha - Nd_2Zn_{17}$
U1	755	$L + Laves_C15 \rightarrow NdMg_3 + Nd(Mg, Zn)$
E1	735	$L \rightarrow Nd(Mg, Zn) + NdMg_3 + \tau 3$
U2	727	$L + NdZn_2 \rightarrow NdZn_3 + \tau 3$
E2	722	$L \rightarrow Nd(Mg, Zn) + NdZn_2 + \tau 3$
U3	716	$L + NdZn_3 \rightarrow Nd_3Zn_{11} + \tau 3$
P2	694	$L + Nd_3Zn_{11} + Nd_{13}Zn_{58} \rightarrow \tau 7$
U4	688	$L + Nd_3Zn_{11} \rightarrow \tau 3 + \tau 7$
U5	665	$L + Nd_{13}Zn_{58} \rightarrow Nd_3Zn_{22} + \tau 7$
P3	612	$L + \tau 3 + \tau 7 \rightarrow \tau 4$
U6	610	$L + \tau 7 \rightarrow Nd_3Zn_{22} + \tau 4$
U7	548	$L + \alpha - Nd_2Zn_{17} \rightarrow Nd_3Zn_{22} + Laves_C14$
U8	544	$L + \alpha - Nd_2Zn_{17} \rightarrow NdZn_{11} + Laves_C14$
U9	516	$L + Nd_5Mg_{41} \rightarrow NdMg_3 + (Mg)$
U10	509	$L + NdMg_3 \rightarrow (Mg) + \tau 3$
P4	488	$L + \tau 3 + \tau 4 \rightarrow Nd(Mg, Zn)_{12}$
U11	482	$L + \tau 3 \rightarrow Nd(Mg, Zn)_{12} + (Mg)$
P5	456	$L + Nd_3Zn_{22} + Laves_C14 \rightarrow \tau 5$
U12	449	$L + Nd_3Zn_{22} \rightarrow \tau 4 + \tau 5$
U13	443	$L + Nd(Mg, Zn)_{12} \rightarrow \tau 4 + (Mg)$
U14	413	$L + Laves_C14 \rightarrow Mg_2Zn_3 + \tau 5$
P6	359	$L + \tau 5 + Mg_2Zn_3 \rightarrow \tau 2$
U15	355	$L + \tau 4 \rightarrow (Mg) + \tau 5$
U16	351	$L + \tau 5 \rightarrow (Mg) + \tau 2$
U17	350	$L + Mg_2Zn_3 \rightarrow \tau 2 + Mg_{12}Zn_{13}$
U18	345	$L + Mg_{12}Zn_{13} \rightarrow \tau 2 + Mg_{51}Zn_{20}$
E3	345	$L \rightarrow Mg_{51}Zn_{20} + \tau 2 + (Mg)$
max1	~788	$L \rightarrow NdMg_3 + \tau 3$
max2	~766	$L \rightarrow NdZn_2 + \tau 3$
max3	~741	$L \rightarrow Nd(Mg, Zn) + \tau 3$
max4	~588	$L \rightarrow Laves_C14 + \alpha - Nd_2Zn_{17}$

Sm-Mg-Zn system

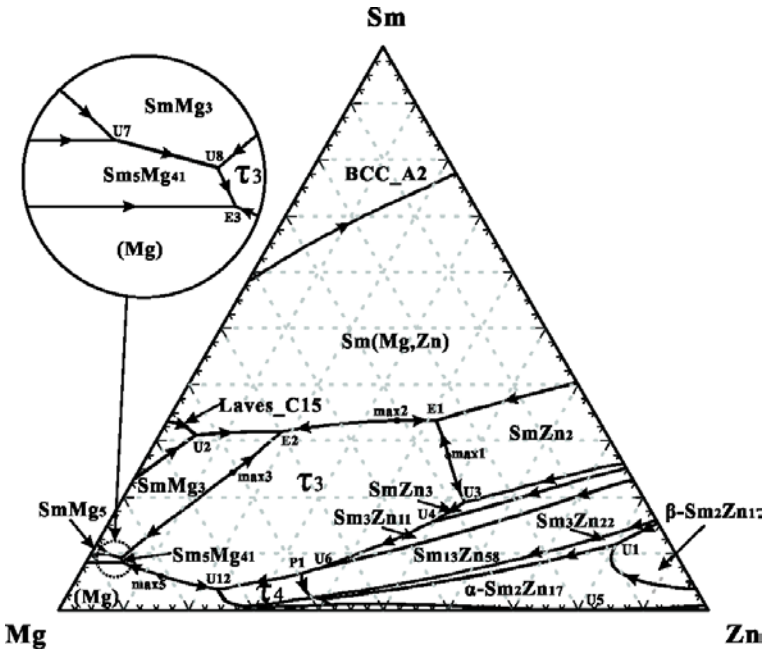

Figure A5.9 Tentative calculated liquidus projection for Sm-Mg-Zn system (mole fraction)

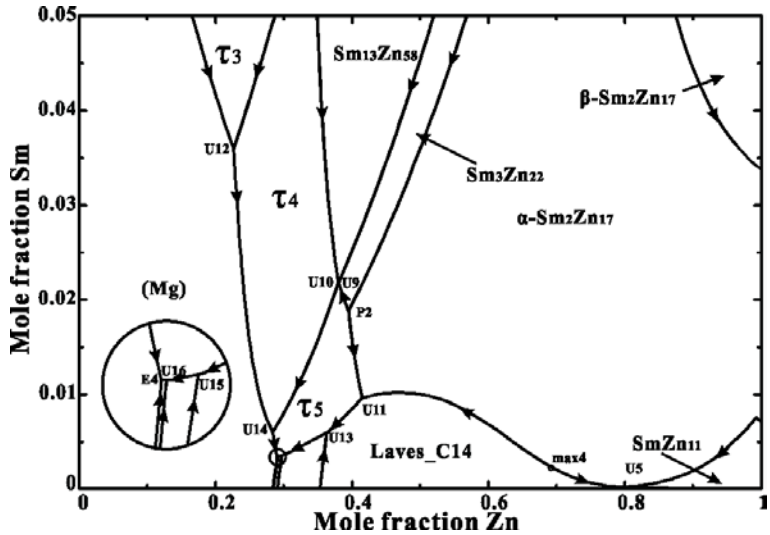

Figure A5.10 Enlargement of part of Fig. A5.9

Table A5.5 Tentative calculated invariant reactions, maxima and minima in the Sm-Mg-Zn system

Type	**Temperature (^{o}C)**	**Reaction**
U1	863	$L+\beta-Sm_2Zn_{17}\rightarrow Sm_3Zn_{22}+\alpha-Sm_2Zn_{17}$
E1	712	$L\rightarrow Sm(Mg,Zn)+SmZn_2+\tau 3$
U2	695	$L+Laves_C15\rightarrow Sm(Mg,Zn)+SmMg_3$
E2	693	$L\rightarrow Sm(Mg,Zn)+SmMg_3+\tau 3$
U3	685	$L+SmZn_2\rightarrow SmZn_3+\tau 3$
U4	655	$L+SmZn_3\rightarrow Sm_3Zn_{11}+\tau 3$
U5	543	$L+\alpha-Sm_2Zn_{17}\rightarrow Laves_C15+SmZn_{11}$
U6	529	$L+Sm_3Zn_{11}\rightarrow \tau 3+Sm_{13}Zn_{58}$
U7	515	$L+SmMg_5\rightarrow SmMg_3+Sm_5Mg_{41}$
P1	510	$L+\tau 3+Sm_{13}Zn_{58}\rightarrow \tau 4$
U8	498	$L+SmMg_3\rightarrow Sm_5Mg_{41}+\tau 3$
E3	489	$L\rightarrow \tau 3+(Mg)+Sm_5Mg_{41}$
P2	464	$L+\alpha-Sm_2Zn_{17}+Sm_3Zn_{22}\rightarrow \tau 5$
U9	458	$L+Sm_3Zn_{22}\rightarrow \tau 5+Sm_{13}Zn_{58}$
U10	458	$L+Sm_{13}Zn_{58}\rightarrow \tau 4+\tau 5$
U11	453	$L+\alpha-Sm_2Zn_{17}\rightarrow Laves_C14+\tau 5$
U12	434	$L+\tau 3\rightarrow (Mg)+\tau 4$
U13	410	$L+Laves_C14\rightarrow Mg_2Zn_3+\tau 5$
U14	357	$L+\tau 4\rightarrow (Mg)+\tau 5$
U15	349	$L+Mg_2Zn_3\rightarrow Mg_{12}Zn_{13}+\tau 5$
U16	343	$L+Mg_{12}Zn_{13}\rightarrow \tau 5+Mg_{51}Zn_{20}$
E4	343	$L\rightarrow Mg_{51}Zn_{20}+\tau 5+(Mg)$
max1	~742	$L\rightarrow SmZn_2+\tau 3$
max2	~716	$L\rightarrow Sm(Mg,Zn)+\tau 3$
max3	~708	$L\rightarrow SmMg_3+\tau 3$
max4	~587	$L\rightarrow Laves_C14+\alpha-Sm_2Zn_{17}$
max5	~496	$L\rightarrow (Mg)+\tau 3$

Y-Mg-Zn system

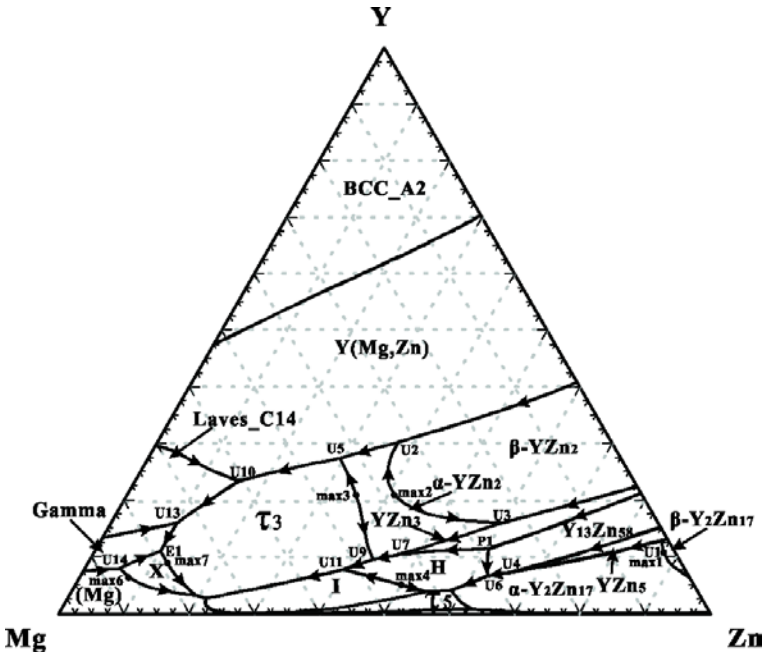

Figure A5.11 Tentative calculated liquidus projection for Y-Mg-Zn system (mole fraction)

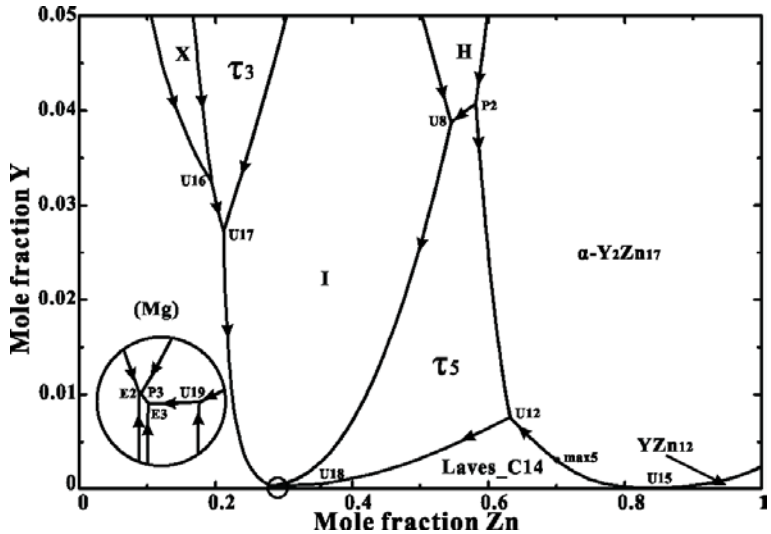

Figure A5.12 Enlargement of part of Fig. A5.11

Table A5.6 Tentative calculated invariant reactions, maxima and minima in the Y-Mg-Zn system

Type	**Temperature (^{o}C)**	**Reaction**
U1	877	$L+\beta-Y_2Zn_{17}\rightarrow\alpha-Y_2Zn_{17}+YZn_5$
U2	752	$L+\beta-YZn_2\rightarrow\alpha-YZn_2+Y(Mg,Zn)$
U3	752	$L+\beta-YZn_2\rightarrow\alpha-YZn_2+YZn_3$
P1	704	$L+Y_{13}Zn_{58}+YZn_3\rightarrow H$
U4	703	$L+YZn_5\rightarrow\alpha-Y_2Zn_{17}+Y_{13}Zn_{58}$
U5	683	$L+\alpha-YZn_2\rightarrow Y(Mg,Zn)+\tau3$
U6	677	$L+Y_{13}Zn_{58}\rightarrow\alpha-Y_2Zn_{17}+H$
U7	636	$L+YZn_3\rightarrow\alpha-YZn_2+H$
P2	629	$L+\alpha-Y_2Zn_{17}+H\rightarrow\tau5$
U8	618	$L+H\rightarrow I+\tau5$
U9	615	$L+\alpha-YZn_2\rightarrow H+\tau3$
U10	608	$L+Y(Mg,Zn)\rightarrow Laves_C14+\tau3$
U11	590	$L+H\rightarrow I+\tau3$
U12	581	$L+\alpha-Y_2Zn_{17}\rightarrow Laves_C14+\tau5$
U13	555	$L+Laves_C14\rightarrow Gamma+\tau3$
U14	539	$L+(Mg)\rightarrow X+Gamma$
E1	529	$L\rightarrow X+Gamma+\tau3$
U15	505	$L+\alpha-Y_2Zn_{17}\rightarrow Laves_C14+YZn_{12}$
U16	464	$L+X\rightarrow\tau3+(Mg)$
U17	448	$L+\tau3\rightarrow I+(Mg)$
U18	413	$L+Laves_C14\rightarrow\tau5+Mg_2Zn_3$
U19	351	$L+Mg_2Zn_3\rightarrow\tau5+Mg_{12}Zn_{13}$
P3	346	$L+I+\tau5\rightarrow Mg_{51}Zn_{20}$
E2	346	$L\rightarrow Mg_{51}Zn_{20}+I+(Mg)$
E3	346	$L\rightarrow Mg_{51}Zn_{20}+\tau5+Mg_{12}Zn_{13}$
max1	~880	$L\rightarrow\alpha-Y_2Zn_{17}+\beta-Y_2Zn_{17}$
max2	~752	$L\rightarrow\alpha-YZn_2+\beta-YZn_2$
max3	~716	$L\rightarrow\alpha-YZn_2+\tau3$
max4	~628	$L\rightarrow H+I$
max5	~585	$L\rightarrow\alpha-Y_2Zn_{17}+Laves_C14$
max6	~585	$L\rightarrow X+(Mg)$
max7	~534	$L\rightarrow X+\tau3$

Gd-Mg-Zn system

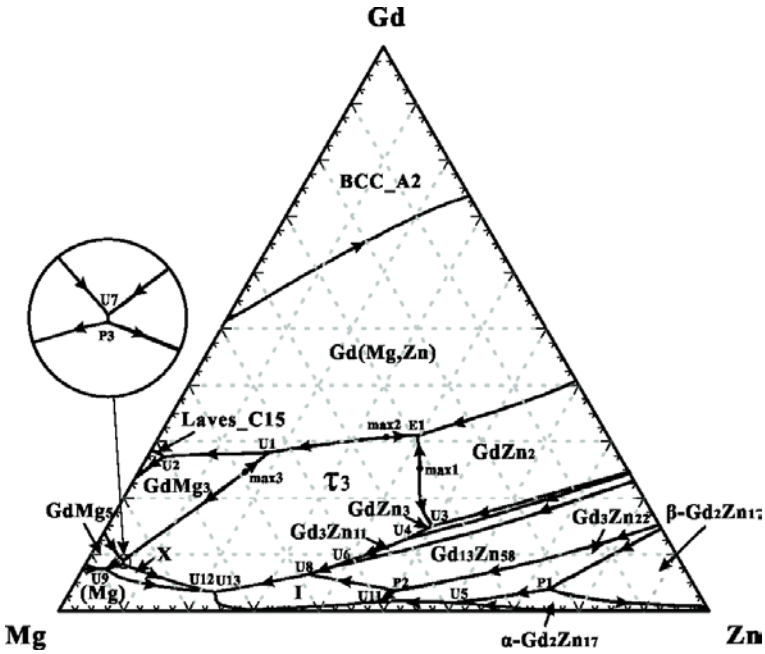

Figure A5.13 Tentative calculated liquidus projection for Gd-Mg-Zn system (mole fraction)

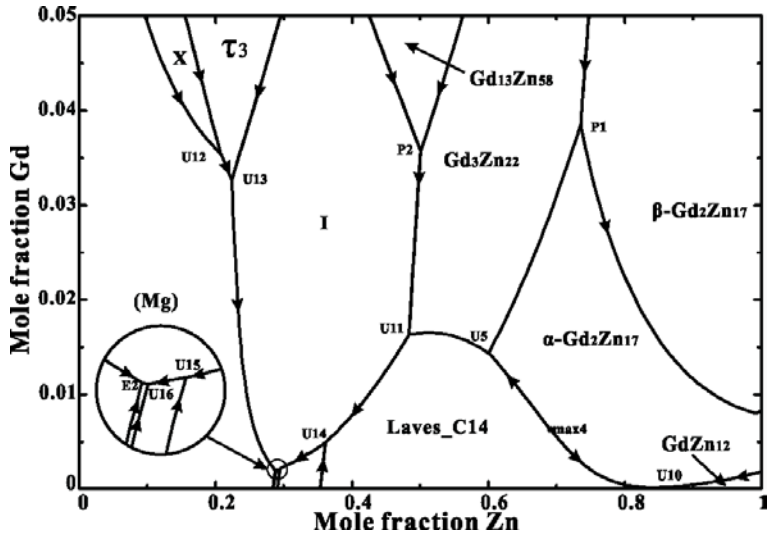

Figure A5.14 Enlargement of part of Fig. A5.13

Table A5.7 Tentative calculated invariant reactions, maxima and minima in the Gd-Mg-Zn system

Type	**Temperature (^{o}C)**	**Reaction**
E1	764	$L \rightarrow Gd(Mg,Zn) + GdZn_2 + \tau 3$
U1	748	$L + \tau 3 \rightarrow Gd(Mg,Zn) + GdMg_3$
U2	732	$L + Gd(Mg,Zn) \rightarrow Laves_C15 + GdMg_3$
P1	727	$L + Gd_3Zn_{22} + \beta - Gd_2Zn_{17} \rightarrow \alpha - Gd_2Zn_{17}$
U3	670	$L + GdZn_2 \rightarrow GdZn_3 + \tau 3$
U4	642	$L + GdZn_3 \rightarrow Gd_3Zn_{11} + \tau 3$
U5	565	$L + \alpha - Gd_2Zn_{17} \rightarrow Gd_3Zn_{22} + Laves_C14$
U6	558	$L + Gd_3Zn_{11} \rightarrow Gd_{13}Zn_{58} + \tau 3$
P2	554	$L + Gd_3Zn_{22} + Gd_{13}Zn_{58} \rightarrow I$
U7	541	$L + GdMg_3 \rightarrow GdMg_5 + \tau 3$
U8	529	$L + Gd_{13}Zn_{58} \rightarrow I + \tau 3$
P3	527	$L + GdMg_5 + \tau 3 \rightarrow X$
U9	523	$L + GdMg_5 \rightarrow (Mg) + X$
U10	505	$L + \alpha - Gd_2Zn_{17} \rightarrow GdZn_{12} + Laves_C14$
U11	497	$L + Gd_3Zn_{22} \rightarrow I + Laves_C14$
U12	451	$L + X \rightarrow (Mg) + \tau 3$
U13	438	$L + \tau 3 \rightarrow (Mg) + I$
U14	410	$L + Laves_C14 \rightarrow Mg_2Zn_3 + I$
U15	350	$L + Mg_2Zn_3 \rightarrow Mg_{12}Zn_{13} + I$
U16	345	$L + Mg_{12}Zn_{13} \rightarrow Mg_{51}Zn_{20} + I$
E2	345	$L \rightarrow Mg_{51}Zn_{20} + I + (Mg)$
max1	~777	$L \rightarrow GdZn_2 + \tau 3$
max2	~768	$L \rightarrow Gd(Mg,Zn) + \tau 3$
max3	~752	$L \rightarrow GdMg_3 + \tau 3$
max4	~584	$L \rightarrow \alpha - Gd_2Zn_{17} + Laves_C14$

Tb-Mg-Zn system

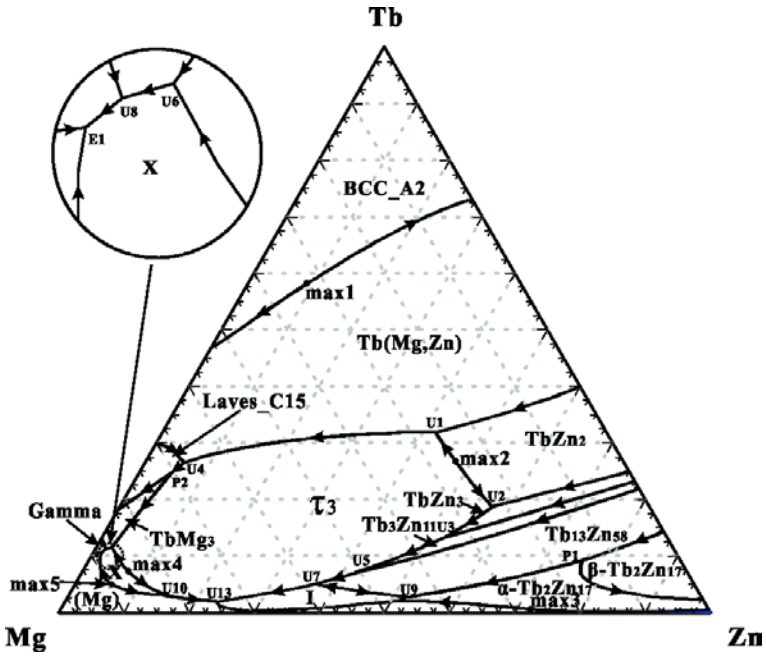

Figure A5.15 Tentative calculated liquidus projection for Tb-Mg-Zn system (mole fraction)

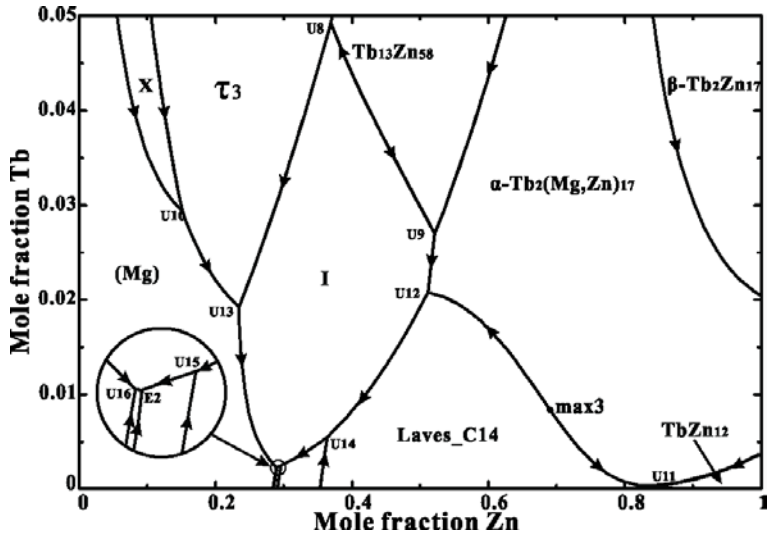

Figure A5.16 Enlargement of part of Fig. A5.15

Table A5.8 Tentative calculated invariant reactions, maxima and minima in the Tb-Mg-Zn system

Type	**Temperature (^{o}C)**	**Reaction**
U1	783	$L + TbZn_2 \rightarrow Tb(Mg, Zn) + \tau 3$
P1	772	$L + Tb_{13}Zn_{58} + \beta - Tb_2Zn_{17} \rightarrow \alpha - Tb_2Zn_{17}$
U2	729	$L + TbZn_2 \rightarrow TbZn_3 + \tau 3$
U3	671	$L + TbZn_3 \rightarrow Tb_3Zn_{11} + \tau 3$
U4	645	$L + Tb(Mg, Zn) \rightarrow Laves_C15 + \tau 3$
P2	637	$L + Laves_C15 + \tau 3 \rightarrow TbMg_3$
U5	577	$L + Tb_3Zn_{11} \rightarrow Tb_{13}Zn_{58} + \tau 3$
U6	537	$L + \tau 3 \rightarrow TbMg_3 + X$
U7	531	$L + Tb_{13}Zn_{58} \rightarrow I + \tau 3$
U8	527	$L + TbMg_3 \rightarrow Gamma + X$
U9	524	$L + Tb_{13}Zn_{58} \rightarrow \alpha - Tb_2Zn_{17} + I$
E1	523	$L \rightarrow Gamma + X + (Mg)$
U10	517	$L + X \rightarrow \tau 3 + (Mg)$
U11	512	$L + \alpha - Tb_2Zn_{17} \rightarrow TbZn_{12} + Laves_C14$
U12	479	$L + \alpha - Tb_2Zn_{17} \rightarrow I + Laves_C14$
U13	439	$L + \tau 3 \rightarrow I + (Mg)$
U14	410	$L + Laves_C14 \rightarrow I + Mg_2Zn_3$
U15	349	$L + Mg_2Zn_3 \rightarrow I + Mg_{12}Zn_{13}$
U16	344	$L + (Mg) \rightarrow I + Mg_{51}Zn_{20}$
E2	344	$L \rightarrow I + Mg_{51}Zn_{20} + Mg_{12}Zn_{13}$
max1	~862	$L \rightarrow Bcc_A2 + Tb(Mg, Zn)$
max2	~805	$L \rightarrow TbZn_2 + \tau 3$
max3	~584	$L \rightarrow Laves_C14 + \alpha - Tb_2Zn_{17}$
max4	~574	$L \rightarrow X + \tau 3$
max5	~570	$L \rightarrow X + (Mg)$

Dy-Mg-Zn system

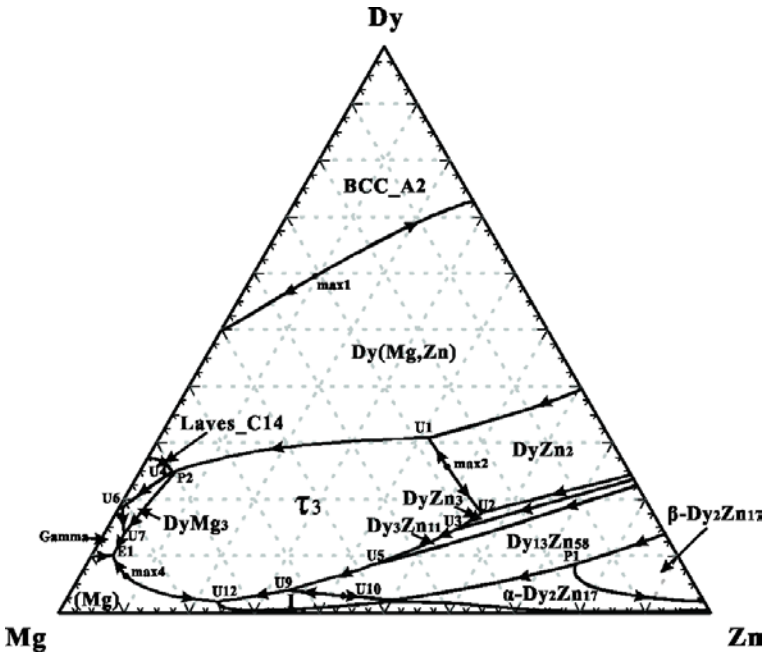

Figure A5.17 Tentative calculated liquidus projection for Dy-Mg-Zn system (mole fraction)

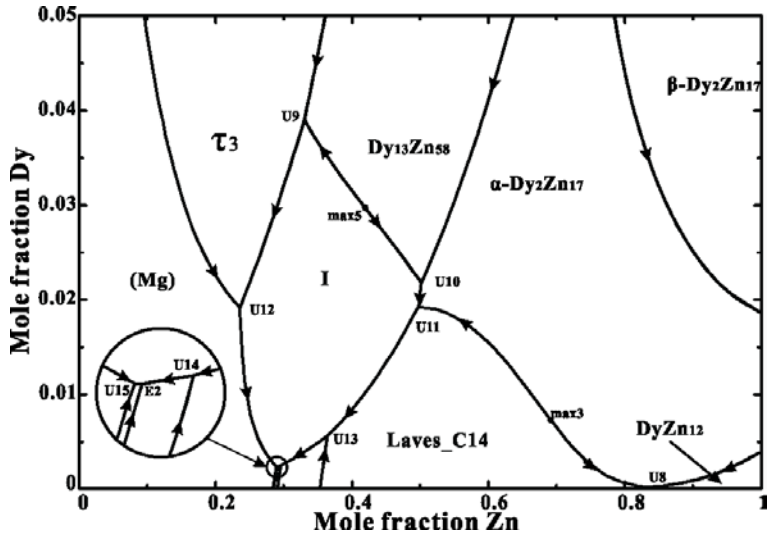

Figure A5.18 Enlargement of part of Fig. A5.17

Table A5.9 Tentative calculated invariant reactions, maxima and minima in the Dy-Mg-Zn system

Type	**Temperature (^{o}C)**	**Reaction**
U1	792	$L + DyZn_2 \rightarrow Dy(Mg, Zn) + \tau 3$
P1	833	$L + Dy_{13}Zn_{58} + \beta - Dy_2Zn_{17} \rightarrow \alpha - Dy_2Zn_{17}$
U2	722	$L + DyZn_2 \rightarrow DyZn_3 + \tau 3$
U3	692	$L + DyZn_3 \rightarrow Dy_3Zn_{11} + \tau 3$
P2	649	$L + Dy(Mg, Zn) + \tau 3 \rightarrow DyMg_3$
U4	647	$L + Dy(Mg, Zn) \rightarrow DyMg_3 + Laves_C14$
U5	610	$L + Dy_3Zn_{11} \rightarrow Dy_{13}Zn_{58} + \tau 3$
U6	605	$L + Laves_C14 \rightarrow DyMg_3 + Gamma$
U7	577	$L + DyMg_3 \rightarrow \tau 3 + Gamma$
E1	539	$L \rightarrow \tau 3 + Gamma + (Mg)$
U8	510	$L + \alpha - Dy_2Zn_{17} \rightarrow DyZn_{12} + Laves_C14$
U9	507	$L + Dy_{13}Zn_{58} \rightarrow I + \tau 3$
U10	507	$L + Dy_{13}Zn_{58} \rightarrow I + \alpha - Dy_2Zn_{17}$
U11	498	$L + \alpha - Dy_2Zn_{17} \rightarrow I + Laves_C14$
U12	436	$L + \tau 3 \rightarrow I + (Mg)$
U13	410	$L + Laves_C14 \rightarrow I + Mg_2Zn_3$
U14	349	$L + Mg_2Zn_3 \rightarrow I + Mg_{12}Zn_{13}$
U15	344	$L + (Mg) \rightarrow I + Mg_{51}Zn_{20}$
E2	344	$L \rightarrow I + Mg_{51}Zn_{20} + Mg_{12}Zn_{13}$
max1	~899	$L \rightarrow Bcc_A2 + Dy(Mg, Zn)$
max2	~899	$L \rightarrow DyZn_2 + \tau 3$
max3	~584	$L \rightarrow Laves_C14 + \alpha - Dy_2Zn_{17}$
max4	~551	$L \rightarrow \tau 3 + (Mg)$
max5	~546	$L \rightarrow Dy_{13}Zn_{58} + I$

Ho-Mg-Zn system

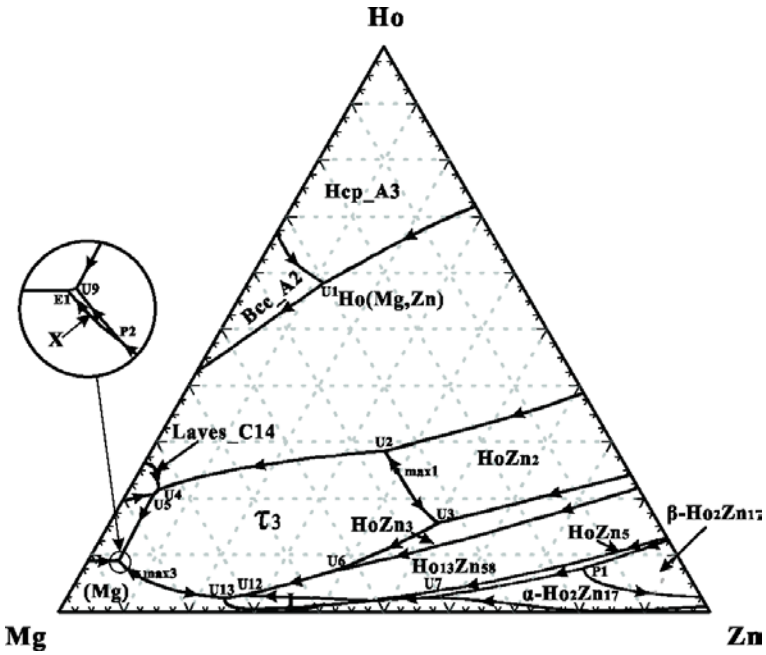

Figure A5.19 Tentative calculated liquidus projection for Ho-Mg-Zn system (mole fraction)

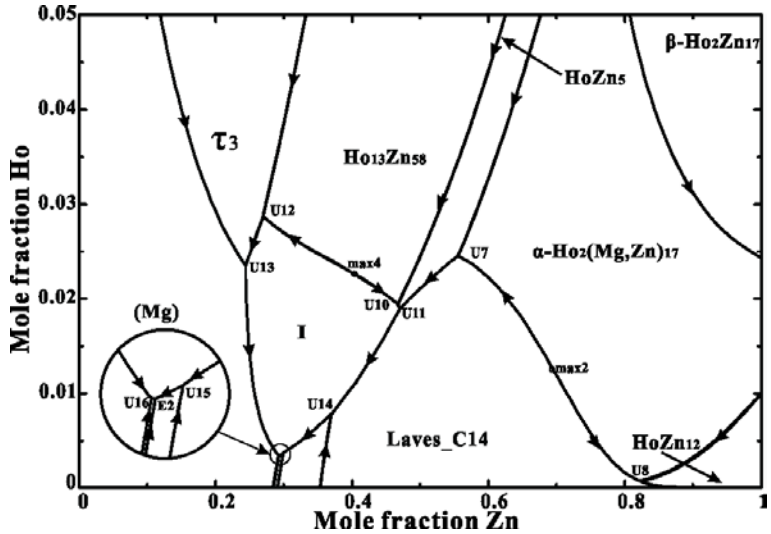

Figure A5.20 Enlargement of part of Fig. A5.19

Table A5.10 Tentative calculated invariant reactions, maxima and minima in the Ho-Mg-Zn system

Type	**Temperature (^{o}C)**	**Reaction**
U1	892	$L + Hcp_A3 \rightarrow Ho(Mg,Zn) + Bcc_A2$
U2	770	$L + HoZn_2 \rightarrow Ho(Mg,Zn) + \tau 3$
P1	750	$L + HoZn_5 + \beta - Ho_2Zn_{17} \rightarrow \alpha - Ho_2Zn_{17}$
U3	705	$L + HoZn_2 \rightarrow HoZn_3 + \tau 3$
U4	588	$L + Ho(Mg,Zn)_2 \rightarrow Laves_C14 + \tau 3$
U5	581	$L + Laves_C14 \rightarrow Gamma + \tau 3$
U6	573	$L + HoZn_3 \rightarrow Ho_{13}Zn_{58} + \tau 3$
U7	524	$L + \alpha - Ho_2Zn_{17} \rightarrow HoZn_5 + Laves_C14$
P2	523	$L + (Mg) + \tau 3 \rightarrow X$
U8	519	$L + \alpha - Ho_2Zn_{17} \rightarrow HoZn_{12} + Laves_C14$
U9	517	$L + \tau 3 \rightarrow X + Gamma$
E1	517	$L \rightarrow X + Gamma + (Mg)$
U10	475	$L + Ho_{13}Zn_{58} \rightarrow HoZn_5 + I$
U11	473	$L + HoZn_5 \rightarrow Laves_C14 + I$
U12	451	$L + Ho_{13}Zn_{58} \rightarrow \tau 3 + I$
U13	430	$L + \tau 3 \rightarrow (Mg) + I$
U14	407	$L + Laves_C14 \rightarrow I + Mg_2Zn_3$
U15	348	$L + Mg_2Zn_3 \rightarrow I + Mg_{12}Zn_{13}$
U16	343	$L + (Mg) \rightarrow I + Mg_{51}Zn_{20}$
E2	343	$L \rightarrow I + Mg_{51}Zn_{20} + Mg_{12}Zn_{13}$
max1	~781	$L \rightarrow HoZn_2 + \tau 3$
max2	~580	$L \rightarrow Laves_C14 + \alpha - Ho_2Zn_{17}$
max3	~527	$L \rightarrow \tau 3 + (Mg)$
max4	~486	$L \rightarrow I + Ho_{13}Zn_{58}$

Er-Mg-Zn system

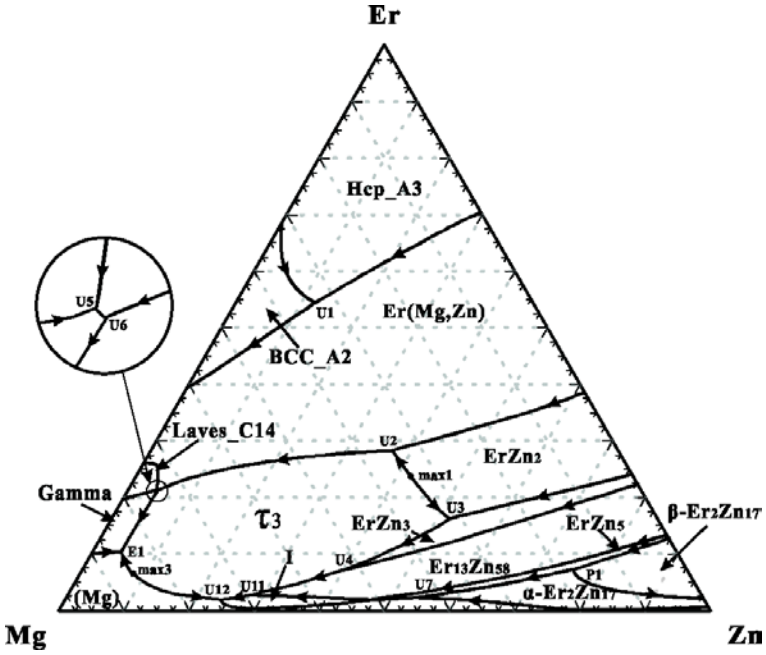

Figure A5.21 Tentative calculated liquidus projection for Er-Mg-Zn system (mole fraction)

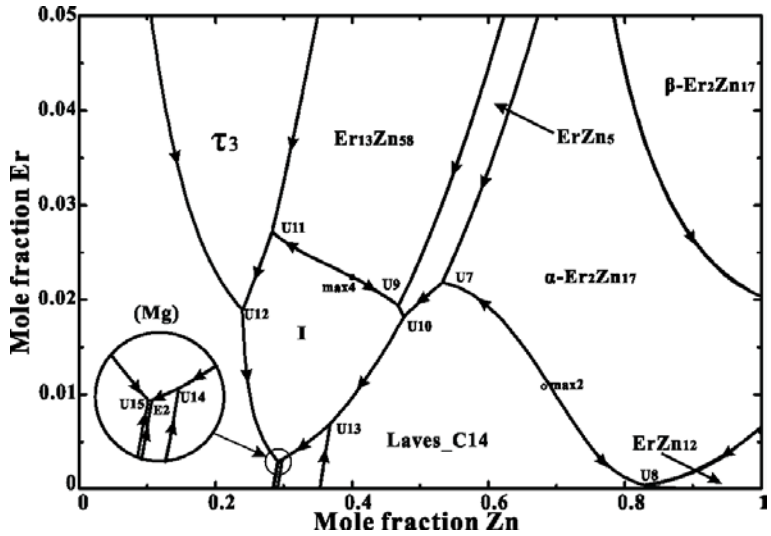

Figure A5.22 Enlargement of part of Fig. A5.21

Table A5.11 Tentative calculated invariant reactions, maxima and minima in the Er-Mg-Zn system

Type	**Temperature (^{o}C)**	**Reaction**
U1	881	$L + Hcp_A3 \rightarrow Er(Mg,Zn) + Bcc_A2$
U2	774	$L + ErZn_2 \rightarrow Er(Mg,Zn) + \tau 3$
P1	750	$L + ErZn_5 + \beta - Er_2Zn_{17} \rightarrow \alpha - Er_2Zn_{17}$
U3	719	$L + ErZn_2 \rightarrow ErZn_3 + \tau 3$
U4	589	$L + ErZn_3 \rightarrow Er_{13}Zn_{58} + \tau 3$
U5	568	$L + Laves_C14 \rightarrow Er(Mg,Zn) + Gamma$
U6	567	$L + Er(Mg,Zn) \rightarrow \tau 3 + Gamma$
E1	532	$L \rightarrow \tau 3 + Gamma + (Mg)$
U7	514	$L + \alpha - Er_2Zn_{17} \rightarrow Laves_C14 + ErZn_5$
U8	513	$L + \alpha - Er_2Zn_{17} \rightarrow Laves_C14 + ErZn_{12}$
U9	485	$L + Er_{13}Zn_{58} \rightarrow I + ErZn_5$
U10	479	$L + ErZn_5 \rightarrow I + Laves_C14$
U11	469	$L + Er_{13}Zn_{58} \rightarrow I + \tau 3$
U12	434	$L + \tau 3 \rightarrow I + (Mg)$
U13	408	$L + Laves_C14 \rightarrow I + Mg_2Zn_3$
U14	348	$L + Mg_2Zn_3 \rightarrow I + Mg_{12}Zn_{13}$
U15	344	$L + (Mg) \rightarrow I + Mg_{51}Zn_{20}$
E2	343	$L \rightarrow I + Mg_{51}Zn_{20} + Mg_{12}Zn_{13}$
max1	~785	$L \rightarrow ErZn_2 + \tau 3$
max2	~582	$L \rightarrow Laves_C14 + \alpha - Er_2Zn_{17}$
max3	~545	$L \rightarrow \tau 3 + (Mg)$
max4	~497	$L \rightarrow I + Er_{13}Zn_{58}$

Tm-Mg-Zn system

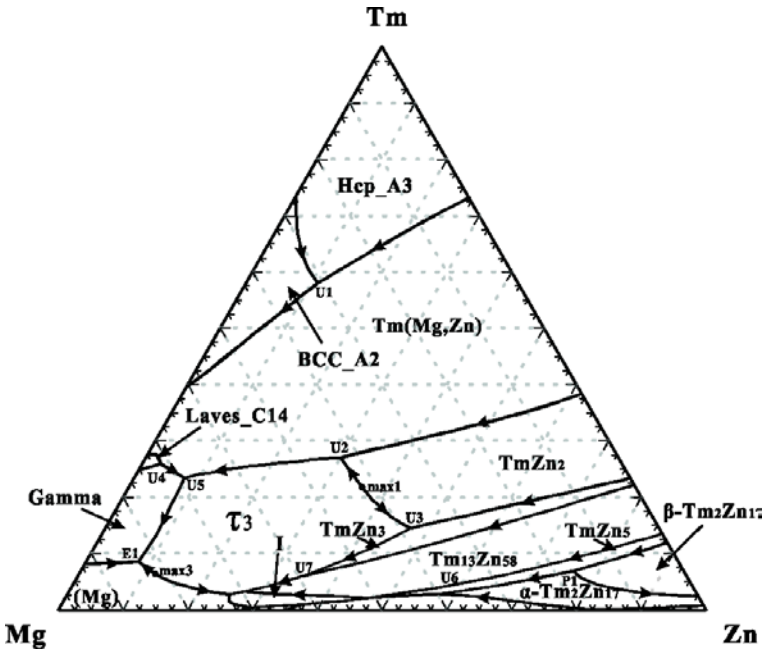

Figure A5.23 Tentative calculated liquidus projection for Tm-Mg-Zn system (mole fraction)

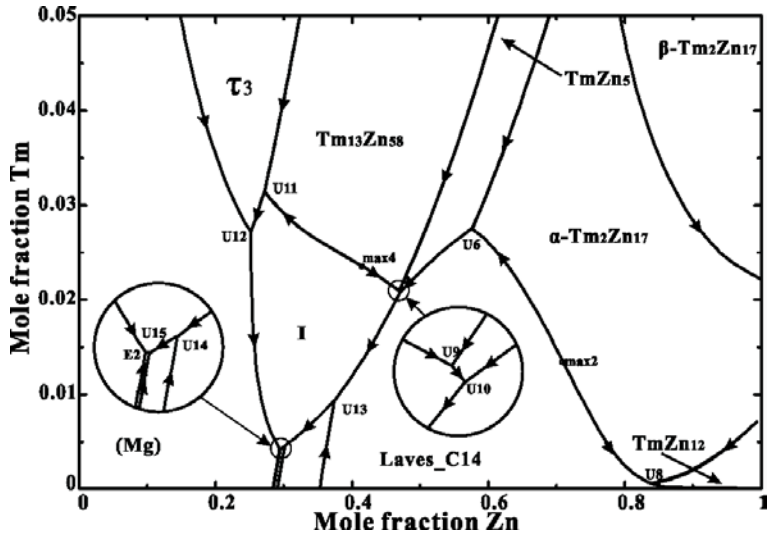

Figure A5.24 Enlargement of part of Fig. A5.23

Table A5.12 Tentative calculated invariant reactions, maxima and minima in the Tm-Mg-Zn system

Type	**Temperature (^{o}C)**	**Reaction**
U1	843	$L + Hcp_A3 \rightarrow Tm(Mg, Zn) + Bcc_A2$
P1	727	$L + TmZn_5 + \beta - Tm_2Zn_{17} \rightarrow \alpha - Tm_2Zn_{17}$
U2	711	$L + TmZn_2 \rightarrow Tm(Mg, Zn) + \tau 3$
U3	664	$L + TmZn_2 \rightarrow TmZn_3 + \tau 3$
U4	577	$L + Laves_C14 \rightarrow Tm(Mg, Zn) + Gamma$
U5	571	$L + Tm(Mg, Zn) \rightarrow \tau 3 + Gamma$
U6	529	$L + \alpha - Tm_2Zn_{17} \rightarrow Laves_C14 + TmZn_5$
U7	525	$L + TmZn_3 \rightarrow Tm_{13}Zn_{58} + \tau 3$
E1	510	$L \rightarrow \tau 3 + Gamma + (Mg)$
U8	501	$L + \alpha - Tm_2Zn_{17} \rightarrow Laves_C14 + TmZn_{12}$
U9	467	$L + Tm_{13}Zn_{58} \rightarrow I + TmZn_5$
U10	467	$L + TmZn_5 \rightarrow I + Laves_C14$
U11	442	$L + Tm_{13}Zn_{58} \rightarrow I + \tau 3$
U12	426	$L + \tau 3 \rightarrow I + (Mg)$
U13	406	$L + Laves_C14 \rightarrow I + Mg_2Zn_3$
U14	347	$L + Mg_2Zn_3 \rightarrow I + Mg_{12}Zn_{13}$
U15	342	$L + Mg_{12}Zn_{13} \rightarrow I + Mg_{51}Zn_{20}$
E2	342	$L \rightarrow I + Mg_{51}Zn_{20} + (Mg)$
max1	~728	$L \rightarrow TmZn_2 + \tau 3$
max2	~577	$L \rightarrow Laves_C14 + \alpha - Tm_2Zn_{17}$
max3	~516	$L \rightarrow \tau 3 + (Mg)$
max4	~478	$L \rightarrow I + Tm_{13}Zn_{58}$

Lu-Mg-Zn system

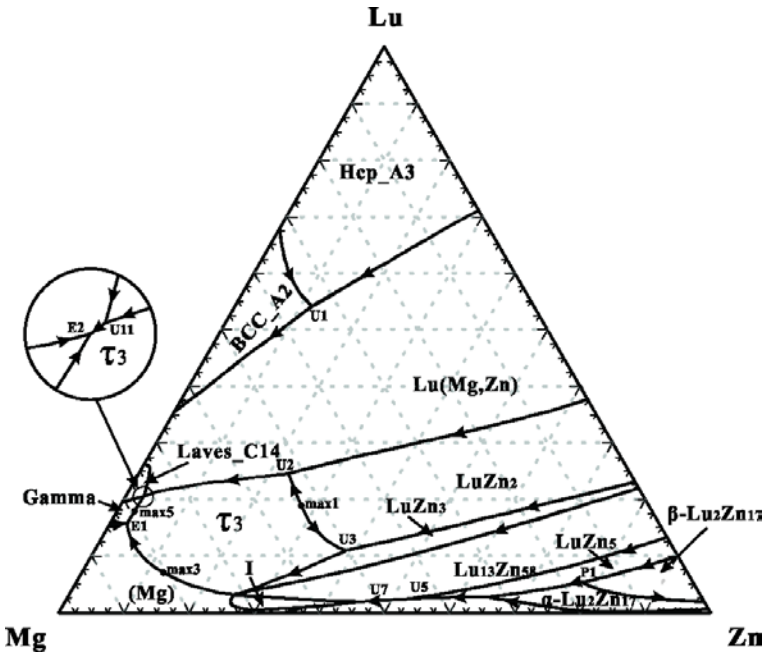

Figure A5.25 Tentative calculated liquidus projection for Lu-Mg-Zn system (mole fraction)

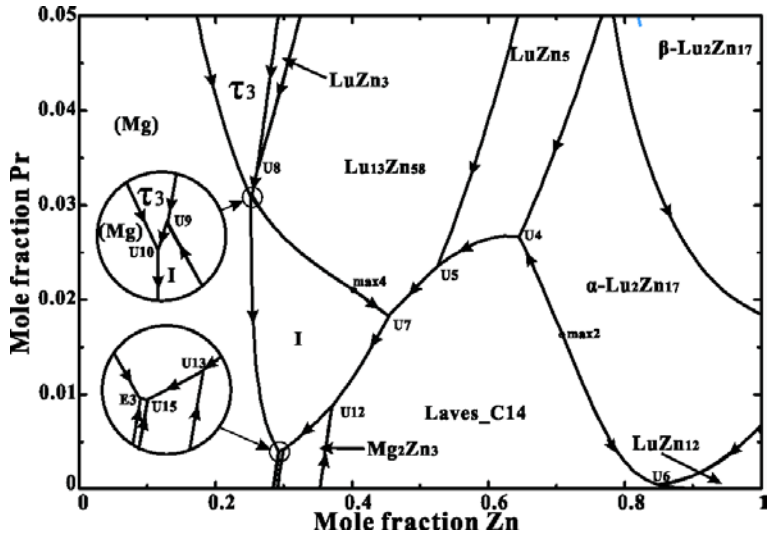

Figure A5.26 Enlargement of part of Fig. A5.25

Table A5.13 Tentative calculated invariant reactions, maxima and minima in the Lu-Mg-Zn system

Type	**Temperature (^{o}C)**	**Reaction**
U1	867	$L + Hcp_A3 \rightarrow Lu(Mg,Zn) + Bcc_A2$
P1	700	$L + LuZn_5 + \beta - Lu_2Zn_{17} \rightarrow \alpha - Lu_2Zn_{17}$
U2	652	$L + LuZn_2 \rightarrow Lu(Mg,Zn) + \tau 3$
U3	605	$L + LuZn_2 \rightarrow LuZn_3 + \tau 3$
U4	561	$L + \alpha - Lu_2Zn_{17} \rightarrow Laves_C14 + LuZn_5$
U5	509	$L + LuZn_5 \rightarrow Tm_{13}Zn_{58} + Laves_C14$
U6	488	$L + \alpha - Lu_2Zn_{17} \rightarrow Laves_C14 + LuZn_{12}$
U7	463	$L + Lu_{13}Zn_{58} \rightarrow I + Laves_C14$
U8	435	$L + LuZn_3 \rightarrow Lu_{13}Zn_{58} + \tau 3$
U9	425	$L + Lu_{13}Zn_{58} \rightarrow I + \tau 3$
U10	424	$L + \tau 3 \rightarrow I + (Mg)$
E1	409	$L \rightarrow \tau 3 + Gamma + (Mg)$
U11	408	$L + Lu(Mg,Zn) \rightarrow \tau 3 + Laves_C14$
U12	407	$L + Laves_C14 \rightarrow I + Mg_2Zn_3$
E2	406	$L \rightarrow \tau 3 + Gamma + Laves_C14$
U13	348	$L + Mg_2Zn_3 \rightarrow I + Mg_{12}Zn_{13}$
U14	343	$L + Mg_{12}Zn_{13} \rightarrow I + Mg_{51}Zn_{20}$
E3	343	$L \rightarrow I + Mg_{51}Zn_{20} + (Mg)$
max1	~669	$L \rightarrow LuZn_2 + \tau 3$
max2	~574	$L \rightarrow Laves_C14 + \alpha - Lu_2Zn_{17}$
max3	~503	$L \rightarrow \tau 3 + (Mg)$
max4	~470	$L \rightarrow I + Lu_{13}Zn_{58}$
max5	~412	$L \rightarrow \tau 3 + Gamma$